جامعة سيدي محمد بن عبد الله بفاس
UNIVERSITÉ SIDI MOHAMED BEN ABDELLAH DE FES

كلية العلوم ظهر المهراز فاس
FACULTE DES SCIENCES DHAR EL MAHRAZ FES

N° d'ordre : 09/2023

Centre des Etudes : ***Sciences et Techniques et Sciences Médicales***

Formation Doctorale : ***Ressources Naturelles et Développement Durable***

Discipline : ***Géologie du Quaternaire***
Spécialité : ***Géosciences et Ressources Naturelles***
Laboratoire : ***LIEME***

THÈSE DE DOCTORAT

Titre de la thèse : Approche de la stratigraphie séquentielle dans le déchiffrage climatique et néotectonique dans les dépôts lacustres : cas d'Ifrah et d'Imouzzer Kandar (Moyen Atlas, Maroc)

Présentée par :

Azennoud Khalil

Soutenue le 04-02-2023 devant le jury :

Rhoujjati Ali	PES	Université Cadi Ayyad (FST)	Président
Nutz Alexis	PH	Université Aix Marseille (France)	Rapporteur & examinateur
Larbi Boudad	PES	Université Mohammed V (FS)	Rapporteur & examinateur
Dridri abdallah	PES	Université Sidi Mohamed Ben Abdellah (FSDM)	Rapporteur & examinateur
Benkaddour Abdelfattah	PES	Université Cadi Ayyad (FST)	Examinateur
Oukassou Mostafa	PES	Université Hassan II (FS Ben M'Sik)	Examinateur
Cheddadi Rachid	PES	Directeur de Recherche (CNRS, France)	Examinateur
Ait Brahim Yassine	PH	Université Mohammed VI polytechnique, Ben Guerir	Examinateur
Boushaba Abdellah	PES	Université Sidi Mohamed Ben Abdellah (FSDM)	Invité
Baali Abdennasser	PES	Université Sidi Mohamed Ben Abdellah (FSDM)	Directeur de thèse

Année Universitaire : 2022-2023

Résumé de la thèse

Bien que divers par leur nature et origine, les systèmes lacustres sont des lieux privilégiés pour la réception et la préservation des signatures allocycliques tels que les pulsations tectoniques et les forçages climatiques à différentes fenêtres temporelles (échelles orbitale, suborbitale et instantanée). Néanmoins, l'examen de déchiffrage de ces signatures cycliques reçues et préservées dans les sédiments est très délicat et exige d'approcher une méthodologie s'appuyant sur un travail de terrain et au laboratoire à la fois extensif et minutieux. Parallèlement à cette logique, le travail mené apporte un coup d'essai où deux exemples-types de systèmes lacustres, situés dans le Moyen Atlas septentrional (Nord du Maroc), à dominante lithologique et contexte morpho-structural différents sont examinés : un système lacustre où la sédimentation est détritico-biochimique se développant sur une structure comparable à celle d'un hémi-graben (lac Ifrah) et un système fluviolacustre à dominante lithologique carbonatée, tufs calcaires (Imouzzer Kandar). L'interprétation des systèmes de dépôts, l'identification des cycles et cortèges sédimentaires par rapport à la variation du niveau de base et de l'accommodation ainsi qu'à l'examen des déformations synsédimentaires sont élaborés moyennant l'usage conventionnel d'une analyse sédimentologique, stratigraphique séquentielle et géologique structurale détaillée. Couplée à cette approche plutôt axée sur le travail de terrain, une étude basée sur de nombreux marqueurs paléoenvironnementaux (matière organique, ostracodes, macro-charbons, phases minérales, K, A, K/Al, Fe/Mn) est également adoptée et faisant objet du travail extensif au laboratoire.

Dans l'exemple-type du lac Ifrah où la dépression est développée moyennant la subsidence cumulative causée par la faille maîtresse du système en hémi-graben, l'examen des déformations 'ductiles' et cassantes synsédimentaires a permis de décrypter les signatures de la paléo-séismicité à l'échelle régionale et celles des pulsations tectoniques à l'échelle du bassin. L'application des relations structurales d'échelle au système en hémi-graben a permis d'estimer, *a priori*, l'accommodation due à la subsidence du compartiment inférieur et le soulèvement du compartiment supérieur de part et d'autre de la faille maîtresse. Par extension, un modèle d'ouverture du bassin du lac Ifrah est proposé sur la base d'une combinaison des observations structurales à l'échelle régionale et des données géophysiques, pétrographiques et géodynamiques de la littérature. L'exploitation de ces perspectives, en plus de l'emploi, sur le même endroit, d'une approche sédimentologique et stratigraphique conventionnelle, complémentée par l'étude micropaléontologique (ostracodes) et géochimique élémentaire, a donné accès à l'extraction des signatures des forçages orbital (*viz*., précession et obliquité), suborbital (oscillation de type Dansgaard-Oeschger, événements de Heinrich) et tectonique (basculement différentiel du compartiment inférieur). L'approche appliquée à l'étude de cas serait d'une grande convenance par rapport aux reconstitutions paléoclimatiques et néotectoniques dans des contextes similaires.

Quant au site d'Imouzzer Kandar, l'analyse sédimentologique et séquentielle, complémentée par une étude multi-proxy, appliquée aux tufs calcaires fluviolacustres développés durant les derniers *ca*. 5000 années dans un contexte géomorphologique impliquant un système en barrage-retenue d'une dimension considérable (kilométrique), a démontré le control exclusif des paramètres climatiques sur la sédimentation et sur l'accommodation potentielle. Deux événements froids d'ampleur global (événements de Bond 4.6 ka et 2.7 ka) sont extraits de ces registres géologiques pour la première fois. L'étude a souligné le grand potentiel des tufs calcaires dans l'archivage des signatures du forçage climatique suborbital.

Mots clés : pulsations tectoniques et forçages climatiques ; Systèmes lacustres ; Tufs calcaires ; Stade Isotopique Marin-3 ; Stratigraphie séquentielle ; Structures de déformations synsédimentaires ; Moyen Atlas ; Maroc.

Abstract

While diverse in nature and origin, lake systems are ideal recipients of allocyclic signatures such as tectonic pulses and climate forcing at different time windows (orbital, suborbital and instantaneous scales). Nevertheless, deciphering these cyclic signatures is extremely difficult and requires the adoption of a methodology based upon extensive and meticulous fieldwork and laboratory work. In line with this reasoning, the herein conducted work examines two typical examples of lake systems in the northern Middle Atlas (northern Morocco), each with a different lithological dominance and morpho-structural setting: a lacustrine system involving cyclic clastic-biochemical sedimentation developing upon a half-graben-like structural setting (lake Ifrah); and a carbonate-dominated fluviolacustrine system, tufa deposits (Imouzzer Kandar). Interpretation of depositional systems, delineation of sedimentary cycles and systems tracts with respect to base level and accommodation variation, along with investigation of 'ductile' and brittle soft-sediment deformations are carried out through the conventional application of thorough sedimentological, sequence stratigraphic and structural geological analyses. In conjunction with this rather fieldwork-oriented approach, extensive laboratory work has been conducted in order to build results of numerous palaeoenvironmental markers (organic matter, ostracods, macro-charcoal, mineral phases, K, A, K/Al, Fe/Mn).

In the typical example of lake Ifrah, where the depression is developed through master fault cumulative subsidence in a half-graben-like structural setting, examination of synsedimentary 'ductile' and brittle soft-sediment deformations has allowed extraction of regional-scale palaeoseismic signals and basin-scale tectonic pulses since the Marine Stage Isotope-3. The application of structural scaling relationships to the half-graben-like system allowed a preliminary estimation of the accommodation due to the hanging-wall subsidence and footwall uplift on either side of the master fault. By extension, a model explaining the mechanism behind the initiation of lake Ifrah Basin is proposed based upon a combination of regional structural observations and geophysical, petrographic and geodynamic data from the literature. Building on these insights, in addition to the use of a conventional sedimentological and stratigraphic approach at the same location, complemented by a micropalaeontological (ostracod-based) and elemental geochemical analyses, the signatures of orbital (*viz*., precession and obliquity), suborbital (Dansgaard-Oeschger-type oscillation, Heinrich Events), and tectonic (differential tilting of the hanging-wall) forcing have been deciphered. The approach applied to the case study would be of great effectiveness in deciphering climatic and neotectonics' signatures in comparable settings.

Regarding the example of the Imouzzer Kandar site, the sedimentological and sequence analysis, coupled with a multi-proxy approach, applied to fluviolacustrine tufa deposited during the last ca. 5000 years, with geomorphological setting involving a barrage-dammed-area system of considerable dimension (kilometre), demonstrates exclusive climate control on sedimentation and potential accommodation. Two cold relapses events (Bond Events 4.6 and 2.7 ka) have been extracted for the first time from these archives. The case study highlighted the great potential of tufa in capturing signals of suborbital climate forcing.

Keywords: Tectonic pulses and climate forcing; Lacustrine systems; Tufa; Marin Isotope Stage-3; Sequence stratigraphy; Soft-sediment deformation structures; Middle Atlas; Morocco.

Remerciements

L'aide et le soutien dans la science est une vertu à nul autre second. Il s'agit d'un acte qui propulse les frontières de la science. Dans cette lumière, l'exploit de ce travail n'aurait jamais eu le jour sans l'influence concrète de plusieurs personnes et organismes dont j'ai l'honneur de pouvoir leur adresser avec beaucoup d'émotion les expressions de remerciements les plus distinguées.

Au premier abord, j'exprime ma profonde reconnaissance à mon professeur **Abdennasser Baali** pour les efforts colossaux qu'il a déployés dans la direction du travail. Merci pour votre soutien et votre ouverture corps et âme, merci pour le long temps consacré dans les relectures en me donnant les conseils avisés et mille mercis pour la confiance que vous m'accordez. Je ne peux passer sans l'évocation de vos interventions en guise de produire l'environnement adéquat de travail et d'approcher tout ce qui est loin, qui ont de loin contribué à l'aboutissement du travail.

Je souhaiterais remercier l'organisme d'accueil, la présidence de l'**Université Sidi Mohamed Ben Abdellah,** pour son soutien financier des quatre datations au radiocarbone faites en Lituanie. Dans le même sens, je remercie vivement et chaleureusement **Amine Couscous** pour son intervention amicale dans la procédure, et **Julius Pažolis**, directeur du laboratoire de datation (Vinius Radiocarbon), d'avoir aimablement accepté de remplacer trois échantillons ayant échoué à procurer la quantité requise.

J'adresse mes sincères remerciements au professeur M^{me} **Naima Bachiri** d'avoir cordialement accordé de m'accueillir et m'accompagner dans le cadre d'un stage dans son laboratoire d'analyse palynologique. Malgré l'échec à cause de la pandémie, les deux mois de stage m'ont permis d'acquérir des connaissances incommensurables surtout dans le plan pratique, mille mercis madame. Dans le même sens, je souhaiterais remercier l'organisme d'accueil, **Faculté des Sciences Ben M'Sik** et son doyen, professeur **Mohammed Talbi**, le chef de département de Géologie, professeur **Mohammed Raji** et le responsable du laboratoire, professeur **Rachid Essamoud**. J'en profite de l'occasion pour remercier vivement les chercheurs experts **Rachid Cheddadi** et **Maria Fernanda Sanchez Goñi** pour la discussion scientifique et les précieuses informations qui m'ont aimablement transmises concernant le protocole d'analyse, merci mes seniors chercheurs.

Je souhaiterais également adresser mes reconnaissances les plus distinguées au professeur **Fransesc Mezquita-Joanes** pour ses efforts considérables déployés dans la détermination des ostracodes et leurs significations écologiques, et au professeur **Alexis Nutz** et au docteur **Stratos Delogkos** pour les discussions fructueuses aux sujets de la stratigraphie séquentielle et de la géologie

structurale. Je suis placé dans l'obligation d'annoncer que plusieurs aspects du travail ont été inspirés des travaux d'**Alexis Nutz** tant sur le plan forme (illustrations, enchainement logique des sections) que sur le plan contenu scientifique (sédimentologie et stratigraphie).

Des remerciements spéciaux sont destinés à mon cher professeur et ami **Yassine Ait Brahim** qui, à partir du jour où j'ai appris à le connaître, m'a beaucoup aidé tant sur le plan personnel que sur le plan académique, merci **Yassine**.

J'exprime mes remerciements les plus distingués au professeur **Ali Rhoujjati** d'avoir accepté de présider la soutenance et les rapporteurs de la thèse, professeurs **Alexis Nutz**, **Larbi Boudad** et **Abdallah Dridri**. J'adresse également les expressions de gratitude les plus raffinées aux autres membres du jury qui ont accepté d'examiner ce travail, professeurs **Rachid Cheddadi**, **Abdelfattah Benkaddour**, **Mostafa Oukassou** et **Yassine Ait Brahim** ainsi qu'à mon cher professeur **Abdellah Boushaba**.

Je remercie tous les doctorants que j'ai rencontrés et avec lesquels j'ai passé des bons moments en échangeant des connaissances et expériences sur le terrain et au laboratoire. Un merci particulier à **Youssra Ahouach** et à **Soukaina Targhi** pour leur aide incommensurable au laboratoire.

En fin, mais pas des moindres, je remercie ma famille, mes tantes, mes oncles et mes cousines et cousins, particulièrement mon père spirituel **My Ahmed**, mes tantes **Houriya**, **Maryama** et **Badia**, mon oncle **Taïb**, mes cousines **Afaf**, **Souhad** et **Siham**, de m'avoir soutenu tout au long de ce parcours. Un grand merci à mes frères, **Naoufal** et **Yassir**, et à ma **mère** à qui je donne ma vie de par tout ce qu'elle a fait pour nous depuis le décès de mon père, *Allah Irahmou*, très tôt dans notre enfance et sa jeunesse, merci perle mère.

Je finirais ces remerciements avec une petite pensée pour mon **père**, **Jaouad**. Tu es parti bien trop tôt. J'espère que, de là où tu es, tu gardes un œil sur nous et que je ne te déçois pas. Je te dédie ce travail.

SOMMAIRE

Résumé ____ *I*
Abstract ____ *II*
Remerciements ____ *IV*
Préface ____ *XIII*

CHAPITRE I ____ *1*
INTRODUCTION GENERALE ____ *1*
1 Systèmes lacustres à dominante détritico-carbonatée ____ *4*
1.1 Processus réguliers et événements extrêmes ____ **5**
1.1.1 Processus physiques réguliers ____ 5
1.1.2 Processus biochimiques ____ 7
1.1.3 Événements extrêmes et dépôts associés ____ 8
1.2 Sédimentation et environnements de dépôt ____ **9**
1.2.1 Lacs dominés par l'activité détritique ____ 9
1.2.2 Lacs dominés par l'activité biologique authigénique ____ 11
1.3 Facteurs de contrôle de la sédimentation et modèle hydro-stratigraphique ____ **12**
2 Sédimentation fluviolacustre à dominante carbonatée : tufs calcaires ____ *15*

CHAPITRE II ____ *21*
PLACE DU MOYEN ATLAS DANS SON CONTEXTE GEOLOGIQUE ET CLIMATIQUE ET METHODOLOGIE ____ *21*
1 Présentation de la zone d'étude ____ *22*
1.1 Cadre géologique ____ **22**
1.2 Cadre climatique et paléoclimatique ____ **26**
1.2.1 Circulation atmosphérique globale et position du Maroc dans celle-ci ____ 26
1.2.2 Climat actuel du Moyen Atlas ____ 27
1.2.3 Histoire climatique depuis le Stade Isotopique Marin 3 (SIM-3) de l'Afrique du NO : données des géoarchives lacustres et spéléothèmes ____ 28
2 Méthodologie ____ *31*
2.1 Choix des sites ____ **34**
2.2 Collecte d'informations ____ **34**
2.3 Cadre chronologique et datations ____ **35**
2.4 Analyses chimiques au laboratoire : *proxies* géochimiques et biologiques ____ **36**
2.4.1 Préparation pour étude taxonomique et morphotypique des ostracodes et macro-charbon 36
2.4.2 Prétraitement pour analyse spectroscopique : ICP-OES ____ 36
2.4.3 Dosage de la matière organique et des carbonates de calcium ____ 37

CHAPITRE III ____ *42*
Soft-sediment deformation structures recognised in a reverse-drag associated with normal faulting (Lake Ifrah, Northwest Africa): Palaeoseismic assessment and neotectonic implications 43

Khalil Azennoud[a,], Abdennasser Baali[a], Hicham El Asmi[b], Yassine Ait Brahim[c], Oualid Hakam[a], Aziz Hayati[b], Touria El Kamel[a]* 43
Abstract 43
1 Introduction 44
2 Geological and tectonic background 46
3 Facies assessment 49
3.1 Unit 1 52
3.2 Unit 2 54
3.3 Unit 3 57
4 Sedimentary deformation structures 57
4.1 Load structures 58
4.2 Hybrid 'ductile'-brittle deformations 60
4.3 Neptunian dykes and normal faults 65
4.4 Bed-parallel slip and associated domino-style faults 68
4.5 Shrinkage cracks 71
5 Discussion 72
5.1 Trigger mechanism 72
5.1.1 Endogenic triggers: Context- and trigger-based approaches 72
5.1.2 Exogenic trigger: Palaeoseismic implication 74
5.2 Tectonic implications 77
5.2.1 Master fault slip behaviour and tectonic controls on sedimentation 77
5.2.2 Scaling relationships: Spatial and temporal basin-scale implications 78
5.2.3 Regional-scale neotectonic implications 81
6 Conclusions 83
Supplement material 84
References (supplement materiel) 87
Acknowledgment 89
References (article) 89

CHAPITRE IV 106
Disentangling orbital, sub-orbital, and tectonic signatures from lacustrine sediments developed upon a half-graben (Lake Ifrah Basin, Northwest Africa): Insights into lowest-rank T-R sequences for interior basins 107
Khalil Azennoud[a,], Abdennasser Baali[a], Francesc Mesquita-Joanes[b], Hicham El Asmi[c], Yassine Ait Brahim[d]* 107
Abstract 107
1 Introduction 108
2 Geological context and present-day climate 109
3 Materials and methods 111
3.1 Sedimentological, stratigraphic, and petrographic analyses 111
3.2 Biological, geochemical proxies, and chronological framework 111
4 Sedimentologic and stratigraphic analyses 112
4.1 Sedimentologic analysis 113

4.1.1 Facies Association 1 (FA1, lacustrine offshore deposits) 113
Carbonate and organic-rich facies 119
4.1.2 Facies association 2 (FA2, low-energy bench and ramp lacustrine deposits) 122
4.1.3 Facies association 3 (FA3, lacustrine wave-influenced nearshore deposits) 126
4.1.4 Facies association 4 (FA4, Gilbert-type delta deposits) 130
4.1.5 Facies association 5 (FA5, fluvial/alluvial deposits) 132
4.2 Sequence analysis and facies models 136
4.2.1 Stratigraphic sequence 1: Lower mud – upper carbonate sequence 137
4.2.2 Stratigraphic sequence 2: hybrid to clastic-dominated sequence 139
4.2.3 Stratigraphic sequence 3: lower carbonate-upper fine-to-coarse-clastic sequence 140
5 Discussion 144
5.1 Basin configuration 144
5.2 Controls on sedimentation and stacking patterns 147
5.2.1 Influence of tectonics 148
5.2.2 Role of climate: Orbital and sub-orbital forcing 149
5.3 What insights are to be drawn into sequence stratigraphy from the case study? 155
6 Conclusions 157
Acknowledgement 158
References 158

CHAPITRE V 174
Climate controls on tufa deposition over the last 5000 years: A case study from Northwest Africa 175
Khalil Azennoud[a,], Abdennasser Baali[a], Yassine Ait Brahim[b], Youssra Ahouach[a], Oualid Hakam[a]* ***175***
Abstract 175
1 Introduction 176
2 Structural, geologic and climatic context 177
3 Methods and material studied 179
3.1 Sedimentological and petrographic analysis 179
3.2 Geochemical and biological proxies 179
3.3 Dating 180
4 Results and analysis 181
4.1 Proxy results, facies and facies association analysis 181
4.1.1 Fluvial non-tufa FA: F-nT 182
4.1.2 Fluvial-palustrine FA: FP1 183
4.1.1 Fluvial s.s. tufa: F1 184
4.1.2 Palustrine-lacustrine FA: L1 189
4.1.1 Fluvial-palustrine FA: FP2 190
4.2 Petrographic analysis: lamination pattern 193
4.2.1 Laminations in oncoids 194
4.2.2 Lamination in stromatolites 196
4.3 Sequence analysis 197
4.3.1 Depositional Sequence 1: fluvial-dominated interval 198

4.3.2 Depositional Sequence 2: lacustrine-dominated interval 199
4.4 Evolutionary facies model 200
4.4.1 Incision event(s), the start of a new stage of sedimentation: Middle Holocene 200
4.4.2 First tufa occurrence, accelerated aggradation rate: from ca. 4.6 to 2.7 cal kyr B.P. 201
4.4.3 Active overflow, progradation pattern: from ca. 2.7 cal kyr B.P. onwards 201
5 Discussion 205
5.1 Lamination pattern 205
5.1.1 Lamination in oncoids 205
5.1.2 Lamination in stromatolites 206
5.2 Paleoclimate implications 207
5.2.1 Orbital to millennial timescale variability 208
5.2.2 Abrupt climate change: possible solar imprints and/or internal forcing cyclicity within tufa records 213
6 Conclusions 214
Supplement material 215
1 Age/depth model 215
2 Facies associations in log2 (N33° 43' 54.15"; W5° 0' 41.35") 216
2.1 Palustrine FAs: P1 and P2 216
2.2 Palustrine-lacustrine FA: L2 218
3 Facies association in log3 (N33° 44' 12.27"; W5° 0' 54.96"): Barrage cascade FA (B-C) 218
4 Facies associations in log4 (N33° 44' 17.03"; W5° 1' 5.80"): fluvial FAs (F2 and F3) 220
Acknowledgments 220
References 221

CHAPITRE VI 232
SYNTHÈSE ET CONCLUSIONS 232
Synthèse 233
1 Apport de l'approche sédimentologique et stratigraphique séquentielle conventionnelle 234
2 Apport des proxies et des SSDSs 236
Conclusions et perspectives 237

REFERENCES 241
CHAPITRE I ET II 241

ANNEXE 253
GENERALITÉS SUR LA SÉDIMENTATION LACUSTRE ET FLUVIOLACUSTRE 253
1 Systèmes lacustres à dominante détritico-carbonatée 254
1.1 Processus réguliers et événements extrêmes 254
1.1.1 Processus physiques 254
1.1.2 Processus chimiques et biochimiques 261
1.1.3 Événements extrêmes et dépôts associés 263
1.2 Sédimentation et environnements de dépôts 265

1.2.1 Lacs dominés par la sédimentation détritique 265
1.2.2 Lacs dominés par l'activité biologique authigénique 267
2 Sédimentation fluviatile à fluvio-lacustre à dominante carbonatée : tufs calcaires 271
2.1 Contexte de formation : aspects chimiques et biochimiques 272
2.2 Association de faciès et environnements de dépôts : séquences de faciès élémentaires 274
2.3 Modèles conceptuels de faciès 277
2.3.1 'low-gradient, non-stepped, fluvial and fluvio-lacustrine facies model' 278
2.3.2 'High-gradient and stepped fluvial conditions' 281
Références 283

Préface

Bien que nombreux sont les géoarchives capables d'enregistrer les signatures des forçages allocycliques comme les pulsations tectoniques et le climat, l'examen de leur déchiffrage est délicat. Ainsi, les signaux des forçages tectoniques et climatiques ne peuvent s'extraire concurremment du registre géologique que si ceci présente une extension idéale rappelant le principe de 'Boucle d'or' où toutes les fréquences de la variabilité du forçage climatique (orbital et suborbital) peuvent être captées et préservées, d'une part, et que, de l'autre part, les conséquences des pulsations tectoniques, structures surtout cassantes donc discontinues dans l'espace, sont susceptibles d'être détectées. Dans ce sens, les lacs constituent de lieux privilégiés où leur registre sédimentaire est capable de tracer la cyclicité à la fois tectonique et climatique dans différentes échelles temporelles. Qui plus est, l'examen du déchiffrage de cette cyclicité deviendrait aisé avec l'usage, couplé à une analyse sédimentologique détaillée, de la stratigraphie séquentielle conventionnelle où les cycles des variations du niveau de base/l'accommodation sont potentiellement susceptibles d'être ajustées avec (i) les paramètres modulant l'insolation (*viz*., précession et obliquité) et (ii) les pulsations tectoniques instantanées. De même, l'application d'une approche basée sur une multitude d'indicateurs ou proxies paléoenvironnementaux, facilement manipulable dans le contexte des lacs, certes conduira à mieux cerner le facteur de contrôle climatique. C'est dans cette logique que ce projet de doctorat s'est ébauché en s'appuyant sur deux exemples-types de systèmes lacustres situés dans le Moyen Atlas septentrional au Nord du Maroc : un système lacustre évoquant une sédimentation à mixture détritico-biochimique se développant sur une structure rappelant celle d'un hémi-graben (lac Ifrah), et un système fluviolacustre à dominante carbonatée, tufs calcaires (Imouzzer Kandar). Ces deux exemples-types à lithologies et contextes morpho-structuraux différents sont ainsi choisis pour tester concurremment leur aptitude à capter les signaux des forçages climatiques et tectoniques dans deux fenêtres temporelles différentes : échelle orbitale à millénaire dans le cas du lac Ifrah et échelle millénaire à centennal pour le cas d'Imouzzer Kandar.

Afin de guider dans les normes de l'art la perquisition scientifique, un enchaînement d'idées délibérément jugé logique à suivre est adopté dans cette dissertation. Ainsi, le **premier chapitre** ouvre la porte vers une présentation concise de l'état de l'art concernant les systèmes lacustres où plus de détail est déplacé vers l'**Annexe**. Après avoir mentionné d'emblée le degré de diversité de l'origine des dépressions où existent les lacs, une limitation aux systèmes lacustres d'origine tectonique et fluviatile à dominante détritico-biochimique et exclusivement carbonatée, respectivement, est procédée dans la suite du chapitre. La première section est dédiée au premier cas de figure où est rapportée les grands traits qui englobent la sédimentation là-dedans (processus physiques réguliers et

extrêmes et processus biochimiques), expliquant les différents modèles de faciès et classifications qui y sont systématiquement identifiés. La deuxième section donne l'état de connaissance concernant l'approche sédimentologique dédiée aux tufs calcaires en contexte fluviolacustre sur la base d'une bibliographie récemment aboutie. Faute de place, des références clés d'importance cruciale par rapport aux interprétations présentées plus loin sont fournies.

Le **chapitre 2** expose des généralités sur la zone d'étude, le Moyen Atlas, et sur la méthodologie adoptée dans ce projet de doctorat. L'histoire géodynamique polyphasée du Moyen Atlas, en tant que domaine structural à l'échelle de la géologie du Maroc, depuis le Mésozoïque est concisément présentée, rappelant uniquement les grands traits et conséquences tectono-sédimentaires de cette histoire polyphasée. Par la suite, après avoir remémoré la place du territoire marocain dans la circulation atmosphérique générale et le climat modern du Moyen Atlas, une synthèse sur l'histoire paléoclimatique à l'échelle régionale (i.e., Méditerranée occidentale) depuis le Stade Isotopique Marin-3 est présentée sur la base des données extraites de diverses géoarchives (sédiments lacustres et marins et spéléothèmes) et méthodologies (palynologie, géochimie isotopique, micropaléontologie). Dans la deuxième section est présenté un aperçu sur la méthodologie adoptée en soulignant le rôle prépondérant du travail de terrain de prime abord, puis celui du laboratoire.

Les **chapitres 3**, **4** et **5**, constituent le cœur du travail. Chaque chapitre est un article soit déjà publié (**chapitres 3** et **5**) soit soumissionné (**chapitre 4**). Le cas du lac Ifrah est présenté dans les **chapitres 3** et **4**, alors que celui du site d'Imouzzer Kandar est illustré dans le **chapitre 5**. Brièvement, le **chapitre 3** livre un cas de figure montrant l'influence des événements extrêmes (paléo-séismes et pulsations tectoniques) sur la sédimentation selon les dires d'une analyse détaillée des déformations 'ductiles' et cassantes synsédimentaires ('*soft-sediment deformations*'). Le **chapitre 4** présente en partie l'exploit des perspectives tirées du chapitre précédent et son emploi, combiné à une approche sédimentologique et stratigraphique séquentielle détaillée, dans la question ultime qu'envisage ce projet de doctorat, à savoir le décryptage des signatures climatiques et tectoniques. Le **chapitre 5** illustre un exemple typique où le climat est démontré être le facteur de contrôle principal sur la sédimentation et, intéressement, sur l'accommodation potentielle. Qui plus est, l'empreinte de deux événements froids rapides (*événements de Bond*) marquant l'Holocène, où l'origine est systématiquement démontrée être associée aux vêlages extensifs de la calotte glaciaire groenlandaise ainsi qu'au blocage de la circulation thermohaline, a été identifiée pour la première fois dans les tufs calcaires (événements 4.6 ka et 2.7 ka), ce qui encourage davantage le recours à ces géoarchives une fois les changements climatiques du passé sont investigués.

Le dernier chapitre, **chapitre 6**, recombine toutes les perspectives tirées des trois chapitres qui le précédent sous forme d'une synthèse et conclusions ainsi qu'aux futurs travaux à mener et qui vont dans le sens soit de réplication soit d'approfondissement de la perquisition scientifique envisagée dans le cadre de ce doctorat, chose qui va certes repousser les frontières de notre perception *vis-à-vis* de la cause.

CHAPITRE I

INTRODUCTION GENERALE

Les environnements continentaux sont divers et variés ce qui rend impossible de les couvrir exhaustivement dans un seul œuvre académique. Ainsi, en allant des régions polaires ou montagnards où les processus glaciaires priment et commandent l'édification d'une géomorphologie emblématique (e.g., cirque glaciaire, verrous, eskers, drumlins) aboutissant à des tillites et/ou moraines, jusqu'aux régions désertiques où le vent se présente comme l'artiste des sculptures typiques à ces endroits (e.g., barkhane, seifs, roches en champignon), en passant par les régions tempérées où la disponibilité en eaux stimule l'altération chimique (bisiallitisation, ou fersiallitisation en climat méditerranéen), le transport et le dépôt par voie hydrique, aboutissant à des systèmes fluviatiles et lacustres d'importance à nul autre second. Qui plus est, l'altération chimique très prononcée dans la région équatoriale où l'hydrolyse des silicates est complète (allitisation), siège de fortes précipitations et d'importante énergie calorique reçue des rayons solaires, conduit à des sols très développés. Néanmoins, comme cité d'emblée, notre attention sera portée uniquement sur les systèmes lacustres qui, eux même, présentent une complexité incommensurable et peuvent se générer dans différents contextes et régions.

Un lac peut être défini comme "une masse d'eau stagnante intérieure au continent occupant une dépression sur la croûte terrestre" (traduit d'après Kelts, 1988, p. 3). Les lacs représentent 3% de la surface continentale globale (Downing et al., 2006). Les dépressions occupées par ceux-ci ont de nombreuses origines (Hutchinson, 1957; Branstrator, 2009; Sladen et Chiarella, 2020). Néanmoins, 90% de tous les bassins lacustres actuels sont issus de processus tectoniques et glaciaires (Cohen, 2003), alors que 8% de la surface qu'occupe les lacs actuels est dédiée aux processus fluviatiles (Meybeck, 1995).

Les processus tectoniques produisent des rifts continentaux (exemple du lac Tanganyika, en Afrique de l'Est), des bassins associés aux décrochements (dans les zones de relais, i.e., bassin en pull-apart, e.g., mer morte en Jordanie, ou d'extrémité, i.e., quadrant de dilatation, e.g., Hoang Sa Basin en Chine, ainsi que l'exemple du bassin du lac Ifrah, chapitre 3), des bassins d'avant-pays (e.g., bassin plio-quaternaire de Saiss au Maroc et la fameuse formation de 'Eocene Green River' aux États-Unis) et des lacs intra-arc (e.g., le lac Titicaca en Bolivie).

L'érosion glaciaire et l'endiguement par les dépôts glaciaires donnent naissance à des grands lacs proglaciaires (e.g., le lac Agassiz, au centre de l'Amérique du Nord), à des vallées glaciaires (e.g., Wastwater, Cumbria, Royaume-Uni) et à des lacs de type « kettle » (e.g., les lacs d'eau douce et salée peu profonds de Saskatchewan, Canada).

Les processus fluviatiles constituent la troisième catégorie la plus importante de mécanismes de formation des dépressions abritant les lacs. Alors qu'ils représentent 8% de la superficie totale des lacs du monde, les lacs d'origine fluviatile occupent seulement 0,3 % de leur volume total (Meybeck, 1995). De ce fait, ils sont presque invariablement peu profonds (Herdendorf, 1990). Néanmoins, les lacs d'origine fluviatile sont des éléments courants de la géomorphologie des cônes alluviaux, des plaines d'inondation et des deltas présentant une dimension considérable, et constituent probablement la deuxième classe la plus courante, après les lacs glaciaires, en termes de nombre de lacs individuels (Cohen, 2003, p. 42). Qui plus est, associés aux processus biochimiques, de larges et extensifs systèmes lacustres peuvent s'instaurer en arrière d'édifices qualifiés de « barrages-cascades » où l'accrétion verticale est susceptible de créer de l'espace derrière (Pedley, 1990 ; Ford et Pedley, 1996 ; Gourari, 2001; Vázquez-Urbez et al., 2012 ; Arenas et al., 2014 ; Azennoud et al., 2022a) (chapitre 5).

Les 2% restants comprennent les lacs issus de la dissolution dans les milieux karstiques [lacs du Moyen Atlas (Maroc) sont, entièrement ou partiellement, d'origine karstique, exemple des lacs Iffer et Afourgagh qui se développent sur des dolines ; Baali, 1998], les lacs générés par l'activité volcanique et hydrothermale (les lacs de maar et de cratère comme le lac Taupo, en Nouvelle-Zélande) et les lacs qui ont d'autres origines (e.g., déflation, processus côtiers, impact de météorites, etc.) (Renaut et al., 2010, p. 541).

En fait, une fois étudiés, les sédiments lacustres peuvent servir de registre où les conditions hydrologiques locales, la nature du substrat rocheux et l'état physico-chimique qu'a connu le lac sont archivés. De plus, le fait que ces milieux aquatiques sont aussi des écosystèmes où faune (e.g., ostracodes, bivalves, gastéropodes), flore (e.g., charophytes, diatomées) et microorganismes (e.g., cyanobactéries, certaines bactéries eucaryotes) peuvent proliférer et s'adapter à différentes conditions hydrodynamiques, chimiques et physiques (notion de sous-environnement) rend prometteur le recours à ces biomarqueurs et permet de cerner plus précisément les conditions hydrodynamiques, chimiques et physiques qu'a vécu le lac pendant son histoire d'existence. En outre, la signature géochimique (élémentaire et isotopique) des sédiments ou restes bio-minéralisés de la faune (e.g., carapaces et tests) et de la flore (e.g., oogones des charophytes) constituent des marqueurs particuliers (proxies) des conditions paléoenvironnementales. Par conséquent, l'étude sédimentologique et biostratigraphique couplée d'une approche multi-proxy du registre sédimentaire lacustre est une démarche à la fois compréhensible et prometteuse permettant le décryptage des signaux des changements environnementaux, chose très précieuse aux échelles de la science et de la vie humaine.

Par ailleurs, la diversité des systèmes lacustres complique leur investigation et donc exige une approche approfondie qui doit s'appuyer sur un ensemble de considérations et d'outils pour enfin pouvoir dresser avec succès les modèles de faciès de dépôts, très spécifiques et différents d'un cas à l'autre. Ainsi, (i) la compréhension des processus inhérents aux systèmes lacustres en question est une matière indispensable, (ii) l'usage d'une description conventionnelle des faciès basée sur de nombreuses publications clés et sur le degré de compréhension du premier point est une nécessité, (iii) l'organisation de facies génétiquement liés en un assemblage vertical (association de faciès) reflétant un système de dépôt interprété, par inférence, en terme d'environnement ou sous-environnement de dépôt, et en fin (iv) le rassemblement de tous ces approches particulières seraient très informatif et surtout instructif pour pouvoir contraindre et conceptualiser un modèle de faciès généralisant les particularités. Ce raisonnement par induction est entièrement adopté le long du trajet et stations pris dans ce travail.

Partant de ces aspects, le présent travail est limité à l'étude de deux contextes de systèmes de dépôt : (i) un système de dépôt lacustre d'origine tectonique et à lithologie mixte (détritico-carbonatée) et (ii) un système de dépôt fluviolacustre à dominante biocarbonatée. L'objectif primordial de cette étude est le déchiffrage des signatures climatiques (orbitales et suborbitales) et tectoniques moyennent une démarche qui fait appel à l'approche sédimentologique et stratigraphique séquentielle complémentée par l'utilisation des marqueurs paléoenvironnementaux (proxies biologiques et géochimiques). Alors qu'un aperçu sur cette démarche (méthodologie) est présenté dans le chapitre suivant, le présent chapitre expose brièvement les principaux aspects sur la sédimentation dans les deux contextes de dépôt que le lecteur doit connaître avant de foncer sur le cœur de ce travail (chapitres 3-5). Néanmoins, afin d'éviter l'alourdissement du texte et de maintenir le cap, une présentation plus détaillée par rapport à ces aspects est déplacée vers l'Annexe où des références plus riches et mieux placées sont fournies, le cas échéant.

1 Systèmes lacustres à dominante détritico-carbonatée

Les systèmes lacustres à dominante détritico-carbonatée sont le siège à la fois de processus purement physiques [aboutissant à la composante détritique (clastique) et aux caractères morphologiques et structurales qui lui sont associés (e.g., structures sédimentaires, géométrie des dépôts)] et d'autres purement biochimiques (contribuant à la sédimentation biochimique, généralement carbonatée). De ce fait, les systèmes lacustres sont des écosystèmes, où la chaîne trophique est bien développée, avant d'être considérés comme un milieu de dépôt, imitant ainsi en partie leurs homologues marins. Dès lors, la compréhension de ces processus physiques (réguliers et extrêmes) et

biochimiques, présentés avec plus de détail en Annexe, dans un tel environnement de dépôt est nécessaire pour contraindre les différents sous-environnements de dépôts et modèles de faciès, inhérents de ceux-ci.

1.1 Processus réguliers et événements extrêmes

1.1.1 Processus physiques réguliers

Les processus physiques hydrodynamiques réguliers, contribuant à la redistribution des sédiments dans le bassin, sont commandés par le vent, les propriétés rhéologiques des cours d'eau affluant vers le lac et la gravité. Les conséquences de ces processus contrôlent l'occurrence, l'extension et le caractère des faciès et systèmes de dépôts. Conformément à cette considération, Nutz et al. (2016) ont proposé une classification ternaire qui se base sur la dynamique sédimentaire dominant le bassin (Fig. I.1) : systèmes lacustres à dominante éolienne (*'wind-driven waterbodies'*) ; systèmes lacustres à dominante fluviatile (*'river-driven waterbodies'*) ; systèmes lacustres dominés par les processus gravitaires sous-aquatiques (*'gravity-driven waterbodies'*).

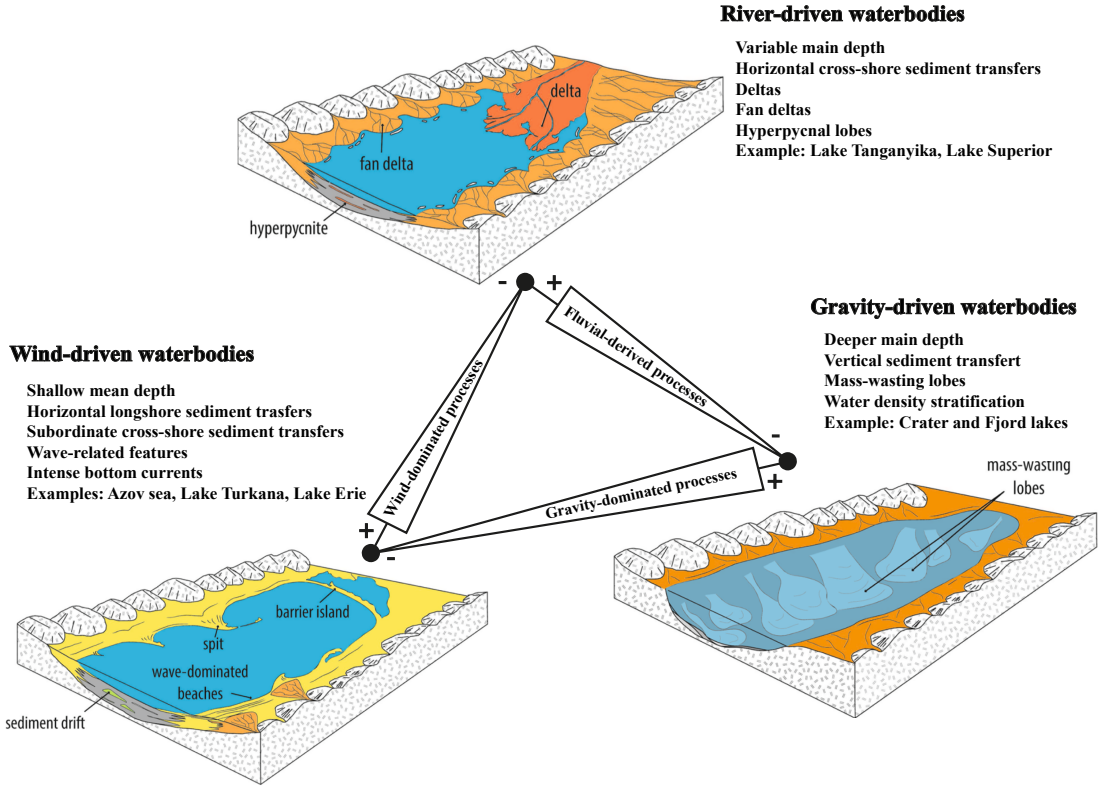


***Figure I.1**. Ternary classification for lacustrine systems based on physical sedimentary dynamics (after Nutz et al., 2016, adapted).*

***Figure I.1**. Classification ternaire des systèmes lacustres basée sur la dynamique sédimentaire (d'après Nutz et al., 2016, adaptée).*

Le régime thermal, et la conséquente stratification thermique, des eaux des lacs constitue un facteur déterminant dans l'accumulation et la préservation de la matière organique. Considérant le paroxysme de la densité de l'eau douce à 4°C, la variation saisonnière de la température peut enclencher le brassage de la colonne d'eau aussitôt que les densités de la partie superficielle (épilimnion) et profonde (hypolimnion) de la colonne d'eau s'inversent ou s'avoisinent (Fig. I.2 ; *voir* Annexe). En tenant compte du nombre de brassage induit annuellement, les limnologistes ont établi une classification descriptive (e.g., Hutchinson, 1957; Håkanson, 1982; Lewis Jr., 1983; Wetzel, 2001) en distinguant : lacs monomictiques (brassage une seule fois par année) ; lacs dimictiques (brassage deux fois par année, généralement au printemps et en automne) ; lacs polymictiques (lacs peu profonds se stratifiant temporairement pour des périodes courtes, mais se brassant librement le reste de l'année) ; et lacs meromictique (lacs restant d'ordinaire stratifiés tout au long de l'année, Fig. I.2 ; Hakala, 2004). Généralement, le brassage des eaux lacustres induit de nombreux effets déterminants qui influencent à la fois l'écologie du milieu et le mode de sédimentation (Renaut et al., 2010) (*voir* Annexe).

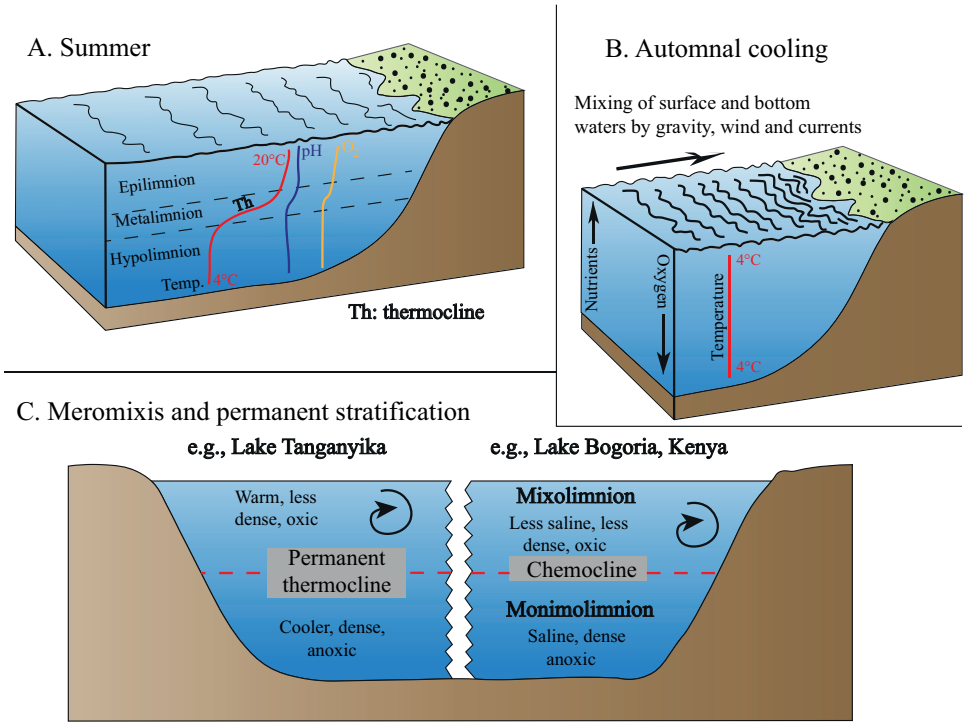


Figure I.2. *Stratification in lakes. **A**. Vertical profile of temperature, pH and oxygen in a typical perennial lake during warm summer months. Warm, less dense surface waters lie upon denser cooler waters, separated by the thermocline. **B**. Breakdown of stratification during winter months when surface waters cool to 4°C and attain their maximum density. Surface and bottom waters can be mixed by wind induced currents, waves and gravity. **C**. Meromixis (stable stratification) can develop when surface waters are consistently warmer than the cooler, dense bottom waters or when relatively less saline surface waters lie upon denser more saline brines. Redrawn after Renaut et al. (2010).*

Figure I.2. *Stratification des eaux des lacs. **A**. Profil vertical de température, pH et oxygène pour un lac permanent typique pendant la saison chaude. Durant cette saison, une couche d'eau chaude, moins dense repose sur une couche froide et plus dense, séparées par la thermocline. **B**. Rupture de stratification pendant la saison froide lorsque les eaux de surface atteignent 4°C, ainsi atteignant leur densité maximum. Les eaux de surfaces et de fond peuvent dès lors se mélanger*

*facilement via les courants induits par le vent, vagues et gravité. **C**. Meromixisme (stratification stable) peut se développer lorsque les eaux de surface sont constamment plus chaudes que les eaux de fond (cas du lac Tanganyika), ou lorsque les eaux de surface relativement moins salines reposent sur des eaux de fond plus salines (plus denses ; exemple du lac Bogoria). Redessinée d'après Renaut et al. (2010).*

1.1.2 Processus biochimiques

La chimie des eaux des lacs dépend de plusieurs facteurs comme, entre autres, la géologie de la zone distributrice, le climat contrôlant le degré d'altération chimique ainsi qu'à l'état hydrologique du bassin lacustre modulant le temps de résidence (Dean et al., 2007; Verrecchia, 2007; Rosenbaum et Kaufman, 2009). En effet, le caractère doux des eaux se présente chaque fois un drainage ouvert est maintenu (i.e., le lac est hydrologiquement ouvert) et la somme des entrées (précipitations directes, ruissèlements, recharge par la nappe) équivaut celle des sorties (flux sortant et évaporation) (Fig. I.3A et B). En revanche, un lac salé est conditionné si le bassin lacustre est hydrologiquement fermé en permanence, favorisant ainsi le stockage des solutés transportés par le réseau de drainage depuis le bassin versant après hydrolyse et dissolution de la roche mère. En outre, la disponibilité en éléments nutritifs sépare l'état eutrophe (disponibilité importante en nutriments) de l'état oligotrophe (limitation en nutriments), eux même influencés par l'état hydrologique du lac (Fig. I.3A_1 et B_2) (Einsele, 2000). Alors que la précipitation de certaines espèces (sels) par voie purement chimique (sursaturation par rapport à l'espèce via évaporation) caractérisent les lacs salés hydrologiquement fermés (Renaut et al., 2010), la précipitation de certaines espèces de carbonates (*viz*., calcite et aragonite) et de silicates (silice hydratée, opale) peut être induite ou contrôlée biologiquement en cas d'eau douce (Müller et Wagner, 1978; Kempe et Kazmierczak, 1990; Merz, 1992; Robbins et Blackwelder, 1993; Arp et al., 2010; Gierlowski-Kordesch, 2010) (*voir* Annexe).

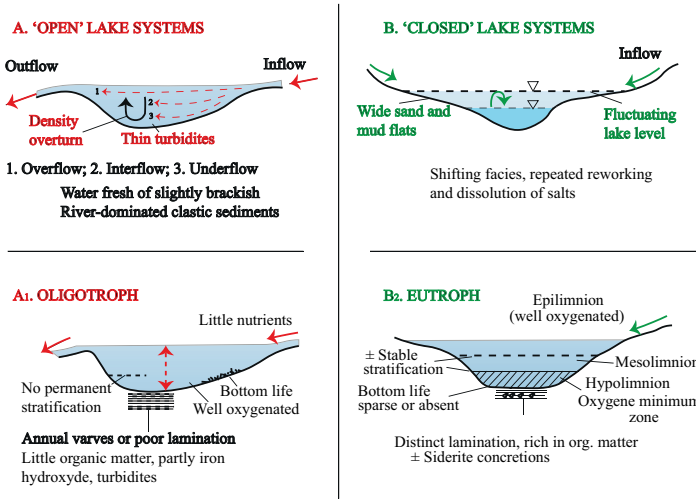


***Figure I.3**. Overview of different lake systems. **A**. Open system with inflow and outflow; the lake water chemistry is river-dominated. **A1**. Well oxygenated, oligotrophic lake (poor in nutrients). **B**. Closed systems without outflow; concentration of dissolved species commonly increasing with lowering lake water level and time. **B2**. Stable stratification of lake water and eutrophic conditions with oxygen-deficient bottom water. Redrawn after Einsele (2000, p. 77).*

***Figure I.3**. Aperçu sur les différents systèmes lacustres. **A**. Système ouvert avec flux entrant et flux sortant ; la chimie du lac est dominée par celle du cours d'eau. **A1**. Lac oligotrophe (pauvre en nutriments) bien oxygéné. **B**. Système fermé (sans flux sortant) ; l'augmentation de la concentration des espèces chimiques est fonction de la variation du niveau d'eau modulée par l'évaporation/précipitation. **B2**. Stratification stable de la colonne d'eau et installation des conditions d'eutrophie (disponibilité importante en nutriments) avec déplétion en oxygène des eaux de fond.*

1.1.3 Événements extrêmes et dépôts associés

La sédimentation dans les bassins lacustres peut être contrôlée ou modifiée par des pulsations périodiques des événements extrêmes qui sont d'origine soit géodynamique (e.g., tremblements de terre, tsunamis, éruptions volcaniques) soit climatique (e.g., crues, hurricans, avalanches) (*voir* Annexe et Sabatier et al., 2022; Fig. I.4). Alors que certains de ces événements peuvent déclencher des mouvements gravitaires des sédiments et ainsi aboutissant à des dépôts de transport de masse ('*mass-transport deposits*'), d'autres peuvent être directement impliqués dans la déformation synsédimentaire et stationnaire des sédiments à l'état mou ('*soft-sediment deformations*'). En effet, il s'agit de déformations 'ductiles' ou cassantes déclenchées par l'événement (e.g., séisme, avalanche) et guidées par des forces internes ou externe (forces motrices; Owen, 1987) après que le sédiment hôte (toujours à l'état mou) voit sa résistance au cisaillement diminue ou devenant nulle (mécanisme de déformation, *liquidization*, *sensu* Allen, 1977). Celles-ci, baptisées en anglais '*soft-sediment deformation structures*' (SSDSs), reçoivent un grand intérêt dans ce projet de doctorat et sont exhaustivement communiquées dans le chapitre 3. Une très bonne exposition sur les SSDSs peut être trouvée dans le bouquin précurseur par Allen (1982, volume B, p. 343-393) et l'article fondateur par Owen (1987). D'autres révisions qui peuvent intéresser le lecteur sur le sujet des SSDSs, les processus de déformation et leur classification, sont, entre autres : Plaziat et al. (1990) ; Collinson (1994, 2019) ; Greb et al. (2002) ; Montenat et al. (2007) ; Van Loon (2009, 2014) ; Owen et al. (2011) ; Owen et Moretti (2011) ; Waldron et Gagnon (2011) ; Dechen et Aiping (2012) ; Moretti et al. (2014) ; Topal et Özkul (2014) ; He et Qiao (2015) ; Menzies et al. (2016) ; Shanmugam (2017).

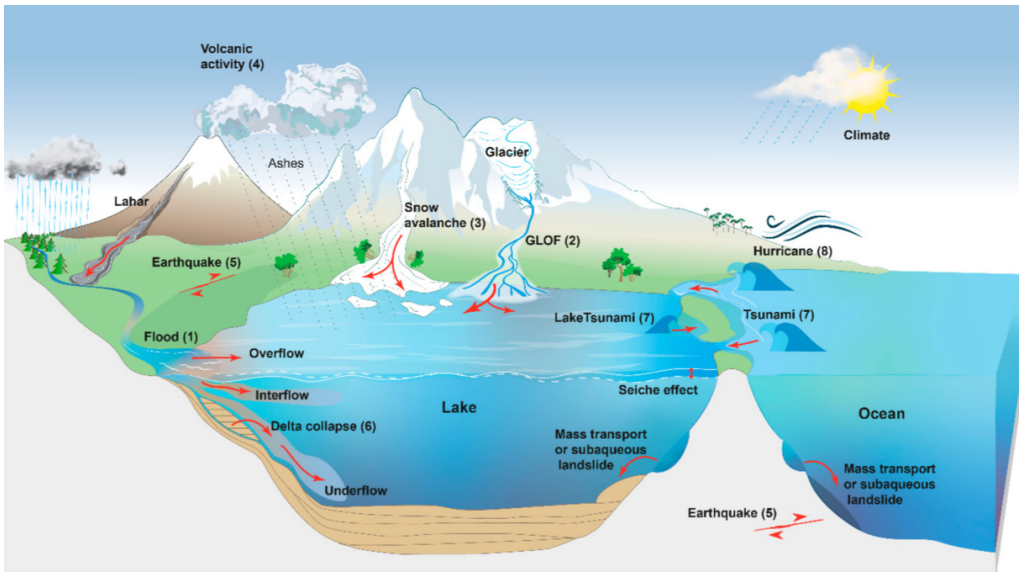


Figure I.4. *Processes at the origin of event deposits in lake systems. GLOFs: glacial-lake outburst floods. After Sabatier et al. (2022).*

***Figure I.4**. Processus sur l'origine des dépôts d'événements extrêmes dans les systèmes lacustres. GLOFs : 'glacial-lake outburst floods' (crue associée à la rupture d'un barrage glaciaire retenant un lac glaciaire). D'après Sabatier et al. (2022).*

1.2 Sédimentation et environnements de dépôt

Du fait que les lacs sont considérés à la fois comme des réceptacles des sédiments allochtones et sièges d'une production authigénique guidée biologiquement et/ou chimiquement, le caractère de la sédimentation doit refléter le relief, le climat, l'hydrologie et la lithologie des roches directement impliquées dans les processus de drainage caractérisant le système lacustre. En effet, ceci serait tant et si bien marqué que le registre lacustre exhibe une cyclicité entre dépôts détritiques et biochimiques ; le chapitre 4 livre un exemple de celle-ci. De ce fait, cerner les processus qui aboutissent aux composantes détritiques et biochimiques de la cyclicité est inéluctable pour le déchiffrage des facteurs contrôlant celle-ci.

1.2.1 Lacs dominés par l'activité détritique

La dominance de la composante détritique dans les archives lacustres est un signe de prédominance des processus physiques guidés par le vent, les cours d'eau débordant leurs charges sédimentaires dans le lac et mouvement gravitaires résumés dans la figure I.1. Ceux-ci, en assurant la redistribution de la charge de fond et en suspension des cours d'eau entrants le lac, conduisent à l'instauration d'une pléthore de sous-environnements qui peuvent être regroupés en deux zonations qui se distinguent hydrodynamiquement et bathymétriquement (Fig. I.5) : zone littorale ('*nearshore enironment*') et zone profonde ('*offshore environment*'). Les caractères faciologiques des dépôts dans les deux zonations sont en fonction du niveau de l'énergie guidé par le vent, de la topographie du bassin lacustre et des caractéristiques rhéologiques des eaux et sédiments gagnant le lac. Plus de détails sur les deux zonations et l'explication de la figure I.5 sont déplacés vers l'Annexe. De plus, un exemple concret et surtout exhaustif où le lecteur peut consulter est fourni par Nutz et al. (2017, 2020) pour le lac Turkana en Kenya (système de rift Est africain).

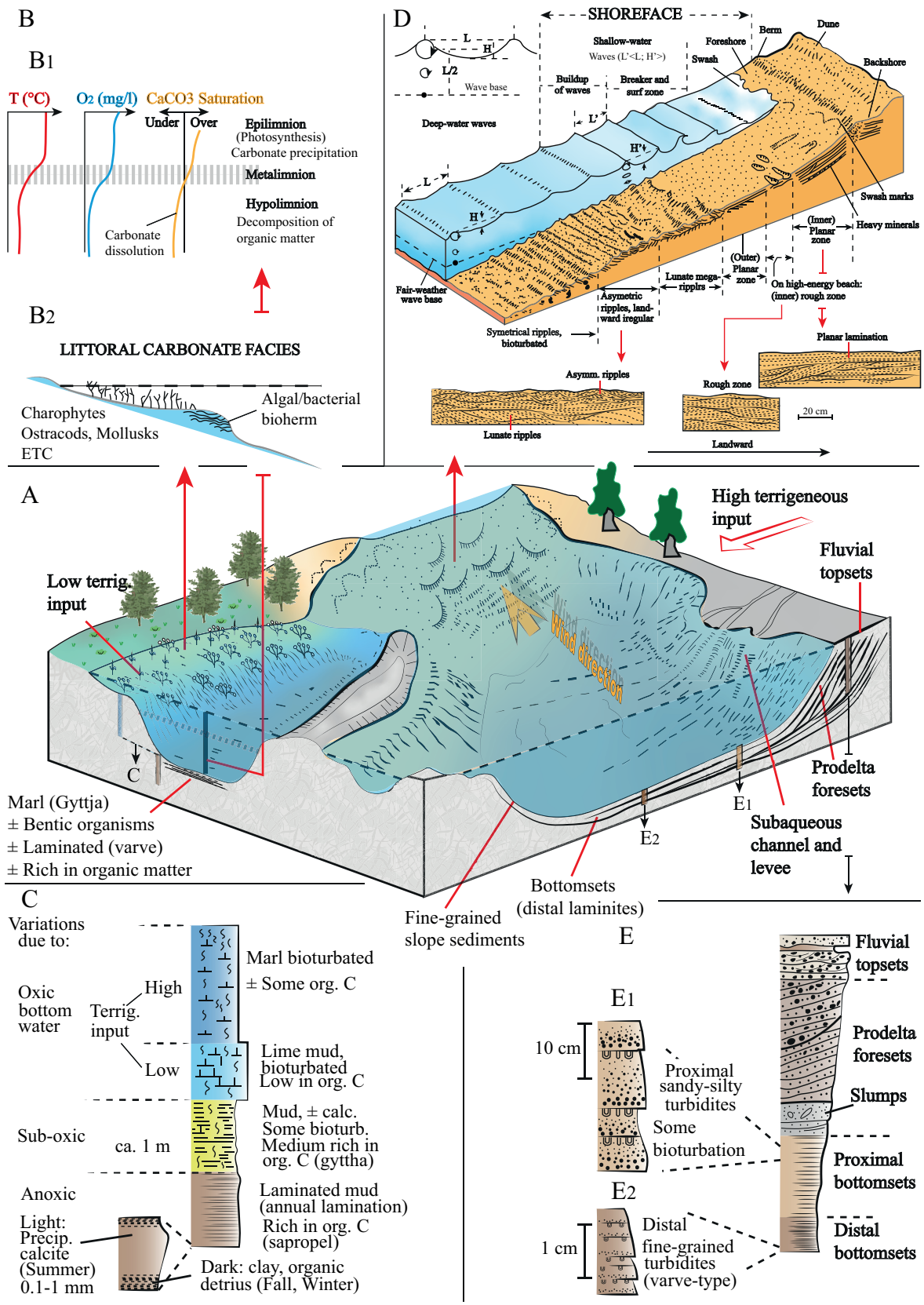


Figure I.5. *Conceptual facies model.* ***A***. *3D drawing of the depositional systems for open to balanced lake system (not close or underfilled system) with clastic- (river-driven and wind-driven physical processes) and biochemical-dominated settings.* ***B1***. *Some characteristics of the epi- and hypolimnion of hard-water lakes allowing calcite precipitation in summer time.* ***B2***. *Littoral carbonate facies (see* ***Fig. I.6*** *for more details).* ***C***. *Idealised stratigraphic log showing variation in facies from the littoral zone (**B2**) towards the profundal (offshore) setting in hard-water lake due to changing terrigenous input*

and oxygenation of bottom water in biochemical-dominated settings. Note the occurrence of annual lamination (varve). ***D****. Nearshore wind-driven clastic-dominated depositional system showing transition from deep-water waves to shallow-water waves and swash (backwash) in the shoreface zone and associated bedforms and internal sedimentary structures.* ***E****. Idealised stratigraphic log of river-dominated depositional system showing ideal coarsening-upward sequence (detrital clastic-dominated basin-fill), with* ***(E1)*** *proximal and* ***(E2)*** *distal (varve-like) turbidites. Redrawn with modification after Einsele (2000, his* ***Figs. 2.29*** *and* ***3.1****).*

Figure I.5*. Modèle conceptuel de faciès.* ***A.*** *Illustration en perspective montrant les différents systèmes de dépôt potentiellement rencontrés dans les systèmes lacustres hydrologiquement fermés ou balancés (systèmes fermés sont exclus), avec domination détritique terrigène (processus physiques gouvernés soit par le vent ou par le cours d'eau entrant) ou biochimique.* ***B1****. Quelques caractéristiques de l'épilimnion et l'hypolimnion des eaux lacustres à caractère dure permettant la précipitation de la calcite pendant la saison l'été.* ***B2****. Facies carbonaté de la zone littorale (plus de précision en* ***Fig. I.6****).* ***C****. Log stratigraphique idéalisé montrant une variation de faciès depuis la zone littorale* ***(B2)*** *jusqu'à la zone profonde comme réponse au changement de l'apport détritique ainsi que l'oxygénation du fond de lac dans un système de dépôt à dominante biochimique. Note la présence des laminites (lamines saisonnières ou varves).* ***D****. Système de dépôt de la zone littorale de haute-énergie à dominance détritique montrant la transition depuis les vagues des eaux profondes jusqu'aux vagues des eaux peu profondes et zone de plage.* ***E****. Log stratigraphique de système de dépôt dominé par les processus fluviaux (remplissage dominé par le détritisme) montrant une séquence à granoclassement négatif, avec des dépôts de turbidites* ***(E1)*** *proximaux et* ***(E2)*** *distaux (lamines semblables aux varves). Redessinée avec modification d'après Eisele (2000, ses* ***Figs. 2.29*** *et* ***3.1****).*

1.2.2 Lacs dominés par l'activité biologique authigénique

La sédimentation biochimique en domaine lacustre dépend forcément du chimisme de l'eau qui, à son tour, influe sur la biocénose benthique et pélagique apte à se développer dans les zones littorale et centrale (Kelts and Hsü, 1978; Dean, 1981; Renaut et al., 2010). Ainsi, les eaux lacustres riches en ions alcalino-terreux, spécialement les ions ca^{2+}, sont favorables pour la croissance des organismes sécréteurs de tests calcaires (précipitation biocontrôlée), alors que les lacs pauvres en Ca^{2+} mais relativement riches en silice dissout et en nutriments (comme P et NO^{-}_{3}) favorisent plutôt une production considérable en silice opale biogénique. En outre, la productivité biologique authigénique et la préservation de la matière organique dans la zone centrale sont intimement liés au statuts nutritionnel (e.g., eutrophie, oligotrophie) et thermique (i.e., stratification thermique et nombre de brassages annuels) des eaux lacustres ainsi qu'à l'importance des apports détritiques gagnant le lac. Le caractère faciologique des dépôts carbonatés constitutifs de la zone littorale dépend de la pente et du niveau d'énergie aboutissant à la définition de quatre modèle de faciès (Fig. I.6 ; Platt and Wright, 1991) ; des détails sur les deux zonations (littorale et centrale) et l'explication de la figure I.6 sont déplacés vers l'Annexe.

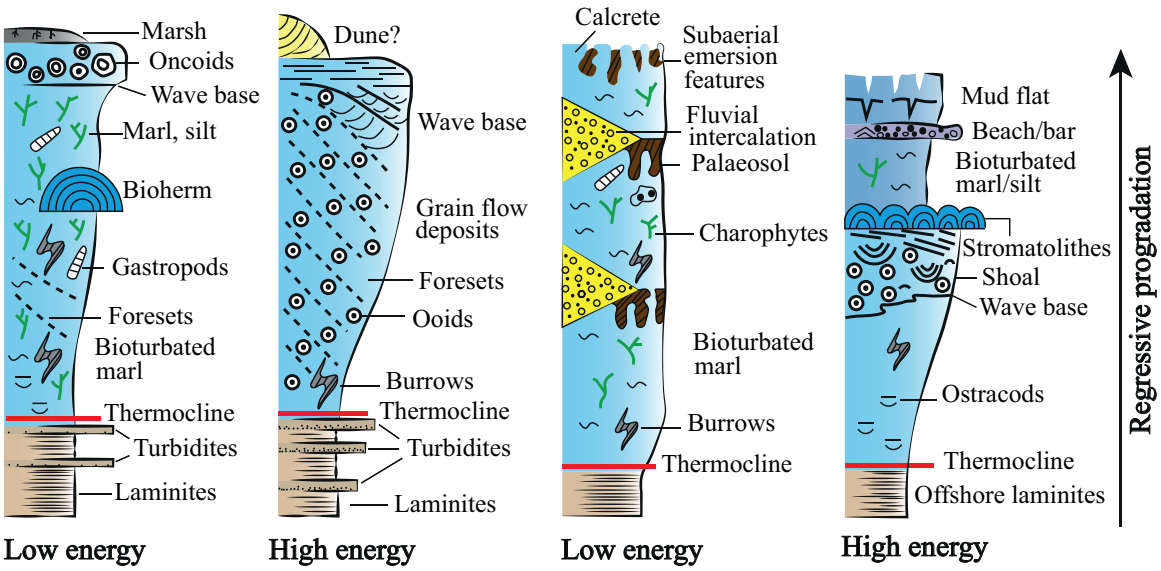


***Figure I.6**. Ideal vertical sequences (facies models) of lacustrine carbonates and associated facies showing typical shallowing upwards conditioning a regressive progradation of marginal lacustrine ramp and bench. Redrawn after Platt et Wright (1991, **Fig. 2**) (see also Renaut et al., 2010, **Fig. 5**).*

***Figure I.6**. Séquences verticales idéales (modèles de faciès) des carbonates lacustres et faciès associés montrant un passage vers des conditions de plus en plus peu profondes du bas en haut conditionnant une progradation régressive des faciès marginaux de 'ramp' et 'banc'. Redessinée d'après Platt et Wright (1991, **Fig. 2**) (voir aussi Renaut et al., 2010, **Fig. 5**).*

1.3 Facteurs de contrôle de la sédimentation et modèle hydro-stratigraphique

Bien qu'une multitude de facteurs puissent interagir (Fig. I.7), la sédimentation lacustre est principalement contrôlée par la tectonique et le climat (Kelts, 1988; Strecker et al., 1999; Bohacs et al., 2000; Changsong et al., 2001; Pietras et al., 2003; Keighley et al., 2003; Anselmetti et al., 2006). Ces deux facteurs s'expriment spécialement dans la régulation des sources d'eau entrant le bassin lacustre (eaux de ruissèlement, eaux souterraines, précipitations directes) (Rosen, 1994; Winter, 2003) ainsi que la charge sédimentaire transportée (charge de fond, charge en suspension, solutés dissouts) (Gierlowski-Kordesch, 2010). L'influence tectonique et l'hydro(géo)logie du bassin lacustre ainsi que le facteur climatique et les processus biologiques (e.g., productivité planctonique) modulent la mosaïque des potentiels sous-environnements dans n'importe quel bassin lacustre (Bohacs et al., 2000; Cohen, 2003).

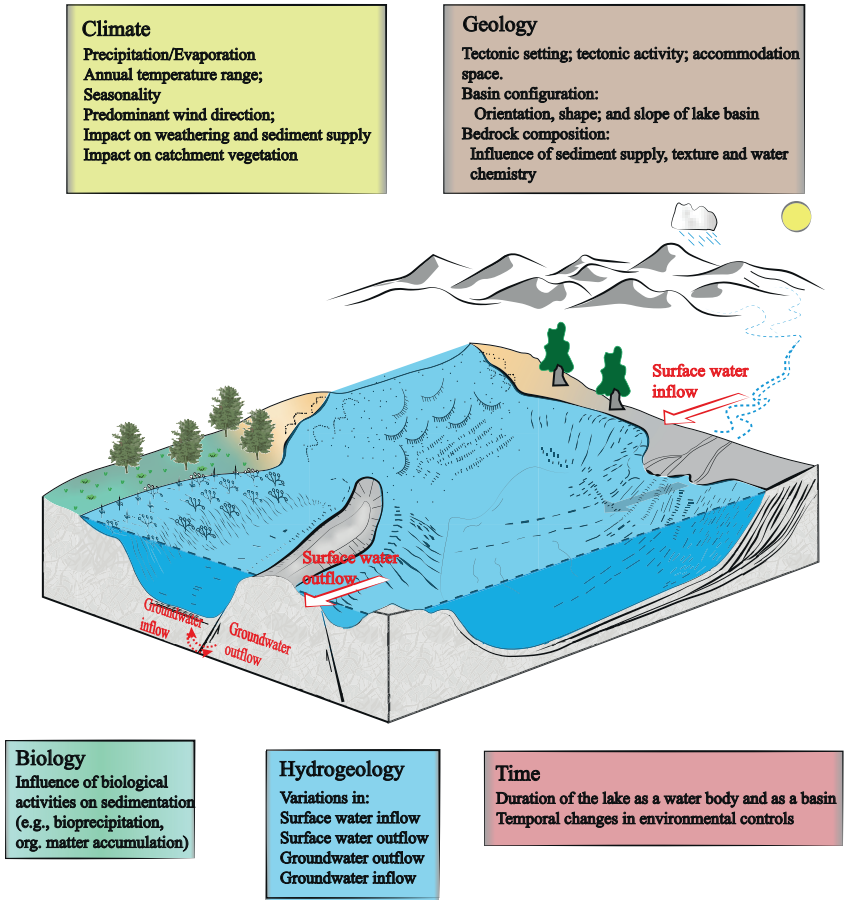


Figure I.7*. Main controls on lacustrine sedimentation. After Renaut et al. (2010, **Fig. 2**, modified).*

Figure I.7*. Principaux facteurs de contrôle de la sédimentation lacustre. D'après Renaut et al. (2010, **Fig. 2,** modifiée).*

La configuration du bassin et les processus hydrodynamiques internes des eaux lacustres, notamment l'activité des vagues et courants, stratification thermique de la colonne d'eau et l'hydrodynamisme des flux entrants (e.g., écoulements en nappe ou concentrés, courants de densité impliquant les dépôts de masse), influent sur la charge sédimentaire entrée, et ainsi sur la (re)distribution de celle-ci dans le bassin (Renaut et al., 2010). En outre, l'importance du drainage dans le bassin versant du système lacustre et l'état hydrologique du bassin (soit ouvert ou fermé), contrôlent à la fois le chimisme et le détritisme du lac, et influencent directement la production et la préservation de la matière organique (*cf., supra*) (Renaut et al., 2010).

En effet, le climat détermine le rapport évaporation/précipitation, le volume des eaux de surface et leur charge sédimentaire, la 'livraison' de particules sédimentaires par les agents de transport (en particulier eau et vent) ainsi que, en moindre mesure, l'afflux des solutés atmosphériques (e.g., chlorides) (Bohacs et al., 2000, 2007; Renaut et al., 2010). En revanche, la tectonique est considérée comme le principal facteur de contrôle de l'espace d'accommodation potentiel (i.e., maximale ; Bohacs et al., 2000; Catuneanu, 2017) ainsi que du drainage général du bassin lacustre, notamment les entrées et sorties impliquant la nappe souterraine (Renaut et al., 2010 ; Fig. I.7). De plus, son

interaction avec le substrat rocheux détermine la composition et l'échelle spatiale du bassin lacustre (étendue d'eau et son bassin versant associée). Ceci, à son tour, module à la fois la composition et la texture (i.e., granulométrie) des sédiments entrants, et le faciès hydrochimique des eaux du lac (Renaut et al., 2010).

Finalement, il faut noter que les effets de la tectonique et du climat sur la sédimentation et processus lacustres sont plutôt enchevêtrés, ce qui rend difficile leur décryptage depuis les sédiments. Ils peuvent produire les mêmes effets sur la productivité organique et la vie aquatique et subaquatique en général, la distribution et typologie (détritique, donc allochtone, ou authigénique, donc autochtone) des faciès organiques (e.g., tourbe vs sapropèle). Dès lors, par rapport à de nombreux systèmes de dépôts, les lacs sont à la fois divers et très complexes.

Comptant sur les conséquences des principaux facteurs de contrôle (Fig. I.7), la balance entre (i) l'évolution de l'espace d'accommodation potentiel, conditionné par la hauteur de la crête de sortie ('*outflow ridge*' ; un acte généralement tectonique), et (ii) la variation de la tranche d'eau, définissant l'espace accommodation effectif (*voir* Catuneanu, 2017) qui est directement associée aux apports des sédiments et de l'eau depuis le bassin versant (un acte généralement climatique), gouverne l'occurrence, la distribution et le caractère des corps sédimentaires dans un bassin lacustre (Bohacs et al., 2000). Ceci conduisait à l'essor d'une classification à base stratigraphique (séquentielle) mais considère aussi l'état hydrologique (i.e., ouvert, fermé ou balancé) à des échelles du temps généralement larges, correspondant à celle du remplissage de bassin (séquence de 1er ordre, *sensu* Catuneanu, 2019). En conséquence, trois types de bassins lacustres ont été définis (Fig. I.8) : '*underfilled lake basin*' ; '*balanced lake basin*' ; '*overfilled lake basin*' (Carroll et Bohacs, 1999; Bohacs et al., 2000, 2007; Zavala et al., 2022). Les caractères typiques de chaque classe sont résumés dans Hanneman et Wideman (2010) et modifié par Zavala et al. (2022).

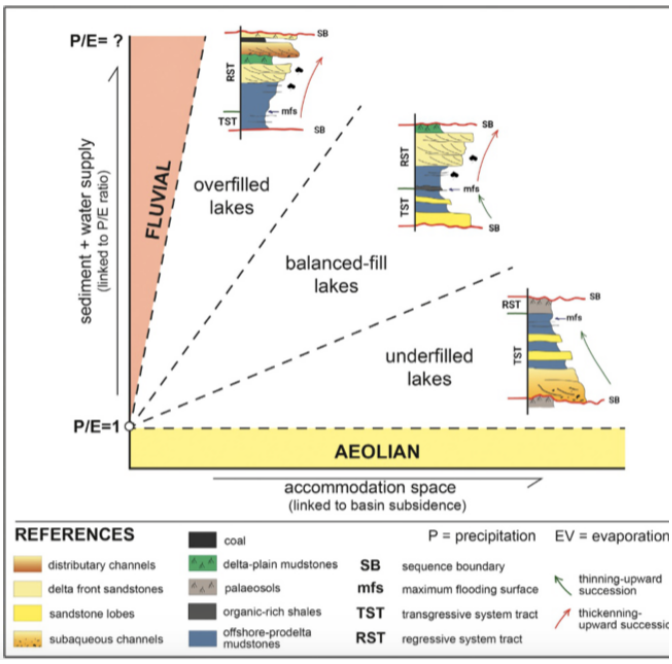


***Figure I.8**. Underfilled, balanced-filled and overfilled lake-basin types, and their stacking patterns. The type of lacustrine basin is a function of the relationship between subsidence (tectonic-controlled) and sediment/water supply (climate-driven). The precipitation/evaporation ratio and the relative lake level (effective accommodation space) determine whether a lacustrine basin will operate as an underfilled, balanced-fill, or overfilled lake, resulting in different stacking pattern trends. After Zavala et al. (2022).*

***Figure I.8**. Trois types de bassins lacustres, 'sous-rempli', 'à remplissage équilibré' et 'sur-rempli', et leurs modes d'empilement. Le type du bassin lacustre est fonction de la balance entre la subsidence (contrôlée par la tectonique) et les apports en eau et sédiments (gouvernés par le climat). Le rapport précipitation/évaporation et le niveau lacustre relatif (espace effectif d'accommodation) déterminent si un bassin lacustre fonctionnera comme un lac 'sous-rempli', 'à remplissage équilibré' ou 'sur-rempli', ce qui se traduira par des tendances différentes en matière de modes d'empilement. D'après Zavala et al. (2022).*

Le déchiffrage des principaux facteurs de contrôle à partir du registre lacustre est la question fondamentale que ce présent projet de doctorat tente à résoudre. Pour ce faire, l'usage de la stratigraphie séquentielle s'est avéré indispensable afin de bien cerner les différents corps sédimentaires ou cortèges sédimentaires (comptant sur l'évolution du niveau lacustre à l'échelle du temps orbitale et suborbitale) et les surfaces qui l'encadrent. De plus, une discussion à propos de la configuration du bassin lacustre en question, et par rapport à la classification hydro-stratigraphique mentionnée plus haut, est une démarche inéluctable puisque les signaux des facteurs externes au système (tectonique et climat) dépendent forcément de cette configuration et de l'état hydrologique du bassin ; les bassins lacustres 'surchargés' ('*overfilled basin-type*') ne sont pas en mesure d'enregistrer l'évolution absolue du climat (*voir* Hanneman et Wideman, 2010).

2 Sédimentation fluviolacustre à dominante carbonatée : tufs calcaires

Les dépôts de carbonates biogènes en domaine fluviatile actuel et ancien enregistrent une pléthore de systèmes de dépôts qui varient de contextes purement fluviatiles à fluviolacustres et exclusivement lacustres à palustres (Arenas-Abad et al., 2010). Compte tenu de la température ambiante, des conditions d'eau relativement froide à tiède ainsi que l'origine météorique du CO_2, les carbonates fluviolacustres sont classés comme des 'travertins météogènes' (Pentecost et Viles, 1994;

Pentecost, 2005), aussi dénommés '*tufas*'(ou tufs calcaires) (Pedley, 1990; Ford et Pedley, 1996). Le terme tufs calcaires est communément attribué aux faciès contenant des restes de plantes incrustés ou imprégnés de carbonates de calcium (Arenas-Abad et al., 2010). En effet, Pedley (1990) a délibérément recommandé à ce que le terme 'tufs calcaires' soit employé pour les carbonates biogènes associés aux systèmes fluviatiles et fluviolacustres où l'origine de $\mathbf{CO_2}$ est météorique. Dans leur publication fondatrice, Arenas-Abad et al. (2010) ont proposé une classification descriptive en termes de faciès sur la base des caractéristiques texturales, en s'appuyant sur le vocabulaire développé par Dunham (1962) et Embry et Klovan (1971). Les relations génétiques entre les faciès reflétant des environnements ou sous-environnements de dépôt ont été exprimées sous forme d'association de faciès ou 'séquence' de faciès (Fig. I.9). Les détails sur le contexte de formation ainsi que les associations et modèles de faciès sont placés dans l'Annexe. Pour l'aspect pétrographique, le lecteur peut consulter la thèse de Julie Dabkowski (2011, et références y afférentes) où une description exhaustive et très pédagogique de l'examen microscopique des faciès des tufs calcaires est fournie.

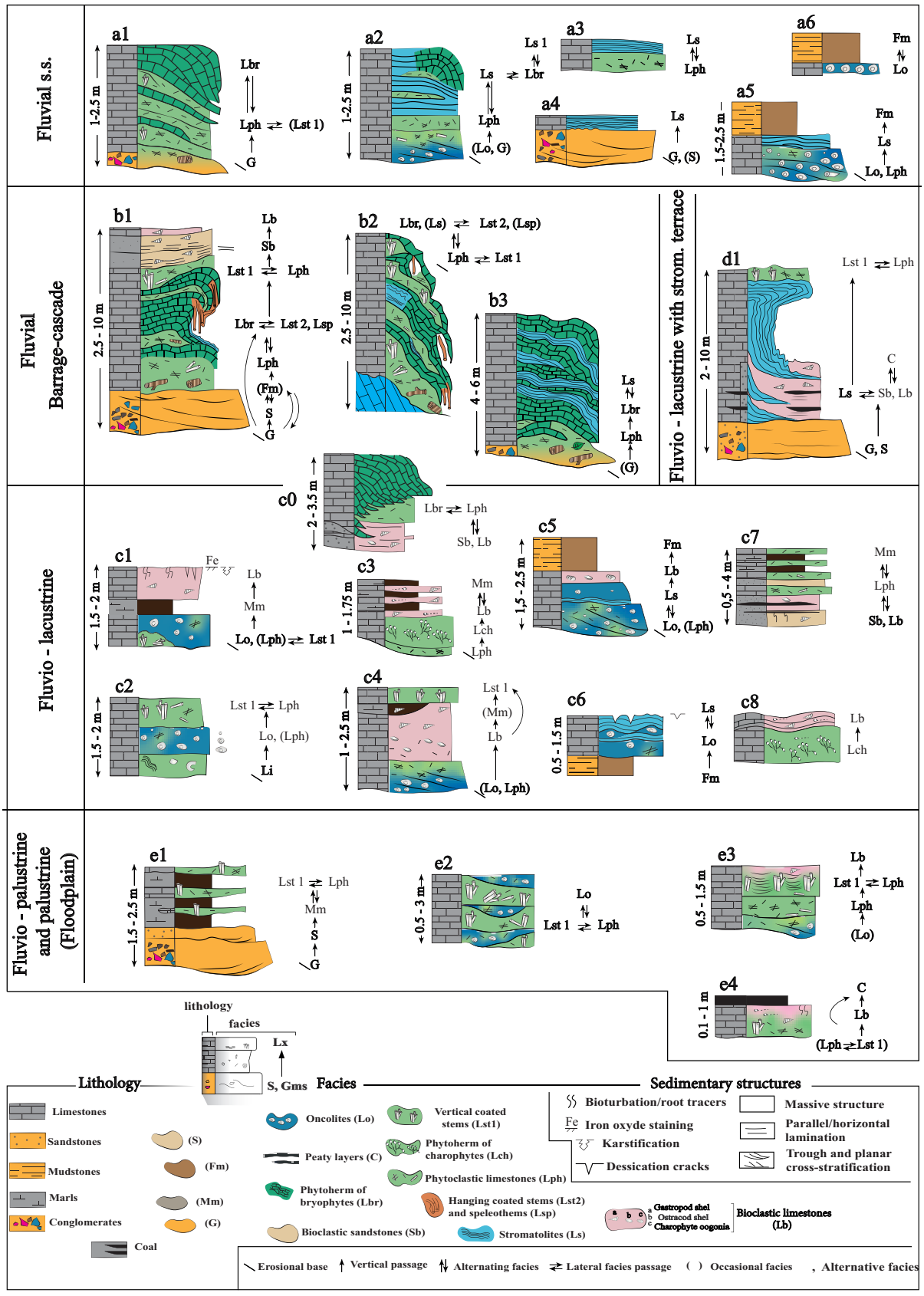


Figure I.9. *Some of the most characteristic facies sequences for fluvial s.s., fluvio-lacustrine, and fluvio-palustrine carbonate systems. Compiled after Arenas- Abad et al. (2010, and references therein) Vázquez-Urbez et al. (2012), and Arenas et al. (2014).*

***Figure I.9**. Séquences de faciès typiques des systèmes carbonatés fluviatiles s.s., fluviolacustres et fluviopalustres. Compilé d'après Arenas-Abad et al. (2010, et références y afférentes) Vázquez-Urbez et al. (2012), et Arenas et al. (2014).*

En termes de conservation de faciès et registre géologique, les dépôts de tufs calcaires ou travertins météogènes qui se développent sous conditions d'un gradient topographique modéré (deuxième variété du modèle proposé par Arenas et al., 2014, *voir* Annexe) sont les mieux conservés, et donc les mieux placés pour donner des réponses sur le passé géologique, climatique et tectonique de la région considérée. Ainsi, en raison d'un dégazage exceptionnellement élevé de CO_2 (Zhang et al., 2001, 2012; Chen et al., 2004) et du développement de mousses qui sont jugées être des contributeurs à des taux les plus élevés de bio-calcification (Pentecost, 1998), le taux d'accrétion important au niveau des barrages crée en aval un niveau de base local, et ainsi de l'espace disponible pour être rempli par une sédimentation fine bioclastique susceptible de conservation (i.e., espace d'accommodation). De plus, l'extension et la profondeur de la tranche d'eau sont en fonction du taux d'aggradation au niveau du barrage. Dès lors, un taux élevé (faible) d'aggradation aurait conditionné en arrière une étendue d'eau extensive (réduite) et profonde (peu profonde). Cet aspect, bien exprimé sous gradient topographique modéré, a suscité une réflexion de notre part sur la mise en application d'un outil qui peut élucider l'interaction entre le style d'empilement inféré au niveau d'un barrage à dimensions considérables (i.e., aggradation, progradation ou dégradation) et la variation de l'espace d'accommodation créé en arrière de cet édifice. Cet outil est bel et bien la stratigraphie séquentielle haute résolution. L'application de celle-ci dans un tel contexte constitue l'un des apports majeurs qu'a adressé ce projet de doctorat pour la première fois à l'échelle de la science dédiée au carbonates fluviolacustres. En fait, les relations entre extension et profondeur de la retenue et le style d'entablement au niveau du barrage ont été déjà présentés, ainsi qu'aux paramètres les contrôlant, par Arenas et al. (2014 ; Fig. I.10). En effet, le rapport aggradation/progradation, contrôlant l'espace d'accommodation derrière, est directement lié à la décharge d'eau (volume d'eau traversant une section du chenal) et à la vitesse de l'écoulement d'eau ; des valeurs élevées (modérées à faibles) auraient conditionné la progradation (aggradation) de l'édifice, tandis que des valeurs très élevés (très faibles à nuls) auraient conditionné sa dégradation (stabilité) (Arenas et al., 2014) (Fig. I.10). Outre la conjoncture attractive de l'usage de la stratigraphie séquentielle, un contexte impliquant une retenue extensive et profonde endiguée par un large barrage-cascade où l'aggradation est maintenue, est susceptible de capturer, enregistrer et surtout préserver des signaux de contrôles, en l'occurrence climatiques à l'échelle du temps orbitale, voire même suborbitale. En effet, il a été largement démontré que les pulsations d'occurrence des tufs calcaires suivent en général les paramètres orbitaux de

Milankovitch (e.g., Arenas et al., 2014; Dabkowski et al., 2015; Nutz et al., 2019). Cependant, le décryptage des signaux à l'échelle centennale (*événements de Bond*) ou même à l'échelle multimillénaire des interglaciaires n'a pas été délibérément et explicitement élaboré. Ce défaut de contribution constitue un autre apport majeur qu'a adressé ce projet de doctorat (chapitre 5).

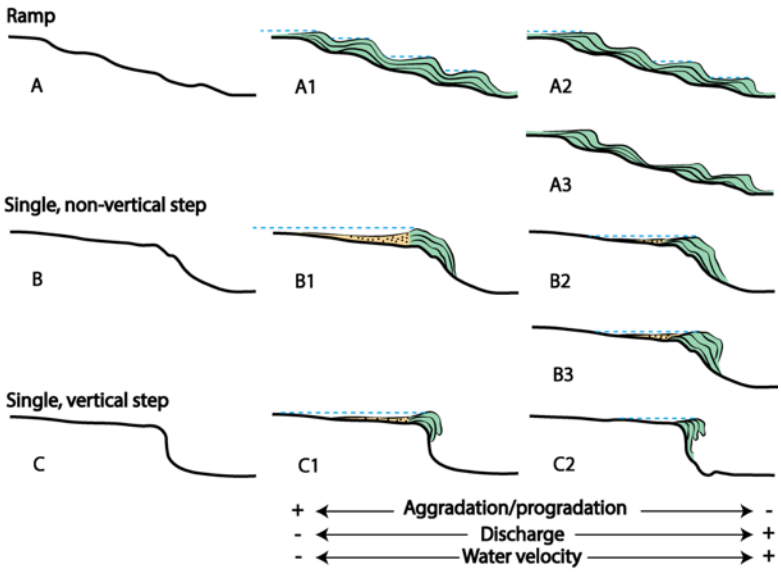


***Figure I.10**. Proposed patterns of growth style of cascades as a function of the slope break (knickpoint) geometry and the aggradation/progradation ratio. After Arenas et al. (2014).*

***Figure I.10**. Différents modes d'empilement au niveau des cascades en fonction de la géométrie de la rupture de pente ('knickpoint') et le rapport aggradation/progradation. D'après Arenas et al. (2014).*

Au final, il est à noter que, par faute de place, elle a été omise la présentation d'un aperçu sur la variabilité climatique à l'échelle des fluctuations glaciaire/interglaciaire et stadiaire/interstadiaire (pour une configuration totalement glaciaire) ainsi qu'à la périodicité des événements froids (i.e., '*Ice Rafting Events*') marquant le présent interglaciaire, l'Holocène. Cependant, une connaissance minimale sur ce sujet est inéluctable afin de contraindre l'apport scientifique de cette dissertation (surtout pour les chapitres 4 et 5). Pour cela on a le plaisir de référer à deux bouquins beaucoup mieux placés et élaborés par des séniors chercheurs en domaine de paléoclimatologie, à savoir (i) 'Paleoclimatology' par Giles **Ramstein et al. (2021)** [document fournissant une base scientifique pertinente pour comprendre l'histoire climatique de de la Terre depuis l'apparition des continents, en exposant tous les facteurs ou 'acteurs' qui interagissent dans l'archivage de cette histoire] et (ii) 'Paleoclimatology : Reconstructing climate of the Quaternary' 3ème édition par **Raymond S. Bradley (2015)** [un excellent document où le lecteur peut trouver la présentation théorique des principes de paléoclimatologie ainsi que les variabilités climatiques, à l'échelle chronostratigraphique du Quaternaire, observées et inférées par les archives naturelles].

CHAPITRE III

PLACE DU MOYEN ATLAS DANS SON CONTEXTE GEOLOGIQUE ET CLIMATIQUE ET METHODOLOGIE

1 Présentation de la zone d'étude

Les sites où cette étude est menée appartiennent au Moyen Atlas septentrional (Nord du Maroc, Fig. II.1) dont l'histoire géologique et climatique n'est autre que celle de la chaîne moyen atlasique entière. Sa position géographique, siège de téléconnexions entre différentes oscillations météorologiques d'échelle synoptique, lui confère une importance particulière sur le plan paléoclimatique pendant le Quaternaire.

1.1 Cadre géologique

De point de vue structural, le Moyen Atlas est une chaîne intraplaque à tendance NE-SW, subdivisé en deux sous-domaines morpho-structuraux (Martin, 1981) (Fig. II.1) : Moyen Atlas Tabulaire (MAT) au Nord-Ouest faiblement déformé, conditionnant un relief relativement modéré sous forme de plateaux séparés par des structures cassantes ; et Moyen Atlas Plissé (MAP) à relief beaucoup plus accusé, conditionnant un emplacement successif de rides et de dépressions (anticlinaux et synclinaux). Les deux sous-domaines morpho-structuraux sont séparés par l'Accident Nord Moyen Atlasique (ANMA). Parallèlement à ceci, d'autre accidents structurent le Moyen Atlas de part et d'autre de l'ANMA selon une direction compatible avec les contraintes qui ont joué pendant l'orogenèse hercynienne (i.e., NW-SE) (Charrière, 1990). Parmi ceux-ci, un accident ayant une importance plus spécifique dans le cadre de recherche sépare le MAT en deux, l'Accident de Tizi n'Tretten (ATT). Les deux sites sont inclus dans le MAT et sont situés de part et d'autre de l'ATT.

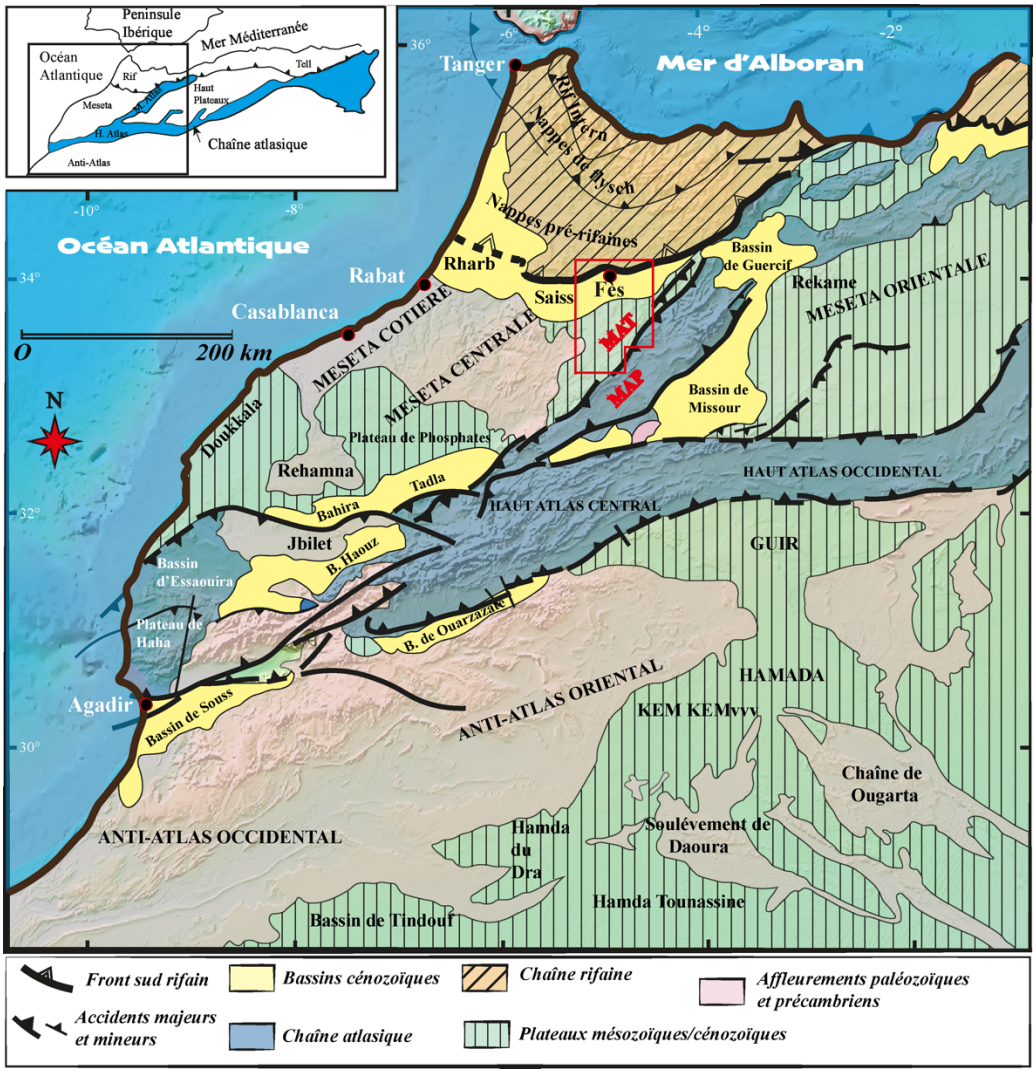


Figure II.1. *Carte des domaines morpho-structuraux du Nord du Maroc montrant l'extension de la chaîne atlasique et bassins et plateaux l'encadrant. MAT : Moyen Atlas Tabulaire ; MAP : Moyen Atlas Plissé. Le tracé en rouge indique l'emplacement de la* ***figure 1****, chapitre 3. D'après Hafid et al. (2006) et Michard et al. (2008), adaptée.*

De point de vue évolution tectono-sédimentaire, les structures majeures, en partie héritées de l'orogenèse varisque, ont servi de place pour accommoder le rifting de l'Atlas téthysien au cours du Trias lors de la dislocation de la Pangée (Mattauer et al., 1977), créant ainsi de l'espace pour des dépôts significatifs d'évaporites synrift, de dépôts volcano-détritiques et de basaltes tholéiitiques qui recouvrent en discordance les schistes et grès paléozoïques déformés (Figs. II.2 et II.3) (Ouarhache et al., 2000, 2012 ; Laville et al., 2004). Lors de l'avortement du rift de l'Atlas téthysien, l'extension lente contrôlée par la subsidence thermique s'est poursuivie durant le Lias inférieur et moyen, conditionnant la mise en place des carbonates de plateforme post-rift (Charrière, 1990 ; Ouarhache et al., 2012) qui dominent en affleurement la surface, notamment dans le MAT (Fig. II.2 et II.3) (Martin, 1981). Ces derniers ont été individualisés dans de tels contextes d'extension grâce à la tectonique en blocs basculés conduisant au développement d'hémi-grabens limités par des crêtes des lèvres supérieures ('*hanging-*

walls') de failles normales maîtresses (Frizon de Lamotte et al., 2008). Là encore, ils ont constitué des places pour des transgressions subséquentes qui sont soit localisées du Barrémien-Aptien (golfe du Moyen Atlas Nord) soit généralisées du Cénomanien-Turonien (Charrière et Vila, 1991 ; Charrière et al., 1998). Du Bathonien jusqu'au début du Crétacé inférieur, le Moyen Atlas émerge et la sédimentation devient continentale, donnant lieu aux fameux 'couches rouges' à dominante fluviatile (Fig. II.3) (Frison de Lamote et al., 2008). Depuis l'ébauche de la convergence entre la plaque d'Afrique et celle de l'Eurasie à la fin du Crétacé (Rosenbaum et al., 2002 ; Fernàndez et al., 2019), un régime compressif avec deux climax atteints pendant l'Éocène moyen et le Plio-quaternaire (Frizon de Lamotte et al., 2000) a conduit à une inversion de la configuration jadis développée avec crêtes et dépressions successifs en anticlinaux accommodés par des chevauchements senestres et synclinaux dans le MAP, respectivement, et en décrochement à composante transtensive dans le MAT, sculptant ainsi les principales structures observées actuellement (e.g., Ait Brahim et al., 2002) (Fig. II.1) ; cet état de répartition inégale des déformations entre le MAP et le MAT (i.e., fort relief vs. faible relief, respectivement) trouve son explication dans le fait que le MAT a été plus stable que le MAP pendant l'extension mésozoïque (Gomez et al., 1996, 1998). Toutefois, la tectonique extensive dans le Moyen Atlas a repris pendant le Miocène moyen entraînant ainsi la néoformation de plusieurs bassins inondés (Fig. II.2) (Hinaje, 2004) et servant de voie pour guider vers la surface le volcanisme alcalin néogène-quaternaire du Moyen Atlas (Fig. II.2) (El Azzouzi et al., 2010 ; Hinaje et al., 2019). Dès lors, cette histoire géodynamique polyphasée du Moyen Atlas depuis le début du Mésozoïque conditionna la mise en place de deux discordances angulaires séparant trois cycles tectono-sédimentaires (Mésozoïque, Paléogène et Néogène-Quaternaire) (Fig. II.3).

Pour une lecture plus exhaustive sur les différents aspects de l'évolution géodynamique des domaines structuraux du Maroc (montrés en partie dans la figure II.1) depuis l'Archéen, le lecteur peut référer au fameux bouquin de Michard et al. (2008, et références y afférentes).

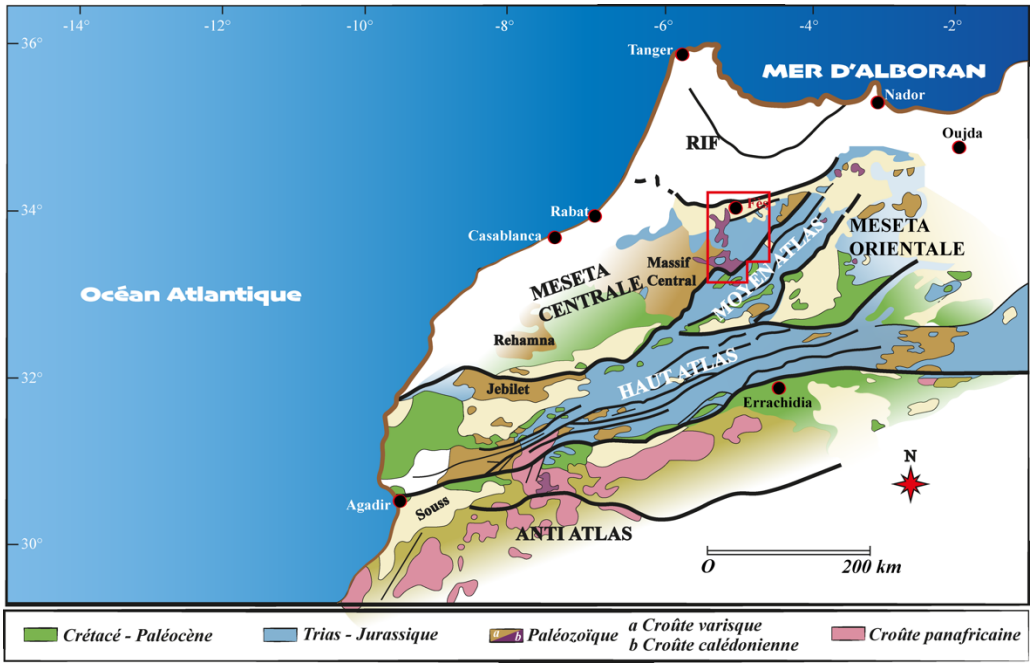


Figure II.2. *Carte géologique simplifiée du Moyen Atlas et bassins et plateaux qui l'encadrent. Le tracé en rouge indique l'emplacement de la* ***figure 1****, chapitre 3. D'après Frizon de Lamotte et al. (2004) et Michard et al. (2008), adaptée.*

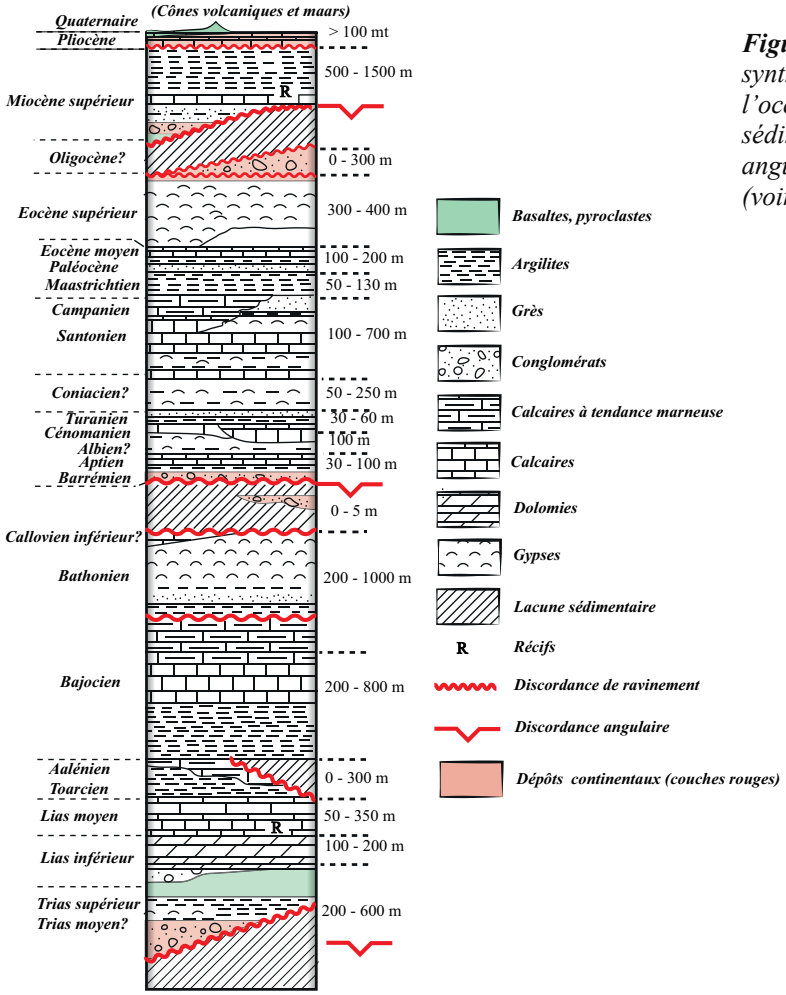


Figure II.3. *Log stratigraphique synthétique du Moyen Atlas montrant l'occurrence de trois cycles tectono-sédimentaires (séparés par les discordances angulaires). D'après Charrière et al. (2011) (voir aussi Michard et al., 2008,* ***Fig. 4.11****).*

De manière contradictoire, l'élévation relativement élevée du Moyen Atlas et du Haute Atlas par rapport aux autres Atlas du Maghreb n'est pas compatible avec le raccourcissement tectonique calculé (10 % ou moins, Gomez et al., 1998 ; Frizon de Lamotte et al., 2009). Pour rendre compte de cette anomalie d'altitude, une composante de flottabilité mantellique sous le Moyen Atlas a été proposée (e.g., Teixell et al., 2005 ; Missenard et al., 2006) et confirmée sur la base de la tomographie sismique (e.g., Bezada et al., 2014 ; Palomeras et al., 2014 ; Miller et al, 2015). Cette anomalie géothermique en dessous du Moyen Atlas explique incontestablement l'apparition du volcanisme néogène-quaternaire (Bosch et al., 2014) (Figs. II.2 et II.3) ; ce dernier point a reçu un grand intérêt de notre part et fait objet du chapitre 3 (Azennoud et al., 2022b).

1.2 Cadre climatique et paléoclimatique

1.2.1 Circulation atmosphérique globale et position du Maroc dans celle-ci

Appartenant à une zone qualifiée astronomiquement de 'zone habitable' dans le système solaire où l'eau est présente sous ses trois états physiques, la Terre connait à sa surface une dynamique dans ses enveloppes fluides (océan et atmosphère) très particulière lui discriminant des autres planètes et lunes du système solaire ayant une composante fluide dynamique (e.g., Vénus, Jupiter, Titan). L'acteur principal de cette mise en scène singulière dans le théâtre du système solaire est le cycle de l'eau. Ainsi, évaporation, condensation et fusion de la molécule d'eau assurent un transfert de chaleur (énergie), surtout sous sa forme latente, depuis la zone intertropicale jusqu'aux hautes latitudes, tamponnant ainsi partiellement l'écart thermique latitudinal. En effet, à cause de la rotation de la Terre et sa rotondité, inclinant à générer un gradient de pression latitudinal, la troposphère se présente avec une dynamique en trois cellules transporteuses d'humidité et de chaleur latente dans chaque hémisphère (cellules de Hadley, de Ferrel et Polaire) où la position latitudinale et longitudinale de leurs extrémités (membres descendants ou ascendants, i.e., anticyclones et dépressions, respectivement) conditionnent des oscillations synoptiques modulant extensivement la climatologie et la météorologie des zones proches (e.g., ONA, *cf. infra*) (Fig. II.4). De plus, au voisinage de la tropopause où les cellules communiquent, un gradient altitudinal de pression fort enclenche des vents zonaux dits courants jets ('*jet streams*', y compris les vents d'Ouest, ou '*westerlies*', Fig. II.4) jouant un rôle crucial dans la téléconnexion entre les régions très loin du monde selon plusieurs mécanismes (e.g., ondes de Rossby). En outre, la zone où les vents de surface (les alizés) des deux hémisphères communiquent est appelée Zone de Convergence Intertropicale ('ITCZ') ou équateur météorologique (Fig. II.4). La dynamique atmosphérique influence aussi en partie la circulation océanique de surface qui, à son tour, transfère l'excès de chaleur (sous sa forme sensible cette fois-ci) de l'équateur vers les

hautes latitudes où les eaux dites 'profondes' se forment, conduisant à une circulation connue sous le vocable de 'circulation thermohaline' très importante en climatologie et paléoclimatologie. Au final, il faut mentionner que les positions latitudinales de l'ITCZ, des dépressions et des anticyclones ainsi que les vents zonaux associés varient avec les saisons (Fig. II.4), mais aussi à travers le temps géologique.

En particulier, étant situé entre les latitudes subtropicales et moyennes, le territoire marocain est extensivement influencé par la position de l'anticyclone subtropicale des Açores, surtout durant la période froide de l'année (Fig. II.5). De plus, l'influence de la mer méditerranéenne est considérable dans l'enclenchement des averses du printemps comme la convection dans le bassin est prononcée durant la période chaude de l'année.

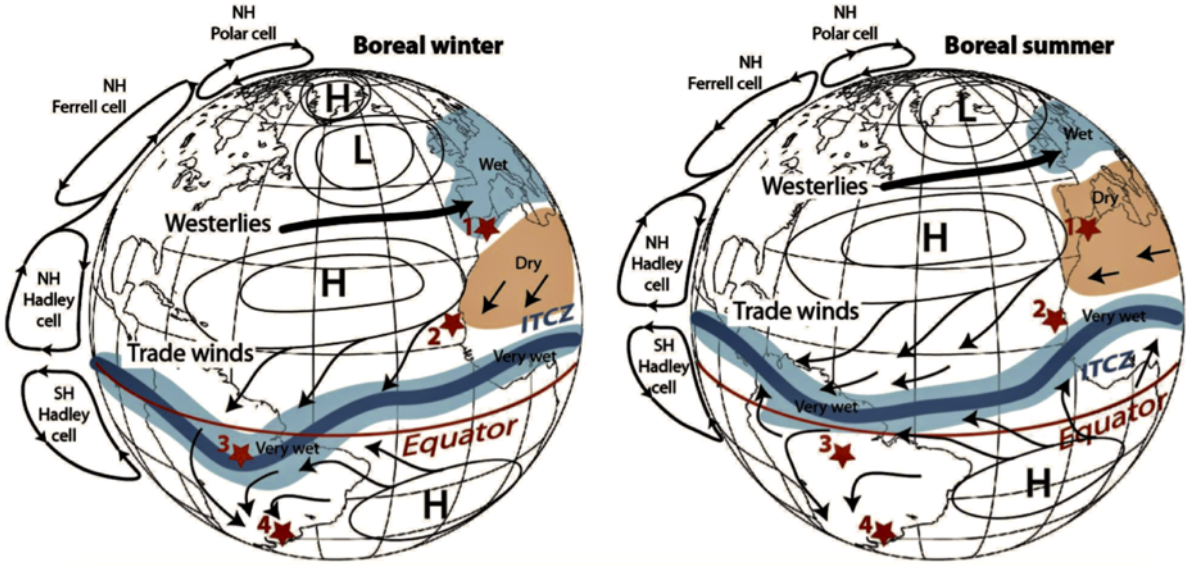


***Figure II.4**. Conceptual schematic of atmospheric teleconnections across the Atlantic (after J. Wassenburg, unpublished document). Sea level pressure centres and associated atmospheric circulation patterns in the Atlantic region based on figures from Tjallingii et al. (2008) and (Wang et al., 2017). Air rises at the intertropical convergence zone (ITCZ), and descends at the Azores High, where it causes very wet and dry conditions, respectively. Red stars indicate the Northwest Africa region (1), paleoclimate records affected by the North African monsoon (2) (Tjallingii et al., 2008), and the SASM (Cruz et al., 2005; Wang et al., 2017), 3 and 4, respectively.*

***Figure II.4**. Schéma conceptuel des téléconnexions atmosphériques à travers l'océan Atlantique (d'après un document non publié de J. Wassenburg). Les positions des centres de pressions au niveau marin, et configurations de la circulation atmosphérique associées, dans le domaine atlantique sont d'après des figures de Tjallingii et al. (2008) et Wang et al. (2017). L'air monte dans la zone de convergence intertropicale ('ITCZ') et descend dans l'anticyclone des Açores, où il provoque respectivement des conditions très humides et sèches. Les étoiles rouges indiquent la région de l'Afrique du Nord-Ouest (1), les enregistrements paléoclimatiques affectés par la mousson nord-africaine (2) (Tjallingii et al., 2008), et le SASM (Cruz et al., 2005 ; Wang et al., 2017), 3 et 4, respectivement.*

1.2.2 Climat actuel du Moyen Atlas

Dans son ensemble, le Moyen Atlas est caractérisé par un climat tempéré avec un été chaud, i.e., type Csa selon la classification de Köppen (Köppen, 1900 ; Kottek et al., 2006), avec des précipitations annuelles d'environ 683 mm et une température moyenne de 12,1°C

(http://www.climate-data.org/). En général, la dynamique des précipitations en Afrique du Nord-Ouest (NO) est modulée par la position latitudinale et longitudinale et par le gradient de pression à la surface entre l'anticyclone subtropical des Açores et la dépression de l'Island modulant la trajectoire des vents d'Ouest (‘*westerlies*’, Figs. II.4 et II.5). Ainsi, la déviation des vents d'Ouest vers le Nord (Sud) résulte en des conditions arides (humides) pendant l'hiver en Afrique du Nord-Ouest (Fig. II.5). Le climat méditerranéen avec des étés chauds et secs et des hivers humides est lié à la migration saisonnière Nord-Sud de l'anticyclone des Açores et au positionnement correspondant à des vents d'ouest porteurs d'humidité (Fig. II.5). Ainsi, la quantité de précipitations hivernales dans le Nord du Maroc est fortement couplée à l'état de l'Oscillation Nord-Atlantique (ONA) (Knippertz et al., 2003; Ait Brahim et al., 2018; Hakam et al., 2022).

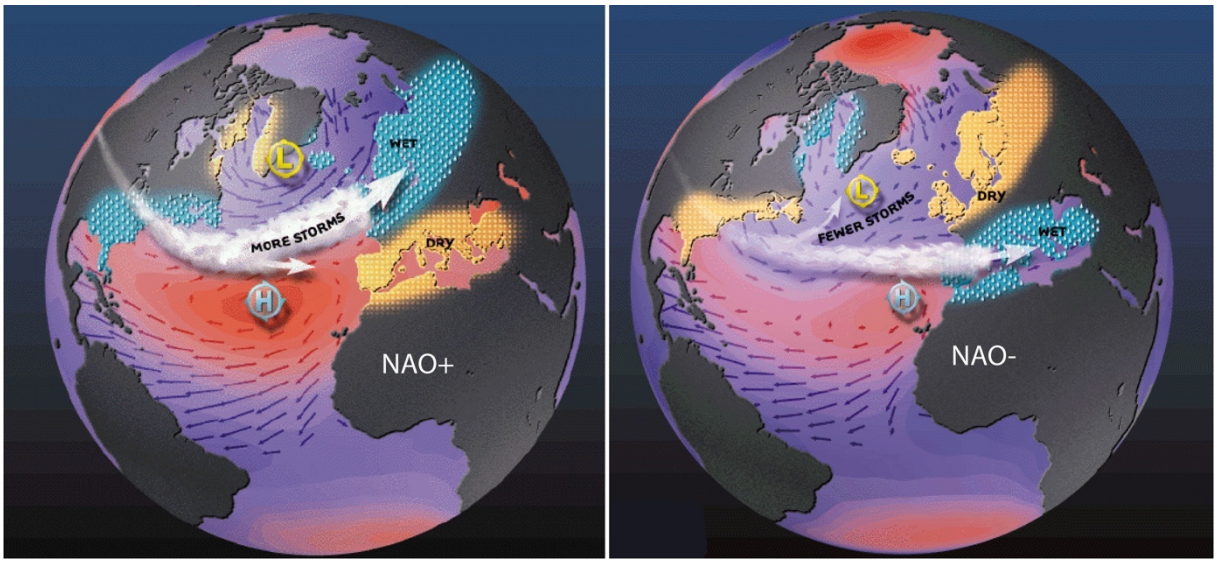


Figure II.5*. Schéma conceptuel rappelant les impacts associés aux deux phases de l'Oscillation Nord-Atlantique (ONA). Reproduite d'après des pages descriptives 'Internet du Lamont Doherty Earth Observatory', Martin Visbeck.*

1.2.3 Histoire climatique depuis le Stade Isotopique Marin 3 (SIM-3) de l'Afrique du NO : données des géoarchives lacustres et spéléothèmes

La question du décryptage des signaux de la variabilité climatique à travers l'Holocène dans l'Afrique du NO a été confiée aux sédiments lacustres (Lamb et al., 1995, 1999; Baali, 1998; Cheddadi et al., 1998, 2009; Rhoujjati et al., 2010, 2012; Nourelbait et al., 2014, 2016; Tabel et al., 2016; Campbell et al., 2017; Zielhofer et al., 2017a, 2017b, 2019; Abdellah et al., 2021) et aux spéléothèmes (Wassenburg, 2016; Ait Brahim et al., 2017, 2018, 2019; Sha et al., 2019, 2021). En fait, l'influence de l'ONA a été soulignée comme le mécanisme principal de modulation des précipitations dans la région (Wassenburg, 2016; Zielhofer et al., 2017a, 2017b, 2019; Ait Brahim et al., 2018, 2019). En outre, les données palynologiques suggèrent des conditions plutôt arides (dominance de plantes en C4) durant l'Holocène inférieur (i.e., 11.7-8.2 cal ka BP) suivi d'une période plus humide durant

l'Holocène moyen et une partie de l'Holocène supérieur (Lamb and van der Kaars, 1995; Nourelbait et al., 2014; Campbell et al., 2017), et une aridification pendant l'Holocène tardif (Nourelbait et al., 2016) accusée partiellement par l'action anthropique (Lamb and van der Kaars, 1995; Cheddadi et al., 1998; Nourelbait et al., 2014). Cependant, ces interprétations basées sur les données paléobotaniques sont partiellement contradictoires avec les données paléolimnologiques et géochimiques isotopiques des spéléothèmes, notamment en ce qui concerne le début de l'Holocène (Lamb and van der Kaars, 1995; Campbell et al., 2017; Zielhofer et al., 2017b; Ait Brahim et al., 2019). Ainsi, prenant l'exemple du lac Sidi Ali (Sud du MAP), le niveau lacustre inféré durant l'Holocène inférieur aurait été plus élevé alors que les données polliniques de la même carotte suggèrent l'installation d'une végétation steppique (plantes en C4; Campbell et al., 2017; Zielhofer et al., 2017b). De même, les données isotopiques suggèrent des hivers humides durant l'Holocène inférieur, à l'instar d'une situation prolongée avec un indice négatif de l'ONA (Ait Brahim et al., 2019). Cette contradiction est expliquée par la saisonnalité très prononcée pendant l'Holocène inférieur (Lamb and van der Kaars, 1995) modulée en partie par la position du solstice d'été proche du périhélie de l'orbite terrestre (i.e., faible précession) et par une forte obliquité. De ce fait, le niveau lacustre élevé durant l'Holocène inférieur serait dû à une surcharge de la nappe souterraine pendant la saison pluviale, en accord avec les données isotopiques, alors que la limitation de la biomasse à photosynthèse en C3 serait une réponse d'un assèchement très prononcé pendant la saison estivale (forte insolation et faibles précipitations). Le développement subséquent d'une végétation boisée typique du Moyen Atlas (cèdre de l'Atlas et chêne vert) suivrait la cadence de la baisse de la saisonnalité dans l'hémisphère nord (Lamb and van der Kaars, 1995). Par ailleurs, des données isotopiques récentes, contradictoires à ce qu'on a jadis pensé (Kuhlmann et al., 2004), suggèrent un déplacement de la Zone de Convergence Intertropicale ('ITCZ') jusqu'aux côtes d'Essaouira (31°N) (Sha et al., 2019), mais jamais atteignant le Moyen Atlas (32-33°N) (Ait Brahim et al., 2019) pendant la Période Humide Africaine. Ceci suggère à son tour que les précipitations estivales ont été toujours modulées par la cyclogenèse méditerranéenne, loin de l'influence de la Mousson Ouest Africaine durant l'ensemble de l'Holocène.

Alors que notre conception de la variabilité climatique à travers l'Holocène dans le Moyen Atlas est devenue de plus en plus claire avec la compilation de différents géoarchives et méthodologies, celle du dernier glaciaire et tardiglaciaire est beaucoup loin d'être fondée. En fait, le climat glaciaire de l'Afrique du Nord-Ouest et de la Méditerranée occidentale a été reconstitué principalement pour les SIM-3 et SIM-2 sur la base de sédiments marins carottés du bassin d'Alboran (Cacho et al., 1999; Moreno et al., 2002, 2005; Sánchez Goñi et al., 2002, 2008; Martrat et al., 2004; Bout-Roumazeilles

et al., 2007; Jimenez-Espejo et al., 2008; Fletcher and Sánchez Goñi, 2008; Eynaud et al., 2009; Naughton et al., 2009). Les reconstitutions soulignent que le climat sous sa configuration glaciaire est beaucoup plus fluctuant comparé à l'interglaciaire. Ainsi, les oscillations à l'échelle millénaire du signal isotopique de l'oxygène de la molécule d'eau produit des carottes de glace en Groenland (fluctuations dites de Dansgaard-Oeschger, D-O ; Dansgaard et al., 1993) sont répliquées à partir des sédiments marins du bassin d'Alboran. Elles reflètent des fluctuations climatiques entre périodes humides et sèches bien exprimées à travers le SIM-3. En effet, les données disponibles suggèrent que les interstadiaires D-O (également désignés par interstadiaires Groenlands) étaient relativement chauds et humides, alors que les stadiaires D-O (ou stadiaires Groenlands) étaient plus secs dans la région de la mer d'Alboran (Sánchez Goñi et al., 2002 ; Moreno et al., 2005 ; Fletcher and Sánchez Goñi, 2008). Qui plus est, périodes avec un refroidissement prononcé et des conditions plus arides dans la Méditerranée occidentale auraient coïncidé avec les événements les plus froids de la période glaciaire désignés par 'événements de Heinrich' initialement découverts à partir des sédiments marins de l'Atlantique du Nord (Heinrich, 1988; Bond et al., 1992; Broecker et al., 1992).

À ce jour, seules quelques reconstitutions du climat depuis des géoarchives terrestres couvrant une partie du dernier glaciaire sont disponibles pour la Méditerranée occidentale et l'Afrique du Nord-Ouest (Rhoujjati et al., 2010; Moreno et al., 2012; Reddad et al., 2013; Nourelbait et al., 2014; Tabel et al., 2016; Lacey et al., 2016; Damnati and Reddad, 2017). En particulier, les données actuelles des géoarchives lacustres au niveau du Moyen Atlas suggèrent un climat généralement froid et sec de 29 à 12 cal ka BP (Rhoujjati et al., 2010; Reddad et al., 2013; Nourelbait et al., 2014; Tabel et al., 2016). Du côté de la péninsule ibérique, à notre connaissance, seulement quelques reconstitutions depuis les sédiments lacustres à résolution considérable couvrant les derniers 50 ka sont disponibles. Ainsi, Lacey et al. (2016) détectaient des fluctuations du niveau lacustre au cours du SIM-3, et des hauts niveaux ('*highstands*') inhabituels au cours du SIM-2. De leur côté, Vegas et al. (2010) ont corrélé les phases sèches aux événements de Heinrich et les phases humides aux interstadiaires D-O. Néanmoins, ces enregistrements manquent d'une haute résolution nécessaire pour discuter avec confiance les fluctuations de haute fréquence et présentent des incertitudes analytiques souvent importantes, parfois liées au manque de matériel datable lui-même ; ceci donne aux spéléothèmes l'avantage d'être mieux placés pour produire des séries temporelles de très haute résolution (parfois arrivant jusqu'à l'échelle de la saison) et souvent considérés lors de comparaisons des courbes des proxies paléoclimatiques à l'échelle de l'hémisphère. À notre connaissance, il n'existe aucune reconstitution à l'heure actuelle du climat terrestre qui permettrait de tirer des conclusions solides, basées sur des séries chronologiques à

haute résolution, sur les conditions climatiques à l'échelle des fluctuations interstadiaires/stadiaires (D-O, événements de Heinrich) en Afrique du Nord-Ouest, à l'instar de l'Holocène.

2 Méthodologie

Le décryptage des signaux climatiques et tectoniques à partir des sédiments déposés dans un bassin où l'espace d'accommodation varie en fonction de la variation d'un niveau d'eau plus ou moins stagnante (e.g., lac, mer) exige de suivre une démarche conventionnelle dédiée au domaine d'analyse des bassins ('*basin analysis*') (Allen et Allen, 2013, partie 3; Miall, 2013). Ainsi, une étude sédimentologique détaillée doit être menée dont l'objectif est de reconstituer les paléoenvironnements de dépôt et les conditions hydrodynamiques dans l'intervalle considérée du temps. Néanmoins, l'analyse sédimentologique doit suivre une démarche conventionnelle alimentée par un raisonnement inductif imitant celui présenté dans le premier chapitre et dans l'Annexe (i.e., du faciès au modèle de faciès en passant par le système de dépôt). De plus, l'interaction entre l'évolution latérale des systèmes de dépôts et la variation de l'accommodation constitue une approche indispensable pour la mise au point de la cyclicité sédimentaire, chose qui ouvre grand la porte vers l'examen de l'empreinte des signaux climatiques et tectoniques. Cette démarche constitue l'intérêt de la stratigraphie séquentielle (*sensu* l'école Exxon) appliquée initialement en domaine marin (e.g., Vail et al., 1977; Payton, 1977; Posamentier et al., 1988; Van Wagoner et al., 1988) et adaptée ensuite au contexte lacustre (e.g., Prosser, 1993; Carroll and Bohacs, 1999; Strecker et al., 1999; Bohacs et al., 2000, 2007; Hanneman and Wideman, 2010; Nutz et al., 2020; Zavala et al., 2022). Les deux approches (sédimentologie et stratigraphie) demandent à cor et à cri un travail de terrain colossal et surtout minutieux visant à collecter des informations (observations) de l'échelle du millimètre au kilomètre. Néanmoins, bien qu'il forme la base de l'investigation, le travail de terrain n'est pas suffisant pour entièrement aboutir dans la perquisition scientifique. Par ailleurs, comme déjà mentionné dans l'introduction, la faune et la flore plus les proxies géochimiques peuvent servir d'outils pour un déchiffrage plus délicat des conditions paléoenvironnementales. En conséquence, l'intégration des méthodes conventionnelles de terraine et le travail de laboratoire certes abouterai à des conclusions prometteuses par rapport à la cause définie d'emblée.

Suivant cette logique, ce projet de thèse a consacré une large période pour un travail minutieux de terrain comptant sur plusieurs expéditions d'exploration, de mise au point et de vérifications. De plus, des campagnes d'échantillonnage ont été menées pour analyses au laboratoire à l'université et ailleurs (Casablanca, Espagne, Lituanie, États-Unis).

Le travail de terrain consiste à :

- choisir les sites les mieux représentatifs pour mener l'investigation par rapport aux objectifs cités (étape d'exploration) ;
- mener une investigation sédimentologique et stratigraphique séquentielle conventionnelle selon un consensus accordé internationalement entre les sédimentologues et experts de la stratigraphie séquentielle (étape de mises au point) ;
- faire des retours chaque fois nécessaire aux sites choisis pour vérifications ou approfondissement des observations en rapport avec les interprétations conduites dans la deuxième étape (étape de vérifications) (Fig. II.6).

Le travail du laboratoire consiste à :

- préparer délicatement des échantillons pour les datations par radiocarbone et par série U/Th ;
- préparer les échantillons (prétraitement) pour analyse spectroscopique (ICP-AES, DRX, pour étude géochimique élémentaire et minéralogique, respectivement) ;
- préparer les échantillons pour analyse micropaléontologique (détermination taxonomique d'ostracodes jusqu'au niveau de l'espèce) et observations sous microscope électronique à balayage (MEB) ;
- préparer les échantillons pour mener l'étude du macro-charbon (comptage et détermination morphotypique) ;
- mener des analyses pour le dosage de la matière organique et carbonates ;
- préparer (i) les lames minces de roches pour étude pétrographique et (ii) les échantillons de roches dures (oncolithes et stromatolithes) pour des investigations nanoscopiques sous le MEB (Fig. II.6).

Les résultats ainsi obtenus sont traités et interprétés. Cela consiste en leur translation en forme de diagrammes représentatifs au moyen d'un logiciel de DAO (e.g., Adobe Illustrator) (Fig. II.6). L'interprétation des résultats a demandé une recherche bibliographique approfondie et extensive par rapport à plusieurs disciplines envisagées dans le cadre de ce doctorat (e.g., pétrographie des tufs calcaires et autres carbonates continentaux, stratigraphie séquentielle, environnements de dépôts lacustres, principes de paléoclimatologie et données mises à jour sur l'évolution du climat à travers la période considérée). Les résultats ainsi traités et interprétés sont publiés ou en phase de révision ('*Under Review*') dans des revues internationales d'impact élevé (Palae-3 et Sedimentary Geology) et communiqués au sein de la communauté scientifique (e.g., PAGES, IAS) (Fig. II.6).

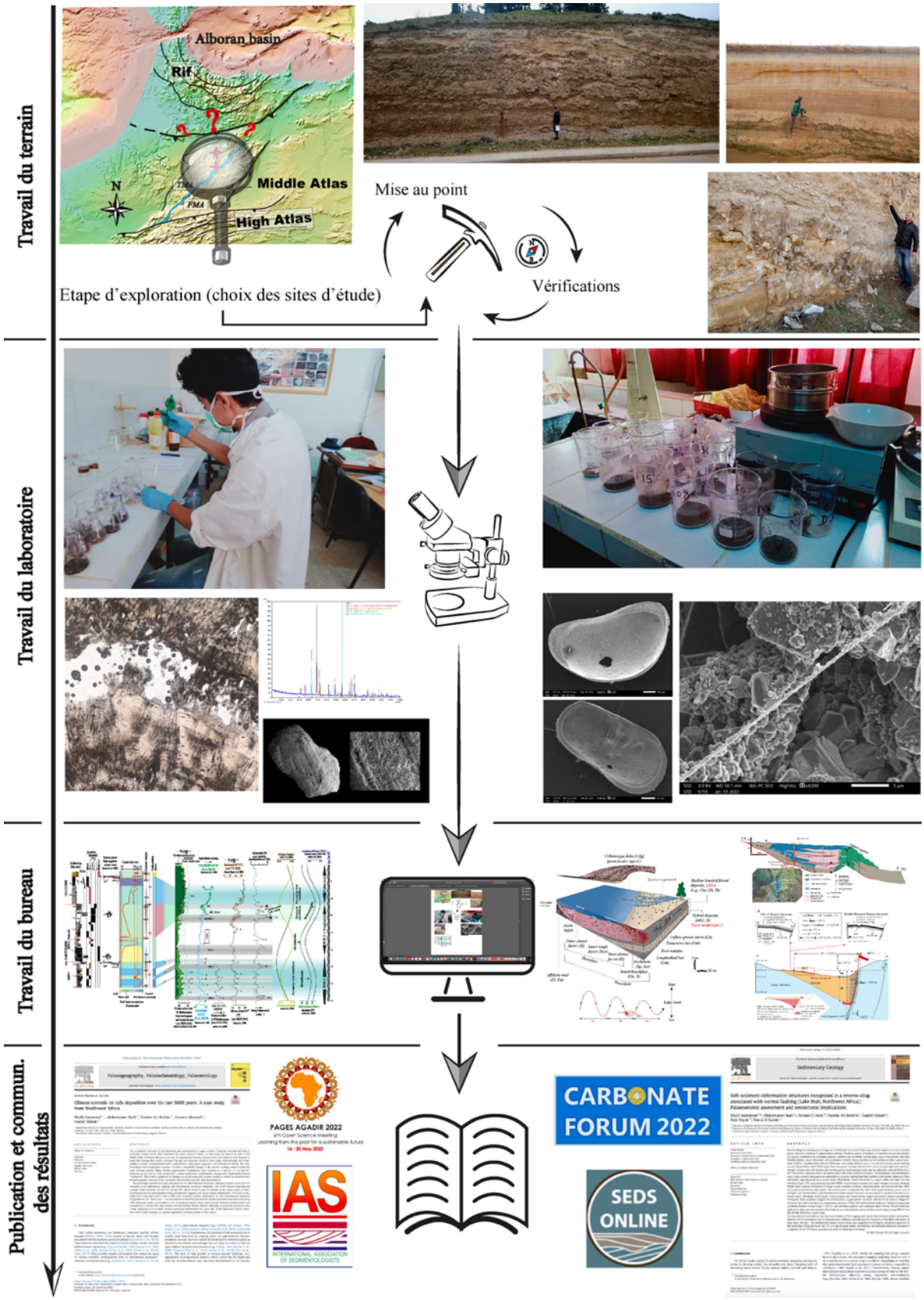


Figure II.6. *Schéma illustrant la méthodologie suivie depuis la génération des résultats (travail de terrain et au laboratoire) jusqu'à leurs publications et communications dans des rencontres internationales.*

2.1 Choix des sites

Sur la base de plusieurs expéditions dans le Moyen Atlas, avant et après l'ébauche de ce projet de doctorat, les sites d'Imouzzer Kandar et du lac Ifrah ont été délibérément jugés être les mieux convenables pour atteindre les objectifs cités d'emblée. Ainsi, les dépôts des tufs calcaires développés sous la ville d'Imouzzer Kandar donnent l'image du système à retenue extensive ('*extensive dammed area*') se développant derrière un large barrage-cascade (ressemblant à la variété B1, Fig. I.10). De plus, un affleurement disponible proche du centre de la ville révèle au premier regard quelques particularités faciologiques intrigantes (e.g., occurrence périodique d'un niveau riche en matière organique, faciès **C**) avec une préservation typique des dépôts (Chapitre 5). Parallèlement, le site du lac Ifrah exprime, au sens strict du terme, une situation à la fois structurale et sédimentologique extrêmement typique. En effet, la géométrie du lac et de son bassin (elliptique et en forme de parallélogramme, respectivement) ainsi qu'au contexte tectonique à l'échelle de la région, suscitent la curiosité de l'analyseur des bassins. En outre, la géométrie asymétrique du profil topographique d'un tracé traversant le lac perpendiculairement à son grand axe (marges à différents gradients topographique) exprime la géométrie d'un hémi-graben potentiellement évoquant le contrôle d'une faille maîtresse ('*master fault*') sur l'espace d'accommodation et sur la sédimentation elle-même au niveau de la dépression où existe le lac Ifrah. Cette géométrie asymétrique conditionnant une marge lacustre avec faible gradient topographique permettrait aux sédiments déposés sur cette marge de garder les traces de variations du niveau du lac à une échelle temporelle probablement orbitale, et donc peut conduire à élucider les interactions potentielles entre les différents facteurs de contrôle (surtout climatiques et tectoniques).

2.2 Collecte d'informations

Les sites ainsi choisis ont été sujets à une analyse sédimentologique et stratigraphique (séquentielle) approfondie. L'approche est conventionnelle et basée sur des publications clés et recommandations publiées dans des revues d'impact très élevé en domaine de géosciences (e.g., Earth Science Reviews) et largement accepté par la communauté scientifique. Ainsi, l'analyse des faciès sédimentologiques et de leurs déformations syn-dépôts suit les publications clés de, entre autre, Dunham (1962), Clifton et al. (1971), Middleton and Hampton (1973), Miall (1977), Allen (1982), Owen (1987), Platt and Wright (1991), Horton and Schmitt (1996), Freytet and Verrecchia (2002), Alonso-Zarza (2003), et finalement Arenas-Abad et al. (2010) au sujet des tufs calcaires. Des exemples de base imitant cette approche conventionnelle, d'où le présent travail s'est largement inspiré, sont livrés par Alexis Nutz (et co-auteurs) dans plusieurs travaux récemment publiés (e.g., Nutz et al.,

2015b, 2017, 2019, 2020). De même, l'analyse stratigraphique séquentielle adoptée dans ce projet de thèse suit les travaux et recommandations extensivement acceptés par la communauté scientifique (Carroll and Bohacs, 1999; Bohacs et al., 2000, 2007; Keighley et al., 2003; Catuneanu, 2006, 2019; Hanneman and Wideman, 2010; Catuneanu et al., 2011).

2.3 Cadre chronologique et datations

La discussion des empreintes climatiques à partir d'une série sédimentaire et leur calage dans la chronologie calendaire exigent un contrôle d'âge par des datations absolues de plusieurs niveaux. Dans ce sens, quatre datations par radiocarbone ont été menées au laboratoire de Vilnius Radiocarbone en Lituanie sur les dépôts de tufs calcaires les plus récents (dernière génération) du site d'Imouzzer Kandar. Les échantillons ont été prélevés intacts à la main dans quatre niveaux stratigraphiques riches en fragments de macro-charbons. Ces derniers ont été soigneusement sélectionnées pour accomplir un minimum de 10 mg, en ne prenant que ceux ne présentant pas de traces taphonomiques significatives pour s'assurer que les résultats reflètent au plus près l'âge du dépôt du niveau lithologique. Au laboratoire de datation (Vilnius Radiocarbon), après graphitisation à l'aide d'un équipement de graphitisation automatisé AGE-3 (IonPlus AG), les échantillons ont été analysés par un accélérateur de spectrométrie de masse ('AMS' en anglais) à étage unique (SSAMS, NEC, USA).

Les datations ^{14}C obtenues sont calibrées à l'aide du programme OxCal v.4.4 (Ramsey et Lee, 2013) en utilisant la courbe d'étalonnage IntCal20 (Reimer et al., 2020) avec un intervalle de confiance correspondant à 2σ (95.4% de probabilité). Le modèle âge/profondeur a été construit sur la base d'une simulation de Monte Carlo en utilisant le programme StalAge (Scholz and Hoffmann, 2011). Néanmoins le modèle d'âge n'a pas été pris en considération pour des raisons citées plus loin (*voir* chapitre 5).

Dans le même site, les générations plus anciennes ont aussi reçu un grand intérêt de notre part. Ainsi, outre le travail extensif de terrain et de laboratoire (préparation de plusieurs lames minces de roches), cinq datations par la technique U/Th ont été menées sur des stromatolithes et des oncolithes à l'université de Minnesota (États-Unis). Cette technique est récemment améliorée par Cheng et al. (2013) pour aboutir à des datations des matériaux carbonatés (notamment les carbonates des spéléothèmes) tellement précises que l'erreur est inférieure à 1 ‰. Les résultats ont permis de contraindre, *a priori*, le cadre chronologique des différentes générations des tufs calcaires à l'échelle des affleurements levés (depuis 500 ka BP). Néanmoins, ces résultats, couplés à ceux des observations sédimentologiques et pétrographiques, n'ont pas été communiqués dans le cadre de cette thèse en guise de les finaliser avec d'autres résultats d'analyses plus approfondies (isotopes et éléments traces) ainsi

que de mener plus de datations pour augmenter davantage la résolution temporelle. Cela ne peut avoir le jour (i) sans l'aide d'une collaboration extensive avec des experts en géochimie et en paléoclimatologie et (ii) sans le mettre dans le cadre d'un projet financé par un organisme international, qui, évidemment, demandent du temps et d'une expertise plus approfondie.

Quant au site d'Ifrah, le cadre chronologique de la série sédimentaire étudiée a pu être construit en faisant la corrélation de l'affleurement considéré (rivage SW) avec une carotte sédimentaire datée et étudiée par Cheddadi et al. (2009) et Rhoujjati et al. (2010), extraite d'une localisation distante d'un km (rivage NW). La corrélation est faite en prenant en considération l'influence fluviatile dans chaque localisation, l'occurrence des niveaux carbonatés/marneux, la variation de la granulométrie en fonction de la profondeur (*voir* chapitres 3 et 4). La confiance en cette corrélation est justifiée de par la proximité des deux localisations ainsi que la taille du bassin lacustre qui suggère une réponse plutôt généralisée sur l'ensemble du bassin lacustre par rapport à un agent de contrôle extérieur (un forçage climatique par exemple conduisant à l'occurrence des niveaux carbonatés/marneux).

2.4 Analyses chimiques au laboratoire : *proxies* géochimiques et biologiques

Les échantillons prélevés, emballés et référencés des deux sites ont subi un traitement chimique par des acides pour (i) leur préparation à l'étude taxonomique des ostracodes et comptage et détermination morphotypique des fragments de macro-charbon, (ii) le prétraitement pour analyse spectroscopique, ainsi que (iii) le dosage de la matière organique et des carbonates de calcium.

2.4.1 Préparation pour étude taxonomique et morphotypique des ostracodes et macro-charbon

Une quantité de 10 g de chaque échantillon est traitée avec 3% H_2O_2 pendant une semaine puis tamisée à l'aide des tamis de mailles de 100 µm. Le refus est analysé sous la loupe binoculaire pour le comptage des ostracodes et macro-charbon. La détermination morphotypique des particules de macro-charbon est faite selon les classifications élaborées par Enache et Cumming (2006, 2007) et Mustaphi et Pisaric (2014). Les valves d'ostracodes extraites de chaque échantillon ont été soumises à une étude taxonomique par Pr. Fransesc Mezquita-Joanes (Université de Valencia, Espagne).

2.4.2 Prétraitement pour analyse spectroscopique : ICP-OES

Avant d'être analysés par spectroscopie de plasma à couplage inductif ('ICP-OES') avec le système MORIBA Jobin Yvon – ACTIVA à la Citée de l'Innovation Fès (Fig. II.7D), les échantillons ont subi un prétraitement par des acides au laboratoire du département de Géologie de la Faculté des

Sciences Dhar Mahraz. La technique consiste en une attaque de chaque échantillon broyé de 1 g par 3 ml d'acide chlorhydrique (HCl, 12.1 *M*), 1 ml d'acide nitrique (HNO_3, 16 *M*) et 2 ml de l'eau oxygénée (H_2O_2, 9.97 *M*) (Fig. II.7A). A chaque attaque, l'échantillon est gardé 15 min après avoir atteint le point de l'ébullition (jusqu'à 120°C) dans d'un bain de sables (Fig. II.7B). Après refroidissement, le contenu minéral est filtré et ajusté à 50 ml avec de l'eau distillée et conditionné dans des flacons (Fig. II.7C) pour être introduit dans l'appareillage de spectroscopie (Fig. II.7D). Les éléments chimiques choisis à être dosés par la spectroscopie sont Al, K, Fe et Mn. Les résultats sont exprimés soit sous forme de rapports sans unité (K/Al, Fe/Mn) soit sous forme élémentaire en mg/g (i.e., ppm). Ils sont utilisés comme des marqueurs des conditions paléoenvironnementales, e.g., érosion, intensité du drainage, altération chimique, condition d'oxydo-réduction (*voir* Davies et al., 2015).

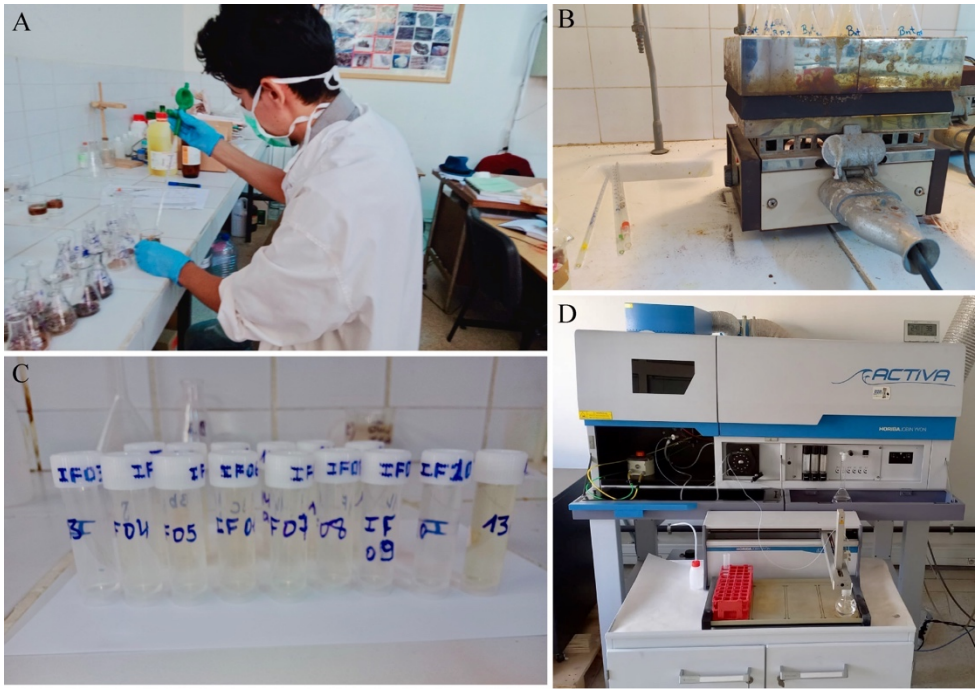


Figure II.7*. Photos montrant les différentes étapes de la préparation des échantillons pour l'analyse spectroscopique.* ***A****. Étape de l'attaque par acides.* ***B****. Bain de sable pour le chauffage et stimulation de l'attaque par acides.* ***C****. Échantillons préparés pour l'analyse spectroscopique.* ***D****. Appareillage utilisé pour le dosage spectroscopique des éléments chimiques.*

2.4.3 Dosage de la matière organique et des carbonates de calcium

La quantification du carbone organique est basée sur la méthode d'oxydation humide à l'acide chromique de Walkley et Black (1934) (*voir* Allison, 1965, et FAO, 2020). Avant chaque titrage de 1 g d'échantillon, la suspension est filtrée pour permettre de discerner plus précisément le point de virage. Pour la détermination de la teneur en carbonate de calcium, 1 g de chaque échantillon est placé dans un flacon attaché à l'appareil classique de Bernard (*voir* Dreimanis, 1962). La concentration de $CaCO_3$ est déterminée indirectement, avec une précision de ±0,1, à partir du volume de gaz CO_2 dégazé, corrigé aux conditions de pression et de température standard, et des masses moléculaires de

$CaCO_3$ et de CO_2 (Dreimanis, 1962). La manipulation est répétée trois fois pour aboutir à plus de précision.

De par son efficacité dans le décryptage de la dynamique de la végétation passée et, conséquemment, les changements bioclimatiques, l'inclusion de l'analyse palynologique a été envisagée. En effet, dans le cadre d'un stage se tenant début 2020, j'ai commencé une analyse palynologique sur les échantillons des tufs calcaires du site d'Imouzzer Kandar au département de Géologie de la Faculté des Sciences Ben M'Sik (Casablanca), sous la direction du **Pr. Bachiri Naima** et par l'assistance de **Targhi Soukaina**. Malheureusement, en raison de la pandémie et de la fermeture durable des universités, le stage n'a pas atteint la fin escomptée et a finalement été annulé.

Les trois chapitres qui suivent constituent le cœur du travail fait pour ce projet de doctorat dont chacun correspond à un article, soit déjà publié (chapitres 3 et 5) soit progressant dans la révision par les paires (chapitre 4). L'exemple du lac Ifrah est communiqué dans les chapitres 3 et 4, alors que celui d'Imouzzer Kandar est présenté dans le chapitre 5. Chaque chapitre constitue un aboutissement par rapport à la cause fixée, à savoir : déchiffrage des facteurs de contrôle de la nature et de l'organisation des sédiments.

Dès lors, une enquête géologique structurale menée à la fois sur les sédiments lacustres mous ('*soft-sediment*') qui enregistrent l'intervalle du temps considéré (MIS-3-Holocène) et le substrat rocheux (liasique) fait objet du chapitre 3. Les relations entre (i) la tectonique à l'échelle régionale et locale, (ii) la paléo-séismicité et les déformations 'ductiles' synsédimentaires ainsi que (iii) les pulsations tectoniques à l'échelle du bassin et les déformations cassantes synsédimentaires y sont élucidés. Le signal tectonique et son contrôle sur la sédimentation y est présenté. Le contrôle géologique structural (un système structural identique à celui d'un hémi-graben en présence d'une faille maîtresse) sur la géométrie du bassin et sa typologie hydro-stratigraphique (*sensu* Bohacs et al., 2000) y est également envisagé. De plus, des implications néotectoniques à l'échelle régionale et une hypothèse proposant un modèle expliquant l'ouverture du bassin sont également présentées.

Le chapitre 4 représente une extension du chapitre 3 où une approche sédimentologique et stratigraphique séquentielle détaillée est adoptée. Cinq systèmes de dépôts et modèles de faciès ont été reconstitués sur la base de l'étude sédimentologique, alors que trois cycles du niveau lacustre à l'échelle orbitale ont été inférés selon les dires de l'approche stratigraphique séquentielle conventionnelle. L'usage de cette dernière a démontré son utilité dans le déchiffrage de la cyclicité de l'accommodation/sédimentation et son ajustement par rapport aux paramètres modulant l'insolation (*viz.*, précession et obliquité). Le forçage suborbital est également montré. De plus, le recours aux proxies géochimiques (*viz.*, K/Al, Fe/Mn) et à la micropaléontologie (étude taxonomique des ostracodes) s'est avéré très prometteur dans le traçage des surfaces de nature cryptique ayant une signification déterminante en stratigraphie séquentielle (e.g., surface d'inondation maximale, '*maximum flooding surface*').

Dans le chapitre 5 est présenté un exemple d'un système fluviolacustre carbonaté (tufs calcaires, travertins météogènes) avec une géomorphologie emblématique (imitant la variété B1, Fig. I.10) conduisant à une préservation typique des dépôts ainsi qu'aux signaux des forçages externes, surtout ceux du climat, durant les dernières 5000 années. Afin d'aboutir justement dans l'extraction des signatures climatiques, une étude sédimentologique détaillée (suit la logique présentée dans le chapitre de l'introduction) et stratigraphique séquentielle, combinée à une étude multi-proxy sur la

base d'indicateurs paléoenvironnementaux biologiques (matière organique, ostracodes et macro-charbon) et géochimiques/minéralogiques (K, K/Al, DRX). Les résultats soulignent l'exclusive intervention du forçage climatique dans la modulation de l'espace potentiel d'accommodation dans la retenue, faisant ainsi exception à la règle de l'art ; l'espace potentiel (ou maximum) de l'accommodation dans les bassins sédimentaires est généralement contrôlé par la tectonique (Bohacs et al., 2000). Ainsi, décharge hydrique annuelle et température et précipitations estivales, tous auraient contribué à moduler le taux d'accrétion au niveau du barrage ainsi que l'accommodation au niveau de la retenue, chose qui s'est clairement imprimée dans les cortèges sédimentaires selon les dires de l'analyse séquentielle. Fait intéressant à noter, une périodique occurrence d'un niveau lithologique organique enregistre, pour la première fois à l'échelle de la science dédiée aux tufs calcaires, l'empreinte de deux événements de refroidissement centennal connus sous le vocable de '*Ice Rafting Events*' ou '*Bond Events*' (événement de 4.6 ka et de 2.7 ka). La fréquence d'occurrence de ces niveaux lithologiques devient relativement plus élevée durant les derniers deux millénaires, probablement enregistrant l'empreinte solaire à l'instar des données isotopiques des spéléothèmes étudiés proche du site d'Imouzzer.

CHAPITRE IIII

SOFT-SEDIMENT DEFORMATION STRUCTURES RECOGNISED IN A REVERSE-DRAG ASSOCIATED WITH NORMAL FAULTING (LAKE IFRAH, NORTHWEST AFRICA): PALAEOSEISMIC ASSESSMENT AND NEOTECTONIC IMPLICATIONS

Soft-sediment deformation structures recognised in a reverse-drag associated with normal faulting (Lake Ifrah, Northwest Africa): Palaeoseismic assessment and neotectonic implications

Khalil Azennoud[a,*], Abdennasser Baali[a], Hicham El Asmi[b], Yassine Ait Brahim[c], Oualid Hakam[a], Aziz Hayati[b], Touria El Kamel[a]

[a] Laboratory of Engineering, Electrochemistry, Modelling and Environment, Faculty of Sciences Dhar EL Mahraz, Sidi Mohamed Ben Abdellah University, P.O. Box 1796, Atlas, Fez 30000, Morocco

[b] Laboratory of Geosciences, Environment and Associated Resources, Faculty of Sciences Dhar EL Mahraz, Sidi Mohamed Ben Abdellah University, P.O. Box 1796, Atlas, Fez 30000, Morocco

[c] International Water Research Institute, University of Mohammed VI Polytechnic, Benguerir, Morocco

Published in: Sedimentary Geology 106264 (2022b)

Abstract

Reverse-drags in extensional settings are emblematic structures that may provide imprints of (neo)tectonic pulses, and even evidence of palaeoseismic activity. The direct pieces of evidence of (neo)tectonic activity therein are mostly reported to be *subsidiary grabens*, *synthetic* and *antithetic normal faults*, and/or *bed-parallel slip* that brittlely deform newly deposited soft-sediments, therefor being classified as soft-sediment deformation structures (SSDSs). Liquidization-induced SSDSs are, reasonably, likely to occur in such tectonically active settings as well. Nonetheless, both SSDSs types have not gained enough interest from structural geologist and sedimentologist communities. We hereby address this gap by investigating brittle and liquidization-induced SSDSs from late Pleistocene-Holocene fluvio-lacustrine beds (Lake Ifrah, northern Morocco). Sedimentation and deformation occur upon a *reverse-drag* anticline connected to a master normal fault that borders a half-graben structure (Ifrah sub-basin) superimposed on a master basin (Ifrah Basin), itself connected to a major strike-slip fault (the Tizi n'Tretten Fault, TTF). Liquidization-induced SSDSs involve *load structures* and *water-escape structures*, whereas brittle deformations encompass *shrinkage cracks, subsidiary grabens*, *neptunian dykes*, and *bed-parallel slip* (BPS) and associated *domino-style faults*. The deformation mechanism for both SSDS types involves either loss of strength upon liquidization (*load structures*

and *water-escape structures*) or an increase in applied (internal or external) shear (*shrinkage cracks, faults*). Facies analysis and conventional trigger assessment allowed deciphering endogenic from exogenic triggers for deformation. Liquidization has been inferred to be seismic-triggered whereby the deformed beds are considered seismites. While BPS deformed brittlely late Pleistocene deposits (probably Marine Isotope Stage 3, MIS-3) and *subsidiary grabens* and *neptunian dykes* involve Middle Holocene sediments, they are considered to be linked to two flexural-slip events of the *reverse-drag* during MIS-3? and the Middle Holocene, respectively.

Scaling relationships between the structural entities of the *hanging-wall-master fault-footwall* system allowed estimation of the subsidence due to hanging-wall collapses, and thereby the initiation of the Ifrah sub-basin (at least since 260 kyr). The rhomboidal-shaped master basin was suggested to belong to a dilational quadrant of the associated strike-slip fault, the TTF, at a tip-damage region. Accordingly, we highlight structural isolation of a segment of the TTF that is synchronous with the Ifrah Basin initiation.

Keywords: soft-sediment deformation structures, *reverse-drag*, seismites, normal faulting, dilational quadrant, Northwest Africa.

1 Introduction

In interior basins subject to active tectonics, lacustrine settings are prone to develop within the downthrown block (hanging-wall) of bounding-basin normal faults (master faults) (Carroll and Bohacs, 1999; Keighley et al., 2003). Whilst the ongoing slip along a master fault is maintained, the associated hanging-wall may bend to form a structure known as a *reverse-drag* or a *rollover*, depending on whether the associated master fault geometry is planar or listric, respectively (Schlische, 1995; Spahić et al., 2011). Furthermore, flexural pulses thereof have widely been reported to spawn plenty of evidence for brittle deformation affecting newly deposited soft-sediments (e.g., Hamblin, 1965; White et al., 1986; McClay, 1990), hence classified as soft-sediment deformation structures (SSDSs) (*sensu* Allen, 1982 and Van Loon, 2009). These may concern *synthetic/antithetic faults*, *subsidiary grabens* (Hamblin, 1965; Barnett et al., 1987) or, more interestingly, *bed-parallel slips* (Watterson et al., 1998; Delogkos et al., 2018). To our knowledge, 'ductile' deformation (*sensu* Owen, 1987, p. 20) however has not explicitly been studied in the frame of the classical SSDSs analysis within such structural settings that ostensibly demonstrate a component of synsedimentary tectonic control, and hence very likely to hold imprints of palaeoseismic activity. We hereby focus on this gap in order to draw emphasis on how far from the SSDSs analysis (both 'ductile' and brittle) we can assess the

palaeoseismicity, and address the neotectonic implication(s) thereof, in a region known to be tectonically active (Northwest Africa).

Indeed, the application of SSDSs has greatly improved comprehension of the past allocyclic (e.g., palaeoseismicity) and autocyclic (e.g., flooding, or storm recurrence) processes (Montenat et al., 2007; Obermeier, 2009; Moretti et al., 2016) relative to different depositional environments on Earth, such as: fluvial (Rana et al., 2016; Rossetti et al., 2017), aeolian (Moretti, 2000; Bryant et al., 2013, 2016), palustrine (Ezquerro et al., 2015), lacustrine (e.g., Törő and Pratt, 2016; Alsop et al., 2016), marine (e.g., Moretti et al., 2011; Basilone et al., 2016) environments, and even on planet Mars (Wheatley et al., 2019; Chan et al., 2019). Their occurrence requires (i) loss of strength (liquidization, *sensu* Allen, 1977) of a cohesionless water-saturated host bed (i.e., deformation mechanism, Obermeier, 2009; Moretti and Ronchi, 2011) or increase of stress field outside or inside until overcoming the strength of a cohesive material (Collinson, 1994; Pratt and Ponce, 2019), (ii) existence of a driving force system (*sensu* Owen, 1987), and (iii) a trigger mechanism for loss of strength (Owen, 1987; Owen et al., 2011). This latter is indeed the centrepiece that appeals to the broader academic authorship, including the herein presented work, as to its implication in understanding short-lived (cyclic) processes related or not to the depositional environment. With respect to this latter point, many possible processes can trigger loss of strength (Van Loon, 2009) and be classified as endogenic (e.g., overloading, cyclic storms, tidal actions) or exogenic (impacts, earthquakes) (Owen et al., 2011; Moretti et al., 2014). However, deciphering the responsible trigger for liquidization from the final morphology is a difficult task and requires a comprehensive understanding of all aspects that might interfere before and during deformation to build the eventual morphology (e.g., environmental setting, host bed properties). SSDSs interpreted as earthquake-induced (i.e., seismites, *sensu* Seilacher, 1969) have received a central place in several reports by sedimentary and engineer geologists worldwide, as they provide promising clues in understanding palaeoseismic and tectonic history of the studied case (e.g., Sims, 1975; Allen, 1986; Rodríguez-Pascua et al., 2000; García-Tortosa et al., 2011; Basilone et al., 2016). In particular, lacustrine-dominated deposits are considered to be the most relevant archives that provide information on past earthquakes, since many endogenic triggers (e.g., tidal and storm actions) are unlikely to operate in such settings (Sims, 1975; Moretti and Sabato, 2007).

In this study, we conducted conventional sedimentary facies and SSDSs analyses on a typical case that involves a lacustrine basin (Ifrah Basin). The lacustrine sedimentation occurs upon a *reverse-drag* in conjunction with a basin-border normal fault within a tectonically active region nearing a slow

plate boundary (Middle Atlas, Morocco, Fig.1), where only two comparable studies have been carried out (Plaziat and Ahmamou, 1998; Benabbou et al., 2018). We described the morphology and interpreted the deformation mechanisms and driving force systems of the 'ductile' and brittle deformation structures with more emphasis pointed to regional palaeoseismicity and basin-scale tectonics (scaling relationships). The results reveal promising conclusions on how far the inclusion of SSDSs in such interior basin analysis studies is required to draw the tectonic and palaeoseismic history of the concerned region. Besides, as the Ifrah Basin is connected to a major strike-slip fault (the Tizi n'Tretten fault), the further focus was concisely placed on regional-scale tectonics and previous structural geologic studies (e.g., Kim and Sanderson, 2006) to propose a model for the basin initiation.

2 Geological and tectonic background

Lake Ifrah is a small (1 km^2) and shallow (around 2 m deep) lake located in the Middle Atlas tectonic province (33° 33' 32.42" N, 4° 55' 50.36" W; 1616 m asl), which is an intracontinental mountain belt where the main structures are striking NE-SW, inherited from a polyphase geodynamic evolution since the Variscan orogeny (Frizon de Lamotte et al., 2008, and references therein). Two main sub-structural domains are distinguished according to the deformation degree that accommodates each one (Martin, 1981; Arboleya et al., 2004) (Fig. 1): the north-western Tabular Middle Atlas (TMA), where Lake Ifrah is located, relatively weakly deformed by left-lateral strike-slip (including the Tizi n'Tretten Fault, the subject of this study) and normal faults, resulting in a broadly flat high plateau (average topography of 1300 m asl); and the south-western Folded Middle Atlas (FMA), separated from the TMA by the so-cold North Middle Atlas Fault (NMAF), where the large part of deformation was accommodated by thrust folds with a sinistral component, giving way to a pronounced succession of anticline ridges (exceeding 3000 m asl) and syncline depressions.

In fact, upon the break-up of Pangea, the present-day observed major structures, partly inherited from the Variscan orogeny, have served as loci to accommodate the Tethyan Atlas rifting during the Triassic period (Mattauer et al., 1977), creating space for significant synrift deposition of evaporites, volcano-detrital deposits, and tholeiitic basalts that unconformably overlie deformed Palaeozoic schists and sandstones (Ouarhache, 1987; Ouarhache et al., 2000, 2012; Laville et al., 2004). Upon the Tethyan Atlas rifting abortion, slow extension controlled by thermal subsidence has continued during the Early-Middle Liassic, giving way to post-rift platform carbonates (Charrière, 1990; Ouarhache et al., 2012) mapped to dominate in thickness and surface outcrops, especially in the TMA (Fig. 1; Martin, 1981). Thanks to the NMAF with south-eastward vergence, maximum active subsidence has

been accommodated in the FMA during the Middle Jurassic (Middle Bajocian to late Bathonian), resulting in the isolation of the FMA from the emerged TMA and the deposition of first marine then continental (red beds) sediments partly filling the depocentres (Charrière et al., 1994; Frizon de Lamotte et al., 2008). These latter have been individualised in such extensional settings through block faulting and tilting with the development of half-grabens bounded by ridges in hanging-walls of major normal faults (Frizon de Lamotte et al., 2008), akin to the rigid domino model (e.g., Nur et al., 1986; Vendeville et al., 1987). Since the Africa-Eurasia plate convergence began at late Cretaceous (Rosenbaum et al., 2002; Fernàndez et al., 2019), a compressional regime with two climaxes reached during the mid-Eocene and Pliocene-Quaternary (Frizon de Lamotte et al., 2000) has led to an inversion of the border block faults and the associated depocentres into thrust anticlines with sinistral component and depression synclines in the FMA, respectively, and strike-slip faults with transtensional regime in the TMA, thus sculpting the main observed structure (e.g., Ait Brahim et al., 2002) (Fig. 1); this horizontal strain partitioning (*sensu* Gomez et al., 1998) finds its explanation in the fact that the TMA has been more stable than the FMA during the Mesozoic extension (Gomez et al., 1996, 1998). However, extensional tectonics in the Middle Atlas resumed during the Middle Miocene, resulting in the neoformation of several flooded basins (Hinaje, 2004) and partly giving way for Neogene-Quaternary alkaline volcanism in the Middle Atlas to reach the surface (Fig. 1; El Azzouzi et al., 2010; Hinaje et al., 2019). Conflictingly, the relatively high elevation of the Middle Atlas is not compatible with the modest tectonic shortening (10% or lower, Gomez et al., 1998; Frizon de Lamotte et al., 2009). Mantle component of buoyancy was proposed (e.g., Teixell et al., 2005; Missenard et al., 2006; Fig. 1) and confirmed based on seismic tomography (e.g., Bezada et al., 2014; Palomeras et al., 2014; Miller et al., 2015) to account for the high Middle Atlas elevation and to explain the occurrence of Neogene-Quaternary volcanism (e.g., Bosch et al., 2014) (Fig. 1; this is further considered in the discussion section and supplement material). Historical and instrumental data indicate active seismicity where most of the seismic foci are concentrated in the Rif belt (northernmost Morocco) and at the transition between the Rif and the Middle Atlas (Medina and Cherkaoui, 1991; Peláez et al., 2007; Mourabit et al., 2014; Poujol et al., 2014, 2017) (Fig. 1).

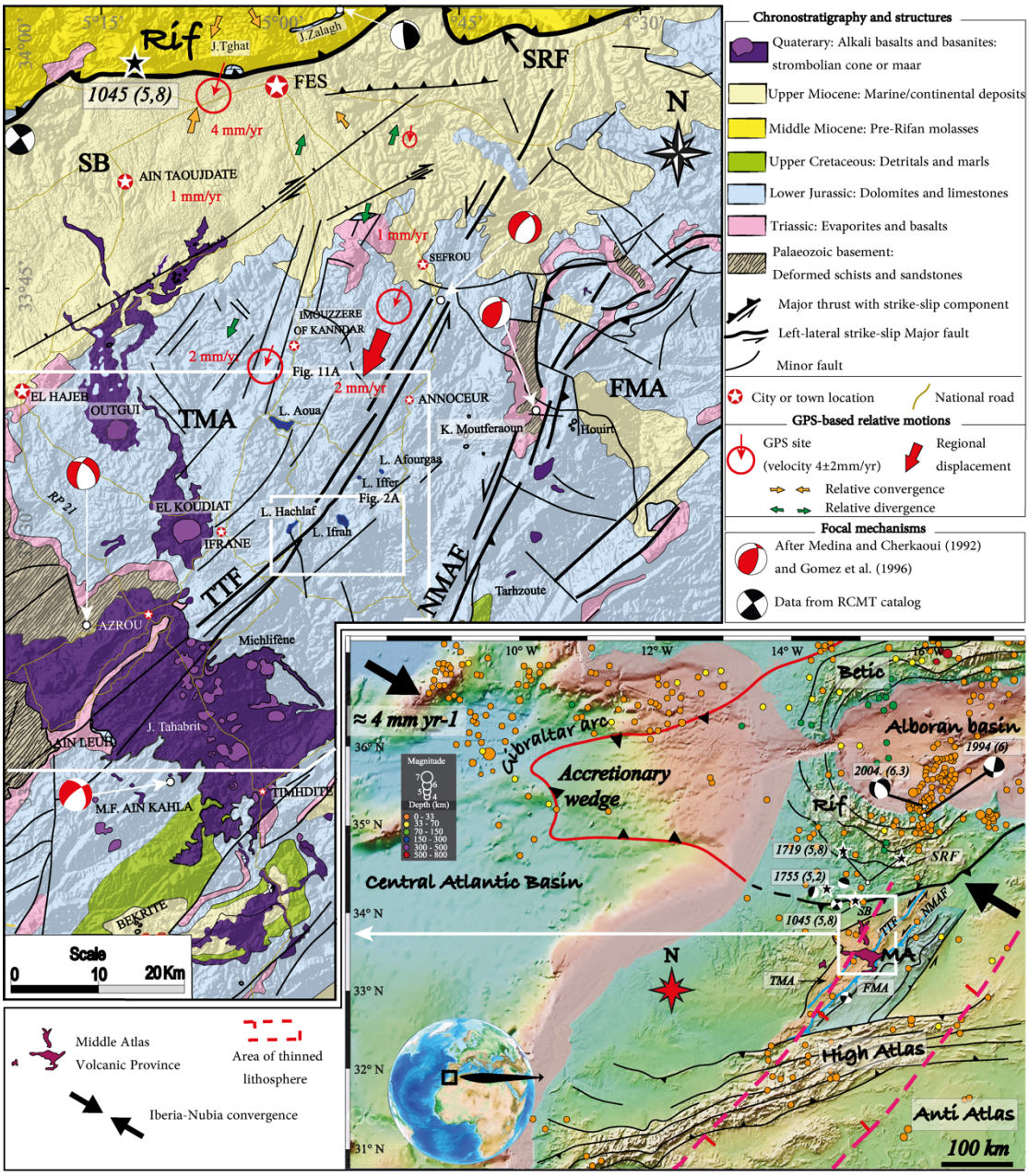


Figure 1. *Structural framework of Northwest Africa and Gibraltar arc, a regional geological map of the western central Middle Atlas, and the location of the Ifrah Basin. Seismicity is from the National Earthquake Information Centre catalogue of crustal earthquakes with magnitudes above 4 (1976–2022; https://earthquake.usgs.gov/earthquakes/search/). Seismotectonic map with major faults drawn on SRTM30 PLUS DEM. Focal mechanisms are from the RCMT catalogue (http://www.bo.ingv.it/RCMT/searchRCMT.html) and Medina and Cherkaoui (1992) and Gomez et al. (1996). GPS-based motions are from Chalouan et al. (2014). Stars represent historical principal earthquakes since 1045 CE in the Rif-Middle Atlas transition (SRF). Lithospheric thinning and Quaternary intra-plate mafic volcanism are shown. MA: Middle Atlas; TMA: Tabular Middle Atlas; FMA: Folded Middle Atlas; SRF: Southern Rif Front; TTF: Tizi n'Tretten Fault; NMAF: North Middle Atlas Fault; SB: Saiss Basin.*

In particular, the Ifrah Basin, located in the north-eastern half of the TMA (Fig. 1), demonstrates a rhomboidal shape with a surface area exceeding 20 km^2 and the main axis trending SW-NE (Fig. 2A). It is bordered by master normal and strike-slip faults. In fact, to its NW side, the basin is connected to the Tizi n'Tretten (hereafter referred to as TTF, Fig. 2A), which is considered to

be the most important structure crosscutting lengthwise the entire TMA. Its NE and SW sides are bordered by normal faults striking SE-NW (Fig. 2A). Interestingly, the lake water body with an elliptical shape is restricted to the NE side of the basin (Fig. 2A, B). This shape and position are controlled by one of the NE border basin faults, which receives the most interest in this study (hereafter referred to as the master fault, Fig. 2B).

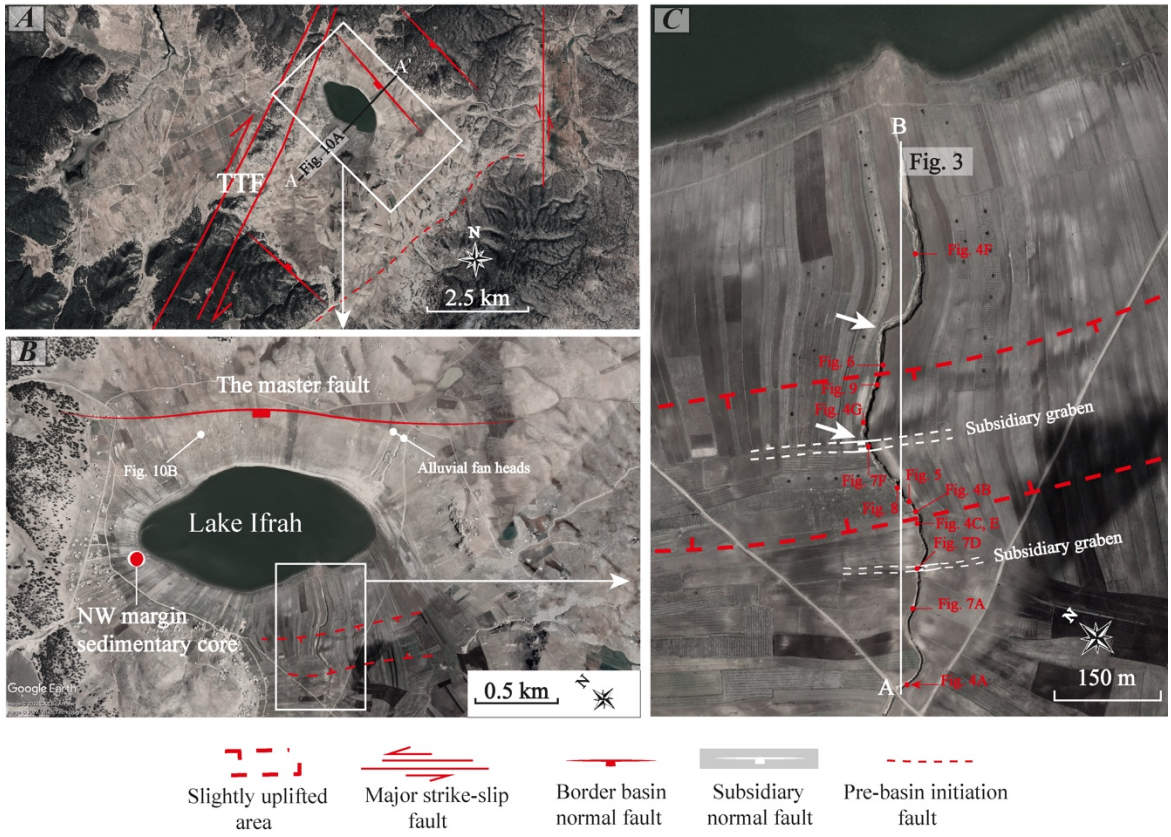


***Figure 2**. Structural framework of the Ifrah Basin and location of the studied outcrop. **A**: The main structures that enclose the Ifrah Basin, including the NE border basin fault (the master fault, **B**). Note the elliptical shape of the water body and its restriction on the NE side of the basin. **B**: The master fault is delineated thanks to direct and indirect evidence (e.g., alluvial fan head, damage zone,* see ***Fig. 10B**). Note the locations of the NW margin sedimentary core (after Rhoujjati et al., 2010) and the SW margin studied outcrop (**C**). **C**: Locations of figures and the cross section shown in **Figure 3**, and delineation of the* subsidiary grabens *discussed in the text. A slight uplift of the surface is to be noted. White arrows indicate drainage anomalies. The basin scale master structures are deliberately dealt with in the discussion section. TTF: Tizi n'Tretten Fault.*

3 Facies assessment

Observation and description of facies (and SSDSs) have been made possible along a gully generally striking SW-NE and exposing an average of 3 m in depth of sediments along a distance of ca. 1 km at the SW lake margin (Fig. 2C). Particularly, the gully direction and incision depth change in accordance to the present-day topography, that is, drainage anomalies with sub-orthogonal shapes and maximum incision depth occur where the topography reveals slight doming with reverse slope dip (i.e., landward) (Fig. 2C). Conventional facies analysis for the available outcrop has been performed

based on numerous key publications and summarised in table 1. Facies that appear to be genetically linked were combined into a facies association, or at the subunit level. Three allostratigraphic units have been raised (Fig. 3). They reflect a significant shift in sedimentation patterns and lake states that are separated by well-recognised, relatively long-term subareal unconformities. Facies and facies associations (subunits) are described and interpreted from the bottom (unit 1) to the top (unit 3) of the stratigraphic succession. The chronological framework of the described subunits was made based on their correlation with an available dated core retrieved from the NW margin (Rhoujjati et al., 2010; Fig. 2B). Accounting for the current lake size and the different degrees of fluvial influence on the two lake margins, the correlation has been based on granulometry variation, inferred depth, and the occurrence of carbonaceous beds (Fig. 3). More detailed descriptions and further interpretations are in chapter 4 (Azennoud et al., *Under Review*).

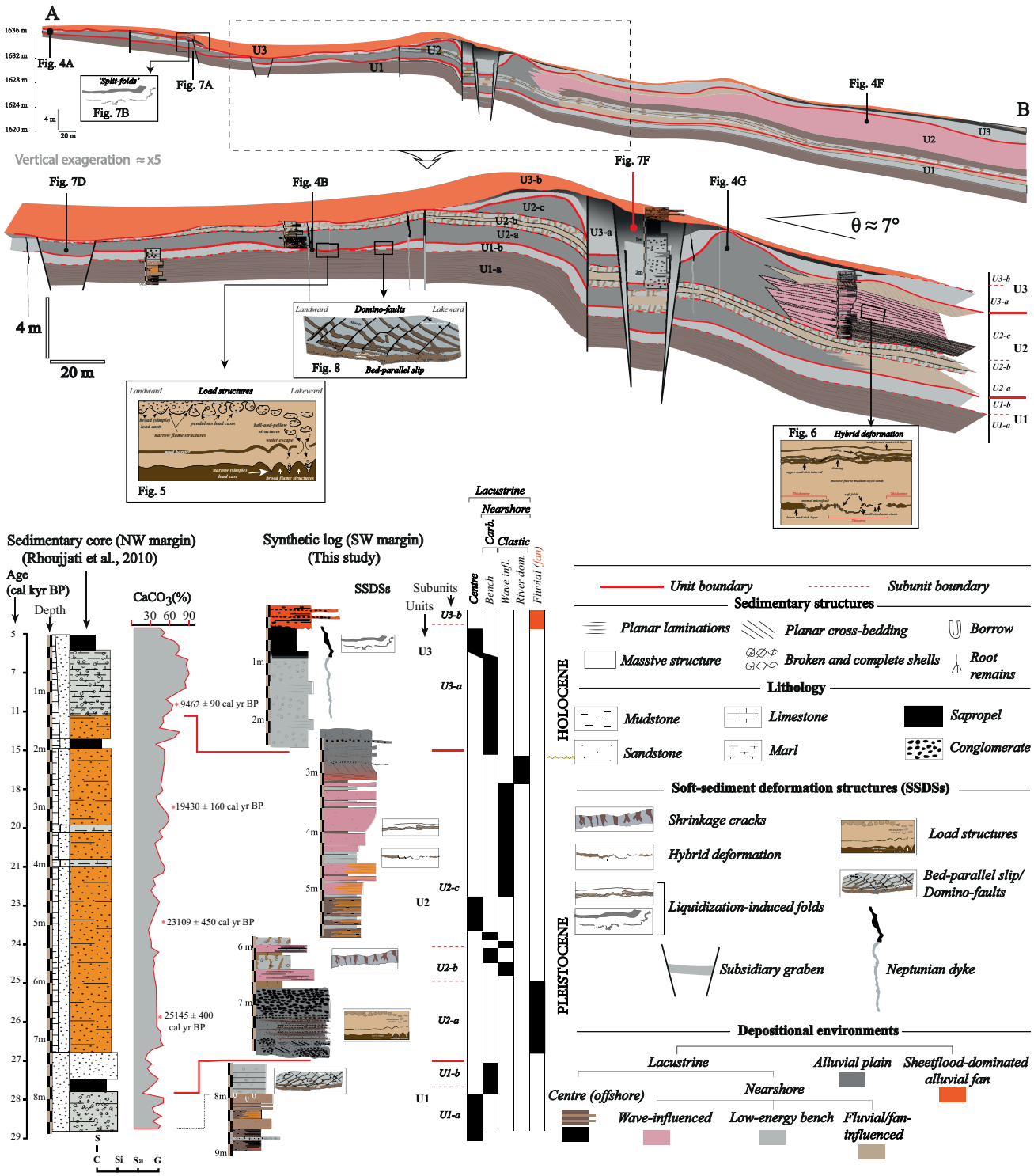


Figure 3. *Allostratigraphic cross-section of the SW margin studied outcrop and correlations with the NW margin sedimentary core (after Rhoujjati et al., 2010), locations in Figure 2. Note the reverse slope (i.e., landward dip) of the topographic surface. The subsidiary graben fault openings are exaggerated. Subunit codes and most figure locations are shown. The chronological framework of the deformation is illustrated. The Greek letter θ refers to the rotation angle (see discussion), accounting for the vertical exaggeration. Texture and lithology abbreviations: P: sapropel; C: clay; Si: silts; Sa: sand; G: gravel.*

3.1 Unit 1

The lowest unit (**U1**) is subdivided into a lower clastic-dominated subunit, **U1-a**, and an upper carbonate-dominated subunit, **U1-b**. **U1-a** is formed broadly by an alternating succession of cm-thick laminated mudstone and dm-thick beigy massive sandstone (Fig. 4B, D). Mm- to cm-scale laminations in the mudstone are recognisable by their variation in colour (blackish to brownish) and sand content. Sandstone lacks internal structures and, aligning with mudstone, shows no erosional features at its boundaries (Fig. 4D). On the other hand, **U1-b** consists of m-scale greyish bioclastic marl with a homogeneous internal structure (Fig. 4C, E; *see* also Fig. 8). Its upper boundary has been widely truncated, to the point of being completely eroded in some places.

Mudstone is formed throughout the suspension fall-out process of fines in subaqueous settings, away from the effect of storms and fair-weather waves (Nutz et al., 2015; Birgenheier et al., 2017). The settling process of fines is assumed to be associated with continuous deposition with periodic change (probably seasonal or decadal) in sediment supply (Pickering et al., 1986), although the contribution of occasional (low-density) turbidity currents is not completely excluded (Gierlowski-Kordesch, 2010). Aligning with this latter, the massive sandstone is more likely to reflect *en masse* deposition (Lowe, 1982) from subaqueous, non-cohesive (sandy), debris flow (Shanmugam, 1996; Talling et al., 2012) that might be generated by inertia-dominated underflows or hyperpycnal flows during dense fluvial floods (Mutti et al., 2003; Zavala et al., 2011). Accordingly, laminated mudstone and massive sandstone are interpreted to reflect a lacustrine offshore environment associated with active clastic supply (Potter et al., 1980; Peters and Loss, 2012; Nutz et al., 2020). **U1-b** reflects a moderate clastic component and active authigenic bio-controlled and bio-induced calcite precipitation, implying optimum conditions with active water drainage and warmer temperatures (Platt and Wright, 1991; Gierlowski-Kordesch, 2010). This would have resulted in a higher sedimentation rate in the lakeshore (the photic zone), promoting the development of a carbonate bench-like build-up in a low-energy setting (Platt and Wright, 1991). Referring to the dated core and the $CaCO_3$ curve from the same core (Rhoujjati et al., 2010; Fig. 3), **U1-b** would be deposited before ca. 28 cal yr. BP (perhaps during MIS-3).

***Table 1**. Synopsis of the facies descriptions and interpretations from the bottom (**U1-a**) to the top (**U3-b**) of the stratigraphic succession.*

Subunit code	Facies	Facies and bedding characters	Interpretation	Depositional environment
U1-a	Laminated mudstone	Tabular bodies; cm- to dm-scale thick, several metres in lateral extent; remarkable planar mm- to cm-thick laminations	Deposition from suspension-fallout in low-energy settings; occasional small turbidity currents (Nutz et al., 2015)	Lake offshore (centre associated with activ clastic supply (Potter et al., 1980)
	Massive sandstone	Tabular bodies; interbedded with laminated mudstone; non-erosive bases, poorly sorted and containing some outsized granules	en masse deposition by frictional freezing from plastic (laminar) flow (Lowe, 1982)	
U1-b	Bioclastic marl	Grey bed with variable thickness (dm- to m-thick); frequent fresh water shells; low to moderate clastic component; unconformable upper boundary	High biologic (authigenic) productivity with moderate clastic input in marginal setting (high sedimentation rate in the photic zone)	Low-energy bench margin (Platt and Wright, 1991)
U2-a	Sand-gravel alternation	Planar interbedded dm-thick laminated sandstone and one clast-thick horizontally bedded orthoconglomerate; lack of vegetation markers	Tractional deposition in upper flow regime (Allen, 1982); unconfined flow	Sheetflow and confin flow deposits in a bra plain in the vicinity o the lake shoreline
	Normally graded orthoconglomerate	Lenticular beds with erosional bases; dm- to m-thick and few meters in lateral extent; moderately sorted with a matrix-filled framework, sometimes with openwork texture; flattened clasts are well oriented [a(t), b(i)]; matrix consists of sands	Tractional and rapid grain-by-grain deposition from the turbulent fluidal (Newtonian) flow with high energy and high clast (bedload) supply; confined flow	
U2-b	Sand-marl alternation	Tabular interbedded dm-thick laminated sandstone and shrinkage cracked marl	Deposition from tractional flow associated with active clastic supply; moderate biological productivity associated with moderate clastic input	Shifts from clastic to carbonate-dominated lacustrine nearshore
		Interbedded planar bed of cm- to dm-thick horizontally-bedded gravels	Tractional and rapid grain-by-grain deposition from the turbulent fluidal	Subareal conditions; braided alluvial plain where broadly

	Sand-gravel-gravel alternation	and laminated sandstone, with lenticular bodies of dm- to m-thick channelized normally-graded orthoconglomerates; the presence of root remains	(Newtonian) flow with high energy and high clast supply	unconfined flow wou dominate (Nutz et al. 2020).
U2-c	Planar laminated sandstone	Tabular dm-thick beds; moderately sorted fine to coarse-grained sand; occasional fresh-water shells; moderate bioturbation (faint lamination)	Tractional deposition from strong shoreward wave surges (outer planar facies *sensu* Clifton et al., 1971)	Relatively high-energ lake shoreface environment (Clifton al., 1971; Nutz et al., 2020)
	Wave-ripple laminated sandstone		Tractional deposition from symmetrical orbital velocity (inner rough facies, *sensu* Clifton et al., 1971) in the upper part of the surf zone	
	Bioclastic marl	Same as U1-b, except that here this is erosive based	Same as U1-b	Same as U1-b
U3-a	Organic-rich mud (sapropel)	Dark-coloured bed with variable thickness (dm- to m-thick); considerable lateral extension; highly bioturbated; lack vegetation marker	High bio-productivity and preservation (non-oxygenating setting)	Lake centre (offshore
U3-b	Sand-gravel alternation	Planar interbedded dm-thick laminated sandstone and horizontally bedded orthoconglomerate; moderate bioturbation	Tractional deposition from diluted sheetflow/sheetflood in upper flow regime conditions	lower reaches of sheetflood-dominatec alluvial fan (Blair an McPherson, 2009)

3.2 Unit 2

Three separate subunits mark the middle allostratigraphic unit (**U2**), **U2-a**, **U2-b,** and **U2-c**. The lowest subunit, **U2-a**, is formed by a succession of planar cross-stratified pebbly sandstone, near-horizontal cm-thick beds of planar laminated sandstone, and horizontally-stratified gravels that are overlain by dm- to m-thick beds of normally graded orthoconglomerate (Fig. 4B). The flattened clasts composing the orthoconglomerate framework are well-oriented with clast fabric a(t)b(i) type, and the matrix consists mainly of sand. These deposits contain root remains but lack shell fragments. **U2-b** is composed of an alternating succession of clastic beds made by laminated sandstone and carbonate deposits consisting of shrinkage cracked marl (this is considered as a deformed bed and hence is taken separately in the next section) (Fig. 4B, E). **U2-c** exhibits a basinward shift in facies. Interbedded planar beds made by cm- to dm-thick horizontally-bedded gravel and laminated sandstone, with lenticular bodies of dm- to m-thick channelized normally-graded orthoconglomerate, were recognized proximally (Fig. 4G). More distally, a succession of tabular dm-thick beds consisting mainly of

moderately sorted fine to coarse-grained sandstone with occasional freshwater broken mollusc and bivalve shells was observed. Internal sedimentary structures involve both planar and wave-ripple laminations (Fig. 4F, H), although locally massive beds with poorly visible planar laminations associated or not with moderate bioturbation were also observed.

The alternating succession of laminated sandstone and stratified gravels overlain by normally-graded orthoconglomerate within the **U2-a** reflects more likely sheetflow and confined flow deposits in a braid-plain at the vicinity of the lake shoreline. The laminated sandstone and disturbed marl forming the **U2-b** are interpreted to reflect changes from clastic to carbonate-dominated nearshore**.** The lack of shell fragments and the presence of root remains in subunit **U2-c** suggest subareal conditions. In particular, this is likely to reflect a braided alluvial plain where broadly unconfined flow would dominate (Nutz et al., 2020). In turn, the presence of freshwater broken shells in the distal facies association of this subunit suggests a lacustrine wave-influenced nearshore environment (Nutz et al., 2020). Near horizontal planar laminations reflect tractional deposition from strong shoreward wave surges (asymmetric orbital velocity) in the lower part of the surf zone (Clifton et al., 1971). Wave-ripple laminations indicate tractional deposition from oscillatory current with symmetrical orbital velocity in the upper part of the surf zone (Clifton et al., 1971). Both facies reveal a relatively high-energy shoreface environment (Clifton et al., 1971; Clifton, 2006; Nutz et al., 2020). Considering the dated data from Rhoujjati et al. (2010), **U2** would be formed between ca. 27 and 12 cal yr. BP.

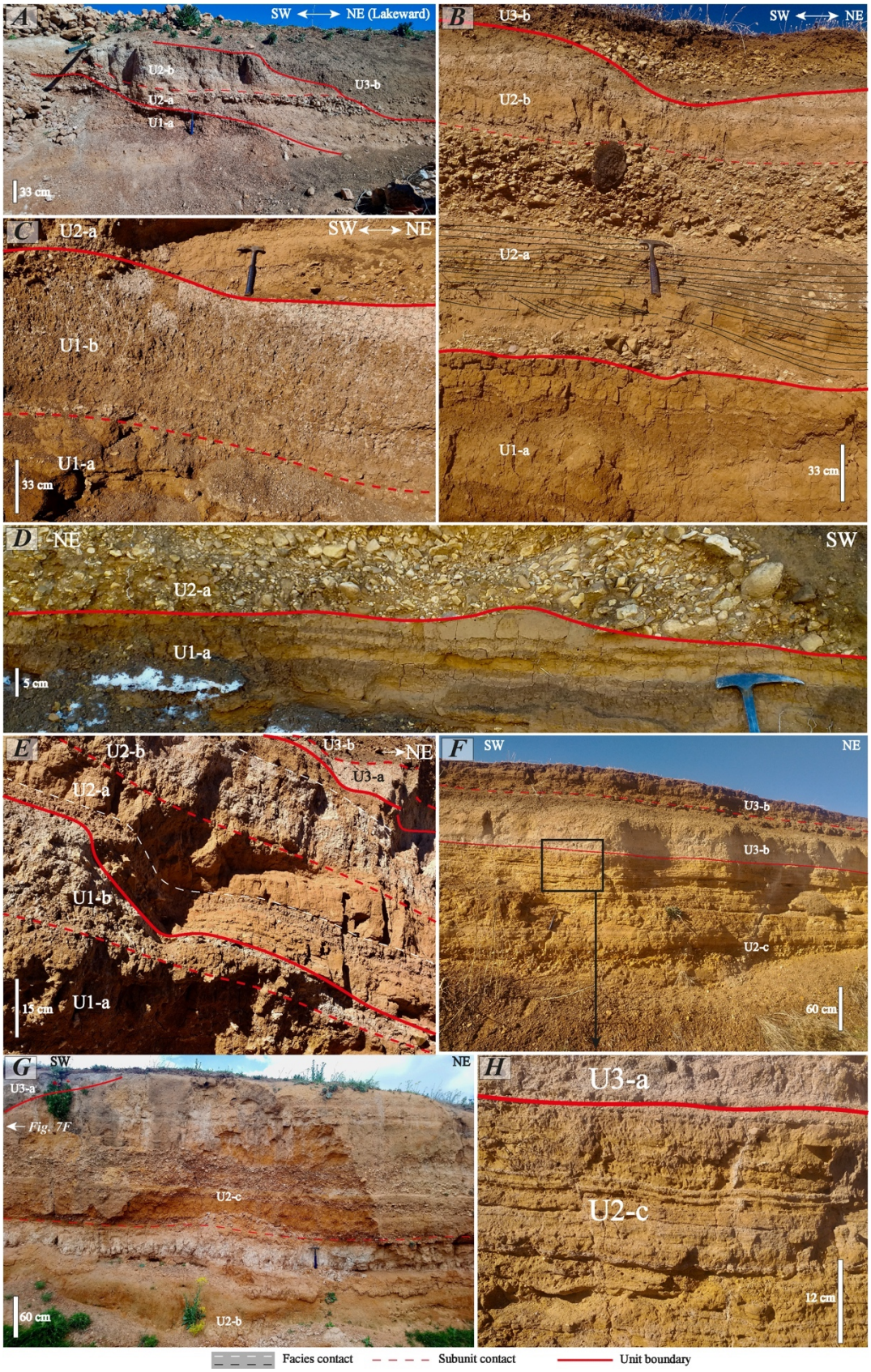


Figure 4. *Mesoscale field views of sedimentary facies and allostratigraphic units from the SW margin outcrop.* ***A-E****: Field views showing subunits* ***U1-a***, ***U1-b***, ***U2-a***, ***U2-b***, *and* ***U3-b*** *from the outcrop proximal stretch. The upper bounding surface of the lowest unit is erosive to varying degrees along dip.* ***F-H****: Field views from the distal stretch of the outcrop showing the lateral facies change of the subunit* ***U2-c*** *from fluvial-dominated (proximally,* ***G****) to wave-influenced nearshore (distally,* ***F*** *and* ***H****) (see locations in Fig. 2C)*

3.3 Unit 3

The upper unit (**U3**) is subdivided into a lower carbonate-organic subunit, **U3-a**, and an upper clastic-dominated subunit, **U3-b**. **U3-a** consists of m-scale, but variable in thickness, bed of bioclastic marl (resembling that of **U1-b**) overlain by sub-metric organic-rich and bioturbated bed lacking root remains or other vegetation-indicative markers (Fig. 7F). These deposits are seen and inferred to have considerable lateral extension relative to the basin. The subunit **U3-b** is made by a bioturbated alternation of tabular beds of cm-thick laminated sandstone and one clast-thick horizontal orthoconglomerate (Fig. 4A, B). This subunit overlaps the whole stratigraphic succession.

The lower marl bed is interpreted similarly to the one forming the subunit **U1-b** (i.e., low-energy bench-like margin according to Platt and Wright, 1991). The transition toward the organic-rich bed may indicate either a trend to lake shrinkage, the materialisation of which could be seen as an establishment of marshy conditions (*see* Platt and Wright, 1991), or rather an extensive lake state that would make this deposit interpreted as a sapropel facies, formed in profundal setting (lake centre). The former interpretation, however, is precluded by the relatively considerable bed extension and lack of root remains. In turn, **U3-b** is likely to reflect the distal reach of a sheetflood-dominated alluvial fan (Blair and McPherson, 2009), where the lack of erosional bases suggests laminar flow and deposition from traction in upper flow regime (Allen, 1982). Correlation with the dated data from Rhoujjati et al. (2010) suggests that the subunit **U3-a** would be deposited during the Early to Middle Holocene. While alluvial fan deposits have not been recognised in the NW margin, subunit **U3-b** is more likely to form later, perhaps during the Upper Holocene.

4 Sedimentary deformation structures

Along dip, sedimentary deformation structures of different types were recognised. While the present-day state of the sediments described above shows no-evidence of early to late lithification, all of the deformation preserved therein must involve unlithified sediments. Namely, these include deformation with ‘ductile’ (*sensu* Owen, 1987, p. 20) or brittle behaviour with the ‘ductile’ behaviour may encompass either hydroplastic (Lowe, 1975) or viscous behaviour depending on the cohesion state of the host material. As they involve loose lithologies, they are considered soft-sediment deformation structures (SSDSs) as per the pioneering generic definition (Allen, 1982; Owen, 1987; Van Loon, 2009) that does not regard whether the host sediment involves loss of strength or not (*cf.*, Maltman, 1984, and Shanmugam, 2017). Their deformation mechanisms, driving force systems, and trigger agents may differ depending on the mechanical, rheological, and lithological properties of the

host bed for each deformation structure. Description and interpretation of each SSDS are presented in the following subsections and summarised in table 2.

4.1 Load structures

Interestingly, cm- to dm-scale *load structures* were observed to involve three successive different lithologies (three members, *sensu* Anketell et al., 1970) with reverse densities, including offshore (mud and sand, "a" and "b" members) and fluvial ("c" member) deposits of the subunits **U1-a** and **U2-a**, respectively (Fig. 5). Particularly, lakeward increase in complexity from *simple* and *broad load casts*, *narrow flame structures*, and *pendulous load casts*, towards *ball-and-pillow structures* at the interface between fluvial and offshore deposits (sandy granules, "c" member, and fine to medium-grained sands, "b" member), was recognised (Fig. 5). Likewise, this basinward increase in deformation (*deformation series*, *sensu* Owen, 2003) has been observed at the interface between mud ("a" member) and sand ("b" member) with unusual *broad flame* and *narrow load casts* (cusps-like features). It is worth noting that the base of the "a" member is still planar (Fig. 5B). Within member 'b", cm-thick cohesive mud-rich layers are plastically deformed, giving way to particular *folds* and *cusps* (*see* next subsection), revealing water-escape processes and appears to be causally linked to downward movement of *pseudonodules* (sourced from "c") crossing the mud (barrier permeability) layers (Fig. 5B, C).

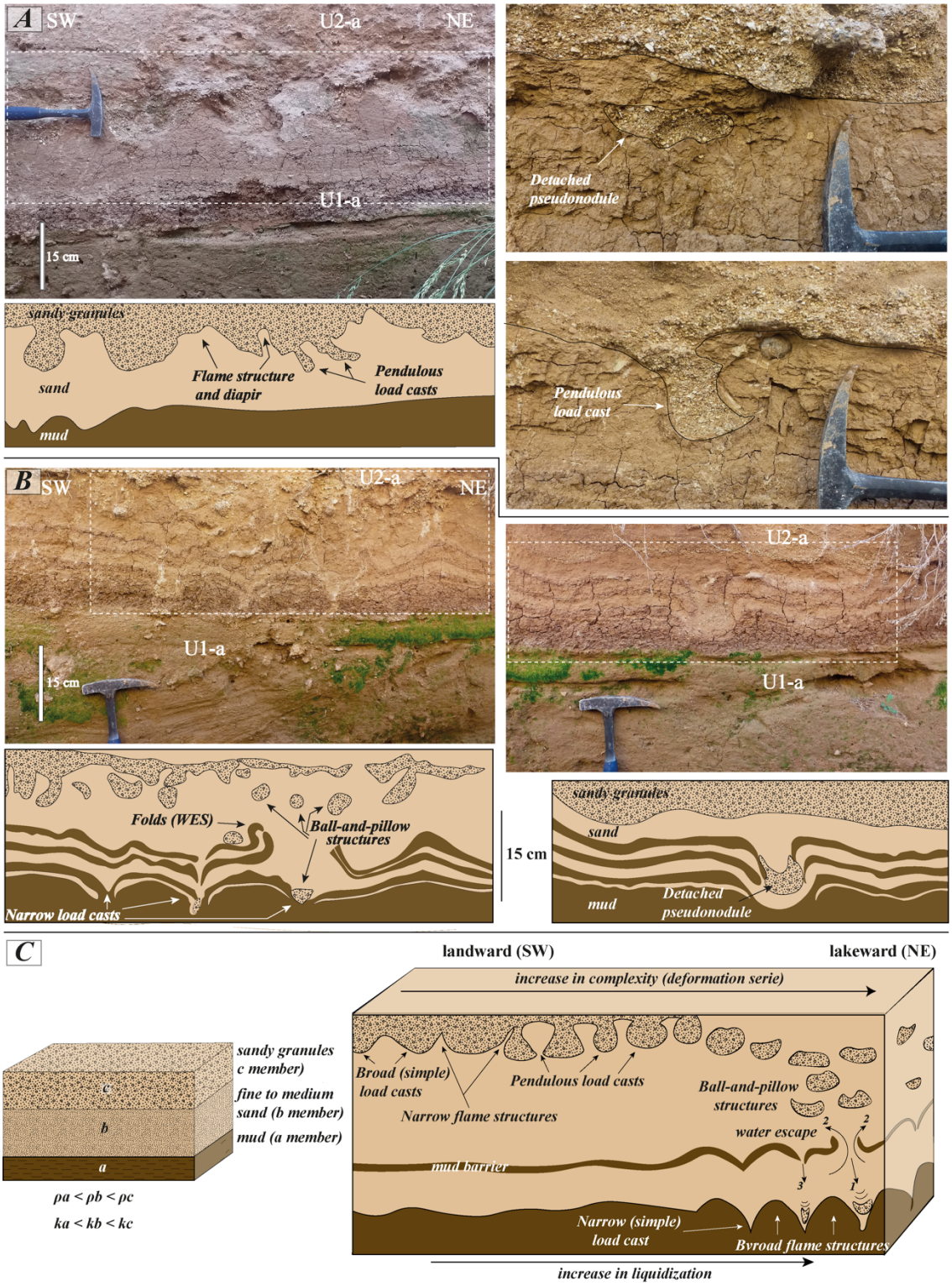


Figure 5. *Load structures, involving three lithologies (members) with reverse densities.* ***A****: Simple load casts and flames, pendulous load casts and detached pseudonodules developed at the interface between* ***U1-a*** *and* ***U2-a****.* ***B****: Synchronous loading and water-escape processes within* ***U1-a****.* ***C****: Drawn diagram demonstrating an increase in deformation complexity basinward. The numbers represent the sequence of events related to the downward sinking of detached pseudonodules into liquidised sandstone of subunit* ***U1-a*** *and upward water-escape beneath the mud permeability barrier. The Greek ρ and κ letters refer to the density and kinematic viscosity of each member, respectively. WES: water escape structures.*

With the involvement of three lithological members with reverse densities, the *broad* (*narrow*) *load casts* (*flame structures*) at the interface between “b” and “c”, and the *narrow* (*broad*) *load casts*

(*flame structures*) at the interface between "a" and "b" suggest a multi-member (c, b, a) system in which the kinematic viscosities increase from the lower to the upper member (Anketell et al., 1970) (Fig. 5C); such a system represents Rayleigh-Taylor instability. The deformation mechanism requires a reduction in the sediment strength upon liquidization (Allen, 1977). More precisely, localised fluidization of member "b" is evidenced through the development of *narrow flame structures* (*see* Owen, 2003) and typically through the occurrence of *water-escape-generated folds*. This suggests that, in accordance with Owen (1996), deformation driven by water-escape processes was superimposed on deformation driven by the Rayleigh-Taylor instability. In turn, the lower member (mud) needs thixotropy or incomplete liquefaction for its reduction in strength to occur, although the contribution of downwards migrating *pseudonodules* should be considered. As the reverse densities are well expressed, the driving force systems (*sensu* Owen, 1987) must be mainly fed by the gravitational potential energy (density loading, Owen 2003), although the observed irregular morphologies at the interface between sand and sandy granules do not rule out a partial contribution of unequal loading (*sensu* Allen, 1982) as a possible secondary driving force system (*see* Moretti and Ronchi, 2011). The basinward increase in deformation complexity is likely to be related to a basinward increase in liquidization of the "b" member. This is probably linked to differential water saturation of the involved sediments as the lake would be in an areally restricted state at the time of deformation (the deformation occurred during deposition of fluvial sediments, "c", above offshore deposits, "b" and "a"). Accordingly, high water-saturation state and density contrast (strong driving force) would have promoted *detached pseudonodules* to pierce repeatedly into the lower members, forming the *ball-and-pillow structures* basinward. Besides, the relatively higher thickness of the "b" member would have made the fluidized state longer.

4.2 Hybrid 'ductile'-brittle deformations

Soft-sediment folds are shown to occur periodically across the stratigraphic units. They can be coupled with *load structures* (Fig. 5B) or *normal faults* (Fig. 7B), or they can involve multi-layered systems composed of mud-rich and sand beds. This latter is illustrated in figure 6, where the upper and lower mud-rich levels are laterally extensive deformed layers, and the sandy beds present faint planar lamination to massive structures within the subunit **U2-c**. Remarkably, the lower mud-rich layer exhibits a lateral passage of *hybrid hydroplastic-brittle deformation* with *micro-faults* and *soft-sediment folds*, locally split into some separate small-sized *auto-clasts* (Fig. 6). Lateral thinning of the host layer was remarked as well. In turn, the upper mud-rich interval reveals no brittle or fragmentation but locally *doming* and *folding*. Above, a non-deformed cm-thick mud layer is marked and separated

from the underlying mud-rich interval by a sandy bed that exhibits thickness variation, hence mismatching the underlying forms (Fig. 6). Soft-sediment folding in unit **U2-b** and **U3-a**, developing in the footwall of a *normal fault,* reveals a discontinuous pattern marked by fragmentation into several folded pieces, herein termed '*split-folds'* (Fig. 7B). The sandy layer involved in loading-driven deformation (member "b", Fig. 5) in subunit **U1-a** contains deformed mud-rich levels (*see* the previous subsection). They display both *upward-directed fold limbs*, linked to burst-out of the cohesive mud layers, and *downward-directed cusp-like features*, linked directly to the sink of pseudonodules.

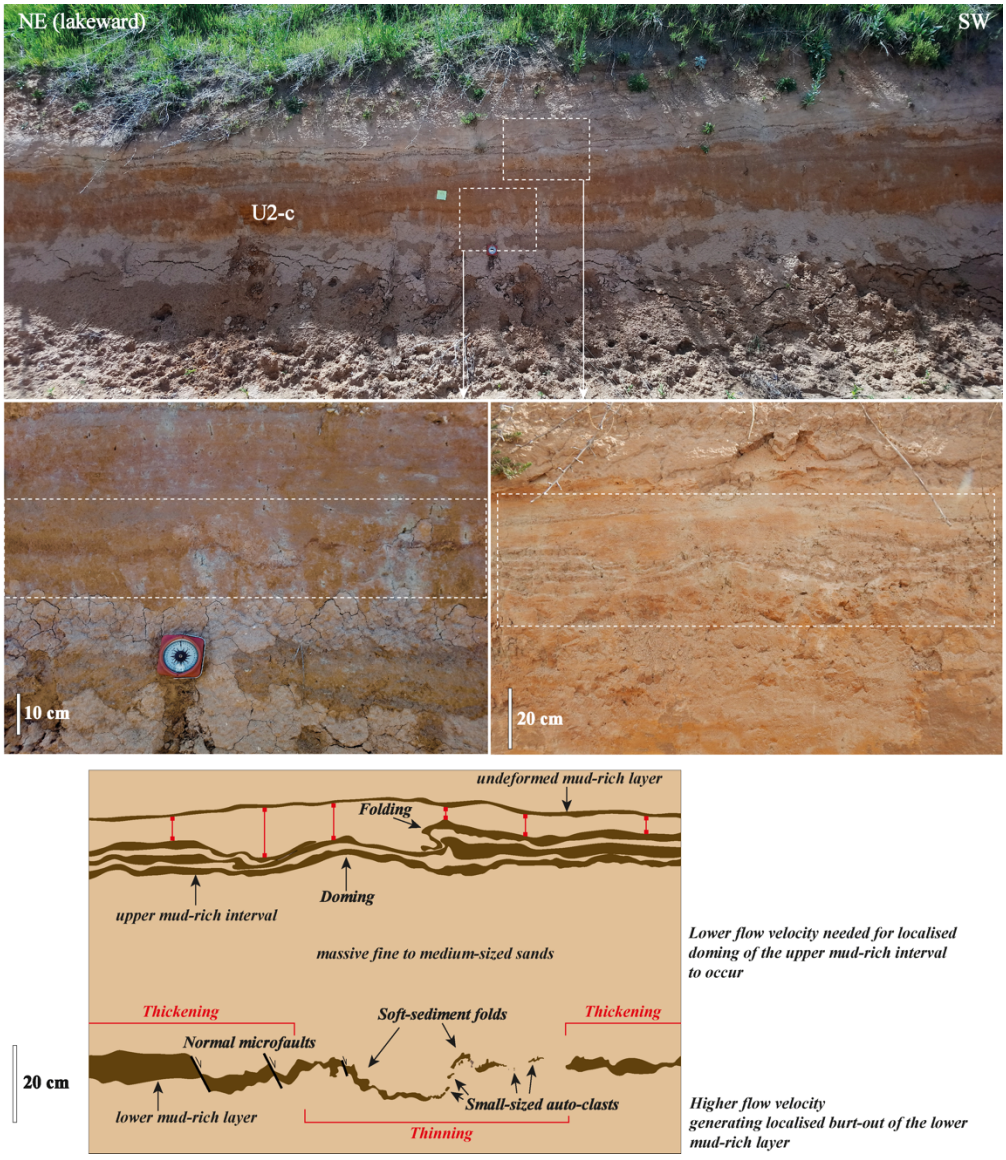


***Figure 6**. Hybrid hydroplastic-brittle deformation structures in a multi-layered system within subunit **U2-c** (distal part). Note the difference in deformation pattern between the lower and upper mud-rich layers. Note also the occurrence of a sandy bed with variable thickness (portrayed by the variation in length of the red brackets) separating the lower deformed multi-layered system below from an undeformed mud layer above.*

The faint planar lamination and massive structures of sand beds in figure 6 evidence localised fluidization (e.g., Lowe, 1975). The lateral passage of *hybrid hydroplastic-brittle deformation*

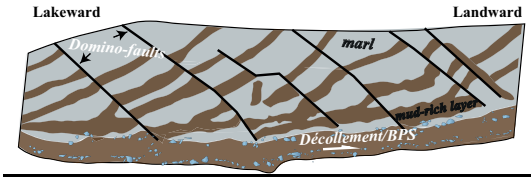
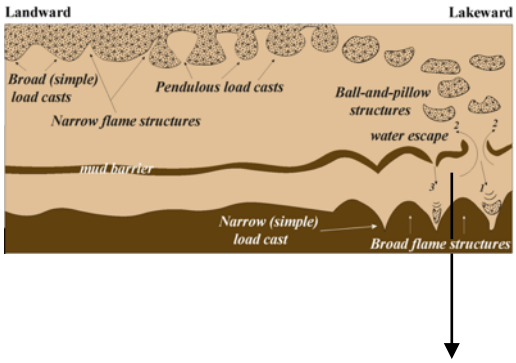
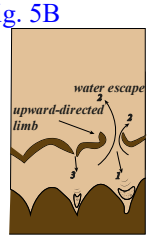
structures, namely *micro-faults*, *soft-sediment folds*, and *auto-clasts*, affecting the lower mud level is ascribed to the anisotropic rheology of the host bed (Törő and Pratt, 2016). This might be related to localised growth of water-filled voids (Nichols et al., 1994; Moretti et al., 1999), which developed upon localised fluidization of the sandy bed below, and eventually to localised burst-out and breaking up of the cohesive mud layer into separate small *auto-clasts* (Nichols et al., 1994). Localised fluidization and, consequently, differential bed expansion and bulk density might be involved in causing soft-sediment folding and a change in layer thickness. The occurrence of *normal micro-faults* excludes alternative driving force systems that may involve lateral movement of sand beds, the tangential shear (*see* Allen, 1982, Volume II, p. 378). Between localised growing water-filled voids, the mud (host) layer would not be liable to plastic deformation, provided the initial cohesive behaviour of this layer. According to Nichols et al. (1994), breaking up of the cohesive layer into small *auto-clasts* requires a (superficial) flow velocity of the fluidized sediment significantly greater than the flow velocity needed for fluidization to occur (minimum fluidization velocity). Therefore, it is conceivable that fluidization of the lower sand bed would have resulted in high flow velocity. In contrast, the upper mud interval, marking no water-escape features, would imply a flow velocity of the fluidized upper sand bed just beyond that required to counteract the weight of the particles (minimum fluidization), which is needed to give rise to the so-recognised small *doming* and *folding*. This contrast in fluidization state between the two sand beds may be attributed to the minimum fluidization velocity of each bed (Allen, 1982; Nichols et al., 1994), with the upper sand layer having the highest value (Fig. 6). While the sand bed, separating the undeformed mud layer above from the deformed multi-layered system below, exhibits remarkable variation in thickness, the hybrid deformation is thereby suggested to occur immediately below the subaqueous surface (*see* Alsop et al., 2022), therefore providing a bracket on the age of the deformation, which is notably tied to the estimated age of the host unit (i.e., between 27 and 12 cal kyr BP) (Fossen, 2010; Alsop et al., 2022). Besides, due to lack of its evidence, shallow sub-surface sliding between the deformed and undeformed layers is discounted as being an alternative interpretation that would suggest a rather apparent undeformed state of the overlying beds (*see* Alsop et al., 2022).

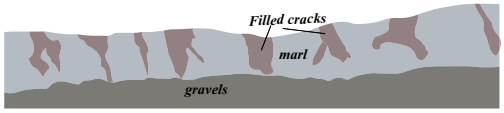
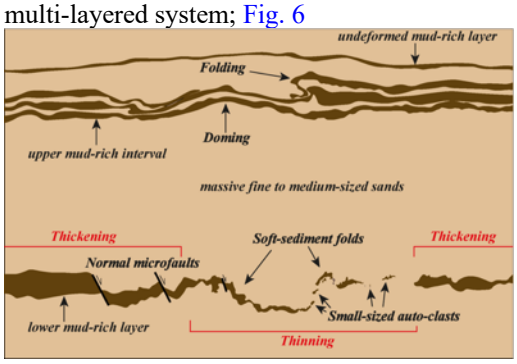
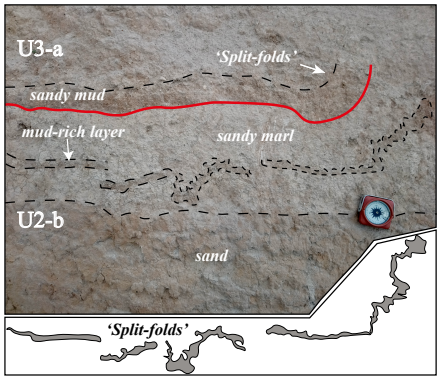
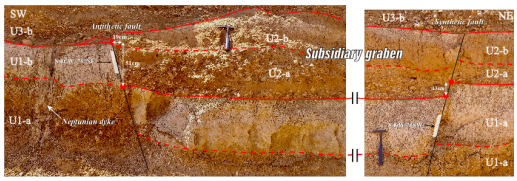
Within member "b" of figure 5B, the collapse and upward bending of the mud layers reveals a dramatic water-escape-generated burst-out. However, the collapse of the host layers and the water-escape process must be genetically linked to, and immediately follow, the downward drift of the *pseudonodules* across the host layers. In turn, the *cusp-like structures* pointing downward appear to be unrelated to water-escape processes. On the other hand, the '*split-folds'* generation that involves the

mud and sandy mud layers and developed in the footwall (Fig. 7B) seems to be synchronised with the brittle deformation accommodated by the *normal fault* alongside.

To summarise, fluidization of the sandy layers is involved in all *soft-sediment folding deformation*. This liquidization style provides both a driving force (the upward component of fluid drag) and a deformation mechanism (Allen, 1982; Owen, 1996).

***Table 2**. Summary of the soft-sediment deformations structures recognised from the SW margin of Lake Ifrah.*

Sedimentary deformation structures; Figures	**Host sub-unit(s)**	**Description**	**Deformation mechanism; driving force systems**	**Trigger mechanism (of liquidization) or origin of brittle deformation**
Bed-parallel slip and associated *domino-style faults*; Fig. 8 	**U1-b**	high-angle, unfolded, subparallel, normal-fault blocs of planar geometry; basal *décollement*/*bed-parallel slip*	frictional sliding	Partial response to the strain due to the *reverse-drag* flexure (Delogkos et al., 2018)
Load structures; Fig. 5 	**U1-a, U2-a**	Cm- to dm-scale *load structures* of different types (*load cast*, *pendulous load cast and ball-and-pillow*); lakeward increase in complexity (deformation series, *sensu* Owen, 2003)	Liquidization (liquefaction and localised fluidization); density loading (gravitation force) (Owen 2003); possible unequal loading (Allen,1982); basinward increase in liquidization	Seismic chock
Water escape-generated folds; Fig. 5B 	**U1-a**	Upward-directed limbs, linked to burst-out of the cohesive mud layers	Fluidization of the lower sand layer; vertical shear tied to water escape process	Seismic chock
Shrinkage (*desiccation*) *cracks; Fig. 9*	**U2-b**	Filled *shrinkage cracks*, mostly V-shaped in	Dewatering of the muddy component; increase in	Endogenic (basin-related) origin

		vertical view; some openings exceed 10 cm in diameter; mostly parallel-sided; filling material consists of sand coming from above	tensile stress (due to dewatering) until surpassing the tensile strength of the host bed (Morris et al., 1992)	
Hybrid hydroplastic-brittle deformation in a multi-layered system; Fig. 6 	**U2-c**	Soft-sediment folding, *microfaults*, small-scale *auto-clasts* and doming are involved in deformation in a multi-layered system composed of mud-rich and sand beds; lateral thinning and thickening	Localised fluidization (Nichols et al., 1994); vertical shear stress due to the upward component of fluid drag during fluidization (Owen, 1987)	Seismic chock
Fault-linked deformation: '*split-folds*'; *Fig. 7B* 	**U2-b, U3-a**	Discontinuous deformation pattern within the footwall side of a *normal fault* (*antithetic fault*); fragmentation into folded pieces affecting mud and sandy mud layers	Localised fluidization of the (sandy) marl bed; vertical shear stress	Seismic shock contemporaneous to tectonic activity
Subsidiary graben, mode fracture III; Fig. 7D, F 	All but **U3-b**	*Normal faults* with opposing dip direction forming downthrown bloc; sharp and near planar slip plane; faults dipping lakeward (landward) always exhibit the higher (lower) dip separation	Frictional sliding after that the differential stress (σ1-σ3) overcomes the strength of the involved sediments; tectonic uplift and tilting	Partial response to the strain due to the *reverse-drag* flexure
Neptunian dyke, mode fracture I; Fig 8D, Fig. 7D, F	All except **U3-b**	Broadly vertical, V-shaped, opening, few cm to	Subaqueous infilling of fractures that develop in an extensional	Partial response to the strain due to the *reverse-drag* flexure

		submetric in diameter; filling through the collapse of soft-sediment (overlying sediment of **U3-a**)	regime (Moretti and Sabato, 2007)	

4.3 Neptunian dykes and normal faults

Tensional features such as *neptunian dykes* and *soft-sediment normal faults* have been widely recognised over the studied outcrop. *Normal faults* are a few metres deep, having near planar and sharp slip face planes and with sub-metric dip separation and throws (usually 15-50 cm; Fig. 7). They share a similar azimuth as the master fault, SE-NW (Fig. 2). In two instances, faults dipping towards each other and creating a downthrown block were typically recognised and ascribed to small-scale *grabens*. The *faults* that dip lakeward always portray the higher dip separation relative to their conjugates (dipping landward). Besides, a basinward increase in fault offsets was recognised. In addition to demonstrating a vertical displacement along the slip planes, they usually accommodate a lateral displacement (opening) of a few centimetres to several decimetres filled by material coming from above (marl and organic-rich sediments of the subunit **U3-a**). These filled-up openings are encountered in other instances without demonstrating vertical displacement and respecting the defined structures as *neptunian dykes* (Lehner, 1991), and are typically shown to be vertical, except for one case where it is seen to be diverted through piercing the domino-fault host bed (Fig. 8D), described in the next subsection. They are sealed by the sheetflood deposits of the upper unit (**U3-b**).

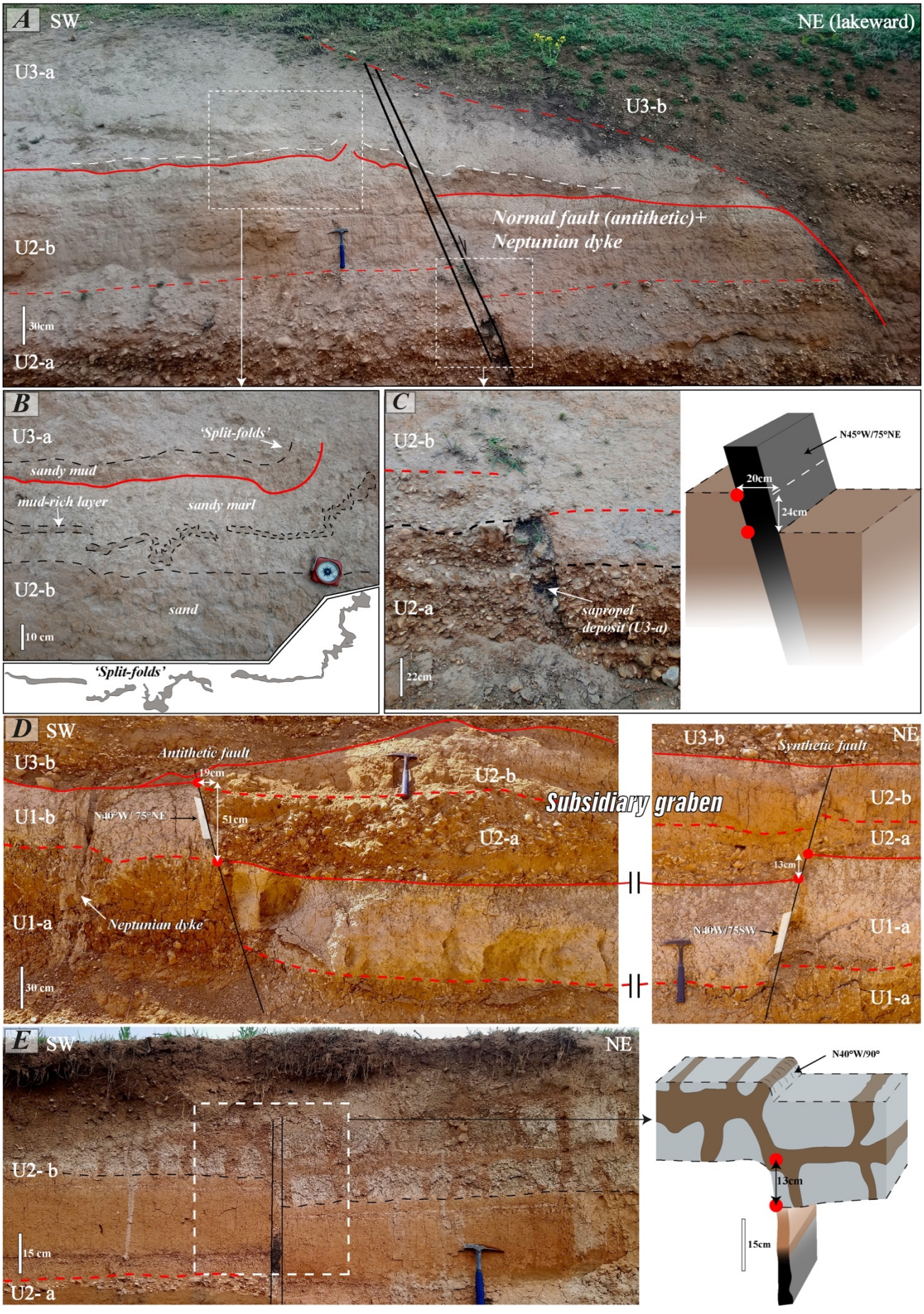

A
SW
NE (lakeward)
U3-a
U3-b
Normal fault (antithetic)+
Neptunian dyke
U2-b
30cm
U2-a
B
U3-a
'Split-folds'
sandy mud
mud-rich layer
sandy marl
U2-b
sand
10 cm
'Split-folds'
C
U2-b
U2-a
sapropel
deposit (U3-a)
22cm
N45°W/75°NE
20cm
24cm
D
SW
U3-b
Antithetic fault
19cm
U2-b
U1-b
N40°W/ 75°NE
51cm
U2-a
U1-a
Neptunian dyke
30 cm
Subsidiary graben
U3-b
Synthetic fault
NE
U2-b
U2-a
13cm
N40W/75SW
U1-a
U1-a
E
SW
NE
U2- b
15 cm
U2- a
N40°W/90°
13cm
15cm

***Figure** 7. Field views of antithetic and synthetic normal faults, subsidiary grabens (mode III fractures), and neptunian dykes (mode I fractures), as well as their associated hydroplastic deformation structures (locations in Fig. 2C). **A**: Isolated antithetic normal fault demonstrating vertical frictional sliding (mode fracture III) and opening (mode fracture I) synchronously filled by material coming from above (neptunian dyke). **B**: Close-up view of (**A**) showing split folds in the footwall side of the fault. **C**: Close-up view of (**A**), showing that the filling material is originated from subunit **U3-a** (sapropel deposit). **D**, **F** and **G**: subsidiary grabens exhibiting (**F** and **G**) or no (**D**) submetric opening. Note the difference in dip separation between antithetic and synthetic faults. **E**: Vertical fault demonstrating frictional sliding and opening. The subunit codes are shown. Thick red lines (solid) refer to unit-bounding surfaces; thin red lines (dashed) refer to subunit surfaces; thin white or black lines (dashed) refer to facies' contacts.*

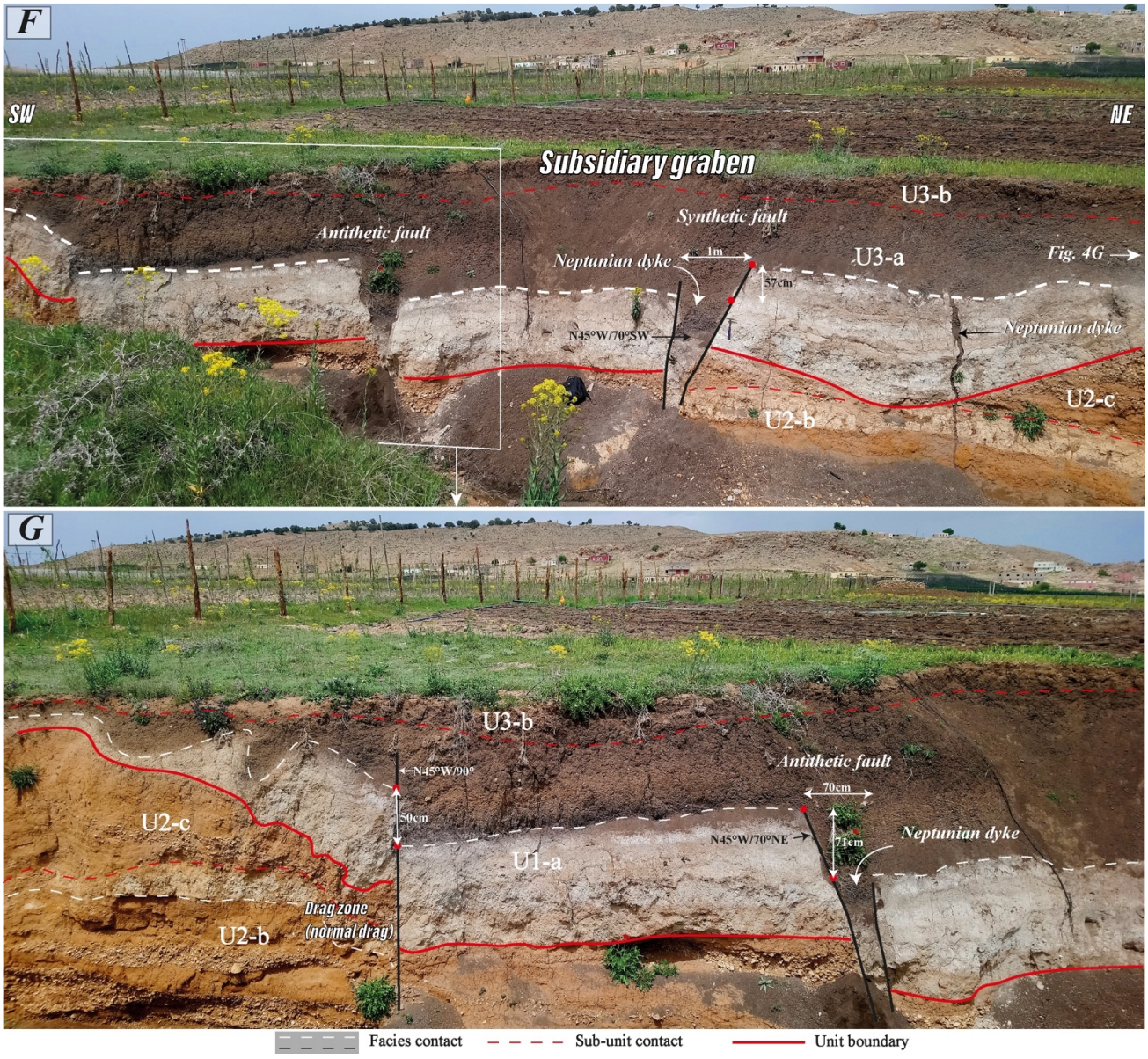


***Figure** 7. (Continued)*

The direct association of *normal faults* and *neptunian dykes* (mode III and I fracture, respectively), along with the shared direction with respect to the border margin fault (the master fault), NW-SE, suggests a common tectonic origin (or event), accommodating a NE-SW-directed extension (Lehner, 1991; Fossen, 2010). Indeed, *neptunian dykes* are commonly considered to form through subaqueous infilling of fractures that develop in extensional regimes (e.g., Moretti and Sabato, 2007),

and are commonly used as kinematic indicators of normal movement (e.g., Davis et al., 2011; Martinelli et al., 2019). The small-scale *grabens* appear to be *subsidiary* and developed within the hanging-wall side of the master fault, suggesting a genetic relationship (Hamblin, 1965). Indeed, the higher offset that portrays the lakeward dipping faults with respect to those dipping landward (*antithetic* and *synthetic faults*, respectively, according to Peacock et al., 2016), as well as the overall increase in the fault offsets basinward, suggest a brittle deformation response as the hanging-wall side of the master fault bends to form a large-scale *rollover* anticline or *reverse-drag*, depending on the geometry of the master fault (listric or planar, respectively; Xiao and Suppe, 1992; Schlische, 1995; Spahić et al., 2011). Considering the limited width of the master fault (ca. 3 km), along with the scale and the subsidiary nature of the basin relative to the Tizi n'Tretten Fault (TTF, Figs. 1 and 2), suggesting extensional deformation at the upper crust, it is unlikely to consider a classical listric fault that detaches and exhibits no displacement gradient along its slip plane (Shelton, 1984; Dula Jr, 1991). Alternatively, the hanging-wall flexing is more likely to be primarily linked to a decrease in displacement field in the direction normal to the master fault with elliptical displacement contours (Barnett et al., 1987; Grasemann et al., 2005). Nevertheless, the observed localised landward direction of the slop dip (Fig. 3) formed upon the last folding event of the *reverse-drag* suggests a slightly curved or mildly listric fault (Schlische, 1995). Involving Early to Middle Holocene lithologies, the *reverse-drag* folding event and associated *subsidiary grabens* and *neptunian dykes* are suggested to have occurred during the Middle Holocene.

4.4 Bed-parallel slip and associated domino-style faults

Rotational extension structures were observed disrupting locally the bioclastic marl of the subunit **U1-b**. They consist of high-angle, unfolded, subparallel, normal-fault blocks of planar geometry dipping landward (SW) and associated with a basal up-dip directed (SW) *bed-parallel slip* (BPS) or *décollement* (Fig. 8). A truncation surface (a unit-bounding surface) downcutting irregularly into the marl bed and component marker horizons (Fig. 8A, D) and hence separating this bed from the fluvial deposits above (demonstrating higher energy level, thereby conditioning the truncation surface), the subunit **U2-a** (involved in loading deformation lakeward). As a result, the host bed has not been preserved entirely laterally, and in some cases, it is eroded completely, prohibiting lateral tracking of the deformation (e.g., Figs. 3 and 8A). However, undisrupted stretches of this host bed were observed more proximally (*see* Figs. 4B and 5, and locations in Fig. 2C), suggesting a restricted spatial character of this deformation style.

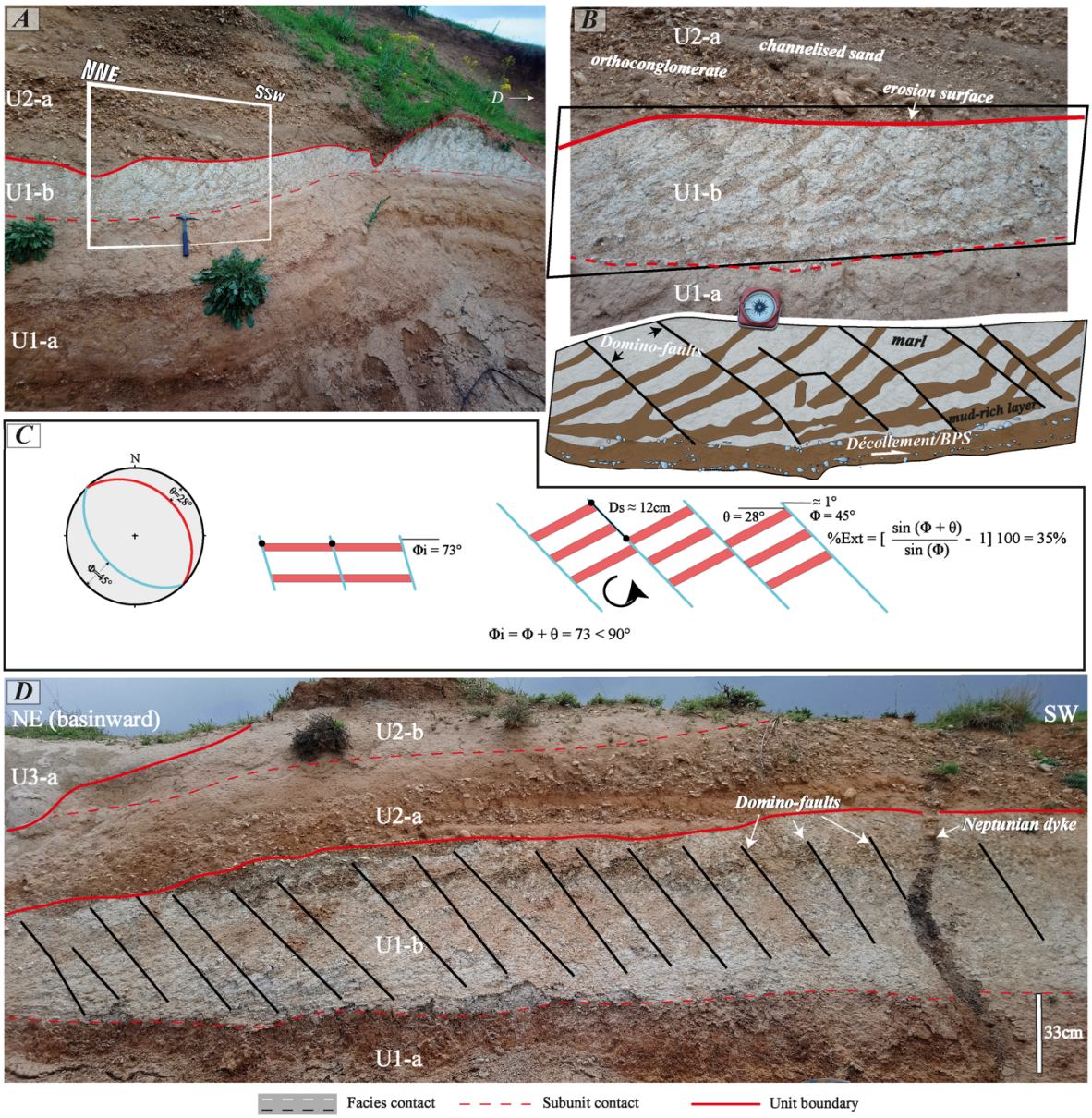


Figure 8. *Bed-parallel slip (BPS) and associated domino-style faults (location in* ***Fig. 2C****). **A**: Mesoscale field view showing brittle deformation within the subunit **U1-b**. Note the truncation pattern of the unit-bounding surface at the top of the host bed. **B**: Close-up view outlined in (**A**), with corresponding drawn diagram showing domino-style faulting linked to a basal BPS (décollement). **C**: Geometric relations to estimate horizontal extension (after Wernicke and Burchfiel, 1982). **D**: Lateral continuity (cf., text) of the deformation (few metres landward of (**A**)). Note how one of the domino-faults conditioned the diverting of the subsequent neptunian dyke. Subunit codes are shown. Thick red lines (solid) refer to unit-bounding surfaces.*

Interestingly, this extensional pattern could be reconciled with the rigid domino model that describes a simultaneous rotation in the same sense of fault-bounded blocks (dominos) (Wernicke and Burchfiel, 1982; Nur et al., 1986; Axen, 1988; Jackson et al., 1988). In this respect, high-angle *normal faults* can be regarded as a secondary synthetic fault set relative to the basal *décollement* surface (*bed-parallel slip*) that contributes to the landward lengthening and disruption of the bioclastic marl (Reinoso et al., 2020). Restoration (rigid rotation) into a horizontal attitude of the marker horizons (mud layers) suggests a dip of around 73° of *secondary normal faults*, which is compatible with the

Andersonian fault theory (Anderson, 1951). The hydroplastic behaviour of the competent mud layer promoting the *décollement* displacement (Alsop et al., 2018) would serve as a mobile medium and thus solve the (second) compatibility problem related to boundary conditions of the domino model (*see* Fossen, 2010, p. 336). According to the geometric relations proposed by Wernicke and Burchfiel (1982), the calculated horizontal extension for the domino-style structure is around 35% (Fig. 8C).

The generation of this rotational extension (domino-faults) could either be gravity-driven, which would have resulted in a translational glide (Basilone et al., 2016), or tectonically-induced as related to the flexural-slip mechanism (Watterson et al., 1998; Delogkos et al., 2018). While *bed-parallel slips* can simply be gravity-driven (Alsop et al., 2020), a landward dipping palaeoslope is required in the case study to generate the landward dipping strata-bound domino-faults (*see* Fossen, 2010, pp. 337). In contrast, flexural-slip folding with an up-dip sense of the *bed-parallel slip* is compatible with the present-day slope (lakeward). Considering the structural setting that involves folding of the hanging-wall block of the master fault (previous subsection), and given the present-day slope dip of the host unit (≈ 1° NE, lakeward), it is unlikely to consider a reverse slope that would have been created following a folding event (slip increment(s)); if this was so, the reverse slope of the host bed (**U1-b**) would be more accentuated instead of revealing lakeward slope dip. Alternatively, the *bed-parallel slip* associated with *domino-style faults* (or bookshelf faults) is likely to reflect a partial response (accommodation) of a flexural-slip pulse, but without an uplift component contrary to the one that would have created the present-day topography (involving a reverse slope, Fig. 3) and triggered the *subsidiary grabens* and *neptunian dykes*. As such, we consider dip-slip and bed-parallel slip faulting as response mechanisms of *reverse-drag* flexural pulses, with the fact that dip-slip faulting (giving way to *subsidiary grabens*) accommodates in the hanging-wall more significant displacement increment (or cumulative increments) along the master fault.

Compared to the loading deformation, the *domino-faults* would have been created previously before the truncation surface (separating **U1** from **U2**) was formed. Standing on prior dating (Rhoujjati et al., 2010) and correlations (Fig. 3), the deformation is suggested to be previous to 28 ka cal BP (probably during the Marine Isotope Stage 3, MIS-3). Accordingly, it is inferred that two *reverse-drag* folding events associated with two displacement increments (or cumulative increments) would have developed during the late Pleistocene (MIS-3?) and Middle Holocene, evidencing basin-scale neotectonic activity and potentially providing clues to understand the tectonic history of the basin, including its onset (*see* discussion).

4.5 Shrinkage cracks

Within the subunit **U2-b**, the marl beds are pierced continually and regularly by filled *shrinkage cracks*. Although some of them have a U shape, most of the *shrinkage cracks* are V-shaped in vertical view, tapering downward with a maximum width of usually a few cm, with an average of 3 cm, but can exceed, in some instances, 10 cm. They are almost regularly separated from each other, with an average spacing of about 10 cm, where the filling is mostly bridged (Fig. 9B) or less commonly unbridged (Fig. 9A) (*sensu* Allen 1982). The filling material consists of coarser sediments (medium to coarse sands), ostensibly coming from above.

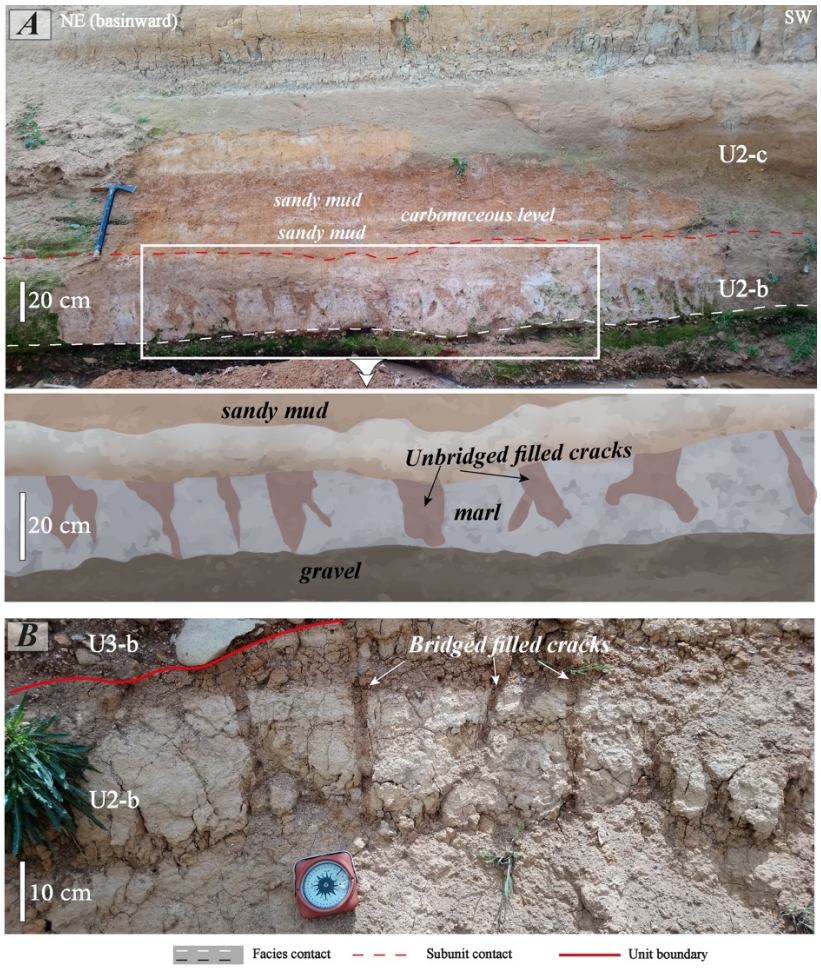


***Figure 9**. Unbridged (**A**) and bridged (**B**) filled shrinkage cracks affecting the sandy marl of subunit **U2-b**. Thick red lines (solid) refer to unit-bounding surfaces; thin red lines (dashed) refer to subunit surfaces; thin white or black lines (dashed) refer to facies' contacts.*

The relative higher width and the predominance of V shape that tapers downward of the filled cracks, together with the absence of deformation in the host bed, suggest subareal shrinkage rather than syneresis cracking processes (Plummer and Gostin, 1981; Pratt, 1998). According to this, it is suggested that during desiccation (dewatering) of the muddy component of the host bed (marl), the volume of which tends to reduce and a tensile failure comes to happen once the increasing tensile stress surpasses the tensile strength of the host bed, surface cracking develops (Morris et al., 1992;

Tang et al., 2021). This declines downward from a maximum at the surface until the compressional lithostatic force takes over (Allen, 1982; Tang et al., 2021), thus giving rise to the remarkable V shape (Plummer and Gostin, 1981).

5 Discussion

5.1 Trigger mechanism

Although not all SSDSs from Lake Ifrah involve loss of strength upon liquidization as a deformation mechanism (e.g., neptunian dykes, normal faults), their collective application in assessing the palaeoseismicity and neotectonic activity in the case study could be of major benefit. Thus, while m-scale brittle structures may serve as direct proxies to appreciate the basin-scale neotectonic pulses, liquidization-linked hydroplastic and viscous deformation can be used to assess the past seismic signals whereby considered to be seismic-triggered. However, assigning such a liquidization trigger to earthquakes is not a straightforward approach (Owen et al., 2011; Moretti et al., 2014) and, in some cases, becomes more challenging (Shanmugam, 2016) as many possible triggers, related or not to the depositional context (endogenic or exogenic, respectively; Leeder, 1987; Owen et al., 2011), can be conceivably involved in building the same eventual morphology. Therefore, a more realistic and particularly objective tripartite approach, accounting for the depositional setting (context-based), discussion of all possible trigger agents (trigger-based), and reference to some criteria that may be specific to the studied case and hence employed as supporting evidence for an assigned trigger (criteria-based), has been recommended (Owen et al., 2011; Moretti et al., 2014) and hereby strictly applied to assess the palaeoseismicity in the region.

5.1.1 Endogenic triggers: Context- and trigger-based approaches

Many endogenic triggers for liquidization have been documented to be possible in fluvio-lacustrine settings. Overloading due to rapid deposition (Lowe, 1975; Owen and Moretti, 2008), a sudden change in the water table (Guhman and Pederson, 1992; Holzer and Clark, 1993), the cyclic effect of storms and strong waves (e.g., Molina et al., 1998; Alfaro et al., 2002), and uneven loading due to channelised erosion in more fluvial-dominated settings (Dasgupta, 1998), are the most common triggers in non-glacial areas. On the other hand, some endogenic processes can operate to deform unconsolidated sediments during or shortly after deposition without implying liquidization (Ezquerro et al., 2015).

The present-day lake water body of the Ifrah Basin is very small (1 km in surface area), and the main fluvio-lacustrine deposits are restricted to the NE side of the basin. Therefore, the available fetch of the lake is not prone to holding storms and strong waves. Moreover, although the subunit **U2-c** reflects relatively high-energy nearshore conditions, lacustrine deposits from the available outcrop lack evidence of extreme hydrodynamic events (no hummocky or swaley cross stratification has been recognised). Besides, the hybrid deformation inferred and found to occur at the surface and within relatively high-energy nearshore conditions (distal part of **U2-c**) reveals undisturbed beds just above the deformed horizons with similar lithologies (sand-mud multi-layered system, Fig. 6), thus discarding an endogenic trigger agent (Moretti and Ronchi, 2011) for the hybrid deformation.

Rapid deposition is particularly likely to cause the creation of *load structures* in fluvio-lacustrine conditions (Moretti and Sabato, 2007; Owen and Moretti, 2008). In fact, the *load structures*, involving the offshore sand-mud succession of **U1-a** and sand-gravel-dominated deposits of **U2-a**, are suitable to invoke overloading-triggered liquefaction. However, the horizontal stratification, along with the well-marked flat-clast imbrication that characterises the subunit **U2-a**, suggests deposition from a tractive flow rather than *en masse* deposition, hence discarding a potential overloading effect (Ezquerro et al., 2016). On the other hand, the development of the erosional surface separating the fluvial from offshore deposits may induce unequal loading and hence trigger the liquefaction of the sand below, giving rise to some particular *load structures* (Dasgupta, 1998; Moretti and Ronchi, 2011). Nevertheless, the geomorphologies of *load structures* described from Lake Ifrah are not compatible with those that are prone to form under unequal loading effects (e.g., *recumbent flames*, *see* Dasgupta, 1998). Therefore, the liquidization mechanism inducing *simple load casts* and *ball-and-pillow structures* is not considered to be triggered by an endogenic agent. Accordingly, the distal occurrence, with a basinward increase in deformation complexity, of *load structures* (from *simple load casts* to *ball-and-pillow structures*) is interpreted to be related to an increase in water saturation basinward as the lake level during deformation (time of **U2-a** deposition) has considerably dropped.

Sudden variation in groundwater level is unlikely to be a trigger mechanism for liquidization since morphologies induced by this process, such as *sand boils* (Guhman and Pederson, 1992; Holzer and Clark, 1993) and *clastic pipes* (Netoff and Shroba, 2001; Wheatley et al., 2016), are absent. Furthermore, this trigger mechanism is more effective in exclusive fluvial settings (Holzer and Clark, 1993). Other triggers related to periglacial environments (thawing of permafrost, unequal loading near marginal ice cover; Harris et al., 2000; Le Heron et al., 2005) or associated with very large-scale basins

(e.g., tidal effects, tsunamis; Greb and Archer, 2007; Matsumoto et al., 2008) are easily excluded, given the latitudinal position and the small scale of the studied basin.

Some natural endogenic processes can deform unlithified beds without involving loss of strength. *Desiccation cracks*, for instance, are considered to reflect periodic emersions (Allen, 1982; Ezquerro et al., 2015) and to be induced by internal applied tensile stress that exceeds the tensile strength of the host bed and decreases downward (Morris et al., 1992; Tang et al., 2021), thereby sculpting the filled-up V-shaped morphologies seen in vertical section (Plummer and Gostin, 1981).

Neptunian dykes can also form without involving liquidization. They demonstrate the passive collapse of sediment into open fractures (mode I fractures) and are commonly used as markers of extensional tectonic activity (Moretti and Sabato, 2007; Berra and Felletti, 2011). An alternative interpretation that may involve collapse associated with karstic sinkhole formation (Moretti et al., 2011) is discarded even if the Liasic bedrock is observed to hold well-recognised large-scale morphologies induced by karstic activity. This is attested by their association with *normal faults* and their direction being compatible with the master structures bounding the basin. Additionally, their geometry (planar) is inconsistent with the elliptical structures that develop in relation to sinkhole activity (*see* Moretti et al., 2011). Therefore, m-scale brittle deformations are undoubtedly ascribed to tectonic activity.

In such growing hanging-wall anticlines, co-seismic slips along horizontal discontinuities are not uncommon (Aydin and Du, 1995; Berberian et al., 2000). However, BPS in the case study is unlikely to be considered as co-seismic or seismic-triggered that would cause the sediments above to slide downdip, since dips of the associated *domino-faults* are not compatible with the BPS dip. Furthermore, co-seismic shaking mechanism would generate multiple vertically stacked BPS planes along the marker horizons of the host bed (mud-layers in Fig. 8B) rather than cross-cutting them (Weinberger et al., 2016; *see* alsop et al., 2020, p. 13). Therefore, the BPS and associated *domino-faults*, along with *neptunian dykes* and *subsidiary grabens*, again, are assigned undoubtedly to two separate flexural-slip pulses of the *reverse-drag*, thereby recording synsedimentary basin-related tectonic events.

5.1.2 Exogenic trigger: Palaeoseismic implication

After having assigned some non-liquidization-requiring deformations to basin-related processes (desiccation, faulting), and discarded the possibility of the most potential endogenic processes (e.g., overloading, strong waves effect) in triggering liquidization, it remains to consider an

exogenic trigger for liquefaction and fluidization. Meteorite impact (Simms, 2007), and volcanic (Zhou et al., 2017) or tectonically-induced (e.g., Rossetti et al., 2017) earthquakes are the most possible exogenic agents. Possible meteorite impacts are ostensibly discarded due to the lack of their evidence. Given the current state of knowledge, the most recent alkaline mafic eruptions resulting in scattered strombolian cones and maars (i.e., explosive eruptions, hence likely to generate earthquakes) in the Middle Atlas is reported to be older than 0.6-0.5 Myr (Harmand and Cantagrel, 1984; El Azzouzi et al., 2010), which is very far from the herein considered depositional period (late Pleistocene-Holocene). Regarding the seismotectonic context of the study area, fault stick-slip-related earthquakes are the most likely exogenic mechanism that would trigger liquidization. Therefore, loss of strength upon an increase in pore fluid pressure is best explained by the cyclic passage of seismic waves generating chaotic compressive-tensile stresses. Additionally, this mechanism explains, accounting also for the rheological heterogeneity, the *hybrid deformation* with randomly-oriented *folds* and cm-scale brittle structures, (El Taki et al., 2012; Törő et al., 2015; Törő and Pratt, 2016). Accordingly, deformed horizons that involve liquidization (e.g., *load structures*, *water-escape* SSDSs, *hybrid deformation structures*) are considered seismites (Seilacher, 1969, 1984).

To fully ascertain the seismic involvement in triggering liquidization, we discuss the several criteria that have therefore been suggested (criteria-based approach, Owen et al., 2011) (e.g., Sims, 1975; Obermeier, 1996; Mazumder et al., 2006; Montenat et al., 2007; Owen and Moretti, 2011; Moretti et al., 2014). However, it is important to stress at the outset that these criteria are neither straightforward diagnostic in themselves nor easy to verify in most instances (Owen and Moretti, 2011), thus prompting caution whenever applied (Moretti et al., 2014). While some of the criteria do meet when considering the local context of the study area, others do not. First, the regional context of the study area is known to be tectonically and seismically active (Medina and Cherkaoui, 1991; Chalouan et al., 2014; Poujol et al., 2014, 2017), hence fulfilling one of the most promising proposed criteria. The occurrence of *soft-sediment faults* and *neptunian dykes* also supports the neotectonic influence. Second, the liquidization-induced deformation morphologies are comparable with (i) those reproduced in the laboratory with shaking tables modelling earthquake effects (Moretti et al., 1999; Dasgupta and Chatterjee, 2019) (for instance, compare Fig. 5B and C of this paper with Fig. 5F of Dasgupta and Chatterjee, 2019), and (ii) those proved to be seismically-triggered in natural cases (e.g., Ezquerro et al., 2015; Meng et al., 2021). Third, lateral continuity of deformation structures is expected to occur whenever a seismic origin is investigated, particularly where the host sediment seems to be liquefiable. However, initial properties such as degree of saturation may influence liquefaction

potential and, interestingly, may not be evident from the deformed deposits (Moretti et al., 2011). According to this, the lateral discontinuity of the *load structures* observed to form distally during the deposition of the subunit **U2-a** is likely to be linked to low saturation of the involved sediments in the proximal stretch of the outcrop as the lake level was lower during this time-lapse, therefore not excluding a seismic origin. Fourth, as earthquakes are recurrent events, their imprints in sedimentary successions should be recognised in vertical repetition (Moretti et al., 2011). This is consistent with the deformations concerned, especially for the *hybrid deformation structures* developed within **U2-c** that involve a vertical succession of deformed and undeformed horizons with similar lithologies.

Zonation in the complexity of deformation morphologies relative to the epicentral distance is suggested to be the most supportive criterion for seismic origin, albeit mostly non-applicable (Owen and Moretti, 2011). In fact, the limited size of the studied basin precluded lateral deformation tracking. However, recent data from Lake Iffer (Benabbou et al., 2018), about 6 km north of Lake Ifrah (Figs. 1 and 11A), suggest promising remarks. Given the similar lithologies and time interval between the two locations, well-developed *water-escape structures* with metre-scale *clastic dykes* in Lake Iffer appear to be coeval with the *load structures* in Lake Ifrah (both are, chrono-stratigraphically, shortly younger than 29 cal kyr BP, *see* their Fig. 3). Furthermore, extensive *dish structures* from the Saiss Basin (Plaziat and Ahmamou, 1998), about 35 km further north (*see* location in Fig. 1), have been recognised to affect Pliocene sandstones. As a result, besides suggesting a likely zonation in deformation complexity (Rodríguez-Pascua et al., 2000), these findings point to a northward location of the potential epicentres; more studies should be conducted, however, at nearby sites to verify this assumption. This is in fact consistent with recent investigations that have emphasised higher seismic activity at the transition between the Rif and the Middle Atlas, known as the South Rif Front (SRF, Fig. 1; Medina and Cherkaoui, 1992; Moratti et al., 2003; Poujol et al., 2017), in response to the convergence between Africa and Iberia since the Cretaceous (Dewey et al., 1989; Lonergan and White, 1997; Fernàndez et al., 2019). Indeed, at least four historical earthquakes of Mw > 5.5 have been reported to have occurred in this transitional zone, not far from Lake Ifrah, over the last millennium (Moratti et al., 2003; Peláez et al., 2007; Poujol et al., 2017; Fig. 1). Furthermore, instrumental data from the Middle Atlas based on regional observation of stress (focal mechanisms) between 1970 and 1992 revealed that the majority of instrumental seismicity is localised in the Rif (including the SRF) and High Atlas (very far from the studied site, Fig. 1) with strike-slip and reverse faulting solutions, whereas the Middle Atlas shows little seismicity, concentrated in its north-western and southern

borders with normal faulting solutions (Tadili and Ramdani, 1986; Medina and Cherkaoui, 1991, 1992).

In line with these insights, the sedimentological results presented here allow us to consider that the present-day state of seismicity would be persistent for at least the entire late Pleistocene and Holocene period. That is, most of the slip events (co-seismic ruptures) able to generate earthquakes that would induce liquefaction (Mw > 5) were accommodated by thrust and strike-slip movements in the northern part of the Middle Atlas, which may lead to a striking (transtensional?) neotectonic implication for the central part of the Middle Atlas, including the studied basin.

5.2 Tectonic implications

5.2.1 Master fault slip behaviour and tectonic controls on sedimentation

According to previous evidence, the space made available for sedimentation (the accommodation concept) within the Ifrah Basin is largely controlled by the amount of the episodic displacement increments along the NE border basin fault (the master fault) and the associated elastic-flexural response of the *reverse-drag*. This master fault striking SE-NW is inferred to accommodate most of the recent extension along the basin, thus prompting a half-graben geometry (Fig. 10A). This is supported by the shape of the lake (elliptical), the position (NE) and the direction of the maximum axis (NW-SE) of the water body relative to the basin (Fig. 2). Additionally, the clear-cut combination of an *antithetic normal fault* with liquidization-induced soft-sediment deformation (Fig. 7A, B) suggests regional co-seismic faulting. Therefore, and accounting for the slip hardening (Beeler et al., 2001), the occurrence at the uppermost part of the crust as the fault length is ca. 3 km (i.e., small normal stress; Marone and Scholz, 1988), and the fact that part of the residual strike-slip displacement is periodically transferred from the master strike-slip fault (into which the basin is attached, the TTF) upon large slip events (high magnitude earthquakes) into the border basin faults (Storti et al., 2003), we consider that the master fault responsible for the elastic and brittle deformation in the hanging-wall upon flexural-slip folding should involve short-lived periodic slip events (stick-slip behaviour) separated by near-continuously long-period of slow displacement (stable sliding behaviour) (Azzaro et al., 2020). On the other hand, the two significant *reverse-drag* flexural-slip events reported to occur during the late Pleistocene (MIS-3?) and Middle Holocene are followed by sharp lake shrinkage. This is evidenced by basin-scale erosional surfaces followed by deposition of fluvial and sheetflood-dominated fan deposits, which form the subunits **U2-a** and **U3-b**, respectively. This episodic instantaneous lake shrinkage is unambiguously caused by tilting (Strecker et al., 1999) and even

localised uplift of the hanging-wall upon flexural-slip folding. According to Delogkos et al. (2022), it is possible to estimate the rotation angle of the host bed (angle of tilting in this case, **θ**) associated with flexural-slip of hanging-wall *reverse-drag*, given the involved average bed thickness (above the bed-parallel slip surface, **t**) and the magnitude of the BPS (**s**), such that:

$$s = tan\,\theta * t \qquad 1)$$

Given the thickness of the host subunit **U1-b**, at around 1 m, and the magnitude of the BPS that is inferred from the dip separation of horizon markers from the domino model, about 12 cm, an angular amount of tilting of about 6° is required in order to drive the observed BPS upon the late Pleistocene (MIS-3?) flexural event. Besides, while this modelled relationship is dedicated to BPS associated with, but not restricted to, *reverse-drag* flexural-slip, the average amount of dip separation accommodated by the *subsidiary normal faults* (ca. 1 m) upon the Middle Holocene flexural event is consistent with the bed thickness of the involved sediment (ca. 10m) and the observed angle of bed rotation (θ ≈ 7°) (Figs. 3 and 10A).

Based on these findings, it is suggested that the two *reverse-drag* folding events observed in the basin would have controlled the temporary base level fall upon tilting and uplifting and are contemporaneous with, and genetically related to, regional-scale episodes of significant displacement that provide more clastic material from the damage zones (wall damage zones) of major strike-slip and reverse faults (Kim et al., 2004; Wibberley et al., 2008). Between these tectonic episodes, and accounting also for other prominent controls (e.g., climate), the lake had been becoming more extended into which a lacustrine-dominated nearshore environment was prone to develop (**U1-a**, **U1-b**, **U2-b**, **U2-c**, **U3-a**), although with episodic liquidization deformation that is inferred to be earthquake-triggered.

5.2.2 Scaling relationships: Spatial and temporal basin-scale implications

Based on indirect evidence from field observation (e.g., scarp, damage zone, alluvial fan head, Figs. 3B and 10B) and geometric considerations, the master fault bounding the concerned half-graben has been delineated and considered to be an Andersonian fault, although with slightly curved geometry; a progressive decrease in dip from 60° to 30° is required to control the geometry observed far from the fault (i.e., the position of the depocentre, localised reverse slope). By admitting this departure reasoning, it is possible to infer unknown geometric entities from known ones as they are considered to be kinematically interdependent and contribute all to forming the final structural morphology. Indeed, based on fractal (i.e., scale-independent) analysis of several normal fault examples, Doutsos and Koukouvelas (1998) have explicitly demonstrated these relationships between

the geometric entities associated with *reverse-drag* folding. Thus, the hanging-wall reverse-drag radius (or wavelength, **r1**) is directly related to the maximum displacement ($\mathbf{d_{max}}$) along the master fault, such that:

$$log(\boldsymbol{d_{max}}) = 1.02 * log(\boldsymbol{r1}) - 2.1 \qquad 2)$$

Given a *reverse-drag* radius of 1319 m (horizontal distance between the tangent point to the surface of the *reverse-drag* and the master fault, Fig. 10A), the maximum displacement is estimated to be 192 m. Indeed, while considering the *displacement-length* scaling relationship (Cowie and Scholz, 1992), the $\boldsymbol{\gamma = d_{max}/L}$ ratio of ca. 0.06, with a fault length (**L**) of about 3 km, is consistent with the typical values from Earth faults (*see* compilations by Schultz and Fossen, 2002, Fossen, 2020, and, for normal faults, Schultz et al. 2006, 2008). Likewise, a footwall uplift (**u**), which is an unknown geometric entity due to footwall vulnerability to erosion, can be estimated knowing the maximum displacement, such that:

$$log(\boldsymbol{d_{max}}) = 0.99 * log(\boldsymbol{u}) + 1.22 \qquad 3)$$

That is:

$$log(\boldsymbol{u}) = \frac{log(\boldsymbol{d_{max}}) - 1.22}{0.99} \qquad 4)$$

which yields an estimated value of 59 m, compatible with the constructed cross section while accounting for the vertical scale exaggeration and the geomorphology nearing the fault (Fig. 10A). According to these outcomes, it is now possible to estimate the other fault geometric components (Fig. 10A): the maximum hanging-wall subsidence (**s**) is estimated at 124 m; the fault throw (**u**+**s**) approximates 183 m; and the fault heave would contribute to an extension of 100 m, approximately. According to recent compilations for carbonate rocks, and considering the maximum displacement (>100 m), the *displacement-thickness* ($\mathbf{d_{max}}$-**T**) scaling relationship of the fault damage zone follows a power law with an exponent of 0.82, such that: $\boldsymbol{T = 1.6 * d_{max}^{0.82}}$ (*see* Mayolle et al., 2019, Fig. 7), which yields an estimated value of ca. 119 m (Fig. 10A).

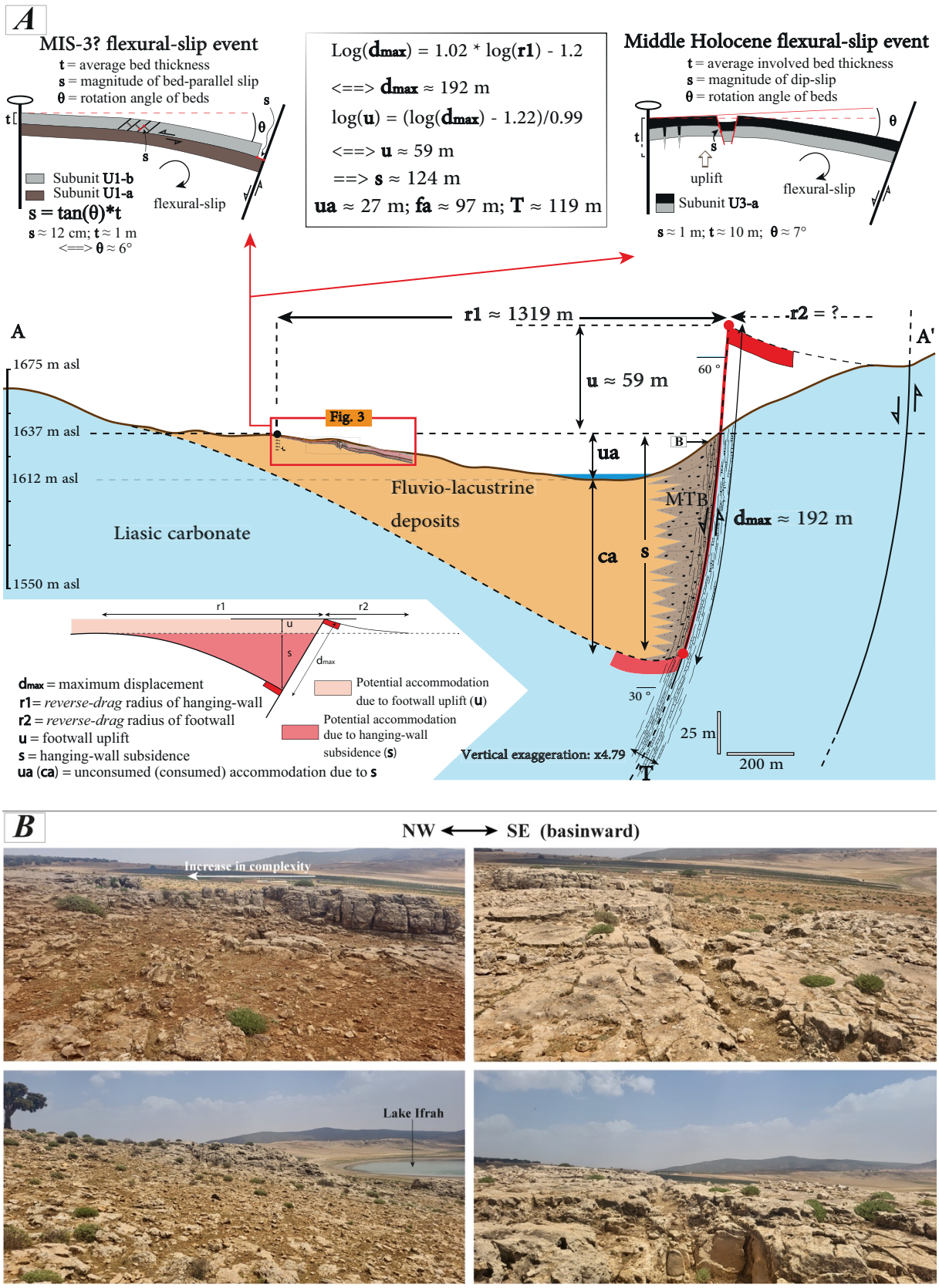


Figure 10. *Scaling relationships between structural entities in the hanging-wall master fault-footwall system (see* ***Figs.*** *2A and 11B for location of the cross section).* ***A****: Drawn diagram portraying the subsident half-graben structure with the master fault and the reverse-drag, as well as the scaling relationships between structural entities forming this half-graben (**s**, and **r1**) and these with the footwall side of the master fault (**u**, **r2**, **dmax**) according to Doutsos and Koukouvelas (1998). The two flexural-slip events with (Middle Holocene) or without (MIS-3?) an uplift component are shown; the equation that*

*relates **s** with **θ**, and **t** is from Delogkos et al. (2022). Because of the interference with other border basin faults (such as the one shown on the right side), the reverse-drag radius of the footwall (**r2**) was not calculated. **B**: Field views revealing the master-fault-related damage zone on the hanging-wall side (see **Fig. 3B** for location). Note the variation in the damage zone complexity towards the fault core (i.e., NW, see the top-left picture); the fault core was not tracked due to access limitation. **T**: damage zone thickness; **ua (ca):** unconsumed (consumed) accommodation, respectively, due to the hanging-wall collapse (**s**); MTB: mass transport breccia.*

The maximum subsidence (**s**) defines the maximum accommodation space due to hanging-wall collapse in interior basins (Catuneanu, 2017). Besides, it is recognised that the rate of subsidence overcomes that of sedimentation by ca. 28 % [(**ua**/**s**)*100, Fig. 10A, where **ua** refers to the unconsumed accommodation], thus conditioning an underfilled basin end-member (*sensu* Carroll and Bohacs, 1999 and Bohacs et al., 2000), controlled principally by tectonic subsidence (Kelts, 1988). Referring to the sedimentary core retrieved from the NW margin of the lake (Rhoujjati et al., 2010), and given the provided distances and time control (ca. 9 m of sediments deposited between ca. 29 and 5 ka. cal BP.), a maximum consumed accommodation space (**ca**, Fig. 10A) of about 97 m, and the fact that this part of the lake is near the depocentre (placed within the main direction of the lake, *see* location Fig. 2B) and not subjected to erosion (as opposed to the herein studied south-western shoreline), it is assumed that the sedimentation in the basin would be initiated approximately at 260 ka BP. However, while accounting for potential pervasive lake droughts or sedimentation hiatuses, the timing of sedimentation initiation must be considered older. Regardless of what it is suspected, the timing of the basin initiation that would have been first accommodated by master faults other than the one dealt with herein (e.g., the SW border basin fault that seems to be dormant for a while) should be further older. In fact, it is assumed that the rhomboidal shape of the basin (the master Ifrah Basin) would have been created earlier, then superimposed by the herein concerned half-graben structure (thus considered to be hierarchically a subsidiary basin, Fig. 11D) that would have accommodated most of the extension since at least 260 kyr BP.

5.2.3 Regional-scale neotectonic implications

Continental basins associated with major strike-slip faults (transtensional regime) are largely considered as a sort of large-scale damage zones refer to as linking- (e.g., pull-apart basin) or tip-damage zone (normal faults, large-scale equivalents of wing cracks) (Kim and Sanderson, 2006; Choi et al., 2016). Although it is observed from a nearby example (*stepover*, Lake Aoua basin, Fig. 11A), normal faulting due to stress concentration in releasing *bends* or *stepovers* (Cunningham and Mann, 2007) is easily discarded in the case of the Ifrah Basin since this neither involves a curvature (or bend) of the associated fault (TTF), nor a slip transfer between two major strike-slip faults. Alternatively, we assume that the Ifrah Basin belongs to a dilational quadrant of the major strike-slip fault, TTF, at a tip-

damage region (Reches and Lockner, 1994; Kim and Sanderson, 2006). Indeed, map scale observations from satellite imaging reveal typical structures with high and low angles (normal faults and horsetail splays with synthetic motion, respectively), relative to the major fault, that are reported to develop at the tip of strike-slip in the dilational quadrant (*see* examples in Kim et al., 2006) (Fig. 11A, C). Slightly far from the inferred dilational quadrant, the exact fault tip location appears to be linked to the contractional quadrant where thrust faults develop (large-scale equivalents of solution surfaces) at a very high angle to the strike-slip fault (Fig. 11A, C). Accordingly, while the TTF is reported to be a lithospheric-scale tectonic structure (Miller and Becker, 2014), inherited earlier from the Variscan orogeny (Piqué et al., 1987; Charrière, 1990) and later reactivated from the synrift Jurassic normal faults during the Cenozoic Africa-Eurasia convergence (Gomez et al., 2000; Piqué et al., 2002), and mapped to crosscut lengthwise the entire Middle Atlas (Martin, 1981; Fig. 1, *see* section 2), we hereby suggest structural isolation of the northern part of this major tectonic feature where most of the displacement would have been accommodated. Therefore, considering the seismotectonic inferences from the studied section, it would be plausible to conclude that the basin-scale hanging-wall flexural events that separate several regional-scale high-magnitude earthquake-induced SSDSs (at least two given the reported results) suggest that the residual strike-slip displacement is transferred to the NE master fault after several co-seismic ruptures along the isolated segment of the TTF. Besides, the onset of this structural reorganisation of the TTF must be synchronous with the initiation of the Ifrah Basin. Indeed, a combination of a variety of outcomes from (i) geodetic constraints (Fadil et al., 2006; Tahayt et al., 2008; Vernant et al., 2010; Koulali et al., 2011), (ii) mantle dynamic considerations beneath the Middle Atlas and the Nubia-Iberia convergence zone (Fullea et al., 2010; Missenard and Cadoux, 2012; Gutscher et al., 2012; Alpert et al., 2013; Bezada et al., 2013, 2014; Miller et al., 2013; Kaislaniemi and van Hunen, 2014; Palomeras et al., 2014; Villaseñor et al., 2015), and (iii) petrographic insights regarding the Middle Atlas volcanism during the Quaternary (Harmand and Cantagrel, 1984; El Azzouzi et al., 2010; Bosch et al., 2014), collectively highlight a striking relationship between the Ifrah Basin initiation and the geodynamic context that implies interdependently (i) lithosphere thinning, (ii) slab rollback, and (iii) mantle lithosphere-derived alkaline volcanism; as being slightly moving out from the core results of the paper, the full discussion of these aspects with reference to more key publications is moved to the supplement material.

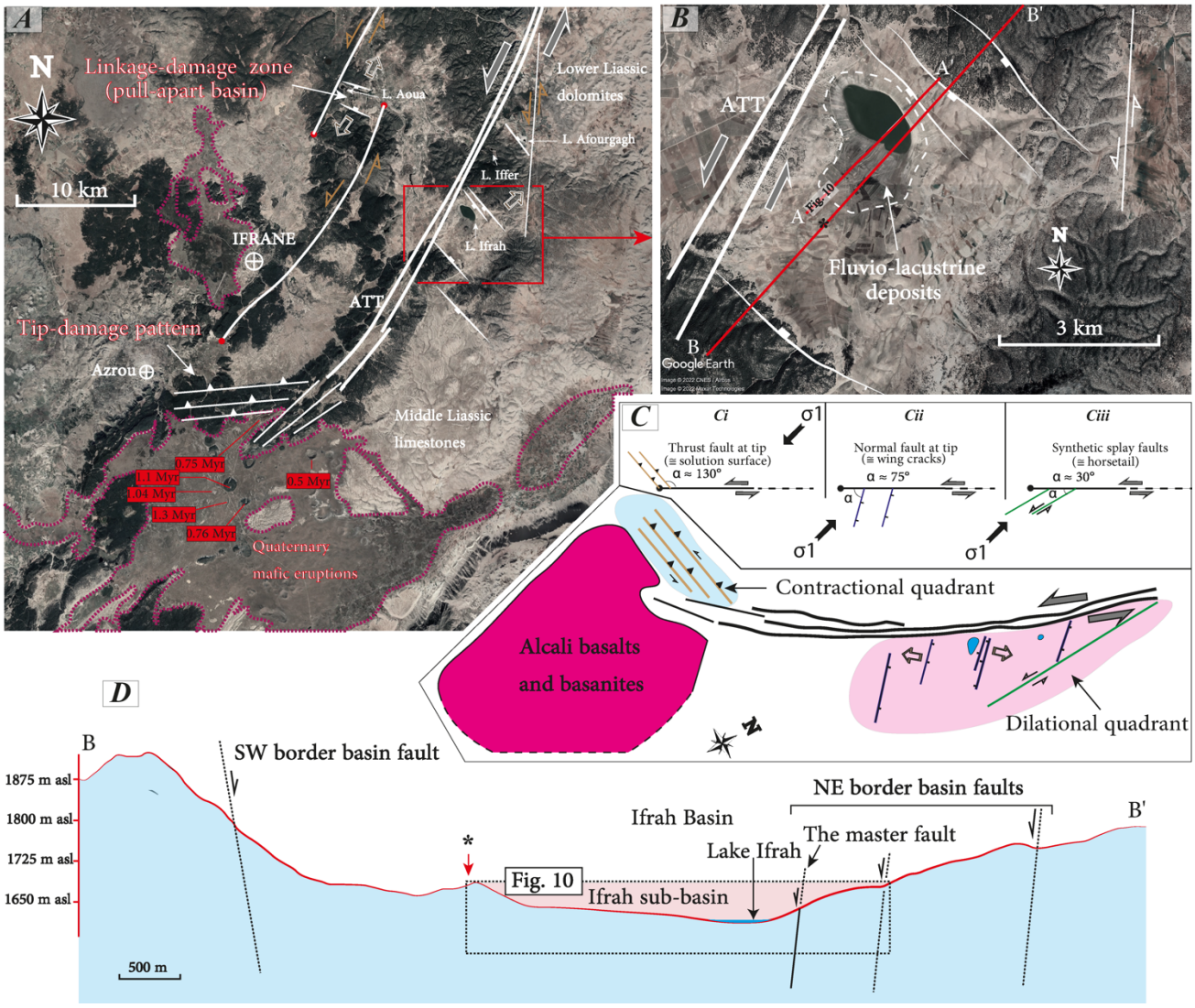


***Figure 11**. Map- and basin-scale structural considerations pointing to a mechanism for basin initiation. **A**: Satellite image (Google Earth pro, 2016) portraying an example of a transtensional regime localised in a linking-damage zone forming a pull-apart basin (Lake Aoua) and a transpersonal regime at the herein suggested tip-damage zone (contractional quadrant). Note the location of the Ifrah basin and the contractional quadrant relative to the position of the area covered by the Quaternary volcanism (Azrou field). **B**: Satellite image of the Ifrah Basin outlined in (**A**) showing the main master structures, as well as delineating the fluvio-lacustrine deposits and the location of the cross section shown in **Figure 10A**. **C**: Drawn diagram portraying a proposed model for the main structures associated to the Tizi n'Tretten Fault (TTF) and delineated in (**A**). The large-scale structures and laboratory-scale structures that develop at tip damage-zones can be compared; thrusts developing in the contractional quadrant are similar to solution surfaces (**Ci**); normal faults (**Cii**) and synthetic splay faults (**Ciii**) developing in the dilational quadrant are similar to wing cracks and horsetail, respectively. The basin initiation and the position of the tip-damage zone is considered to be at least partly linked to the volcanic eruption sealing locally the TTF; this mafic volcanism accounts for the location of the dilational quadrant. **D**: Cross section outlined in (**B**) highlighting the subsidiary nature of the half-graben structure (shown in **Fig. 10A**) relative to the master Ifrah Basin.*

6 Conclusions

'Ductile' and brittle SSDSs have been recognised in a typical structural setting involving a *reverse-drag* folding driven by a border basin normal fault (the master fault). This latter appears to accommodate most of the recent extension in the basin, creating a half-graben structure that provided

space for lacustrine sediments to develop. The master basin where the half-graben is superimposed is connected to a major strike-slip fault (the Tizi n'Tretten fault, TTA).

Three allostratigraphic units, having deposited since MIS-3, was raised from the studied outcrop (south-western lake margin). They reveal changes in sedimentation patterns and are separated by relatively long-term subareal unconformities. 'Ductile' deformations include *load structures* and *water-escape structures*, formed during deposition of the middle unit (**U2**) and are framed between two *reverse-drag* flexure events that resulted in brittle deformations, namely (i) *bed-parallel slip* and associated *domino-style faults*, and (ii) *subsidiary grabens* and associated *neptunian dykes*, formed during late Pleistocene (unit **U1**, MIS-3?) and Middle Holocene (unit **U3**), respectively. 'Ductile' SSDSs that form upon liquidization (thixotropy, liquefaction, and localised fluidization) are inferred to be seismically-induced.

Given the *reverse-drag* radius, scaling relationships were applied to the master fault, which is inferred to be Andersonian with mildly listric geometry. Calculation results allowed drawing dimensions of the structural entities that characterise the *hanging-wall-master fault-footwall* system (e.g., footwall uplift, hanging-wall subsidence, damage-zone thickness). According to these results and considering the time control on deposition at the vicinity of the depocentre, it is inferred that the half-graben structure (Ifrah subsidiary basin) would have been initiated at least since 260 kyr BP and hence that of the master Ifrah Basin must be earlier. Based on large-scale structural observations, the master Ifrah Basin belongs to a dilational quadrant of the major strike-slip fault, TTF, at a tip-damage region. As such, we highlight structural isolation of the northern segment of the TTF. Interestingly, the initiation thereof is seen to be linked to the geodynamic context between Nubia and Iberia.

Supplement material

According to the discussion in subsection 5.2.3., the onset of the structural reorganisation of the Tizi n'Tretten Fault must be synchronous with the initiation of the Ifrah Basin. Two pieces of evidence, which seem to be independent (but see below), may be invoked in explaining this first-time quoted contention.

Present-day plate motion indicated by geodetic constraints suggests a southward drift component (≈ 3 mm yr^{-1}) of the Rif and northern part of the Middle Atlas in a fixed Nubia frame (Fadil et al., 2006; Tahayt et al., 2008; Vernant et al., 2010; Koulali et al., 2011) as a possible result of a southward-directed rollback of a residual slab beneath the Alboran-Rif region (Vernant et al., 2010; Bezada et al., 2013; Palomeras et al., 2014) in a pattern of toroidal flow-dominated subduction (Gutscher et al., 2012; Alpert et al., 2013; Miller et al., 2013); the trench retreat velocity of the Alboran

slab remains however below the slow velocity of the Nubia-Iberia convergence, Since late Miocene (Peral et al., 2022). This motion is approximately normal to the present-day direction of Nubia-Iberia convergence (4.3 ± 0.5 mm yr^{-1} at an azimuth of 116 ± 6°, McClusky et al., 2003). Palaeostress constraints from micro-tectonic analysis show near consistency with this present-day state for the Pliocene-Quaternary (Ait Brahim et al., 2002; Hinaje, 2004), although with a possible counter-clockwise rotation of 20° (i.e., a southward drift of the Euler pole) since ca. 3 Myr (Calais et al., 2003). In fact, the south-westward motion of the west-side block of the TTF is explicitly confirmed from GPS constraints with an average interseismic velocity of ca. 2 mm yr^{-1} (Chalouan et al., 2014, Fig. 8). It is, therefore, plausible to conclude that a considerable amount of strain upon the Nubia-Iberia convergence would be accommodated in the northern part of the Middle Atlas by SW-NE trending faults as supposed to act as lateral ramps (including the TTF and NMAF, Fig. 1) in foreland domain (Chalouan et al., 2014). This is consistent with our sedimentological data as well as industrial and historical seismicity in the region that suggests a conspicuous concentration of seismic foci in the transition between the Rif and Middle Atlas (Medina and Cherkaoui, 1991; Poujol et al., 2017).

Another possible explanation that seems to be plausible in conditioning the purported structural isolation of the northern segment of the TTF may invoke local "tectonic insulation". In fact, several pulses of intraplate ("anorogenic") igneous activity have been reported to occur since the Early Tertiary in the circum-Mediterranean region (Lustrino and Wilson, 2007). The Middle Atlas Volcanic Province with alkaline intraplate geochemical affinity is the largest and youngest volcanic area in Morocco (Frizon de Lamotte et al., 2008; Bosch et al., 2014; Fig. 1). They consist mainly of alkali basalts and basanites giving way to several strombolian cones and mares at the surface, following an SSE-NNW and SE-NW trends (Fig. 1). They are considered as derived from low-degree partial melting of a metasomatized thinned mantle lithosphere base (El Azzouzi et al., 2010; Bosch et al., 2014), below which the asthenosphere shows conspicuously low *P*-wave (Fullea et al., 2010; Bezada et al., 2014; Villaseñor et al., 2015) and *S*-wave velocity anomaly (Palomeras et al., 2014). Excepting some patchy earlier eruptions, the main recent volcanic pulse in the Middle Atlas (Azrou field, about 20 km south of the Ifrah Basin, Fig. 11A) lasts between 1.3 and 0.5 Myr according to the K-Ar dating method (Harmand and Cantagrel, 1984; El Azzouzi et al., 2010). Therefore, considering the location (crosscutting normally the TTF, Figs. 1 and 11A), the age and the mafic/incompatible-rich nature (i.e., denser, thus yielding higher shear strength) of the Quaternary volcanism, it is suggested that a sort of "tectonic insulation" would be created as a result of a local decrease in anisotropy and crustal weakness. In other words, sealing through the freezing of molten mafic material within lithospheric-

scale discontinuities (including locally the TTF and the SE-NW-trending grabens initiated through the Miocene extensional phase, Hinaje et al., 2019) would have strengthened locally this tectonic features and made the surrounding area behaving as a resistant block, thus decreasing crustal weakness locally. As such, regional stress would be transferred northward from the volcanic field without, or with minor, strain accommodation ("tectonic insulation"), giving way to a northern isolated segment (but attached to the volcanic province) of the TTF. In fact, minor strain accommodation is suggested from the occurrence of some calcite-filled openings with slight normal motion (mode I-III fractures) aligning with the far-field σ1 (NNW-SSE) that involve maar-derived deposits (Hinaje et al., 2019). Considering the oblique direction of the TTF relative to the far-field maximum compressive stress, the "tectonic insulation" assumption account for both the slightly distant location of the dilational quadrant (where the Ifrah Basin were initiated) relative to the inferred tip and the location of the inferred compressional quadrant Fig. 11A, C).

Finally, even though these two aforementioned mechanisms for the structural isolation assumption appear to be independent, they might be indirectly linked to each other through a common genetic process. In fact, the generation of the partial melting that lies beneath the Azrou volcanic field was demonstrated to be related to a piecewise delamination of the subcontinental mantle lithosphere (Bezada et al., 2014), giving way to a maximum lithosphere thinning (Fullea et al., 2010). Otherwise, although Edge-Driven Convection (EDC) seems to be a plausible mechanism to explain lithosphere thinning and mantle melting regarding the regional geological setting (presence of the West African Craton, Missenard and Cadoux, 2012; Kaislaniemi and van Hunen, 2014), mantle seismic imaging beneath the Middle Atlas did not support this and, instead, it was suggested that the EDC is more likely to drive the regional upwarping in the Anti Atlas domain (*see* Bezada et al., 2014). According to Bezada et al. (2014), besides the small contribution of tectonic shortening, instability of the mantle lithosphere would be enhanced by rollback-related toroidal flow around the Alboran slab by helping focus mantle upwelling beneath the Middle Atlas (*see* for comparison seismic imaging in Bezada et al., 2014, and 3D-modeling results in Piromallo et al., 2006). Subcrustal eclogite loading through the freezing of molten basalts as a result of the asthenosphere upwelling is likely to further enhance the lithosphere instability and initiate the delamination (Krystopowicz and Currie, 2013; Bezada et al., 2014). Therefore, we report a possible example where the initiation of a strike-slip related basin would follow a complex tectonic process that is directly or indirectly related to both horizontal lithospheric motion and vertical asthenospheric upwelling, which are both driven by slab rollback in a slow plate convergence boundary.

References (supplement materiel)

Ait Brahim, L., Chotin, P., Hinaj, S., Abdelouafi, A., El Adraoui, A., Nakcha, C., Dhont, D., Charroud, M., Sossey Alaoui, F., Amrhar, M., Bouaza, A., Tabyaoui, H., Chaouni, A., 2002. Paleostress evolution in the Moroccan African margin from Triassic to Present. Tectonophysics 357, 187–205. https://doi.org/10.1016/S0040-1951(02)00368-2

Alpert, L.A., Miller, M.S., Becker, T.W., Allam, A.A., 2013. Structure beneath the Alboran from geodynamic flow models and seismic anisotropy. Journal of Geophysical Research: Solid Earth 118, 4265–4277. https://doi.org/10.1002/jgrb.50309

Bezada, M.J., Humphreys, E.D., Davila, J. m., Carbonell, R., Harnafi, M., Palomeras, I., Levander, A., 2014. Piecewise delamination of Moroccan lithosphere from beneath the Atlas Mountains. Geochemistry, Geophysics, Geosystems 15, 975–985. https://doi.org/10.1002/2013GC005059

Bezada, M.J., Humphreys, E.D., Toomey, D.R., Harnafi, M., Dávila, J.M., Gallart, J., 2013. Evidence for slab rollback in westernmost Mediterranean from improved upper mantle imaging. Earth and Planetary Science Letters 368, 51–60. https://doi.org/10.1016/j.epsl.2013.02.024

Bosch, D., Maury, R.C., El Azzouzi, M., Bollinger, C., Bellon, H., Verdoux, P., 2014. Lithospheric origin for Neogene–Quaternary Middle Atlas lavas (Morocco): Clues from trace elements and Sr–Nd–Pb–Hf isotopes. Lithos 205, 247–265. https://doi.org/10.1016/j.lithos.2014.07.009

Calais, E., DeMets, C., Nocquet, J.-M., 2003. Evidence for a post-3.16-Ma change in Nubia–Eurasia–North America plate motions? Earth and Planetary Science Letters 216, 81–92. https://doi.org/10.1016/S0012-821X(03)00482-5

Chalouan, A., Gil, A.J., Galindo-Zaldívar, J., Ahmamou, M., Ruano, P., de Lacy, M.C., Ruiz-Armenteros, A.M., Benmakhlouf, M., Riguzzi, F., 2014. Active faulting in the frontal Rif Cordillera (Fes region, Morocco): Constraints from GPS data. Journal of Geodynamics 77, 110–122. https://doi.org/10.1016/j.jog.2014.01.002

El Azzouzi, M., Maury, R.C., Bellon, H., Youbi, N., Cotten, J., Kharbouch, F., 2010. Petrology and K-Ar chronology of the Neogene-Quaternary Middle Atlas basaltic province, Morocco. Bulletin de la Societe Geologique de France 181, 243–257. https://doi.org/10.2113/gssgfbull.181.3.243

Fadil, A., Vernant, P., McClusky, S., Reilinger, R., Gomez, F., Ben Sari, D., Mourabit, T., Feigl, K., Barazangi, M., 2006. Active tectonics of the western Mediterranean: Geodetic evidence for rollback of a delaminated subcontinental lithospheric slab beneath the Rif Mountains, Morocco. Geology 34, 529–532. https://doi.org/10.1130/G22291.1

Frizon de Lamotte, D., Zizi, M., Missenard, Y., Hafid, M., Azzouzi, M.E., Maury, R.C., Charrière, A., Taki, Z., Benammi, M., Michard, A., 2008. The Atlas System, in: Michard, André, Saddiqi, O., Chalouan, A.,

Lamotte, D.F. de (Eds.), Continental Evolution: The Geology of Morocco: Structure, Stratigraphy, and Tectonics of the Africa-Atlantic-Mediterranean Triple Junction, Lecture Notes in Earth Sciences. Springer, Berlin, Heidelberg, pp. 133–202. https://doi.org/10.1007/978-3-540-77076-3_4

Fullea, J., Fernàndez, M., Afonso, J.C., Vergés, J., Zeyen, H., 2010. The structure and evolution of the lithosphere–asthenosphere boundary beneath the Atlantic–Mediterranean Transition Region. Lithos, The lithosphere/asthenosphere boundary: Nature, formation and evolution 120, 74–95. https://doi.org/10.1016/j.lithos.2010.03.003

Gutscher, M.-A., Dominguez, S., Westbrook, G.K., Le Roy, P., Rosas, F., Duarte, J.C., Terrinha, P., Miranda, J.M., Graindorge, D., Gailler, A., Sallares, V., Bartolome, R., 2012. The Gibraltar subduction: A decade of new geophysical data. Tectonophysics 574–575, 72–91. https://doi.org/10.1016/j.tecto.2012.08.038

Harmand, C., Cantagrel, J.M., 1984. Le volcanisme alcalin tertiaire et quaternaire du moyen atlas (Maroc): chronologie K/Ar et cadre géodynamique. Journal of African Earth Sciences (1983) 2, 51–55. https://doi.org/10.1016/0899-5362(84)90019-8

Hinaje, S., 2004. Tectonique cassante et paléochamps de contraintes dans le Moyen Atlas et le Haut Atlas central (Midelt-Errachidia) depuis le Trias jusqu'à l'Actuel. Université Mohammed V, Rabat.

Hinaje, S., El Fartati, M., Yaagoub, D., Amrani, S., Gharmane, Y., El Fellah Idrissi, B., 2019. Paleocontraintes et contexte tectonique de mise en place du volcanisme alcalin neogene et quaternaire du Moyen Atlas (Maroc). European Scientific Journal May 448–466.

Kaislaniemi, L., van Hunen, J., 2014. Dynamics of lithospheric thinning and mantle melting by edge-driven convection: Application to Moroccan Atlas mountains. Geochemistry, Geophysics, Geosystems 15, 3175–3189. https://doi.org/10.1002/2014GC005414

Koulali, A., Ouazar, D., Tahayt, A., King, R.W., Vernant, P., Reilinger, R.E., McClusky, S., Mourabit, T., Davila, J.M., Amraoui, N., 2011. New GPS constraints on active deformation along the Africa–Iberia plate boundary. Earth and Planetary Science Letters 308, 211–217. https://doi.org/10.1016/j.epsl.2011.05.048

Krystopowicz, N.J., Currie, C.A., 2013. Crustal eclogitization and lithosphere delamination in orogens. Earth and Planetary Science Letters 361, 195–207. https://doi.org/10.1016/j.epsl.2012.09.056

Lustrino, M., Wilson, M., 2007. The circum-Mediterranean anorogenic Cenozoic igneous province. Earth-Science Reviews 81, 1–65. https://doi.org/10.1016/j.earscirev.2006.09.002

McClusky, S., Reilinger, R., Mahmoud, S., Ben Sari, D., Tealeb, A., 2003. GPS constraints on Africa (Nubia) and Arabia plate motions. Geophysical Journal International 155, 126–138. https://doi.org/10.1046/j.1365-246X.2003.02023.x

Medina, F., Cherkaoui, T.E., 1991. Focal mechanisms of the Atlas earthquakes, and tectonic implications. Geologische Rundschau 80, 639–648. https://doi.org/10.1007/bf01803691

Miller, M.S., Allam, A.A., Becker, T.W., Di Leo, J.F., Wookey, J., 2013. Constraints on the tectonic evolution of the westernmost Mediterranean and northwestern Africa from shear wave splitting analysis. Earth and Planetary Science Letters 375, 234–243. https://doi.org/10.1016/j.epsl.2013.05.036

Missenard, Y., Cadoux, A., 2012. Can Moroccan Atlas lithospheric thinning and volcanism be induced by Edge-Driven Convection?: Edge-Driven Convection in Morocco? Terra Nova 24, 27–33. https://doi.org/10.1111/j.1365-3121.2011.01033.x

Palomeras, I., Thurner, S., Levander, A., Liu, K., Villasenor, A., Carbonell, R., Harnafi, M., 2014. Finite-frequency Rayleigh wave tomography of the western Mediterranean: Mapping its lithospheric structure. Geochemistry, Geophysics, Geosystems 15, 140–160. https://doi.org/10.1002/2013GC004861

Peral, M., Fernàndez, M., Vergés, J., Zlotnik, S., Jiménez-Munt, I., 2022. Numerical modelling of opposing subduction in the Western Mediterranean. Tectonophysics 830, 229309. https://doi.org/10.1016/j.tecto.2022.229309

Piromallo, C., Becker, T.W., Funiciello, F., Faccenna, C., 2006. Three-dimensional instantaneous mantle flow induced by subduction. Geophysical Research Letters 33. https://doi.org/10.1029/2005GL025390

Poujol, A., Ritz, J.-F., Vernant, P., Huot, S., Maate, S., Tahayt, A., 2017. Which fault destroyed Fes city (Morocco) in 1755? A new insight from the Holocene deformations observed along the southern border of Gibraltar arc. Tectonophysics 712, 303–311.

Tahayt, A., Mourabit, T., Rigo, A., Feigl, K.L., Fadil, A., McClusky, S., Reilinger, R., Serroukh, M., Ouazzani-Touhami, A., Sari, D.B., Vernant, P., 2008. Mouvements actuels des blocs tectoniques dans l'arc Bético-Rifain à partir des mesures GPS entre 1999 et 2005. Comptes Rendus Geoscience 340, 400–413. https://doi.org/10.1016/j.crte.2008.02.003

Vernant, P., Fadil, A., Mourabit, T., Ouazar, D., Koulali, A., Davila, J.M., Garate, J., McClusky, S., Reilinger, R., 2010. Geodetic constraints on active tectonics of the Western Mediterranean: Implications for the kinematics and dynamics of the Nubia-Eurasia plate boundary zone. Journal of Geodynamics, WEGENER 2008 - Proceedings of the 14th General Assembly of Wegener 49, 123–129. https://doi.org/10.1016/j.jog.2009.10.007

Villaseñor, A., Chevrot, S., Harnafi, M., Gallart, J., Pazos, A., Serrano, I., Córdoba, D., Pulgar, J.A., Ibarra, P., 2015. Subduction and volcanism in the Iberia–North Africa collision zone from tomographic images of the upper mantle. Tectonophysics, Special issue on Iberia geodynamics: An integrative approach from the Topo-Iberia framework 663, 238–249. https://doi.org/10.1016/j.tecto.2015.08.042

Acknowledgment

The authors cordially thank Prof. Ian Alsop and the anonymous reviewer for the fruitful and constructive review that helped improve the quality of the manuscript and Prof. Massimo Moretti for efficient editorial handling. KA and BA as principal investigators thank Dr. Stratos Delogkos for his fruitful discussion and recommendations about BPS and associated domino-faults. Prof. Haakon Fossen is gratefully acknowledged for his extensive efforts to disseminate his expertise among the early-career research community.

References (article)

Ait Brahim, L., Chotin, P., Hinaj, S., Abdelouafi, A., El Adraoui, A., Nakcha, C., Dhont, D., Charroud, M., Sossey Alaoui, F., Amrhar, M., Bouaza, A., Tabyaoui, H., Chaouni, A., 2002. Paleostress evolution in the Moroccan African margin from Triassic to Present. Tectonophysics 357, 187–205. https://doi.org/10.1016/S0040-1951(02)00368-2

Alfaro, P., Delgado, J., Estévez, A., Molina, J., Moretti, M., Soria, J., 2002. Liquefaction and fluidization structures in Messinian storm deposits (Bajo Segura Basin, Betic Cordillera, southern Spain). International Journal of Earth Sciences 91, 505–513.

Allen, J.R.L., 1986. Earthquake magnitude-frequency, epicentral distance, and soft-sediment deformation in sedimentary basins. Sedimentary Geology 46, 67–75. https://doi.org/10.1016/0037-0738(86)90006-0

Allen, J.R.L., 1982. Sedimentary structures, their character and physical basis. Elsevier.

Allen, J.R.L., 1977. The possible mechanics of convolute lamination in graded sand beds. Journal of the Geological Society 134, 19–31.

Alpert, L.A., Miller, M.S., Becker, T.W., Allam, A.A., 2013. Structure beneath the Alboran from geodynamic flow models and seismic anisotropy. Journal of Geophysical Research: Solid Earth 118, 4265–4277. https://doi.org/10.1002/jgrb.50309.

Alsop, G.I., Marco, S., Levi, T., 2022. Recognising surface versus sub-surface deformation of soft-sediments: Consequences and considerations for palaeoseismic studies. Journal of Structural Geology 154, 104493. https://doi.org/10.1016/j.jsg.2021.104493.

Alsop, G.I., Marco, S., Weinberger, R., Levi, T., 2016. Sedimentary and structural controls on seismogenic slumping within mass transport deposits from the Dead Sea Basin. Sedimentary Geology, The environmental significance of soft-sediment deformation 344, 71–90. https://doi.org/10.1016/j.sedgeo.2016.02.019.

Alsop, G.I., Weinberger, R., Marco, S., 2018. Distinguishing thrust sequences in gravity-driven fold and thrust belts. Journal of Structural Geology 109, 99–119. https://doi.org/10.1016/j.jsg.2018.01.005.

Alsop, G.I., Weinberger, R., Marco, S., Levi, T., 2020. Bed-parallel slip: Identifying missing displacement in mass transport deposits. Journal of Structural Geology 131, 103952. https://doi.org/10.1016/j.jsg.2019.103952.

Anderson, E.M., 1951. The dynamics of faulting and dyke formation with applications to Britain: Edinburgh. Oliver and Boyd 206.

Anketell, J.M., Ceg\la, J., Dżu\lyński, S., 1970. On the deformational structures in systems with reversed density gradients, in: Annales Societatis Geologorum Poloniae. pp. 3–30.

Arboleya, M.L., Teixell, A., Charroud, M., Julivert, M., 2004. A structural transect through the High and Middle Atlas of Morocco. Journal of African Earth Sciences, Key Points on African Geology 39, 319–327. https://doi.org/10.1016/j.jafrearsci.2004.07.036.

Axen, G.J., 1988. The geometry of planar domino-style normal faults above a dipping basal detachment. Journal of Structural Geology 10, 405–411. https://doi.org/10.1016/0191-8141(88)90018-1.

Aydin, A., Du, Y., 1995. Surface rupture at a fault bend: the 28 June 1992 Landers, California, earthquake. Bulletin of the Seismological Society of America 85, 111–128. https://doi.org/10.1785/BSSA0850010111.

Azzaro, R., Bonforte, A., D'Amico, S., Guglielmino, F., Scarfì, L., 2020. Stick-slip vs. stable sliding fault behaviour: A case-study using a multidisciplinary approach in the volcanic region of Mt. Etna (Italy). Tectonophysics 790, 228554. https://doi.org/10.1016/j.tecto.2020.228554.

Barnett, J.A.M., Mortimer, J., Rippon, J.H., Walsh, J.J., Watterson, J., 1987. Displacement Geometry in the Volume Containing a Single Normal Fault1. AAPG Bulletin 71, 925–937. https://doi.org/10.1306/948878ED-1704-11D7-8645000102C1865D.

Basilone, L., Sulli, A., Gasparo Morticelli, M., 2016. The relationships between soft-sediment deformation structures and synsedimentary extensional tectonics in Upper Triassic deep-water carbonate succession (Southern Tethyan rifted continental margin — Central Sicily). Sedimentary Geology, The environmental significance of soft-sediment deformation 344, 310–322. https://doi.org/10.1016/j.sedgeo.2016.01.010.

Beeler, N.M., Lockner, D.L., Hickman, S.H., 2001. A Simple Stick-Slip and Creep-Slip Model for Repeating Earthquakes and its Implication for Microearthquakes at Parkfield. Bulletin of the Seismological Society of America 91, 1797–1804. https://doi.org/10.1785/0120000096.

Benabbou, M., Alaoui, B.L., Baali, A., 2018. Structures de déformation hydroplastique d'origine sismique dans les dépôts lacustres du Pléistocène supérieur de dayet Iffer (Moyen Atlas, Maroc). Quaternaire. Revue de l'Association française pour l'étude du Quaternaire 29, 295–310.

Berberian, M., Jackson, J.A., Qorashi, M., Talebian, M., Khatib, M., Priestley, K., 2000. The 1994 Sefidabeh earthquakes in eastern Iran: blind thrusting and bedding-plane slip on a growing anticline, and active tectonics of the Sistan suture zone. Geophysical Journal International 142, 283–299. https://doi.org/10.1046/j.1365-246x.2000.00158.x.

Berra, F., Felletti, F., 2011. Syndepositional tectonics recorded by soft-sediment deformation and liquefaction structures (continental Lower Permian sediments, Southern Alps, Northern Italy): stratigraphic significance. Sedimentary Geology 235, 249–263.

Bezada, M.J., Humphreys, E.D., Davila, J. m., Carbonell, R., Harnafi, M., Palomeras, I., Levander, A., 2014. Piecewise delamination of Moroccan lithosphere from beneath the Atlas Mountains. Geochemistry, Geophysics, Geosystems 15, 975–985. https://doi.org/10.1002/2013GC005059.

Bezada, M.J., Humphreys, E.D., Toomey, D.R., Harnafi, M., Dávila, J.M., Gallart, J., 2013. Evidence for slab rollback in westernmost Mediterranean from improved upper mantle imaging. Earth and Planetary Science Letters 368, 51–60. https://doi.org/10.1016/j.epsl.2013.02.024.

Birgenheier, L.P., Horton, B., McCauley, A.D., Johnson, C.L., Kennedy, A., 2017. A depositional model for offshore deposits of the lower Blue Gate Member, Mancos Shale, Uinta Basin, Utah, USA. Sedimentology 64, 1402–1438. https://doi.org/10.1111/sed.12359.

Blair, T.C., McPherson, J.G., 2009. Processes and Forms of Alluvial Fans, in: Parsons, A.J., Abrahams, A.D. (Eds.), Geomorphology of Desert Environments. Springer Netherlands, Dordrecht, pp. 413–467. https://doi.org/10.1007/978-1-4020-5719-9_14.

Bohacs, K.M., Carroll, A.R., Neal, J.E., Mankiewicz, P.J., 2000. Lake-basin type, source potential, and hydrocarbon character: an integrated sequence-stratigraphic-geochemical framework. Lake basins through space and time: AAPG Studies in Geology 46, 3–34.

Bosch, D., Maury, R.C., El Azzouzi, M., Bollinger, C., Bellon, H., Verdoux, P., 2014. Lithospheric origin for Neogene–Quaternary Middle Atlas lavas (Morocco): Clues from trace elements and Sr–Nd–Pb–Hf isotopes. Lithos 205, 247–265. https://doi.org/10.1016/j.lithos.2014.07.009.

Bryant, G., Cushman, R., Nick, K., Miall, A., 2016. Paleohydrologic controls on soft-sediment deformation in the Navajo Sandstone. Sedimentary Geology, The environmental significance of soft-sediment deformation 344, 205–221. https://doi.org/10.1016/j.sedgeo.2016.06.005.

Bryant, G., Monegato, G., Miall, A., 2013. An example of liquefaction-induced interdune sedimentation from the early Jurassic Navajo Sandstone, USA. Sedimentary Geology 297, 50–62. https://doi.org/10.1016/j.sedgeo.2013.09.001.

Carroll, A.R., Bohacs, K.M., 1999. Stratigraphic classification of ancient lakes: Balancing tectonic and climatic controls. Geology 27, 99–102.

Catuneanu, O., 2017. Chapter One - Sequence Stratigraphy: Guidelines for a Standard Methodology, in: Montenari, M. (Ed.), Stratigraphy & Timescales, Advances in Sequence Stratigraphy. Academic Press, pp. 1–57. https://doi.org/10.1016/bs.sats.2017.07.003.

Chalouan, A., Gil, A.J., Galindo-Zaldívar, J., Ahmamou, M., Ruano, P., de Lacy, M.C., Ruiz-Armenteros, A.M., Benmakhlouf, M., Riguzzi, F., 2014. Active faulting in the frontal Rif Cordillera (Fes region, Morocco): Constraints from GPS data. Journal of Geodynamics 77, 110–122. https://doi.org/10.1016/j.jog.2014.01.002.

Chan, M.A., Wheatley, D.F., Okubo, C.H., 2019. Dynamic fluids under pressure on Earth and Mars: Records of soft-sediment deformation 2019, P43F-3521.

Charrière, A., 1990. Héritage hercynien et évolution géody- namique alpine d'une chaîne intracontinentale : le Moyen Atlas au sud-est de Fes (Maroc). Thèse de Doctorat d'État, Université Toulouse III – Paul Sabatier, Toulouse, 589 p.

Charrière, A., Dépêche, F., Feist, M., Grambast-Fessard, N., Jaffrezo, M., Peybernès, B., Ramalho, M., 1994. Microfaunes, microflores etpaléoenvironnements successifs dans la formation d'El Mers (Bathonien-?Callovien) du synclinal de Skoura (Moyen-Atlas, Maroc). Geobios 27, 157–174. https://doi.org/10.1016/S0016-6995(94)80002-2.

Choi, J.-H., Edwards, P., Ko, K., Kim, Y.-S., 2016. Definition and classification of fault damage zones: A review and a new methodological approach. Earth-Science Reviews 152, 70–87. https://doi.org/10.1016/j.earscirev.2015.11.006.

Clifton, H.E., 2006. A Reexamination of Facies Models for Clastic Shorelines. https://doi.org/10.2110/pec.06.84.0293.

Clifton, H.E., Hunter, R.E., Phillips, R.L., 1971. Depositional structures and processes in the non-barred high-energy nearshore. Journal of Sedimentary Research 41, 651–670. https://doi.org/10.1306/74D7231A-2B21-11D7-8648000102C1865D.

Collinson, J., 1994. Sedimentary deformational structures, in: The Geological Deformation of Sediments. Springer, pp. 95–125.

Cowie, P.A., Scholz, C.H., 1992. Displacement-length scaling relationship for faults: data synthesis and discussion. Journal of Structural Geology 14, 1149–1156. https://doi.org/10.1016/0191-8141(92)90066-6.

Cunningham, W.D., Mann, P., 2007. Tectonics of strike-slip restraining and releasing bends. Geological Society, London, Special Publications 290, 1–12. https://doi.org/10.1144/SP290.1

Dasgupta, P., 1998. Recumbent flame structures in the Lower Gondwana rocks of the Jharia Basin, India — a plausible origin. Sedimentary Geology 119, 253–261. https://doi.org/10.1016/S0037-0738(98)00058-X.

Dasgupta, P., Chatterjee, A., 2019. Formation of water-escape structure during shock-induced fluidization: The role of permeability contrast. Journal of Structural Geology 124, 1–7. https://doi.org/10.1016/j.jsg.2019.04.002.

Davis, G.H., Reynolds, S.J., Kluth, C.F., 2011. Structural geology of rocks and regions. John Wiley & Sons.

Delogkos, E., Childs, C., Manzocchi, T., Walsh, J.J., 2018. The nature and origin of bed-parallel slip in Kardia Mine, Ptolemais Basin, Greece. Journal of Structural Geology 113, 115–133. https://doi.org/10.1016/j.jsg.2018.05.015.

Delogkos, E., Roche, V., Walsh, J.J., 2022. Bed-parallel slip associated with normal fault systems. Earth-Science Reviews 230, 104044. https://doi.org/10.1016/j.earscirev.2022.104044.

Dewey, J.F., Helman, M.L., Knott, S.D., Turco, E., Hutton, D.H.W., 1989. Kinematics of the western Mediterranean. Geological Society, London, Special Publications 45, 265–283. https://doi.org/10.1144/GSL.SP.1989.045.01.15.

Doutsos, T., Koukouvelas, I., 1998. Fractal analysis of normal faults in northwestern Aegean area, Greece. Journal of Geodynamics, G.C.P. King 26, 197–216. https://doi.org/10.1016/S0264-3707(97)00052-5.

Dula Jr, W.F., 1991. Geometric models of listric normal faults and rollover folds. AAPG bulletin 75, 1609–1625.

El Azzouzi, M., Maury, R.C., Bellon, H., Youbi, N., Cotten, J., Kharbouch, F., 2010. Petrology and K-Ar chronology of the Neogene-Quaternary Middle Atlas basaltic province, Morocco. Bulletin de la Societe Geologique de France 181, 243–257. https://doi.org/10.2113/gssgfbull.181.3.243..

Ezquerro, L., Moretti, M., Liesa, C.L., Luzón, A., Simón, J.L., 2015. Seismites from a well core of palustrine deposits as a tool for reconstructing the palaeoseismic history of a fault. Tectonophysics 655, 191–205. https://doi.org/10.1016/j.tecto.2015.05.025

Fadil, A., Vernant, P., McClusky, S., Reilinger, R., Gomez, F., Ben Sari, D., Mourabit, T., Feigl, K., Barazangi, M., 2006. Active tectonics of the western Mediterranean: Geodetic evidence for rollback of a delaminated subcontinental lithospheric slab beneath the Rif Mountains, Morocco. Geology 34, 529–532. https://doi.org/10.1130/G22291.1

Fernàndez, M., Torne, M., Vergés, J., Casciello, E., Macchiavelli, C., 2019. Evidence of Segmentation in the Iberia–Africa Plate Boundary: A Jurassic Heritage? Geosciences 9, 343. https://doi.org/10.3390/geosciences9080343

Fossen, H., 2020. Chapter 8 - Fault classification, fault growth and displacement, in: Scarselli, N., Adam, J., Chiarella, D., Roberts, D.G., Bally, A.W. (Eds.), Regional Geology and Tectonics (Second Edition). Elsevier, pp. 119–147. https://doi.org/10.1016/B978-0-444-64134-2.00007-9.

Fossen, H., 2010. Deformation bands formed during soft-sediment deformation: Observations from SE Utah. Marine and Petroleum Geology 27, 215–222. https://doi.org/10.1016/j.marpetgeo.2009.06.005.

Frizon de Lamotte, D., Saint Bezar, B., Bracène, R., Mercier, E., 2000. The two main steps of the Atlas building and geodynamics of the western Mediterranean. Tectonics 19, 740–761. https://doi.org/10.1029/2000TC900003.

Frizon de Lamotte, D., Zizi, M., Missenard, Y., Hafid, M., Azzouzi, M.E., Maury, R.C., Charrière, A., Taki, Z., Benammi, M., Michard, A., 2008. The Atlas System, in: Michard, André, Saddiqi, O., Chalouan, A., Lamotte, D.F. de (Eds.), Continental Evolution: The Geology of Morocco: Structure, Stratigraphy, and Tectonics of the Africa-Atlantic-Mediterranean Triple Junction, Lecture Notes in Earth Sciences. Springer, Berlin, Heidelberg, pp. 133–202. https://doi.org/10.1007/978-3-540-77076-3_4.

Frizon de Lamotte, D.F., Leturmy, P., Missenard, Y., Khomsi, S., Ruiz, G., Saddiqi, O., Guillocheau, F., Michard, A., 2009. Mesozoic and Cenozoic vertical movements in the Atlas system (Algeria, Morocco, Tunisia): An overview. Tectonophysics, The geology of vertical movements of the lithosphere 475, 9–28. https://doi.org/10.1016/j.tecto.2008.10.024.

Fullea, J., Fernàndez, M., Afonso, J.C., Vergés, J., Zeyen, H., 2010. The structure and evolution of the lithosphere–asthenosphere boundary beneath the Atlantic–Mediterranean Transition Region. Lithos, The lithosphere/asthenosphere boundary: Nature, formation and evolution 120, 74–95. https://doi.org/10.1016/j.lithos.2010.03.003.

García-Tortosa, F.J., Alfaro, P., Gibert, L., Scott, G., 2011. Seismically induced slump on an extremely gentle slope (<1°) of the Pleistocene Tecopa paleolake (California). Geology 39, 1055–1058. https://doi.org/10.1130/G32218.1.

Gierlowski-Kordesch, E.H., 2010. Chapter 1 Lacustrine Carbonates, in: Alonso-Zarza, A.M., Tanner, L.H. (Eds.), Developments in Sedimentology, Carbonates in Continental Settings: Facies, Environments, and Processes. Elsevier, pp. 1–101. https://doi.org/10.1016/S0070-4571(09)06101-9.

Gomez, F., Allmendinger, R., Barazangi, M., Er-Raji, A., Dahmani, M., 1998. Crustal shortening and vertical strain partitioning in the Middle Atlas Mountains of Morocco. Tectonics 17, 520–533. https://doi.org/10.1029/98TC01439.

Gomez, F., Barazangi, M., Bensaid, M., 1996. Active tectonism in the intracontinental Middle Atlas Mountains of Morocco: synchronous crustal shortening and extension. Journal of the Geological Society 153, 389–402. https://doi.org/10.1144/gsjgs.153.3.0389.

Gomez, F., Beauchamp, W., Barazangi, M., 2000. Role of the Atlas Mountains (northwest Africa) within the African-Eurasian plate-boundary zone. Geology 28, 775–778. https://doi.org/10.1130/0091-7613(2000)28<775:ROTAMN>2.0.CO;2.

Grasemann, B., Martel, S., Passchier, C., 2005. Reverse and normal drag along a fault. Journal of Structural Geology 27, 999–1010. https://doi.org/10.1016/j.jsg.2005.04.006.

Greb, S.F., Archer, A.W., 2007. Soft-sediment deformation produced by tides in a meizoseismic area, Turnagain Arm, Alaska. Geology 35, 435–438. https://doi.org/10.1130/G23209A.1.

Guhman, A.I., Pederson, D.T., 1992. Boiling sand springs, Dismal River, Nebraska: Agents for formation of vertical cylindrical structures and geomorphic change. Geology 20, 8–10. https://doi.org/10.1130/0091-7613(1992)020<0008:BSSDRN>2.3.CO;2.

Gutscher, M.-A., Dominguez, S., Westbrook, G.K., Le Roy, P., Rosas, F., Duarte, J.C., Terrinha, P., Miranda, J.M., Graindorge, D., Gailler, A., Sallares, V., Bartolome, R., 2012. The Gibraltar subduction: A decade of new geophysical data. Tectonophysics 574–575, 72–91. https://doi.org/10.1016/j.tecto.2012.08.038.

Hamblin, W.K., 1965. Origin of "Reverse Drag" on the Downthrown Side of Normal Faults. GSA Bulletin 76, 1145–1164. https://doi.org/10.1130/0016-7606(1965)76[1145:OORDOT]2.0.CO;2.

Harmand, C., Cantagrel, J.M., 1984. Le volcanisme alcalin tertiaire et quaternaire du moyen atlas (Maroc): chronologie K/Ar et cadre géodynamique. Journal of African Earth Sciences (1983) 2, 51–55. https://doi.org/10.1016/0899-5362(84)90019-8.

Harris, C., Murton, J., Davies, M.C.R., 2000. Soft-sediment deformation during thawing of ice-rich frozen soils: results of scaled centrifuge modelling experiments. Sedimentology 47, 687–700. https://doi.org/10.1046/j.1365-3091.2000.00322.x.

Hinaje, S., 2004. Tectonique cassante et paléochamps de contraintes dans le Moyen Atlas et le Haut Atlas central (Midelt-Errachidia) depuis le Trias jusqu'à l'Actuel. Université Mohammed V, Rabat.

Hinaje, S., El Fartati, M., Yaagoub, D., Amrani, S., Gharmane, Y., El Fellah Idrissi, B., 2019. Paleocontraintes et contexte tectonique de mise en place du volcanisme alcalin neogene et quaternaire du Moyen Atlas (Maroc). European Scientific Journal May 448–466.

Holzer, T.L., Clark, M.M., 1993. Sand boils without earthquakes. Geology 21, 873–876. https://doi.org/10.1130/0091-7613(1993)021<0873:SBWE>2.3.CO;2.

Jackson, J.A., White, N.J., Garfunkel, Z., Anderson, H., 1988. Relations between normal-fault geometry, tilting and vertical motions in extensional terrains: an example from the southern Gulf of Suez. Journal of Structural Geology 10, 155–170. https://doi.org/10.1016/0191-8141(88)90113-7.

Kaislaniemi, L., van Hunen, J., 2014. Dynamics of lithospheric thinning and mantle melting by edge-driven convection: Application to Moroccan Atlas mountains. Geochemistry, Geophysics, Geosystems 15, 3175–3189. https://doi.org/10.1002/2014GC005414.

Kelts, K., 1988. Environments of deposition of lacustrine petroleum source rocks: an introduction. Geological Society, London, Special Publications 40, 3–26. https://doi.org/10.1144/GSL.SP.1988.040.01.02.

Kim, Y.-S., Peacock, D.C.P., Sanderson, D.J., 2004. Fault damage zones. Journal of Structural Geology 26, 503–517. https://doi.org/10.1016/j.jsg.2003.08.002.

Kim, Y.-S., Sanderson, D.J., 2006. Structural similarity and variety at the tips in a wide range of strike–slip faults: a review. Terra Nova 18, 330–344. https://doi.org/10.1111/j.1365-3121.2006.00697.x.

Koulali, A., Ouazar, D., Tahayt, A., King, R.W., Vernant, P., Reilinger, R.E., McClusky, S., Mourabit, T., Davila, J.M., Amraoui, N., 2011. New GPS constraints on active deformation along the Africa–Iberia plate boundary. Earth and Planetary Science Letters 308, 211–217. https://doi.org/10.1016/j.epsl.2011.05.048.

Laville, E., Pique, A., Amrhar, M., Charroud, M., 2004. A restatement of the Mesozoic Atlasic Rifting (Morocco). Journal of African Earth Sciences 38, 145–153. https://doi.org/10.1016/j.jafrearsci.2003.12.003.

Le Heron, D.P., Sutcliffe, O.E., Whittington, R.J., Craig, J., 2005. The origins of glacially related soft-sediment deformation structures in Upper Ordovician glaciogenic rocks: implication for ice-sheet dynamics. Palaeogeography, Palaeoclimatology, Palaeoecology 218, 75–103. https://doi.org/10.1016/j.palaeo.2004.12.007.

Leeder, M., 1987. Sediment deformation structures and the palaeotectonic analysis of sedimentary basins, with a case-study from the Carboniferous of northern England. Geological Society, London, Special Publications 29, 137–146. https://doi.org/10.1144/GSL.SP.1987.029.01.12

Lehner, B.L., 1991. Neptunian dykes along a drowned carbonate platform margin: an indication for recurrent extensional tectonic activity? Terra Nova 3, 593–602. https://doi.org/10.1111/j.1365-3121.1991.tb00201.x.

Lonergan, L., White, N., 1997. Origin of the Betic-Rif mountain belt. Tectonics 16, 504–522. https://doi.org/10.1029/96TC03937.

Lowe, D.R., 1982. Sediment gravity flows; II, Depositional models with special reference to the deposits of high-density turbidity currents. Journal of Sedimentary Research 52, 279–297. https://doi.org/10.1306/212F7F31-2B24-11D7-8648000102C1865D.

Lowe, D.R., 1975. Water escape structures in coarse-grained sediments. Sedimentology 22, 157–204.

Maltman, A., 1984. On the term “soft-sediment deformation.” Journal of Structural Geology 6, 589–592. https://doi.org/10.1016/0191-8141(84)90069-5.

Marone, C., Scholz, C.H., 1988. The depth of seismic faulting and the upper transition from stable to unstable slip regimes. Geophysical Research Letters 15, 621–624. https://doi.org/10.1029/GL015i006p00621.

Martin, J., 1981. Le Moyen Atlas central étude géomorphologique. Editions du Service géologique du Maroc.

Martinelli, M., Bistacchi, A., Balsamo, F., Meda, M., 2019. Late Oligocene to Pliocene Extension in the Maltese Islands and Implications for Geodynamics of the Pantelleria Rift and Pelagian Platform. Tectonics 38, 3394–3415. https://doi.org/10.1029/2019TC005627..

Mattauer, M., Tapponnier, P., Proust, F., 1977. Sur les méchanismes de formation des chaînes intracontinentales. L'example des chaînes atlasiques du Maroc. Bull. Soc. géol. France, (VII) 19.

Mayolle, S., Soliva, R., Caniven, Y., Wibberley, C., Ballas, G., Milesi, G., Dominguez, S., 2019. Scaling of fault damage zones in carbonate rocks. Journal of. Structural Geology 124, 35–50. https://doi.org/10.1016/j.jsg.2019.03.007

Mazumder, R., van Loon, A.J. (Tom), Arima, M., 2006. Soft-sediment deformation structures in the Earth's oldest seismites. Sedimentary Geology 186, 19–26. https://doi.org/10.1016/j.sedgeo.2005.12.002.

McClay, K.R., 1990. Extensional fault systems in sedimentary basins: a review of analogue model studies. Marine and Petroleum Geology 7, 206–233. https://doi.org/10.1016/0264-8172(90)90001-W.

Medina, F., Cherkaoui, T.E., 1992. Mécanismes au foyer des séismes du Maroc et des régions voisines (1959-1986). Conséquences tectoniques. Eclogae Geol. Helv 85, 433–457.

Medina, F., Cherkaoui, T.E., 1991. Focal mechanisms of the Atlas earthquakes, and tectonic implications. Geologische Rundschau 80, 639–648. https://doi.org/10.1007/bf01803691.

Meng, J., Jiang, Z., Yang, Y., Nian, T., 2021. Soft-sediment deformation structures in a lacustrine depositional context: An example from the Eocene Dongying Depression in the Bohai Bay Basin, East China. Sedimentary Geology 426, 106039. https://doi.org/10.1016/j.sedgeo.2021.106039.

Miller, M.S., Allam, A.A., Becker, T.W., Di Leo, J.F., Wookey, J., 2013. Constraints on the tectonic evolution of the westernmost Mediterranean and northwestern Africa from shear wave splitting analysis. Earth and Planetary Science Letters 375, 234–243. https://doi.org/10.1016/j.epsl.2013.05.036.

Miller, M.S., Becker, T.W., 2014. Reactivated lithospheric-scale discontinuities localize dynamic uplift of the Moroccan Atlas Mountains. Geology 42, 35–38. https://doi.org/10.1130/G34959.1.

Miller, M.S., O'Driscoll, L.J., Butcher, A.J., Thomas, C., 2015. Imaging Canary Island hotspot material beneath the lithosphere of Morocco and southern Spain. Earth and Planetary Science Letters 431, 186–194. https://doi.org/10.1016/j.epsl.2015.09.026.

Missenard, Y., Cadoux, A., 2012. Can Moroccan Atlas lithospheric thinning and volcanism be induced by Edge-Driven Convection?: Edge-Driven Convection in Morocco? Terra Nova 24, 27–33. https://doi.org/10.1111/j.1365-3121.2011.01033.x.

Missenard, Y., Zeyen, H., Frizon de Lamotte, D., Leturmy, P., Petit, C., Sébrier, M., Saddiqi, O., 2006. Crustal versus asthenospheric origin of relief of the Atlas Mountains of Morocco. Journal of Geophysical Research: Solid Earth 111. https://doi.org/10.1029/2005JB003708.

Molina, J.M., Alfaro, P., Moretti, M., Soria, J.M., 1998. Soft-sediment deformation structures induced by cyclic stress of storm waves in tempestites (Miocene, Guadalquivir Basin, Spain). Terra Nova 10, 145–150. https://doi.org/10.1046/j.1365-3121.1998.00183.x.

Montenat, C., Barrier, P., Ott d'Estevou, P., Hibsch, C., 2007. Seismites: An attempt at critical analysis and classification. Sedimentary Geology 196, 5–30. https://doi.org/10.1016/j.sedgeo.2006.08.004.

Moratti, G., Piccardi, L., Vannucci, G., Belardinelli, M.E., Dahmani, M., Bendkik, A., Chenakeb, M., 2003. The 1755 "Meknes" earthquake (Morocco): field data and geodynamic implications. Journal of

Geodynamics, Active Faults: Analysis, Processes and Monitoring 36, 305–322. https://doi.org/10.1016/S0264-3707(03)00052-8.

Moretti, M., 2000. Soft-sediment deformation structures interpreted as seismites in middle-late Pleistocene aeolian deposits (Apulian foreland, southern Italy). Sedimentary Geology 135, 167–179. https://doi.org/10.1016/S0037-0738(00)00070-1.

Moretti, M., Alfaro, P., Caselles, O., Canas, J.A., 1999. Modelling seismites with a digital shaking table. Tectonophysics 304, 369–383.

Moretti, M., Alfaro, P., Owen, G., 2016. The environmental significance of soft-sediment deformation structures: key signatures for sedimentary and tectonic processes. Sedimentary Geology, The environmental significance of soft-sediment deformation 344, 1–4. https://doi.org/10.1016/j.sedgeo.2016.10.002.

Moretti, M., Owen, G., Tropeano, M., 2011. Soft-sediment deformation induced by sinkhole activity in shallow marine environments: A fossil example in the Apulian Foreland (Southern Italy). Sedimentary Geology 235, 331–342.

Moretti, M., Ronchi, A., 2011. Liquefaction features interpreted as seismites in the Pleistocene fluvio-lacustrine deposits of the Neuquén Basin (Northern Patagonia). Sedimentary Geology 235, 200–209.

Moretti, M., Sabato, L., 2007. Recognition of trigger mechanisms for soft-sediment deformation in the Pleistocene lacustrine deposits of the Sant'Arcangelo Basin (Southern Italy): seismic shock vs. overloading. Sedimentary Geology 196, 31–45.

Moretti, M., (Tom) van Loon, A.J., Liu, M., Wang, Y., 2014. Restrictions to the application of 'diagnostic' criteria for recognizing ancient seismites. Journal of Palaeogeography 3, 162–173. https://doi.org/10.3724/SP.J.1261.2014.00050.

Morris, P.H., Graham, J., Williams, D.J., 1992. Cracking in drying soils. Can. Geotech. J. 29, 263–277. https://doi.org/10.1139/t92-030.

Mourabit, T., Abou Elenean, K.M., Ayadi, A., Benouar, D., Ben Suleman, A., Bezzeghoud, M., Cheddadi, A., Chourak, M., ElGabry, M.N., Harbi, A., Hfaiedh, M., Hussein, H.M., Kacem, J., Ksentini, A., Jabour, N., Magrin, A., Maouche, S., Meghraoui, M., Ousadou, F., Panza, G.F., Peresan, A., Romdhane, N., Vaccari, F., Zuccolo, E., 2014. Neo-deterministic seismic hazard assessment in North Africa. J Seismol 18, 301–318. https://doi.org/10.1007/s10950-013-9375-2.

Mutti, E., Tinterri, R., Benevelli, G., Biase, D. di, Cavanna, G., 2003. Deltaic, mixed and turbidite sedimentation of ancient foreland basins. Marine and Petroleum Geology, Turbidites: Models and Problems 20, 733–755. https://doi.org/10.1016/j.marpetgeo.2003.09.001.

Netoff, D.I., Shroba, R.R., 2001. Conical sandstone landforms cored with clastic pipes in Glen Canyon National Recreation Area, southeastern Utah. Geomorphology 39, 99–110. https://doi.org/10.1016/S0169-555X(00)00096-9.

Nichols, R.J., Sparks, R.S.J., Wilson, C.J.N., 1994. Experimental studies of the fluidization of layered sediments and the formation of fluid escape structures. Sedimentology 41, 233–253.

Nur, A., Ron, H., Scotti, O., 1986. Fault mechanics and the kinematics of block rotations. Geology 14, 746–749. https://doi.org/10.1130/0091-7613(1986)14<746:FMATKO>2.0.CO;2.

Nutz, A., Ghienne, J.-F., Schuster, M., Dietrich, P., Roquin, C., Hay, M.B., Bouchette, F., Cousineau, P.A., 2015. Forced regressive deposits of a deglaciation sequence: Example from the Late Quaternary succession in the Lake Saint-Jean basin (Québec, Canada). Sedimentology 62, 1573–1610.

Nutz, A., Schuster, M., Barboni, D., Gassier, G., Van Bocxlaer, B., Robin, C., Ragon, T., Ghienne, J.-F., Rubino, J.-L., 2020. Plio-Pleistocene sedimentation in West Turkana (Turkana Depression, Kenya, East African Rift System): Paleolake fluctuations, paleolandscapes and controlling factors. Earth-Science Reviews 211, 103415. https://doi.org/10.1016/j.earscirev.2020.103415.

Obermeier, S.F., 2009. Chapter 7 Using Liquefaction-Induced and Other Soft-Sediment Features for Paleoseismic Analysis, in: International Geophysics, Paleoseismology. Academic Press, pp. 497–564. https://doi.org/10.1016/S0074-6142(09)95007-0.

Obermeier, S.F., 1996. Use of liquefaction-induced features for paleoseismic analysis — An overview of how seismic liquefaction features can be distinguished from other features and how their regional distribution and properties of source sediment can be used to infer the location and strength of Holocene paleo-earthquakes. Engineering Geology 44, 1–76. https://doi.org/10.1016/S0013-7952(96)00040-3.

Ouarhache, D., 1987. Etude geologique dans le paleozoique et le trias de la bordure nw du cauuse moyen-atlasique (s et w de fes,maroc) (These de doctorat). Toulouse 3.

Ouarhache, D., Charriere, A., Chalot-Prat, F., El-Wartiti, M., 2000. Sédimentation détritique continentale synchrone d'un volcanisme explosif dans le Trias terminal à infra-Lias du domaine atlasique (Haute Moulouya, Maroc) (Late Triassic to infra-Liassic continental detrital sedimentation synchronous with an explosive volcanic event in the Atlas area [Hgh Moulouya, Morocco]). Journal of African Earth Sciences 31, 555–570. https://doi.org/10.1016/S0899-5362(00)80007-X.

Ouarhache, D., Charriere, A., Chalot-prat, F., Wartiti, M.E., 2012. Triassic to early Liassic continental rifting chronology and process at the southwest margin of the Alpine Tethys (Middle Atlas and High Moulouya, Morocco); correlations with the Atlantic rifting, synchronous and diachronous. Bulletin de la Societe Geologique de France 183, 233–249. https://doi.org/10.2113/gssgfbull.183.3.233

Owen, G., 2003. Load structures: gravity-driven sediment mobilization in the shallow subsurface. Geological Society, London, Special Publications 216, 21–34.

Owen, G., 1996. Experimental soft-sediment deformation: structures formed by the liquefaction of unconsolidated sands and some ancient examples. Sedimentology 43, 279–293.

Owen, G., 1987. Deformation processes in unconsolidated sands. Geological Society, London, Special Publications 29, 11–24.

Owen, G., Moretti, M., 2011. Identifying triggers for liquefaction-induced soft-sediment deformation in sands. Sedimentary Geology 235, 141–147. https://doi.org/10.1016/j.sedgeo.2010.10.003.

Owen, G., Moretti, M., 2008. Determining the origin of soft-sediment deformation structures: a case study from Upper Carboniferous delta deposits in south-west Wales, UK. Terra Nova 20, 237–245.

Owen, G., Moretti, M., Alfaro, P., 2011. Recognising triggers for soft-sediment deformation: Current understanding and future directions. Sedimentary Geology, Recognising triggers for soft-sediment deformation: Current understanding and future directions 235, 133–140. https://doi.org/10.1016/j.sedgeo.2010.12.010.

Palomeras, I., Thurner, S., Levander, A., Liu, K., Villasenor, A., Carbonell, R., Harnafi, M., 2014. Finite-frequency Rayleigh wave tomography of the western Mediterranean: Mapping its lithospheric structure. Geochemistry, Geophysics, Geosystems 15, 140–160. https://doi.org/10.1002/2013GC004861.

Peacock, D.C.P., Nixon, C.W., Rotevatn, A., Sanderson, D.J., Zuluaga, L.F., 2016. Glossary of fault and other fracture networks. Journal of Structural Geology 92, 12–29. https://doi.org/10.1016/j.jsg.2016.09.008.

Peláez, J.A., Chourak, M., Tadili, B.A., Brahim, L.A., Hamdache, M., Casado, C.L., Solares, J.M.M., 2007. A Catalog of Main Moroccan Earthquakes from 1045 to 2005. Seismological Research Letters 78, 614–621. https://doi.org/10.1785/gssrl.78.6.614.

Peters, S.E., Loss, D.P., 2012. Storm and fair-weather wave base: A relevant distinction? Geology 40, 511–514. https://doi.org/10.1130/G32791.1.

Pickering, K., Stow, D., Watson, M., Hiscott, R., 1986. Deep-water facies, processes and models: a review and classification scheme for modern and ancient sediments. Earth-Science Reviews 23, 75–174. https://doi.org/10.1016/0012-8252(86)90001-2.

Piqué, A., Dahmani, M., Jeannette, D., Bahi, L., 1987. Permanence of structural lines in Morocco from Precambrian to Present. Journal of African Earth Sciences (1983) 6, 247–256. https://doi.org/10.1016/0899-5362(87)90066-2.

Piqué, A., Tricart, P., Guiraud, R., Laville, E., Bouaziz, S., Amrhar, M., Ouali, R.A., 2002. The Mesozoic-Cenozoic Atlas belt (North Africa): an overview. Geodinamica Acta 15, 185–208. https://doi.org/10.1080/09853111.2002.10510752.

Platt, N.H., Wright, V.P., 1991. Lacustrine Carbonates: Facies Models, Facies Distributions and Hydrocarbon Aspects, in: Lacustrine Facies Analysis. John Wiley & Sons, Ltd, pp. 57–74. https://doi.org/10.1002/9781444303919.ch3.

Plaziat, J.-C., Ahmamou, M., 1998. Les différents mécanismes à l'origine de la diversité des séismites, leur identification dans le Pliocène du Saïss de Fès et de Meknès (Maroc) et leur signification tectonique. Geodinamica Acta 11, 183–203.

Plummer, P.S., Gostin, V.A., 1981. Shrinkage cracks; desiccation or synaeresis? Journal of Sedimentary Research 51, 1147–1156. https://doi.org/10.1306/212F7E4B-2B24-11D7-8648000102C1865D.

Potter, P.E., Maynard, J.B., Pryor, W.A., 1980. Sedimentology of Shale. Springer New York, New York, NY. https://doi.org/10.1007/978-1-4612-9981-3.

Poujol, A., Ritz, J.-F., Tahayt, A., Vernant, P., Condomines, M., Blard, P.-H., Billant, J., Vacher, L., Tibari, B., Hni, L., Idrissi, A.K., 2014. Active tectonics of the Northern Rif (Morocco) from geomorphic and geochronological data. Journal of Geodynamics, SI : Geodynamic evolution of the Alboran domain 77, 70–88. https://doi.org/10.1016/j.jog.2014.01.004.

Poujol, A., Ritz, J.-F., Vernant, P., Huot, S., Maate, S., Tahayt, A., 2017. Which fault destroyed Fes city (Morocco) in 1755? A new insight from the Holocene deformations observed along the southern border of Gibraltar arc. Tectonophysics 712, 303–311.

Pratt, B.R., 1998. Syneresis cracks: subaqueous shrinkage in argillaceous sediments caused by earthquake-induced dewatering. Sedimentary Geology 117, 1–10. https://doi.org/10.1016/S0037-0738(98)00023-2.

Pratt, B.R., Ponce, J.J., 2019. Sedimentation, earthquakes, and tsunamis in a shallow, muddy epeiric sea: Grinnell Formation (Belt Supergroup, ca. 1.45 Ga), western North America. GSA Bulletin 131, 1411–1439. https://doi.org/10.1130/B35012.1.

Rana, N., Sati, S.P., Sundriyal, Y., Juyal, N., 2016. Genesis and implication of soft-sediment deformation structures in high-energy fluvial deposits of the Alaknanda Valley, Garhwal Himalaya, India. Sedimentary Geology, The environmental significance of soft-sediment deformation 344, 263–276. https://doi.org/10.1016/j.sedgeo.2016.06.012.

Reches, Z., Lockner, D.A., 1994. Nucleation and growth of faults in brittle rocks. Journal of Geophysical Research: Solid Earth 99, 18159–18173. https://doi.org/10.1029/94JB00115.

Reinoso, F., Díaz-Alvarado, J., Fernández, C., 2020. Structural characteristics of the “Puquios chaos” and its relationship with the Andean middle Cretaceous extensional tectonics at 27°S, northern Chile. Journal of South American Earth Sciences 98, 102454. https://doi.org/10.1016/j.jsames.2019.102454.

Rhoujjati, A., Cheddadi, R., Taïeb, M., Baali, A., Ortu, E., 2010. Environmental changes over the past c. 29,000 years in the Middle Atlas (Morocco): A record from Lake Ifrah. Journal of Arid Environments 74, 737–745. https://doi.org/10.1016/j.jaridenv.2009.09.006.

Rodríguez-Pascua, M.A., Calvo, J.P., De Vicente, G., Gómez-Gras, D., 2000. Soft-sediment deformation structures interpreted as seismites in lacustrine sediments of the Prebetic Zone, SE Spain, and their potential use as indicators of earthquake magnitudes during the Late Miocene. Sedimentary Geology 135, 117–135. https://doi.org/10.1016/S0037-0738(00)00067-1.

Rosenbaum, G., Lister, G.S., Duboz, C., 2002. Relative motions of Africa, Iberia and Europe during Alpine orogeny. Tectonophysics 359, 117–129. https://doi.org/10.1016/S0040-1951(02)00442-0.

Rossetti, D.F., Alves, F.C., Valeriano, M.M., 2017. A tectonically-triggered late Holocene seismite in the southern Amazonian lowlands, Brazil. Sedimentary Geology 358, 70–83. https://doi.org/10.1016/j.sedgeo.2017.07.003.

Schlische, R.W., 1995. Geometry and Origin of Fault-Related Folds in Extensional Settings 1. AAPG Bulletin 79, 1661–1678. https://doi.org/10.1306/7834DE4A-1721-11D7-8645000102C1865D

Schultz, R.A., Fossen, H., 2002. Displacement–length scaling in three dimensions: the importance of aspect ratio and application to deformation bands. Journal of Structural Geology 24, 1389–1411. https://doi.org/10.1016/S0191-8141(01)00146-8.

Schultz, R.A., Okubo, C.H., Wilkins, S.J., 2006. Displacement-length scaling relations for faults on the terrestrial planets. Journal of Structural Geology, Faulting and fault-related processes on planetary surfaces 28, 2182–2193. https://doi.org/10.1016/j.jsg.2006.03.034.

Schultz, R.A., Soliva, R., Fossen, H., Okubo, C.H., Reeves, D.M., 2008. Dependence of displacement–length scaling relations for fractures and deformation bands on the volumetric changes across them. Journal of Structural Geology 30, 1405–1411. https://doi.org/10.1016/j.jsg.2008.08.001.

Seilacher, A., 1984. Sedimentary structures tentatively attributed to seismic events. Marine geology 55, 1–12.

Seilacher, A., 1969. Fault-graded beds interpreted as seismites. Sedimentology 13, 155–159.

Shanmugam, G., 2017. Global case studies of soft-sediment deformation structures (SSDS): Definitions, classifications, advances, origins, and problems. Journal of Palaeogeography 6, 251–320. https://doi.org/10.1016/j.jop.2017.06.004.

Shanmugam, G., 2016. The seismite problem. Journal of Palaeogeography 5, 318–362. https://doi.org/10.1016/j.jop.2016.06.002.

Shanmugam, G., 1996. High-density turbidity currents; are they sandy debris flows? Journal of Sedimentary Research 66, 2–10. https://doi.org/10.1306/D426828E-2B26-11D7-8648000102C1865D

Shelton, J.W., 1984. Listric Normal Faults: An Illustrated Summary1. AAPG Bulletin 68, 801–815. https://doi.org/10.1306/AD461426-16F7-11D7-8645000102C1865D

Simms, M.J., 2007. Uniquely extensive soft-sediment deformation in the Rhaetian of the UK: Evidence for earthquake or impact? Palaeogeography, Palaeoclimatology, Palaeoecology, Triassic-Jurassic Boundary events: problems, progress, possibilities 244, 407–423. https://doi.org/10.1016/j.palaeo.2006.06.037

Sims, J.D., 1975. Determining earthquake recurrence intervals from deformational structures in young lacustrine sediments, in: Developments in Geotectonics. Elsevier, pp. 141–152.

Spahić, D., Exner, U., Behm, M., Grasemann, B., Haring, A., Pretsch, H., 2011. Listric versus planar normal fault geometry: an example from the Eisenstadt-Sopron Basin (E Austria). Int J Earth Sci (Geol Rundsch) 100, 1685–1695. https://doi.org/10.1007/s00531-010-0583-5.

Storti, F., Holdsworth, R.E., Salvini, F., 2003. Intraplate strike-slip deformation belts. Geological Society, London, Special Publications 210, 1–14. https://doi.org/10.1144/GSL.SP.2003.210.01.01.

Strecker, U., Steidtmann, J.R., Smithson, S.B., 1999. A Conceptual Tectonostratigraphic Model for Seismic Facies Migrations in a Fluvio-Lacustrine Extensional Basin1. AAPG Bulletin 83, 1320–1336. https://doi.org/10.1306/00AA99F8-1730-11D7-8645000102C1865D.

Tadili, B.A., Ramdani, M., 1986. La Sismicite du Moyen Atlas. Gerlands Beiträge zur Geophysik 95, 469–476.

Tahayt, A., Mourabit, T., Rigo, A., Feigl, K.L., Fadil, A., McClusky, S., Reilinger, R., Serroukh, M., Ouazzani-Touhami, A., Sari, D.B., Vernant, P., 2008. Mouvements actuels des blocs tectoniques dans l'arc Bético-Rifain à partir des mesures GPS entre 1999 et 2005. Comptes Rendus Geoscience 340, 400–413. https://doi.org/10.1016/j.crte.2008.02.003.

Talling, P.J., Masson, D.G., Sumner, E.J., Malgesini, G., 2012. Subaqueous sediment density flows: Depositional processes and deposit types. Sedimentology 59, 1937–2003. https://doi.org/10.1111/j.1365-3091.2012.01353.x.

Tang, C.-S., Zhu, C., Cheng, Q., Zeng, H., Xu, J.-J., Tian, B.-G., Shi, B., 2021. Desiccation cracking of soils: A review of investigation approaches, underlying mechanisms, and influencing factors. Earth-Science Reviews 216, 103586. https://doi.org/10.1016/j.earscirev.2021.103586.

Teixell, A., Ayarza, P., Zeyen, H., Fernàndez, M., Arboleya, M.-L., 2005. Effects of mantle upwelling in a compressional setting: the Atlas Mountains of Morocco. Terra Nova 17, 456–461. https://doi.org/10.1111/j.1365-3121.2005.00633.x.

Törő, B., Pratt, B.R., 2016. Sedimentary record of seismic events in the Eocene Green River Formation and its implications for regional tectonics on lake evolution (Bridger Basin, Wyoming). Sedimentary Geology 344, 175–204.

Törő, B., Pratt, B.R., Renaut, R.W., 2015. Tectonically induced change in lake evolution recorded by seismites in the Eocene Green River Formation, Wyoming. Terra Nova 27, 218–224. https://doi.org/10.1111/ter.12150

Van Loon, A.J., 2009. Soft-sediment deformation structures in siliciclastic sediments: an overview.

Vendeville, B., Cobbold, P.R., Davy, P., Choukroune, P., Brun, J.P., 1987. Physical models of extensional tectonics at various scales. Geological Society, London, Special Publications 28, 95–107. https://doi.org/10.1144/GSL.SP.1987.028.01.08.

Vernant, P., Fadil, A., Mourabit, T., Ouazar, D., Koulali, A., Davila, J.M., Garate, J., McClusky, S., Reilinger, R., 2010. Geodetic constraints on active tectonics of the Western Mediterranean: Implications for the kinematics and dynamics of the Nubia-Eurasia plate boundary zone. Journal of Geodynamics, WEGENER 2008 - Proceedings of the 14th General Assembly of Wegener 49, 123–129. https://doi.org/10.1016/j.jog.2009.10.007.

Villaseñor, A., Chevrot, S., Harnafi, M., Gallart, J., Pazos, A., Serrano, I., Córdoba, D., Pulgar, J.A., Ibarra, P., 2015. Subduction and volcanism in the Iberia–North Africa collision zone from tomographic images of the upper mantle. Tectonophysics, Special issue on Iberia geodynamics: An integrative approach from the Topo-Iberia framework 663, 238–249. https://doi.org/10.1016/j.tecto.2015.08.042.

Watterson, J., Childs, C., Walsh, J.J., 1998. Widening of fault zones by erosion of asperities formed by bed-parallel slip. Geology 26, 71–74. https://doi.org/10.1130/0091-7613(1998)026<0071:WOFZBE>2.3.CO;2.

Weinberger, R., Levi, T., Alsop, G.I., Eyal, Y., 2016. Coseismic horizontal slip revealed by sheared clastic dikes in the Dead Sea Basin. Bulletin of the Geological Society of America 128, 1193–1206. https://doi.org/10.1130/B31415.1.

Wernicke, B., Burchfiel, B.C., 1982. Modes of extensional tectonics. Journal of Structural Geology 4, 105–115. https://doi.org/10.1016/0191-8141(82)90021-9.

Wheatley, D.F., Chan, M.A., Okubo, C.H., 2019. Clastic pipes and mud volcanism across Mars: Terrestrial analog evidence of past martian groundwater and subsurface fluid mobilization. Icarus 328, 141–151. https://doi.org/10.1016/j.icarus.2019.02.002.

Wheatley, D.F., Chan, M.A., Sprinkel, D.A., 2016. Clastic pipe characteristics and distributions throughout the Colorado Plateau: Implications for paleoenvironment and paleoseismic controls. Sedimentary Geology, The environmental significance of soft-sediment deformation 344, 20–33. https://doi.org/10.1016/j.sedgeo.2016.03.027.

White, N.J., Jackson, J.A., McKenzie, D.P., 1986. The relationship between the geometry of normal faults and that of the sedimentary layers in their hanging walls. Journal of Structural Geology 8, 897–909. https://doi.org/10.1016/0191-8141(86)90035-0.

Wibberley, C.A.J., Yielding, G., Toro, G.D., 2008. Recent advances in the understanding of fault zone internal structure: a review. Geological Society, London, Special Publications 299, 5–33. https://doi.org/10.1144/SP299.2.

Xiao, H., Suppe, J., 1992. Origin of rollover (1). AAPG bulletin 76, 509–529.

Zavala, C., Arcuri, M., Meglio, M.D., Diaz, H.G., Contreras, C., 2011. A Genetic Facies Tract for the Analysis of Sustained Hyperpycnal Flow Deposits 31–51. https://doi.org/10.1306/13271349St613438.

Zhou, Y.-Q., Peng, T.-M., Zhou, T.-F., Zhang, Z.-K., Tian, H., Liang, W.-D., Yu, T., Sun, L.-F., 2017. Soft-sediment deformation structures related to volcanic earthquakes of the Lower Cretaceous Qingshan Group in Lingshan Island, Shandong Province, East China. Journal of Palaeogeography 6, 162–181. https://doi.org/10.1016/j.jop.2017.02.002.

CHAPITRE IV

DESENTANGLING ORBITAL, SUBORBITAL, AND TECTONC SIGNATURES FROM LACUSTRINE SEDIMENTS DEVELOPPED UPON A HALF-GRABEN (LAKE IFRAH, NORTHWEST AFRICA): INSIGHTS INTO LOWEST RANK T-R SEQUENCES FOR INTERIOR BASINS

Disentangling orbital, sub-orbital, and tectonic signatures from lacustrine sediments developed upon a half-graben (Lake Ifrah Basin, Northwest Africa): Insights into lowest-rank T-R sequences for interior basins

Khalil Azennoud[a,*], Abdennasser Baali[a], Francesc Mesquita-Joanes[b], Hicham El Asmi[c], Yassine Ait Brahim[d]

[a] Laboratory of Engineering, Electrochemistry, Modelling and Environment, Faculty of Sciences Dhar EL Mahraz, Sidi Mohamed Ben Abdellah University, P.O. Box 1796, Atlas, Fez 30000, Morocco

[b] University of Valencia, Valencia, Spain

[c] Laboratory of Geosciences, Environment and Associated Resources, Faculty of Sciences Dhar EL Mahraz, Sidi Mohamed Ben Abdellah University, P.O. Box 1796, Atlas, Fez 30000, Morocco

[d] International Water Research Institute, University of Mohammed VI Polytechnic, Benguerir, Morocco

* Corresponding author: Khalil.azennoud@usmba.ac.ma

Under Review in Sedimentary Geology

Abstract

Lacustrine settings constitute a promising recipient of allocyclic signals such as those of climate and tectonics. Possible decryption of these signatures stems from careful scrutiny of the sedimentation dynamics (temporary base-level variations), lake-level fluctuations (accommodation), and resulting strata bounding surfaces. This is wholly achievable thanks to the conventional sequence-stratigraphic approach that gives credit to all of these fundamental aspects. However, due to discrepancies between marine, to which this approach has been initially dedicated, and lacustrine settings (especially regarding the physical scale), deciphering climate from tectonic forcing becomes unwieldy in such interior basins. The present work deals with this challenge and provides insights from a case study where lacustrine sedimentation occurs on a tectonically active half-graben within a key climate region (Lake Ifrah, Northwest Africa). We conducted conventional sedimentological and high-resolution sequence-stratigraphic analyses, integrated with palaeolimnological proxies (geochemical elements and ostracods). Up to five facies models (accounting for lithological domination, wind-driven energy, and lake-level state) and three lowest rank T-R sequences, deposited since the Marine Isotope Stage-3 (MIS-3), have been identified. Periods with sustained high lake levels appear to be mainly precession-paced (as during MIS-3 and the Early Holocene), although the role of obliquity is shown to influence the hydrological budget as well. Furthermore, sedimentation dynamics are shown to respond to millennial timescale climate variability associated with North Atlantic cooling events

(Dansgaard-Oeschger stadials, Heinrich Events) and, interestingly, to enhanced Saharan winds during the deglacial period. On the other hand, tectonism had a rather instantaneous effect on lake level and sedimentation. Two tectonic pulses marking instantaneous differential hanging-wall subsidence have triggered a sharp drop in relative lake level, hence conditioning a forced regression.
We highlight the importance of the conventional high-resolution sequence stratigraphy in shaping our understanding of the cyclic interplay between orbital/sub-orbital and tectonic forcing, so as the resulting sedimentation dynamics and lake-level cycles in lacustrine settings. We stress the role of the forced regression concept and associated systems tract and bounding surfaces, as well as the importance of using ostracods and geochemical proxies to trace transgressions and cryptic surfaces with sequence-stratigraphic significance, such as the maximum flooding surface, in lacustrine settings.

Keywords: orbital and sub-orbital forcing; tectonic pulses; sequence stratigraphy, lowest rank T-R sequences, interior basins, Northwest Africa

1 Introduction

Lacustrine-sediment archives have long been proven to hold significant imprints of tectonic and climate over the past geological times (e.g., Bohacs et al., 2000; Cohen, 2003; Nutz et al., 2017, 2022; Bernhart Owen et al., 2019). A legitimate understanding of key processes and sedimentary response-records (e.g., Anadón et al., 1991; Gierlowski-Kordesch and Kelts, 1994) has paved the way to draw reasonable hydro-stratigraphic models for lake basins, fuelled by the sequence stratigraphy approach (Carroll and Bohacs, 1999; Bohacs et al., 2000; Zavala et al., 2022). Indeed, adaptations of sequence stratigraphy (*sensu* Exxon school) to lacustrine settings has been the subject of numerous works as the standard basics of the approach are, reasonably, not breached in lacustrine settings (e.g., accommodation/base-level concept, shoreline migration, strata stacking patterns, bounding surfaces), although discrepancies exist amongst lacustrine and marine settings (Oviatt et al., 1994; Carroll and Bohacs, 1999; Strecker et al., 1999; Changsong et al., 2001; Keighley et al., 2003; Anselmetti et al., 2006; Gracia et al., 2021; Zavala et al., 2022). Notably, the response of the lacustrine sedimentation dynamics (i.e., temporary base-level, *sensu* Barrell, 1917) and water level (i.e., accommodation, *sensu* Jervey, 1988) to external forcing (tectonic pulses and climate) is faster than in marine settings (Scholz et al., 1990; Strecker et al., 1999), thereby rendering delicate the recording process of these external signals in the sediment geoarchives as so their decryption.

In fact, the tectonic influence on strata stacking patterns is more prominent in half-graben settings where the hanging-wall subsidence pulses (i.e., incremental tectonic tilting) are prone to instantaneously drop the relative lake level (e.g., Prosser, 1993; Strecker et al., 1999). On the other hand, cyclic sedimentation of biochemical and clastic rocks has been considered climate-sensitive (Cecil, 1990) and orbitally-paced (Cecil, 1990; Ashley et al., 2014; de Wet et al., 2015). However, although reasonably assumed, obliquity and precession controls on this lithological cyclicity have not explicitly been proved, with the use of different palaeoclimatic data (e.g., pollens, dust proxies, isotopes) from various natural archives (e.g., speleothems, marine sediments, ice cores). To our knowledge, although a potential imprint of sub-orbital forcing from this cyclicity is likely to be involved (e.g., solar irradiation minima, volcanic eruptions), its decryption is mostly omitted or underestimated. Besides, subsidence pulses in tectonically active settings (e.g., half-graben) are likely to mimic, even though partially, the climatic effect. As the present work deals with mixed clastic-biochemical lacustrine succession in tectonically active settings, we carefully address these challenges while discussing the forcing mechanisms.

The present work delivers an example where a complex, but decipherable, interplay between climate, on both orbital and sub-orbital timescales, and tectonism operate to control the sedimentation dynamics and accommodation in an interior basin. The sedimentation occurs upon an active half-graben setting, and regionally laying on a key climate region (Lake Ifrah, Middle Atlas, Northwest Africa). We conducted conventional sedimentological and high-resolution sequence-stratigraphic analyses, complemented with palaeolimnological proxies. The results demonstrated a striking modulation of sedimentation dynamics/accommodation with climate forcing on both orbital (involving precession and obliquity) and sub-orbital (involving the cooling events) timescales since the Marine Isotope Stage-3 (MIS-3). Furthermore, tectonic pulses revealed their striking influence in controlling instantaneous forced regressions and clastic delivery into the basin. We finally emphasise the role of conventional high-resolution sequence stratigraphy whenever dealing with such lacustrine settings.

2 Geological context and present-day climate

Lake Ifrah Basin (hereafter shortened to Ifrah Basin) is located in the north-western Middle Atlas tectonic province, northern Morocco (33°33′ 32.42″ N, 4°55′ 50.36″ W; 1616 m asl; Fig. 1). To its north-east side a small (1 km^2) and shallow (2 m) lake is established, Lake Ifrah, which receives the most interest in this paper. Regionally, the Middle Atlas is an intracontinental mountain range structured into two main sub-structural domains trending SW-NE and separated by the so-called North Middle Atlas Fault (NMAF; Fig. 1) (Martin, 1981): Tabular Middle Atlas (TMA) with smooth relief

to the NW; and Folded Middle Atlas (FMA) with accentuated relief to the SE. This structuration resulted from a polyphase geodynamic evolution since the Variscan orogeny, with a tectonic inversion from a broad extensional regime during the Mesozoic upon the break-up of Pangea (Mattauer et al., 1977; Charrière, 1990; Frizon de Lamotte et al., 2008; Ouarhache et al., 2012), towards a general compressional regime since late Cretaceous upon Africa-Eurasia convergence (Frizon de Lamotte et al., 2000; Ait Brahim et al., 2002; Fernàndez et al., 2019). The extensional regime during the Mesozoic has led to the extensive and thick succession of platform carbonates (Liassic dolomites and limestones, Fig. 1), which are well-marked in the TMA where the Ifrah Basin is located. Locally, the initiation of the Ifrah Basin has been tentatively proposed to occur in conjunction with the Quaternary mafic volcanic eruptions (*see* Bosch et al., 2014) during the Middle Pleistocene (Azennoud et al., 2022b). More details about the geodynamic evolution of the Middle Atlas and the context of the Ifrah Basin initiation are provided by Azennoud et al. (2022b).

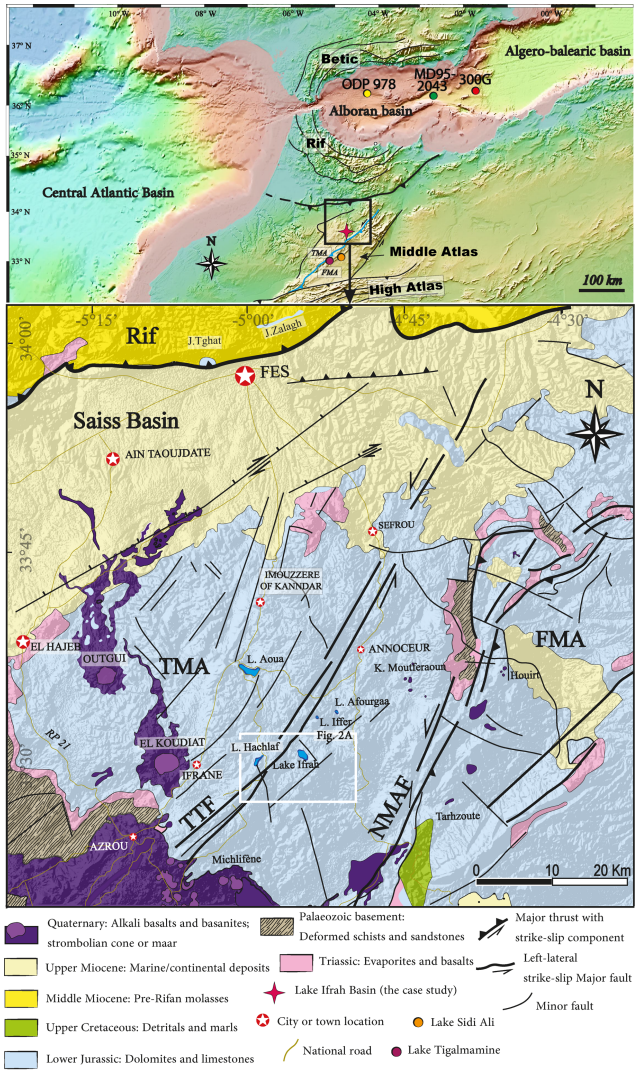


Figure 1. *Geographical locations and geological settings of the Lake Ifrah Basin and other sites referred to in the text. Topographic/bathymetric map based on SRTM30 PLUS. TMA: Tabular Middle Atlas; FMA: Folded Middle Atlas; TTF: Tizi n'Tretten Fault; NMAF: North Middle Atlas Fault (separates TMA and FMA).*

The Lake Ifrah site is characterised by temperate climate with warm summer, that is within the Mediterranean climate type Csa according to köppen classification (Köppen, 1900; Kottek et al., 2006), with annual precipitation of ca. 683 mm and mean temperature of 12.1°C (www.climate-data.org). Being confined between 1400 and 1800 m a.s.l. in the Middle Atlas Mountains, and dominated by *Quercus rotundifolia*, Lake Ifrah site is included within the supra/upper-Mediterranean bioclimatic stage, that is, humid to sub-humid bioclimate according to (Benabid, 1982).

3 Materials and methods

3.1 Sedimentological, stratigraphic, and petrographic analyses

Facies analysis is based on mesoscale field observations and microscopic examinations, according to conventional methodology (*see* Nutz et al., 2019, 2020). Sequence-stratigraphic approach has been conducted as per the recent basin-specific methodology ascribed by Catuneanu et al. (2011), using the T-R model where the sequence bounding surface is defined to be the maximum regression surface. The micro-texture analysis of two palustrine carbonate levels was examined under an optical petrographic microscope. One ground and sieved (63 µm meshes) sample of sand was analysed for mineralogical determination by X-ray diffraction (XRD) using Panalatycal X'Pert PRO Powder Diffractometer equipped with X'Celerator Ultrafast Scintillation Detector at "Cité de l'Innovation Fès". The qualitative determination of mineral major phases was performed using MATCH software and Crystallography Open Database (COD).

3.2 Biological, geochemical proxies, and chronological framework

Twenty-one samples of 10 g each (from log-3 and the marl layer in log-2, Fig. 3) were treated with 3% H_2O_2 for one week and sieved with 100 µm meshes. The residues were analysed using a binocular microscope for ostracod counting and determination. Up to nine species have been determined and used as proxies for lake-level variation (*see* below). Selected ostracod specimens were examined by Scanning Electron Microscope (SEM) using a Quanta 200 FEI equipped with an EDAX probe for surface microanalysis at "Cité de l'Innovation Fès". Eighteen samples of 1 g each (from log-3) were pre-treated for elemental analysis performed with ICP-OES system MORIBA Jobin Yvon - ACTIVA equipment, at "Cité de l'Innovation Fès". The pre-treatment includes digestion of each ground and sieved sample (1 g) with 3 ml of HCl (12.1 M), 1 ml of HNO_3 (16 M), and 2 ml H_2O_2 (9.97 M) for carbonates and organic matter elimination and leaching of the elements of interest. At each digestion, samples were kept at least 15 min after reaching the boiling point (up to 120 ◦ C). After

cooling, the mineralised content was filtered and adjusted to 50 ml with distilled water, hence being prepared for the spectroscopic analysis. The elements of interest used are potassium, aluminium, iron, and manganese. K and Al were used as proxies for drainage network and clastic input, Al/K ratio was used as a proxy for chemical weathering, and Fe/Mn was used as an indicator of lake-bottom reducing conditions (*see* Davies et al., 2015).

The chronological framework of the described depositional systems and sequences was made based on their correlation with an available dated core retrieved from the NW margin (Rhoujjati et al., 2010; Fig. 2B). Accounting for the current lake size and the different degrees of fluvial influence on the two lake margins, the correlation has been based on granulometry variation, inferred depth, and the occurrence of carbonaceous beds (Fig. 3) (*see* Azennoud et al., 2022b).

4 Sedimentologic and stratigraphic analyses

Eight stratigraphic sections were measured from the SW lake margin (Fig. 2) and subjected to a thorough sedimentologic and sequence-stratigraphic investigations. The sedimentological analysis includes (i) conventional facies analysis based on numerous key publications and (ii) combining genetically linked facies such that they depict a specific depositional environment. The sequence analysis has been conducted based on key publications and recommendations. Analysis of soft-sediment deformations has been dealt with separately in another paper (Azennoud et al., 2022b), along with palaeoseismic and regional-scale tectonic implications.

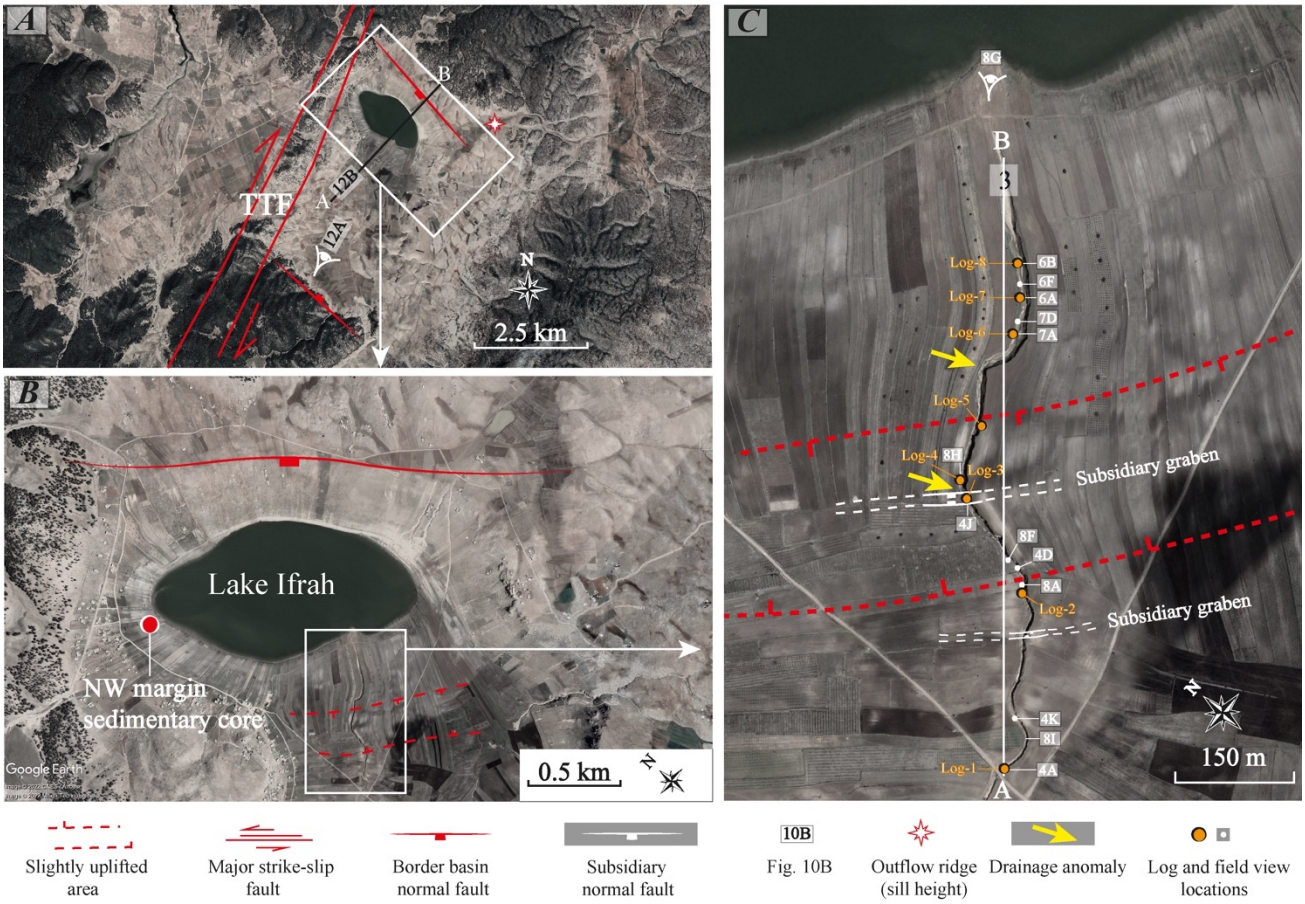


Figure 2. *Simplified structural framework of the Ifrah Basin and locations of the studied outcrop (SW lake margin) and NW lake margin sedimentary core (after Rhoujjati et al., 2010). **A**: Main structures shaping the Ifrah Basin. Note the elliptical shape of the water body and its restriction on the NE side of the basin. The vision field of the perspective view and location of the cross-section shown in **Figure 10** are indicated. **B-C**: locations of the NW lake margin sedimentary core (studied by Rhoujjati et al., 2010) and the SW margin outcrop (studied here), as well as the cross-section shown in **Figure 9**, logs (**Fig. 3**), and field views portrayed in some figures. TTF: Tizi n'Tretten Fault.*

4.1 Sedimentologic analysis

Fifteen sedimentary facies were identified from the studied logs. The main feature descriptions and interpretations of each facies are summarised in table 1. They differ chiefly by (i) their lithological nature (i.e., detrital, carbonaceous, or organic), (ii) their texture/grain size (e.g., muds, sands, gravels, packstones, wackstones), and (iii) their internal sedimentary structures (e.g., grading/sorting, wave/current ripples, upper/lower plane bed).

4.1.1 Facies Association 1 (FA1, lacustrine offshore deposits)

Deposits that characterise FA1 are m-thick succession of dm-thick couplets of laminated mudstone (Fl) and massive sandstone (Sm) (Fig. 4B-D). Mudstone exhibit alternating mm- to cm-scale dark-coloured (blackish to brownish) laminations, recognisable by their slight variation in colours and sand content. Sandstone is beigy and shows no internal structures. Both deposits have planar geometry

and show no erosional boundaries at the scale of the outcrop (i.e., several metres). They were largely identified from the proximal sections (log-1 and log-2).

Organised mudstone is formed throughout the grain-by-grain or aggregate settling process of fines in subaqueous settings, below the influence of the storm and the fair-weather waves (Pickering et al., 1986; Birgenheier et al., 2017). This defines the (lacustrine) offshore environment (Peters and Loss, 2012; Nutz et al., 2020). The settling process of fines may be associated with (i) (low-density) turbidity currents or (ii) more continuous deposition with periodic fluctuations in the influx of terrigenous sediments (Pickering et al., 1986). Indeed, the observed variation in colours and sand content, defining the laminations, is diagnostic evidence of periodic changes in clastic input within a continuous sedimentation background, although the occurrence of occasional small (low-density) turbidity currents is not completely excluded (Sturm and Matter, 1978; Gierlowski-Kordesch, 2010; Nutz et al., 2015b; Zavala and Arcuri, 2016; Pan et al., 2020). In all cases, the occurrence of sandy laminae points out the fluvial influence. Likewise, sand beds lacking internal structures are more likely to reflect subaqueous, non-cohesive (sandy), debris-flow processes (Shanmugam, 1996; Talling et al., 2012) that may be generated by inertia-dominated underflows or hyperpycnal flows during dense fluvial floods (Mutti et al., 2003; Zavala et al., 2011; Zavala, 2020). Deposition of this sandy debrite was initiated when the excess pore pressure was lost enough to cause frictional freezing of the surge-like or episodic plastic flow (Lowe, 1982; Mutti et al., 2003; Talling et al., 2012). Sand-sized grains are supported by their interaction throughout the life of the plastic flow (Middleton and Hampton, 1973). Accordingly, the succession of these mud and sand couplets is likely to reflect remote (Gilbert-type) delta sedimentation (Zavala et al., 2021; Budai et al., 2021).

The rhythmic nature of both deposits and their recognition within the proximal logs suggest lake extension phase with relatively important offshore domain and flooding events generating periodic turbidity currents (Wu et al., 2022) and sandy debris flows. Comparison with the dated core (Rhoujjati et al., 2010) suggests deposition of this facies association prior to 28 cal kyr BP.

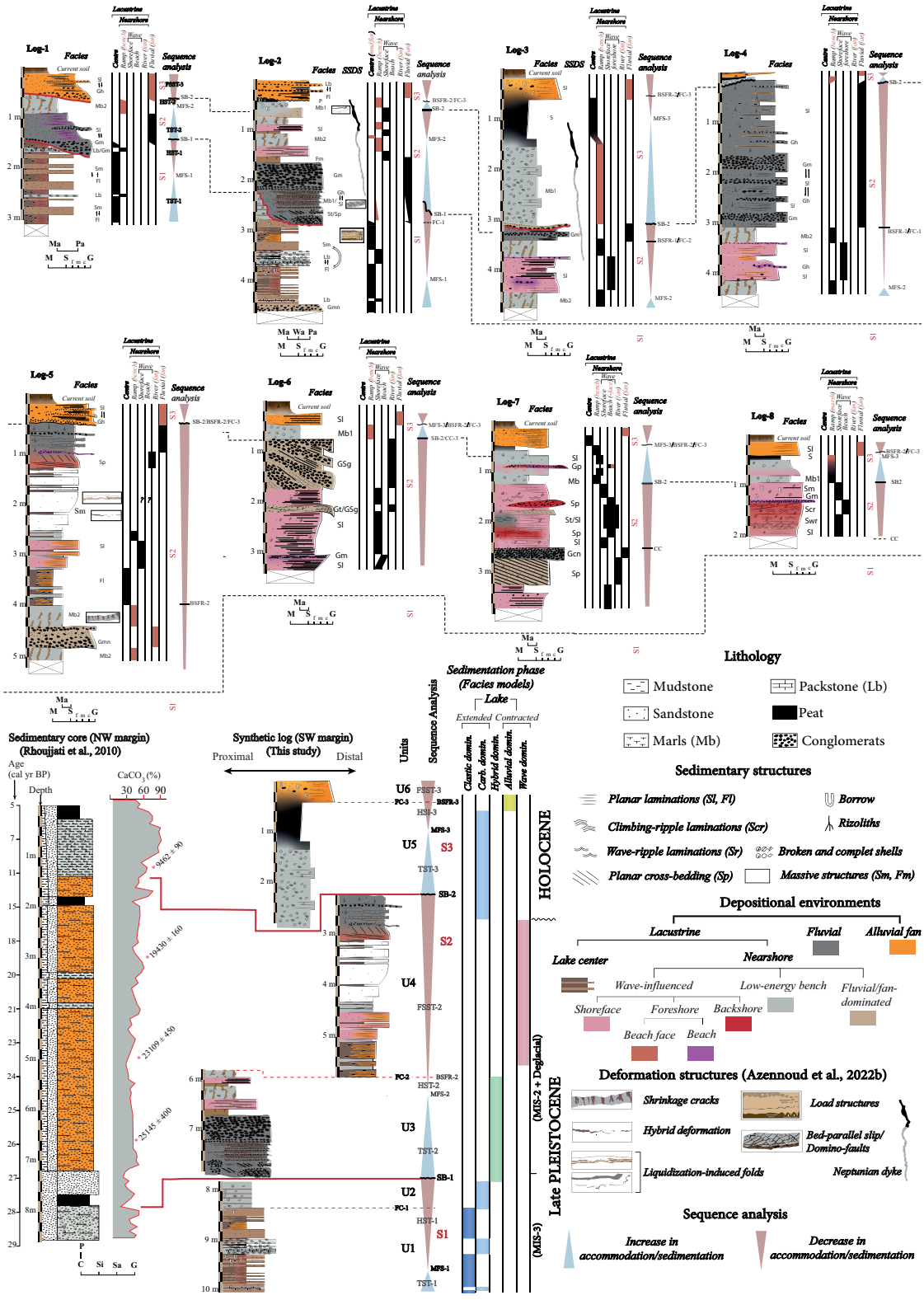


Figure 3. *Measured logs 1 to 8 from the SW lake margin (see **Fig. 1** for locations). Five depositional environments have been depicted from conventional facies analysis (**table 1**) and allowed delineation of three lowest rank T-R sequences and their systems tracts component. Available absolute ages are from the NW lake margin core (Rhoujjati et al., 2010) and correlations with the herein presented logs are based on lithologies and $CaCO_3$ curve. Textures and lithology: M: mud; $S_{f,m,c}$: sand (fine, middle, coarse); G: gravel; Ma: marl; W: wackstone; Pa: packstone. Systems tracts' and bounding surfaces' abbreviations: TST: transgressive systems tract; HST: highstand systems tract; FSST: Falling-stage systems tract; SB: sequence boundary; MFS: maximum flooding surface; FC: within trend (or not) facies contact; BSFR: basal surface of forced regression.*

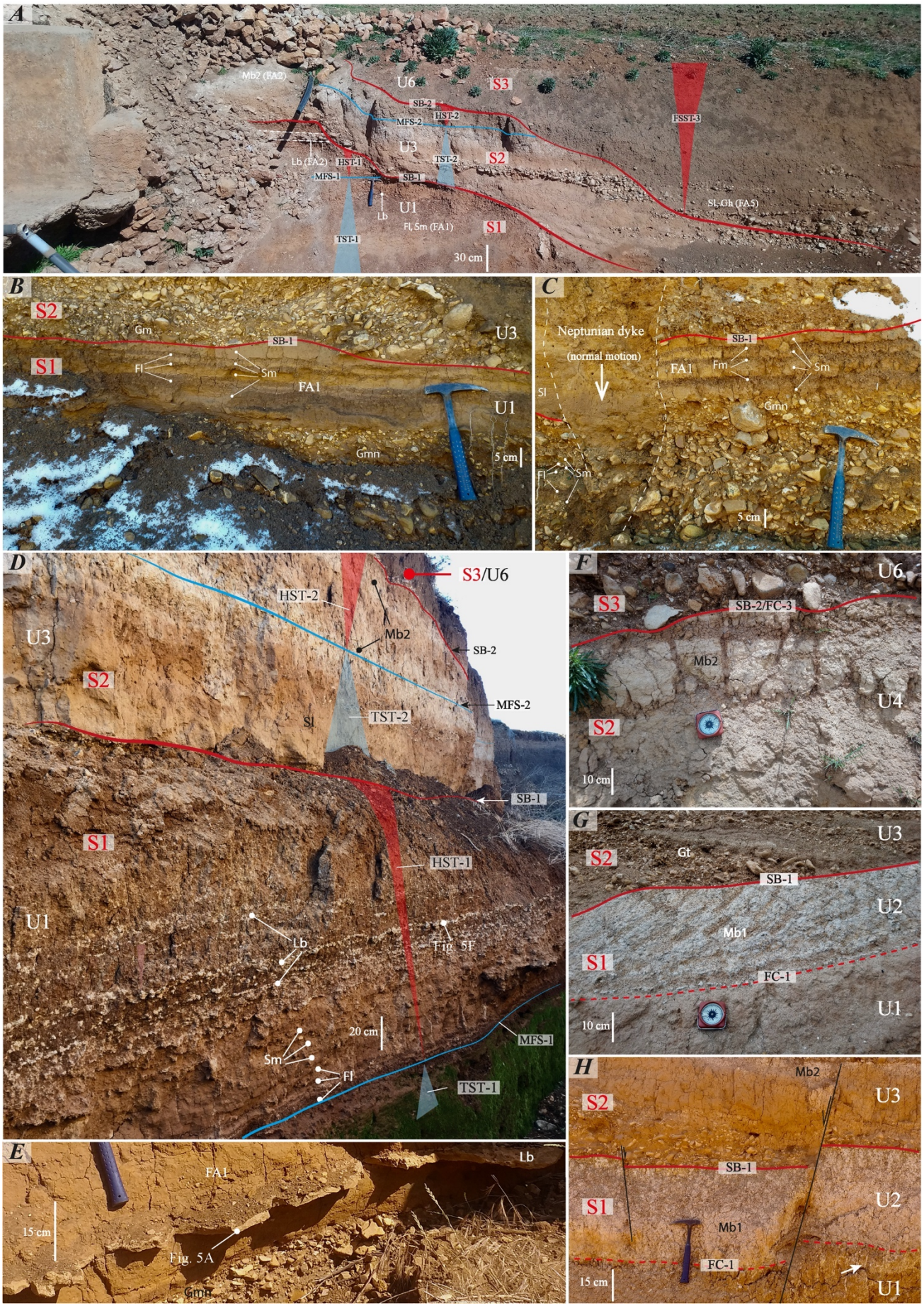
***Table 1**. Synopsis of the facies descriptions and interpretations*

Facies, conventional code, abundance, and figure(s)	**Geometry of deposits, textural characteristic and sedimentary structures**	**Interpretation**	**Associated facies**	**Depositional environment and deposit significance**
Mudstones				
Massive mudstones, **Fm**:	Tabular bodies; cm- to dm-scale thick, several metres in lateral extent; contain desiccation cracks and rhizoliths; structureless, although crudely laminated in some instances	Deposition from suspension in shallow standing water with periodic emersions	**Mb**, **Gcu**	Mud flat, low-energy lacustrine backshore
Laminated mudstones, **Fl**:	Tabular bodies; cm- to dm-scale thick, several metres in lateral extent; remarkable planar mm- to cm-thick laminations	Deposition from suspension-fallout in low-energy settings; occasional small turbidity currents	**Sl**, **Lb**	Lake centre (offshore) associated with active clastic supply (Potter et al., 1980)
Sandstones				
Horizontally laminated sandstones, **Sl:**	Tabular bodies; fine to medium-grained sands; cm- to dm-scale thick, meter to several meters in lateral extent; remarkable planar lamination; they can be (i) well sorted and associated with **Sr** and **Sp** or (ii) poorly to moderately sorted with outsized pebble-cobble clasts	(i) Tractional deposition from strong shoreward wave surges (outer planar facies *sensu* Clifton et al., 1971) in the lower part of the surf zone (Clifton et al., 1971);	**(i) Swr**, **Sp**	(i) Shoreface (Clifton et al., 1971)
		(ii) Deposition from tractional current in the lower part of the upper flow regime ($0.84 < Fr < 1$; Allen, 1982; Southard and Boguchwal, 1990)	**(ii) Gh**	(ii) Lower reach of sheetflood-dominated fan (Blair and McPherson, 2009); braid-plain of small-scale delta
Wave-ripple laminated sandstones, **Swr**	Tabular bodies; well-sorted fine to medium-grained sands; cm- to dm-thick and, several meters in lateral extent; symmetrical (i) and (ii) asymmetrical wave ripples	Tractional deposition from (i) symmetrical orbital velocity (inner rough facies, *sensu* Clifton et al., 1971) in the upper part of the surf zone, or (ii) asymmetrical orbital velocity	**Sl**	(i) Shoreface; (ii) offshore-shoreface transition (Clifton et al., 1971; Clifton, 2006)

Climbing-ripple cross-aminated sandstones, **Scr**	Lenticular bed; moderately sorted fine to medium sands; dm-thick and few metres in lateral extent; high angle of climb with lakeward dip	Deposition from traction and, significantly, from suspension with landward-directed current in lower flow regime; supercritical climb (Hunter, 1977), i.e., high aggradation from suspended load relative to bedload (type B *sensu* Ashley et al., 1982); washover process	**Sr**	Washover deposits; backshore
Massive sandstones, **Sm**	Lenticular or parallel-sided beds; sorted fine to coarse-grained sand; beds can be: (i) markedly massive, with non-erosive bases, poorly sorted, and containing some outsized granules, and interbedded with laminated mud beds (ii) markedly massive, moderately sorted, interbedded with deformed mud beds (iii) moderately bioturbated with poorly visible laminations (ichnofabric index 3 *sensu* Droser and Bottjer, 1986**)** and dominated medium-sized vertical borrows	(i) *en masse* deposition by frictional freezing from plastic (laminar) flow (Lowe, 1982) (ii) loss of granular cohesion and fluidization conditioned by mud barrier (iii) bioturbation akin to the continental Skolithos *ichnofacies* group 2 (*sensu* Scott et al., 2012); biogenic reworking balances the sedimentation rate and energy regime (moderate energy) (Collinson, 2019)	(i) **Fl** (ii) **Sl**, **Fl** (iii) **Fl**, **Fwr**	(i) Subaqueous sandy debris flow deposits (Shanmugam, 1996); lake offshore (ii) lake nearshore (iii) moderate-energy shoreface; sublittoral to littoral near “river” mouth (Scott et al., 2012)
Planar cross-bedded sandstones, **Sp**	Planar to lenticular beds; moderately to well sorted medium to coarse-grained sand with freshwater shell fragments; internal structures in beds can be: (i) high-angle oblique stratification dipping lakeward; (ii) moderate-angle (10°) oblique stratification dipping lakeward; (iii) high-angle oblique stratification dipping landward with sparse granules	(i) Tractional deposition from stronger wave backwash (lakeward wave surges) relative to wave uprush (inner planar facies *sensu* Clifton, 1971) in moderate-energy swash zone; slipface process (Postma, 1990) (ii) same as (i) but in high-energy swash zone (iii) landward progradation from avalanching	(i) **Sl**, **Gh, Gcn** (ii) **Sl**, **Gh**, **Gcn** (iii) **Swr**	(i) Small scale moderate-energy reflected beach-face (Wright et al., 1979); Prograding small scall Gilbert-type delta (Postma, 1990) (ii) Small scale high-energy dissipative beach-face (Wright et al., 1979) (iii) washover deposits; backshore

Conglomerates				
Coarse-tail normal graded matrix-supported conglomerates, **Gmn**	Beds have planar, non-erosive bases, dm- to thick, and several metres in lateral extent; crude coarse-tail normal grading; poorly to moderately sorted; upward increase in matrix content; clasts lack orientation	Deposition by cohesive freezing (Lowe, 1982) and post-debris flow suspension fallout from flow with pseudoplastic behaviour (Horton and Schmitt, 1996; Nemec and Steel, 1984); short-distance subaqueous flow	**Fl**, **Mb2**	Sub-aqueous debris flow (Nemec and Steel, 1984) near a gravely fan delta
Massive to crudely normal-graded clast-supported conglomerates, **Gm**	Lenticular beds with erosional bases and interbedded with facies **Sl** and **Gh**, with or without root remains; dm- to m-thick and few meters in lateral extent; moderately sorted with matrix-filled framework, sometimes with openwork texture; flattened clasts are well oriented [a(t), b(i)]; matrix consists of sands	Tractional and rapid grain-by-grain deposition from turbulent fluidal (Newtonian) flow with high energy and high clast (bedload) supply	**Sl**	Channels in alluvial plain braid-plain of small-scale delta
Graded to massive cross-bedded gravel and sand couplets, **GSg**	Lobe-shaped m-thick body formed by interbedded dm-thick oblique clinoforms (foresets) of orthoconglomerates and sands separated by well-developed near-horizontal beds (topsets and bottomsets)	Slipface processes (graine flow) (Postma, 1990)		Prograding small-scale Gilbert-type delta (Postma, 1990) with non-uniform supply following autogenic process (Kleinhans, 2005)
Horizontally bedded orthoconglomerates, **Gh**	Tabular, dm-thick beds, sometimes one clast-thicks; moderately to well-sorted pebble-cobble; no grading; no erosional bases; recognized stratification and interbedding with facies **Sl**; clasts are horizontally-oriented and show no imbrication	Tractional deposition from diluted sheetflow/sheetflood in upper flow regime conditions; wave-generated winnowing process (lag deposit)	(i) **Sl**, **Gcn** (ii) **Sp** (iii) **Sl**	(i) Braid-plain of small-scale delta; (ii) beach lag deposits (ii) lower reaches of sheetflood-dominated alluvial fan (Blair and McPherson, 2009)

Carbonate and organic-rich facies				
Bioclastic marls, **Mb**:				
Homogeneous, **Mb1**	Grey bed with variable thickness (dm- to m-thick); frequent shells of ostracods, gastropods, and bivalves; frequent charophyte oogonium; low to moderate clastic component; unconformable upper or lower boundary	High biologic (authigenic) productivity with moderate clastic input in marginal setting (high sedimentation rate in the photic zone); active landscape weathering	**P**	Low-energy bench margin (Platt and Wright, 1991)
Disturbed, **Mb2**	Tabular, dm-thick (20- to 40) with relatively constant thickness; moderate bioclastic and clastic component; disturbed with filled casts; conformable boundaries	Moderate rate and landscape weathering	**Fm**	
Bioclastic limestones, **Lb**	Planar to lenticular dm-thick wackstone to packstone very low detrital content; traces of secondary processes (i) ostracod-rich wackstone: very frequent (limited) ostracods (charophytes); widespread mottling (Fe-Mn staining) (ii) charophyte-rich packstone: very frequent charophyte remains; widespread subaerial exposure features (e.g., fenestral and alveolar septal structures, microkarst cavities, pseudo-microkarsts)	High biologic (authigenic) productivity with very low clastic input (low sedimentation rate) subject to periodic sub-areal exposure; generally semi-arid conditions with highly variable evaporation/precipitation ratio	**Fl, Sm**	Palustrine setting (Alonso-Zarza, 2003); ostracod-rich (charophyte-rich) sub-facies indicates relatively more (less) profundal and less (more) variable settings (Gierlowski-Kordesch, 2010); low-energy ramp margin (Platt and Wright, 1991)
Organic-rich facies: **S** (sapropel); **P** (peat)	Dark-coloured bed with variable thickness; very bioturbated; highly-rich in organic matter (i) absence of root remains (distally) (ii) frequent root remains (proximally)	High bio-productivity and/or preservation (non-oxygenating setting)	**Mb**	(i) Profundal conditions (sapropel, **S**) (ii) Marshy lake margin (peat deposits, **P**); low-energy bench margin (Platt and Wright, 1991)


A
Mb2 (FA2)
U6
S3
SB-2
HST-2
MFS-2
FSST-3
U3
TST-2
S2
Lb (FA2)
HST-1
MFS-1
SB-1
Lb
U1
Fl, Sm (FA1)
S1
Sl, Gh (FA5)
TST-1
30 cm
B
S2
Gm
SB-1
U3
S1
Fl
Sm
FA1
U1
Gmn
5 cm
C
Neptunian dyke
(normal motion)
SB-1
FA1
Fm
Sm
Sl
Gmn
Fl
Sm
5 cm
D
S3/U6
HST-2
Mb2
SB-2
U3
S2
MFS-2
Sl
TST-2
SB-1
S1
HST-1
U1
Lb
Fig. 5F
20 cm
MFS-1
Sm
Fl
TST-1
F
U6
S3
SB-2/FC-3
Mb2
U4
S2
10 cm
G
U3
S2
Gt
SB-1
U2
Mb1
S1
FC-1
U1
10 cm
H
Mb2
U3
S2
SB-1
U2
S1
Mb1
FC-1
15 cm
U1
E
FA1
Lb
15 cm
Fig. 5A
GmH

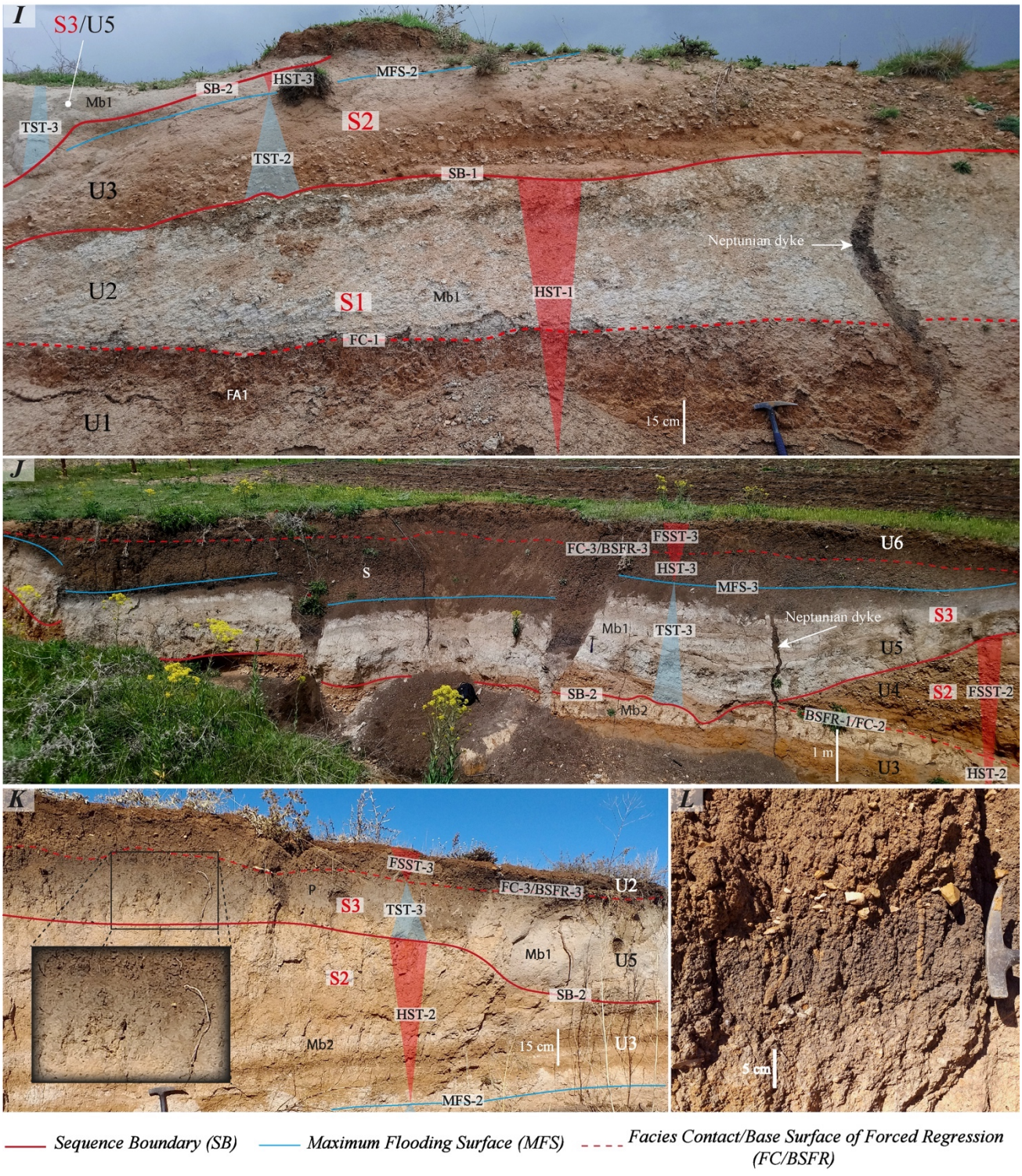


Figure 4. *Field views of various facies associations (FA1-FA2), units (U1-U6), and sequences (S1-S3) and their systems tracts component and bounding surfaces from the studied outcrop (Fig. 2 for locations). **A**: Within proximal stretch field view, logged in log-1. **B-C**: detail of the offshore facies association (FA1) showing the alternating massive sand (Sm) and laminated mud (Fl). This alternation is interrupted by coarse tail paraconglomerate (Gmn) indicating subaqueous debris flow. Note the occurrence of a neptunian dyke (**C**) with normal motion. **D**: Field view showing m-thick succession of offshore (Sm, Fl) and palustrine (Lb) facies of the lower sequence (S1) and fluvial to lacustrine deposits of the middle sequence (S2), separated by SB-1. **E**: Close-up view of the ostracod-rich limestone bed that stratigraphically occurs below the charophyte-rich one shown in **D** (log-2). **F-J**: Field views showing the two types of marl, Mb1, showing brittle deformation (**G**) and vertical burrows piercing into the lower offshore deposits (arrow, **H**), and Mb2 with filled cracks (**F**). Compare Mb1 and Mb2 in **J**. The organic-rich facies in **J** lack root remains, thereby interpreted as sapropel deposits (S). **K-L**: Proximal field views showing bioturbation (vegetation remains, **K**, and vertical burrows, **L**) affecting proximally the*

*same organic-rich facies shown in **J**, thereby interpreted as peat deposits (P). Sequences and their systems tract components and surfaces, along with units and their bounding surfaces (FC or SB) are indicated. See **Table 1** for facies codes. Designation of sequence stratigraphy abbreviations is in **Figure 3** caption.*

4.1.2 Facies association 2 (FA2, low-energy bench and ramp lacustrine deposits)

FA2 consists of dm- to m-thick greyish bioclastic marl (Mb), dm-thick bioclastic wackstone to packstone (Lb), and blackish organic-rich facies (S). Four stratigraphic levels of marl deposits were recognised from the fieldwork (synthetic log in Fig. 3). They show some similarities and many differences in terms of clastic component, faunal richness, and internal structures (Fig. 4J). The higher and lower stratigraphic levels (Mb1) are m-scale with variable thickness, rich (poor) in bioclasts (detrital component), and associated with erosive boundaries (Fig. 4G-J). Interestingly, the base of the lower marl bed exhibits typical medium-sized vertical burrows, that is, 4–9 mm in diameter according to Scott et al. (2012) (Fig. 4H). Ostracods are very abundant (>500 indiv./8g) with a predominance of the species *Neglecandona* sp. (Meisch et al., 2019), a species close to *N. neglecta* and to *N. dalmatina* but clearly different from these, perhaps corresponding to an as yet undescribed new species, and *Ilyocypris gibba* (*see* sub-section 4.2.3 and Fig. 10). *Darwinula stevensoni, Herpetocypris* cf. *helenae, Candona candida, Pseudocandona albicans, Cypridopsis vidua, Cyclocypris* cf. *laevis* and *Herpetocypris brevicaudata* were also identified, yet with minor frequency. Facies Mb1 shows a homogeneous internal structure, although the lower one locally shows brittle deformation materialised by a bed-parallel slip associated with domino-style faults (Fig. 4G; *see* Azennoud et al., 2022b). Those in the middle (Mb2) are dm-thick (20 to 40 cm) with tabular geometry and slight lakeward increase in thickness, richer in detrital component (mostly sand-sized), and bounded by conformable surfaces (Fig. 4D, F and J). Compared to Mb1, Mb2 is poorer in ostracods (<100 indiv./8g), and other aquatic animals, with the predominance of the species *I. gibba* and *Neglecandona* sp. This facies is pierced throughout by regularly spaced, commonly V-shaped and pointed downward sandy injections (Fig. 4F, J), giving rise to an internal structure similar to that of filled cracks described by Tanner (1998). The maximum openings width can exceed 10 cm in some instances. Bioclastic limestone, with a very low clastic component, encompasses two sub-facies types distinguishable by their faunal/floral biocenoses and resulted textures, and by the later vegetation influence. Hence, charophyte-rich limestone with packstone texture and ostracod-rich limestone with wackstone texture were distinguished. they are observed to interrupt FA1 (Fig. 4A, D and E). Hand samples of these two sub-facies indicate differences in vegetation influence during or shortly after deposition, with well-marked root traces (filled or not with spar) recognised in the charophyte-rich sub-facies (Fig. 5). In thin section, both samples reveal primary (lacustrine) and secondary (paedogenic and diagenetic) features

according to previous petrographic key publications (Freytet and Verrecchia, 2002; Alonso-Zarza, 2003). The wackstone to packstone texture (Dunham, 1962) is made up by ostracod, occasional bivalve shells, and calcified charophytes stems, altogether included in a peloidal-clotted micrite matrix (Fig. 5). Later modification through paedogenic and diagenetic processes is attested by the widespread expression of mottling (Fe- and Mn-staining, especially in ostracod-rich sub-facies), fenestral and alveolar septal structures (mostly in charophyte-rich sub-facies), cracks, and less commonly poorly-developed pseudo-microkarst (*sensu* Plaziat and Freytet, 1978) (Fig. 5); the ungenuine character of the microkarst (i.e., the "pseudo" prefix thereof) is evidenced by the vertically elongated and cylindrical shape of the voids (Plaziat and Freytet, 1978), although the rounded margins suggest a minor contribution of dissolution (Platt, 1989) (Fig. 5A). Cavities (fenestral, root and desiccation cracks) are partially or completely filled by Fe-stained microspar, occupying the outermost ("vadose silts", Dunham, 1969), and equant spar crystals, occupying the innermost and occasionally associated with quartz grains and limestone fragments (Fig. 5C, I). Micrite recrystallisation to spar calcite (cement) is very common. This is evidenced by the presence as "ghosts" of some calcified charophyte stems (Fig. 5C) and peloidal-clotted micrite forming the matrix (Fig. 5B, G). Finally, the organic-rich facies reveals variable thickness (dm- to m-thick) and along dip variation in vegetation remains content, with a moderate amount of root debris in the proximal stretch (log-2, Fig. 4K, L) and a lack of plant remains more distally (Log-3, Fig. 4J). Besides, it has been directly seen or inferred from neptunian dykes (Fig. 4I; *see* also Azennoud et al., 2022b) to overlap the upper level of bioclastic marl (Mb1). All of these deposits show considerable extension relative to the basin.

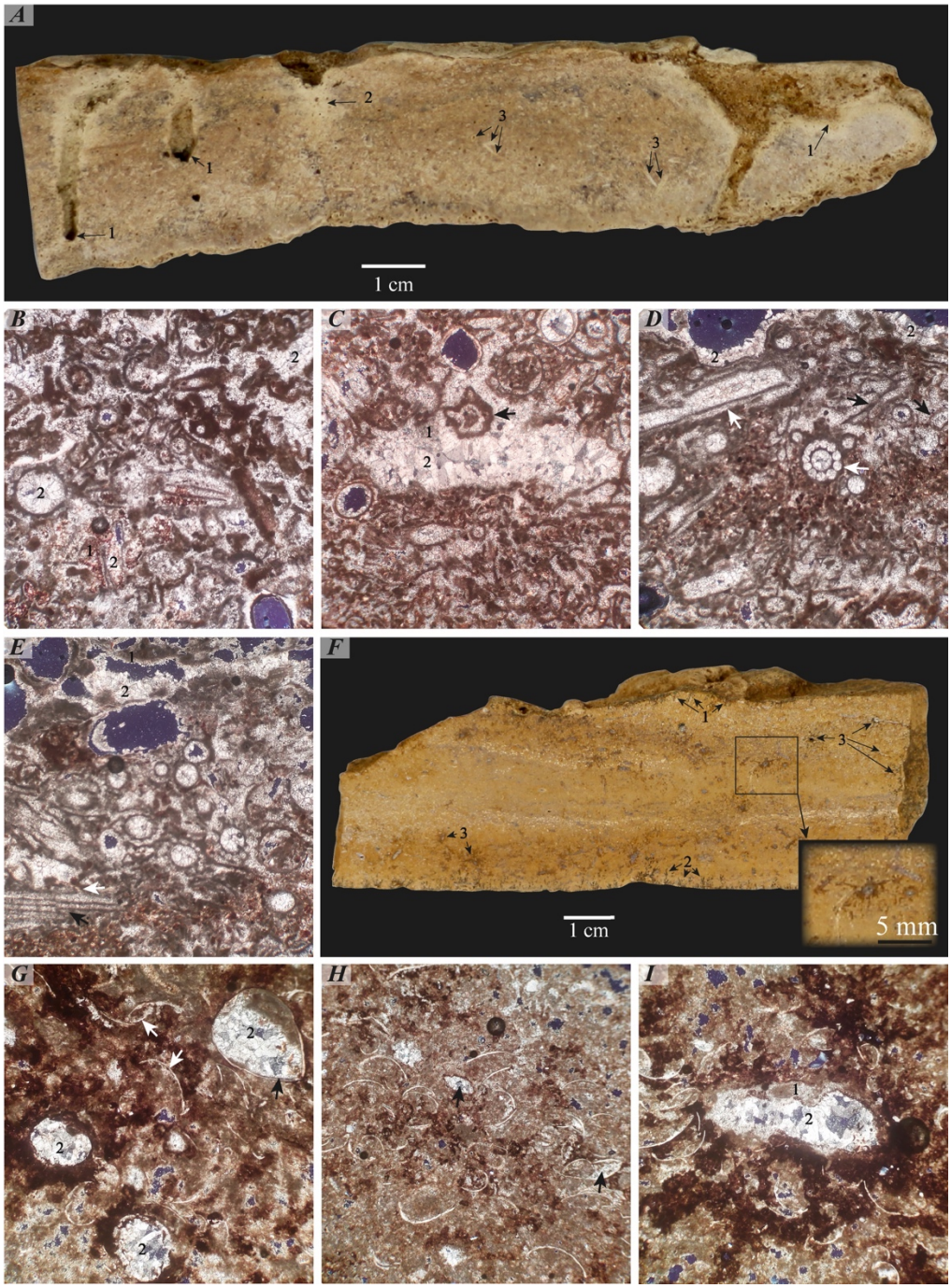


***Figure 5**. Hand samples and photomicrographs of palustrine bioclastic limestone of facies association FA2. The diagonal of each microphotograph is 4 mm. **A-E**: Charophyte-rich packstone. **A**: Hand sample indicating vertical cylinder-shaped cavities (pseudo-microkarst) with rounded margins (1). Some cavities are filled up with spar (2) or intraclastic debris (3); calcified charophyte stems (4) can be recognised. **B-E**: Photomicrographs showing well-developed calcified charophyte stems (white arrows, **D**), "ghosts" of calcified stems (black arrow, **C**), alveolar septal (black arrow, **D**) and fenestral structures (**E**). Note the small fragment in **E** (black arrow) showing alternating laminae of dark micrite and equant microspar developing on charophyte leave (i.e., shoots of limited growth); the indicated small protrusion (white arrow) may correspond to calcified secondary laterals (i.e., stipulodes) of the chara sp. Microspar (1) and spar (2) form the fill of voids. Recrystallisation of micrite to microspar spar is common (e.g., see **B** and the black arrow, **C**). Note the well-developed Fe-staining (e.g., lower third of **B** and **E**). **F-I**: Ostracod-rich wackstone. **F**: Hand sample showing uppermost small desiccation cracks (1), lowermost dendrite-like Mn-staining (2), and filled up with spar and iron circum-stained cavities (3 and inset). **G-I**: Photomicrographs showing articulated and disarticulated ostracod shells (white arrow, **G**), and occasional bivalve (black arrow, **G**) in a peloidal-clotted micrite. Stained microspar ("vadose silts", 1) and equant spar (2) form the fill of the cavities and the voids of some articulated ostracod shells (arrows in **H**). Note the well-expressed mottling around voids.*

The carbonate component of marl is formed through biochemical precipitation of carbonates by means of charophytes and associated epiphyte microorganisms (including cyanobacteria), planktonic organisms, and small animals (e.g., ostracods, gastropods, bivalves) (Freytet and Verrecchia, 2002). Homogeneous marl with a high biogenic component (Mb1) is more likely to reflect low-energy carbonate bench margin according to the facies model proposed by Platt and Wright (1991). The moderate clastic component along with the active authigenic bio-controlled and bio-induced calcite precipitation suggest optimum conditions with active water drainage and warmer temperatures (Platt and Wright, 1991; Gierlowski-Kordesch, 2010). This scenario may have led to higher sedimentation rate on the lake-shore and, subsequently, to the bench formation. Referring to Scott et al. (2012), the moderate-sized vertical burrows, being similar to the continental ichnofacies Skolithos group 2, suggest prograding shoreline conditions (slight water body contraction) upon the transition from the offshore deposits below into the bench deposits above. On the other hand, disturbed marl with moderate biogenic component (Mb2) suggests cooler conditions. This may have promoted the development of bench-like build-up with a very gentle slope break towards the lake centre in a very low-energy setting. Their disturbance by regularly spaced filled cracks was interpreted to reflect subareal desiccation rather than subaqueous shrinkage (synaeresis) processes (Azennoud et al., 2022b). The co-occurrence in prevalence of *I. gibba* with *Neglecandona* sp. suggests deposition in the littoral zone as *I. gibba* prefers shallow water and *Neglecandona* spp., and particularly the widespread *N. neglecta,* occur from the shallow littoral zone down to the great depth (Meisch, 2000). This is also supported by the occurrence of *Herpetocypris* cf. *helenae* (but *cf.,* sub-section 4.2.3), which prefers the littoral zone of lakes (Meisch, 2000).

Later modification of the primary bioclastic limestone by mechanical (desiccation), chemical (mottling and calcite recrystallisation), and biological (pseudo-microkarst, alveolar septae, and fenestral structures) processes and features point to palustrine conditions as defined by Freytet and Plaziat (1982). The predominance of mottling processes (Fe and Mn mobilisation caused by Eh changes due to water table fluctuation, Freytet and Plaziat, 1982) and the absence of complex features such as well-developed pseudo-microkarst and flat pebble breccias (intraclasts) suggest a "*less developed palustrine limestone*", *sensu* Alonso-Zarza (2003), and, in terms of time of exposure, a morphological stage 1 according to Alonso-Zarza et al. (2012). The well-expressed diagenetic processes (cementation and recrystallisation) are interpreted to reflect post-deposition phreatic influence, synchronous with lake-level rise as suggested by the pursued deposition of the offshore

succession (Fig. 4A, D). While charophyte-rich sub-facies suggest deposition in the littoral zone (i.e., photic zone; Gierlowski-Kordesch, 2010), ostracod-rich sub-facies, on the other hand, indicates non-paedogenically modified (profundal) lacustrine settings (Alonso-Zarza, 2003; Gierlowski-Kordesch, 2010) during deposition of the primary features mentioned above. According to the lake facies models proposed by Platt and Wright (1991), this depositional setting would mimic the low-energy ramp-like lacustrine margin.

Lacking plant remains, the organic-rich facies in the distal stretch is more likely to reflect profundal environment, where conditions are suitable for the organic material to accumulate and preserve, giving way to lacustrine sapropel deposits (S). In turn, the presence of vegetation relics in the proximal stretch is to suggest marshy conditions where the accumulation of the organic matter and its poor biodegradation would favour peat formation (P). Accordingly, the vertical passage of homogeneous bioclastic marl to organic-rich facies in log-3 is likely to reflect a rise in lake level (lake extension) and/or a change in palaeoenvironmental conditions that would have enhanced the biological activity (*see* below). Besides, this may reflect an abrupt change in paleoclimatic settings (Cecil et al., 1985). The variation in thickness was controlled by the configuration of the palaeosurface.

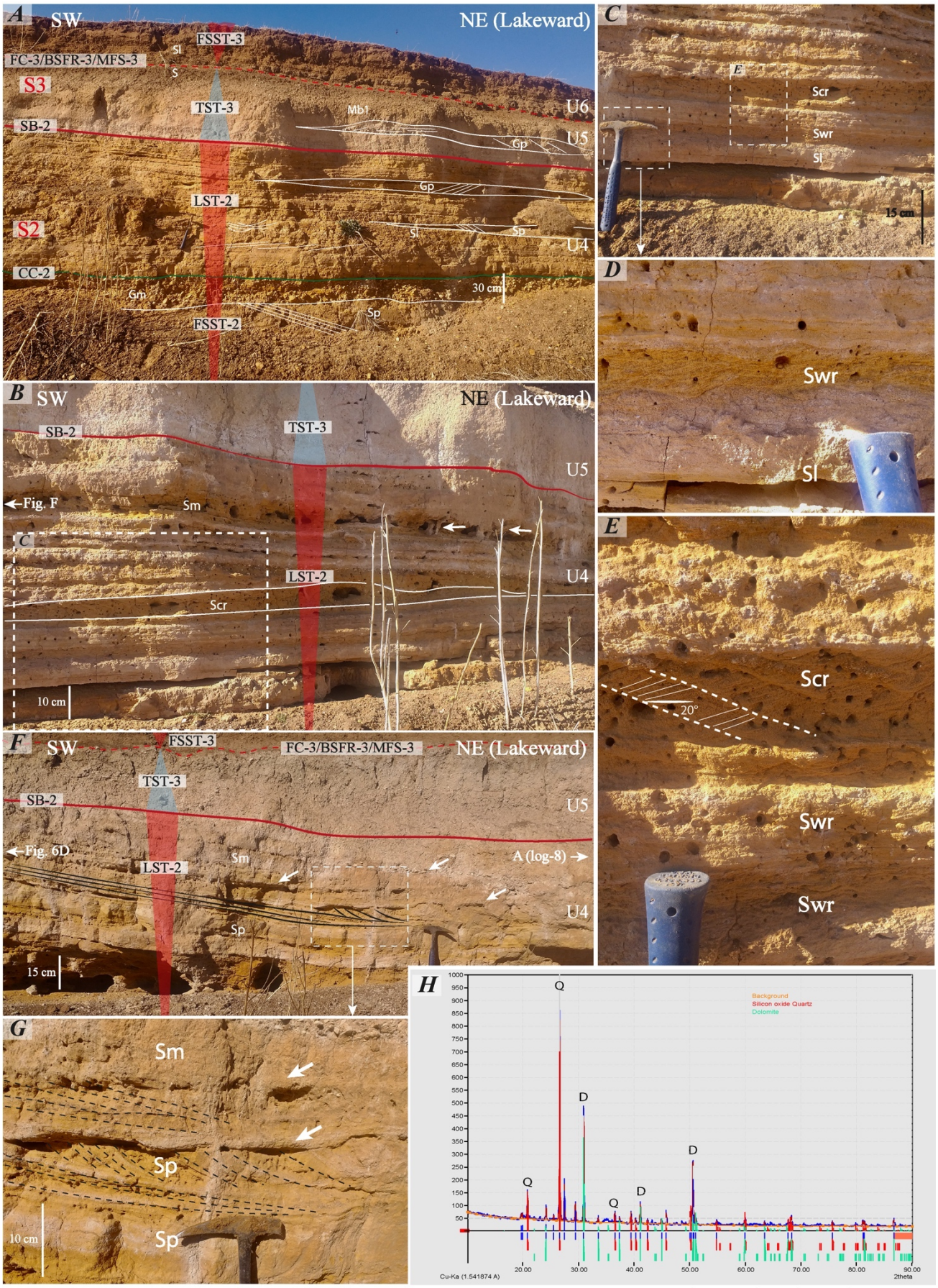
The large extension of these deposits relative to the basin scale suggests a general lake extension during time of their deposition.

4.1.3 Facies association 3 (FA3, lacustrine wave-influenced nearshore deposits)

Facies association 3a (FA3a, lake shoreface). Deposits of FA3a consist mainly of tabular, moderately sorted fine to coarse-grained m-thick sandstone with occasional freshwater broken mollusc and bivalve shells. Alternating carbonaceous layers were also recognised. Internal sedimentary structures involve both planar (Fl) and wave-ripple (Fwr) laminations (Fig. 6D). However, massive beds (Sm) with poorly visible planar laminations associated or not with moderate bioturbation were also observed, especially at the tops of the distal logs (log-7 and log-8; Fig. 6B). Massive structure was shown to be associated with soft-sediment deformation structures in shoreface sandstone (log-5; Azennoud et al., 2022b, their Fig. 6). Bioturbation consists mainly of medium-sized vertical burrows (*sensu* Scott et al., 2012). The sand-sized grains are made of dolomite, detrital calcite and quartz akin to the mineralogical signature of the bedrock (Liasic carbonates) (Figs. 1 and 6H). Altogether, these deposits are extensively shown from the distalmost logs (log-5-log-8), whereas less commonly in the proximal stretch (log-2, Fig. 8B).

The presence of freshwater broken shells indicates lacustrine wave-influenced nearshore environment (Nutz et al., 2020) akin to marine settings (Gracia et al., 2021). Near horizontal planar laminations reflect tractional deposition from strong shoreward wave surges (asymmetric orbital velocity) in the lower part of the surf zone, akin to the "outer planar facies" of Clifton et al. (1971). Wave-ripple laminations indicate tractional deposition from oscillatory current with either (i) symmetrical orbital velocity in the upper part of the surf zone, akin to the "inner rough facies" of Clifton et al. (1971) or asymmetrical orbital velocity in the offshore-shoreface transition, giving rise to asymmetrical ripples (Clifton et al., 1971; Weleschuk and Dashtgard, 2019; Xue et al., 2021). Both facies reveal a relatively high-energy shoreface environment (Clifton et al., 1971; Clifton, 2006; Nutz et al., 2020). The occasional occurrence of carbonaceous beds indicates lower-energy conditions and minor clastic supply. As for the bioturbated sandstone (Sm), the still visible planar laminations with medium-sized vertical burrows suggest moderate biological reworking, which may be akin to ichnofabric index 3 according to Droser and Bottjer (1986), and a continental ichnofacies type *Skolithos* group 2 (Scott et al., 2012). According to Scott et al. (2012), this bioturbated sandstone is likely to reflect sublittoral to littoral near "river" mouth. Alternatively, this may be compared to "river"-fed lower-energy shoreface environment (Scott et al., 2012), regarding also the planar lamination, where the sedimentation rate balances the bioturbation. The massive structure seen to be unrelated to bioturbation was interpreted as due to liquefaction and local fluidization (*see* Azennoud et al., 2022b).

Facies association 3b (FA3-b, lake foreshore deposits). FA2-b consists of tabular, dm- to m-thick, moderately to well-sorted, medium to coarse-grained sandstone beds with occasional broken shell remains. Internal structures of sandstone beds involve two varieties of near-planar, yet slightly concave upward, cross-stratifications (Sp): (i) high-angle (20°-30°) oblique stratification, and (ii) moderate angle (10°) oblique stratification (Fig. 6F, G). The stratification dips lakeward in both varieties. Associated with these deposits, granule coarse sandstone (arrows in Fig. 6F, G) or one clast-thick beds with horizontal, well-sorted pebble- to cobble-sized gravels were observed locally. Deposits of this facies association are restricted to the distal part of the studied outcrop (log-5-log-8).



Sequence Boundary (SB) *Correlative Conformity (CC)* *Facies Contact/Base Surface of Forced Regression (FC/BSFR)*

Figure 6. *Distal stretch. Field views and X-Ray Diffraction diagram of the wave-influenced nearshore deposits.* ***A****: Field view logged in log-7.* ***B-E****: Mesoscale and close-up views of the shoreface (Swr, Sl) and backshore (Scr) sandstone deposits. The field view shown in* ***B*** *is logged in log-8. Note the upward increase in bioturbation materialised by vertical burrows, giving way to massive structure (arrows,* ***B****).* ***F-G****: Mesoscale and close-up view showing high- and moderate-angle slightly upward concave oblique stratification (Sp) defining the foreshore (beach-face) deposits, along with associated beach deposits (white arrows). Note the upward increase in bioturbation.* ***H****: X-Ray diffractogram of a nearshore sandstone sample showing the dominance of dolomite (D) and quartz (Q). Sequences and their systems tract components and surfaces, along with units and their bounding surfaces (FC or SB) are indicated. See* ***Table 1*** *for facies codes. Designation of sequence stratigraphy abbreviations is in* ***Figure 3*** *caption.*

The occasional presence of broken shells attests to lacustrine wave-influenced nearshore environment (Nutz et al., 2020). High-angle oblique stratification with sparse fine gravels reflects tractional deposition from stronger wave backwash (lakeward wave surges) relative to wave uprush in moderate-energy swash zone (inner planar facies *sensu* Clifton, 1971). As such, this suggests (small scale) moderate-energy reflected beach-face (Wright et al., 1979) sub-environment. Otherwise, low-angle oblique stratification rather reflects dissipative beach-face accretion in higher energy foreshore environment (Wright et al., 1979; Nutz et al., 2020). Granule coarse-grained sandstone and one clast-thick gravel deposits reflect more likely winnowing process developed in beach environment.

Facies association 3c (FA3-c, lake backshore deposits). Deposits of FA3-c are made up of dm-thick beds of moderately sorted, fine to medium-grained sandstone and pebbly sandstone with infrequent broken shells. Along the outcrop, two types of facies were identified. The first type exhibits lenticular bodies of pebbly sandstone with high-angle oblique stratification (facies Sp) that dips landward (Fig. 6A). The second type consists of lenticular beds of climbing-ripples laminated sandstone with high critical angle of climb (>15°) that dips lakeward, and stoss side preservation (Fig. 6B, E). Both types are pinched out laterally and vertically by wavy-ripples cross-laminated sandstone (Swr), planar laminated sandstone (Sl), or lakeward-dipping low-angle oblique stratified sandstone (Sp). Deposits of FA3-c, like the other nearshore deposits, are limited to the distal portion of the studied outcrops.

Freshwater shell fragments reflect a lacustrine nearshore domain (Nutz et al., 2020). The landward dip of oblique stratification of pebbly sandstone suggests washover deposits that imply landward progradation driven by overwash avalanching (Nutz et al., 2017, 2020). Similarly, the high value, and lakeward dip, of the critical angle of climb imply supercritical climb (Hunter, 1977; Jobe et al., 2012) and deposition (i) through significant suspension fallout with high aggradation (type B according to Ashley et al., 1982) in upper flow regime, and (ii) from landwards-directed flows (overwash flows, Matias and Masselink, 2017). The constant angle of climb, the lack of hummocky and swaley cross-stratification, and the small-scale lake basin, all point to regular and persistent overwash flows in relatively high-energy settings (lack of bioturbation) rather than storm-related overwash episodes. Besides, the lakeward passage of this facies towards low-angle oblique stratified

sandstone suggests an implication of infragravity waves as they dominate at dissipative beach-faces (Wright et al., 1979; Baumann et al., 2017). Accordingly, the overwash processes are indicative of the backshore environment (Nutz et al., 2020).

Overall, the limited occurrence of nearshore deposits in the distal part, the vertical transitions between shoreface, foreshore and backshore deposits, together with the increase in bioturbation more distally and upward (i.e., upper part of Fig. 6B and F), suggest a progressive lake contraction, superimposed by small-scale lake-level fluctuations, under a background reduction in wind-generated waves.

4.1.4 Facies association 4 (FA4, Gilbert-type delta deposits)

FA4-a sediments are composed of dm- to m-thick alternating beds of conglomerate and sandstone. They consist of m-thick, one lobe-shaped set formed by (i) sigmoidal clinoforms with moderate-angle of alternating massive to normally graded clast-supported conglomerate (orthoconglomerate) and sandstone beds (facies GSg), and (ii) dm-thick planar of cross-stratified coarse-grained to granule sandstone (Sp) with straight foresets dipping lakeward. Clinoforms are dipping lakeward but show asymptotic lower contact. They are separated upwards and downwards by well-developed planar beds. This is observed strictly on the distal stretch. The strike planar geometry of the foresets forming the cross-stratified sandstone (Sp) of this facies association makes this latter clearly distinguished from that of the beach-face where foresets show slight upward concave curvature (compare Fig. 6G with Fig. 7E).

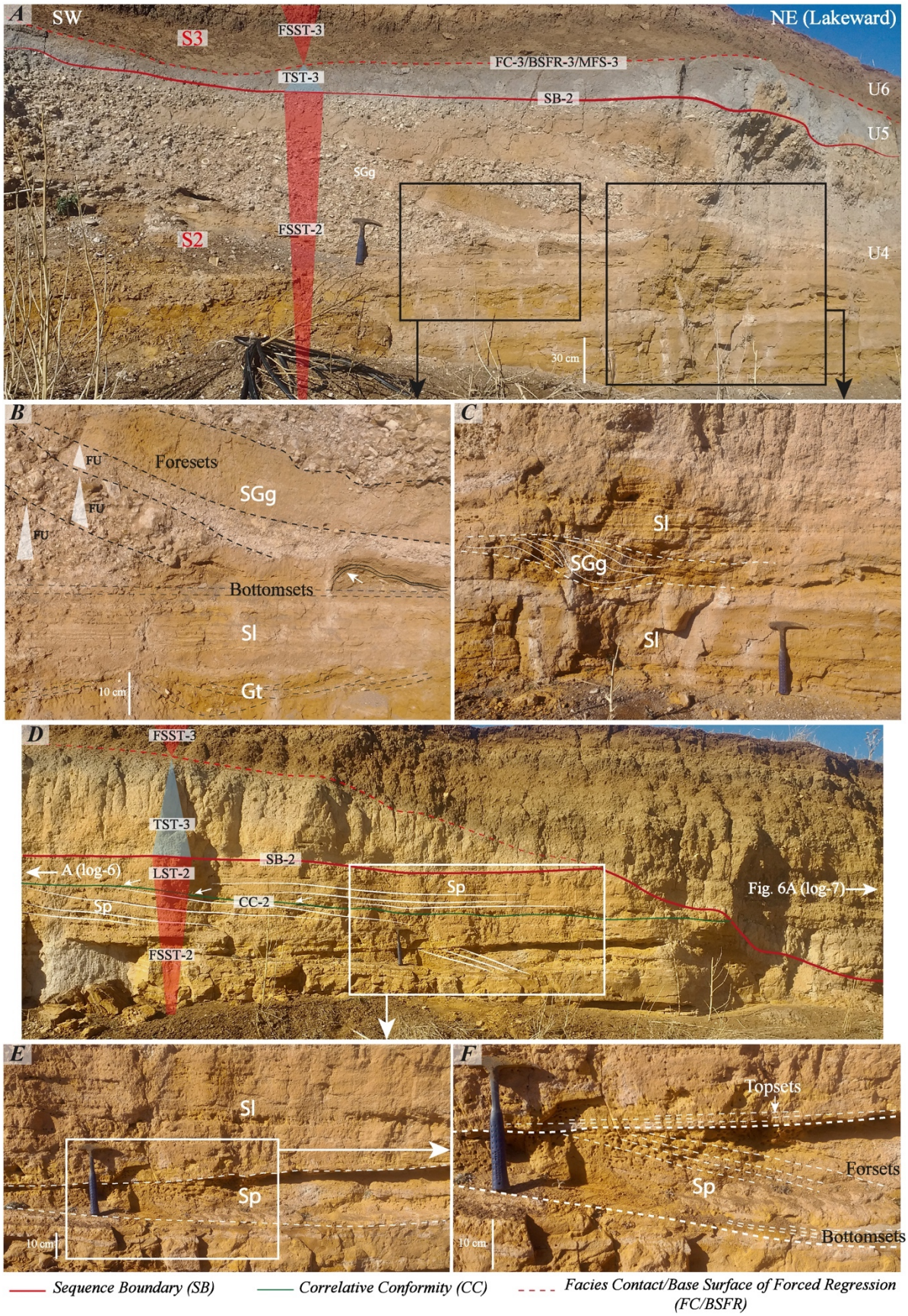


***Figure 7**. Distal stretch. Field views of Gilbert-type delta deposits. **A-C**: Mesoscale and close-up field views logged in log-6 showing interbedded larger-scaled (**A**) and smaller scaled clinoforms (**C**) with slight asymptotic base contact (**B**) forming the foresets of the classical Gilbert-type delta. **D-E**: Smaller scaled sandstone delta lobe with planar foreset and angular*

*base contact. Sequences and their systems tract components and surfaces, along with units and their bounding surfaces (FC or SB) are indicated. See **Table 1** for facies codes. Designation of sequence stratigraphy abbreviations is in **Figure 3** caption.*

The sigmoidal clinoforms, combined with the planar beds by which they are separated, more likely mimic the architecture of a small-scale shallow-water Gilbert-type delta where the clinoforms form the foresets and the planar beds build the bottomsets and the topsets (Postma, 1990; Zavala et al., 2021; Budai et al., 2021). The depositional mechanism of these interbedded foresets implies slipface processes where grain flow and avalanching dominate (Nemec, 1990; Postma, 1990). The observed quasi-cyclicity of sand and gravel foresets can be generated by several allocyclic processes, including wave reworking and seasonal fluctuations (e.g., Rojas and Le Roux, 2005), or it might be the result of autogenic processes (Kleinhans, 2005). In fact, experiment findings have emphasised the role of the feeder system (line or point feeding, Postma, 1990), and its width relative to the basin depth in modulating autogenic processes of the foresets (Kleinhans, 2005). Similarly, planar bedded (granule) sandstone is likely to reflect slipface processes of finer sediments giving way to one lobe of planar foresets. Indeed, the straight planar foresets exclude another alternative that may involve a lobate set of migrating 3D-dune, since the observed grain size (coarse sand to granule sand) would imply deposition from traction in upper flow regime (Southard and Boguchwal, 1990) where the separation eddy must be strong, thereby favouring asymptotic basal contact (Collinson, 1970; Miall, 1977) rather than the observed angular contact. In turn, while involving coarser sediments, the asymptotic lower contacts at the toesets observed from the first type deposits are likely to relate to both the greater momentum gaining of granules and pebbles as they slip onto the foresets and the loss of which further downslope (Sohn et al., 1997).

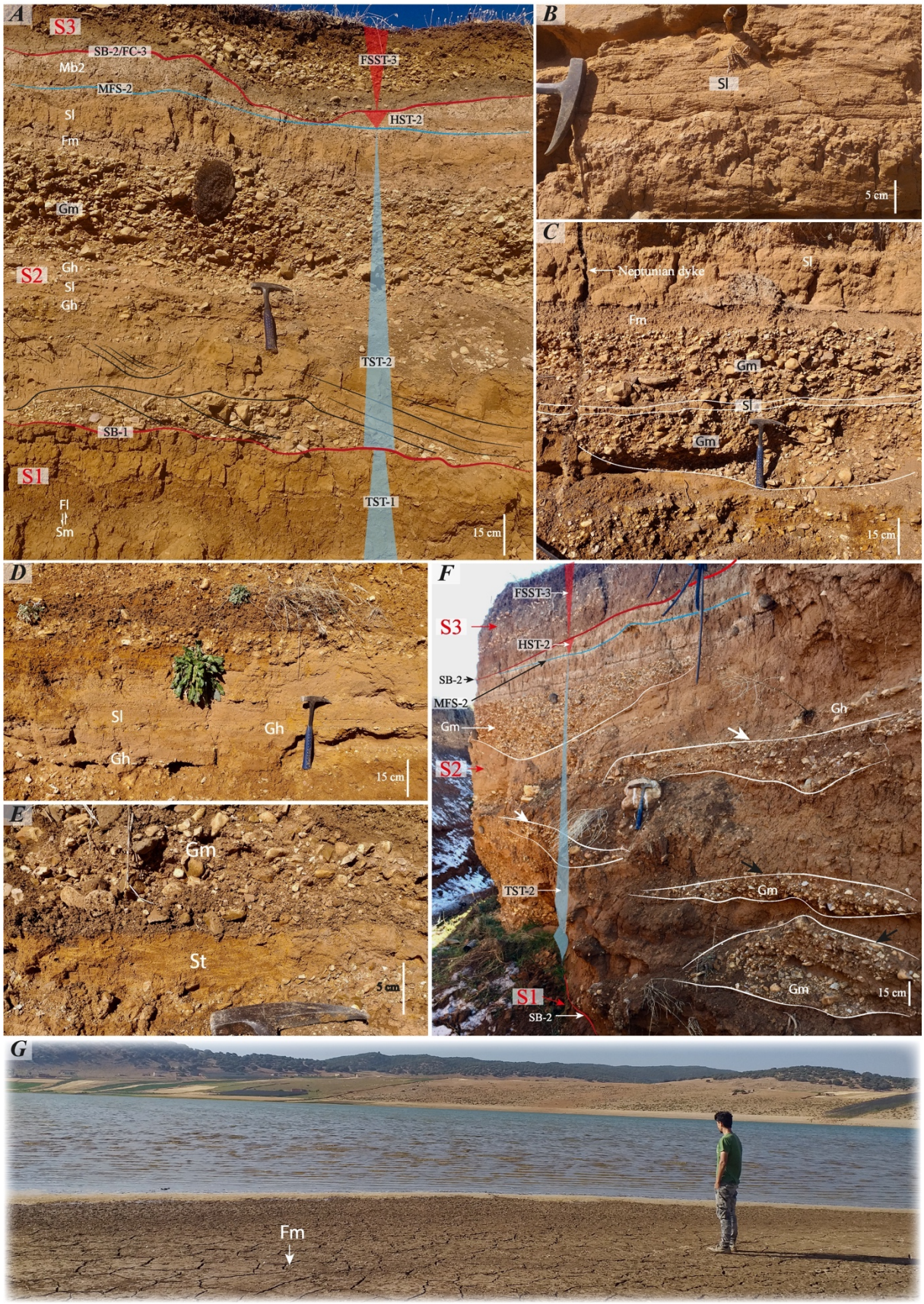
4.1.5 Facies association 5 (FA5, fluvial/alluvial deposits)

Facies association 5a (FA5-a, fluvial deposits). Along dip (Fig. 8A, G), This is formed by a succession of (i) laterally limited lenticular dm-thick bodies of orthoconglomerate with faint planar cross-bedding and localised openwork texture (Fig. 8A), (ii) conglomerate with trough cross-stratification (Gt, Fig. 4G, upper third) and sandstone with trough cross lamination (St, Fig. 8E) and cross-bedding (Sp, Fig. 8A), (iii) alternation of broadly lenticular cm-thick beds of planar laminated coarse-grained sandstone (Sl) and one clast thick flat-lying strata of gravels (Gh) (Fig. 8D) that rest gradationally upon the former facies and are overlain by (iv) laterally extensive dm- to m-thick beds of well-sorted massive to crudely normal-graded and horizontal orthoconglomerate with tightly packed flat-lying clasts (Gm), and (v) cracked massive mud (Fm). Above this succession occur a sub-metre

thick bed of shoreface deposits (Fig. 8B). Along strike (Fig. 8F), field views indicate sharp lateral and vertical facies change amongst the facies recognised along dip, with individualised erosive-based lenticular bodies of massive conglomerate (Gm), separated by horizontally-bedded conglomerate (Gh) and laminated to massive sandstone (Sl) (Fig. 8F). The lenticular bodies are of two shapes: ones with convex-up top (Fig. 8F, black arrows) and others with slightly flat tops (Fig. 8F, white arrows). Scouring is common, and cross-bedded sand generally accumulates into the resulting hollows (Fig. 8A, arrows). The common disc-shaped clasts composing the orthoconglomerate framework are well-imbricated with clast fabric a(t)b(i) type, whereas the matrix content is low and consists mainly of sand. Broadly, these successive deposits lack freshwater shell fragments, however demonstrating well-preserved root remains. They appear to occur below and above the disturbed marl beds (Mb2).

The low matrix content, as well as the well-expressed clast sorting and roundness, suggest a considerable texture maturity of the gravel deposits (Nemec and Steel, 1984). This implies deposition from fluidal (Newtonian) flow in fluvial rather than alluvial fan settings (Nemec and Steel, 1984). Indeed, poorly-defined cross-stratification in orthoconglomerate with openwork texture, and well-defined imbrication of the tightly packed clasts in laterally extensive orthoconglomerate have been commonly used as diagnostic for transverse bar and longitudinal bar development, respectively, in a braided river system (Rust, 1972; Smith, 1974; Miall, 1977). According to Smith (1974), the nearly flat and convex-up tops of the lenticular bodies seen along strike (i.e., slightly normal to palaeoflow, hence to the downstream growth axis) seem to correspond to transverse and longitudinal unit bars, respectively (*see* Smith, 1974, his Fig. 14). Defining a crude stratification, thin successive strata of imbricated gravels and coarse-grained laminated sandstone suggest enhanced downstream growth of diffuse gravel sheets (*sensu* Hein and Walker, 1977) during high flow velocity separated by periods of deposition from tractive flow in lower flow regime of finer sediments (coarse sand) as the flow decreases in velocity (Hein and Walker, 1977). This is suggested to occur in shallow braided fluvial settings (Eynon and Walker, 1974), wherein sheetflow is common. In fact, the vertical transition from bar to thin horizontal stratification development has been modelled to be water discharge-dependent (Hein and Walker, 1977); the more the discharge is high the more the vertical growth of diffuse gravel sheets is impeded. Trough cross-laminated sandstone (and orthoconglomerate) are likely to form in side channels (Eynon and Walker, 1974) from tractive flow in lower flow regime (Allen, 1982). The mud forms through settling processes of fines in calm subaqueous conditions, whereas cracking suggests periodic subareal conditions. Considering the general fluvial setting below and the occurrence of shoreface deposits above, along with the upward decrease in energy level, it is suggested therefore

that the massive mud deposits are likely to occur in very low energy settings probably in mudflat backshore environment as it develops in present-day conditions (Fig. 8G).



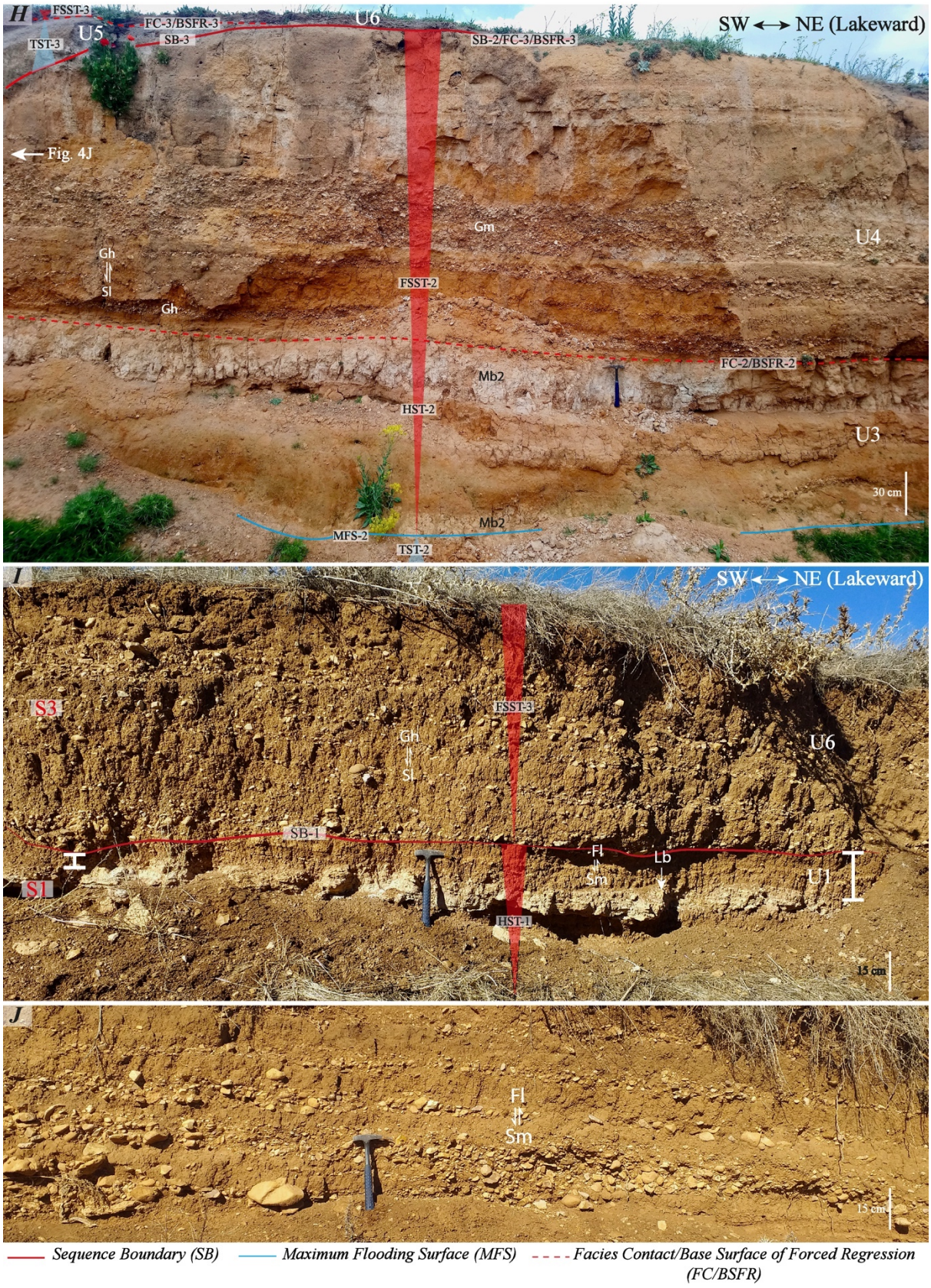


Figure 8. *Field views of the fluvial and alluvial fan deposits.* ***A-F****: Proximal stretch.* ***A****: Along dip cross section (parallel to palaeoflow) logged in log-2 showing different fluvial facies.* ***B****: Shoreface planar laminated sandstone overlying the fluvial deposits.* ***C-E****: Close-up field views of the fluvial facies.* ***F****:Along strike cross section showing lenticular bodies with flat (white arrows) and convex-up (black arrows) tops separated by laminated sandstone and horizontal orthoconglomerate.* ***G****: Picture of the SW lake margin revealing relatively low energy settings, thereby affording the*

*development of mudflat deposits (cracked massive fines, Fm) in the backshore lake environment. **H**: Distal stretch field view logged in log-4 showing a succession of fluvial deposits that occur above the disturbed marl (Mb). **I-J**: Proximal stretch field views showing alternations of laminated sand and thin strata of flat-lying gravel of the sheetflood-dominated fan deposits. Sequences and their systems tract components and surfaces, along with units and their bounding surfaces (FC or SB) are indicated. Note the difference in length between the two brackets in **I** suggesting a slight onlap between the SB-1 surface and underlying offshore deposits. See **Table 1** for facies codes. Designation of sequence stratigraphy abbreviations is in **Figure 3** caption.*

Facies association 5b (FA5-b, alluvial fan deposits). FA5-b consists of an erosive-based succession of alternating tabular beds of cm-thick laminated sandstone (Sl) and thin strata of horizontally bedded clast-supported conglomerate (Gh, Fig. 8H). The clasts composing the framework of this latter are well-sorted and tightly packed, whilst their imbrication is common (Fig. 8H). They show a decrease in size from the base strata upwards (Fig. 8H) and from the proximal stretch downstream where they die out (compare Fig. 8H with Fig. 6A). Compared to the fluvial conglomerate, the one composing this facies association show less textural maturity. Generally, this sedimentary succession appears to overlap the whole stratigraphic section. Otherwise, occasional coarse-tail normal-graded clast to matrix-supported conglomerate (Gmn) have been observed to interrupt the offshore deposits with slight increase in matrix upwards.

This facies association is likely to reflect the distal reach of sheetflood-dominated alluvial fan (Blair and McPherson, 2009), where the lack of erosional bases of the component planar strata suggests sediment-laden laminar flow and deposition from traction in upper flow regime (Allen, 1982). Otherwise, the slight upwards increase in the matrix content in coarse-tail clast to matrix-supported conglomerate suggests subaqueous debris flow deposits that may have evolved partially towards high-density turbidity flow (Nemec and Steel, 1984; Ito, 2019). The deposition mechanism would involve cohesive freezing (Lowe, 1982) that might be followed by rapid suspension fallout from the flow with pseudo-plastic behaviour (Horton and Schmitt, 1996).

4.2 Sequence analysis and facies models

Conventional interpretation of facies successions has led implicitly to depict multiple relatively long-term extension/contraction lake cycles. As such, to basically define and highlight the framework of the depositional character and, eventually, the controlling factor of each lake-level cycle, conventional sequence analysis was carefully applied as per the model-independent and basin-specific methodology prescribed by Catuneanu et al., (2011) and reviewed recently by Catuneanu (2019). In fact, regarding the small scale of the sedimentary basin where the autogenic processes, if any, are short-lasting events, as well as for the sake of simplicity, we consider the T-R sequence model (*sensu* Embry and Johannessen, 1993) in which a sequence is typically equated to a full allocycle of

accommodation succession (*sensu* Neal and Abreu, 2009) that include a negative value (subareal unconformity); autogenic processes may modify the character of the depositional elements, but not substantially the shoreline trajectories, within the large scale allogenic-controlled framework. The sequence bounding surface is considered to reflect the maximum regression (lake contraction) that is likely to match, with slight diachroneity yet, a subareal unconformity that would develop landward. Accordingly, three lowest hierarchical rank T-R sequences (the depositional systems include only sedimentological scale cycles; Catuneanu, 2019) with mixed clastic-carbonate depositional elements have been identified. In addition, the component systems tracts, along with their bounding surfaces and inferred stratigraphic staking patterns, depend upon the specific interplay between accommodation rate (i.e., lake level shifts, A) and sedimentation rate (i.e., temporary base-level changes, S), and so on the A/S ratio (the balance between creation and consumption of space; Catuneanu, 2006). Thus, intervals of high lake level would include the transgressive (highstand) systems tract with $A/S > 1$ ($A/S \approx 1$), whilst those of low lake level would include the falling-stage (lowstand) systems tract with $A/S < 0$ ($A/S \approx 1$).

Aligning with this rather shoreline trajectory-based stratigraphic approach, hence not necessarily fitting with the inner lithological specificities and shifts, within trend (or not) facies contact bounding allostratigraphic units have been identified in order to emphasise changes in the characters and sedimentation patterns (e.g., carbonate/clastic, high/low energy) of the depositional systems. The outcome of this approach has led to conceptual constructions of the different facies' models.

4.2.1 Stratigraphic sequence 1: Lower mud – upper carbonate sequence

Being typically recognised in the proximal stretch, the first cycle of lake level, sequence 1 (S1), is marked by a transition from offshore dominated mud and sand (FA1) to bench carbonate deposits (FA2) (Fig. 9). The lower bounding surface is not delineated due to limited data, whereas the upper sequence boundary (SB1, Fig. 4A, D) coincides with a maximum regressive surface and a subareal unconformity marking the negative trend of accommodation, thereby completing the full cycle (Fig. 9). Additionally, SB-1 subtly onlaps this sequence (Fig. 8I), suggesting a slight tilting of lake floor before the development of the boundary surface. Within the sequence, an overall change in the stacking pattern is inferred to indicate a transgressive interval (transgressive systems tract, TST-1), marking lake extension, followed by a normal regressive interval (highstand systems tract, HST-1), pointing out general stillstand conditions with a slight progradation as suggested by the occurrence of the Skolithos ichnofacies. These systems tracts are bounded by a maximum flooding surface (MFS-1) placed within the lower offshore dominated deposits (cryptic surface between the two limestone sub-

facies, log-2, Fig. 4D). Besides, this sequence reveals two allostratigraphic units separated by within-trend (within the HST-1) facies contact (FC-1), with a clastic-dominated lower unit (U1) and a bioturbated carbonate-dominated upper unit (U2; Fig. 4G-I). Both units mark soft and brittle deformation structures, *viz*. load structures and domino-style faults (Fig. 4G), respectively (*see* Azennoud et al., 2022b).

Compared with the dated data from the NW lake margin core (Rhoujjati et al., 2010), it is suggested that this sequence is likely to have had developed before 28 cal. kyr BP. The general trend of the stacking pattern marks a general lake extension phase during the TST-1 and HST-1, hence suggesting humid conditions with frequent 'river' floods (Wu et al., 2022), under lower wind-driven energy settings. However, the within-trend facies contact (FC-1) indicates a prominent environmental shift from high allogenic sediment supply towards a rather sediment starvation (condensed section) and enhanced authigenic processes. The sediment starvation would have afforded the aforementioned bioturbation development (*Skolithos* ichnofacies). Accordingly, we propose a sedimentary system change from low-energy clastic-dominated extended lake (facies model type-1) to low-energy carbonate-dominated extended lake (facies model type-2) (Fig. 11).

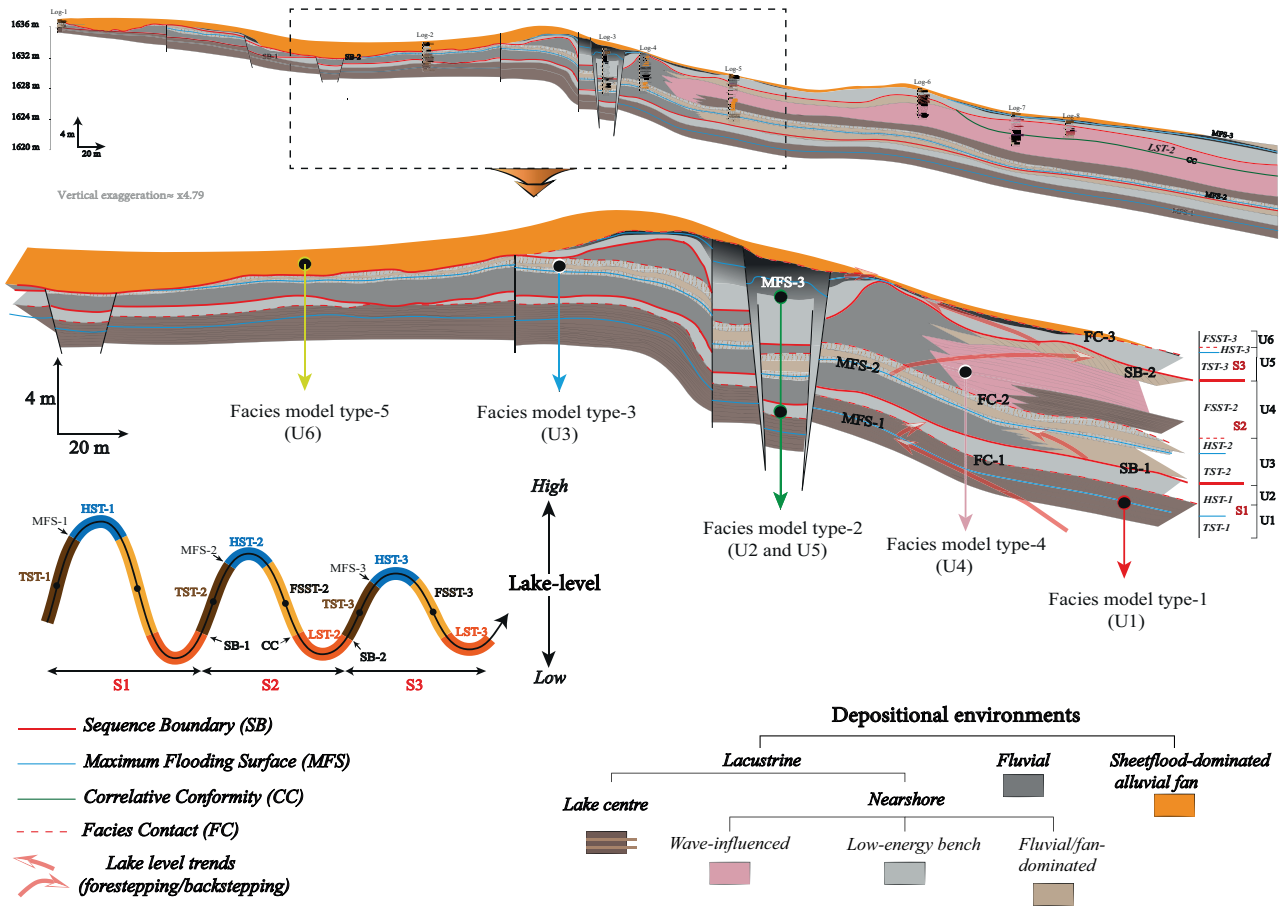


***Figure 9**. Cross section (outlined in **Fig. 2**) summarising the various depositional systems, T-R sequences, and allostratigraphic units of the SW lake margin.*

4.2.2 Stratigraphic sequence 2: hybrid to clastic-dominated sequence

The second lake-level fluctuation, developing sequence 2 (S2) and slightly onlapping S1, is marked by a lower backstepping transgressive interval (TST-2, Fig. 8A) that afforded shift from fluvial (FA5-a) to nearshore deposits (FA3-a), and an upper forestepping regressive interval (Fig. 9). The regressive interval can be subdivided into a highstand normal regression (HST-2, Fig. 4D, K), marking an overall stillstand higher lake level and a continuous deposition of nearshore sediments, a forced regression (falling-stage systems tract, FSST-2, Figs. 7 and 8H), revealing a progressive lake contraction and a general downstepping, and a lowstand normal regression (lowstand systems tract, LST-2) (Fig. 9). This latter is typically noticed to be restricted to the distalmost portion of the available data (log-7 and 8, Figs. 6 and 7) indicating both (i) a progressive decrease in energy and sedimentation rate that afforded the observed increase in bioturbation upward (Fig. 6B, F), and (ii) a slight upstepping component (see the vertical passage from delta to shoreface deposits in log-7, Figs. 6A, and 7D). Besides, it is noteworthy that all of these stacking patterns nest small scale (sedimentological scale, *sensu* Catuneanu, 2019) lake-level variation. In fact, the surface delineating the transition from the FSST-2 to the LST-2 corresponds to the correlative conformity (CC) as defined by Van Wagoner et

al. (1988), and hereby marks a change from river-born sediments (lake-level fall) into shoreface deposits (relative lake-level rise upon a relatively low sedimentation rate), thus onlapping the delta lower front sediments bellow (Fig. 7D, arrows). On the other hand, the change from HST-2 (below) to FSST-2 (above) delineates the lacustrine basal surface of forced regression (BSFR-2; Hunt and Tucker, 1992; Nutz et al., 2015b), and hereby marks a sharp change, or facies contact (FC-2), from nearshore to shallow braided river deposits (log-4, Fig. 8H). Transgressive and regressive intervals are separated by a maximum flooding surface (MFS-2), placed at the middle of the lower disturbed marl (Mb2, Fig. 4D) and marks the maximum lake extension. The upper sequence boundary (SB-2) represents a maximum regression surface that coincides landward with a subareal unconformity (erosional or non-depositional hiatal surface, e.g., Figs. 4K and 8F), and lakeward with a change from exclusively clastic deposits into carbonate sediments (e.g., Figs. 6 and 7), expressing a sharp passage towards lower sedimentation rate versus higher accommodation. The fluvial terms of the TST-2 are deliberately demonstrated to be implicated in the generation of load structures observed within the lower sequence (*see* Azennoud et al., 2022b). Likewise, the FSST-2 reveal evidence of fluidization and water escape structures (Azennoud et al., 2022b).

According to the dated nearby core (Rhoujjati et al., 2010), it is suggested that S2 is formed between ca. 27 and ca. 12 cal. kyr BP. Involving hybrid lithology with clastic and carbonate deposits, the lower part of this sequence (between SB-1 and BSFR-1) indicates fluctuating higher lake levels and energy conditions. The upper part (between BSFR and the SB-2), in turn, marks clastic-dominated setting with lower lake levels and high-energy conditions. As such, we propose a sedimentary system shift from low-energy hybrid-dominated extended lake (facies model type-3) towards high-energy clastic-dominated contracted lake (facies model type-4) (Fig. 11). This later can be considered as a variety of 'wind-driven waterbody' category of the recently proposed classification for lakes by Nutz et al. (2015a, 2016), although with less prominent morpho-sedimentological features (e.g., spit, barrier inland) due to the small physical scale of the case study.

4.2.3 Stratigraphic sequence 3: lower carbonate-upper fine-to-coarse-clastic sequence

The youngest sequence (S3) is made by a lower carbonate and organic-dominated transgressive and highstand normal regression intervals and an upper clastic-dominated forced regression interval (Fig. 9). In fact, insights from ostracod fauna (Fig. 10), *viz*. the upward disappearance and decrease in frequency of *Herpetocypris* cf. *helenae* and *Ilyocypris gibba*, respectively, and the upward increase in frequency of *Neglecandona* sp., suggest that the lower carbonate interval reveals continuous lake-level increase; while *Neglecandona* spp., and particularly *N. neglecta,* occur in lakes from the shallow

littoral zone down to the great depth (60 m), *Herpetocypris helenae and Ilyocypris gibba* prefer the littoral zone of lakes (Meisch, 2000). As such, the maximum flooding surface must be placed somewhere within the upper organic layer as a cryptic surface. Indeed, results of elemental geochemistry reveal concluding remarks (Fig. 10A). Thus, potassium and aluminium both indicate upward increasing values, thereby suggesting increasing sediment input (Kylander et al., 2011; Boës et al., 2011), synchronous with increasing watershed drainage, which eventually would prompt lake-level rise. Likewise, the Al/K ratio indicates a slight upward increase, suggesting a moderate watershed weathering enhancement (Burnett et al., 2011; Davies et al., 2015), which is compatible with the lake state and character (higher lake level and bio-productivity). The Fe/Mn profile shows a steady lower half and a subsequence upward increase thereafter with a maximum value placed within the organic-rich facies, suggesting maximum anaerobic conditions (Boyle, 2001), hence delineating the MFS-3. In accordance with Zecchin et al. (2021, 2022) for marine settings, here it is stressed the effective usefulness of micropaleontological analysis (using ostracods) and geochemical proxies (especially the Fe/Mn ratio) in tracing cryptic surfaces such as the MFS in lacustrine settings as well. On the other hand, the facies contact between the organic-rich (lacustrine) and clastic-rich (subareal fan) deposits (FC-3), being erosional, marks the basal surface of forced regression (BSFR-3) and merges in places with MFS-3. Otherwise, the current lake depositional state represents a lowstand interval with low-energy setting that favoured mudflat deposits in backshore environment (Fig. 8G). The lower stratigraphic intervals (TST-3 and HST-3) are typically affected by normal faults with decametric to sub-metric offsets (Fig. 4J) and neptunian dykes with carbonate and organic-rich filling material of the lower intervals of this sequence (e.g., Fig. 4I, J; *see* Azennoud et al., 2022b).

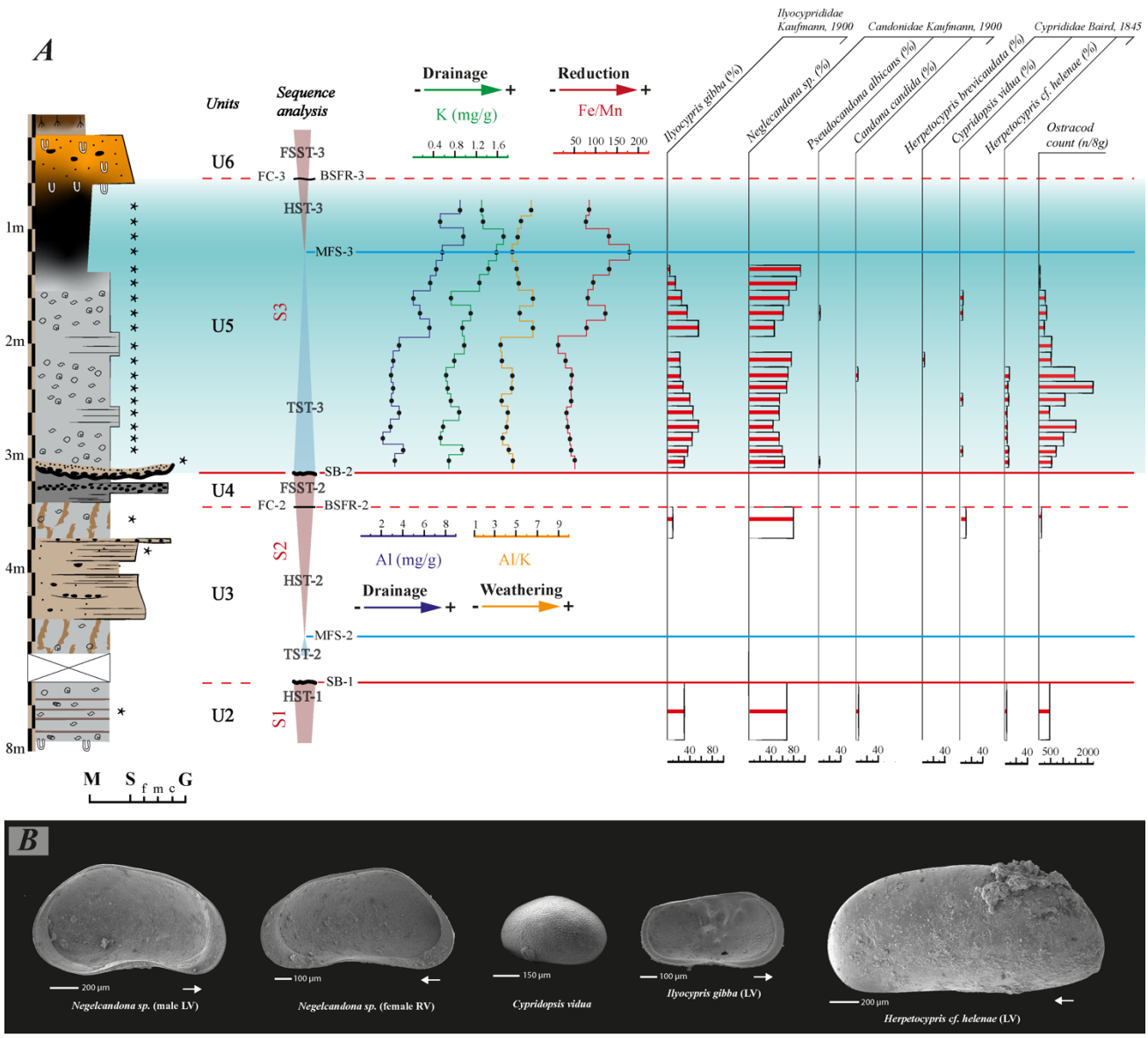


Figure 10. *Transgressive trend (TST-3) inferred from geochemical proxies and ostracod biomarkers.* ***A****: Palaeolimnological proxies (Geochemical elements/ratio and ostracod species) against sequence analysis from log-1 inferring lake-level variations and delineating the cryptic, in nature, maximum flooding surface, MFS-3 (peak in Fe/Mn curve).* ***B****: Scanning Electron Microscope (SEM) images of some specimens of ostracods. Systems tract and texture designations are in* ***Figure 3*** *caption.*

Correlated to the dated core (Rhoujjati et al., 2010), the latest lake-level cycle is likely to belong to the Holocene (ca. 12 cal kyr BP onwards). According to the facies analysis, the lower transgressive and highstand intervals correspond to a low-energy carbonate-dominated extended lake (facies model type-2), whereas the falling-stage and the current lowstand intervals mimic a low-energy, fan-dominated contracted lake (facies model type-5) (Fig. 11). The normal faults (and neptunian dykes), affecting peculiarly the lower stratigraphic intervals, reveal evidence of neotectonics activity that is to be considered in conditioning the forced regression and in generating the fan deposits that characterize this interval.

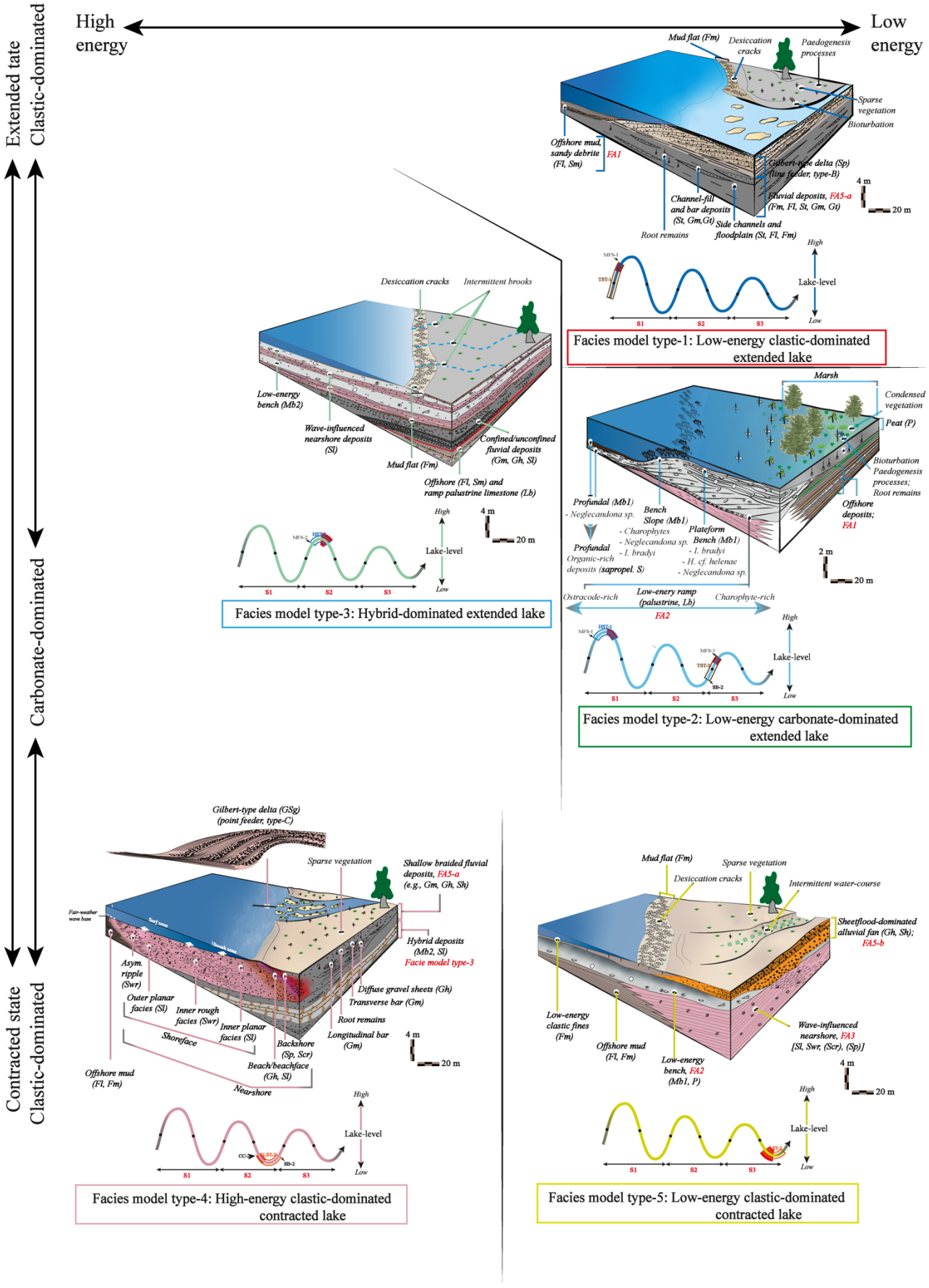


Figure 11. *Five facies models proposed for the studied SW lake margin outcrop based on energy level (wind-driven), dominant lithology (clastic- vs. carbonate-dominated), and general water body state (extended vs. contracted).*

5 Discussion

The Ifrah Basin may provide a unique example of a small-scale interior basin where climate and tectonism are prone to interchangeably act in controlling the occurrence, extension, and character of the depositional systems, rendering very informative their imprint and preservation. This is fairly true especially if we consider the typical local and regional settings of the case study. Thus, the local structural configuration of the lacustrine basin involves sedimentation upon a *reverse-drag* associated with active normal faulting (Azennoud et al., 2022b). Regionally, the studied case is included within a seismically and tectonically active area, nearing plate boundary between Nubia and Eurasia (e.g., Chalouan et al., 2014; Poujol et al., 2017). Besides, the Northwest Africa region is known to be a key climate region (Knippertz et al., 2003), and especially a key North Atlantic Oscillation (NAO) region (Wassenburg, 2016; Zielhofer et al., 2017; Ait Brahim et al., 2018, 2019; Azennoud et al., 2022a; Hakam et al., 2022), which render this region very sensitive to global and synoptic-scale climate variability, both on orbital and sub-orbital timescales. Accordingly, our focus of interest should be hereafter on disentangling climatic from tectonic signals as they are the main independent allocyclic controls on sedimentation and stacking patterns in interior basins (Cojan, 1993; Shanley and McCabe, 1994; Carroll and Bohacs, 1999; Keighley et al., 2003; Pla-Pueyo et al., 2009; Alonso-Zarza et al., 2012). However, assessment of the local specific features that the basin configuration may encompass (e.g., lake basin type, *sensu* Carroll and Bohacs, 1999 and Bohacs et al., 2000) is of necessity before pursuing the discussion into the controlling factors; sedimentation in overfilled basin is not suitable to record the absolute climate conditions. Finally, we address the question of why the application of standard sequence stratigraphy, accompanying thorough structural and sedimentologic analyses, in such small-scale interior basin may be a robust approach to better frame the depositional systems, thereby making easier decryption of the allocyclic-control signals.

5.1 Basin configuration

First and foremost, the lacustrine sedimentation occurs upon a folded hanging-wall subsidence linked to a border basin master fault, thereby sculpting a half-graben with near flat fault-opposite lake margin (SW margin) wherein the herein presented observations have been made. Folding of the hanging-wall block gave way to a *reverse-drag* structure where at least two flexural-slip pulses would have occurred during the considered bracketed time (Azennoud et al., 2022b, their Fig. 10A). Generally, as defined to be the difference in elevation between the lowest point in the basin and its outflow ridge (sill), potential accommodation is a determinant parameter that controls in part the

hydrologic closeness/openness of an interior basin (Carroll and Bohacs, 1999; Keighley et al., 2003). It is mainly tectonic-paced but could be subjected to considerable modification upon erosion of the sill or sedimentation in the depocentre, especially during long-term periods of tectonic quiescence. Relative lake-level changes (accommodation s.s., Catuneanu, 2017), however, is another major parameter that conditions the hydrologic openness of a lake basin since overbalanced water budget may enhance overflowing throughout the sill, especially during tectonic quiescence. Unlike the sill height, relative lake level is predominantly controlled by climate (*viz*. precipitation/evaporation ratio; Bohacs et al., 2000), albeit short-lasting tectonic pulses could cause the shoreline and depocentre to instantaneously relocate upon lake-floor tilting (Keighley, 2003; *see* below). Accordingly, in sequence stratigraphic terms, while the lake-level variation directly paces the shoreline trajectory and thereby the sedimentary stacking patterns (Catuneanu, 2017), composing lower rank sequences (Catuneanu, 2019), the potential accommodation has a crucial implication on the basin fill timing (Bohacs et al., 2000) and therefore on the first-order cycle (*sensu* Catuneanu, 2019, p. 371). Accounting for these insights, and based on scaling-relationships applied to the hanging-wall-master fault-footwall structural system carried out by Azennoud et al., (2022b) on the study case, insightful conclusions can be drawn (Fig.12). Thus, the present-day maximum subsidence, that is the maximum accommodation, due to hanging-wall-collapses (**s**, Fig. 12) corresponds to 124 m (Azennoud et al., 2022b), wherein 97 m has been already consumed (consumed accommodation, **ca**, Fig. 12B) and 27 m is the accommodation that still available due to hanging-wall collapses (unconsumed accommodation due to **s**, **ua**, Fig. 12B) including 2 m, the current water depth, which defines the subaqueous accommodation (*sensu* Catuneanu, 2017, p. 9) directly tied to the sequence stratigraphy framework, in contrary to the rest of the available accommodation due to **s** (subareal accommodation, Catuneanu, 2017). Consequently, while considering ongoing hanging-wall subsidence upon the bracketed time, that is a lower value of **s** as we dive into the past, the maximum lake levels during the three sequences are very likely to overcome the available accommodation due to hanging-wall subsidence; the relative maximum lake-level values ($\Delta\mathbf{L_m}$) are very close to the present-day **ua** (Fig. 12B); $\Delta\mathbf{L_m}$ values are estimated by abstracting the absolute elevation of the inferred shoreline of the considered maximum lake level (**L_m-1-L_m-3)** from the absolute elevation of the present-day lake level (**L-0**, *viz*. 1614 m a.s.l.) (Fig. 12B). As such, unless we account for the footwall uplift, the basin would be classified as overfilled or balanced. In fact, scaling-relationships, again, suggest that about 59 m of the accommodation would be created due to footwall uplift (**u**, Fig. 12B). As per the definition quoted above, the potential accommodation would be 86 (**ua** + **u**). Considering the 3D configuration of the

basin, the effective sill height (1973 m a.s.l., Fig. 12A) does not coincide however with the theoretical elevation of the footwall (Fig. 12B), most likely due to enhanced erosion in areas where faults connect. As such, the present-day potential accommodation would be estimated to be 61 m, which far surpasses the maximum relative lake levels during the considered sedimentation time. During this time, the lake basin is therefore classified as underfilled and hence being suitable to confidently record the allocyclic controls. However, as we further consider deeper times, periods of water overflow should not be considered uncommon, since evidence of lacustrine deposits is observed to occur onto the outflow ridge (see dark colour in Fig. 12A). This would basically explain the water chemical state that does not involve saline or even brackish signatures as it is typically expected to be in the case of underfilled basin end-member (Bohacs et al., 2000; Zavala et al., 2022).

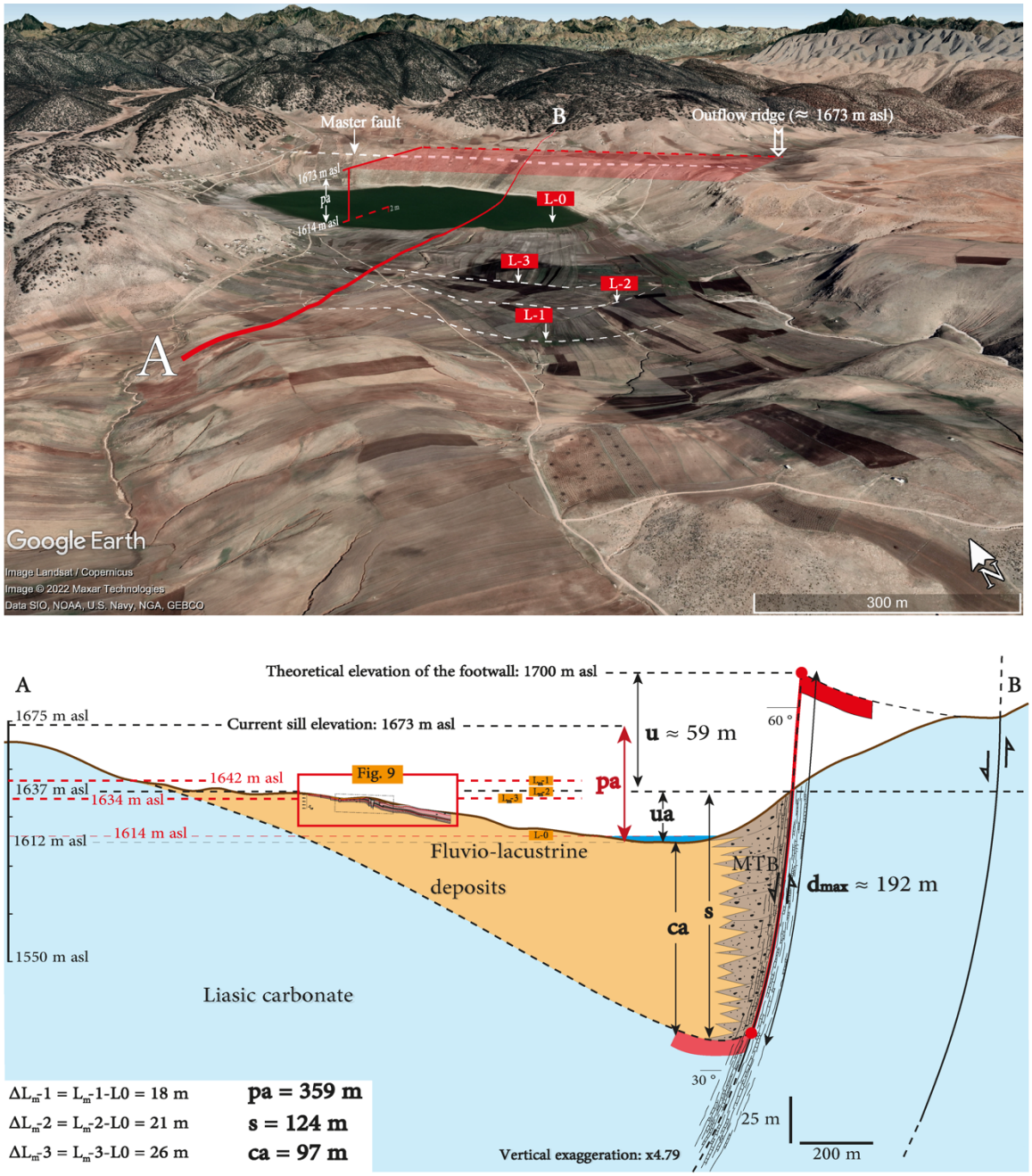


Figure 12. *Basin configuration.* ***A****: Relationship between the potential accommodation (pa) and maximum lake levels during periods of maximum flooding (Lm-1, Lm-2, and Lm-3) relative to the present-day lake level (L-0). The height of the outflow ridge with regards to the maximum lake levels of the concerned period suggests an underfilled basin.* ***B****: Quantification of some geometric entities linked to the half-graben settings conducted by Azennoud et al. (2022b) along with the relative lake levels (relative to the L-0) suggesting a considerable amplitude of variations (ca. 21.66 ± 4 m), yet under the outflow ridge. The effective outflow ridge does not coincide with the theoretical elevation of the footwall most probably due to erosion. MTB: mass-transport breccias* ***s****: subsidence due to hanging-wall collapses;* ***u****: uplift due to footwall;* ***ca****: consumed accommodation;* ***ua****: unconsumed accommodation.*

5.2 Controls on sedimentation and stacking patterns

Integration of conventional facies and sequence-stratigraphic analyses has led to the identification of three long-term lake-level cycles nesting different depositional systems that are summarised in five facies models, each with specific character and extension reflecting a variety of

depositional controls. Hydrologic closeness of the lake basin during the time of deposition makes deciphering allocyclic controls from the deposits assured. We hereafter discuss tectonic and climate as considered to be the main allocyclic controlling factors on stratigraphy.

5.2.1 Influence of tectonics

Tectonic pulses are prone to cause an instantaneous relocation of the shoreline through fault-block tilting (Strecker et al., 1999; Keighley et al., 2003), hence modifying the stratigraphy and component systems tracts (Catuneanu, 2019). According to a thorough sedimentological and structural analyses conducted on the same studied sediments (Azennoud et al., 2022b), two flexural-slip folding events of the *reverse-drag* have been recognised (Fig. 13). Thus, the bed-parallel slip and associated domino-faults, deforming the subunit **U1-a** and fossilised by the fluvial sediments of the subunit **U2-a**, was interpreted to reflect a partial accommodation of a flexural-slip pulse of the *reverse-drag* prior to 28 cal kyr BP (Azennoud et al., 2022b) (Fig. 13). Furthermore, tilting of the lake basin-floor was estimated at 6° without an uplift component (Azennoud et al., 2022b), which causes the observed subtle onlap (Fig. 8I). Generally, unlike in continental passive margin (infinite water volume), subsidence in a half-graben context, where lacustrine settings are prone to develop (finite water volume), is simultaneous with restriction of the water body area, and hence instantaneous regression of the shoreline (Strecker et al., 1999). Typically, while considering the near-flat south-western margin of the lake basin and the amount of incremental tilting upon the *reverse-drag* flexural pulse in the Ifrah Basin, the shoreline would instantaneously and considerably regress downdip in the south-western margin, thereby conditioning a sharp shoreline trajectory inflexion and, subsequently, a change from highstand to forced regression. This conceived scenario is strikingly imprinted in the sediment archive. Thus, the marl bed hosting the domino-faults and bed-parallel slip and recording a highstand interval is separated from the fluvial deposits above by a significant erosion surface (a sequence boundary, SB-1). Therefore, the sharp facies change and shoreline trajectory inflexion, the occurrence of the (basin-scale) significant subareal unconformity, and the resulting stacking pattern change was directly controlled by the flexural-slip pulse of the *reverse-drag*, hence recording a direct tectonic signature (Frostick and Steel, 1994).

Another flexural pulse of the *reverse-drag*, yet with an uplift component, has been depicted from the sedimentary succession (Azennoud et al., 2022b) (Fig. 13). Hence, the soft-sediment normal faults and neptunian dykes, involving marl and sapropel deposits of U5 of the Middle Holocene (Azennoud et al., 2022b), record sharp shoreline regression and thereby sharp stacking pattern change from upstepping (highstand) to downstepping (forced regression) (Fig. 13). This tectonic pulse

confidently would explain the sharp facies change (FC-3) from lake offshore organic-rich sediments (sapropel) to subareal clastic deposits (sheetflood-dominated fan) in the distal stretch where no evidence of erosion has been recognised between the two deposits.

In addition, as the *reverse-drag* flexural pulses are connected to regional-scale episodes of significant displacement (Azennoud et al. 2022b), it is conceivable that more clastic material from the damage zones of major strike-slip and reverse faults in the vicinity of the basin would be provided upon each significant displacement increment, hence conditioning the shallow braided system and sheetflood-dominated fan deposits above SB-1 and FC-3, respectively.

5.2.2 Role of climate: Orbital and sub-orbital forcing

Interestingly, the periodic recurrence of biochemical- (limestone, marl, and organic-rich) and clastic-dominated beds in the study case raises the question as to why such a sharp facies change would take place and how this cyclicity can be originally paced? In his key publication, Cecil (1990) addressed successfully this question by emphasising the role of precession and obliquity (his "short-term cycles") in modulating the sediment flux and hydrological balance and thereby conditioning the stratigraphic repetition of the climate-sensitive rocks observed in the case studied therein. Adoption of Cecil' paper considerations (his Fig. 1), along with the outcomes presented here, allow some insights to be confidently drawn at the outset. Thus, during high lake levels, clastic deposits reflect wet periods, whereas organic-rich beds (sapropel) depict a considerable positive hydrological balance. Palustrine limestone, interrupting offshore clastic beds in the lower sequence, marks sub-humid to semi-arid conditions (a Goldilocks situation qualified to be "just right", Ashley et al., 2014; de Wet et al., 2015). Marl deposits, in turn, would reflect humid conditions between those required to drain a sufficient amount of fine-grained sediments into the basin and those needed for the authigenic biochemical precipitation to be considerably preserved as much as dilution by the clastic component is sufficiently reduced. Clastic-dominated deposits during falling-stage and lowstand periods would reflect sub-humid to semi-arid conditions, whereas the driest time-lapses would be indicated by the extensive lake shrinkage and consequent development of desiccation cracks as seen in the middle sequence (S2). However, deciphering the responsible driving mechanisms for such stratigraphic periodicity must be tackled further whereby a concrete visualisation of the cause-and-effect concept would be successfully drawn. The next subsections deliberately address this point for the three lake-level cycles and component depositional systems depicted herein.

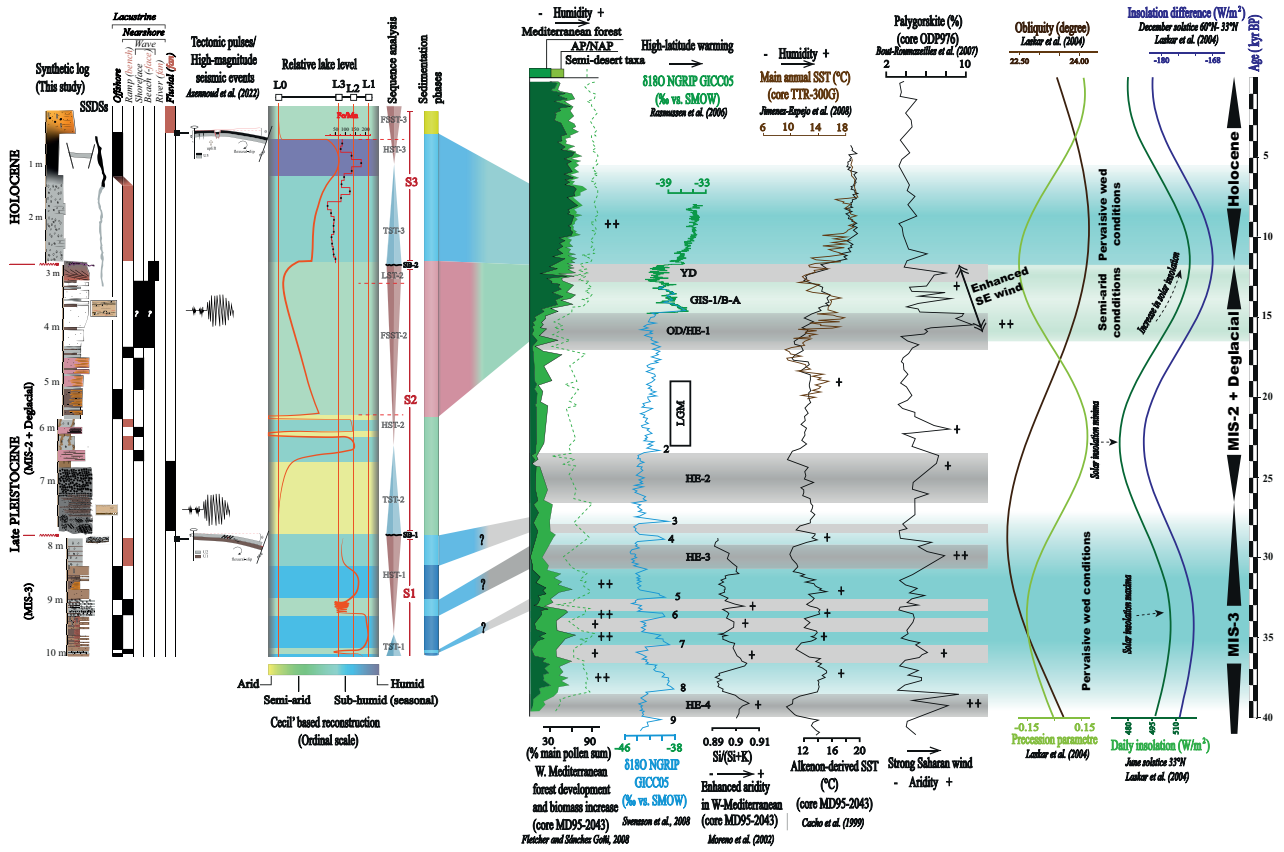


Figure 13. *Correlations of sedimentary data (details in **Fig. 3**), sequence-stratigraphic analysis (details in **Figs. 3** and **10**), inferred lake level variation (details in **Figs. 9** and **12**), seismo-tectonic insights (after Azennoud et al., 2022b), and sedimentary facies models (details in **Fig. 11**), from this case study, with insolation outcomes (after Laskar et al., 2004) and palaeoclimatic data from Greenland ice cores (Rasmussen et al., 2006; Svensson et al., 2008) and Alboran marine cores (Bout-Roumazeilles et al., 2007; Cacho et al., 1999; Fletcher and Sánchez Goñi, 2008; Jimenez-Espejo et al., 2008; Moreno et al., 2002) for the considered time interval. Cecil' based considerations have been applied to the case study to qualitatively draw rock-based hydroclimate reconstructions. Numbers Greenland Interstadials; the GIS-1: Greenland Interstadial-1; YD: Younger Dryas; B-A: Bølling–Allerød; LGM: Late Glacial Maximum; HE-1: Heinrich Event-1.*

5.2.2.1 Orbital signature

Broadly, sustained high lake levels occurred during deposition of the lower (S1) and upper (S3) sequences. Chrono-stratigraphically, these two time periods correspond with MIS-3 and Early Holocene, respectively. Besides, the upper sequence is broadly more clastic-starved than the lower one. On the other hand, the middle sequence (S2), probably covering part of the MIS-2 and the last deglacial period, broadly records low lake levels, with the exception made by the highstand (alternation of filled-cracked marl and nearshore laminated sand) appears to be not pervasive and demonstrates high-frequency/magnitude fluctuations. These sustained high lake levels interestingly occurred during maxima in Northern Hemisphere summer insolation, arising from obliquity maxima and/or precession minima (Berger and Loutre, 1991; Laskar et al., 2004) (Fig. 13); MIS-3 (Early Holocene) high summer insolation is in phase with precession minima (precession minima and obliquity maxima). Furthermore, they both occur during peaks, yet continuously negatives, of winter insolation gradient between high- and mid-latitude (60°N and 33°N, respectively, Fig. 13) (Laskar et al., 2004) and follow

proportionally the long-term fluctuation of the W-Mediterranean forest development (Combourieu Nebout, 2002; Fletcher and Sánchez Goñi, 2008; Camuera et al., 2019) (Fig. 13). Orbitally-paced humid conditions mark therefore the W-Mediterranean region during MIS-3 and the Early Holocene. This is also suggested from speleothem-derived results that demonstrated rainfall enhancement during peaks in obliquity and/or precession minima in North Africa (Hoffmann et al., 2016; Rogerson et al., 2019). Increasing winter insolation at latitude 60°N relative to 33°N is prone to weaken the geostrophic gradient between Iceland Low and Azores High, leading to pervasive wetter conditions in W-Mediterranean (Hoffmann et al., 2016) akin to a negative NAO-like pattern (Wanner et al., 2001). The general higher clastic-starvation of the upper sequence relative to the lower one during high lake levels is in sync with summer insolation at 33°N, winter insolation gradient between 60°N and 33°N, and biomass development in W-Mediterranean (Fig. 13); the upper sequence occurs during higher summer insolation, higher winter insolation gradient, and more enhanced biomass development relative to the lower sequence. As such, it is suggested that upon biomass development enhancement during periods of higher summer insolation and winter gradient insolation between high- and mid-latitudes, arising from precession minima and obliquity maxima (the Early Holocene in this case), transport of fine-grained clastic elements is limited, thereby promoting sediment starvation (in accordance with Cecil' considerations (1990). On the other hand, periods with low summer insolation, low winter insolation gradient, and lower vegetation density are in sync with broadly low lake levels and higher clastic component (the middle sequence). Within this long-term scenario of lake level and sediment-starvation fluctuation is superimposed a short-term variability (perhaps multicentennial to multimillennial timescale) that is evident in the patterns of occurrences of the different sedimentation phases (facies models).

5.2.2.2 Sub-orbital signatures

First lake-level cycle. Typically, the lower T-R sequence, developed during MIS-3, encompasses a lower mud-rich interval, yet interrupted by periods of clastic sediment-starvation and development of palustrine carbonate layers, and an upper carbonate-rich interval. The mud-rich beds of the lower interval reflect wet periods whereby upland response to drainage network would be enhanced (Suchecki et al., 1988; Ashley et al., 2014), generating frequent 'river' floods and basinward turbidites (Wu et al., 2022), while the palustrine carbonate layers thereof indicate semi-arid to sub-humid conditions with marked seasonality (Cecil, 1990; Platt and Wright, 1992; Tanner, 2010; Alonso-Zarza et al., 2012), promoting periodic subareal exposure under tectonic quiescence (de Wet et al., 2015). The marl bed composing the upper interval reflects hydrological conditions between those

giving way to the offshore mud and those conditioning the palustrine settings. Regionally, northern Africa during MIS-3 was experiencing increased effective rainfall that allowed speleothem growth in present-day arid areas, although intercepted by millennial timescale periods of isotopically less negative rainfall (Hoffmann et al., 2016; Rogerson et al., 2019) in sync with (i) North Atlantic cooling phases (Rasmussen et al., 2006, 2014; Svensson et al., 2008), (ii) cooling phases of the Alboran Sea surface (lower SST, Fig. 13; Cacho et al., 1999) and deep water (lower DWT; Cacho et al., 2006, Fig. 4e), (iii) a decrease in vegetation density in the W-Mediterranean borderlands (Fletcher and Sánchez Goñi, 2008), and (iv) increase in Saharan aeolian dust transport (Moreno et al., 2002; Bout-Roumazeilles et al., 2007) (Fig. 13). The opposite is true for periods of isotopically more negative rainfall depicted from speleothems (*see* Hoffmann et al., 2016). Collectively, this cooling/warming fluctuations during MIS-3 mimic the Dansgaard-Oeschger (D-O) frequencies (Dansgaard et al., 1993; Bond and Lotti, 1995) with stadials (interstadials) correspond regionally to increased moisture limitation (availability), Mediterranean cooling (warming) phases, reduction (increase) in forest development and increase (decrease) in Saharan dust transport, and locally to palustrine limestone or marl (mud-rich) deposition. Periods with prominent cooling and more arid conditions in W-Mediterranean are in phase with the Heinrich Events first depicted from North Atlantic deep-marine sediments (Heinrich, 1988; Bond et al., 1992; Broecker et al., 1992). Accounting for these insights and the chronostratigraphic considerations (Fig. 13), the charophyte-rich palustrine limestone, demonstrating more pervasive sub-areal exposure relative to the ostracod-rich one, is likely to develop during the more prominent arid periods akin to those of Heinrich Events (probably the HE-3 one). Stratigraphically below and above that, the ostracod-rich limestone and bioclastic marl are likely to develop during D-O (or Greenland) stadials (probably the ones between the GIS-5 and 6, and 3 and 4, respectively, Fig. 13), although with the consideration that the marl bed can form during warming phases and hence during the GIS-3 as well.

Second lake-level cycle. The most prominent short-term fluctuations typify the middle T-R sequence (S2). While the lower (transgressive interval) and upper (falling-stage and lowstand intervals) parts of S2 are marked by water volume restriction and clastic domination, the middle (highstand) interval shows a rather general pattern of higher lake level and a striking alternation of nearshore marl and laminated sand separated by periods of extensive lake shrinkage (affording conditions for desiccation cracking to occur). Accounting for the time control on the subareal unconformity separating this sequence from the lower one, the arid interval that conditioned the lower

part of S2 is likely to occur during the Heinrich Event-2 (HE-2, Fig. 13), a period reported as severely cold and extremely arid in W-Mediterranean (Cacho et al., 1999; Combourieu Nebout, 2002; Goñi-Sánchez et al., 2002; Allard et al., 2021). Warming of the Alboran Sea (Jimenez-Espejo et al., 2008) right after the Late Glacial Maximum (LGM, 23-19 cal Kyr BP; Mix et al., 2001) synchronous with a slight increase in temperature over Greenland (Meese et al., 1997) might reflect a common forcing mechanism that would have modulated the occurrence of marl deposits at the middle part of the sequence. Although periods with enhanced Saharan winds are well recorded to occur during late HE-2 and LGM (Fig. 13; Bout-Roumazeilles et al., 2007), suggesting a control on wind-driven nearshore development, the relationship between the climate-controlling factors and sedimentation during this period (between HE-2 and HE-1) is not clear enough to build reasonable assumptions.

Key findings mark the final oscillations of the last glacial period (late HE-1 to Younger Dryas) with remarkable Saharan wind/aridity enhancement (Bout-Roumazeilles et al., 2007; Fink et al., 2013) (Fig. 13). Furthermore, enhanced northward Saharan dust transport has been seen to be synchronous with strengthening and northward shift of north-westerly winds during stadials (Cacho et al., 2000; Moreno et al., 2002) and with higher NAO index in a modern situation (Moulin et al., 1997). Moreover, pervasive aridity with extended landscape vegetation clearance has been reported to dominate the Middle Atlas during this period (Lamb et al., 1989; Cheddadi et al., 2009; Rhoujjati et al., 2010; Nourelbait et al., 2014; Tabel et al., 2016). Considering the most likely atmospheric configuration during periods of enhanced Saharan dust transport according to Bout-Roumazeilles et al. (2007), it is expected that summer Saharan winds carrying dust (including the palygorskite mineral) would have crossed north-westwardly the Middle Atlas before being turned due to Coriolis effect towards the western part of the Mediterranean whose signature has been depicted. Given the chronostratigraphic setting, the high-energy low lake level clastic-dominated nearshore facies model (Facies model type-4, Fig. 11) characterising the falling-stage and lowstand intervals of the middle sequence, fits well with the palaeoclimatic data that suggest collectively enhancement (reduction) of W-Mediterranean summer winds (hydrological budget); it is not clear however how a peak of Saharan dust in W-Mediterranean would exist during interstadial conditions akin to those giving way to the Bølling–Allerød interstadial. The slight increase in lake level resulting in the lowstand interval might be in sync with slight shift to humid conditions in W-Mediterranean during the Bølling–Allerød (Camuera et al., 2021).

Interestingly, given the elongated state of the lake where the major axis is striking SE-NW (Fig. 2) and the analytical mathematical considerations developed by Winant (2004) and complemented so

far by Toffolon (2013), clockwise secondary circulation at the cross-section plan relative to the inferred direction of the Saharan winds (facing north-westwardly the Middle Atlas) would be prone to develop during this time interval, and hence promote establishment of the wind-influenced nearshore at the SW lake margin. Moreover, steady upwelling would have been developed at the left side of the lake (i.e., SW margin) relative to the wind direction (north-westward) during periods of higher wind intensity (*see* Toffolon, 2013), which is of great consistency with the sedimentological observations that pointed out development of steady washover processes giving way to uncommon climbing ripples with high angle of climb dipping lakeward (Fig. 6).

Third lake-level cycle. The transition from the middle to the upper T-R sequences is marked by a subareal unconformity (well-expressed landwards) and a sharp increase in carbonate content. Chronostratigraphically, this corresponds to the glacial termination-Holocene transition (Rhoujjati et al., 2010). Lake-level rise (transgressive systems tract, TST-3) is inferred according to biochemical proxies and ostracod markers (Fig. 10A) with a maximum in lake-level (maximum flooding surface, MFS-3) aligns with a minimum in lake bottom oxygenation (peak in Fe/Mn), whereby hypolimnion conditions would have been prone to develop aiding organic matter preservation. The highstand interval above traces a slight lake-level fall with continuous organic matter deposition, yet with increasing lake bottom oxygenation (decrease in Fe/Mn, Figs. 10 and 13), and unconformably separated from the above clastic-dominated falling-stage interval (FSST-3), marking a forced regression.

Palaeolimnological data from nearby sites (Lake Tigalmamine and Lake Sidi Ali, locations in Fig. 1) suggest lake-level rise during the Early Holocene (11.7-8.2 cal kyr BP, Walker et al., 2019) whose maximum was attained at around 8 cal kyr BP (Lamb and van der Kaars, 1995; Lamb et al., 1995; Zielhofer et al., 2017). According to a myriad of records, based upon diverse proxies and archives, the Early Holocene has been demonstrated to experience higher seasonality than present-day in the Middle Atlas with cool and humid wintertime (Lamb and van der Kaars, 1995; Zielhofer et al., 2017, 2019; Ait Brahim et al., 2019), akin to modern negative NAO-like pattern (Ait Brahim et al., 2019), and warm and dry summertime (Cheddadi et al., 1998; Nourelbait et al., 2014; Tabel et al., 2016; Campbell et al., 2017), affording conditions for drought-tolerant steppic and sclerophyll taxa (e.g., evergreen *Quercus*) to develop (Lamb and van der Kaars, 1995; Campbell et al., 2017). This is consistence with summer insolation, arising from low precession and high obliquity (Berger and Loutre, 1991; Laskar et al., 2004), low December insolation difference between latitudes 60°N and

33°N (Laskar et al., 2004), hence low-pressure gradient conditioning in part a pervasive negative NAO-like state (Hoffmann et al., 2016), and with climate simulation (Renssen et al., 2009) imparting the role that plays precession and obliquity in modulating the hydrological budget in the Mediterranean basin (Bosmans et al., 2015, 2020). Maximum lake level around 8 cal kyr BP in lake Tigalmamine (Lamb and van der Kaars, 1995) and Sidi Ali (Zielhofer et al., 2017) is consistent with speleothem data from a nearby site that suggest a peak in winter precipitation at ca. 8.2 cal kyr BP (Ait Brahim et al., 2019) that corresponds to a North Atlantic ice-rafting cold event (*viz*. Bond Event 5; Bond et al., 1997, 2001; Wanner et al., 2011). Collectively, it is suggested that the transgressive interval and the occurrence of marl mimic the orbital curves, and the maximum flooding surface is likely to reflect a North Atlantic cooling event. Such a lithological imprint (high degree of organic matter preservation) of abrupt cooling events during the Holocene has been recently reported from fluviolacustrine tufa deposits in a nearby site (Azennoud et al., 2022a).

Shift into the Mid-Holocene is marked by a progressive decrease in winter precipitation (Zielhofer et al., 2017; Ait Brahim et al., 2019) and in summer drought (Campbell et al., 2017), leading to gradual recruitment of woody vegetation. Strikingly, this coincides with synoptic scale atmospheric and oceanic reorganisation in the North Atlantic realm (Wassenburg, 2016) in response to the demise of the Laurentide Ice Sheet (Carlson et al., 2008). This is partly consistent with our palaeolimnological data that suggest a progressive decrease in lake level and a slight increase in chemical weathering (increase in Al/K ratio) during the highstand interval, suggesting a decrease in woody vegetation clearance. However, while this climate forcing would suggest a more gradual lake-level change signal so far, the instantaneous drop in lake-level and the subsequent establishment of the falling-stage interval represents confidently a signal of a tectonic pulse as evidenced by Azennoud et al. (2022b).

5.3 What insights are to be drawn into sequence stratigraphy from the case study?

As it fundamentally sheds light on the interplay between sedimentation and accommodation rates and exclusively gives credit to strata bounding surfaces (Catuneanu, 2020), sequence stratigraphy methodology, formulated initially for marine settings (e.g., Brown Jr and Fisher, 1977; Payton, 1977; Posamentier et al., 1988; Van Wagoner et al., 1988), is justified to be confidently applied to lacustrine settings as the basic requirements of the approach are met (Bohacs et al., 2007; Hanneman and Wideman, 2010; Nutz et al., 2020; Zavala et al., 2022). However, many discrepancies between marine and lacustrine settings exist and hence drive considerable restrictions and adaptations whenever the

sequence-stratigraphic approach is applied to lakes. Physical scale, time control on water-level variations, and degree of tectonic influence draw the main differences between marine and lacustrine settings (Scholz et al., 1990; Strecker et al., 1999). Unless glaciomarine influences are demonstrated to be part of the sedimentation (e.g., Nutz et al., 2015b), employment of the genuine forced regression and the resulting falling-stage systems tract and bounding surfaces (basal surface of forced regression and correlative conformity, *sensu* Van Wagoner et al., 1988) has been omitted in lake settings, while kept are the transgression genuine concept and the two-component of normal regression (e.g., Strecker et al., 1999; Bohacs et al., 2000; Zavala et al., 2022). The reasons thereof might be related, again, to the rapid drop in lake level in conjunction with, if any, low-gradient lake basin, the small physical scale of the basin, and the downstepping component of the falling-stage systems tract. Collectively, these specific aspects would cause landward preservation of deposits to be uncertain and expression of the stacking pattern basinward to be poor (confusion between forced regression and lowstand normal regression is expected). Well-expression of transgressions with respect to forced regressions in lacustrine settings may see its explanation in the fact that, contrasting marine settings, enhanced sedimentation routinely occurs during transgressions where sediment and water are more available (Zavala et al., 2022). However, in the case study presented herein, we tentatively demonstrated that not only falling-stage systems tracts can be imprinted in small-scale lakes, but their implication in disentangling climatic from tectonic forcing is of importance. Thus, differential subsidence upon *reverse-drag* flexures conditioned instantaneous forced regression in the lower and upper T-R sequences (S1 and S3, respectively), with a well-expressed falling-stage systems tract in the case where sub-humid conditions are established (occurrence of sheetflood-dominated fan deposits marking the FSST-3 of the upper sequence). On the other hand, climatic-driven downstepping marks progressive lake-level fall with well-preserved wave-influenced nearshore and Gilbert-type delta deposits. Interestingly, tracking of lake transgressions on multimillennial timescale in such settings can be performed using key ostracod species coupled with chemical weathering, drainage and redox geochemical proxies (K, Al, AL/K, and Fe/Mn), whereby the MFS is expected to correspond to maximum lake-bottom reduction (peak in Fe/Mn).

As a whole, the use of high-resolution sequence-stratigraphic approach in such interior basin has set forth the striking tuning of lowest-rank T-R sequences and component systems tracts with precession and obliquity orbital parameters. Furthermore, it is suggested that an exclusive climatic control on a lowest-rank T-R sequence is expected to output well-preserved standards systems tracts

and associated bounding surfaces, whereby the shoreline trajectory can be readily tracked (example of the middle sequence, S2).

6 Conclusions

Integration of detailed sedimentological and sequence-stratigraphic analyses in a typical tectonically-generated small-scale interior basin permitted a fair understanding of spatiotemporal variability in sedimentation dynamics and associated forcing mechanisms. Three lowest-rank T-R sequences and up to five facies models have been raised. Each T-R sequence reflects a full cycle of accommodation, whereas the facies conceptual models have been constructed based on lake level (higher *v*. lower), energy level (wind-driven), and dominant lithology (carbonate-dominated *v*. clastic-dominated). They demonstrated a complex, but decipherable, interplay between climate forcing, on both orbital and sub-orbital timescales, and tectonism. Hence, periods of sustained high lake levels have been shown to be precession-paced (MIS-3 and Early Holocene). The role of obliquity has been also shown in modulating the hydrological budget: higher (lower) obliquity enhanced (reduced) summer insolation in Northern Hemisphere, and thus the evaporation, example of the Early Holocene (MIS-3). Lithology appears to be the response of a complex interplay between climate parameters (evaporation/precipitation) and vegetation. Besides, sedimentation dynamics have been suggested to respond to millennial timescale climate variability (D-O, Heinrich Events, Bond Events) and, interestingly, to enhanced Saharan winds during the deglacial period. On the other hand, tectonism had a rather instantaneous effect on lake level and sedimentation. Two tectonic pulses marking instantaneous differential subsidence have triggered a sharp drop in relative lake level and hence conditioned a forced regression.

The use of high-resolution sequence stratigraphy in such small-scale interior basin has demonstrated its importance in driving fair understandings of the interplay between orbital, sub-orbital and tectonic forcing, so as the resulting sedimentation dynamics. Furthermore, while this approach fairly gives credit to strata bounding surfaces, scrutinising deeply, in the frame of sequence stratigraphy, surfaces that mark a sharp change in shoreline trajectory (such as the basal surface of forced regression) would be a necessary step to build a concrete understanding of the aforementioned interplay. We highlighted the effective usefulness of ostracods and geochemical proxies (especially the Fe/Mn ratio) in tracing transgressions and cryptic surfaces such as the MFS in lacustrine settings. We therefore recommend the use of sequence-stratigraphic approach in similar cases as it is standardised by Catuneanu et al. (2011), with more emphasis here pointed to the importance of the forced regression concept and associated systems tract and bounding surfaces.

Acknowledgement

The geochemical analyses carried out in this work were supported thanks to the Laboratory of Engineering, Electrochemistry, Modelling and Environment, Faculty of Sciences Dhar EL Mahraz, Sidi Mohamed Ben Abdellah University (Morocco).

References

Ait Brahim, L., Chotin, P., Hinaj, S., Abdelouafi, A., El Adraoui, A., Nakcha, C., Dhont, D., Charroud, M., Sossey Alaoui, F., Amrhar, M., Bouaza, A., Tabyaoui, H., Chaouni, A., 2002. Paleostress evolution in the Moroccan African margin from Triassic to Present. Tectonophysics 357, 187–205. https://doi.org/10.1016/S0040-1951(02)00368-2

Ait Brahim, Y., Wassenburg, J.A., Cruz, F.W., Sifeddine, A., Scholz, D., Bouchaou, L., Dassié, E.P., Jochum, K.P., Edwards, R.L., Cheng, H., 2018. Multi-decadal to centennial hydro-climate variability and linkage to solar forcing in the Western Mediterranean during the last 1000 years. Sci Rep 8, 17446. https://doi.org/10.1038/s41598-018-35498-x

Ait Brahim, Y., Wassenburg, J.A., Sha, L., Cruz, F.W., Deininger, M., Sifeddine, A., Bouchaou, L., Spötl, C., Edwards, R.L., Cheng, H., 2019. North Atlantic Ice-Rafting, Ocean and Atmospheric Circulation During the Holocene: Insights From Western Mediterranean Speleothems. Geophysical Research Letters 46, 7614–7623.

Allard, J.L., Hughes, P.D., Woodward, J.C., 2021. Heinrich Stadial aridity forced Mediterranean-wide glacier retreat in the last cold stage. Nat. Geosci. 14, 197–205. https://doi.org/10.1038/s41561-021-00703-6

Allen, J.R.L., 1982. Sedimentary structures, their character and physical basis. Elsevier.

Alonso-Zarza, A.M., 2003. Palaeoenvironmental significance of palustrine carbonates and calcretes in the geological record. Earth-Science Reviews 60, 261–298.

Alonso-Zarza, A.M., Meléndez, A., Martín-García, R., Herrero, M.J., Martín-Pérez, A., 2012. Discriminating between tectonism and climate signatures in palustrine deposits: lessons from the Miocene of the Teruel Graben, NE Spain. Earth-Science Reviews 113, 141–160.

Anadón, P., Cabrera, Ll., Julià, R., Marzo, M., 1991. Sequential Arrangement and Asymmetrical Fill in the Miocene Rubielos de Mora Basin (Northeast Spain), in: Lacustrine Facies Analysis. John Wiley & Sons, Ltd, pp. 257–275. https://doi.org/10.1002/9781444303919.ch13

Anselmetti, F.S., Ariztegui, D., Hodell, D.A., Hillesheim, M.B., Brenner, M., Gilli, A., McKenzie, J.A., Mueller, A.D., 2006. Late Quaternary climate-induced lake level variations in Lake Petén Itzá, Guatemala, inferred from seismic stratigraphic analysis. Palaeogeography, Palaeoclimatology, Palaeoecology 230, 52–69. https://doi.org/10.1016/j.palaeo.2005.06.037

Ashley, G.M., De Wet, C.B., Domínguez-Rodrigo, M., Karis, A.M., O'Reilly, T.M., Baluyot, R., 2014. Freshwater Limestone In An Arid Rift Basin: A Goldilocks Effect. Journal of Sedimentary Research 84, 988–1004. https://doi.org/10.2110/jsr.2014.80

Ashley, G.M., Southard, J.B., Boothroyd, J.C., 1982. Deposition of climbing-ripple beds: a flume simulation. Sedimentology 29, 67–79. https://doi.org/10.1111/j.1365-3091.1982.tb01709.x

Azennoud, K., Baali, A., Ait Brahim, Y., Ahouach, Y., Hakam, O., 2022a. Climate controls on tufa deposition over the last 5000 years: A case study from Northwest Africa. Palaeogeography, Palaeoclimatology, Palaeoecology 586, 110767. https://doi.org/10.1016/j.palaeo.2021.110767

Azennoud, K., Baali, A., El Asmi, H., Brahim, Y.A., Hakam, O., Hayati, A., El Kamel, T., 2022b. Soft-sediment deformation structures recognised in a reverse-drag associated with normal faulting (Lake Ifrah, Northwest Africa): Palaeoseismic assessment and neotectonic implications. Sedimentary Geology 106264. https://doi.org/10.1016/j.sedgeo.2022.106264

Barrell, J., 1917. Rhythms and the measurements of geologic time1. GSA Bulletin 28, 745–904. https://doi.org/10.1130/GSAB-28-745

Baumann, J., Chaumillon, E., Bertin, X., Schneider, J.-L., Guillot, B., Schmutz, M., 2017. Importance of infragravity waves for the generation of washover deposits. Marine Geology 391, 20–35. https://doi.org/10.1016/j.margeo.2017.07.013

Benabid, A., 1982. Bref aperçu sur la zonation altitudinale de la végétation climacique du Maroc. Ecologia mediterranea 8, 301–315.

Berger, A., Loutre, M.F., 1991. Insolation values for the climate of the last 10 million years. Quaternary Science Reviews 10, 297–317. https://doi.org/10.1016/0277-3791(91)90033-Q

Bernhart Owen, R., Renaut, R.W., Muiruri, V.M., Rabideaux, N.M., Lowenstein, T.K., McNulty, E.P., Leet, K., Deocampo, D., Luo, S., Deino, A.L., Cohen, A., Sier, M.J., Campisano, C., Shen, C.-C., Billingsley, A., Mbuthia, A., Stockhecke, M., 2019. Quaternary history of the Lake Magadi Basin, southern Kenya Rift: Tectonic and climatic controls. Palaeogeography, Palaeoclimatology, Palaeoecology 518, 97–118. https://doi.org/10.1016/j.palaeo.2019.01.017

Birgenheier, L.P., Horton, B., McCauley, A.D., Johnson, C.L., Kennedy, A., 2017. A depositional model for offshore deposits of the lower Blue Gate Member, Mancos Shale, Uinta Basin, Utah, USA. Sedimentology 64, 1402–1438. https://doi.org/10.1111/sed.12359

Blair, T.C., McPherson, J.G., 2009. Processes and Forms of Alluvial Fans, in: Parsons, A.J., Abrahams, A.D. (Eds.), Geomorphology of Desert Environments. Springer Netherlands, Dordrecht, pp. 413–467. https://doi.org/10.1007/978-1-4020-5719-9_14

Boës, X., Rydberg, J., Martinez-Cortizas, A., Bindler, R., Renberg, I., 2011. Evaluation of conservative lithogenic elements (Ti, Zr, Al, and Rb) to study anthropogenic element enrichments in lake sediments. J Paleolimnol 46, 75–87. https://doi.org/10.1007/s10933-011-9515-z

Bohacs, K.M., Carroll, A.R., Neal, J.E., Mankiewicz, P.J., 2000. Lake-basin type, source potential, and hydrocarbon character: an integrated sequence-stratigraphic-geochemical framework. Lake basins through space and time: AAPG Studies in Geology 46, 3–34.

Bohacs, K.M., Grabowski Jr, G., Carroll, A.R., 2007. Lithofacies architecture and variations in expression of sequence stratigraphy within representative intervals of the Green River Formation, Greater Green River Basin, Wyoming and Colorado.

Bond, G., Heinrich, H., Broecker, W., Labeyrie, L., McManus, J., Andrews, J., Huon, S., Jantschik, R., Clasen, S., Simet, C., 1992. Evidence for massive discharges of icebergs into the North Atlantic ocean during the last glacial period. Nature 360, 245–249.

Bond, G., Kromer, B., Beer, J., Muscheler, R., Evans, M.N., Showers, W., Hoffmann, S., Lotti-Bond, R., Hajdas, I., Bonani, G., 2001. Persistent solar influence on North Atlantic climate during the Holocene. science 294, 2130–2136.

Bond, G., Showers, W., Cheseby, M., Lotti, R., Almasi, P., DeMenocal, P., Priore, P., Cullen, H., Hajdas, I., Bonani, G., 1997. A pervasive millennial-scale cycle in North Atlantic Holocene and glacial climates. science 278, 1257–1266.

Bond, G.C., Lotti, R., 1995. Iceberg discharges into the North Atlantic on millennial time scales during the last glaciation. Science 267, 1005–1010.

Bosmans, J.H.C., Drijfhout, S.S., Tuenter, E., Hilgen, F.J., Lourens, L.J., Rohling, E.J., 2015. Precession and obliquity forcing of the freshwater budget over the Mediterranean. Quaternary Science Reviews 123, 16–30. https://doi.org/10.1016/j.quascirev.2015.06.008

Bosmans, J.H.C., Ent, R.J. van der, Haarsma, R.J., Drijfhout, S.S., Hilgen, F.J., 2020. Precession- and Obliquity-Induced Changes in Moisture Sources for Enhanced Precipitation Over the Mediterranean Sea. Paleoceanography and Paleoclimatology 35, e2019PA003655. https://doi.org/10.1029/2019PA003655

Bout-Roumazeilles, V., Nebout, N.C., Peyron, O., Cortijo, E., Landais, A., Masson-Delmotte, V., 2007. Connection between South Mediterranean climate and North African atmospheric circulation during the last 50,000 yr BP North Atlantic cold events. Quaternary Science Reviews 26, 3197–3215.

Boyle, J.F., 2001. Inorganic geochemical methods in palaeolimnology, in: Tracking Environmental Change Using Lake Sediments. Springer, pp. 83–141.

Broecker, W., Bond, G., Klas, M., Clark, E., McManus, J., 1992. Origin of the northern Atlantic's Heinrich events. Climate Dynamics 6, 265–273. https://doi.org/10.1007/BF00193540

Brown Jr, L.F.B., Fisher, W.L., 1977. Seismic-Stratigraphic Interpretation of Depositional Systems: Examples from Brazilian Rift and Pull-Apart Basins: Section 2. Application of Seismic Reflection Configuration to Stratigraphic Interpretation 165, 213–248.

Budai, S., Colombera, L., Mountney, N.P., 2021. Quantitative characterization of the sedimentary architecture of Gilbert-type deltas. Sedimentary Geology 426, 106022. https://doi.org/10.1016/j.sedgeo.2021.106022

Burnett, A.P., Soreghan, M.J., Scholz, C.A., Brown, E.T., 2011. Tropical East African climate change and its relation to global climate: a record from Lake Tanganyika, Tropical East Africa, over the past 90+ kyr. Palaeogeography, Palaeoclimatology, Palaeoecology 303, 155–167.

Cacho, I., Grimalt, J.O., Pelejero, C., Canals, M., Sierro, F.J., Flores, J.A., Shackleton, N., 1999. Dansgaard-Oeschger and Heinrich event imprints in Alboran Sea paleotemperatures. Paleoceanography 14, 698–705.

Cacho, I., Grimalt, J.O., Sierro, F.J., Shackleton, N., Canals, M., 2000. Evidence for enhanced Mediterranean thermohaline circulation during rapid climatic coolings. Earth and Planetary Science Letters 183, 417–429. https://doi.org/10.1016/S0012-821X(00)00296-X

Cacho, I., Shackleton, N., Elderfield, H., Sierro, F.J., Grimalt, J.O., 2006. Glacial rapid variability in deep-water temperature and δ18O from the Western Mediterranean Sea. Quaternary Science Reviews, Critical Quaternary Stratigraphy 25, 3294–3311. https://doi.org/10.1016/j.quascirev.2006.10.004

Campbell, J.F.E., Fletcher, W.J., Joannin, S., Hughes, P.D., Rhanem, M., Zielhofer, C., 2017. Environmental Drivers of Holocene Forest Development in the Middle Atlas, Morocco. Front. Ecol. Evol. 5. https://doi.org/10.3389/fevo.2017.00113

Camuera, J., Jiménez-Moreno, G., Ramos-Román, M.J., García-Alix, A., Toney, J.L., Anderson, R.S., Jiménez-Espejo, F., Bright, J., Webster, C., Yanes, Y., Carrión, J.S., 2019. Vegetation and climate changes during the last two glacial-interglacial cycles in the western Mediterranean: A new long pollen record from Padul (southern Iberian Peninsula). Quaternary Science Reviews 205, 86–105. https://doi.org/10.1016/j.quascirev.2018.12.013

Carlson, A.E., LeGrande, A.N., Oppo, D.W., Came, R.E., Schmidt, G.A., Anslow, F.S., Licciardi, J.M., Obbink, E.A., 2008. Rapid early Holocene deglaciation of the Laurentide ice sheet. Nature Geosci 1, 620–624. https://doi.org/10.1038/ngeo285

Carroll, A.R., Bohacs, K.M., 1999. Stratigraphic classification of ancient lakes: Balancing tectonic and climatic controls. Geology 27, 99–102.

Catuneanu, O., 2019. Model-independent sequence stratigraphy. Earth-science reviews 188, 312–388.

Catuneanu, O., 2017. Chapter One - Sequence Stratigraphy: Guidelines for a Standard Methodology, in: Montenari, M. (Ed.), Stratigraphy & Timescales, Advances in Sequence Stratigraphy. Academic Press, pp. 1–57. https://doi.org/10.1016/bs.sats.2017.07.003

Catuneanu, O., 2006. Principles of sequence stratigraphy, 1st ed. ed, Developments in sedimentology. Elsevier, Amsterdam ; Boston.

Catuneanu, O., Galloway, W.E., Kendall, C.G.S.C., Miall, A.D., Posamentier, H.W., Strasser, A., Tucker, M.E., 2011. Sequence stratigraphy: methodology and nomenclature. Newsletters on stratigraphy 44, 173–245.

Cecil, C.B., 1990. Paleoclimate controls on stratigraphic repetition of chemical and siliciclastic rocks. Geology 18, 533–536. https://doi.org/10.1130/0091-7613(1990)018<0533:PCOSRO>2.3.CO;2

Cecil, C.B., Stanton, R.W., Neuzil, S.G., Dulong, F.T., Ruppert, L.F., Pierce, B.S., 1985. Paleoclimate controls on late paleozoic sedimentation and peat formation in the central appalachian basin (U.S.A.). International Journal of Coal Geology 5, 195–230. https://doi.org/10.1016/0166-5162(85)90014-X

Chalouan, A., Gil, A.J., Galindo-Zaldívar, J., Ahmamou, M., Ruano, P., de Lacy, M.C., Ruiz-Armenteros, A.M., Benmakhlouf, M., Riguzzi, F., 2014. Active faulting in the frontal Rif Cordillera (Fes region, Morocco):

Constraints from GPS data. Journal of Geodynamics 77, 110–122. https://doi.org/10.1016/j.jog.2014.01.002

Changsong, L., Eriksson, K., Sitian, L., Yongxian, W., Jianye, R., Yanmei, Z., 2001. Sequence Architecture, Depositional Systems, and Controls on Development of Lacustrine Basin Fills in Part of the Erlian Basin, Northeast China. AAPG Bulletin 85, 2017–2043. https://doi.org/10.1306/8626D0DB-173B-11D7-8645000102C1865D

Charrière, A., 1990. Héritage hercynien et évolution géody- namique alpine d'une chaîne intracontinentale : le Moyen Atlas au sud-est de Fes (Maroc). Thèse de Doctorat d'État, Université Toulouse III – Paul Sabatier, Toulouse, 589 p.

Cheddadi, R., Fady, B., François, L., Hajar, L., Suc, J.-P., Huang, K., Demarteau, M., Vendramin, G.G., Ortu, E., 2009. Putative glacial refugia of Cedrus atlantica deduced from Quaternary pollen records and modern genetic diversity. Journal of Biogeography 36, 1361–1371.

Cheddadi, R., Mamakowa, K., Guiot, J., De Beaulieu, J.-L., Reille, M., Andrieu, V., Granoszewski, W., Peyron, O., 1998. Was the climate of the Eemian stable? A quantitative climate reconstruction from seven European pollen records. Palaeogeography, Palaeoclimatology, Palaeoecology 143, 73–85.

Clifton, H.E., 2006. A Reexamination of Facies Models for Clastic Shorelines. https://doi.org/10.2110/pec.06.84.0293

Clifton, H.E., Hunter, R.E., Phillips, R.L., 1971. Depositional structures and processes in the non-barred high-energy nearshore. Journal of Sedimentary Research 41, 651–670. https://doi.org/10.1306/74D7231A-2B21-11D7-8648000102C1865D

Cohen, A.S., 2003. Lakes as Archives of Earth History, in: Cohen, A.S. (Ed.), Paleolimnology: The History and Evolution of Lake Systems. Oxford University Press, p. 0. https://doi.org/10.1093/oso/9780195133530.003.0005

Cojan, I., 1993. Alternating Fluvial and Lacustrine Sedimentation: Tectonic and Climatic Controls (Provence Basin, S. France, Upper Cretaceous/Palaeocene), in: Alluvial Sedimentation. John Wiley & Sons, Ltd, pp. 425–438. https://doi.org/10.1002/9781444303995.ch27

Combourieu Nebout, N., 2002. Enhanced aridity and atmospheric high-pressure stability over the western Mediterranean during the North Atlantic cold events of the past 50 kyr. Geology 30.

Dansgaard, W., Johnsen, S.J., Clausen, H.B., Dahl-Jensen, D., Gundestrup, N.S., Hammer, C.U., Hvidberg, C.S., Steffensen, J.P., Sveinbjörnsdottir, A.E., Jouzel, J., 1993. Evidence for general instability of past climate from a 250-kyr ice-core record. Nature 364, 218–220.

Davies, S.J., Lamb, H.F., Roberts, S.J., 2015. Micro-XRF core scanning in palaeolimnology: recent developments, in: Micro-XRF Studies of Sediment Cores. Springer, pp. 189–226.

de Wet, C.B., Godfrey, L., de Wet, A.P., 2015. Sedimentology and stable isotopes from a lacustrine-to-palustrine limestone deposited in an arid setting, climatic and tectonic factors: Miocene–Pliocene Opache Formation, Atacama Desert, Chile. Palaeogeography, Palaeoclimatology, Palaeoecology 426, 46–67. https://doi.org/10.1016/j.palaeo.2015.02.039

Droser, M.L., Bottjer, D.J., 1986. A Semiquantitative Field Classification of Ichnofabric: RESEARCH METHOD PAPER. Journal of Sedimentary Research 56.

Dunham, R.J., 1969. Early Vadose Silt in Townsend Mound (Reef), New Mexico.

Dunham, R.J., 1962. Classification of Carbonate Rocks According to Depositional Textures 38, 108–121.

Embry, A.F., Johannessen, E.P., 1993. T–R sequence stratigraphy, facies analysis and reservoir distribution in the uppermost Triassic–Lower Jurassic succession, western Sverdrup Basin, Arctic Canada, in: Vorren, T.O., Bergsager, E., Dahl-Stamnes, Ø.A., Holter, E., Johansen, B., Lie, E., Lund, T.B. (Eds.), Norwegian Petroleum Society Special Publications. Elsevier, pp. 121–146. https://doi.org/10.1016/B978-0-444-88943-0.50013-7

Eynon, G., Walker, R.G., 1974. Facies relationships in Pleistocene outwash gravels, southern Ontario: a model for bar growth in braided rivers. Sedimentology 21, 43–70. https://doi.org/10.1111/j.1365-3091.1974.tb01781.x

Fernàndez, M., Torne, M., Vergés, J., Casciello, E., Macchiavelli, C., 2019. Evidence of Segmentation in the Iberia–Africa Plate Boundary: A Jurassic Heritage? Geosciences 9, 343. https://doi.org/10.3390/geosciences9080343

Fink, H.G., Wienberg, C., De Pol-Holz, R., Wintersteller, P., Hebbeln, D., 2013. Cold-water coral growth in the Alboran Sea related to high productivity during the Late Pleistocene and Holocene. Marine Geology 339, 71–82. https://doi.org/10.1016/j.margeo.2013.04.009

Fletcher, W.J., Sánchez Goñi, M.F.S., 2008. Orbital- and sub-orbital-scale climate impacts on vegetation of the western Mediterranean basin over the last 48,000 yr. Quaternary Research 70, 451–464. https://doi.org/10.1016/j.yqres.2008.07.002

Freytet, P., Plaziat, J.-C., 1982. Continental Carbonate Sedimentation and Pedogenesis - Late Cretaceous and Early Tertiary of Southern France [WWW Document]. URL https://www.schweizerbart.de/publications/detail/isbn/9783510570126/Continental_Carbonate_Sedimentation_and_Pedogenesi (accessed 8.6.22).

Freytet, P., Verrecchia, E.P., 2002. Lacustrine and palustrine carbonate petrography: an overview. Journal of Paleolimnology 27, 221–237. https://doi.org/10.1023/A:1014263722766

Frizon de Lamotte, D., Saint Bezar, B., Bracène, R., Mercier, E., 2000. The two main steps of the Atlas building and geodynamics of the western Mediterranean. Tectonics 19, 740–761. https://doi.org/10.1029/2000TC900003

Frizon de Lamotte, D., Zizi, M., Missenard, Y., Hafid, M., Azzouzi, M.E., Maury, R.C., Charrière, A., Taki, Z., Benammi, M., Michard, A., 2008. The Atlas System, in: Michard, André, Saddiqi, O., Chalouan, A., Lamotte, D.F. de (Eds.), Continental Evolution: The Geology of Morocco: Structure, Stratigraphy, and Tectonics of the Africa-Atlantic-Mediterranean Triple Junction, Lecture Notes in Earth Sciences. Springer, Berlin, Heidelberg, pp. 133–202. https://doi.org/10.1007/978-3-540-77076-3_4

Frostick, L.E., Steel, R.J., 1994. Tectonic Signatures in Sedimentary Basin Fills: An Overview, in: Tectonic Controls and Signatures in Sedimentary Successions. John Wiley & Sons, Ltd, pp. 1–9. https://doi.org/10.1002/9781444304053.ch1

Gierlowski-Kordesch, E., Kelts, K., 1994. Global Geological Record of Lake Basins: Volume 1. Cambridge University Press.

Gierlowski-Kordesch, E.H., 2010. Chapter 1 Lacustrine Carbonates, in: Alonso-Zarza, A.M., Tanner, L.H. (Eds.), Developments in Sedimentology, Carbonates in Continental Settings: Facies, Environments, and Processes. Elsevier, pp. 1–101. https://doi.org/10.1016/S0070-4571(09)06101-9

Gracia, F.-J., Morales, J.-A., Castañeda, C., Plomaritis, T.A., 2021. Shallow lacustrine versus open ocean coastal clastic deposits: Morphosedimentary diagnostic indicators and interpretation. Sedimentary Geology 423, 105981. https://doi.org/10.1016/j.sedgeo.2021.105981

Hakam, O., Baali, A., Ait Brahim, Y., El Kamel, T., Azennoud, K., 2022. Regional and global teleconnections patterns governing rainfall in the Western Mediterranean: case of the Lower Sebou Basin, North-West Morocco. Model. Earth Syst. Environ. https://doi.org/10.1007/s40808-022-01425-3

Hein, F.J., Walker, R.G., 1977. Bar evolution and development of stratification in the gravelly, braided, Kicking Horse River, British Columbia. Can. J. Earth Sci. 14, 562–570. https://doi.org/10.1139/e77-058

Heinrich, H., 1988. Origin and consequences of cyclic ice rafting in the northeast Atlantic Ocean during the past 130,000 years. Quaternary research 29, 142–152.

Hoffmann, D.L., Rogerson, M., Spötl, C., Luetscher, M., Vance, D., Osborne, A.H., Fello, N.M., Moseley, G.E., 2016. Timing and causes of North African wet phases during the last glacial period and implications for modern human migration. Sci Rep 6, 36367. https://doi.org/10.1038/srep36367

Horton, B.K., Schmitt, J.G., 1996. Sedimentology of a lacustrine fan-delta system, Miocene Horse Camp Formation, Nevada, USA. Sedimentology 43, 133–155. https://doi.org/10.1111/j.1365-3091.1996.tb01464.x

Hunt, D., Tucker, M.E., 1992. Stranded parasequences and the forced regressive wedge systems tract: deposition during base-level'fall. Sedimentary Geology 81, 1–9. https://doi.org/10.1016/0037-0738(92)90052-S

Hunter, R.E., 1977. Terminology of cross-stratified sedimentary layers and climbing-ripple structures. Journal of Sedimentary Research 47, 697–706. https://doi.org/10.1306/212F7225-2B24-11D7-8648000102C1865D

Ito, M., 2019. Lithofacies architecture of gravel-wave deposits: Insights into the origins of coarse-grained gravity-flow deposits. Sedimentary Geology 382, 36–46. https://doi.org/10.1016/j.sedgeo.2019.01.004

Jervey, M.T., 1988. Quantitative Geological Modeling of Siliciclastic Rock Sequences and Their Seismic Expression, in: Wilgus, C.K., Hastings, B.S., Posamentier, H., Wagoner, J.V., Ross, C.A., Kendall, C.G.St.C. (Eds.), Sea-Level Changes: An Integrated Approach. SEPM Society for Sedimentary Geology, p. 0. https://doi.org/10.2110/pec.88.01.0047

Jimenez-Espejo, F.J., Martinez-Ruiz, F., Rogerson, M., González-Donoso, J.M., Romero, O.E., Linares, D., Sakamoto, T., Gallego-Torres, D., Rueda Ruiz, J.L., Ortega-Huertas, M., Perez Claros, J.A., 2008. Detrital input, productivity fluctuations, and water mass circulation in the westernmost Mediterranean Sea since the Last Glacial Maximum. Geochemistry, Geophysics, Geosystems 9. https://doi.org/10.1029/2008GC002096

Jobe, Z.R., Lowe, D.R., Morris, W.R., 2012. Climbing-ripple successions in turbidite systems: depositional environments, sedimentation rates and accumulation times. Sedimentology 59, 867–898. https://doi.org/10.1111/j.1365-3091.2011.01283.x

Keighley, D., Flint, S., Howell, J., Moscariello, A., 2003. Sequence Stratigraphy in Lacustrine Basins: A Model for Part of the Green River Formation (Eocene), Southwest Uinta Basin, Utah, U.S.A. Journal of Sedimentary Research 73, 987–1006. https://doi.org/10.1306/050103730987

Kleinhans, M.G., 2005. Autogenic cyclicity of foreset sorting in experimental Gilbert-type deltas. Sedimentary Geology 181, 215–224. https://doi.org/10.1016/j.sedgeo.2005.09.001

Knippertz, P., Christoph, M., Speth, P., 2003. Long-term precipitation variability in Morocco and the link to the large-scale circulation in recent and future climates. Meteorology and Atmospheric physics 83, 67–88.

Köppen, W., 1900. Versuch einer Klassifikation der Klimate, vorzugsweise nach ihren Beziehungen zur Pflanzenwelt. (Schluss). Geographische Zeitschrift 6, 657–679.

Kottek, M., Grieser, J., Beck, C., Rudolf, B., Rubel, F., 2006. World Map of the Köppen-Geiger climate classification updated. Meteorologische Zeitschrift 259–263. https://doi.org/10.1127/0941-2948/2006/0130

Kylander, M.E., Ampel, L., Wohlfarth, B., Veres, D., 2011. High-resolution X-ray fluorescence core scanning analysis of Les Echets (France) sedimentary sequence: new insights from chemical proxies. Journal of Quaternary Science 26, 109–117.

Lamb, H.F., Eicher, U., Switsur, V.R., 1989. An 18,000-Year Record of Vegetation, Lake-Level and Climatic Change from Tigalmamine, Middle Atlas, Morocco. Journal of Biogeography 16, 65–74. https://doi.org/10.2307/2845311

Lamb, H.F., Gasse, F., Benkaddour, A., El Hamouti, N., Van der Kaars, S., Perkins, W.T., Pearce, N.J., Roberts, C.N., 1995. Relation between century-scale Holocene arid intervals in tropical and temperate zones. Nature 373, 134–137.

Lamb, H.F., van der Kaars, S., 1995. Vegetational response to Holocene climatic change: pollen and palaeolimnological data from the Middle Atlas, Morocco. The Holocene 5, 400–408. https://doi.org/10.1177/095968369500500402

Laskar, J., Robutel, P., Joutel, F., Gastineau, M., Correia, A.C.M., Levrard, B., 2004. A long-term numerical solution for the insolation quantities of the Earth. A&A 428, 261–285. https://doi.org/10.1051/0004-6361:20041335

Lowe, D.R., 1982. Sediment gravity flows; II, Depositional models with special reference to the deposits of high-density turbidity currents. Journal of Sedimentary Research 52, 279–297. https://doi.org/10.1306/212F7F31-2B24-11D7-8648000102C1865D

Martin, J., 1981. Le Moyen Atlas central étude géomorphologique. Editions du Service géologique du Maroc.

Matias, A., Masselink, G., 2017. Overwash Processes: Lessons from Fieldwork and Laboratory Experiments, in: Coastal Storms. John Wiley & Sons, Ltd, pp. 175–194. https://doi.org/10.1002/9781118937099.ch9

Mattauer, M., Tapponnier, P., Proust, F., 1977. Sur les méchanismes de formation des chaînes intracontinentales. L'example des chaînes atlasiques du Maroc. Bull. Soc. géol. France, (VII) 19.

Meese, D.A., Gow, A.J., Alley, R.B., Zielinski, G.A., Grootes, P.M., Ram, M., Taylor, K.C., Mayewski, P.A., Bolzan, J.F., 1997. The Greenland Ice Sheet Project 2 depth-age scale: Methods and results. Journal of Geophysical Research: Oceans 102, 26411–26423. https://doi.org/10.1029/97JC00269

Meisch, C., 2000. Freshwater Ostracoda of western and central Europe. Süsswasserfauna von Mitteleuropa 8/3. Spektrum, Gustav Fischer, Heidelberg; Berlin.

Meisch, C., Scharf, B., Fuhrmann, R., Thiery, A., 2019. Neglecandona altoides (Petkovski, 1961) nov. comb. and the genus Neglecandona Krstic, 2006 (Crustacea, Ostracoda, Candonidae). Bulletin de la Société des naturalistes luxembourgeois 121, 237–264.

Miall, A.D., 1977. A review of the braided-river depositional environment. Earth-Science Reviews 13, 1–62. https://doi.org/10.1016/0012-8252(77)90055-1

Middleton, G.V., Hampton, M.A., 1973. Part I. Sediment Gravity Flows: Mechanics of Flow and Deposition 1–38.

Mix, A.C., Bard, E., Schneider, R., 2001. Environmental processes of the ice age: land, oceans, glaciers (EPILOG). Quaternary Science Reviews 20, 627–657. https://doi.org/10.1016/S0277-3791(00)00145-1

Moreno, A., Cacho, I., Canals, M., Prins, M.A., Sánchez-Goñi, M.-F., Grimalt, J.O., Weltje, G.J., 2002. Saharan dust transport and high-latitude glacial climatic variability: the Alboran Sea record. Quaternary Research 58, 318–328.

Moulin, C., Lambert, C.E., Dulac, F., Dayan, U., 1997. Control of atmospheric export of dust from North Africa by the North Atlantic Oscillation. Nature 387, 691–694.

Mutti, E., Tinterri, R., Benevelli, G., Biase, D. di, Cavanna, G., 2003. Deltaic, mixed and turbidite sedimentation of ancient foreland basins. Marine and Petroleum Geology, Turbidites: Models and Problems 20, 733–755. https://doi.org/10.1016/j.marpetgeo.2003.09.001

Neal, J., Abreu, V., 2009. Sequence stratigraphy hierarchy and the accommodation succession method. Geology 37, 779–782. https://doi.org/10.1130/G25722A.1

Nemec, W., 1990. Aspects of sediment movement on steep delta slopes. Coarse-grained deltas 10, 29–73.

Nemec, W., Steel, R.J., 1984. Alluvial and Coastal Conglomerates: Their Significant Features and Some Comments on Gravelly Mass-Flow Deposits 1–31.

Nourelbait, M., Rhoujjati, A., Eynaud, F., Benkaddour, A., Dezileau, L., Wainer, K., Goslar, T., Khater, C., Tabel, J., Cheddadi, R., 2014. An 18 000-year pollen and sedimentary record from the cedar forests of the Middle Atlas, Morocco: POLLEN/SEDIMENTARY RECORD FROM THE MIDDLE ATLAS. J. Quaternary Sci. 29, 423–432. https://doi.org/10.1002/jqs.2708

Nutz, Alexis, Ghienne, J.-F., Schuster, M., Dietrich, P., Roquin, C., Hay, M.B., Bouchette, F., Cousineau, P.A., 2015. Forced regressive deposits of a deglaciation sequence: Example from the Late Quaternary succession in the Lake Saint-Jean basin (Québec, Canada). Sedimentology 62, 1573–1610.

Nutz, A., Kwiecien, O., Breitenbach, S.F.M., Cai, Y., Porta, G.D., Danisch, J., Kabiri, L., Bodin, S., 2019. Fluvio-lacustrine sedimentation in the Agadir-Tissint Feija (Anti-Atlas, Morocco): A promising palaeoclimate archive for the last glacial cycle in northwest Africa. The Depositional Record 5, 362–387. https://doi.org/10.1002/dep2.65

Nutz, A., Ragon, T., Schuster, M., 2022. Cenozoic tectono-sedimentary evolution of the northern Turkana Depression (East African Rift System) and its significance for continental rifts. Earth and Planetary Science Letters 578, 117285. https://doi.org/10.1016/j.epsl.2021.117285

Nutz, A., Schuster, M., Barboni, D., Gassier, G., Van Bocxlaer, B., Robin, C., Ragon, T., Ghienne, J.-F., Rubino, J.-L., 2020. Plio-Pleistocene sedimentation in West Turkana (Turkana Depression, Kenya, East African Rift System): Paleolake fluctuations, paleolandscapes and controlling factors. Earth-Science Reviews 211, 103415. https://doi.org/10.1016/j.earscirev.2020.103415

Nutz, A., Schuster, M., Boës, X., Rubino, J.-L., 2017. Orbitally-driven evolution of Lake Turkana (Turkana Depression, Kenya, EARS) between 1.95 and 1.72 Ma: A sequence stratigraphy perspective. Journal of African Earth Sciences 125, 230–243. https://doi.org/10.1016/j.jafrearsci.2016.10.016

Nutz, A., Schuster, M., Ghienne, J.-F., Roquin, C., Bouchette, F., 2016. Wind-driven waterbodies: a new category of lake within an alternative sedimentologically-based lake classification. J Paleolimnol 59, 189–199. https://doi.org/10.1007/s10933-016-9894-2

Nutz, A., Schuster, M., Ghienne, J.-F., Roquin, C., Hay, M.B., Rétif, F., Certain, R., Robin, N., Raynal, O., Cousineau, P.A., Team, S., Bouchette, F., 2015. Wind-driven bottom currents and related sedimentary bodies in Lake Saint-Jean (Québec, Canada). GSA Bulletin 127, 1194–1208. https://doi.org/10.1130/B31145.1

Ouarhache, D., Charriere, A., Chalot-prat, F., Wartiti, M.E., 2012. Triassic to early Liassic continental rifting chronology and process at the southwest margin of the Alpine Tethys (Middle Atlas and High Moulouya, Morocco); correlations with the Atlantic rifting, synchronous and diachronous. Bulletin de la Societe Geologique de France 183, 233–249. https://doi.org/10.2113/gssgfbull.183.3.233

Oviatt, C.G., McCoy, W.D., Nash, W.P., 1994. Sequence stratigraphy of lacustrine deposits: A Quaternary example from the Bonneville basin, Utah. GSA Bulletin 106, 133–144. https://doi.org/10.1130/0016-7606(1994)106<0133:SSOLDA>2.3.CO;2

Pan, S., Liu, H., Xu, D., Wei, P., Qu, Y., Guan, X., Liu, C., Zhang, S., 2020. Sublacustrine gravity-induced deposits: The diversity of external geometries and origins. Sedimentary Geology 407, 105738. https://doi.org/10.1016/j.sedgeo.2020.105738

Payton, C.E., 1977. Seismic Stratigraphy — Applications to Hydrocarbon Exploration. https://doi.org/10.1306/M26490

Peters, S.E., Loss, D.P., 2012. Storm and fair-weather wave base: A relevant distinction? Geology 40, 511–514. https://doi.org/10.1130/G32791.1

Pickering, K., Stow, D., Watson, M., Hiscott, R., 1986. Deep-water facies, processes and models: a review and classification scheme for modern and ancient sediments. Earth-Science Reviews 23, 75–174. https://doi.org/10.1016/0012-8252(86)90001-2

Pla-Pueyo, S., Gierlowski-Kordesch, E.H., Viseras, C., Soria, J.M., 2009. Major controls on sedimentation during the evolution of a continental basin: Pliocene–Pleistocene of the Guadix Basin (Betic Cordillera, southern Spain). Sedimentary Geology 219, 97–114. https://doi.org/10.1016/j.sedgeo.2009.05.001

Platt, N.H., 1989. Lacustrine carbonates and pedogenesis: sedimentology and origin of palustrine deposits from the Early Cretaceous Rupelo Formation, W Cameros Basin, N Spain. Sedimentology 36, 665–684. https://doi.org/10.1111/j.1365-3091.1989.tb02092.x

Platt, N.H., Wright, V.P., 1992. Palustrine carbonates and the Florida Everglades; towards an exposure index for the fresh-water environment? Journal of Sedimentary Research 62, 1058–1071. https://doi.org/10.1306/D4267A4B-2B26-11D7-8648000102C1865D

Platt, N.H., Wright, V.P., 1991. Lacustrine Carbonates: Facies Models, Facies Distributions and Hydrocarbon Aspects, in: Lacustrine Facies Analysis. John Wiley & Sons, Ltd, pp. 57–74. https://doi.org/10.1002/9781444303919.ch3

Plaziat, J.-C., Freytet, P., 1978. Le pseudo-microkarst pédologique: un aspect particulier des paléo-pedogenéses developpées sur les depôts calcaires lacustres dans le Tertiaire du Languedoc. Comptes Rendués Academie Science Paris 286, 1661–1664.

Posamentier, H.W., Jervey, M.T., Vail, P.R., 1988. Eustatic controls on clastic deposition I—conceptual framework.

Postma, G., 1990. Depositional Architecture and Facies of River and Fan Deltas: A Synthesis, in: Coarse-Grained Deltas. John Wiley & Sons, Ltd, pp. 13–27. https://doi.org/10.1002/9781444303858.ch2

Poujol, A., Ritz, J.-F., Vernant, P., Huot, S., Maate, S., Tahayt, A., 2017. Which fault destroyed Fes city (Morocco) in 1755? A new insight from the Holocene deformations observed along the southern border of Gibraltar arc. Tectonophysics 712, 303–311.

Prosser, S., 1993. Rift-related linked depositional systems and their seismic expression. Geological Society, London, Special Publications 71, 35–66. https://doi.org/10.1144/GSL.SP.1993.071.01.03

Rasmussen, S.O., Andersen, K.K., Svensson, A.M., Steffensen, J.P., Vinther, B.M., Clausen, H.B., Siggaard-Andersen, M.-L., Johnsen, S.J., Larsen, L.B., Dahl-Jensen, D., Bigler, M., Röthlisberger, R., Fischer, H., Goto-Azuma, K., Hansson, M.E., Ruth, U., 2006. A new Greenland ice core chronology for the last

glacial termination. Journal of Geophysical Research: Atmospheres 111. https://doi.org/10.1029/2005JD006079

Rasmussen, S.O., Bigler, M., Blockley, S.P., Blunier, T., Buchardt, S.L., Clausen, H.B., Cvijanovic, I., Dahl-Jensen, D., Johnsen, S.J., Fischer, H., Gkinis, V., Guillevic, M., Hoek, W.Z., Lowe, J.J., Pedro, J.B., Popp, T., Seierstad, I.K., Steffensen, J.P., Svensson, A.M., Vallelonga, P., Vinther, B.M., Walker, M.J.C., Wheatley, J.J., Winstrup, M., 2014. A stratigraphic framework for abrupt climatic changes during the Last Glacial period based on three synchronized Greenland ice-core records: refining and extending the INTIMATE event stratigraphy. Quaternary Science Reviews, Dating, Synthesis, and Interpretation of Palaeoclimatic Records and Model-data Integration: Advances of the INTIMATE project(INTegration of Ice core, Marine and TErrestrial records, COST Action ES0907) 106, 14–28. https://doi.org/10.1016/j.quascirev.2014.09.007

Renssen, H., Seppä, H., Heiri, O., Roche, D.M., Goosse, H., Fichefet, T., 2009. The spatial and temporal complexity of the Holocene thermal maximum. Nature Geosci 2, 411–414. https://doi.org/10.1038/ngeo513

Rhoujjati, A., Cheddadi, R., Taïeb, M., Baali, A., Ortu, E., 2010. Environmental changes over the past c. 29,000 years in the Middle Atlas (Morocco): A record from Lake Ifrah. Journal of Arid Environments 74, 737–745. https://doi.org/10.1016/j.jaridenv.2009.09.006

Rogerson, M., Dublyansky, Y., Hoffmann, D.L., Luetscher, M., Töchterle, P., Spötl, C., 2019. Enhanced Mediterranean water cycle explains increased humidity during MIS 3 in North Africa. Climate of the Past 15, 1757–1769. https://doi.org/10.5194/cp-15-1757-2019

Rojas, E., Le Roux, J.P., 2005. Sedimentary processes on a Gilbert-type delta in Lake Llanquihue, southern Chile. Andean Geology 32, 19–31.

Rust, B.R., 1972. Structure and Process in a Braided River. Sedimentology 18, 221–245. https://doi.org/10.1111/j.1365-3091.1972.tb00013.x

Sánchez Goñi, M., Cacho, I., Turon, J., Guiot, J., Sierro, F., Peypouquet, J., Grimalt, J., Shackleton, N., 2002. Synchroneity between marine and terrestrial responses to millennial scale climatic variability during the last glacial period in the Mediterranean region. Climate Dynamics 19, 95–105. https://doi.org/10.1007/s00382-001-0212-x

Scholz, C.A., Rosendahl, B.R., Scott, D.L., 1990. Development of coarse-grained facies in lacustrine rift basins: Examples from East Africa. Geology 18, 140–144. https://doi.org/10.1130/0091-7613(1990)018<0140:DOCGFI>2.3.CO;2

Scott, J.J., Buatois, L.A., Mángano, M.G., 2012. Chapter 13 - Lacustrine Environments, in: Knaust, D., Bromley, R.G. (Eds.), Developments in Sedimentology, Trace Fossils as Indicators of Sedimentary Environments. Elsevier, pp. 379–417. https://doi.org/10.1016/B978-0-444-53813-0.00013-7

Shanley, K.W., McCabe, P.J., 1994. Perspectives on the sequence stratigraphy of continental strata. AAPG bulletin 78, 544–568.

Shanmugam, G., 1996. High-density turbidity currents; are they sandy debris flows? Journal of Sedimentary Research 66, 2–10. https://doi.org/10.1306/D426828E-2B26-11D7-8648000102C1865D

Smith, N.D., 1974. Sedimentology and Bar Formation in the Upper Kicking Horse River, a Braided Outwash Stream. The Journal of Geology 82, 205–223. https://doi.org/10.1086/627959

Sohn, Y.K., 1997. On traction-carpet sedimentation. Journal of Sedimentary Research 67, 502–509. https://doi.org/10.1306/D42685AE-2B26-11D7-8648000102C1865D

Southard, J.B., Boguchwal, L.A., 1990. Bed configuration in steady unidirectional water flows; Part 2, Synthesis of flume data. Journal of Sedimentary Research 60, 658–679. https://doi.org/10.1306/212F9241-2B24-11D7-8648000102C1865D

Strecker, U., Steidtmann, J.R., Smithson, S.B., 1999. A Conceptual Tectonostratigraphic Model for Seismic Facies Migrations in a Fluvio-Lacustrine Extensional Basin1. AAPG Bulletin 83, 1320–1336. https://doi.org/10.1306/00AA99F8-1730-11D7-8645000102C1865D

Sturm, M., Matter, A., 1978. Turbidites and Varves in Lake Brienz (Switzerland): Deposition of Clastic Detritus by Density Currents, in: Modern and Ancient Lake Sediments. John Wiley & Sons, Ltd, pp. 147–168. https://doi.org/10.1002/9781444303698.ch8

Suchecki, R.K., Hubert, J.F., Birney de Wet, C.C., 1988. Isotopic imprint of climate and hydrogeochemistry on terrestrial strata of the Triassic-Jurassic Hartford and Fundy rift basins. Journal of Sedimentary Research 58, 801–811. https://doi.org/10.1306/212F8E6D-2B24-11D7-8648000102C1865D

Svensson, A., Andersen, K.K., Bigler, M., Clausen, H.B., Dahl-Jensen, D., Davies, S.M., Johnsen, S.J., Muscheler, R., Parrenin, F., Rasmussen, S.O., Röthlisberger, R., Seierstad, I., Steffensen, J.P., Vinther, B.M., 2008. A 60 000 year Greenland stratigraphic ice core chronology. Climate of the Past 4, 47–57. https://doi.org/10.5194/cp-4-47-2008

Tabel, J., Khater, C., Rhoujjati, A., Dezileau, L., Bouimetarhan, I., Carre, M., Vidal, L., Benkaddour, A., Nourelbait, M., Cheddadi, R., 2016. Environmental changes over the past 25 000 years in the southern Middle Atlas, Morocco: PAST ENVIRONMENTAL CHANGES IN MOROCCO. J. Quaternary Sci. 31, 93–102. https://doi.org/10.1002/jqs.2841

Talling, P.J., Masson, D.G., Sumner, E.J., Malgesini, G., 2012. Subaqueous sediment density flows: Depositional processes and deposit types. Sedimentology 59, 1937–2003. https://doi.org/10.1111/j.1365-3091.2012.01353.x

Tanner, 1998. Interstratal dewatering origin for polygonal patterns of sand-filled cracks: a case study from late Proterozoic metasediments of Islay, Scotland: Interstratal dewatering cracks, Islay, Scotland. Sedimentology 45, 71–89. https://doi.org/10.1046/j.1365-3091.1998.00135.x

Tanner, L.H., 2010. Chapter 4 Continental Carbonates as Indicators of Paleoclimate, in: Alonso-Zarza, A.M., Tanner, L. H. (Eds.), Developments in Sedimentology, Carbonates in Continental Settings: Geochemistry, Diagenesis and Applications. Elsevier, pp. 179–214. https://doi.org/10.1016/S0070-4571(09)06204-9

Toffolon, M., 2013. Ekman circulation and downwelling in narrow lakes. Advances in Water Resources 53, 76–86. https://doi.org/10.1016/j.advwatres.2012.10.003

Van Wagoner, J.C., Posamentier, H.W., Mitchum, R.M.J., Vail, P.R., Sarg, J.F., Loutit, T.S., Hardenbol, J., 1988. An overview of the fundamentals of sequence stratigraphy and key definitions.

Wanner, H., Brönnimann, S., Casty, C., Gyalistras, D., Luterbacher, J., Schmutz, C., Stephenson, D.B., Xoplaki, E., 2001. North Atlantic Oscillation – Concepts And Studies. Surveys in Geophysics 22, 321–381. https://doi.org/10.1023/A:1014217317898

Wanner, H., Solomina, O., Grosjean, M., Ritz, S.P., Jetel, M., 2011. Structure and origin of Holocene cold events. Quaternary Science Reviews 30, 3109–3123. https://doi.org/10.1016/j.quascirev.2011.07.010

Wassenburg, J.A., 2016. Major reorganization of the North Atlantic Oscillation during Early Holocene deglaciation. Nat. Geosci. 9. https://doi.org/10.1038/ngeo2767

Weleschuk, Z.P., Dashtgard, S.E., 2019. Evolution of an ancient (Lower Cretaceous) marginal-marine system from tide-dominated to wave-dominated deposition, McMurray Formation. Sedimentology 66, 2354–2391. https://doi.org/10.1111/sed.12601

Winant, C.D., 2004. Three-Dimensional Wind-Driven Flow in an Elongated, Rotating Basin. Journal of Physical Oceanography 34, 462–476. https://doi.org/10.1175/1520-0485(2004)034<0462:TWFIAE>2.0.CO;2

Wright, L.D., Chappell, J., Thom, B.G., Bradshaw, M.P., Cowell, P., 1979. Morphodynamics of reflective and dissipative beach and inshore systems: Southeastern Australia. Marine Geology 32, 105–140. https://doi.org/10.1016/0025-3227(79)90149-X

Wu, Q., Xian, B., Gao, X., Bai, Q., Wang, Z., Liu, J., Chen, P., Li, Y., Rahman, N.U., Tian, R., Zhang, W., Zhang, H., 2022. Differences of sedimentary triggers and depositional architecture of lacustrine turbidites from normal regression to forced regression: Eocene Dongying depression, Bohai Bay Basin, East China. Sedimentary Geology 439, 106222. https://doi.org/10.1016/j.sedgeo.2022.106222

Xue, X., Zhang, Y., Jiang, Z., Wang, L., Wang, S., Jiang, H., 2021. Wave and storm signals in a lacustrine succession and their relationship to paleowind direction (Tanan Depression, Mongolia, early Cretaceous). Sedimentary Geology 419, 105911. https://doi.org/10.1016/j.sedgeo.2021.105911

Zavala, C., 2020. Hyperpycnal (over density) flows and deposits. Journal of Palaeogeography 9, 17. https://doi.org/10.1186/s42501-020-00065-x

Zavala, C., Arcuri, M., 2016. Intrabasinal and extrabasinal turbidites: Origin and distinctive characteristics. Sedimentary Geology 337, 36–54. https://doi.org/10.1016/j.sedgeo.2016.03.008

Zavala, C., Arcuri, M., Di Meglio, M., Zorzano, A., Otharán, G., Irastorza, A., Torresi, A., 2021. Deltas: a new classification expanding Bates's concepts. Journal of Palaeogeography 10, 23. https://doi.org/10.1186/s42501-021-00098-w

Zavala, C., Arcuri, M., Meglio, M.D., Diaz, H.G., Contreras, C., 2011. A Genetic Facies Tract for the Analysis of Sustained Hyperpycnal Flow Deposits 31–51. https://doi.org/10.1306/13271349St613438

Zavala, C., Liu, H., Li, X., Arcuri, M., Di Meglio, M., Zorzano, A., Otharán, G., Hao, B., Wang, Y., 2022. Chapter 16 - Lacustrine sequence stratigraphy: New insights from the study of the Yanchang Formation (Middle-Late Triassic), Ordos Basin, China, in: Yang, R., Van Loon, A.J. (Tom) (Eds.), The Ordos Basin. Elsevier, pp. 309–335. https://doi.org/10.1016/B978-0-323-85264-7.00012-6

Zecchin, M., Caffau, M., Catuneanu, O., 2022. Identification of maximum flooding surfaces at different scales: The case of the Piacenzian to Gelasian Cutro Clay and Strongoli Sandstone (Crotone Basin, southern Italy). Marine and Petroleum Geology 146, 105971. https://doi.org/10.1016/j.marpetgeo.2022.105971

Zecchin, M., Caffau, M., Catuneanu, O., 2021. Recognizing maximum flooding surfaces in shallow-water deposits: An integrated sedimentological and micropaleontological approach (Crotone Basin, southern Italy). Marine and Petroleum Geology 133, 105225. https://doi.org/10.1016/j.marpetgeo.2021.105225

Zielhofer, C., Fletcher, W.J., Mischke, S., De Batist, M., Campbell, J.F., Joannin, S., Tjallingii, R., El Hamouti, N., Junginger, A., Stele, A., 2017. Atlantic forcing of Western Mediterranean winter rain minima during the last 12,000 years. Quaternary Science Reviews 157, 29–51.

Zielhofer, C., Köhler, A., Mischke, S., Benkaddour, A., Mikdad, A., Fletcher, W.J., 2019. Western Mediterranean hydro-climatic consequences of Holocene ice-rafted debris (Bond) events. Climate of the Past 15, 463–475. https://doi.org/10.5194/cp-15-463-2019

CHAPITRE V

CLIMATE CONTROLS ON TUFA DEPOSITION OVER THE LAST 5000 YEARS: A CASE STUDY FROM NORTHWEST AFRICA

Climate controls on tufa deposition over the last 5000 years: A case study from Northwest Africa

Khalil Azennoud[a,*], Abdennasser Baali[a], Yassine Ait Brahim[b], Youssra Ahouach[a], Oualid Hakam[a]

[a]Engineering Laboratory of Organometallic, Molecular Materials and Environment (LIMOME), Faculty of Sciences Dhar EL Mahraz, Sidi Mohamed Ben Abdellah University, P.O. Box 1796 (Atlas), Fez 30000, Morocco.

[b] International Water Research Institute, Université Mohammed VI Polytechnique, Benguerir, Morocco.

Published in: Palaeo-3 110767 (2022a)

Abstract

The occurrence and rate of tufa deposition are controlled by a large number of external and internal factors, including climate which often represents the main allocyclic factor. In this study, the first of its kind in the Middle Atlas (Northern Morocco), we test the dependency between climate factor and Holocene tufa deposits in basin-like settings that involve enlarged barrage and extensive dammed area using sedimentologic and stratigraphic analyses complemented with a paleoclimate multi-proxy approach and radiocarbon dating. The sedimentologic and stratigraphic analyses revealed a remarkable change in the vertical stacking pattern within the main barrage-cascade: higher (lower) Aggradation/Progradation ratio between ca. 4 and ca. 2.7 cal kyr B.P. (between ca. 2.7 and ca. 0.35 cal kyr B.P.), which would have conditioned a transgressive (highstand) interval “basinward". This shift is modulated by changes in precipitation and summer insolation, which is consistent with the petrographic analysis of the laminated microbialites (oncoids and stromatolites).

The previously reported arid and cold period of the Mid-Holocene Transition (between 6 and 5 cal kyr B.P.) is recorded in the sedimentary deposits and demonstrates landscape instability. The North Atlantic high-latitude cooling events between 4.6 and 2.7 cal kyr B.P. (Bond events 2 and 3) resulted in the interruption of (bio-)calcification and the development of fen and sapropel (organic-rich facies) layers, respectively. The 4.2 ka event, might have coincided herein with a fifth-order bounding surface delineating the two depositional sequences recognized on the “basin-scale”. A multi-centennial timescale period with climate optimum conditions coinciding with enhanced calcite precipitation at the downstream-facing of the main barrage (buttress development), and centred at ca. 2 cal kyr B.P. may coincide with the Roman-Iberian Climate Optimum. A recurrent occurrence with a high frequency of sub-humid marshy conditions underscored the upper part of the highstand interval which may reflect solar imprints, as already reported in previous studies in the region.

Keywords: Holocene; abrupt climate change; organic-rich facies; Middle Atlas; Morocco

1 Introduction

Tufa, unlike travertine, are freshwater carbonate (mainly calcite) deposits (Pedley, 1990, 2009) typical of karstic areas and broadly associated with microphytes and macrophytes (Capezzuoli et al., 2014). These archives have been the subject of several studies carried out in the Mediterranean region (e.g., Viles and Goudie, 1990; Goudie et al., 1993; Pedley et al., 1996; Vázquez-Urbez et al., 2012; Arenas et al., 2014b; Toker, 2017). They provide valuable information that widens the scope of various scientific investigations such as sedimentary paleoenvironmental reconstructions (e.g., Arenas et al., 2007, 2014; Toker, 2017), paleoclimate research (e.g., Griffiths and Pedley, 1995; Pedley et al., 1996; Andrews, 2006; Cremaschi et al., 2010; Dabkowski et al., 2015a, 2015b). Furthermore, the potential of tufa accumulation to modify local base-level by creating space for sedimentation (accommodation concept) has been widely demonstrated in stretches named as dammed areas behind tufa barrages that are likely to evolve to form an open shallow lacustrine environment (e.g., Pedley, 1990; Golubić et al., 2008; Vázquez-Urbez et al., 2012; Arenas et al., 2014b; Nutz et al., 2019). The style of tufa growth at barrage-cascade build-ups (i.e., aggradation or progradation pattern), which control the sill height and thus the accommodation rate, has been demonstrated to be directly related to the climate and especially to temperature changes (Pedley et al., 1996; Arenas et al., 2014b; Sancho et al., 2015; Nutz et al., 2019). Additionally, changes in climate and hydrology are proved to have conditioned changes in textures and calcite growth rate of the laminae composing microbialites (i.e., oncoids and stromatolites; e.g., Gradziński, 2010; Berrendero et al., 2016; Arenas and Jones, 2017). However, albeit numerous studies have highlighted the major influence of climate on tufa growth on orbital to millennial timescale, the response of tufa to multi-centennial timescale climate extremes such as North Atlantic ice rafted events (Bond events; Bond el al., 1997) during interglacials remains elusive. Such an investigation would be informative especially when the constructed sedimentary facies model involves extensive dammed areas behind enlarged barrage-cascades build-ups, where deposition could be sustained at the same place (unlike fluvial s.s. settings).

The Middle Atlas (Northern Morocco; Fig. 1A) offers a wide dispersed bedrock dominated by Lias carbonate rocks, which are experiencing active karstification (Tennevin, 1978; Martin, 1981; Du Dresnay, 1988; Baali, 1998; Baali et al., 2007; Michard et al., 2008; Hamdani and Baali, 2019) and,

thus, is suspected to promote large scale tufa deposition (Capezzuolli et al., 2014); Unfortunately, only a few publications focused on Pliocene-Quaternary tufa formations (Ahmamou et al., 1989; El Bouch, 1994; Gourari, 2001; Wackenheim et al., 2020) compared to other regions such as the Iberian Peninsula. Moreover, the Middle Atlas has widely been recognized as a key region for paleoclimate investigation thanks to its geographical position and therefore its sensitivity to record teleconnections between the North Atlantic realm, the Saharan sub-tropical latitudes, and the Mediterranean region (Knippertz et al., 2003; Wassenburg et al., 2013, 2016; Zielhofer et al., 2017a, 2017b; Ait Brahim et al., 2018, 2019). Therefore, future detailed studies upon these continental carbonates within this strategic geological and geographic context would be very interesting and fruitful for sedimentological and paleoclimatic research.

To investigate the linkage between climate and tufa accumulation, and to define the potential of using tufa as promising paleoclimate and paleoenvironmental archive in northwestern Africa, we conducted, for the first time in the Middle Atlas, sedimentologic and stratigraphic analyses using recent classifications and terminologies carried out on the Holocene tufa of Imouzzer Kandar (Northern Middle Atlas) within basin-like settings (dammed area behind enlarged barrage-cascade build-up). Herein, we determined vertical and lateral characteristics and distribution of facies (facies and sequence analyses), then we reconstructed their temporal evolution (evolutionary facies model). Furthermore, we applied a multi-proxy approach with radiocarbon dating on charcoal from the most representative stratigraphic section in order to test the paleoclimatic implications that can be concluded from the sedimentologic analysis.

2 Structural, geologic and climatic context

Imouzzer Kandar is located in the northwest of the Middle Atlas (33° 43' 44" N, 5° 0' 39" W; ca. 1300 m a.s.l.) south of the Rifian foreland basin (Saïss basin). The Middle Atlas is an alpine intracontinental belt that constitutes a major structural domain in northern Morocco. It is subdivided into two different geomorphic entities (Arboleya et al., 2004): (i) northwestern Tabular Middle Atlas (TMA), in which the study site is located, with relatively flat higher relief (average topography of 1300m) and weakly disrupted by normal and thrust faults, and (ii) southwestern Folded Middle Atlas (FMA), where the structure involves a succession of synclines and faulted anticlines (exceeding 3000m) separated from the TMA by the so-called North Middle Atlas Fault (A.N.M.A., Fig. 1A). The major faults, with a left-lateral strike-slip component, broadly trend NE-SW. This structural framework is the evidence of a polyphase geodynamic evolution that involves a progressive inversion

of the Mesozoic Tethys rifting (Favre et al., 1991; Laville et al., 2004; de Lamotte et al., 2009) to a contractional regime accommodated by the convergence between Africa and Eurasia (Rosenbaum et al., 2002). The general trending NE-SW of the major structures are the heritage of the Hercynian orogeny (Charrière, 1990; Piqué and Laville, 1996). The anomalously high elevation of the Moroccan Atlas System (including the TMA) compared to other North African mountain belts was proved to be the result of major lithospheric thinning with a NE-SW trend initiated since the Upper Neogene (Missenard et al., 2006; Babault et al., 2008).

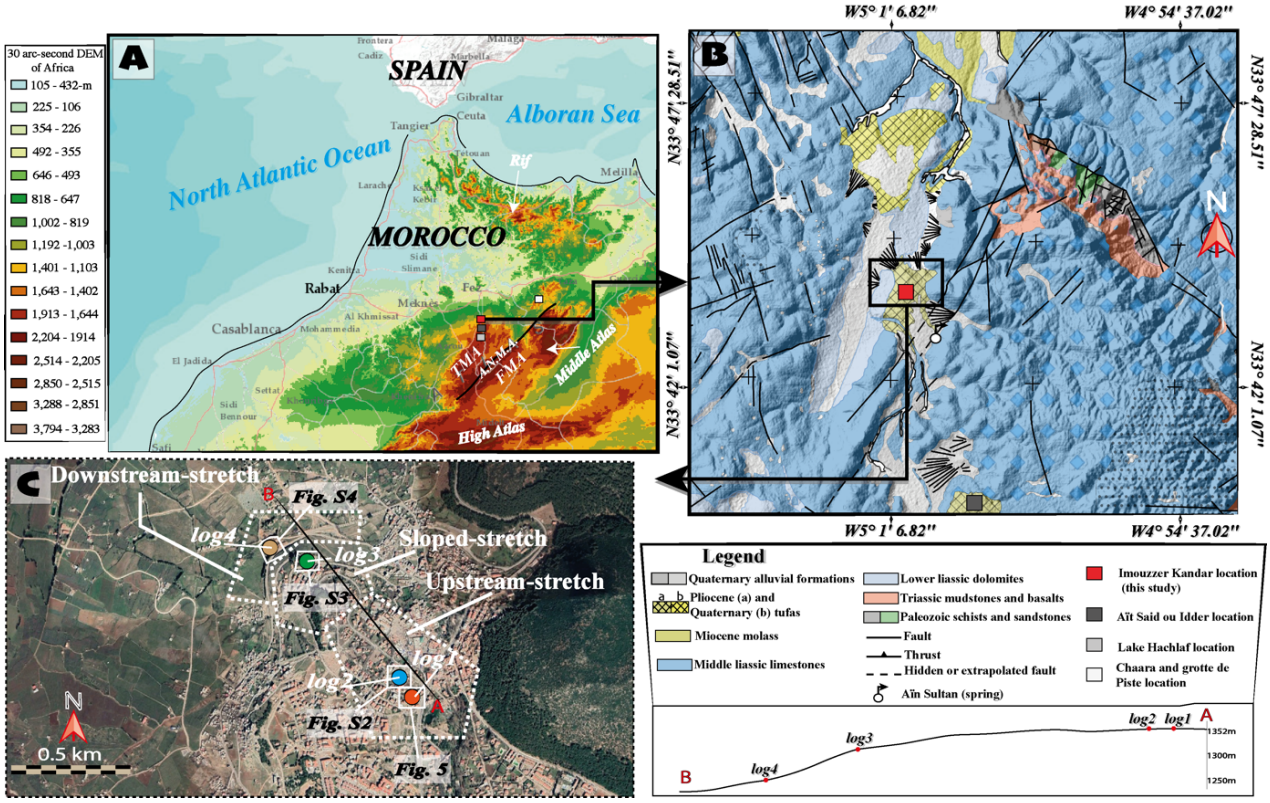


Figure 1. *Geographical locations and geological settings of Imouzzer Kandar, and other sites referred in this study.* ***A****: Geographic situation of Imouzzer Kandar and other sites.* ***B****: Geological context of Imouzzer Kandar.* ***C****: Logs and stretch situations. The DEM map is from https://databasin.org/; the geological map is redrawn from Ennadifi et al., 1975 and Charrière, 1989 using QGIS version 3.12 (Open-Source Geospatial Foundation Project https://qgis.org/fr/site/.); the satellite image is from Google Earth pro, (2016). The relative elevation of each stratigraphic section is presented in the topographic profile. Abbriations: TMA: Tabular Middle Atlas; FMA: Folded Middle Atlas; A.N.M.A.: North Middle Atlas Fault.*

The TMA includes rocks formed from the Paleozoic to the Cenozoic. The Hercynian basement is mainly composed of deformed schists and sandstones and is unconformably overlapped by the Triassic evaporites and tholeiitic basalts that mark evidence of the Tethys rifting (i.e., syn-rift deposits) (Laville et al., 2004; Ouarhache, 1987; Ouarhache et al., 2012). Early and Middle Liasic platform carbonates (dolomites and limestones) dominate in thickness and surface (Fig. 1B). They are considered as post-rift (i.e., the aborted Tethys rift) deposits, which was controlled by thermal subsidence (Laville et al., 2004; Ouarhache et al., 2012). Since then, the Liasic carbonates of the TMA,

unlike those of the FMA, were generally emerged and, therefore, subject to significant weathering, generating a large-scale karstic plateau associated with numerous springs (Tennevin, 1978; Martin, 1981; Baali, 1998; Hamdani and Baali, 2019). These resurgences have contributed to the deposition of a well-preserved and large amount of tufa during the Plio-Quaternary (Charrière, 1990; Gourari, 2001). In some places, Neogene-Quaternary alkaline mafic lavas have sealed the platform rocks (Bosch et al., 2014). These were assumed to be closely related to the lithospheric doming reported above (Teixell et al., 2005; Missenard et al., 2006).

Imouzzer Kandar is characterized by a temperate climate with warm summer, located within the Mediterranean climate type Csa according to Köppen classification (Köppen, 1900; Kottek et al., 2006), with annual precipitation of 612 mm and a mean temperature of 13.5°C (www.climate-data.org).

3 Methods and material studied

3.1 Sedimentological and petrographic analysis

The facies analysis (table 2), sequence analysis (Fig. 10), and the evolutive sedimentary facies model (Fig. 11) are based on mesoscale field and microscopic scale observations according to Arenas-Abad et al., (2010) for tufa facies and Miall (1977, 2014) for non-tufa deposits. The micro-texture analysis and the calcification style of the microbialite (oncoids and stromatolites) laminations were examined under an optical microscope and by Scanning Electron Microscope (SEM) using a Quanta 200 FEI equipped with EDAX probe for surface microanalysis at “la Cité de l’Innovation Fès”. Twenty-eight ground and sieved (63 µm meshes) samples (from log1, Fig. 1C) were analyzed for mineralogical determination by X-ray diffraction (XRD) using Panalatycal X'Pert PRO Powder Diffractometer equipped with X'Celerator Ultrafast Scintillation Detector at “la Cité de l’Innovation Fès”. The qualitative and quantitative determination of mineral major phases was performed using MATCH software and Crystallography Open Database (COD).

3.2 Geochemical and biological proxies

Twenty-one samples of 10g (from log1), were treated with 3% H_2O_2 for one week and sieved with 100 µm meshes. The residues were analyzed using a binocular microscope for macro-charcoal and ostracod counting. Macro-charcoal morphotypes were examined following Enache and Cumming (2006, 2007) and Mustaphi and Pisaric (2014). Subsequently, we focused on three layers of major

interest for this work. Two species typical of spring, ponds fed by spring, and water fed by spring of the order Podocopida Sars (1866) were examined according to Meisch (2000) and Mazzini et al., (2014): (i) *Ilyocypris inermis* Kaufmann (1900), a cold stenothermal (linked to permanently cold water) and mesorheophylic (sustain various velocity) species; and (ii) *Ilyocypris bradyi* Sars (1890), an oligothermophilic (preferring cold water) and mesorheophylic species. Where this latter is found in lake habitat, it is usually reported as discharged from nearby sites (*see* Meisch, 2000). These two species were used as the main proxies to conclude emphasis on water temperature and groundwater contribution, although ostracods diversity is provided on an ordinal scale (Fig. 2). Specimens of macro-charcoal and two specimens of *I. bradyi* were examined by SEM. The determination of organic carbon is based on Walkley and Black (1934) chromic acid wet oxidation method (*see* Allison, 1965, and FAO, 2020). Before each titration, the suspension was filtered to provide more precision in discerning the endpoint. To determine the calcium carbonate content, 1g of each sample is placed in a flask, attached to a Chittick gasometric apparatus and digested with 6*M* (ca. 20% strong) HCl (*see* Dreimanis, 1962, for more detail). The concentration of $CaCO_3$ is determined indirectly, with an accuracy of ±0.1, from the volume of evolved CO_2 gas, corrected to conditions of standard pressure and temperature, and molecular masses of $CaCO_3$ and CO_2 (Dreimanis, 1962); the manipulation has been replicated three times for more precision. Each sample is weighted using an analytical balance with 0.001-g accuracy and placed away from ambient air before weighting. Potassium and aluminium concentrations were performed, after pretreatment, with ICP-OES system MORIBA Jobin Yvon - ACTIVA equipment, at "la Citée de l'Innovation Fès". The pretreatment includes digestion of each ground and sieved sample (1 g) with 3ml of HCl (12.1*M*), 1ml of HNO_3 (16*M*), and 2ml H_2O_2 (9.97*M*) for carbonates and organic matter elimination and leaching of potassium and aluminum. At each digestion, samples were kept at least 15 minutes after reaching the boiling point (up to 120 °C). After cooling, the mineralized content was filtered and adjusted to 50ml with distilled-water, then being prepared for the spectroscopic analysis. K is used as a proxy for physical erosion (Kylander et al., 2011), whereas K/Al is used to investigate changes in weathering (Davies et al., 2015), as K is more water-soluble than Al during mineral weathering (Clift et al., 2014).

3.3 Dating

Four accelerator mass spectrometry dates have been performed on charcoal (table 1) at Vilnius Radiocarbon laboratory (Lithuania). The samples were collected intact by hand from four macro-charcoal-rich stratigraphic levels. Macro-charcoal particles were carefully selected for dating, taking

only those with no significant taphonomic features. Samples were analyzed by a single-stage accelerator mass spectrometer (SSAMS, NEC, USA) after conversion to graphite using Automated Graphitization Equipment AGE-3 (IonPlus AG), at Vilnius Radiocarbon laboratory (Lithuania).

The non-calendar dates were calibrated using the program OxCal v.4.4 (Ramsey and Lee, 2013) and the calibration curve IntCal20 (Reimer et al., 2020) with a confidence interval correspond to 2σ (95.4% probability). The age/depth model was constructed based on Monte Carlo simulation using the StalAge algorithm (Scholz and Hoffmann, 2011; Fig. S1). Due to the lack of precision (see supplement material), resulting from potential erosion-hiatus events that cannot be resolved by a continuous age model, our discussion below is mainly focused on precisely-dated layers to chronologically frame the potential sedimentologic/stratigraphic events that we observe with well-constrained evidence from regional- and global-scale records using a curve-fitting approach.

Table 1*. Conventional and calibrated AMS radiocarbon ages for the southernmost stratigraphic section, log1.*

Sample designation	Laboratory code	Facies type and material dated	Radiocarbon age (^{14}C BP)	Calibrated age (cal. a BP, 2σ)
IM01	FTMC-UR02-1	Matrix-supported conglomerate (facies Gms); charcoal	4617 ± 29	5372 ± 83
IM6-b	FTMC-UR02-6	Peaty muds (facies C); charcoal	4126 ± 28	4673.5 ± 143.5
IM13-b	FTMC-UR02-7	Sapropel depocenter (facies C); charcoal	2595 ± 26	2783 ± 22
IM22	FTMC-UR02-5	Calcite-coated stems (facies Lst1); charcoal	378 ± 27	388 ± 78.5

4 Results and analysis

4.1 Proxy results, facies and facies association analysis

Seventeen sedimentary facies have been identified from the four stratigraphic sections studied here. Code, description and interpretation of each facies are summarized in table 2. These facies are observed in vertical facies associations (FAs), which mark the temporal evolution of the environments and subenvironments at each stratigraphic section. Four fundamental FAs have been raised based on conventional facies analysis. These ranges from relatively high energy free-flowing channel-fill to more stagnant water deposits with more or fewer outflows. In the following, we focus only on the FAs present in log1 (N33° 43' 52.31"; W5° 0' 38.06"), the data from the other three logs are moved to the

supplement material. The description and interpretation of facies association and proxy results are taken from the bottom up of log1.

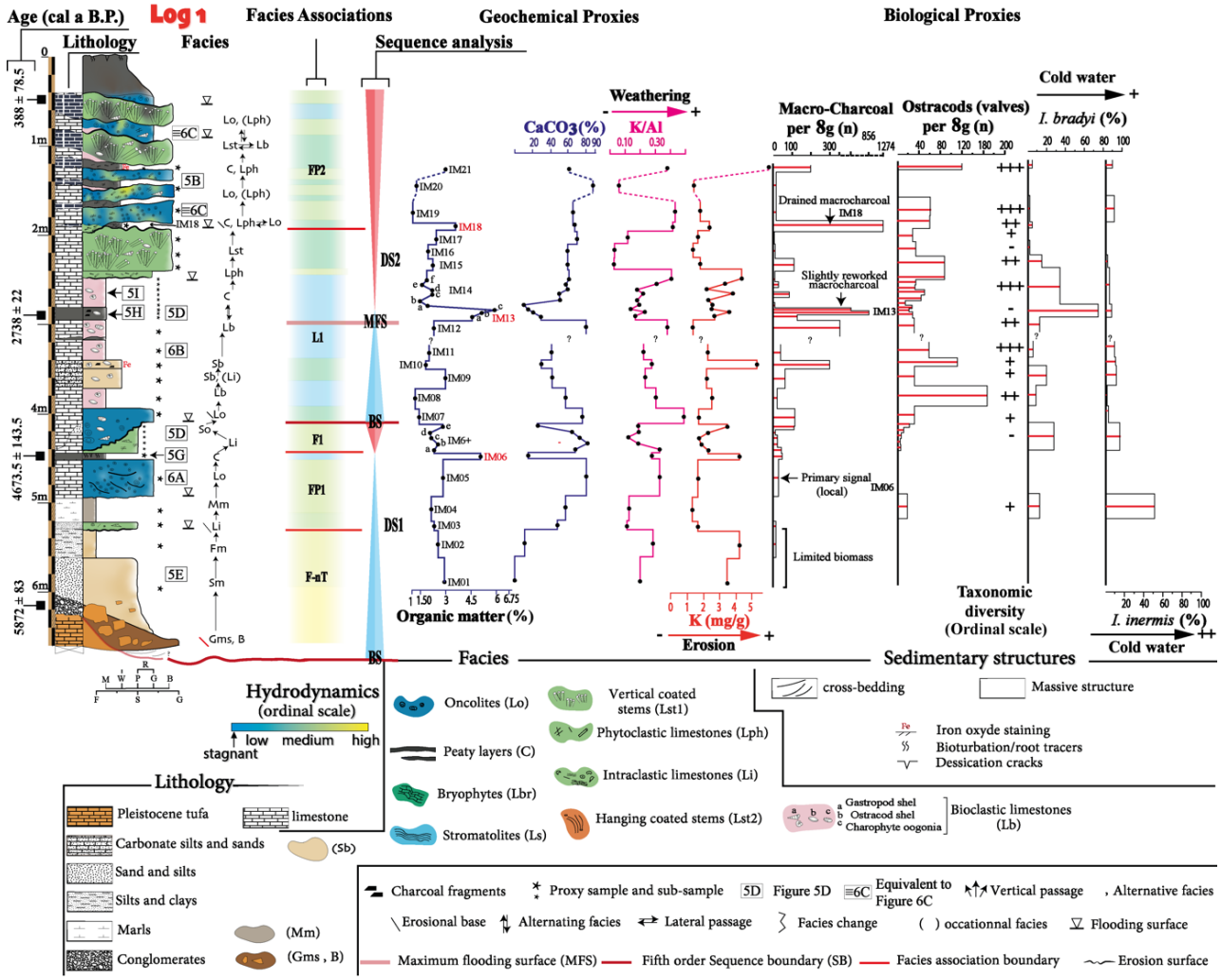


***Figure 2**. Stratigraphic and sedimentologic analysis, with proxy results and hydrodynamic interpretation of facies from log1. Note locations of the SEM samples (IM06, IM13 and IM18) and the dated layers. Facies and facies association codes in Table 2 and Figure 7, respectively. Abbreviations used in the sequence analysis: MFS: Maximum Flooding Surface; DS1(2): Depositional Sequence 1(2). Textures and lithology: F: fines (clays and silts); S: sands; G: gravels; M: mudstones; W: wackstones; P: packstones; G; grainstones; R; rudstones; B: boundstones.*

4.1.1 Fluvial non-tufa FA: F-nT

This facies association includes, from base to top, matrix-supported, poorly sorted conglomerates with breccias (Gms, B), massive sands (Sm), and massive fines (Fm) (**F-nT**; Figs. 5E, 7). These latter exhibit high content of dolomites and quartz (60 and 40%, respectively), a low value of K/Al ratio (ca. 0.20), and the quasi-absence of macro-charcoal and ostracods (Figs. 2, 3).

Facies Gms and Sm at the lower part of log1 reflect the debris-flow process (Miall, 1977, 2014; Miall and Postma, 1997) during landscape slope instability. Upward, massive fines indicate low-energy fluvial deposits. The low K/Al ratio and the high concentration of dolomite and quartz suggest

significant drainage, while the absence of macro-charcoal is probably related to biomass limitation implying previous degraded forest conditions, which is consistent with the facies interpretation above.

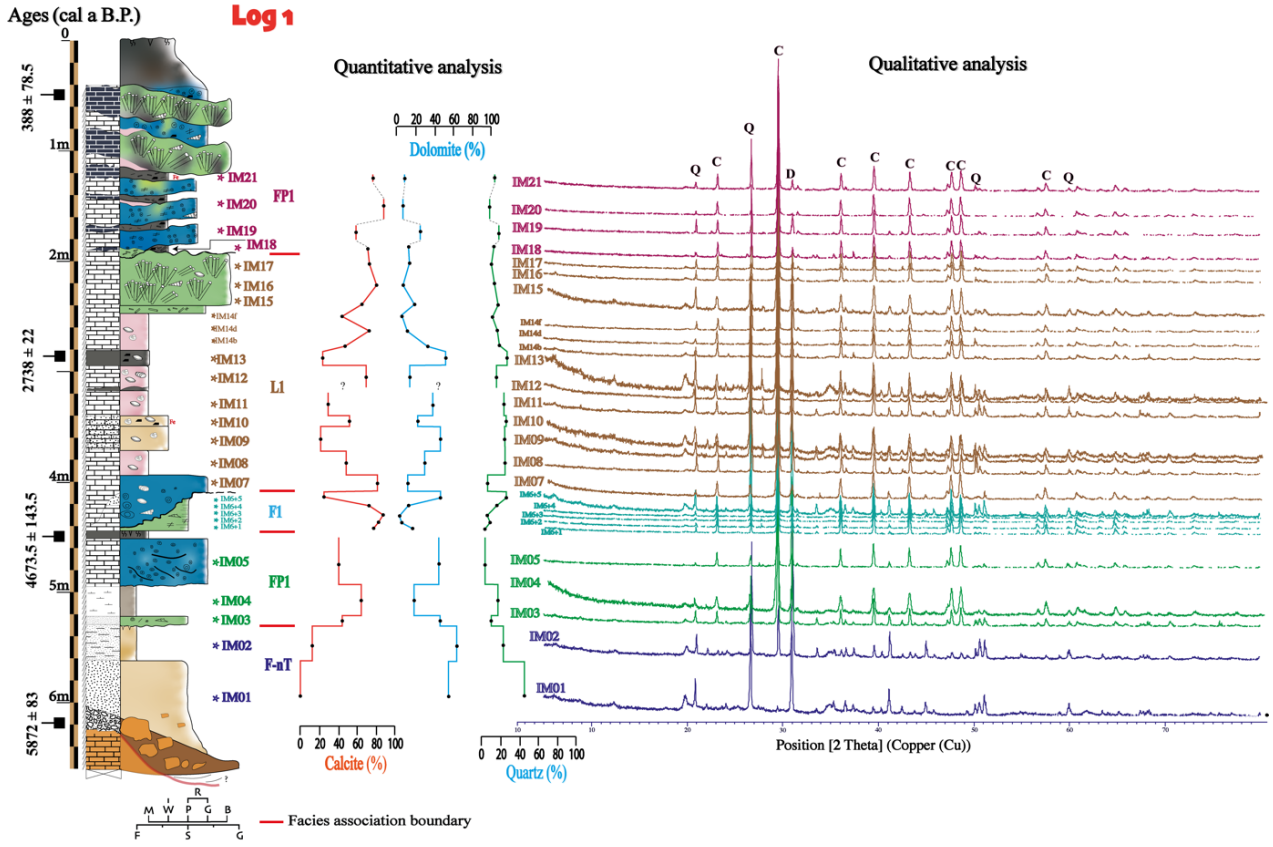


***Figure 3**. X-ray diffraction (XRD) analysis of samples from log1. The colors of the diffractograms (qualitative analysis) match the facies association depicted from the stratigraphic section.*

4.1.2 Fluvial-palustrine FA: FP1

FP1, above **F-nT**, consists of erosive-based intraclasts (Li), massive muds (Mm), and cross-bedded small oncoids (Lo; Figs. 5F, 6A), where the whole is capped by a peaty layer (C) with pedogenic features (e.g., bioturbation, vascular plant rhizomes; Fig. 6G). This facies association reveals, from facies Li to Lo, low content of organic matter (ca. 2%), increasing content of $CaCO_3$ (from 60 to 80%), relatively low values of K (ca. 1.5 g/kg) and K/Al ratio, whereas the XRD analysis shows the dominance of low-Mg calcite (ca. 70%) (Figs. 2, 3). Ostracods occur only in massive marls (ca. 40 n/8g) with the almost dominance of the species *Ilyocypris inermis* (ca. 50%; Fig. 2). The peaty facies reveals high content of organic matter (5.25%), a dominance of charcoal types "S" with visible cell structure and type "B1" with foliated structure (Enache and Cumming, 2007; Mustaphi and Pisaric, 2014), and the absence (or low concentration) of ostracods (Figs. 2, 4A).

FP1 is interpreted as succession deposits that begin with a relatively high energy flow of the watercourse leading to upstream breakage of coeval tufa-bearing deposits and producing intraclasts. Indeed, this is consistent with the concentration of dolomite and quartz mineral phases. Furthermore,

the high concentration of mesorheophilic and coldstenothermal of *I. inermis* in massive marls suggests cooler and low-energy water conditions (Meisch, 2000). Small oncoids (*sensu* Arenas et al., 2007) with cross-bedding are believed to reflect sinuous (decrease in slope) fluvial conditions close to shallow standing water (probably paludal setting). This assumption leads one to consider that local base-level has been already created (buttress concept of Holbrook et al., 2006). Finally, the peaty facies (dated layer to 4673.5 ± 143.5 cal yr B.P., table 1) with vascular plant rhizomes at the top may mirror a minerotrophic mire (i.e., fen) ecosystem (Rydin et al., 2013). It is suggested that the paludification process is the mechanistic process of peat formation, i.e., progressive waterlogging of a previously dry mineral ground (Rydin et al., 2013; Edvardsson et al., 2016), which fits the interpretation above (previous standing water). This is consistent with the macro-charcoal morphotypes, with preserved primary structures, that suggest an in-situ installation of woody-land. However, the low thickness, under peatland threshold (i.e., < 30cm), suggests that the successional process of peat formation was interrupted by allogenic factors (e.g., climate, hydrology) preventing this from progressing up to reaching the ombrotrophic stage (Rydin et al., 2013). This might be related to a sharp climate shift on centennial timescales.

4.1.1 Fluvial s.s. tufa: F1

F1 consists of a vertical passage from intraclasts (Li) towards millimetric oncoids (So) which suggests an increase in the hydrodynamics until causing a partial truncation of this facies association (Figs. 5F, 6A). This is consistent with the K and K/Al results, which reflect increasing drainage (increasing K values) and weathering (decreasing K/Al) (Fig. 2).

***Table 2**. Facies description and interpretation of the Holocene tufa formation present in Imouzzer Kandar.*

Facies, conventional code, abundance, and figure(s)	**Geometry of deposits, textural characteristic and sedimentary structures (mesoscale)**	**Interpretation**	**Depositional sub-environment**
Tufa facies			
Phytoherm tufa of: Stems **Lst**:			
Bunches, **Lst1** •• Figs. 5D and S2B	Lenticular to tabular bodies; dm-scale in thick, m-scale in lateral extent; cm-scale in diameter; empty interior cavities	Calcite-coating of stems after reaching a supersaturated state most likely due to the photosynthetic-effect in stagnant water (Merz-Preiß and Riding, 1999); growing upward	Palustrine, lacustrine margin (Arenas-Abad et al., 2010; Pedley, 1990)
Curtains, **Lst2** •• Figs. 6H, 11A-C and S3G	Dm- to cm-scale in thick, with overhangs, dm-scale in lateral extent; cm-scale in diameter; empty interior cavities	Calcite-coating of stems after reaching a supersaturated state most likely due to the waterfall-effect in flowing water (Zhang et al., 2001); growing downward	Cascade, fast horizontal growth in cascade (Arenas-Abad et al., 2010; Vázquez-Urbez et al., 2012); small cascades in the downstream-facing part of an extent barrage-cascade
Bryophyte, **Lbr** • Figs. 6I and S3G	Commonly hemi-domed bodies; cm- to dm-scale in thick; m-scale in lateral extent; empty interior cavities	Calcite-coating of mosses and other bryophytes after reaching water supersaturation due to biological and physical effect in flowing conditions; growing upward	Cascade, jumps and barrage-cascade with moderate energy (Arenas-Abad et al., 2010)
Stromatolites, **Ls** •• Figs. S3G, 11C	(a) Tabular, lenticular layer, cm-scale in thick with small undulate base and top; variable in lateral extent; commonly with fenestrae (b) Head-shaped, m-scale in vertical and extent; commonly with fenestrae	Bio-induced calcite precipitation or, most likely, through physico-chemical process that involve CO_2 degassing and the subsequent water supersaturation with regards to calcite along with trapping micrite particles, forming mats	(a) Fast flowing fluvial area (Arenas-Abad et al., 2010) (b) Braided fluvial area (Pedley, 2009)
Oncoidal limestones, **Lo** ••• Figs. 5F, 6A and S2-4	Commonly tabular (Fig. S2) and channelized (Figs. 5F, 6D); dm-scale in thick and m-scale in lateral extent; oncoids are locally oblate and most likely sub-spheroidal; commonly non-organized but locally with	Calcite precipitation around a nuclei after reaching a supersaturated state, induced biologically (photosynthetic effect) or physico-chemically (CO_2 degassing)	Slow-flowing water in channel; point-bar; lake-margins (-shores) (Arenas et al., 2007; Arenas-Abad et al., 2010); the symmetric (oblate) shape of oncoids reflect a regular (limited) rotations

	fining-upward (Fig. 5E), coarsening-upward (Fig. S4B) and trough cross-stratification (Fig. 5B)		in more (less) dynamic conditions
Phytoclastic limestones, **Lph** ••• Figs. 5D, S2-4	Tabular and lenticular beds; dm-scale in thick and variable in lateral extent; commonly non-organized	Erosion of phytoherm tufa (Lst1); fragments are transported and deposited in various sub-environments	Agitated and slow flowing area; barrages and palustrine area (Arenas-Abad et al., 2010); downstream-facing of barrage-cascade
Intraclastic limestones, **Li** •• Figs. 5F, S2 and S4	Lenticular and tabular beds; cm-scale in thick and variable in extent; locally with planar stratification (Fig. 5F) and commonly non-organized	Erosion of previous tufa (e.g., Lbr, Lst, Ls) transport and accumulation in various sub-environments	Aggradation in slow flowing and standing water (Arenas et al., 2014a)
Bioclastic limestones, **Lb** •• Figs. 5D and S2B	Tabular beds, cm-scale in thick and variable in extension; massive structures (Fig. 5I)	Calcite micrite accumulation along with entire or broken shells of gastropods and ostracods in stagnant water	Stagnant area commonly dammed by barrages; extensive shallow lake (Arenas et al., 2014a)
Bioclastic sands and silts, **Sb** • Fig. 5D	Tabular beds, cm-scale in thick and variable in extent; massive structures	Accumulation of entire and broken shells of gastropods and ostracods along with sand- and silt-sized coated fragments	Slow flowing water area (downstream barrage-cascade); aggradation in very low angle or nil area dammed by barrages (Arenas-Abad et al., 2010; Vázquez-Urbez et al., 2012)
Oncoidal sands and silts, **So** ••• Fig. 5E, S2E and S4	Tabular or lenticular beds, cm- to dm-scale in thick: massive (Fig. S3E) or laminated structures (Fig. 5E)	Accumulation of sand-sized coated fragments	Flowing water; channel or overbank deposits in cohesive floodplains
Speleothems, **Lsp** • Fig. 11A	Stalactites take the shape of Lst2 with balloon-like structure at edges; stalagmites, downside caves, form head-like structures	Percolation of already saturated water through open-work tufa ceiling (Gradziński et al., 2018)	Caves and small cavities associated with cascades and waterfalls (Arenas-Abad et al., 2010)
Organic-matter rich muds, **C** •• Figs. 5G, H and S2	Lenticular and tabular; cm to dm-scale in thick; associated or not with Lph; massive	Allogenic or autogenic organic-matter accumulation with anoxia conditions	Quiet water with anoxia; minerotrophic fens giving rise to peaty facies ; marshes giving rise to paludal (marshy) facies ; stratificated lakes giving rise to sapropel facies (Pedley et al., 2000)

Paleosol, **P** • Fig. S3	Variable shape; cm-scale in thick	Pervasive sub-areal conditions	Exposed, non-aqueous area
Non-tufa facies			
Matrix-supported conglomerate with breccias, **Gms**, **B** • Fig. 5E	Wedge-shaped; dm-scale in thick; structureless; disorganized	Slumping and debris flow process	Sides of fluvial valley (Miall, 1977)
Massive sands, **Sm** • Fig. 5E	Tabular; cm-scale in thick; structureless	Sediment gravity flow deposits (Miall and Postma, 1997)	Fluvial valley-side
Massive muds and silts, **Fm** • Fig. 5E	Tabular; cm-scale in thick; desiccation cracks	Overbank deposits (Miall, 1977)	Flood-plain, alluvial plain (Miall, 1977, 2014)
Massive marls, **Mm** • Fig. 5E	Tabular; cm-scale in thick; without significant desiccation cracks	Settle-out in still-water conditions (Vázquez-Urbez et al., 2012)	Area of palustrine character

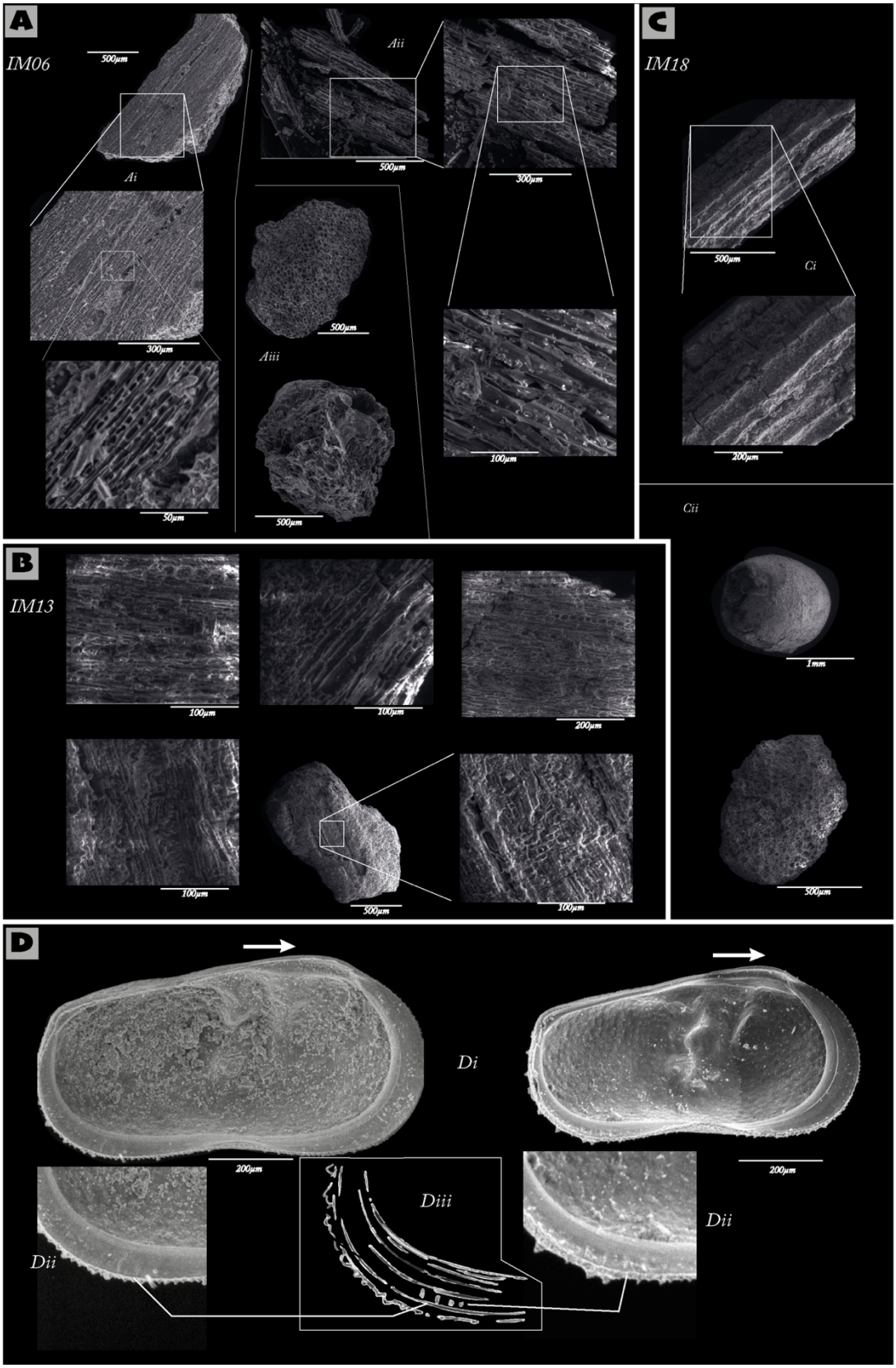


Figure 4. *Scanning electron microscope (SEM) images of some specimens of macro-charcoal and Ilyocypris bradyi.* ***A****: SEM image of macro-charcoal fragments of the reference IM06 (i.e., the peaty facies);* ***Ai****: type "S" charcoal (geometric, visible cell structure, wall porosity) or "B1" (3D block, cellular and foliated);* ***Aii****: type "S" charcoal (wall porosity and fragile) or "B5" (meshed and reticulated);* ***Aiii****: type "E2" charcoal (spheroid and vesiculated).* ***B****: SEM images of macro-charcoal fragments of the reference IM18 showing type "C" charcoal (compact, angular-irregular geometric shape and with no wall porosity).* ***C****: SEM images of macro-charcoal fragments of the reference IM18;* ***Ci****: type "C" charcoal and*

*"B1" (compact and foliated); **Cii**: type "E1" charcoal (rounded and smooth). **D**: SEM images of two specimens of Ilyocypris bradyi valve; **Di**: RV, internal lateral view; **Dii**: detail of the postero-ventral marginal ripplets (PVMR); **Diii**: redrawn schematic PVMR from Mazzini et al., (2014). Locations of the charcoal references are shown in **Figure 2**. The morphotypes "C" and "S" are according to Enache and Cumming (2006); the morphotypes "B1", "B5", "E1", and "E2" are according to Mustaphi and Pisaric (2014).*

4.1.2 Palustrine-lacustrine FA: L1

L1 starts with fining upward oncoids (Fig. 5F) with intraclastic nuclei in nature (Fig. 8A) and ends with boundstones of coated stems (Lst) with the occurrence in a vertical alternation of bioclastic limestones and sandstones (Lb and Sb, respectively), and organic-rich facies (C) at the middle part of this facies association (Figs. 5D, 6B, 7). In general, this reveals moderate values of K/Al and K, except for one peak in facies Sb (IM11, Fig. 2), moderate concentrations of dolomite, and relatively high concentration and diversity of ostracods (Figs. 2, 3). The facies C (IM13; Figs. 2, 4B, 5H) shows a high content of organic matter, low ostracod diversity with the almost dominance of *I. bradyi* (ca. 80%), high concentration of macro-charcoal with the prevalence of types "C" (geometric, compact, and with no porosity wall; Enache and Cumming, 2006) and "B1" (blocky and with a discrete textured surface; Mustaphi and Pisaric, 2014) (Fig. 4B), and peaks in the dolomite and quartz curves (ca. 60 and 20%, respectively) (Fig. 3).

L1 is believed to reflect obvious transitions from marginal (or shore, facies Lo) to central (or offshore) shallow lacustrine (facies Sb, Lb and C) to subsequent palustrine (facies Lst1) subenvironments, typifying the gently sloped ramp with low wave energy model of Platt and Wright (1991). Indeed, the fining upward of oncoids and the subsequent deposition of bioclastic limestones and sandstones indicate waning energy followed by increasing profundal conditions (Ordóñez and García del Cura, 1983; Vázquez-Urbez et al., 2013). On the other hand, the geometry and extension of the deposits, along with the absence of lateral facies change to fluvial s.s. deposits do not support an alternative interpretation involving deposition in ponds (laterally limited standing water) within overbank settings. Indeed, the relatively high concentration and diversity of ostracods in this facies association may witness the establishment of low energy settings (e.g., shallow open lacustrine ecosystem) enabling optimal conditions for the ostracod fauna to thrive. Well-drained conditions and active weathering of the landscape are reflected by the XRD analysis and the K/Al ratio, relatively. Facies C (dated layer to 2738 ± 22 cal yr B.P., table1; Figs. 5D, H) showing no subareal or pedological features (e.g., bioturbation, vascular plant rhizomes) is more likely to reflect relatively profundal stratified lacustrine conditions with high production/(dilution + destruction) ratio (Bohacs et al., 2005) forming sapropel depocenter (*sensu* Pedley et al., 2000). However, the variable "production" here is likely to reflect higher portions of allochthonous organic-rich inputs from the watershed, rather than

autogenic production, during an abrupt period of organic-rich soil drainage within a long-term period of enhanced biologic activity and soil formation. This is consistent with the macro-charcoal analysis of this layer (IM13, Figs. 2, 4B) that exhibits slight reworking features, and with the mineralogical analysis, which suggests active landscape drainage. Therefore, the higher concentration of macro-charcoal within this layer may be linked to the taphonomic process (charcoal transport and deposition), thus reflecting a secondary signal (Patterson et al., 1987; Conedera et al., 2009). The charcoal production, being related to fire events, may be triggered whether by frequent lightning strikes (recurrent storms) or anthropogenically (although this is excluded due to the lack of its evidence) during short-term periods of lower effective humidity with high fuel availability (Huber and Markgraf, 2003).

4.1.1 Fluvial-palustrine FA: FP2

At the upper part of the log, **FP2** shows alternation of phytoclastic organic-rich (Lph, C) facies with oncoids (Lo), overlapped by channelized boundstones of coated stems (Lst1) and oncoids in association with lenticular organic layer (Figs. 5B, C, 7). The organic-rich facies mainly underline truncation surfaces. This facies association reveals substantial fluctuation in proxy results which is consistent with the lithological aspect (Fig. 2). Charcoal morphotypes from one organic-rich layer (IM18, Figs. 2, 4C) clearly show reworking features (e.g., rounded with smooth surface, type "E1", Fig. 4Cii; Mustaphi and Pisaric, 2014).

FP2 is interpreted to reflect fluctuations in a fluvial-marshy subenvironment (see also the lateral "basinward" passage "basinward" to marginal-marshy fluctuations in log 2, Fig 6C and supplement material). The morphotype charcoals in phytoclastic organic-rich layers underlined by erosion surfaces reflect well-drained conditions under cooler temperatures within a marshy subenvironment. Here, the boundstones of coated stems are thought to be formed within relatively stabilized bars (see Fig. 11C), more likely in a braided system close to standing water (shallow lacustrine) margin (see the lateral occurrence of facies Lb in log 2, Fig. S2) marking a slight trend to an overfilled configuration (Nutz et al., 2019). The lateral extension of the frequent alternation between structureless oncoids and marshy facies (occurrence in both "basinward" logs; *see* Fig. S2) suggest substantial changes on the "basin-scale" rather than reflecting strictly limited extensions and lateral facies shifting within overbank settings.

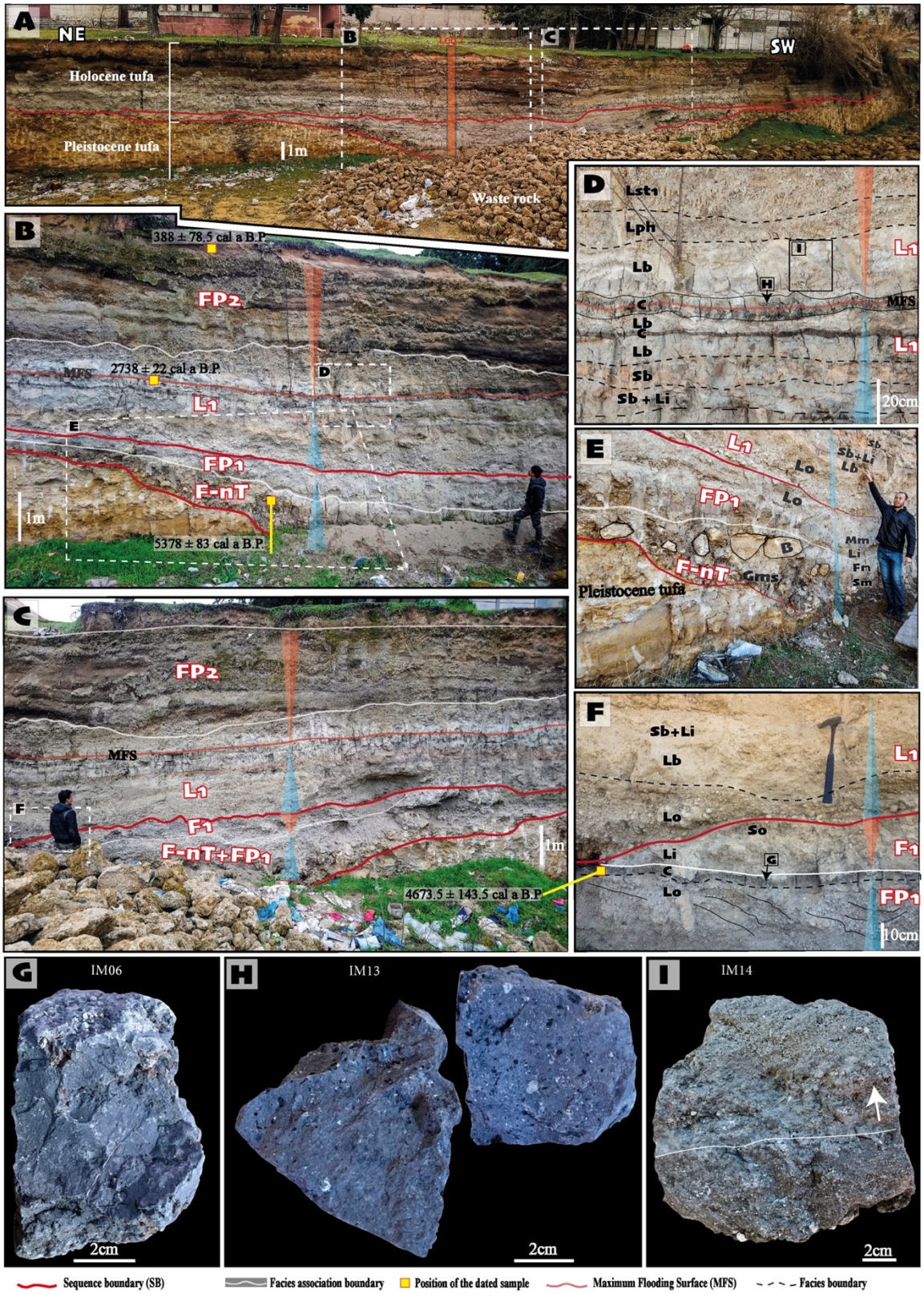


Figure 5. *Upstream stretch (see Fig. 1C). Field views of facies and facies associations (FAs) of log1.* ***A****: Panoramic view of Pleistocene- and Holocene-tufa separated by a major bounding surface.* ***B****: detail of* ***A*** *showing the superposition of FAs and bounding surfaces, with locations of the dated samples; Note the high-frequency occurrence of the organic-rich facies (facies C) at the upper part of the stratigraphic section.* ***C****: Detail of A showing the lateral occurrence of "F1".* ***D****: Close-up view of B showing the superposition of the stagnant-water facies Lb, Sb, C, and Lst1, within "L1". Note the position of the Maximum Flooding Surface (MFS) within the sapropel facies (facies C) delineating the transgressive and highstand intervals.* ***E****: Close-up view of* ***B*** *showing the wedge-shaped body of matrix supported conglomerates with breccias and*

*massive sands (facies Gms, B and Sm) marking the lower part of the stratigraphic section. **F**: Close-up view of **C** showing the sequence boundary delineating the two depositional sequences, "F1", "FP1" and "L1" (partially), and the related facies type. **G**: Hand sample of the dated peaty (fen) facies marking the summit of "FP1" (see **F**); note the presence of bioturbation markers and root remains. **H**: Hand sample of the dated organic-rich (sapropel) facies marking the MFS (see **D**); note the significant occurrence of macro-charcoal. I) hand sample of bioclastic limestone (Lb) marking the passage from shallow lacustrine to palustrine subenvironment; note the decrease (increase) in the concentration of bioclasts (intraclasts) upward. Facies and facies association codes in **Table 2** and **Figure 7**, respectively.*

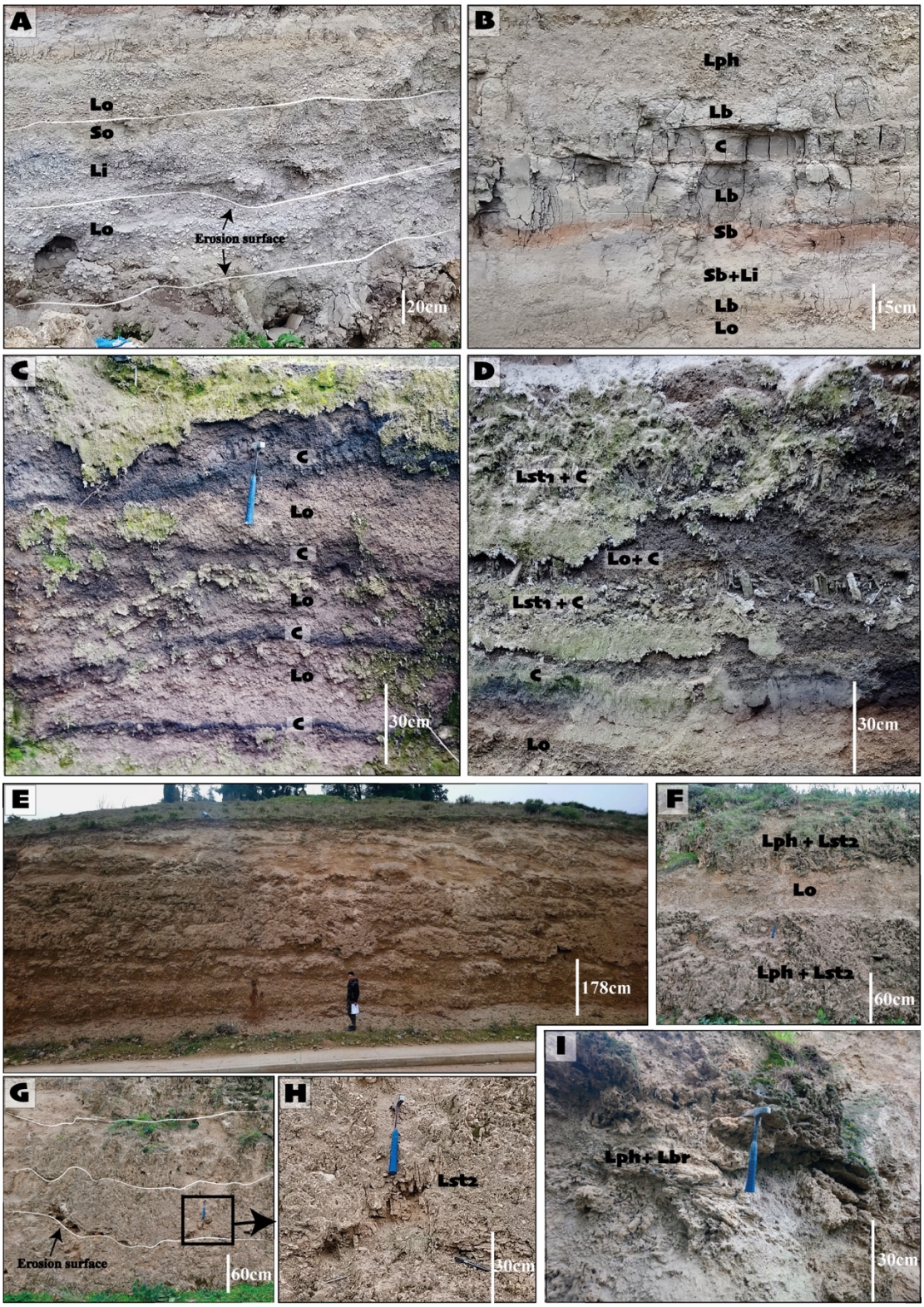


***Figure 6**. Selected field views from the upstream- and sloped stretch. **A-D**: Close-up field views from the upstream stretch showing: (i) fluvial facies (**A**); (ii) central (offshore; Lb, Sb, C) and marginal (shore; Lo, Lph) shallow lacustrine facies (**B**); (iii) alternation of marshy (facies C) and marginal shallow lake (Lo) facies (**C**); and (iv) marshy-palustrine facies (Lst1, Lo, C) (**D**). **A** and **B** are from log1, whereas **C** and **D** are from log2. **E-I**: Field views from the sloped stretch. **E**: Large-scale field views showing the significant thickness of the deposits at the downstream part of the slopped stretch (N33° 44' 16.54"; W5° 1' 0.91"). **F-G**: detail of **E** showing an alternation of phytohermal and oncoidal facies (Lst2, Lo). **H**: detail of phytoherm curtains of hanging stems (Lst2); note the periodic occurrence of erosion surfaces. **I**: Close-up view showing the association of bryophytes and phytoclasts facies (Lbr, Lph) typical of barrage-cascade setting. Facies codes in **Table 2**.*

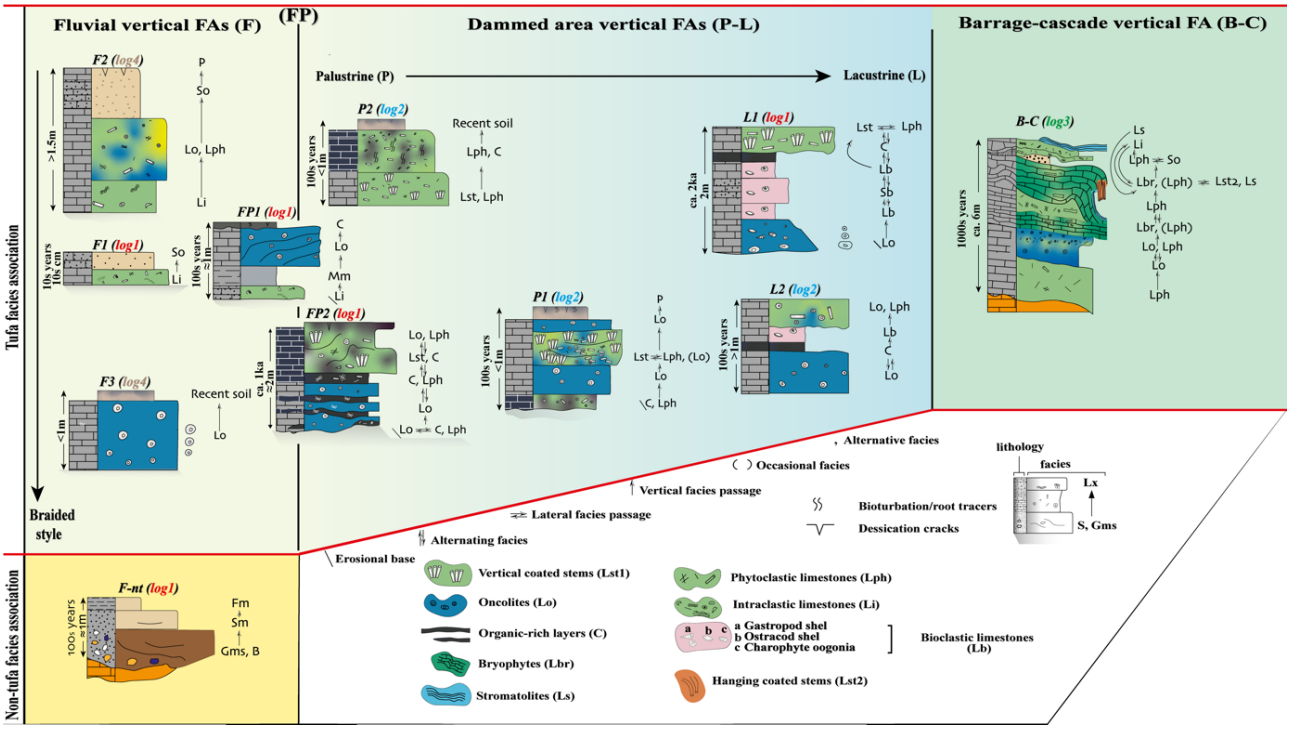


***Figure** 7. Facies associations summarizing the different subenvironments (fluvial s.s., fluvial-palustrine, palustrine-lacustrine, barrage-cascade) present in the Holocene deposits of Imouzzer Kandar.*

4.2 Petrographic analysis: lamination pattern

Microbialite specimens that were the subject of petrographic analysis in this study include oncoids (from log1) and stromatolites (from the sloped stretch; see field views for location, Fig. 11C), which are composed mainly of low-Mg calcite and other subordinate mineral constituting the detrital component, quartz, and dolomite (Figs. 8J, 9J). They exhibit an alternation of slightly undulatory or flat dark and light composite laminae matching the morphology of the substrate or the nucleus (Figs. 8A and 9A-B), although some of these present lateral variation in thickness (especially those that form cortex of oncoids, Fig. 8A). Within these composite intervals (*sensu* Arenas and Jones, 2017) are included several single dark and light laminae (Fig. 9A-C). The thickness, the micro-texture, and the microbial component of the composite laminae differ from one microbialite-type to another.

4.2.1 Laminations in oncoids

The cortex of oncoids, sampled from the base of L1, consists of alternating dark and light composite laminae. These vary laterally in thickness: the underside is thinner whereas the top side is thicker (Fig. 8A), showing a conspicuous asymmetry (Freytet, 2000) and a polar growth (*sensu* Hägele et al., (2006). On the top side, the dark composite laminae are between 0.5 and 2mm, whereas the light ones are between 1 and 3mm. They present several laminae recognizable to the naked eye. The outmost zone is commonly more porous (Fig. 8A, C) resembling the soft (biofilm) zone reported in samples of oncoids from southern Germany by Hägele et al. (2006). In general, the light composite laminae, formed mainly of micrite, are characterized by tightly arranged, erected, not branched and rectilinear parallel calcified filaments (Freytet, 1997, as cited in Dabkowski, 2011) forming tubes with thin coating walls of 1 to 2µm. Two interwoven microbial morphotypes were recognized based on the inner diameter of tubes: morphotype with a smaller (larger) inner diameter of 1 to 3µm (up to 6 µm) (Fig. 8D). The space between tubes is loosely encased by anhedral micritic calcite, defining then interfilamentous porosity. The dark composite laminae, formed mainly of micrite, microspar and spar calcite, are characterized by loosely packed thicker tubes up to 10µm thick, with an inner diameter up to 6µm (Fig. 8E-I), and are preferentially oriented sub-vertical to the depositional surface, with various degree of calcification (Fig. 8E, G). The space between tubes is tightly occupied by micrite and microspar calcite, reducing then the porosity. The coating consists of sub-hederal to euhedral crystals, in which the size increases slightly outwards (Fig. 8F, H). Encrustation is the main mechanism of calcite precipitation. The dark laminae can show some entombed small opening, which may correspond to diatom stalks (Fig. 8I).

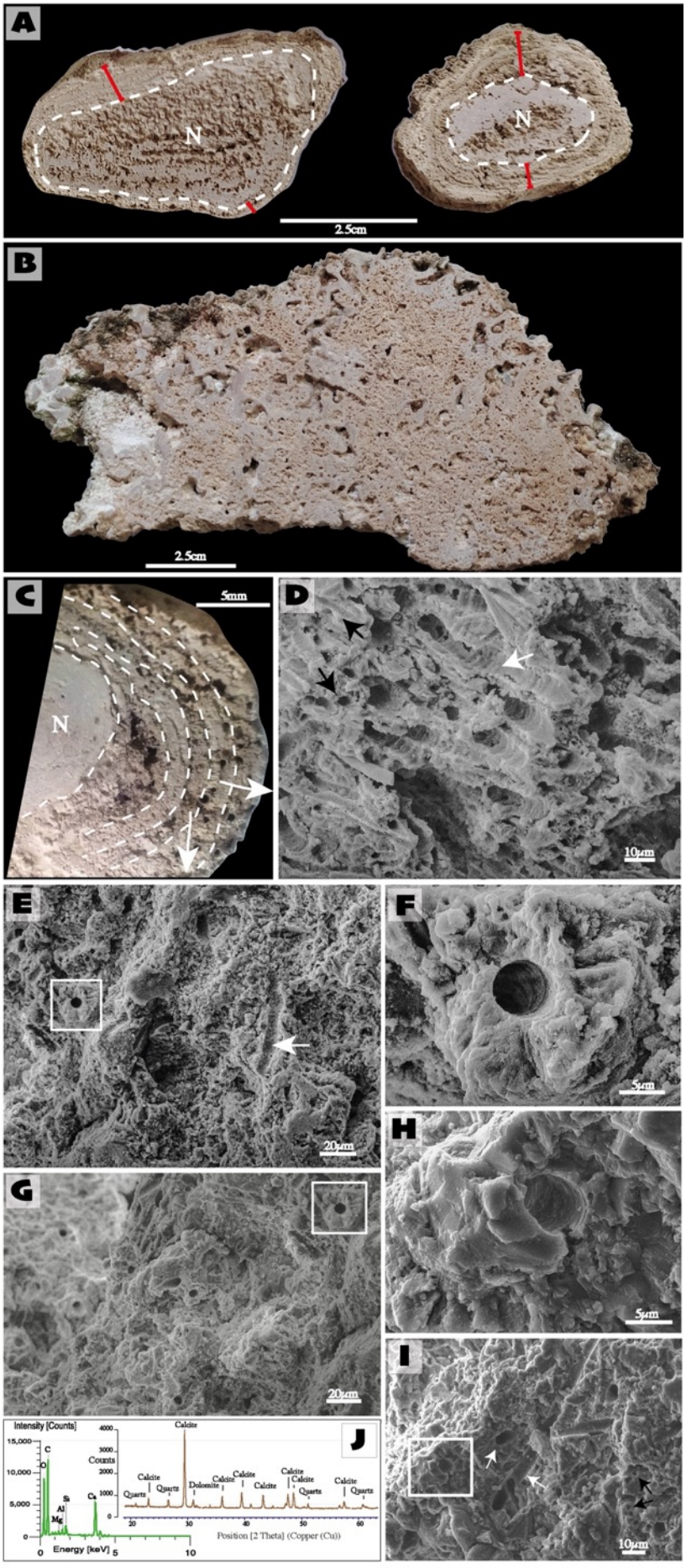


Figure 8. *Morphological characteristics of oncoids (Lo, middle part of log1) and bryophytes (Lbr, sloped stretch), and the calcification pattern of the laminated cortex.* ***A****: Cross-section views of oncoids showing the asymmetrical shape of the cortexes. Note the difference in length of the red brackets.* ***B****: Cross-section view of fossil moss showing a volumetric aspect.* ***C****: Cross-section view showing the laminated cortex of an oncoid specimen from the middle part of log1 (base of DS1). Note the difference in colors and thickness that distinguish a successive couplet of laminae.* ***D****: SEM image of the light laminae showing tightly packed thin tubes developed around filaments of two cyanobacterial morphotypes; the tubes with small (large) diameter indicated by black arrows (white arrows) may correspond to encrustation around Schizothrix calcicola (Calothrix gypsophila). The tubes are normally oriented to the depositional surface.* ***E****,* ***G*** *and* ***I****: SEM images of the dark laminae showing loosely packed thick tubes (may correspond to encrustation around Calothrix gypsophila) oriented in all directions, although with a predominance of the direction normal to the depositional surface.* ***E*** *and* ***H****: detail of calcite tubes showing thick coating with an outward increase of crystal sizes. The small entombed openings in I (black arrows) may correspond to diatom stalks.* ***J****: Elemental (SEM) and mineralogic (XRD) analysis showing consistent peaks with the dominance of low-Mg calcite and, secondarily, quartz and dolomite.*

4.2.2 Lamination in stromatolites

The lamination of the stromatolites, sampled from the sloped stretch, is characterized by an alternation of flat and slightly wavy dense and macrocrystalline composite laminae. In the thin section, the dense composite laminae, 1 to 1.5mm thick, are formed of several well-defined micrite and spar laminae (or "microlaminations" *sensu* Freytet, 1998) sub-parallel to the depositional surface (up to 50 laminae). Spar laminae increase in thickness, at the expense of micrite laminae, upwards (Fig. 9C). The upper boundary surface delineating the dark composite laminae is commonly erosive, and shows wrinkled to arched shapes (*sensu* Freytet, 2000). The macrocrystalline composite laminae, 1.5 to 3mm thick, are formed of large calcite crystals normal to sub-perpendicular to the depositional surface, widen upwards (up to 150µm wide), forming then fan-like texture (or "radial palissadic sparite" *sensu* Freytet, 2000) and displaying competitive growth pattern (Fig. 9C-D). Within these sparry in nature composite laminae, several micritic laminae occur and underline figures of micro-dissolution/erosion (dark color in thin section, Fig. 9C; Freytet, 2000). In general, these composite laminae are more porous than the dense ones, and the porosity is commonly intercrystalline (Fig. 9C). The contact between the dense and macrocrystalline laminae is well-defined (Fig. 9C). In SEM microphotographs, the large crystals have smooth and flat tops and are formed of polyhedron crystals, a few µm in size (Fig. 9D, H, G). Some of these enlarged crystals exhibit entombed openings (Fig. 9F).

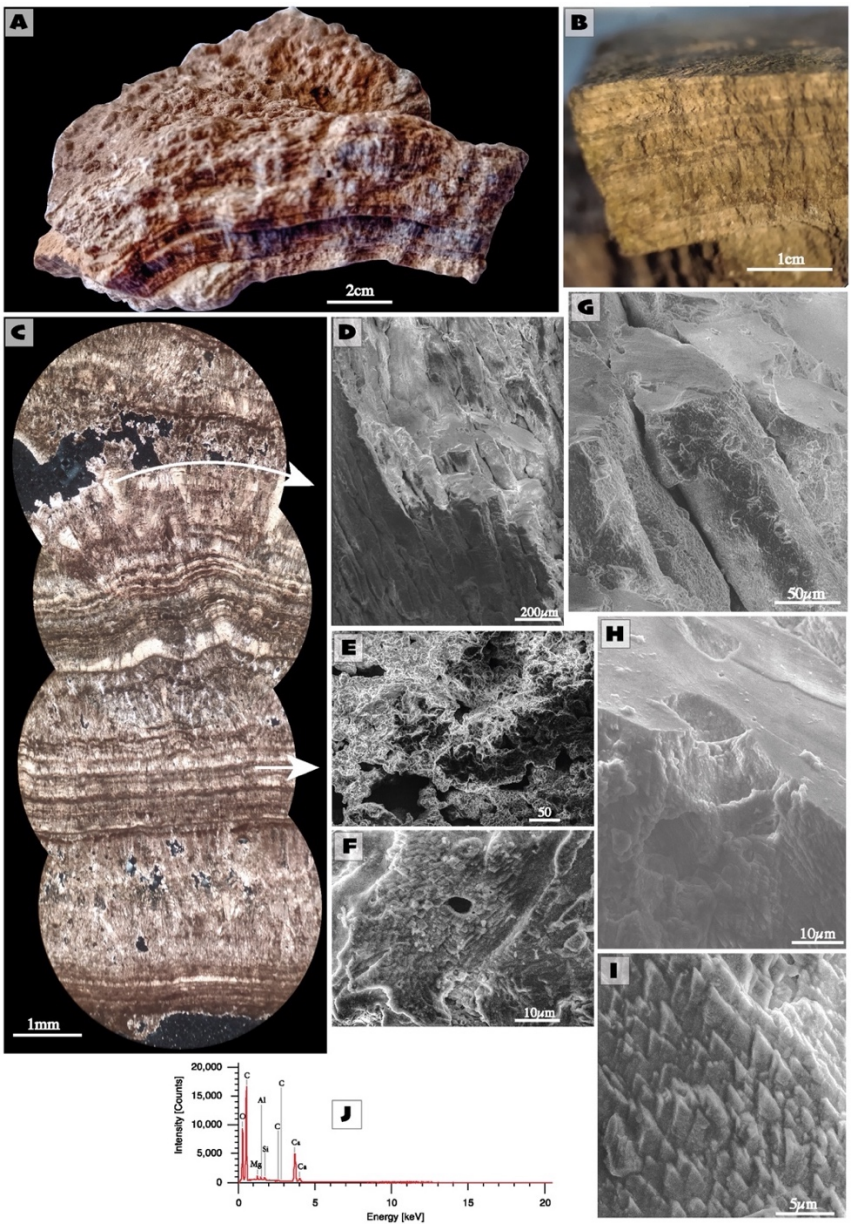


***Figure 9**. Hand samples, optical microscope and SEM images of stromatolites from the sloped stretch. **A-B**: macroscopic view of stromatolites showing a succession of dark and light laminae. **C**: Optical microscope image showing the succession of dark and macrocrystalline composite laminae. **D**, **F-I**: SEM image showing enlarged crystals (**D**) with smooth tops (**G** and **H**) that compose the macrocrystalline composite laminae. The walls are formed of polyhedrons (**I**) and can show entombed openings (**F**). **E**: SEM image of micritic laminae, a component of the dark composite laminae. **J**: Elemental analysis (SEM) suggesting that the low-Mg calcite is the main mineral that form the laminae*

4.3 Sequence analysis

To make the lateral relationship between the different logs and to reconstruct the synoptic architecture of the basin-like deposits, we have applied the conventional sequence analysis according to Bohacs et al. (2000) and Catuneanu et al., (2009), although the use of certain terms (e.g., systems tracts) was omitted. Two fifth-order depositional sequences (i.e., 10^2 -10^4 years; Catuneanu, 2020) on the "basin-scale" (DS1 and DS2, Fig. 10) were recognized considering that a depositional sequence is a full cycle of an increase followed by a decrease in accommodation space, with a subsequence development of a subareal unconformity that delineates the sequence upward (sequence boundary, SB). The SB is of type "A" as is denoted by Keighley et al. (2003), i.e., a physical surface that indicates a sharp change in sedimentation between two sequences with partial truncation of the underlying one.

For that, our approach consisted in analyzing the sedimentary record on the "basin-scale" with regards to the variation of the sill elevation (i.e., barrage or knickpoint height) and the inferred stacking pattern (progradation, aggradation and degradation) at the main barrage.

4.3.1 Depositional Sequence 1: fluvial-dominated interval

At the base of log1, the incision and the subsequent course-grained deposits reflect phases of low accommodation, implying a degradational interval (Catuneanu, 2006, 2020; Currie, 1997). This has been interpreted as either an increase (decrease) in discharge (sediment supply) and/or a tectonic uplift (Shanley and McCabe, 1994; Currie, 1997). The overall finning upward sedimentation, which corresponds to channel-fill deposits followed by minerotrophic peat (Figs. 2, 5E, 6G), reflects an increase in the accommodation rate. Within this trend, two flooding surfaces were identified in the middle (bases of facies Li and Lo; Fig. 2) suggesting superimposed small variations. Over peaty muds, the intraclastic rudstones and oncoidal sands (Figs. 2, 5F) reflect a decrease in accommodation which became negative at the top and allowed a partial truncation (forming the SB). Laterally, log2 does not reach this interval (Fig. S2).

At the downstream-facing of the enlarged barrage, the basal sequence boundary surface separating the Holocene and Pleistocene formations is identified at the lower part of the outcrop (Figs. S3H, 10), whereas the degradational interval in the "basin" has no equivalent herein. This is likely explained by the fact that the paleo-watercourse was slightly located leftward of this outcrop location (*see* Fig. 11A). Otherwise, the increase in accommodation "basinward" may indicate a tendency towards a more closed system. Thus, it is assumed that ongoing aggradation at the sill was active during this time interval. The flooding pulses identified "basinward" may correspond laterally to water overfilling and, thus, collapses of former coated stems close to the sill producing phytoclasts and overflow of oncoids. This is accumulated at the downstream-side (where log3 is measured, Fig. S3) and therefore would have contributed to the decrease in height/width ratio (H/W) of the barrage-cascade architecture (low H/W, Fig. 10). The peaty facies is believed to have no lateral extension downstream the sill since peat formation required anoxic conditions. This implies a limited outflow and minimal temperatures suggesting low discharge and subsequent slow or nil aggradation rate at the sill during the period of peat formation. Within log3, the SB at the top of this sequence might be correlated with the vertical facies change from oncoids towards bryophytes in association with phytoclasts (Fig. S3D, F) and, hence, be considered as correlative conformity (CC, Figs. 10 and S3F, G).

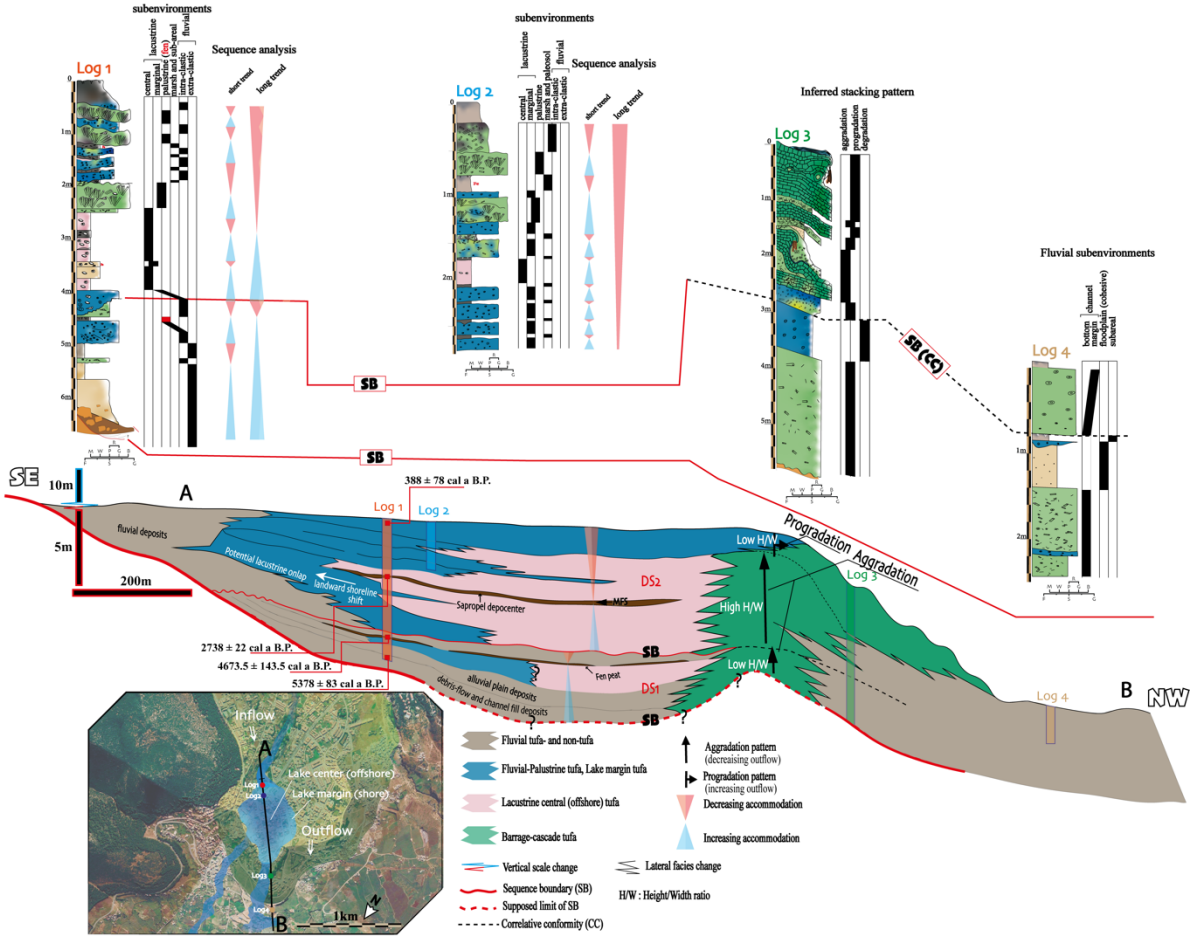


Figure 10. *Stratigraphic architecture of the Holocene tufa formation based on sequence stratigraphy and sedimentologic analysis. The fifth order depositional sequences (DS1 and DS2) and the dated layers locations are indicated at the basin-scale. The satellite image shows the estimated paleolimits of the Holocene paleolake Imouzzer Kandar during the highstand interval. Note the vertical change in scale. See text and other figures for more detail about the abbreviations used here.*

4.3.2 Depositional Sequence 2: lacustrine-dominated interval

Above the sequence boundary marking the termination of **DS1**, the fining-upward up to the sapropel depocenter (facies C) observed in log1 (Fig. 5D, H) correspond to a transgressive interval (Fig. 10). This means that there was a change in the "basin" architecture that would have allowed more potential space for sedimentation. Moreover, the sapropel depocenter (facies C, Fig. 5D), indicating the deepest deposits in the hole stratigraphic formation, is believed to represent a Maximum Flooding Surface (MFS; this is positioned at the middle of the layer, Figs. 2, 5D; Bohacs et al., 2000, 2005); it is noteworthy that log2 does not reach this surface (*see* Fig. S2). Above this, the lacustrine marginal/marshy to fluvial fluctuation deposits reflect a "basin-scale" aggradation pattern that, during periods of higher discharge, is balanced by high outflow over the sill (Shanley and McCabe, 1994; Keighley et al., 2003). Accordingly, this is likely to correspond to a highstand interval (Fig. 10) since the water level is maintained close to and even over the sill height (Bohacs et al., 2000; Catuneanu,

2006, 2020; Hanneman and Wideman, 2010). Laterally, in log2 (Fig. S2), the provided outcrop recording fluvial to marginal (shore, Lo, Lst1), shallow central (offshore) lacustrine (Lb), and marshy (C) conditions is consistent with the highstand interval described above.

Up to about 10's of centimetres above the correlative conformity in log3, the occurrence of bryophytes in association with phytoclasts (Fig. S3E, F) is believed to reflect an aggradation pattern at the sill. Here it is suggested that, firstly, at least 5 m of aggradational stacking is required to produce the space on the "basin-scale" enabling the transgressive interval to be recorded and, secondly, there were low frequency and low amplitude flooding events that limited the production of phytoclasts and intraclasts and their accumulation at the downstream-facing of the enlarged barrage (where log3 is measured). Consequently, this might be correlative with the transgressive interval inferred from the "basin" and is suitable to increase the H/W ratio of the wedge architecture (high H/W, Fig. 10). Otherwise, the dominance of bryophytes at the expense of rudstones and floatstones of intraclasts at the upper third part of log3 (Figs. 6I, S3) indicates a progradation pattern that is likely related to a regular water discharge and active CO_2-degassing in the downstream-facing of the enlarged barrage (Arenas et al., 2015a). This decreases the H/W ratio of the wedge architecture (low H/W, Fig. 10), hence making the barrage-cascade wider and thicker downstream (Fig. 6E). The topographic irregularities at the sloped stretch might be related to flooding events enabling collapses and accumulation of big clasts (e.g., trunks) downstream. This could be, seemingly, coeval with fluvial dominated periods recorded "basinward".

4.4 Evolutionary facies model

The facies and sequence analysis approaches of the Holocene deposits of Imouzzer Kandar have provided a fairly concrete comprehension of the spatial and temporal aspect of the sedimentary processes, thus allowing a sedimentary facies model to be constructed. In general, this corresponds with a "barrage model" in the sense of Pedley (1990), or "moderate-sloped model" with development of large dammed areas within a general stepped context according to Arenas et al. (2014b). In particular, a spatial-temporal evolution of the sedimentary processes and characters from ca. 5 cal kyr B.P. onwards has been observed and inferred. The following sub-sections describe this variability.

4.4.1 Incision event(s), the start of a new stage of sedimentation: Middle Holocene

This interval marks a partial degradation of the previous tufa (i.e., Early Holocene? And/or Pleistocene) through a linear incision of the mean watercourse (Fig. 11A). This bed incision was likely to bring about abrupt entrenchment at the previous knickpoint (a sharp change in topographic gradient)

due to the relatively high resistance of the ordinarily well-cemented barrage build-up in contrast to the upstream sediments, forming a potential small "gorge". Otherwise, It is deduced that through exhibiting prominent hanging curtains of coated stems (Lst2) associated with speleothems (Lsp; see field views, Fig. 11A), the previous tufa pulses may mirror both a strong vertical moss barrage with upstream dammed water bodies model as proposed by Vázquez-Urbez et al. (2012), and a single non-vertical stepped barrage-cascade growth style pattern of type "B3" (with high Aggradation/Progradation ratio), as is described by Arenas et al. (2014b; *see* their Fig. 13).

As a result, downcutting into previous tufa-stages would have created a new space for sedimentation and allowed **F-nT** to be formed following landscape degradation. Large debris (e.g., trunks, extraclastic blocs) may be accumulated at the inferred small "gorge" which may constitute a locus for a higher tufa deposition rate due to enhanced CO_2-degassing (Chen et al., 2004; Vázquez-Urbez et al., 2010; Nutz et al., 2019).

4.4.2 First tufa occurrence, accelerated aggradation rate: from ca. 4.6 to 2.7 cal kyr B.P.

As soon as it is allowed (*viz*., changes to optimal humidity and temperature), tufa growth may begin to occur firstly at the inferred "gorge" associated with large debris. The vertical bryophyte growth and phytoclasts accumulation at the barrage after reaching the previous knickline (the knickline which is not affected by the linear incision) would cause dammed water to expand upstream forming then the transgressive interval with limited overflow. This would favor a rather stable state downstream and even the development of lowest rank subareal unconformity (i.e., paleosol, iron oxide staining; Fig. 11B).

During this interval, facies associations **LP1**, **F1**, **L1** (lower part) "basinward", and **F2** on the downstream stretch, and the lower part of **B-C** on the sloped stretch are assumed to be deposited (Fig. 11B). At the downstream stretch, it is believed that a low-energy intermittent fluvial style is suitable to be developed producing a non-organic cohesive floodplain (*sensu* Nanson and Croke, 1992) with paleosol development (upper part of **F2**; Fig. 11B).

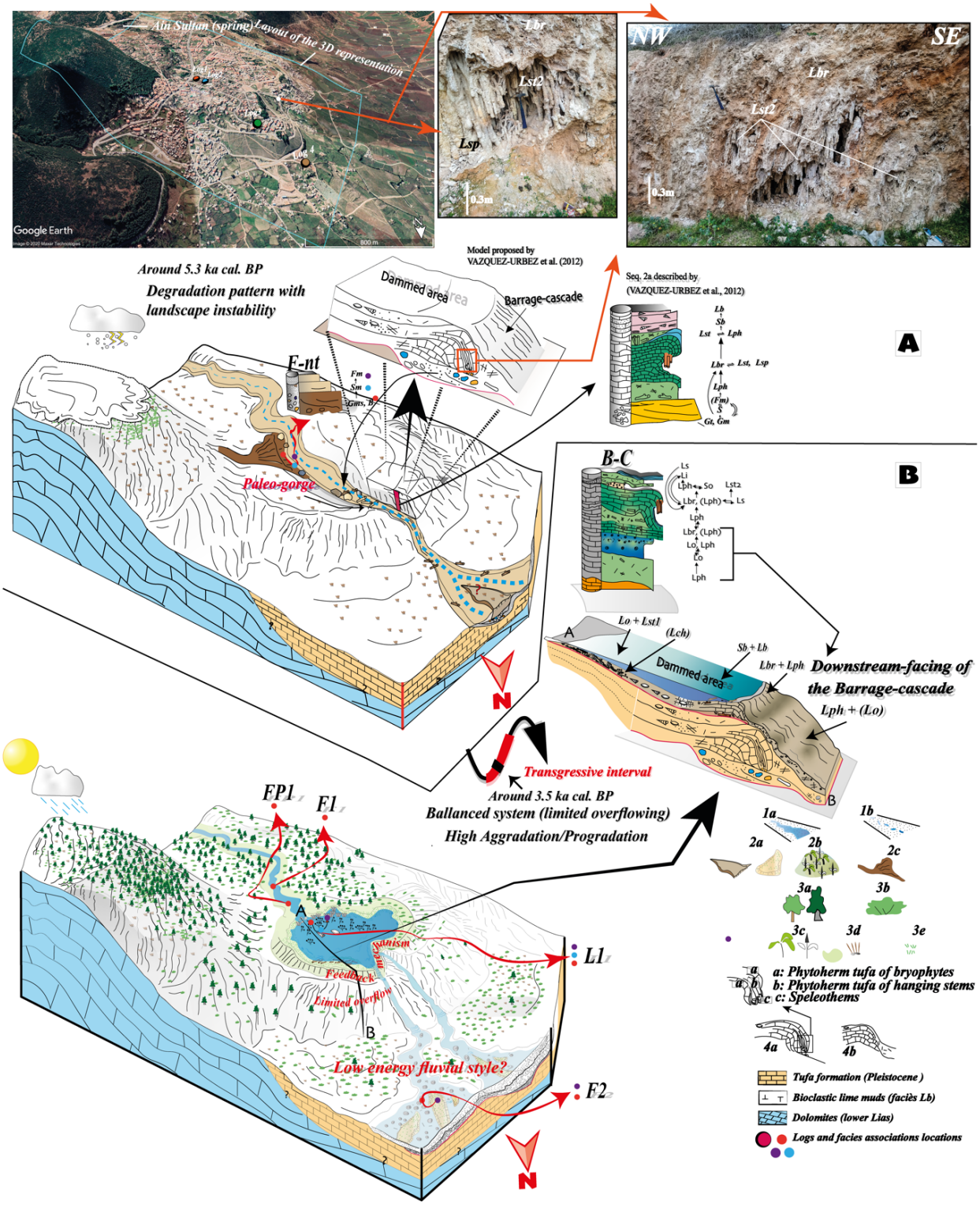
4.4.3 Active overflow, progradation pattern: from ca. 2.7 cal kyr B.P. onwards

Above the transgressive interval, a shift towards active water outflow is observed through field exploratory (*see* field views, Fig. 11C). Indeed, the occurrence of buttresses (*sensu* Pedley, 1990) at the downstream-facing of the enlarged barrage-cascade (Pedley, 1990; Pla-Pueyo et al., 2017) fits this conclusion (Fig. 11C). Therefore, the wedge architecture would be larger since the tufa growth style

shifted from aggradation to progradation at the main barrage (low H/W, Fig. 10). Consequently, the accommodation space decreased "basinward" and lead, considering also the continuous water inflow, to the highstand interval (Fig. 11C).

These conditions would have allowed the deposition of the facies association **L1** (upper part), **L2**, **P1**, **P2**, and **FP2** "basinward", **F3** at the downstream stretch, and the upper part of **B-C** on the sloped stretch. On the downstream stretch, the grossing upward of the oncoids in **F3** (see supplement material) is believed to reflect relatively high energy, which may mirror the braided fluvial style according to Pedley (1990) (Fig. 11C).

According to Arenas et al. (2014b) the stacking shift from aggradation to progradation at the barrage correspond to a transition in the pattern of tufa growth from type "B1" to type "B3" (see their Fig. 10B) with buttresses development at the downstream-facing of the main barrage.


Aïn Sultan (spring)
Layout of the 3D representation
Google Earth
Lbr
Lst2
Lsp
0.3m
NW
SE
Around 5.3 ka cal. BP
Degradation pattern with landscape instability
Model proposed by VAZQUEZ-URBEZ et al. (2012)
Seq. 2a described by (VAZQUEZ-URBEZ et al., 2012)
Dammed area
Barrage-cascade
F-nt
Paleo-gorge
A
B-C
B
Lo + Lst1
(Lch)
Sb + Lb
Lbr + Lph
Downstream-facing of the Barrage-cascade
Lph + (Lo)
Transgressive interval
Around 3.5 ka cal. BP
Ballanced system (limited overflowing)
High Aggradation/Progradation
FP1
F1
L1
F2
Feedback
Limited overflow
Low energy fluvial style?
a: Phytoherm tufa of bryophytes
b: Phytoherm tufa of hanging stems
c: Speleothems
Tufa formation (Pleistocene)
Bioclastic lime muds (faciès Lb)
Dolomites (lower Lias)
Logs and facies associations locations

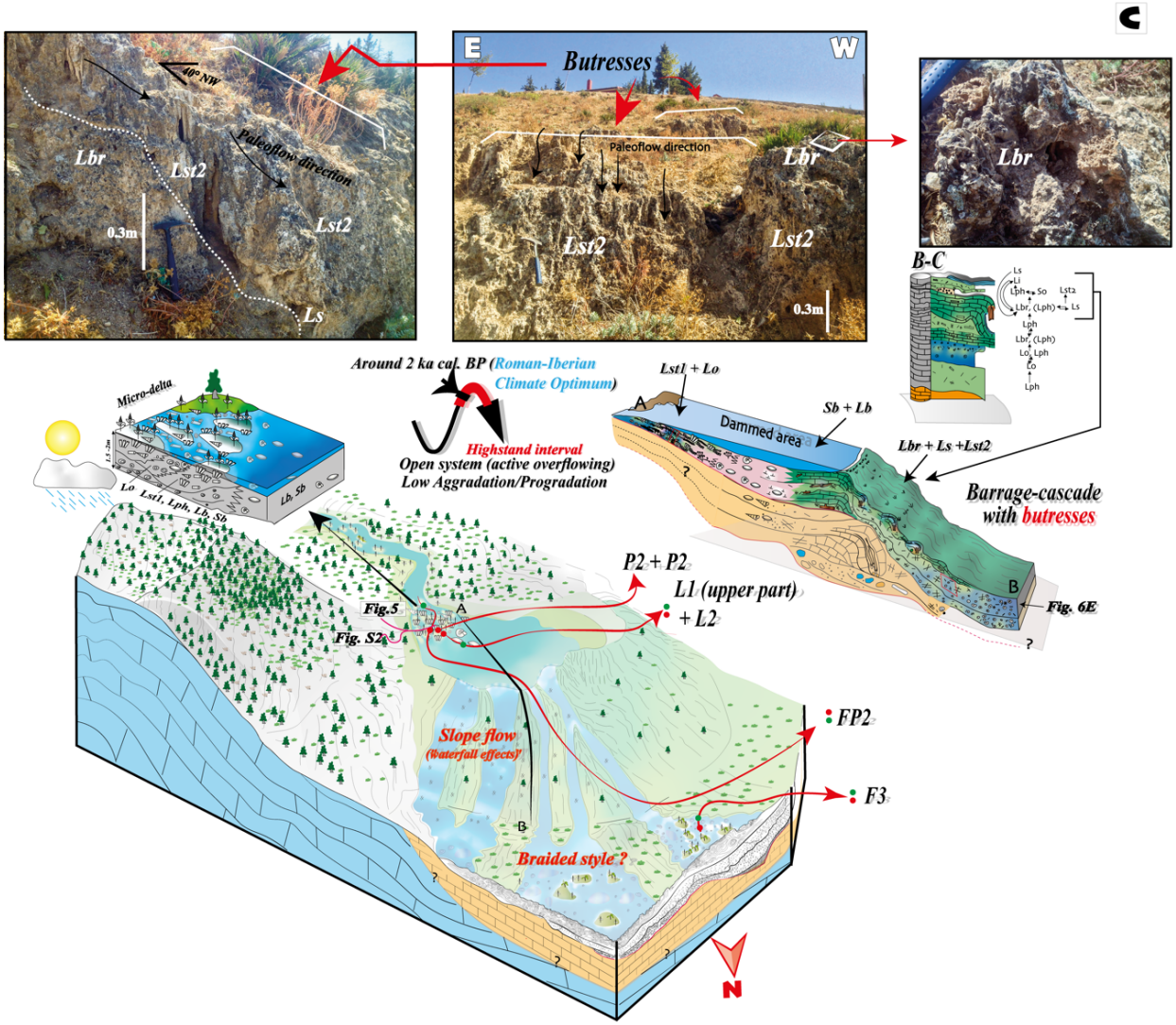


Figure 11. *Evolutive sedimentary facies model inferred from the sedimentological and stratigraphic analysis of the Holocene-tufa formation present in Imouzzer Kandar.* ***A****: Facies model showing the main degradational pattern with slope instability of the landscape during cold and arid period centered at 5.3 ka cal. BP after a long period of linear incision; additional field views of Pleistocene-tufa are presented showing a large development of curtains of hanging stems (Lst2) with speleothems (Lsp).* ***B****: Facies model showing enhanced vertical accretion at the barrage conditioning the transgressive interval basinward between ca. 4 and 2.7 ka cal. BP.* ***C****: Facies model showing active overflow and the attendant progradation pattern at the downstream-facing of the main barrage-cascade conditioning the highstand interval basinward during the period between 2.7 and 0.35 ka cal. BP; buttress development (field view) was enhanced during the known period as "Roman-Iberian Climate Optimum" around 2 ka cal. BP. Note the difference in vertical tufa accretion between Holocene- and Pleistocene-tufa. The relative timing of facies association depositions is given. Legend: 1a) Regular watercourse; 1b) intermittent watercourse; 2a) overbank deposits (cohesive floodplain); 2b) watercourse bar; 2c) proximal alluvial fan; 3a) arboreal vegetation; 3b) shrubby vegetation; 3c) hydrophilous vegetation.3d) steppe vegetation; 3e) bryophyte-dominant vegetation; 4a) barrage-cascade build-up with high vertical growth of bryophyte (Lbr; a) comparable to one of the tufa pulses developed within the Pleistocene epoch (see A) with large hanging stems (Lst2; b) and well-developed speleothems (Lsp; c); 4b) barrage-cascade build-up with moderate vertical growth of bryophytes comparable to the Holocene tufa pulse.*

5 Discussion

5.1 Lamination pattern

5.1.1 Lamination in oncoids

The asymmetric aspect of the cortex indicates a growth towards the top after immobilization (Freytet, 2000) owing to low current energy (Hägele et al., 2006; Arenas et al., 2007). The tightly arranged tubes in light composite laminae are more likely reflecting the warm season, which favors the biomass to develop. This may correspond with the *Phormidium incrustatum* α-type laminae of Freytet and Plet (1996). Otherwise, the loosely packed, but well encrusted, tubes forming the dark composite laminae are likely to reflect the cold season in which the microbial proliferation was limited. This may be compared to *Phormidium incrustatum* β-type laminae of Freytet and Plet (1996). However, taking into account the upward orientation of the filaments observed herein, and the close dependency of the growth direction *Phormidium incrustatum* with the hydrodynamic conditions (Berrendero et al., 2016), it is unlikely that this Oscillatoriale is the main contributor to the fibrous texture of the light composite laminae considering the overall low energy conditions. Instead, it is assumed that the two morphotypes observed in the light composite laminae are similar to the association of the two species *Calothrix gypsophila* (larger holes) and *Schizothrix calcicola* (smaller holes) reported by Hägele et al. (2006) from southern Germany. Hence, cyanobacteria filaments in which tubes are developed in the dark composite laminae may correspond to the species *Calothrix gypsophila*; the non-occurrence of the inferred *Schizothrix calcicola* should be noted. Accordingly, the laminations developed in oncoids are closely related to the biological activity throughout the year (Freytet, 2000), and mark biocenosis changes rather than physiological adaptations of one species (Freytet, 1992; Dabkowski et al., 2010).

The differences in the degree of encrustation observed in both composite laminae may have originated in a seasonal variation in the environmental conditions (e.g., Tw, SI_c; Berrendero et al., 2016; Arenas and Jones, 2017) and/or a variation in the density of calcified cyanobacteria inhabiting the depositional surface (Gradziński, 2010). The tightly packed filamentous moulds in the light composite laminae may mark warmer conditions (warm spring and summer) during which cyanobacteria substantially thrived (Gradziński, 2010). Accordingly, and considering the active apical growth of cyanobacteria, encrustation is maintained upward rather than laterally forming then larger, but narrower, tubes (the feedback mechanism of Gradziński, 2010). Hence, again, the process describing tufa formation for this composite laminae is mediated biologically, it is about organo-

mineralization (Defarge and Trichet, 1995; Dupraz et al., 2009). Small crystals forming the thin tubes are expected to be linked to higher alkalinity and calcite saturation Index (SI_c) along with active nucleation in the vicinity of the sheathed trichomes (Merz-Preiß and Riding, 1999; Turner and Jones, 2005; Arp et al., 2010; Shiraishi et al., 2010; Jimenez-Lopez et al., 2011; Jones and Peng, 2014). In general, tubes associated with smaller crystals are formed during the warmer seasons (Arenas and Jones, 2017). Otherwise, calcite crystals grossing in size outward the walls in the dark composite laminae are assumed to be the result of a decrease in the SI_c as the cyanobacterial influence is decreasing; the large and well-defined crystals at the outer part of the tubes are more influenced by the physicochemical conditions of the bulk water rather than microbial extracellular polymeric substances (Jones and Peng, 2014). The micrite and microspar calcite between the thicker tubes may be deposited through the process involving trapping and binding particles that are eroded from nearby sites. This would be likely to occur considering the season in which the dark composite laminae are assumed to be deposited (i.e., winter season).

In line with these petrographic insights, and regarding the stratigraphic position of the examined samples (base of the transgressive interval), the reported summertime warmer conditions and regular hydrodynamics are consistent with the inferred aggradation pattern at the sill. This explains the tendency towards more profundal conditions "basinward" between ca. 4 and 2.7 cal kyr B.P. This is also consistent with the proxy results (moderate dolomite concentration and lower values of K/Al ratio), which suggests continuous landscape drainage and active weathering providing more alkalis and carbonates.

5.1.2 Lamination in stromatolites

The competitive pattern of the macrocrystalline calcite and the fact that these terminate at the lamination boundary, suggest that these crystals are primarily formed (Gradziński, 2010; Brasier et al., 2011) instead of being the result of diagenesis through aggradational neomorphism as described by Love and Chafetz (1988). Similarly, Freytet (1998, 2000) interpreted the "radial palissadic sparite" as purely primary, physicochemical crystals. Comparative laminae consisting of macrocrystalline calcite have been reported from numerous studies (Pedley, 1992; Arp et al., 2010; Gradziński, 2010; Brasier et al., 2011; Arenas and Jones, 2017). They have suggested that these laminae are formed at sites and during periods that lack microbial colonization, commonly associated with higher energy flow and subsequently high SI_c. The occurrence of sub-periodic micro-dissolution/erosion surfaces that underline micritic laminae suggests sub-periodic flooding events. In turn, the alternation of micrite

and spar microlaminations in the dense composite laminae is previously reported by Freytet (1998, 2000). This has been ascribed to the morphospecies *Broutinella arvernensis* (Freytet, 2000, 1998), which could be equated to two current genus *Schizothrix and Phormidium* (Dabkowski et al., 2010; Freytet, 1998). More precisely, the microlaminations are interpreted to be closely related to the diurnal activity of the genus *Schizothrix* (Freytet, 1998), reflecting, herein, a short-term variability during the summertime.

Accordingly, the macrocrystalline composite laminae, a component of stromatolites formed in the sloped stretch, are deposited during periods with higher energy flow and cold conditions that prevent microbial colonization from starting or continuing. Entombed openings within the spar crystals suggest abortive colonization (*see* Gradziński, 2010). Therefore, the high crystals growth is proposed to be operated during the winter season that experienced higher discharge and lower temperature, which inhibited cyanobacteria to thrive. Indeed, the fact that the sparry meso-crystals are formed of polyhedrons (Fig. 9I) supports the winter-deposits interpretation as is reported by Manzo et al. (2012). Taking into account the slope, the higher crystals growth at such area can be explained by an inorganically-driven mechanism such as "waterfall effects" described by Zhang et al. (2001), which include aeration, low-water-pressure and jet-flow effects (Zhang et al., 2001; Chen et al., 2004).

Finally, it is found that the petrographic insights are consistent with the sedimentologic findings which suggest an active overflowing (progradation pattern) synchronous with the formation of these laminae. The active overflow would promote the "waterfall effect" increasing then the saturation index and the subsequent rapid crystalline growth of calcite in the sloped stretch during the autumn-winter period (relatively high winter discharge within this time-lapse was reported from regional paleoclimate reconstructions, *see infra*). Otherwise, although the microlaminations observed in the dark composite laminae may reflect short-term temporal variability (Kano et al., 2004), calculation of the growth rate would not be concrete as in present-day tufa growth monitoring studies (e.g., Gradziński, 2010; Arenas et al., 2014a; Auqué et al., 2014).

5.2 Paleoclimate implications

Many studies have underlined the importance of climate on the control of the potential space for sedimentation upstream barrage-cascades in fluvial tufa (Pedley, 1990, 2009; Pedley et al., 1996; Arenas et al., 2014b). Indeed, the growth style of the barrage-cascade is directly influenced by climate parameters such as discharge and temperature (Pedley et al., 1996; Zhang et al., 2012; Arenas et al., 2014a, 2014b). On one hand, high water discharges may limit the aggradation and, instead, favor the

progradation or even, in cases with very high-water velocity, the destruction of previously deposited tufa, while very low discharge may limit tufa growth (Arenas et al., 2014a). On the other hand, warmer (cooler) conditions favor vertical (lateral) and narrower (larger) barrages bounded upstream by deeper (shallower) lakes (Pedley et al., 1996).

Intrinsic factors such as the topographic irregularities and the slope have a major impact in controlling the occurrence, character, and extension of tufa pulses (Vázquez-Urbez et al., 2012; Arenas et al., 2014a, 2014b). Indeed, the geomorphological setting (*see* Figs. 1C, 11A) of the studied site, which involves an enlarged line of slope failure (i.e., knickline), is suitable for tufa dammed-lake to be formed. However, this geomorphic factor plays no role in controlling short-term variations within the tufa-pulse itself.

The fact that Holocene tufa, in logged and unlogged outcrops, was not interrupted by coarse-grained clastic sediments, as it was reported in other cases (e.g., Martini and Capezzuoli, 2014), and the absence of soft-sediment deformation structures (SSDSs) that would have been triggered by earthquakes (i.e., giving rise to seismits; Seilacher, 1969; Owen et al., 2011; Brogi et al., 2018) or brittle structure deformations (e.g., normal micro-faults; Brogi et al., 2017), question the tectonic influence over the last 5000 years in controlling the accommodation space in the studied site. Therefore, it is emphasized that the climate was by far the main allocyclic factor that controls the accommodation in the "basin" through controlling the vertical growth of tufa in the barrage-cascade settings during the last 5 ka. The degree of this involvement is examined and evaluated in the following section.

5.2.1 Orbital to millennial timescale variability

5.2.1.1 Middle Holocene: incision and landscape instability

The data from the sedimentological analysis involved a degradational pattern that underline the base of the sediment-infill "basin" during the Mid-Holocene (around 6 ka BP). The remarkable incision at the base reflects relatively long-life conditions that are prone to sustain negative accommodation. Among these, high (low) water discharge (load-supply) could be involved. Afterward, the landscape instability, which is marked by the process leading to mass transport deposits at 5378 ± 83 cal a B.P., marks a drastic climate change towards more arid conditions promoting low accommodation.

The Middle Holocene, 8.2-4.2 cal kyr B.P. (Walker et al., 2019), includes in part the Holocene Thermal Maximum (HTM), between ca. 8 and ca. 6 ka, and the Mid-Holocene Transition (MHT) cold and arid period in the northern continental lands including the Western Mediterranean region (Wanner

et al., 2008; Renssen et al., 2012, 2009; Fletcher and Zielhofer, 2013), between 6 and 5 cal kyr B.P. In the Middle Atlas, the HTM has been shown to correspond with periods of high moisture availability, inferred from pollen-based reconstructions (Lamb and van der Kaars, 1995; Cheddadi et al., 1998; Nourelbait et al., 2014; Tabel et al., 2016), which coincide, conflictingly, with low lake levels (cf. Lamb and van der Kaars, 1995; Lamb et al., 1995, 1999). This has been interpreted by round-year moisture availability (moist summertime; high Precipitation/Evaporation ratio) associated with a decrease in winter precipitation that lowered the water-table level (Lamb and van der Kaars, 1995; Lamb et al., 1995). Such a shift in paleohydrology and moisture availability is likely to be teleconnected with the pervasive positive NAO-like pattern (i.e., reduced precipitation) during wintertime over the Mid-Holocene (Davis and Stevenson, 2007; Ait Brahim et al., 2019), and with the northward shift of the Inter-Tropical Convergence Zone (ITCZ; Haug et al., 2001) in response to a poleward gradient in insolation under a higher obliquity state (Bosmans et al., 2012). This would favor convection over the Mediterranean (Magny et al., 2013; Bosmans et al., 2015, 2020) and northward extension of the African Monsoon precipitation (Bosmans et al., 2012; Sha et al., 2019) during summertime. In turn, the MHT correspond to cold and arid conditions in the Middle Atlas (Lamb and van der Kaars, 1995; Nourelbait et al., 2016; Wackenheim et al., 2020), synchronous with a persistent northward position of the Azores Front (i.e., enhanced subtropical gyre; Repschläger et al., 2017), which would maintain a continuous positive NAO-like state at higher values thus increasing the aridity during wintertime in the Middle Atlas (Ait Brahim et al., 2019).

Accordingly, the aforementioned bed incision and landscape instability events, dated to before 5 ka, fit the regional paleoclimatic data. Hence, the enhanced summertime precipitation (heavy rainstorms) along with the well-developed vegetation cover during the HTM has provided high (low) discharges (load-supply) and promoted pervasive negative accommodation (Fig. 12). Additionally, the slope instability leading to debrites deposition match the reported millennial-scale cold and arid MHT and may be the linear response of the multi-centennial scale 5.2 ka (Bond event 4) North Atlantic cold and dry event (Fig. 12). The low macro-charcoal count and high K concentrations at these levels reflect more vegetation opening, which would limit the fuel availability (Conedera et al., 2009), and active landscape erosion (Kylander et al., 2011), respectively. Moreover, the absence of ostracods (or their low abundance) in the overlying fluvial clastic layer (facies Fm) is most likely related to enhanced suspended load (i.e., turbidity effect; Mezquita et al., 1999; Holmes, 2001; Poquet and Mesquita, 2011). Subsequently, these conditions would have prevented tufa deposition.

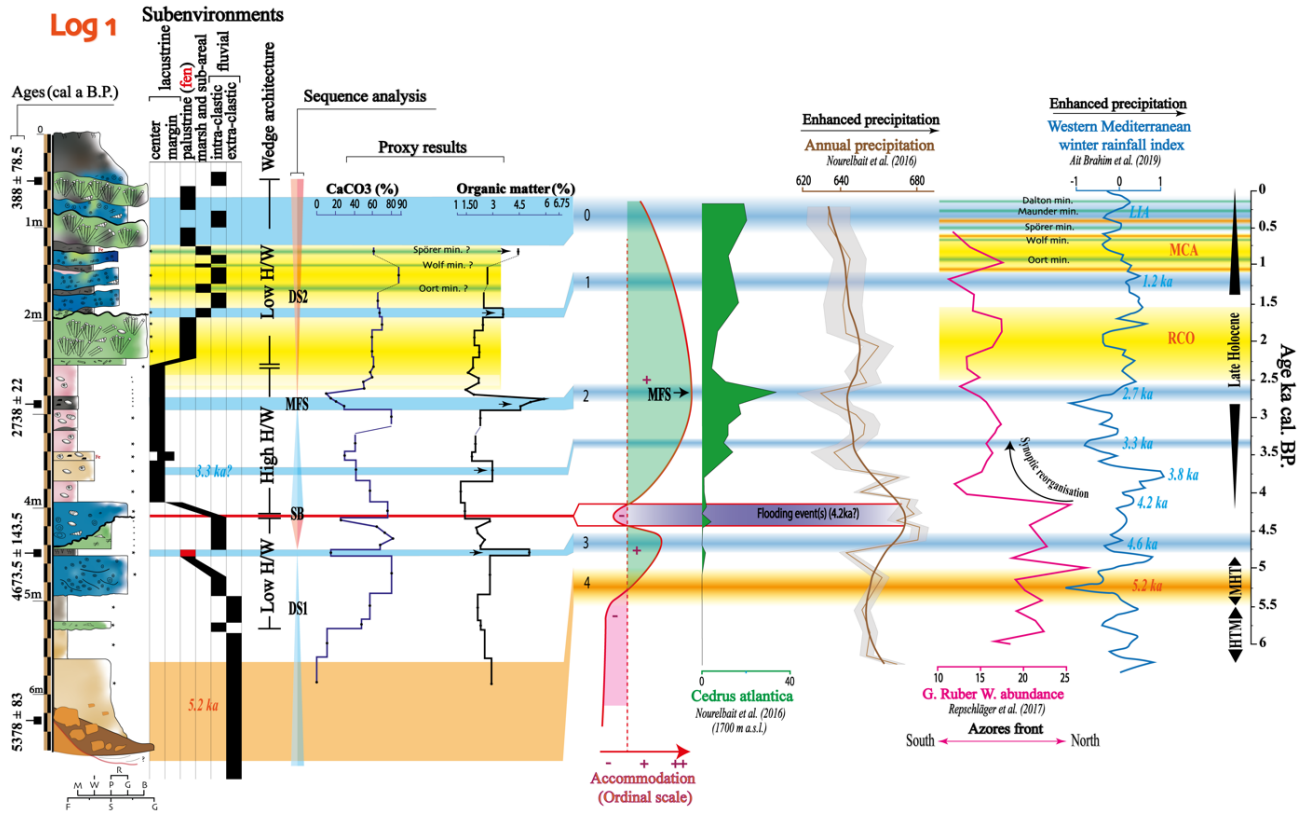


Figure 12. Correlations of the sedimentologic insights, sequence analysis, and proxy results, from this study, with paleoclimate data reported from numerous studies during the last 6 ka cal. BP. The reconstructed annual precipitation from Nourelbait et al. (2016) shows a sharp change in the overall trend at ca. 2.7 cal. kyr B.P. (see also the other reconstructed curves from their **Fig. 3**). A broad reorganization on a synoptic-scale is indicated at ca. 4 cal. kyr B.P. from Repschläger et al. (2017), this is synchronous with the development and the expansion of *Cedrus Atlantis* in the Middle Atlas. The blue curve indicates 70-year smoothing of the winter rainfall index of the Western Mediterranean (Ait Brahim et al., 2019). Solar minima are taken from the solar irradiance curve (Steinhilber et al., 2012). Black arrows show peaks in organic matter content from this study. Blue bars and the integer numbers indicate north Atlantic cold events (Bond et al., 1997, 2001); orange pale bars indicate arid period (5.2 ka, Bond Event 4); yellow bars indicate the Roman-Iberian Climate Optimum (RCO) and Medieval Climate Anomaly (MCA) periods; orange and green colors correspond to multi-decadal arid and humid time spans, respectively, within the MCA (Ait Brahim et al., 2018); the purple bar indicates a suspected flooding event(s) that might correspond with the Bond event 4.2 ka. Changes in the wedge architecture of the main barrage-cascade (Height/width ratio, H/W) and the accommodation evolution are indicated. Other abbreviations: HTM: Holocene Thermal Maximum; MHT: Mid-Holocene Transition.

5.2.1.2 Late Holocene

To address the relationship between the sedimentary process on the studied site and the climate variability during the Late Holocene, a pollen-based quantitative reconstruction study carried out by Nourelbait et al. (2016) at lake Hachlaf (1700m a.s.l.) about 20km away from Imouzzer Kandar was applied. The two sites are within the same meridian; hence, they are not influenced by the E-W drought gradient in the Middle Atlas (the continental effect), which makes the comparison more valuable (*see* locations, Fig. 1A). To ensure the reliability of this relationship, we tested whether these reconstructions have a regional significance or if they depict simply a local effect. Indeed, the authors assume that a reorganization in the main ecosystem and a change in winter precipitation with

progressive increase after ca. 3.7 cal kyr B.P. has been established (Nourelbait et al., 2016). This transition corresponds with a synoptic-scale reorganization in the inter-gyre transport pathways and in the westerly winds belt in the North Atlantic, which is expressed by a southward shift of the Azores Front and the installation of a pervasive negative NAO-like state (Repschläger et al., 2017; Ait Brahim et al., 2019), although with a slight time lag (hysteresis) which may correspond to the vegetation time response (Fig. 12). This reorganization has been reported globally in other synoptic-scale oscillations (e.g., ENSO, PDO), being linked with the North American Monsoon (Jones et al., 2015) and other monsoon systems (McRobie et al., 2015), together with high oscillation within a background southward migration of the ITCZ (Haug et al., 2001). Furthermore, the progressive increase in the pollen-inferred winter temperature (*see* their Fig. 3) fits the orbitally-forced increase in winter insolation at latitude 33°N (Laskar et al., 2004). Hence, the reconstruction data from lake Hachlaf confirm that they reflect a more regional signal, and the onset of the transgressive interval reported from Imouzzer Kandar reflects the aforementioned Late Holocene reorganization (Fig. 12).

5.2.1.2.1 Transgressive interval (between ca. 4 and ca. 2.7 cal kyr B.P.)

The reconstructed annual precipitation (Nourelbait et al., 2016; Fig. 12) indicates a noticeable peak around 4.2 ka. According to that, and regarding its stratigraphic position (above the dated layer to ca. 4.6 ka; Figs. 2, 5F), the sequence boundary surface may correspond with this period (see flooding event(s), Fig. 12). Indeed, this is well reported in the literature as the 4.2 ka cold event (Bond et al., 1997, 2001; Wanner et al., 2011; Bini et al., 2019) and correspond with moderate moist winters in the Middle Atlas (Ait Brahim et al., 2019; Zielhofer et al., 2019). Thus, such cool and moist conditions might have prevented tufa growth and enabled erosion phases that conditioned a fifth-order sequence boundary highlighting the transgressive interval.

Afterward, the reconstruction results show a lower precipitation seasonality index (SI) linked to wetter summertime and less enhanced winter precipitation (Nourelbait et al., 2016). This SI increase progressively until ca. 2.7 ka where it reaches the value 6. Under these regional-scale conditions, and regarding the inferred transgressive interval that would correspond to this period (the MFS is dated to ca. 2.7 cal kyr B.P.; Figs. 2, 5, 11B), it is concluded that the aggradation pattern at the knickpoint may have been enhanced through wetter summer conditions. As the annual precipitation was less enhanced (though with moist summer), and considering that higher tufa growth is more enhanced during the warm season (Vázquez-Urbez et al., 2010; Arenas et al., 2014a; Auqué et al., 2014), it is assumed that during summertime the relatively high summer insolation (compared to the period after ca. 2.7 cal kyr B.P.) along with moist conditions and less hydrological stress would have favored mosses and other

phototrophic organisms to colonize the surface nearby the aquatic zone including the knickpoints (Fig. 11B). Indeed, the high density of the bacterial filaments, forming the light composite laminae of the oncoidal cortex, suggests optimal conditions during the warmer seasons at the beginning of this interval (i.e., at ca., 4 ka. BP), thus reporting the aforementioned synoptic-scale reorganization. Moreover, as the landscape was colonized by dense conifers forest (Cheddadi et al., 1998; Nourelbait et al., 2016, 2014; Campbell et al., 2017), this would have accelerated the dissolution of dolomitic bedrock and the leaching of Ca^{2+} and HCO^{3-} (and Mg^{2+} regarding the Ca-Mg-HCO_3 composition of the regional water-table according to Gourari et al., 2000) which would reach through percolation, along with dissolved CO_2, the groundwater. Moreover, the relatively stable and low values of K/Al ratio (Fig. 2), which is likely to reflect the illite/kaolinite ratio (Burnett et al., 2011; Yarincik et al., 2000) and the moderated concentration of the dolomite and quartz phases, suggesting drained conditions, within this interval are prone to witness this chemical weathering. All of these factors would have enhanced the encrustation process and led to the acceleration rate of the vertical stacking of the barrage-cascade, which would have conditioned the transgressive interval in the dammed area.

5.2.1.2.2 Highstand interval (between ca. 2.7 and ca. 0.3 cal kyr B.P.)

The period after ca. 2.7 cal kyr B.P. indicates a steady SI around 6, low summer precipitation (around 70 mm/season), and relatively high winter precipitation (around 210 mm/season) (Nourelbait et al., 2016). This period chronologically corresponds with the highstand interval inferred from the sequence analysis between the two dated layers (Fig. 5, 10). In particular, the peak at 2 cal kyr B.P. of the reconstructed annual precipitation is prone to reflect a regional climate optimum-like period. Indeed, this has been depicted from lacustrine sediments to infer high lake levels in the Middle Atlas (Lamb and van der Kaars, 1995; Lamb et al., 1999; Détriché et al., 2009; Abdellah et al., 2021) and correspond with the well-known Roman Climate Optimum period (RCO, or Iberian-Roman Humid Period, Fig. 12; Martín-Puertas et al., 2009). The stromatolites, a component of the buttresses in the downstream stretch, evinced high discharge through the occurrence of periodic macrocrystalline composite laminae with well-defined enlarged crystals, and several micro-scale dissolution/erosion surfaces. Periodic higher discharge is witnessed on the meso- and large-scale as well, with the occurrence of periodic erosion surfaces (Fig. 6E-G). Therefore, it is suggested that the development of buttresses and macrocrystalline laminae was favored during the RCO. Otherwise, the high-frequency facies fluctuation between Lo and C at the upper part of the highstand interval may mirror (at least partially) the dry/cold periods within the Medieval Climate Anomaly (MCA) and the Little Ice Age

(LIA) reported from regional studies (Fig. 12) (Esper et al., 2007; Wassenburg et al., 2013; Ait Brahim et al., 2017, 2018; Abdellah et al., 2021).

By examining the long-term trend, tufa deposits have shown a high sensibility level to the millennial timescale climate forcing. However, this overall trend is superimposed by abrupt periods that interrupt calcification (periodic occurrence of facies C).

5.2.2 Abrupt climate change: possible solar imprints and/or internal forcing cyclicity within tufa records

On the "basin-scale", the sedimentologic record (log1 and log2) exhibits a periodic formation of the organic-rich layer, facies C, with a low (high) frequency of occurrence before (after) 2.7 cal kyr B.P. The presence of this stratum within the background process of calcite (bio)precipitation indicates more likely abrupt changes in paleo-environmental/-climatic conditions, which may be the linear response of regional forcing or may reflect, simply, a local effect. Indeed, the strict correspondence, within age errors, of the two dated organic-rich layers (at ca. 2.7 ± 0.02 and ca. 4.6 ± 0.14 cal kyr B.P.; table 1) with the well-known Bond Events 2 and 3 (Bond et al., 1997, 2001) testify the high sensitivity of the site to external forcing mechanisms; this may overcome the disadvantage of the lack of dating in this study and permit the discussion of the multi-centennial scale climate variability. Among these external forcing, the volcanic and solar forcing were shown to be the most dominant drivers of the abrupt events during the last 2.7 ka (including the 2.7 ka event; PAGES 2k Consortium, 2013; Wanner et al., 2015; Kobashi et al., 2017). Indeed, the events 2.7 ka, 1.4 ka, and the LIA coincide with Grand Solar Minima (Steinhilber et al., 2012). The volcanic and solar implications in triggering or amplifying cooling conditions during this period may be favored through the background reduction in the orbitally-paced insolation (Berger and Loutre, 1991; Laskar et al., 2004) and amplified through internal positive feedbacks (Moffa-Sánchez et al., 2014; Kobashi et al., 2017). This makes suitable these events to be recorded in the study area and may explain then the high-frequency of occurrence of the facies C after and not before ca. 2.7 ± 0.02 cal kyr B.P.

Studies from the Middle Atlas have reported that cold and humid multi-decadal periods coincide with solar minima during the last MCA-LIA oscillation (Fig. 12; Wassenburg et al., 2013; Ait Brahim et al., 2017, 2018). According to that, the high-frequency occurrence of facies C, observed at the upper part of the highstand interval in log1 and log2 (Figs. 6C, S2), was likely to be in resonance with solar minima (Fig. 12). The relatively high diversity with low densities of *I. bradyi* and *I. inermis* within the two sampled organic-rich layers in association with phytoclasts (IM18 and IM21, Fig. 2), together with the macro-charcoal morphotypes that exhibit reworking features (IM18, Fig. 4C), may reflect

more humid conditions (marshy subenvironment) under a relative ventilated water column with regards to the previously deposited ones, fen (IM06, Figs. 2, 5G) and sapropel (IM13, Figs. 2, 5H) deposits. These match the regional insights (Fig. 12; Wassenburg et al., 2013; Ait Brahim, 2017). On the other hand, the high density of the running water and spring species *I. bradyi* (ca. 70%) at ca. 2.7 ± 0.02 cal kyr B.P. (IM13, Fig. 2) corroborates the cooler character of the event and may further indicate relatively humid conditions (limited evaporation), since it might implicate, regarding the low abundance and diversity of ostracods (Fig. 2), a reworking process from a nearby spring (probably "Ain Sultan", Fig. 1B) according to Meisch (2000). Indeed, this cold event has been reported in the Middle Atlas (Ait Brahim et al., 2019), and was shown to coincide with a pervasive negative NAO-like pattern in the North-Atlantic realm (Olsen et al., 2012), and to have impacted both hemispheres (Chambers et al., 2007). Accordingly, tufa within enlarged barrage and extensive dammed area is suitable to imprint the respective multi-centennial and multi-millennial Vries-Suess- and Hallstatt-type solar cycles (Steinhilber et al., 2009, 2012; Suess, 1980), already reported from regional studies based on high-resolution ostracod- and speleothems-derived $\delta^{18}O$ (Zielhofer et al., 2017a; Ait Brahim et al., 2018, 2019).

As for the event 4.6 ka, this globally coincides with pervasive high solar irradiance (Steinhilber et al., 2012) and low explosive volcanic eruptions (Kobashi et al., 2017), which suggest that the peaty layer (i.e., IM06, Figs. 2, 5F) may mirror a rather internal forcing of the global climate system (e.g., AMOC oscillation; Schulz et al., 2007; Denton and Broecker, 2008; Thornalley et al., 2009). This abrupt event has been shown from previous studies to coincide with a pervasive positive NAO-like state (Olsen et al., 2012; Ait Brahim et al., 2019), which favored relevant conditions (cold and relatively dry conditions) for fen development, although the abrupt character of the event has prevented this mire type to evolve towards the ombrotrophic mire.

6 Conclusions

In this work, we present a case study of a tufa record in a basin-like setting that involves an enlarged barrage and extensive dammed area from a karstic region in Northwest Africa. We demonstrate that the tufa deposition in this region is highly influenced by climate variability on millennial and multi-centennial timescales over the last 5 kyr B.P. During warmer periods (before ca. 2.7 ± 0.14 cal kyr B.P.), it is inferred that the vertical tufa growth at the barrage was more enhanced (aggradation pattern), which resulted in the deposition of shallow lacustrine facies association at the dammed area behind the barrage (transgressive interval). Contrariwise, during cooler conditions (after ca. 2.7 ± 0.14 cal kyr

B.P.), a more lateral tufa growth (progradation pattern) took place, inducing fluvial-marshy-palustrine facies associations (highstand interval). Furthermore, a multi-centennial scale period with optimum conditions has been recorded (Roman Climate Optimum) and is expected to have favored active overflowing and buttress development at the downstream-facing of the enlarged barrage-cascade. Moreover, our tufa record have a high potential to capture abrupt climate changes, including the Bond event 4.6 ka (2.7 ka), synchronous with pervasive positive (negative) NAO-like pattern, and hence dry (humid) conditions that would have favored fen (sapropel) development.

Finally, we highlight that the climate is the main control on the tufa growth, distribution and character, especially through determining and inferring the vertical stacking variability of a single wedge-shaped architecture that involves enlarged barrage-cascade and extensive dammed-area. Hence, it is highly recommended to reconsider tufa as a valuable archive for deciphering signals of past climate variability, not only the orbital- and millennial-scale signals but also on multi-centennial abrupt changes.

Supplement material

1 Age/depth model

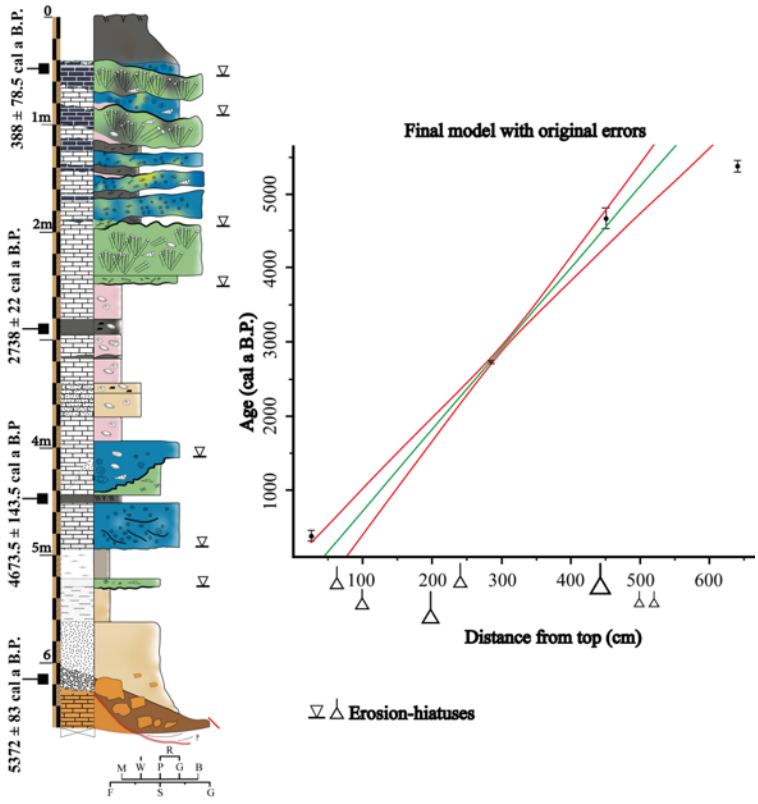


Figure S1. *Log1 and age/depth model. Note the position of the erosion-hiatuses alongside the log and the age model. Note also the high uncertainty of the constructed model that it did not consider erosion-hiatuses; for example, (i) the age uncertainty, at depth 75cm is circa 400 annum which is very high, and (ii) the large margin of negative age values below 70cm. Also, the model considered the fourth dated sample as aberrant (5372 ± 83 cal. a BP), which is not correct in our sense, since both the material and the equipment used for the dating is of high accuracy to give a relevant result.*

2 Facies associations in log2 (N33° 43' 54.15"; W5° 0' 41.35")

2.1 Palustrine FAs: P1 and P2

P1 exhibits a succession of organic-rich facies (C), phytoclasts (Lph), oncoids (Lo) and boundstones of coated stems (Lst1) capped by a paleosol (P), in which Lo (small oncoids) shows massive structures with symmetrical cortex. **P2** starts with facies Lst1 in association with phytoclasts which passes vertically to facies C in association with phytoclasts that contains bioturbation features (Fig. S2).

P1 and **P2** are interpreted to reflect palustrine-marshy conditions. **P1** is likely indicative of hydrodynamic fluctuations in shallow conditions. In fact, organic-rich phytoclasts (facies C, Lph) reflects marshy rather than miry conditions (i.e., without peat formation; Rydin et al., 2013) with low water energy and relatively higher residence time in shallower conditions with regards to other organic-rich layers placed bellow (the peaty and sapropel ones). Upward, subspherical oncoids with symmetrical cortex without channelized structures are thought to reflect more dynamic conditions (e.g., low-energy wind-induced waves) in a lacustrine margin subenvironment. Facies Lst1 reflects palustrine conditions mirroring optimal hydrodynamic which allows the formation and preservation of the coated vertical stems (Arenas-Abad et al., 2010). Likewise, the base of **P2** (Figs. S2, 7) suggests low-energy and shallower conditions that would allow formation and preservation of coated vertical stems (Lst1). However, the occurrence in association of Lph and Lst1 suggests periodic relatively high-water energy, leading to partial breakage of Lst1. Upward, marshy conditions are reflected by the association of both facies C and Lph, and the bioturbation features (Figs. S2, 7).

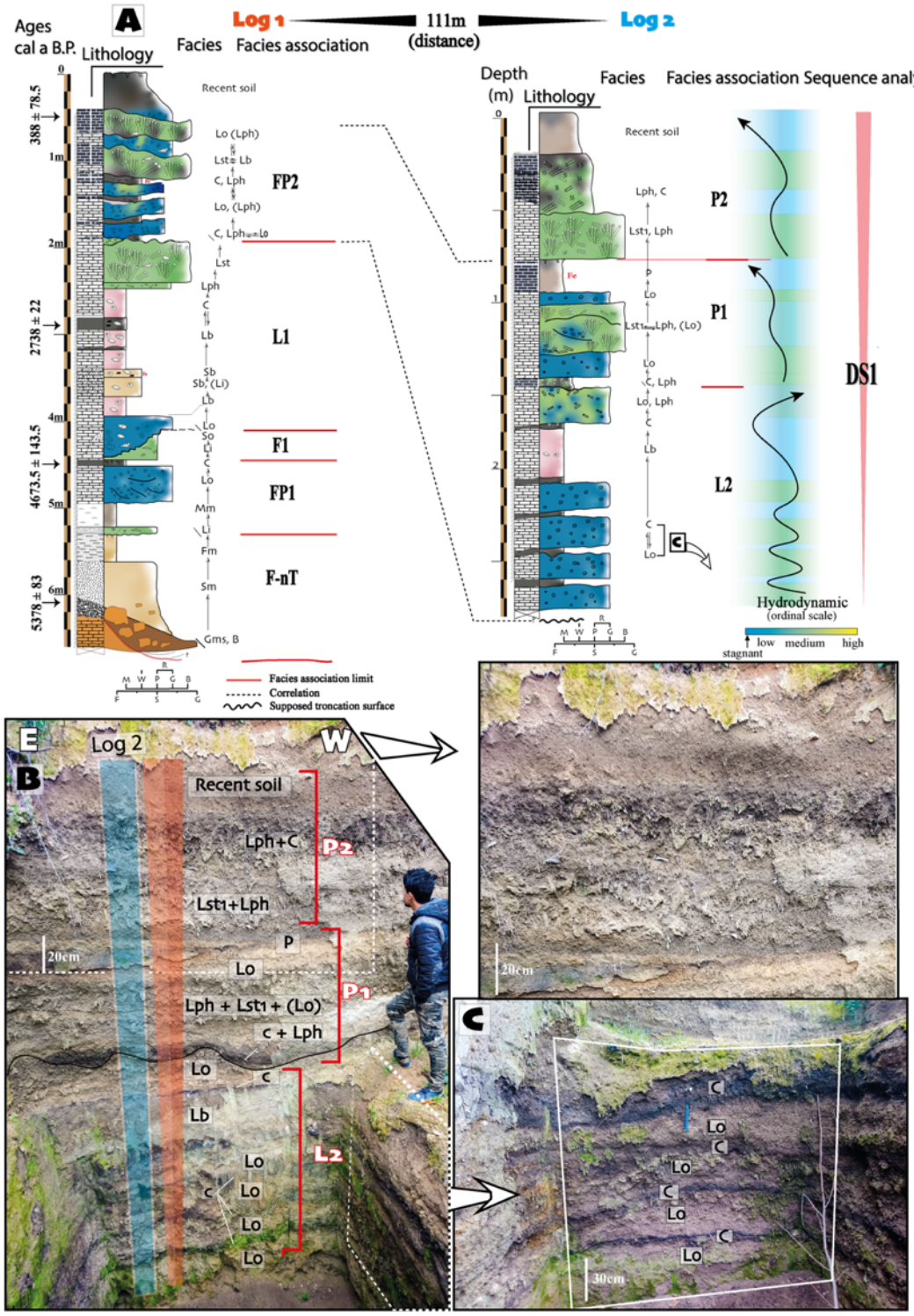


Figure S2. *Upstream-stretch (see for location **Fig. 1C**). Meso-scale field views of the facies and facies associations (FAs) of log2. **A**: Correlation between log1 and log2 based on lithologic similarities and dipping of layers. Note the difference in depth scale of both stratigraphic sections. **B**: Field view showing the vertical succession of facies and FAs of log2. **C**: Field view of the lower part of **B** showing alternation of facies Lo and C. Note the high frequency occurrence of facies C at the hole stratigraphic section marking the upper part of basin-fill deposits. Facies and facies association codes in **Table 2** and **Figure 7**, respectively. Texture and lithology of the stratigraphic section in **Figure 2** caption.*

2.2 Palustrine-lacustrine FA: L2

L2 shows somewhat the same vertical tendency compared to **L1** (*see* Figs. 5, 7), whereas the facies Lst1 is replaced here by Lph (Fig. S2).

L2 represents marginal (shore) and central (offshore) lacustrine subenvironment fluctuations. At the bottom, the alternation of facies C and Lo is likely related to variations in lacustrine margin hydrodynamic. Thus, the transition from facies C to Lo would have mirrored the transition from quiet water conditions with higher residence time (marshy conditions) under cooler temperatures (calcite precipitation interruption), towards more dynamic (e.g., low-energy wind-induced waves) and warmer conditions and still shallow water with more opening conditions. In the middle, the bioclastic limestones (Lb) reflects a progressive pattern towards shallow central (offshore) lacustrine conditions (Vázquez-Urbez et al., 2013). The association of both facies Lo and Lph at the top is most likely reflecting relatively higher and regular hydrodynamics which allowed the symmetric cortex to develop (Lo) and prevented the preservation of vertical coated stems (producing Lph).

3 Facies association in log3 (N33° 44' 12.27"; W5° 0' 54.96"): Barrage cascade FA (B-C)

There is only one facies association in log3, to which we refer to as "**B-C**" (Figs. S3, 7). From bottom to top, this starts with rudstones of phytoclasts (Lph) which are overcame first by floatstones of oncoids (Lo), and then by rudstones of oncoids and phytoclasts (Lo, Lph; Fig. S3). Upward, these are capped by boundstones of bryophytes (Lbr) in association with phytoclasts, and with vertical and lateral alternation with intraclasts (Li), phytoclasts (Lph), oncoidal sands (So), phytoherm of curtains stems (Lst2), and stromatolites (Ls) (Fig. S3E, G, F). Otherwise, the small cascades formed by bryophytes stacking in association with hanging coated stems and stromatolites, were observed at the sloped-stretch (*see* field views, Fig. 11C).

B-C reflects the downstream-facing of barrage-cascade deposits (Pedley, 1990). Indeed, phytoclasts, here, is most likely related to breaks of previous coated stems, which are developed most likely close to outflow points of shallow marginal area following flooding events. It is suspected that a previous aggradation pattern has been performed at the knickpoint (i.e., a sharp change in topographic gradient located upstream close to log3) creating the space upstream for sedimentation. Thus, during periods of low discharge and subsequent low overflowing, palustrine (or lacustrine marginal) conditions may develop close to the knickpoint with subsequent hygrophilous vegetation. Upward, oncoids are thought to be indicative of actively overflowing from the knickpoint, which are synchronous with erosion periods basinward following high discharge. On the other hand, the occurrence of bryophytes at the second half of log3 reflects most likely a prograding pattern in

relatively slow and regular flowing water conditions (Pedley, 1990). The small cascades observed on the sloped-stretch are related to irregularities in the topography caused by collapses and reworkings of some macro-debris (e.g., trunks). These build-ups create buttresses (*sensu* Pedley, 1990) in the downstream-facing of the barrage (Pedley, 1990; Pla-Pueyo et al., 2017).

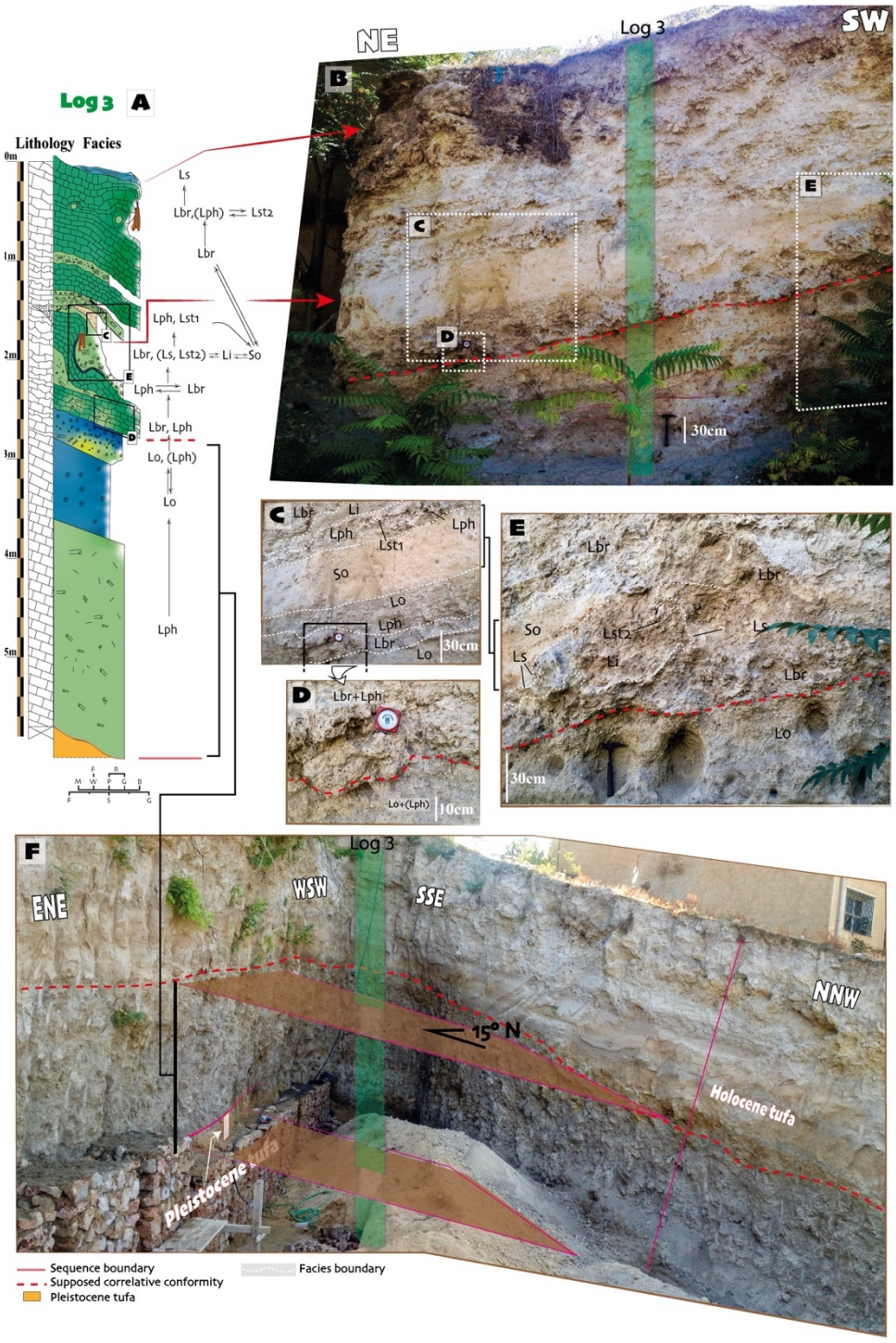


***Figure S3**. sloped-stretch (see for location **Fig. 1C**). **A**: Stratigraphic section (log3) measured from the sloped-stretch. **B**: Field view showing the dip-oriented layers and locations of facies and build-ups presented in log3. **C**: Close-up view of A*

*showing facies type at the middle part of the stratigraphic section. **D**: close-up view indicating bryophytes (Lbr) in association with phytoclasts (Lph). **E**: Meso-scale field view showing small barrage build-up, with the dominance of bryophytes (Lbr), phytoclasts (Lph), stromatolites (Ls) and the sporadic occurrence of hanging stems (Lst2). **F**: field view showing the dip of layers that represent the downstream-facing of the main barrage, and the major sequence boundary that delineates Pleistocene- and Holocene-tufa. Facies codes in **Table 2**; texture and lithology of the stratigraphic section in **Figure 2** caption.*

4 Facies associations in log4 (N33° 44' 17.03"; W5° 1' 5.80"): fluvial FAs (F2 and F3)

F2 consist of the deposition at the base of intraclasts (Li) and shows a transition towards, first, phytoclasts in association with oncoids, then sub-millimetric oncoids (So; Figs. S4, 7). Sporadic subareal exposure features such as marmorization and bioturbations were identified at the summit of **F2** (Fig. S4). **F3** consists of oncoids that exhibit a coarsening upward. According to Ordóñez and Cura (1983), the coarsening upward of oncoids in **F3** (Fig. S4) may be related to an increase of width/depth channel ratio with a limited suspended load or to channel migration, which may mirror the braided style model of Pedley (1990) downstream barrages.

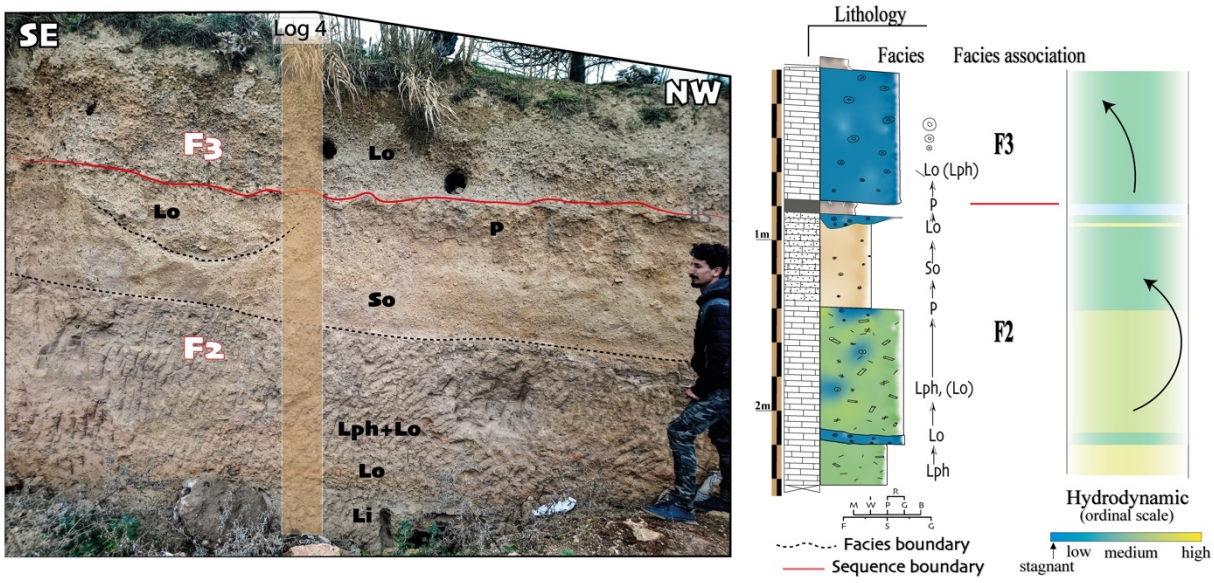


***Figure S4**. Downstream-stretch (see for location **Fig. 1C**). Field view and the corresponding log4. Facies and facies association codes in **Table 2** and **Figure 7**, respectively. Texture and lithology of the stratigraphic section in **Figure 2** caption.*

Acknowledgments

The dating and analysis carried out in this work were supported by the presidency of the University Sidi Mohamed Ben Abdellah; and the Engineering Laboratory of Organometallic, Molecular Materials and Environment, Faculty of Sciences Dhar Mahraz. We would like to thank Fransesc Mezquita-Joanes for his fruitful discussions concerning the ostracod determination and ecological significances, and Hicham el Asmi for his help in the preparation of thin sections. We appreciate the help of Amine Couscous in the radiocarbon dating procedure. We cordially thank Alexis Nutz, the anonymous reviewer and the associate editor Alexander Dickson for their insightful comments and suggestions.

References

Abdellah, H.I., Vidal, L., Benkaddour, A., Rhoujjati, A., Jouve, G., Tachikawa, K., Sonzogni, C., Mazur, J.-C., Paillès, C., Sylvestre, F., 2021. Palaeohydrological changes recorded from a small Moroccan Middle Atlas pond during the last 6000 cal. yr BP: a multi-proxy study. Journal of Paleolimnology 1–19.

Ahmamou, M., Conrad, G., Plaziat, J.-C., 1989. Réinterprétation des conditions de dépôt des calcaires fluviatiles, lacustres et palustres du bassin plio-quaternaire du Saïss de Fès (Maroc). Méditerranée 68, 41–49.

Ait Brahim, Y., 2017. Speleothem records decadal to multidecadal hydroclimate variations in southwestern Morocco during the last millennium. Earth Planet. Sci. Lett. 476. https://doi.org/10.1016/j.epsl.2017.07.045

Ait Brahim, Y., Wassenburg, J.A., Cruz, F.W., Sifeddine, A., Scholz, D., Bouchaou, L., Dassié, E.P., Jochum, K.P., Edwards, R.L., Cheng, H., 2018. Multi-decadal to centennial hydro-climate variability and linkage to solar forcing in the Western Mediterranean during the last 1000 years. Sci Rep 8, 17446. https://doi.org/10.1038/s41598-018-35498-x

Ait Brahim, Y., Wassenburg, J.A., Sha, L., Cruz, F.W., Deininger, M., Sifeddine, A., Bouchaou, L., Spötl, C., Edwards, R.L., Cheng, H., 2019. North Atlantic Ice-Rafting, Ocean and Atmospheric Circulation During the Holocene: Insights From Western Mediterranean Speleothems. Geophysical Research Letters 46, 7614–7623.

Allison, L.E., 1965. Organic Carbon, in: Methods of Soil Analysis. John Wiley & Sons, Ltd, pp. 1367–1378. https://doi.org/10.2134/agronmonogr9.2.c39

Andrews, J.E., 2006. Palaeoclimatic records from stable isotopes in riverine tufas: synthesis and review. Earth-Science Reviews 75, 85–104.

Arboleya, M.L., Teixell, A., Charroud, M., Julivert, M., 2004. A structural transect through the High and Middle Atlas of Morocco. Journal of African Earth Sciences, Key Points on African Geology 39, 319–327. https://doi.org/10.1016/j.jafrearsci.2004.07.036

Arenas, C., Auqué, L., Osácar, C., Sancho, C., Lozano, M.V., Vázquez-Urbez, M., Pardo, G., 2015. Current tufa sedimentation in a high discharge river: a comparison with other synchronous tufa records in the Iberian Range (Spain). Sedimentary Geology 325, 132–157.

Arenas, C., Cabrera, L., Ramos, E., 2007. Sedimentology of tufa facies and continental microbialites from the Palaeogene of Mallorca Island (Spain). Sedimentary Geology 197, 1–27. https://doi.org/10.1016/j.sedgeo.2006.08.009

Arenas, C., Jones, B., 2017. Temporal and environmental significance of microbial lamination: Insights from Recent fluvial stromatolites in the River Piedra, Spain. Sedimentology 64, 1597–1629. https://doi.org/10.1111/sed.12365

Arenas, Concha, Piñuela, L., García-Ramos, J.C., 2015. Climatic and tectonic controls on carbonate deposition in syn-rift siliciclastic fluvial systems: A case of microbialites and associated facies in the Late Jurassic. Sedimentology 62, 1149–1183. https://doi.org/10.1111/sed.12182

Arenas, C., Vázquez-Urbez, M., Auqué, L., Sancho, C., Osácar, C., Pardo, G., 2014a. Intrinsic and extrinsic controls of spatial and temporal variations in modern fluvial tufa sedimentation: A thirteen-year record from a semi-arid environment. Sedimentology 61, 90–132.

Arenas, C., Vázquez-Urbez, M., Pardo, G., Sancho, C., 2014b. Sedimentology and depositional architecture of tufas deposited in stepped fluvial systems of changing slope: Lessons from the Quaternary Añamaza valley (Iberian Range, Spain). Sedimentology 61, 133–171. https://doi.org/10.1111/sed.12053

Arenas-Abad, C., Vázquez-Urbez, M., Pardo-Tirapu, G., Sancho-Marcén, C., 2010. Chapter 3 Fluvial and Associated Carbonate Deposits, in: Developments in Sedimentology. Elsevier, pp. 133–175. https://doi.org/10.1016/S0070-4571(09)06103-2

Arp, G., Bissett, A., Brinkmann, N., Cousin, S., De Beer, D., Friedl, T., Mohr, K.I., Neu, T.R., Reimer, A., Shiraishi, F., 2010. Tufa-forming biofilms of German karstwater streams: microorganisms, exopolymers, hydrochemistry and calcification. Geological Society, London, Special Publications 336, 83–118.

Auqué, L., Arenas, C., Osácar, C., Pardo, G., Sancho, C., Vázquez-Urbez, M., 2014. Current tufa sedimentation in a changing-slope valley: the River Añamaza (Iberian Range, NE Spain). Sedimentary Geology 303, 26–48.

Baali, A., 1998. Genèse et évolution au Plio-Quaternaire de deux bassins intramontagneux en domaine carbonaté méditerranéen. Les bassins versants des dayets Afourgagh et Agoulmam (Moyen Atlas, Maroc) (Thèse Doct. Etat). Thèse d'Etat, Univ. Sidi Mohammed Ben Abdallah, Fès.

Baali, A., Cheddadi, R., Chairi, R., 2007. Evolution sédimentologique, pédologique et paléoclimatique du bassin lacustre de la dayet Agoulmam (Moyen Atlas, Maroc) depuis le Pléistocène (Soltanien) à l'Holocène. Revue Méditerranéenne de l'Environnement 267–280.

Babault, J., Teixell, A., Arboleya, M.L., Charroud, M., 2008. A Late Cenozoic age for long-wavelength surface uplift of the Atlas Mountains of Morocco. Terra Nova 20, 102–107. https://doi.org/10.1111/j.1365-3121.2008.00794.x

Berger, A., Loutre, M.F., 1991. Insolation values for the climate of the last 10 million years. Quaternary Science Reviews 10, 297–317. https://doi.org/10.1016/0277-3791(91)90033-Q

Berrendero, E., Arenas, C., Mateo, P., Jones, B., 2016. Cyanobacterial diversity and related sedimentary facies as a function of water flow conditions: Example from the Monasterio de Piedra Natural Park (Spain). Sedimentary Geology 337, 12–28. https://doi.org/10.1016/j.sedgeo.2016.03.003

Bini, M., Zanchetta, G., Perşoiu, A., Cartier, R., Català, A., Cacho, I., Dean, J.R., Di Rita, F., Drysdale, R.N., Finnè, M., Isola, I., Jalali, B., Lirer, F., Magri, D., Masi, A., Marks, L., Mercuri, A.M., Peyron, O., Sadori, L., Sicre, M.-A., Welc, F., Zielhofer, C., Brisset, E., 2019. The 4.2 ka BP Event in the Mediterranean region: an overview. Clim. Past 15, 555–577. https://doi.org/10.5194/cp-15-555-2019

Bohacs, K.M., Carroll, A.R., Neal, J.E., Mankiewicz, P.J., 2000. Lake-basin type, source potential, and hydrocarbon character: an integrated sequence-stratigraphic-geochemical framework. Lake basins through space and time: AAPG Studies in Geology 46, 3–34.

Bohacs, K.M., Grabowski Jr, G.J., Carroll, A.R., Mankiewicz, P.J., Miskell-Gerhardt, K.J., Schwalbach, J.R., Wegner, M.B., Simo, J.T., 2005. Production, destruction, and dilution—the many paths to source-rock development.

Bond, G., Kromer, B., Beer, J., Muscheler, R., Evans, M.N., Showers, W., Hoffmann, S., Lotti-Bond, R., Hajdas, I., Bonani, G., 2001. Persistent solar influence on North Atlantic climate during the Holocene. science 294, 2130–2136.

Bond, G., Showers, W., Cheseby, M., Lotti, R., Almasi, P., DeMenocal, P., Priore, P., Cullen, H., Hajdas, I., Bonani, G., 1997. A pervasive millennial-scale cycle in North Atlantic Holocene and glacial climates. science 278, 1257–1266.

Bosch, D., Maury, R.C., El Azzouzi, M., Bollinger, C., Bellon, H., Verdoux, P., 2014. Lithospheric origin for Neogene–Quaternary Middle Atlas lavas (Morocco): Clues from trace elements and Sr–Nd–Pb–Hf isotopes. Lithos 205, 247–265. https://doi.org/10.1016/j.lithos.2014.07.009

Bosmans, J.H.C., Drijfhout, S.S., Tuenter, E., Hilgen, F.J., Lourens, L.J., Rohling, E.J., 2015. Precession and obliquity forcing of the freshwater budget over the Mediterranean. Quaternary Science Reviews 123, 16–30. https://doi.org/10.1016/j.quascirev.2015.06.008

Bosmans, J.H.C., Drijfhout, S.S., Tuenter, E., Lourens, L.J., Hilgen, F.J., Weber, S.L., 2012. Monsoonal response to mid-holocene orbital forcing in a high resolution GCM. Climate of the Past 8, 723–740. https://doi.org/10.5194/cp-8-723-2012

Bosmans, J.H.C., Ent, R.J. van der, Haarsma, R.J., Drijfhout, S.S., Hilgen, F.J., 2020. Precession- and Obliquity-Induced Changes in Moisture Sources for Enhanced Precipitation Over the Mediterranean Sea. Paleoceanography and Paleoclimatology 35, e2019PA003655. https://doi.org/10.1029/2019PA003655

Brasier, A.T., Andrews, J.E., Kendall, A.C., 2011. Diagenesis or dire genesis? The origin of columnar spar in tufa stromatolites of central Greece and the role of chironomid larvae. Sedimentology 58, 1283–1302. https://doi.org/10.1111/j.1365-3091.2010.01208.x

Brogi, A., Capezzuoli, E., Kele, S., Baykara, M.O., Shen, C.-C., 2017. Key travertine tectofacies for neotectonics and palaeoseismicity reconstruction: effects of hydrothermal overpressured fluid injection. Journal of the Geological Society 174, 679–699. https://doi.org/10.1144/jgs2016-124

Brogi, A., Capezzuoli, E., Moretti, M., Olvera-García, E., Matera, P.F., Garduno-Monroy, V.-H., Mancini, A., 2018. Earthquake-triggered soft-sediment deformation structures (seismites) in travertine deposits. Tectonophysics 745, 349–365. https://doi.org/10.1016/j.tecto.2018.08.021

Burnett, A.P., Soreghan, M.J., Scholz, C.A., Brown, E.T., 2011. Tropical East African climate change and its relation to global climate: a record from Lake Tanganyika, Tropical East Africa, over the past 90+ kyr. Palaeogeography, Palaeoclimatology, Palaeoecology 303, 155–167.

Campbell, J.F.E., Fletcher, W.J., Joannin, S., Hughes, P.D., Rhanem, M., Zielhofer, C., 2017. Environmental Drivers of Holocene Forest Development in the Middle Atlas, Morocco. Front. Ecol. Evol. 5. https://doi.org/10.3389/fevo.2017.00113

Capezzuoli, E., Gandin, A., Pedley, M., 2014. Decoding tufa and travertine (fresh water carbonates) in the sedimentary record: the state of the art. Sedimentology 61, 1–21.

Catuneanu, O., 2020. Chapter 23 - Sequence stratigraphy, in: Scarselli, N., Adam, J., Chiarella, D., Roberts, D.G., Bally, A.W. (Eds.), Regional Geology and Tectonics (Second Edition). Elsevier, pp. 605–686. https://doi.org/10.1016/B978-0-444-64134-2.00021-3

Catuneanu, O., 2006. Principles of sequence stratigraphy, 1st ed. ed, Developments in sedimentology. Elsevier, Amsterdam ; Boston.

Catuneanu, O., Abreu, V., Bhattacharya, J.P., Blum, M.D., Dalrymple, R.W., Eriksson, P.G., Fielding, C.R., Fisher, W.L., Galloway, W.E., Gibling, M.R., Giles, K.A., Holbrook, J.M., Jordan, R., Kendall, C.G.St.C., Macurda, B., Martinsen, O.J., Miall, A.D., Neal, J.E., Nummedal, D., Pomar, L., Posamentier, H.W., Pratt, B.R., Sarg, J.F., Shanley, K.W., Steel, R.J., Strasser, A., Tucker, M.E., Winker, C., 2009. Towards the standardization of sequence stratigraphy. Earth-Science Reviews 92, 1–33. https://doi.org/10.1016/j.earscirev.2008.10.003

Chambers, F.M., Mauquoy, D., Brain, S.A., Blaauw, M., Daniell, J.R., 2007. Globally synchronous climate change 2800 years ago: proxy data from peat in South America. Earth and Planetary Science Letters 253, 439–444.

Charrière, A., 1990. Héritage hercynien et évolution géody- namique alpine d'une chaîne intracontinentale : le Moyen Atlas au sud-est de Fes (Maroc). Thèse de Doctorat d'État, Université Toulouse III – Paul Sabatier, Toulouse, 589 p.

Charrière, A., 1989. Carte géologique à 1/100 000, Feuille de Sefrou. Notes et Mém. Serv. géol. Maroc 354.

Cheddadi, R., Mamakowa, K., Guiot, J., De Beaulieu, J.-L., Reille, M., Andrieu, V., Granoszewski, W., Peyron, O., 1998. Was the climate of the Eemian stable? A quantitative climate reconstruction from seven European pollen records. Palaeogeography, Palaeoclimatology, Palaeoecology 143, 73–85.

Chen, J., Zhang, D.D., Wang, S., Xiao, T., Huang, R., 2004. Factors controlling tufa deposition in natural waters at waterfall sites. Sedimentary Geology 166, 353–366.

Clift, P.D., Wan, S., Blusztajn, J., 2014. Reconstructing chemical weathering, physical erosion and monsoon intensity since 25 Ma in the northern South China Sea: a review of competing proxies. Earth-Science Reviews 130, 86–102.

Conedera, M., Tinner, W., Neff, C., Meurer, M., Dickens, A.F., Krebs, P., 2009. Reconstructing past fire regimes: methods, applications, and relevance to fire management and conservation. Quaternary Science Reviews 28, 555–576.

Cremaschi, M., Zerboni, A., Spötl, C., Felletti, F., 2010. The calcareous tufa in the Tadrart Acacus Mt. (SW Fezzan, Libya): An early Holocene palaeoclimate archive in the central Sahara. Palaeogeography, Palaeoclimatology, Palaeoecology 287, 81–94. https://doi.org/10.1016/j.palaeo.2010.01.019

Currie, B.S., 1997. Sequence stratigraphy of nonmarine Jurassic–Cretaceous rocks, central Cordilleran foreland-basin system. Geological Society of America Bulletin 109, 1206–1222.

Dabkowski, J., 2011. Analyse géochimique des tufs calcaires en domaine fluviatile ouest européen : reconstitution de variations des paléotempératures et des paléoprécipitations au cours des interglaciaires des stades 11 et 5 (These de doctorat). Paris, Muséum national d'histoire naturelle.

Dabkowski, J., Antoine, P., Limondin-Lozouet, N., Chaussé, C., Carbonel, P., 2010. Les microfaciès du tuf calcaire Eemien (SIM 5e) de Caours (Somme, France): éléments d'analyse paléoécologique du dernier interglaciaire. Quaternaire. Revue de l'Association française pour l'étude du Quaternaire 21, 127–137.

Dabkowski, Julie, Brou, L., Naton, H.-G., 2015. New stratigraphic and geochemical data on the Holocene environment and climate from a tufa deposit at Direndall (Mamer Valley, Luxembourg). The Holocene 25, 1153–1164. https://doi.org/10.1177/0959683615580183

Dabkowski, J., Royle, S.H., Antoine, P., Marca-Bell, A., Andrews, J.E., 2015. High-resolution δ18O seasonality record in a French Eemian tufa stromatolite (Caours, Somme Basin). Palaeogeography, Palaeoclimatology, Palaeoecology 438, 277–284. https://doi.org/10.1016/j.palaeo.2015.08.017

Davies, S.J., Lamb, H.F., Roberts, S.J., 2015. Micro-XRF core scanning in palaeolimnology: recent developments, in: Micro-XRF Studies of Sediment Cores. Springer, pp. 189–226.

Davis, B.A.S., Stevenson, A.C., 2007. The 8.2ka event and Early–Mid Holocene forests, fires and flooding in the Central Ebro Desert, NE Spain. Quaternary Science Reviews 26, 1695–1712. https://doi.org/10.1016/j.quascirev.2007.04.007

Defarge, C., Trichet, J., 1995. From biominerals to" organominerals": The example of the modern lacustrine calcareous stromatolites from Polynesian atolls. BULLETIN-INSTITUT OCEANOGRAPHIQUE MONACO-NUMERO SPECIAL- 265–272.

Denton, G.H., Broecker, W.S., 2008. Wobbly ocean conveyor circulation during the Holocene? Quaternary Science Reviews 27, 1939–1950.

Détriché, S., Bréhéret, J.-G., Soulié-Märsche, I., Karrat, L., Macaire, J.-J., 2009. Late Holocene water level fluctuations of Lake Afourgagh (Middle-Atlas Mountains, Morocco) inferred from charophyte remains. Palaeogeography, palaeoclimatology, palaeoecology 283, 134–147.

Dreimanis, A., 1962. Quantitative gasometric determination of calcite and dolomite by using Chittick apparatus. Journal of Sedimentary Research 32, 520–529. https://doi.org/10.1306/74D70D08-2B21-11D7-8648000102C1865D

du Dresnay, R., 1988. Recent data on the geology of the Middle-Atlas (Morocco), in: Jacobshagen, V.H. (Ed.), The Atlas System of Morocco, Lecture Notes in Earth Sciences. Springer Berlin Heidelberg, Berlin, Heidelberg, pp. 293–320. https://doi.org/10.1007/BFb0011598

Dupraz, C., Reid, R.P., Braissant, O., Decho, A.W., Norman, R.S., Visscher, P.T., 2009. Processes of carbonate precipitation in modern microbial mats. Earth-Science Reviews, Microbial Mats in Earth's Fossil Record of Life: Geobiology 96, 141–162. https://doi.org/10.1016/j.earscirev.2008.10.005

Edvardsson, J., Stoffel, M., Corona, C., Bragazza, L., Leuschner, H.H., Charman, D.J., Helama, S., 2016. Subfossil peatland trees as proxies for Holocene palaeohydrology and palaeoclimate. Earth-Science Reviews 163, 118–140. https://doi.org/10.1016/j.earscirev.2016.10.005

El Bouch, A., 1994. Les travertins du Saïs de Fès et du Causse d'Imouzzère (Maroc nord central): paléoenvironnements quaternaires et anthropisation (These de doctorat). Aix-Marseille 1.

Enache, M.D., Cumming, B.F., 2007. Charcoal morphotypes in lake sediments from British Columbia (Canada): an assessment of their utility for the reconstruction of past fire and precipitation. J Paleolimnol 38, 347–363. https://doi.org/10.1007/s10933-006-9084-8

Enache, M.D., Cumming, B.F., 2006. Tracking recorded fires using charcoal morphology from the sedimentary sequence of Prosser Lake, British Columbia (Canada). Quaternary Research 65, 282–292.

Ennadifi, Y., Boudda, A., du Dresnay, R., Morin, P., Suter, G., 1975. Carte g´eologique a 1/ 100 000, Feuille d'El Hajeb. In: Notes et M´em. Serv. g´eol. Maroc, p. 160.

Esper, J., Frank, D., Buntgen, U., Verstege, A., Luterbacher, J., 2007. Long-term drought severity variations in Morocco. Geophys. Res. Lett. 34. https://doi.org/10.1029/2007GL030844

FAO, 2020. Standard operating procedure for soil organic carbon. Walkley-Black method: titration and colorimetric method. FAO, Rome, Italy.

Favre, P., Stampfli, G., Wildi, W., 1991. Jurassic sedimentary record and tectonic evolution of the northwestern corner of Africa. Palaeogeography, Palaeoclimatology, Palaeoecology, Palaeogeography and Paleoceanography of Tethys 87, 53–73. https://doi.org/10.1016/0031-0182(91)90130-J

Fletcher, W.J., Debret, M., Goñi, M.F.S., 2013. Mid-Holocene emergence of a low-frequency millennial oscillation in western Mediterranean climate: Implications for past dynamics of the North Atlantic atmospheric westerlies. The Holocene 23, 153–166.

Freytet, P., 2000. Distribution and palaeoecology of non marine algae and stromatolites: II, the limagne of allier Oligo-Miocene lake (central France). Annales de Paléontologie 86, 3–57. https://doi.org/10.1016/S0753-3969(00)88723-6

Freytet, P., 1997. Non marine Permian to Holocene algae from France and adjacent country. Part 1. Annales de pal´eontologie (VertInvert) 83, 289–332.

Freytet, P., 1998. Non-marine, Permian to Holocene algae from France and adjacent countries: Part II. Annales de Paléontologie 84, 3–51. https://doi.org/10.1016/S0753-3969(98)80001-3

Freytet, P., 1992. Les cristallisations de calcite associées à des restes végétaux (algues, feuilles) en milieu fluviatile et lacustre, actuel et ancien (tufs et travertins). Bulletin de la Société Botanique de France. Actualités Botaniques 139, 69–74.

Freytet, P., Plet, A., 1996. Modern freshwater microbial carbonates: thePhormidium stromatolites (tufa-travertine) of southeastern Burgundy (Paris Basin, France). Facies 34, 219. https://doi.org/10.1007/BF02546166

Frizon de Lamotte, D.F., Leturmy, P., Missenard, Y., Khomsi, S., Ruiz, G., Saddiqi, O., Guillocheau, F., Michard, A., 2009. Mesozoic and Cenozoic vertical movements in the Atlas system (Algeria, Morocco, Tunisia): An overview. Tectonophysics, The geology of vertical movements of the lithosphere 475, 9–28. https://doi.org/10.1016/j.tecto.2008.10.024

Golubić, S., Violante, C., Plenković-Moraj, A., Grgasović, T., 2008. Travertines and calcareous tufa deposits: an insight into diagenesis. Geologia Croatica 61, 363–378.

Goudie, A.S., Viles, H.A., Pentecost, A., 1993. The late-Holocene tufa decline in Europe. The Holocene 3, 181–186.

Gourari, L., 2001. Etude hydrochimique, morphologique, lithostratigraphique, sédimentologique et pétrographique des dépôts travertino-détritiques actuels et plio-quaternaire du bassin karstique de l'oued Aggaï (Causse de Sefrou Moyen Atlas, Maroc). These Doctorat d'Etat, Université de Fes.

Gourari, L., Alaoui-Mhamdi, M., Boushaba, A., Fedan, B., 2000. Variations des paramètres physico-chimiques des eaux de l'Oued Aggai: significations géo-environnementales et conséquences sur la précipitation des travertins actuels (causse de Sefrou, Moyen-Atlas - Maroc). Journal of African Earth Sciences 30, 283–293. https://doi.org/10.1016/S0899-5362(00)00020-8

Gradziński, M., 2010. Factors controlling growth of modern tufa: results of a field experiment. Geological Society, London, Special Publications 336, 143–191.

Gradziński, M., Bella, P., Holubek, P., 2018. Constructional caves in freshwater limestone: A review of their origin, classification, significance and global occurrence. Earth-Science Reviews 185, 179–201.

Griffiths, H.I., Pedley, H.M., 1995. Did changes in late Last Glacial and early Holocene atmospheric CO2 concentrations control rates of tufa precipitation? The Holocene 5, 238–242.

Hägele, D., Leinfelder, R., Grau, J., Burmeister, E.-G., Struck, U., 2006. Oncoids from the river Alz (southern Germany): tiny ecosystems in a phosphorus-limited environment. Palaeogeography, Palaeoclimatology, Palaeoecology 237, 378–395.

Hamdani, N., Baali, A., 2019. Fracture network mapping using Landsat 8 OLI data and linkage with the karst system: a case study of the Moroccan Central Middle Atlas. Remote Sensing in Earth Systems Sciences 2, 1–17.

Hanneman, D.L., Wideman, C.J., 2010. Chapter 5 Continental Sequence Stratigraphy and Continental Carbonates, in: Alonso-Zarza, A.M., Tanner, L.H. (Eds.), Developments in Sedimentology, Carbonates in Continental Settings: Geochemistry, Diagenesis and Applications. Elsevier, pp. 215–273. https://doi.org/10.1016/S0070-4571(09)06205-0

Haug, G., Hughen, K., Sigman, D., Peterson, L., Rohl, U., 2001. Southward migration of the intertropical convergence zone through the Holocene. Science 293. https://doi.org/10.1126/science.1059725

Holbrook, J., Scott, R.W., Oboh-Ikuenobe, F.E., 2006. Base-level buffers and buttresses: a model for upstream versus downstream control on fluvial geometry and architecture within sequences. Journal of Sedimentary Research 76, 162–174.

Holmes, J.A., 2001. Ostracoda, in: Smol, J.P., Birks, H.J.B., Last, W.M. (Eds.), Tracking Environmental Change Using Lake Sediments. Springer Netherlands, Dordrecht, pp. 125–151. https://doi.org/10.1007/0-306-47671-1_7

Huber, U.M., Markgraf, V., 2003. Holocene Fire Frequency and Climate Change at Rio Rubens Bog, Southern Patagonia, in: Veblen, T.T., Baker, W.L., Montenegro, G., Swetnam, T.W. (Eds.), Fire and Climatic Change in Temperate Ecosystems of the Western Americas, Ecological Studies. Springer, New York, NY, pp. 357–380. https://doi.org/10.1007/0-387-21710-X_13

Jimenez-Lopez, C., Chekroun, K.B., Jroundi, F., Rodríguez-Gallego, M., Arias, J.M., González-Muñoz, M.T., 2011. Myxococcus xanthus Colony Calcification: An Study to Better Understand the Processes Involved in the Formation of this Stromatolite-Like Structure, in: Reitner, J., Quéric, N.-V., Arp, G. (Eds.), Advances in Stromatolite Geobiology, Lecture Notes in Earth Sciences. Springer, Berlin, Heidelberg, pp. 161–181. https://doi.org/10.1007/978-3-642-10415-2_11

Jones, B., Peng, X., 2014. Multiphase calcification associated with the atmophytic cyanobacterium Scytonema julianum. Sedimentary Geology 313, 91–104. https://doi.org/10.1016/j.sedgeo.2014.09.002

Jones, M.D., Metcalfe, S.E., Davies, S.J., Noren, A., 2015. Late Holocene climate reorganisation and the North American Monsoon. Quaternary Science Reviews 124, 290–295. https://doi.org/10.1016/j.quascirev.2015.07.004

Kano, A., Kawai, T., Matsuoka, J., Ihara, T., 2004. High-resolution records of rainfall events from clay bands in tufa. Geology 32, 793–796. https://doi.org/10.1130/G20736.1

Keighley, D., Flint, S., Howell, J., Moscariello, A., 2003. Sequence Stratigraphy in Lacustrine Basins: A Model for Part of the Green River Formation (Eocene), Southwest Uinta Basin, Utah, U.S.A. Journal of Sedimentary Research 73, 987–1006. https://doi.org/10.1306/050103730987

Knippertz, P., Christoph, M., Speth, P., 2003. Long-term precipitation variability in Morocco and the link to the large-scale circulation in recent and future climates. Meteorology and Atmospheric physics 83, 67–88.

Kobashi, T., Menviel, L., Jeltsch-Thömmes, A., Vinther, B.M., Box, J.E., Muscheler, R., Nakaegawa, T., Pfister, P.L., Döring, M., Leuenberger, M., 2017. Volcanic influence on centennial to millennial Holocene Greenland temperature change. Scientific reports 7, 1–10.

Köppen, W., 1900. Versuch einer Klassifikation der Klimate, vorzugsweise nach ihren Beziehungen zur Pflanzenwelt. (Schluss). Geographische Zeitschrift 6, 657–679.

Kottek, M., Grieser, J., Beck, C., Rudolf, B., Rubel, F., 2006. World Map of the Köppen-Geiger climate classification updated. Meteorologische Zeitschrift 259–263. https://doi.org/10.1127/0941-2948/2006/0130

Kylander, M.E., Ampel, L., Wohlfarth, B., Veres, D., 2011. High-resolution X-ray fluorescence core scanning analysis of Les Echets (France) sedimentary sequence: new insights from chemical proxies. Journal of Quaternary Science 26, 109–117.

Lamb, H., Roberts, N., Leng, M., Barker, P., Benkaddour, A., van der Kaars, S., 1999. Lake evolution in a semi-arid montane environment: response to catchment change and hydroclimatic variation. Journal of Paleolimnology 21, 325–343. https://doi.org/10.1023/A:1008099602205

Lamb, H.F., Gasse, F., Benkaddour, A., El Hamouti, N., Van der Kaars, S., Perkins, W.T., Pearce, N.J., Roberts, C.N., 1995. Relation between century-scale Holocene arid intervals in tropical and temperate zones. Nature 373, 134–137.

Lamb, H.F., van der Kaars, S., 1995. Vegetational response to Holocene climatic change: pollen and palaeolimnological data from the Middle Atlas, Morocco. The Holocene 5, 400–408. https://doi.org/10.1177/095968369500500402

Laskar, J., 2004. A long-term numerical solution for the insolation quantities of the Earth. Astron. Astrophys. 428. https://doi.org/10.1051/0004-6361:20041335

Laville, E., Pique, A., Amrhar, M., Charroud, M., 2004. A restatement of the Mesozoic Atlasic Rifting (Morocco). Journal of African Earth Sciences 38, 145–153. https://doi.org/10.1016/j.jafrearsci.2003.12.003

Love, K.M., Chafetz, H.S., 1988. Diagenesis of laminated travertine crusts, Arbuckle Mountains, Oklahoma. Journal of Sedimentary Research 58, 441–445. https://doi.org/10.1306/212F8DB4-2B24-11D7-8648000102C1865D

Magny, M., Combourieu-Nebout, N., De Beaulieu, J.-L., Bout-Roumazeilles, V., Colombaroli, D., Desprat, S., Francke, A., Joannin, S., Ortu, E., Peyron, O., 2013. North–south palaeohydrological contrasts in the central Mediterranean during the Holocene: tentative synthesis and working hypotheses. Climate of the Past 9, 2043–2071.

Manzo, E., Perri, E., Tucker, M.E., 2012. Carbonate deposition in a fluvial tufa system: processes and products (Corvino Valley – southern Italy). Sedimentology 59, 553–577. https://doi.org/10.1111/j.1365-3091.2011.01266.x

Martin, J., 1981. Le Moyen Atlas central étude géomorphologique. Editions du Service géologique du Maroc.

Martini, I., Capezzuoli, E., 2014. Interdigitated fluvial clastic deposits and calcareous tufa testifying an uplift of the catchment area: An example from the Pianizzoli area (southern Tuscany, Italy). Sedimentary Geology 299, 60–73. https://doi.org/10.1016/j.sedgeo.2013.11.001

Martín-Puertas, C., Valero-Garcés, B.L., Brauer, A., Mata, M.P., Delgado-Huertas, A., Dulski, P., 2009. The Iberian–Roman Humid Period (2600–1600 cal yr BP) in the Zoñar Lake varve record (Andalucía, southern Spain). Quaternary Research 71, 108–120.

Mazzini, I., Gliozzi, E., Rossetti, G., Pieri, V., 2014. The Ilyocypris puzzle: A multidisciplinary approach to the study of phenotypic variability. International Review of Hydrobiology 99, 395–408.

McRobie, F.H., Stemler, T., Wyrwoll, K.-H., 2015. Transient coupling relationships of the Holocene Australian monsoon. Quaternary Science Reviews 121, 120–131. https://doi.org/10.1016/j.quascirev.2015.05.011

Meisch, C., 2000. Freshwater Ostracoda of western and central Europe. Süsswasserfauna von Mitteleuropa 8/3. Spektrum, Gustav Fischer, Heidelberg; Berlin.

Merz-Preiß, M., Riding, R., 1999. Cyanobacterial tufa calcification in two freshwater streams: ambient environment, chemical thresholds and biological processes. Sedimentary Geology 126, 103–124.

Mezquita, F., Griffiths, H.I., Sanz, S., Soria, J.M., Piñón, A., 1999. Ecology and distribution of ostracods associated with flowing waters in the eastern Iberian Peninsula. Journal of Crustacean Biology 19, 344–354.
Miall, A., 2014. Fluvial Depositional Systems, Springer Geology. Springer International Publishing, Cham. https://doi.org/10.1007/978-3-319-00666-6
Miall, A.D., 1977. A review of the braided-river depositional environment. Earth-Science Reviews 13, 1–62. https://doi.org/10.1016/0012-8252(77)90055-1
Miall, A.D., Postma, G., 1997. The Geology of Fluvial Deposits, Sedimentary Facies, Basin Analysis and Petroleum Geology. Sedimentary Geology 110, 149.
Michard, A., Saddiqi, O., Chalouan, A., Lamotte, D.F. de (Eds.), 2008. Continental Evolution: The Geology of Morocco: Structure, Stratigraphy, and Tectonics of the Africa-Atlantic-Mediterranean Triple Junction, Lecture Notes in Earth Sciences. Springer-Verlag, Berlin Heidelberg. https://doi.org/10.1007/978-3-540-77076-3
Missenard, Y., Zeyen, H., Frizon de Lamotte, D., Leturmy, P., Petit, C., Sébrier, M., Saddiqi, O., 2006. Crustal versus asthenospheric origin of relief of the Atlas Mountains of Morocco. Journal of Geophysical Research: Solid Earth 111. https://doi.org/10.1029/2005JB003708
Moffa-Sánchez, P., Born, A., Hall, I.R., Thornalley, D.J.R., Barker, S., 2014. Solar forcing of North Atlantic surface temperature and salinity over the past millennium. Nature Geoscience 7, 275–278. https://doi.org/10.1038/ngeo2094
Mustaphi, C.J.C., Pisaric, M.F.J., 2014. A classification for macroscopic charcoal morphologies found in Holocene lacustrine sediments. Progress in Physical Geography: Earth and Environment 38, 734–754. https://doi.org/10.1177/0309133314548886
Nanson, G.C., Croke, J.C., 1992. A genetic classification of floodplains. Geomorphology 4, 459–486.
Nourelbait, M., Rhoujjati, A., Benkaddour, A., Carré, M., Eynaud, F., Martinez, P., Cheddadi, R., 2016. Climate change and ecosystems dynamics over the last 6000 years in the Middle Atlas, Morocco. Clim. Past 12, 1029–1042. https://doi.org/10.5194/cp-12-1029-2016
Nourelbait, M., Rhoujjati, A., Eynaud, F., Benkaddour, A., Dezileau, L., Wainer, K., Goslar, T., Khater, C., Tabel, J., Cheddadi, R., 2014. An 18 000-year pollen and sedimentary record from the cedar forests of the Middle Atlas, Morocco: POLLEN/SEDIMENTARY RECORD FROM THE MIDDLE ATLAS. J. Quaternary Sci. 29, 423–432. https://doi.org/10.1002/jqs.2708
Nutz, A., Kwiecien, O., Breitenbach, S.F.M., Cai, Y., Porta, G.D., Danisch, J., Kabiri, L., Bodin, S., 2019. Fluvio-lacustrine sedimentation in the Agadir-Tissint Feija (Anti-Atlas, Morocco): A promising palaeoclimate archive for the last glacial cycle in northwest Africa. The Depositional Record 5, 362–387. https://doi.org/10.1002/dep2.65
Olsen, J., Anderson, N.J., Knudsen, M.F., 2012. Variability of the North Atlantic Oscillation over the past 5,200 years. Nature Geoscience 5, 808–812.
Ordóñez, S., Cura, M.A.G. del, 1983. Recent and Tertiary Fluvial Carbonates in Central Spain, in: Modern and Ancient Fluvial Systems. John Wiley & Sons, Ltd, pp. 485–497. https://doi.org/10.1002/9781444303773.ch39
Ouarhache, D., 1987. Etude geologique dans le paleozoique et le trias de la bordure nw du cauuse moyen-atlasique (s et w de fes,maroc) (These de doctorat). Toulouse 3.
Ouarhache, D., Charriere, A., Chalot-prat, F., Wartiti, M.E., 2012. Triassic to early Liassic continental rifting chronology and process at the southwest margin of the Alpine Tethys (Middle Atlas and High Moulouya, Morocco); correlations with the Atlantic rifting, synchronous and diachronous. Bulletin de la Societe Geologique de France 183, 233–249. https://doi.org/10.2113/gssgfbull.183.3.233
Owen, G., Moretti, M., Alfaro, P., 2011. Recognising triggers for soft-sediment deformation: current understanding and future directions. Sedimentary Geology 235, 133–140.
PAGES 2k Consortium, 2013. Continental-scale temperature variability during the past two millennia. Nature Geoscience 6, 339–346. https://doi.org/10.1038/ngeo1797
Patterson, W.A., Edwards, K.J., Maguire, D.J., 1987. Microscopic charcoal as a fossil indicator of fire. Quaternary Science Reviews 6, 3–23. https://doi.org/10.1016/0277-3791(87)90012-6
Pedley, H.M., 1990. Classification and environmental models of cool freshwater tufas. Sedimentary Geology 68, 143–154.
Pedley, M., 2009. Tufas and travertines of the Mediterranean region: a testing ground for freshwater carbonate concepts and developments. Sedimentology 56, 221–246.

Pedley, M., 2000. Ambient Temperature Freshwater Microbial Tufas, in: Riding, R.E., Awramik, S.M. (Eds.), Microbial Sediments. Springer, Berlin, Heidelberg, pp. 179–186. https://doi.org/10.1007/978-3-662-04036-2_20
Pedley, M., 1992. Freshwater (phytoherm) reefs: the role of biofilms and their bearing on marine reef cementation. Sedimentary Geology 79, 255–274.
Pedley, M., Andrews, J., Ordonez, S., del Cura, M.A.G., Martin, J.-A.G., Taylor, D., 1996. Does climate control the morphological fabric of freshwater carbonates? A comparative study of Holocene barrage tufas from Spain and Britain. Palaeogeography, Palaeoclimatology, Palaeoecology 121, 239–257.
Piqué, A., Laville, E., 1996. The central Atlantic rifting: Reactivation of Palaeozoic structures? Journal of Geodynamics 21, 235–255. https://doi.org/10.1016/0264-3707(95)00022-4
Pla-Pueyo, S., Viseras, C., Henares, S., Yeste, L.M., Candy, I., 2017. Facies architecture, geochemistry and palaeoenvironmental reconstruction of a barrage tufa reservoir analog (Betic Cordillera, S. Spain). Quaternary International 437, 15–36.
Platt, N.H., Wright, V.P., 1991. Lacustrine Carbonates: Facies Models, Facies Distributions and Hydrocarbon Aspects, in: Lacustrine Facies Analysis. John Wiley & Sons, Ltd, pp. 57–74. https://doi.org/10.1002/9781444303919.ch3
Poquet, J.M., Mesquita, F., 2011. Combined effects of local environment and continental biogeography on the distribution of Ostracoda. Freshwater Biology 56, 448–469.
Ramsey, C.B., Lee, S., 2013. Recent and Planned Developments of the Program OxCal. Radiocarbon 55, 720–730.
Reimer, P.J., Austin, W.E., Bard, E., Bayliss, A., Blackwell, P.G., Ramsey, C.B., Butzin, M., Cheng, H., Edwards, R.L., Friedrich, M., 2020. The IntCal20 Northern Hemisphere radiocarbon age calibration curve (0–55 cal kBP). Radiocarbon 62, 725–757.
Renssen, H., Seppä, H., Crosta, X., Goosse, H., Roche, D.M., 2012. Global characterization of the Holocene Thermal Maximum. Quaternary Science Reviews 48, 7–19. https://doi.org/10.1016/j.quascirev.2012.05.022
Renssen, H., Seppä, H., Heiri, O., Roche, D.M., Goosse, H., Fichefet, T., 2009. The spatial and temporal complexity of the Holocene thermal maximum. Nature Geosci 2, 411–414. https://doi.org/10.1038/ngeo513
Repschläger, J., Garbe-Schönberg, D., Weinelt, M., Schneider, R., 2017. Holocene evolution of the North Atlantic subsurface transport. Climate of the Past 13, 333–344.
Rosenbaum, G., Lister, G.S., Duboz, C., 2002. Relative motions of Africa, Iberia and Europe during Alpine orogeny. Tectonophysics 359, 117–129. https://doi.org/10.1016/S0040-1951(02)00442-0
Rydin, H., Jeglum, J.K., Bennett, K.D., 2013. The biology of peatlands, 2e. Oxford university press.
Sancho, C., Arenas, C., Vázquez-Urbez, M., Pardo, G., Lozano, M.V., Peña-Monné, J.L., Hellstrom, J., Ortiz, J.E., Osácar, M.C., Auqué, L., Torres, T., 2015. Climatic implications of the Quaternary fluvial tufa record in the NE Iberian Peninsula over the last 500ka. Quaternary Research 84, 398–414. https://doi.org/10.1016/j.yqres.2015.08.003
Scholz, D., Hoffmann, D.L., 2011. StalAge – an algorithm designed for construction of speleothem age models. Quat. Geochronol. 6. https://doi.org/10.1016/j.quageo.2011.02.002
Schulz, M., Prange, M., Klocker, A., 2007. Low-frequency oscillations of the Atlantic Ocean meridional overturning circulation in a coupled climate model. Climate of the Past 3, 97–107.
Seilacher, A., 1969. Fault-graded beds interpreted as seismites. Sedimentology 13, 155–159.
Sha, L., Brahim, Y.A., Wassenburg, J.A., Yin, J., Peros, M., Cruz, F.W., Cai, Y., Li, H., Du, W., Zhang, H., Edwards, R.L., Cheng, H., 2019. How Far North Did the African Monsoon Fringe Expand During the African Humid Period? Insights From Southwest Moroccan Speleothems. Geophysical Research Letters 46, 14093–14102. https://doi.org/10.1029/2019GL084879
Shanley, K.W., McCabe, P.J., 1994. Perspectives on the sequence stratigraphy of continental strata. AAPG bulletin 78, 544–568.
Shiraishi, F., Okumura, T., Takahashi, Y., Kano, A., 2010. Influence of microbial photosynthesis on tufa stromatolite formation and ambient water chemistry, SW Japan. Geochimica et Cosmochimica Acta 74, 5289–5304.
Steinhilber, F., Abreu, J.A., Beer, J., Brunner, I., Christl, M., Fischer, H., Heikkilä, U., Kubik, P.W., Mann, M., McCracken, K.G., 2012. 9,400 years of cosmic radiation and solar activity from ice cores and tree rings. Proceedings of the National Academy of Sciences 109, 5967–5971.

Steinhilber, F., Beer, J., Fröhlich, C., 2009. Total solar irradiance during the Holocene. Geophysical Research Letters 36.
Suess, H.E., 1980. The radiocarbon record in tree rings of the last 8000 years. Radiocarbon. 22. https://doi.org/10.1017/S0033822200009462
Tabel, J., Khater, C., Rhoujjati, A., Dezileau, L., Bouimetarhan, I., Carre, M., Vidal, L., Benkaddour, A., Nourelbait, M., Cheddadi, R., 2016. Environmental changes over the past 25 000 years in the southern Middle Atlas, Morocco: PAST ENVIRONMENTAL CHANGES IN MOROCCO. J. Quaternary Sci. 31, 93–102. https://doi.org/10.1002/jqs.2841
Teixell, A., Ayarza, P., Zeyen, H., Fernàndez, M., Arboleya, M.-L., 2005. Effects of mantle upwelling in a compressional setting: the Atlas Mountains of Morocco. Terra Nova 17, 456–461. https://doi.org/10.1111/j.1365-3121.2005.00633.x
Tennevin, M., 1978. Paysages Karstiques du Moyen Atlas Septentrional. Méditerranée 32, 23–32. https://doi.org/10.3406/medit.1978.1767
Thornalley, D.J., Elderfield, H., McCave, I.N., 2009. Holocene oscillations in temperature and salinity of the surface subpolar North Atlantic. Nature 457, 711–714.
Toker, E., 2017. Quaternary fluvial tufas of Sarıkavak area, southwestern Turkey: Facies and depositional systems. Quaternary International, Non-marine Carbonates: A Multidisciplinary Approach 437, 37–50. https://doi.org/10.1016/j.quaint.2016.06.034
Turner, E.C., Jones, B., 2005. Microscopic calcite dendrites in cold-water tufa: implications for nucleation of micrite and cement. Sedimentology 52, 1043–1066. https://doi.org/10.1111/j.1365-3091.2005.00741.x
Vázquez-Urbez, M., Arenas, C., Pardo, G., 2012. A sedimentary facies model for stepped, fluvial tufa systems in the Iberian Range (Spain): the Quaternary Piedra and Mesa valleys. Sedimentology 59, 502–526.
Vázquez-Urbez, M., Arenas, C., Pardo, G., Pérez-Rivarés, J., 2013. The Effect of Drainage Reorganization and Climate On the Sedimentologic Evolution of Intermontane Lake Systems: The Final Fill Stage of the Tertiary Ebro Basin (Spain) SEDIMENTOLOGY OF THE FINAL FILL STAGE OF THE TERTIARY EBRO BASIN. Journal of Sedimentary Research 83, 562–590.
Vázquez-Urbez, M., Arenas, C., Sancho, C., Osácar, C., Auqué, L., Pardo, G., 2010. Factors controlling present-day tufa dynamics in the Monasterio de Piedra Natural Park (Iberian Range, Spain): depositional environmental settings, sedimentation rates and hydrochemistry. International Journal of Earth Sciences 99, 1027–1049.
Viles, H.A., Goudie, A.S., 1990. Tufas, travertines and allied carbonate deposits. Progress in Physical Geography 14, 19–41.
Wackenheim, Q., Limondin-Lozouet, N., Dabkowski, J., Boudad, L., Berger, J.-F., 2020. Reconstructing Mid-Holocene palaeoenvironmental dynamic in the Middle Atlas (Morocco) inferred from non-marine molluscs succession of the Aït Said ou Idder tufa sequence. Quaternaire. Revue de l'Association française pour l'étude du Quaternaire 145–164.
Walker, M., Head, M.J., Lowe, J., Berkelhammer, M., BjÖrck, S., Cheng, H., Cwynar, L.C., Fisher, D., Gkinis, V., Long, A., Newnham, R., Rasmussen, S.O., Weiss, H., 2019. Subdividing the Holocene Series/Epoch: formalization of stages/ages and subseries/subepochs, and designation of GSSPs and auxiliary stratotypes. Journal of Quaternary Science. https://doi.org/10.1002/jqs.3097
Walkley, A., Black, I.A., 1934. AN EXAMINATION OF THE DEGTJAREFF METHOD FOR DETERMINING SOIL ORGANIC MATTER, AND A PROPOSED MODIFICATION OF THE CHROMIC ACID TITRATION METHOD. Soil Science 37, 29–38.
Wanner, H., Beer, J., Bütikofer, J., Crowley, T.J., Cubasch, U., Flückiger, J., Goosse, H., Grosjean, M., Joos, F., Kaplan, J.O., Küttel, M., Müller, S.A., Prentice, I.C., Solomina, O., Stocker, T.F., Tarasov, P., Wagner, M., Widmannm, M., 2008. Mid- to Late Holocene climate change: an overview. Quat Sci Rev 27. https://doi.org/10.1016/j.quascirev.2008.06.013
Wanner, H., Mercolli, L., Grosjean, M., Ritz, S.P., 2015. Holocene climate variability and change; a data-based review. Journal of the Geological Society 172, 254–263. https://doi.org/10.1144/jgs2013-101
Wanner, H., Solomina, O., Grosjean, M., Ritz, S.P., Jetel, M., 2011. Structure and origin of Holocene cold events. Quaternary Science Reviews 30, 3109–3123. https://doi.org/10.1016/j.quascirev.2011.07.010
Wassenburg, J.A., 2016. Major reorganization of the North Atlantic Oscillation during Early Holocene deglaciation. Nat. Geosci. 9. https://doi.org/10.1038/ngeo2767

Wassenburg, J.A., 2013. Moroccan speleothem and tree ring records suggest a variable positive state of the North Atlantic Oscillation during the Medieval Warm Period. Earth Planet. Sci. Lett. 375. https://doi.org/10.1016/j.epsl.2013.05.048

Yarincik, K.M., Murray, R.W., Peterson, L.C., 2000. Climatically sensitive eolian and hemipelagic deposition in the Cariaco Basin, Venezuela, over the past 578,000 years: Results from Al/Ti and K/Al. Paleoceanography 15, 210–228.

Zhang, D.D., Zhang, Y., Zhu, A., Cheng, X., 2001. Physical mechanisms of river waterfall tufa (travertine) formation. Journal of Sedimentary Research 71, 205–216.

Zhang, J., Wang, H., Liu, Z., An, D., Dreybrodt, W., 2012. Spatial–temporal variations of travertine deposition rates and their controlling factors in Huanglong Ravine, China – A world's heritage site. Applied Geochemistry 27, 211–222. https://doi.org/10.1016/j.apgeochem.2011.10.005

Zielhofer, C., Fletcher, W.J., Mischke, S., De Batist, M., Campbell, J.F., Joannin, S., Tjallingii, R., El Hamouti, N., Junginger, A., Stele, A., 2017a. Atlantic forcing of Western Mediterranean winter rain minima during the last 12,000 years. Quaternary Science Reviews 157, 29–51.

Zielhofer, C., Köhler, A., Mischke, S., Benkaddour, A., Mikdad, A., Fletcher, W.J., 2019. Western Mediterranean hydro-climatic consequences of Holocene ice-rafted debris (Bond) events. Climate of the Past 15, 463–475. https://doi.org/10.5194/cp-15-463-2019

Zielhofer, C., von Suchodoletz, H., Fletcher, W.J., Schneider, B., Dietze, E., Schlegel, M., Schepanski, K., Weninger, B., Mischke, S., Mikdad, A., 2017b. Millennial-scale fluctuations in Saharan dust supply across the decline of the African Humid Period. Quaternary Science Reviews 171, 119–135. https://doi.org/10.1016/j.quascirev.2017.07.010

CHAPITRE VI

SYNTHÈSE ET CONCLUSIONS

Synthèse

L'exploit des objectifs définis dans ce projet de doctorat est livré dans les trois chapitres précédents. L'extraction du contrôle tectonique sur la sédimentation via l'analyse des structures de déformations synsédimentaires ('*soft-sediment déformation structures*', SSDSs) depuis le Stade Isotopique-3 (MIS-3) est aboutie dans le chapitre 3 (Azennoud et al., 2022b), alors que le contrôle climatique sur celle-ci est déchiffré au moyen de l'approche sédimentologique et stratigraphique séquentielle, combinée à une approche multi-proxy, est communiquée dans le chapitre 4 (Azennoud et al., *Under Review*). Ces deux chapitres ont livré l'exemple d'un bassin lacustre où l'accommodation potentielle (maximale), et donc la dépression, est principalement contrôlée par les pulsations cumulatives du jeu de la faille maîtresse bordière du bassin, créant une structure en hémi-graben. Le chapitre 5 (Azennoud et al., 2022a) présente un cas typique où à la fois la sédimentation et l'espace disponible pour celle-ci pendant les dernières 5 ka BP ont été fondamentalement forcés par les paramètres climatiques (température estivale, contraste saisonnier des précipitations) dans un contexte fluviolacustre à dominante carbonatée (tufs calcaires).

Les résultats de la démarche conventionnelle suivie ont permis de souligner une pléthore de nouveautés qui ont éclaircis notre perception *vis-à-vis* de l'investigation des formations superficielles quaternaires du Moyen Atlas septentrional. Ainsi, les résultats des datations et des proxies extraits des formations fluviolacustres carbonatées d'Imouzzer Kandar ont permis d'élucider avec certitude considérable et pour la première fois à l'échelle du Moyen Atlas entier (i) l'interaction entre le forçage climatique et la sédimentation, (ii) l'aptitude de ces formations à capturer et à préserver les signatures des événements climatiques rapides à travers l'Holocène ainsi qu'à (iii) l'efficacité de la méthodologie à être appliquée à d'autres formations fluviolacustres carbonatées holocènes du Moyen Atlas pour mettre en vedette la réponse de la sédimentation aux événements bien connus à travers le présent interglaciaire (e.g., la fin de la Période Humide Africaine, l'Optimum Climatique Médiéval, le Petit Âge Glaciaire, les événements de Bond). Parallèlement, les résultats aboutis dans l'étude des sédiments lacustres quaternaires récents du lac Ifrah ont contribué, pour la première fois à l'échelle du Moyen Atlas, à mieux comprendre les relations entre sédimentation lacustre et facteurs de contrôle tectoniques et climatiques. De même, l'application de la méthodologie adoptée pour le cas du lac Ifrah à d'autres systèmes lacustres quaternaires récents dans le Moyen Atlas s'avère efficace dans la réplication de la capture des signatures climatiques et tectoniques à l'échelle du domaine structural, chose qui est nécessaire sur le plan scientifique.

La synthèse présentée ici repousse plus loin les interprétations des résultats en donnant un avis sur leurs implications dans la science et sur le plan des travaux futurs (perspectives).

1 Apport de l'approche sédimentologique et stratigraphique séquentielle conventionnelle

L'approche sédimentologique alimentée par le raisonnement inductif a pu démontrer son utilité dans le décryptage des signatures climatiques, tant en contexte où les pulsations tectoniques sont bien exprimées (lac Ifrah, chapitre 4, Azennoud et al., *Under Review*) qu'en contexte relativement stable par rapport à l'influence tectonique (tufs calcaires d'Imouzzer Kandar, Azennoud et al., 2022b). Cette approche, dont l'analyse commence des faciès pour arriver au modèle de faciès via les systèmes de dépôts, est qualifiée de conventionnelle. Dans le cas du lac Ifrah, la cyclicité détritico-biochimique des sédiments et leur interprétation en termes d'énergie hydrodynamique ont servi d'outils pour mettre en évidence le forçage orbital et suborbital, ainsi qu'aux téléconnexions potentielles entre les hautes et basses latitudes (chapitre 4). Les oscillations millénaires de type Dansgaard-Oeschger en phase avec la fluctuation des conditions humides-arides dans la Méditerranée sont conjecturées être synchrones avec la cyclicité lithologique se développant probablement durant le MIS-3. De plus, l'influence des vents sahariens sur l'évolution des systèmes de dépôts, et précisément sur l'occurrence des conditions de forte énergie hydrodynamique aboutissant au développement des faciès typiques, a été présumée en s'appuyant sur des données régionales. Par ailleurs, l'application de l'approche sédimentologique conventionnelle sur les tufs calcaires en contexte fluviolacustre (chapitre 5, Azennoud et al., 2022a) a mis en évidence l'hyper-sensibilité de ces archives bio-carbonatés *vis-à-vis* du forçage climatique à l'échelle millénaire et centennale (voire décadaire, probablement). Ainsi, l'interruption de la bio-calcification est démontrée être en phase avec les événements froids rapides qui sont associés aux vêlages prononcés des marges de la calotte glaciaire groenlandaise et aux blocages subséquents de la circulation thermohaline.

L'appel à la stratigraphie séquentielle pour la première fois en domaine fluviolacustre carbonaté avec un large système de type barrage-retenue (cas d'Imouzzer Kandar, chapitre 5, Azennoud et al., 2022a) a abouti à des résultats prometteurs. En effet, la variation de l'accommodation au niveau de la retenue et la distinction des cortèges sédimentaires ('*systems tracts*') qui en résultent ont permis d'inférer le mode d'empilement au niveau du barrage (i.e., aggradation/progradation). Un taux d'aggradation élevé (i.e., rapport aggradation/progradation élevé) aurait conditionné le développement d'un *intervalle transgressif.* En revanche, un rapport aggradation/progradation faible (progradation prononcée) aurait favorisé l'installation de conditions palustres marquant le remplissage de la retenue pour donner lieu à un *intervalle de haut niveau.* De plus, la reconnaissance des surfaces significatives en stratigraphie séquentielle comme la *surface d'inondation maximale* ('*maximum flooding surface*') et la *limite de séquence* ('*sequence boundary*') a soutenu l'approche

sédimentologique dans le déchiffrage des signatures climatiques ; exemple de l'événement 2.7 ka (4.2 ka) qui aurait coïncidé avec le développement d'une *surface d'inondation maximale* (*limite de séquence*) séparant l'*intervalle transgressif* (la séquence à dominante fluviatile en bas) de l'*intervalle de haut niveau* (la séquence à dominante lacustre en haut). Dès lors, en débouchant sur une bonne conception de l'interaction entre la variation de l'accommodation et l'organisation architecturale des sédiments, le recours à la stratigraphie séquentielle conventionnelle dans de tels contextes est fortement recommandé.

Dans un autre contexte où l'influence des pulsations tectoniques sur l'organisation spatiale des sédiments est remarquable (cas du lac Ifrah, chapitre 4, Azennoud et al., *Under Review*), l'usage de la stratigraphie séquentielle, en élargissant l'appel aux cortèges sédimentaires et aux surfaces qui les délimitent, a démontré son apport dans le déchiffrage des signatures orbitales et tectoniques. Ainsi, trois cycles d'accommodation, chacun ayant des particularités qui lui sont propres, ont été ajustés avec la courbe de l'insolation (résolue par Laskar et al., 2004), elle-même modulée par les paramètres orbitaux de Milankovich (*viz*., précession et obliquité). Qui plus est, les pulsations tectoniques et les basculements différentiels du compartiment inférieur ('*hanging-wall*') de la faille maîtresse bordant le bassin ont conditionné des déplacements centripètes instantanés du rivage lacustre, et donc l'occurrence des *intervalles de régression forcée* ('*forced regressions*'), ce qui approuve l'appel élargi aux cortèges sédimentaires qui sont communément omis en contexte lacustre.

En résumé, les conclusions tirées des chapitres 4 et 5 débouchent sur la question de l'apport de la sédimentologie et de la stratigraphie séquentielle dans le déchiffrage des signatures climatiques et tectoniques. La combinaison des deux approches permettrait de démêler l'organisation des sédiments en faciès, associations de faciès, systèmes de dépôts puis modèles de faciès, d'une part, et en cortèges sédimentaires, délimités par des surfaces de même importance, puis en séquences de dépôts ou T-R, de l'autre part. Cette démarche, qualifiée de conventionnelle, certes servira d'outil pour cerner les potentielles cyclicités de l'organisation des sédiments et de l'accommodation, rendant ainsi pertinente et pragmatique la comparaison avec les cycles de forçages externes (climatique orbitale ou tectonique). Cependant, bien qu'inéluctable et primordiale, cette démarche n'est scientifiquement pas suffisante pour un aboutissement concret et indisputable. Pragmatiquement parlant, l'extraction qualitative d'un signal climatique à partir d'un niveau lithologique serait plus concrète si l'interprétation se base à la fois sur le caractère faciologique (lithologie, restes de faune et flore et structures et textures sédimentaires) et des indicateurs paléoclimatiques/paléoenvironnementales (proxies biologiques et géochimiques). Par ailleurs, la quantification de la cyclicité des pulsations tectoniques serait plus commode avec le recours à l'analyse structurale des déformations qui affectent les sédiments à l'état mou (déformations cassantes et 'ductiles' synsédimentaires, les SSDSs).

2 Apport des proxies et des SSDSs

Les marqueurs paléoenvironnementaux extraits des dépôts des tufs calcaires (chapitre 5, Azennoud el al., 2022a) ont servi d'outils pour approfondir et mettre en vedette les interprétations déjà dressées sur la base des caractères faciologiques. Ainsi, l'utilisation des deux espèces d'*Ilyocypris* (*inermis* et *bradyi*) a mis en évidence le caractère froid des niveaux lithologiques riches en matière organique qui coïncident exactement avec les fameux événements froids de Bond 2.7 ka et 4.6 ka. De plus, l'analyse morphotypique des fragments de macro-charbon a permis une appréciation des processus taphonomiques, et donc de l'importance du drainage dans le bassin versant. Par ailleurs, les proxies géochimiques (K, Al, K/Al et Fe/Mn) et l'analyse taxonomique des ostracodes appliqués aux sédiments lacustres du lac Ifrah (chapitre 4, Azennoud et al., *Under Review*) ont démontré leur efficacité dans le traçage des intervalles et des surfaces à caractère cryptique (comme l'*intervalle transgressif* et la *surface d'inondation maximale*).

L'analyse structurale des déformations cassantes et 'ductiles' synsédimentaires (SSDSs) affectant les sédiments lacustres du lac Ifrah (chapitre 3, Azennoud et al., 2022b) a permis le déchiffrage de l'activité tectonique et paléo-séismique à l'échelle locale et régionale. L'analyse des déformations 'ductiles' induites par la liquidization (thixotropie, liquéfaction et fluidisation) des sédiments hôtes à l'échelle du bassin lacustre et leur comparaison avec celles d'un bassin voisin (bassin du lac Iffer) suggèrent un gradient de complexité de déformation positif vers le Nord et donc une concentration des épicentres dans la partie nord du Moyen Atlas. De même, l'analyse des déformations cassantes a mis en évidence deux pulsations tectoniques à l'échelle du bassin, conduisant au basculement du compartiment inférieur ('*hanging-wall*') et ainsi causant une inflexion instantanée de la trajectoire temporelle du rivage ('*shoreline trajectory*'). L'implication néotectonique de ces observations est notable. En effet, comme le bassin lacustre est attaché à un décrochement lithosphérique (Accident de Tizi n'Tretten, ATT), les conclusions tirées des SSDSs suggèrent une isolation du segment nord du décrochement où la plupart des ruptures séismiques se sont concentrés au moins durant l'histoire du bassin. Dès lors, l'ouverture du bassin lacustre d'Ifrah est raisonnablement assumée être génétiquement liée à cette isolation où le modèle proposé est celui d'un bassin généré dans le quadrant de dilatation ('*dilational quadrant*') à l'extrémité d'un décrochement (le segment nord de la faille de l'ATT dans l'étude de cas). L'isolation du segment nord de l'ATT, et la subséquente initiation du bassin lacustre d'Ifrah, a été interprétée comme le résultat, au moins en partie, de la mise en place du volcanisme quaternaire au milieu de l'ATT (province de Timahdite-Azrou) qui, en scellant les discontinuités, aurait réduit l'anisotropie et ainsi rendu le milieu plus résistant *vis-à-vis* du champ des contraintes (Azennoud et al., 2022b, matériel supplémentaire).

En résumé, en guise de mettre au point et d'approfondir la perception, le recours aux marqueurs paléoenvironnementaux et à l'analyse des SSDSs, combinés à l'approche sédimentologique et stratigraphique séquentielle conventionnelle, est fortement recommandé pour l'investigation des signatures climatiques et tectoniques dans un bassin continental ('*interior basin*'). En effet, les résultats de l'analyse taxonomique des ostracodes s'avèrent évidents à la fois dans l'interprétation paléoenvironnementale (chapitre 5) et, d'une manière plus frappante, dans l'approche de stratigraphie séquentielle (chapitre 4). De plus, l'étude qualitative des processus taphonomiques inférés des fragments de macro-charbon a servi de support dans l'interprétation des niveaux lithologiques organiques ; distinction entre fagnes ('*fen*'), marais ('*marsh*') et milieu lacustre profond (hypolimnion). En fin, afin d'appréhender les pulsations tectoniques (ainsi que d'estimer l'emplacement des ruptures séismiques potentielles, les hypocentres) et leurs effets sur l'organisation spatiale des sédiments et cortèges sédimentaires [leurs implications dans la configuration (néo)tectonique à l'échelle régionale], le recours à l'analyse des structures de déformations synsédimentaires (SSDSs) est une démarche que l'on qualifie ici d'indispensable.

Conclusions et perspectives

Le Moyen Atlas forme une chaîne intracontinentale où les structures majeures ont connu une histoire évolutive polyphasée. Sa partie nord, le Moyen Atlas septentrional, abrite une multitude de systèmes lacustres quaternaires où l'origine est tectonique et/ou karstique. En outre, par le fait de la prédominance en surface des carbonates mésozoïques, de nombreux systèmes fluviolacustres quaternaires où la sédimentation est à dominante carbonatée (tufs calcaires) sont installés et ainsi livrant passage à un patrimoine scientifique potentiel pour des investigations en domaine des paléo-sciences du Quaternaire. Néanmoins, parallèlement à cet aspect attrayant du Moyen Atlas septentrional, peu de travaux focalisant sur les aspects sédimentologiques et stratigraphiques des dépôts quaternaires et leurs significations paléoclimatiques et néotectoniques ont été menés. Le présent travail tâche que cette lacune soit au moins partiellement comblée en focalisant sur l'étude de deux exemples de contextes de dépôts dans le Moyen Atlas septentrional : (i) un système lacustre à sédimentation détritico-carbonatée impliquant un hémi-graben (site du lac Ifrah) attaché à un décrochement d'échelle lithosphérique (l'Accident de Tizi n'Tretten, ATT) et (ii) un système fluviolacustre à dominante lithologique carbonatée (tufs calcaires, site d'Imouzzer Kandar). Les tufs calcaires ont démontré une haute sensibilité de capture et de préservation des signatures du forçage climatique de haute résolution (échelle centennale à décadaire ?). Ainsi, deux événements froids multi-centennales (événements de Bond 4.6 ka et 2.7 ka) ont été discernés pour la première fois dans les tufs

calcaires et un enregistrement potentiel de la cyclicité solaire de type Vries-Suess est suggéré. Par ailleurs, la cyclicité lithologique des sédiments lacustres se développant dans un contexte structural en hémi-graben (le lac Ifrah) s'est imposée dans le déchiffrage des signatures du forçage orbital et suborbital. Deux événements paléo-séismiques de magnitude élevée et deux pulsations tectoniques à l'échelle du bassin lacustre d'Ifrah depuis le Stade Isotopique Marin-3 (MIS-3) ont été décelés au moyen de l'analyse des structures de déformations synsédimentaires 'ductiles' et cassantes affectant les sédiments lacustres mous ('*soft-sediment deformation structures*', SSDSs). Compte tenu de la situation géologique structurale, l'initiation du bassin lacustre d'Ifrah et les subséquentes pulsations séismo-tectoniques à son échelle sont probablement originaires d'une isolation tectonique du segment nord du décrochement attachant le bassin, l'ATT. Cet événement néotectonique constitue fort probablement l'effet de la mise en place des épanchements volcaniques mafiques du Pléistocène inférieur et moyen scellant les discontinuités tectoniques dans la province de Timahdite-Azrou (milieu de l'ATT et 20 km loin du bassin du lac Ifrah), qui est, à son tour, associée à une anomalie thermique asthénosphérique sous le Moyen Atlas.

Alors que le présent travail tâche à combler partiellement le manque de l'exploitation sur le plan sédimentologique et stratigraphique des formations superficielles quaternaires à l'échelle du Moyen Atlas septentrional, d'autres travaux analogues sont à être menés pour l'ensemble du Moyen Atlas afin de guider la corrélation chronostratigraphique, à l'échelle des fluctuations glaciaires/interglaciaires, des dépôts continentaux moyen-atlasiques avec ceux de la marge continentale atlantique qui sont directement tributaires des variations du niveau marin. Parallèlement, en justifiant le potentiel des géoarchives des deux contextes-types à capturer et à enregistrer les signatures climatiques, d'autres études doivent être conduites sur des contextes similaires à l'échelle de la région et ailleurs afin de tester l'apport abouti dans cette dissertation doctorale sur le plan scientifique philosophique. Par ailleurs, comme il est signalé dans le chapitre 2, le manque grave de données paléoclimatiques sur le dernier glaciaire et interglaciaire à partir des géoarchives dans le Moyen Atlas doit être franchi dans les décades qui suivent. Dès lors, à partir de l'année de soutenance de cette thèse (2023), l'exploitation à cor et à cri du patrimoine scientifique que connait le Moyen Atlas continuera, *inshaellah*, moyennant des collaborations entre paléo-scientifiques quaternaristes à l'échelle nationale et internationale et en s'appuyant sur diverses géoarchives (tufs calcaires, sédiments lacustres et spéléothèmes) et méthodologies [production des séries chronologiques haute résolution, géochimie isotopique et élémentaire (éléments en trace), palynologie, proxies paléolimnologiques (e.g., ostracodes, diatomées), stratigraphie séquentielle haute résolution]. Parallèlement, le décryptage des signatures paléo-séismiques et néotectoniques à partir de l'analyse des structures de déformations 'ductiles' (hydro-plastiques, pseudo-plastiques et fluides) et cassantes des sédiments lacustres sur différents sites

dans le Moyen Atlas avancera dans le sens qui guidera la bonne conception des pulsations tectoniques à l'échelle du domaine structural. À nouveau, une collaboration avec des jeunes géologues structuralistes éminents à l'échelle de la nation est destinée à être fondée à court terme

REFERENCES

CHAPITRE I ET II

Abdellah, H.I., Vidal, L., Benkaddour, A., Rhoujjati, A., Jouve, G., Tachikawa, K., Sonzogni, C., Mazur, J.-C., Paillès, C., Sylvestre, F., 2021. Palaeohydrological changes recorded from a small Moroccan Middle Atlas pond during the last 6000 cal. yr BP: a multi-proxy study. Journal of Paleolimnology 1–19.

Ait Brahim, L., Chotin, P., Hinaj, S., Abdelouafi, A., El Adraoui, A., Nakcha, C., Dhont, D., Charroud, M., Sossey Alaoui, F., Amrhar, M., Bouaza, A., Tabyaoui, H., Chaouni, A., 2002. Paleostress evolution in the Moroccan African margin from Triassic to Present. Tectonophysics 357, 187–205. https://doi.org/10.1016/S0040-1951(02)00368-2

Ait Brahim, Y., 2017. Speleothem records decadal to multidecadal hydroclimate variations in southwestern Morocco during the last millennium. Earth Planet. Sci. Lett. 476. https://doi.org/10.1016/j.epsl.2017.07.045

Ait Brahim, Y., Wassenburg, J.A., Cruz, F.W., Sifeddine, A., Scholz, D., Bouchaou, L., Dassié, E.P., Jochum, K.P., Edwards, R.L., Cheng, H., 2018. Multi-decadal to centennial hydro-climate variability and linkage to solar forcing in the Western Mediterranean during the last 1000 years. Sci Rep 8, 17446. https://doi.org/10.1038/s41598-018-35498-x

Ait Brahim, Y., Wassenburg, J.A., Sha, L., Cruz, F.W., Deininger, M., Sifeddine, A., Bouchaou, L., Spötl, C., Edwards, R.L., Cheng, H., 2019. North Atlantic Ice-Rafting, Ocean and Atmospheric Circulation During the Holocene: Insights From Western Mediterranean Speleothems. Geophysical Research Letters 46, 7614–7623.

Allen, J.R.L., 1982. Sedimentary structures, their character and physical basis, Developments in sedimentology. Elsevier Scientific Pub. Co, Amsterdam ; New York.

Allen, J.R.L., 1977. The possible mechanics of convolute lamination in graded sand beds. Journal of the Geological Society 134, 19–31.

Allen, P.A., Allen, J.R., 2013. Basin analysis: Principles and application to petroleum play assessment. John Wiley & Sons.

Allison, L.E., 1965. Organic Carbon, in: Methods of Soil Analysis. John Wiley & Sons, Ltd, pp. 1367–1378. https://doi.org/10.2134/agronmonogr9.2.c39

Alonso-Zarza, A.M., 2003. Palaeoenvironmental significance of palustrine carbonates and calcretes in the geological record. Earth-Science Reviews 60, 261–298.

Anselmetti, F.S., Ariztegui, D., Hodell, D.A., Hillesheim, M.B., Brenner, M., Gilli, A., McKenzie, J.A., Mueller, A.D., 2006. Late Quaternary climate-induced lake level variations in Lake Petén Itzá, Guatemala, inferred from seismic stratigraphic analysis. Palaeogeography, Palaeoclimatology, Palaeoecology 230, 52–69. https://doi.org/10.1016/j.palaeo.2005.06.037

Arenas, C., Vázquez-Urbez, M., Pardo, G., Sancho, C., 2014. Sedimentology and depositional architecture of tufas deposited in stepped fluvial systems of changing slope: Lessons from the Quaternary Añamaza valley (Iberian Range, Spain). Sedimentology 61, 133–171. https://doi.org/10.1111/sed.12053

Arenas-Abad, C., Vázquez-Urbez, M., Pardo-Tirapu, G., Sancho-Marcén, C., 2010. Chapter 3 Fluvial and Associated Carbonate Deposits, in: Developments in Sedimentology. Elsevier, pp. 133–175. https://doi.org/10.1016/S0070-4571(09)06103-2

Arp, G., Bissett, A., Brinkmann, N., Cousin, S., De Beer, D., Friedl, T., Mohr, K.I., Neu, T.R., Reimer, A., Shiraishi, F., 2010. Tufa-forming biofilms of German karstwater streams: microorganisms, exopolymers, hydrochemistry and calcification. Geological Society, London, Special Publications 336, 83–118.

Azennoud, K., Baali, A., El Asmi, H., Brahim, Y.A., Hakam, O., Hayati, A., El Kamel, T., 2022. Soft-sediment deformation structures recognised in a reverse-drag associated with normal faulting (Lake Ifrah, Northwest Africa): Palaeoseismic assessment and neotectonic implications. Sedimentary Geology 106264. https://doi.org/10.1016/j.sedgeo.2022.106264

Baali, A., 1998. Genèse et évolution au Plio-Quaternaire de deux bassins intramontagneux en domaine carbonaté méditerranéen. Les bassins versants des dayets Afourgagh et Agoulmam (Moyen Atlas, Maroc) (Thèse Doct. Etat). Thèse d'Etat, Univ. Sidi Mohammed Ben Abdallah, Fès.

Bezada, M.J., Humphreys, E.D., Davila, J. m., Carbonell, R., Harnafi, M., Palomeras, I., Levander, A., 2014. Piecewise delamination of Moroccan lithosphere from beneath the Atlas Mountains. Geochemistry, Geophysics, Geosystems 15, 975–985. https://doi.org/10.1002/2013GC005059

Bohacs, K.M., Carroll, A.R., Neal, J.E., Mankiewicz, P.J., 2000. Lake-basin type, source potential, and hydrocarbon character: an integrated sequence-stratigraphic-geochemical framework. Lake basins through space and time: AAPG Studies in Geology 46, 3–34.

Bohacs, K.M., Grabowski Jr, G., Carroll, A.R., 2007. Lithofacies architecture and variations in expression of sequence stratigraphy within representative intervals of the Green River Formation, Greater Green River Basin, Wyoming and Colorado.

Bond, G., Heinrich, H., Broecker, W., Labeyrie, L., McManus, J., Andrews, J., Huon, S., Jantschik, R., Clasen, S., Simet, C., 1992. Evidence for massive discharges of icebergs into the North Atlantic ocean during the last glacial period. Nature 360, 245–249.

Bosch, D., Maury, R.C., El Azzouzi, M., Bollinger, C., Bellon, H., Verdoux, P., 2014. Lithospheric origin for Neogene–Quaternary Middle Atlas lavas (Morocco): Clues from trace elements and Sr–Nd–Pb–Hf isotopes. Lithos 205, 247–265. https://doi.org/10.1016/j.lithos.2014.07.009

Bout-Roumazeilles, V., Nebout, N.C., Peyron, O., Cortijo, E., Landais, A., Masson-Delmotte, V., 2007. Connection between South Mediterranean climate and North African atmospheric circulation during the last 50,000 yr BP North Atlantic cold events. Quaternary Science Reviews 26, 3197–3215.

Broecker, W., Bond, G., Klas, M., Clark, E., McManus, J., 1992. Origin of the northern Atlantic's Heinrich events. Climate Dynamics 6, 265–273. https://doi.org/10.1007/BF00193540

Cacho, I., Grimalt, J.O., Pelejero, C., Canals, M., Sierro, F.J., Flores, J.A., Shackleton, N., 1999. Dansgaard-Oeschger and Heinrich event imprints in Alboran Sea paleotemperatures. Paleoceanography 14, 698–705.

Campbell, J.F.E., Fletcher, W.J., Joannin, S., Hughes, P.D., Rhanem, M., Zielhofer, C., 2017. Environmental Drivers of Holocene Forest Development in the Middle Atlas, Morocco. Front. Ecol. Evol. 5. https://doi.org/10.3389/fevo.2017.00113

Carroll, A.R., Bohacs, K.M., 1999. Stratigraphic classification of ancient lakes: Balancing tectonic and climatic controls. Geology 27, 99–102.

Catuneanu, O., 2019. Model-independent sequence stratigraphy. Earth-science reviews 188, 312–388.

Catuneanu, O., 2017. Chapter One - Sequence Stratigraphy: Guidelines for a Standard Methodology, in: Montenari, M. (Ed.), Stratigraphy & Timescales, Advances in Sequence Stratigraphy. Academic Press, pp. 1–57. https://doi.org/10.1016/bs.sats.2017.07.003

Catuneanu, O., 2006. Principles of sequence stratigraphy, 1st ed. ed, Developments in sedimentology. Elsevier, Amsterdam ; Boston.

Catuneanu, O., Galloway, W.E., Kendall, C.G.S.C., Miall, A.D., Posamentier, H.W., Strasser, A., Tucker, M.E., 2011. Sequence stratigraphy: methodology and nomenclature. Newsletters on stratigraphy 44, 173–245.

Changsong, L., Eriksson, K., Sitian, L., Yongxian, W., Jianye, R., Yanmei, Z., 2001. Sequence Architecture, Depositional Systems, and Controls on Development of Lacustrine Basin Fills in Part of the Erlian Basin, Northeast China. AAPG Bulletin 85, 2017–2043. https://doi.org/10.1306/8626D0DB-173B-11D7-8645000102C1865D

Charrière, A., 1990. Héritage hercynien et évolution géody- namique alpine d'une chaîne intracontinentale : le Moyen Atlas au sud-est de Fes (Maroc). Thèse de Doctorat d'État, Université Toulouse III – Paul Sabatier, Toulouse, 589 p.

Charrière, A., Andreu, B., Ciszak, R., Kennedy, W.J., Rossi, A., Vila, J.-M., 1998. La transgression du Cénomanien supérieur dans la Haute Moulouya et le Moyen Atlas méridional, Maroc. Geobios 31, 551–569.

Charrière, A., Ouarhach, D., El-Arabi, H., 2011. **Volume 4 (Notes & Mém. n° 559) :** Moyen Atlas (6 jours). Haut Atlas central de Beni Mellal à Imilchil (4 jours) / *Middle Atlas (6 days). Central High Atlas from Beni Mellal to Imilchil (4 days).*

Charrière, A., Vila, J.-M., 1991. Découverte d'Aptien marin à foraminifères dans le Moyen-Atlas (Maroc): un golfe mésogéen à travers la Terre des Idrissides? Comptes rendus de l'Académie des sciences. Série 2, Mécanique, Physique, Chimie, Sciences de l'univers, Sciences de la Terre 313, 1579–1586.

Cheddadi, R., Fady, B., François, L., Hajar, L., Suc, J.-P., Huang, K., Demarteau, M., Vendramin, G.G., Ortu, E., 2009. Putative glacial refugia of Cedrus atlantica deduced from Quaternary pollen records and modern genetic diversity. Journal of Biogeography 36, 1361–1371.

Cheddadi, R., Mamakowa, K., Guiot, J., De Beaulieu, J.-L., Reille, M., Andrieu, V., Granoszewski, W., Peyron, O., 1998. Was the climate of the Eemian stable? A quantitative climate reconstruction from seven European pollen records. Palaeogeography, Palaeoclimatology, Palaeoecology 143, 73–85.
Chen, J., Zhang, D.D., Wang, S., Xiao, T., Huang, R., 2004. Factors controlling tufa deposition in natural waters at waterfall sites. Sedimentary Geology 166, 353–366.
Cheng, H., Lawrence Edwards, R., Shen, C.-C., Polyak, V.J., Asmerom, Y., Woodhead, J., Hellstrom, J., Wang, Y., Kong, X., Spötl, C., Wang, X., Calvin Alexander, E., 2013. Improvements in 230Th dating, 230Th and 234U half-life values, and U–Th isotopic measurements by multi-collector inductively coupled plasma mass spectrometry. Earth and Planetary Science Letters 371–372, 82–91. https://doi.org/10.1016/j.epsl.2013.04.006
Clifton, H.E., Hunter, R.E., Phillips, R.L., 1971. Depositional structures and processes in the non-barred high-energy nearshore. Journal of Sedimentary Research 41, 651–670. https://doi.org/10.1306/74D7231A-2B21-11D7-8648000102C1865D
Cohen, A.S., 2003. Lakes as Archives of Earth History, in: Cohen, A.S. (Ed.), Paleolimnology: The History and Evolution of Lake Systems. Oxford University Press, p. 0. https://doi.org/10.1093/oso/9780195133530.003.0005
Collinson, J., 2019. Sedimentary structures. Dunedin Academic Press Ltd.
Collinson, J., 1994. Sedimentary deformational structures, in: The Geological Deformation of Sediments. Springer, pp. 95–125.
Cruz, F.W., Burns, S.J., Karmann, I., Sharp, W.D., Vuille, M., Cardoso, A.O., Ferrari, J.A., Silva Dias, P.L., Viana, O., 2005. Insolation-driven changes in atmospheric circulation over the past 116,000 years in subtropical Brazil. Nature 434, 63–66. https://doi.org/10.1038/nature03365
Dabkowski, J., 2011. Analyse géochimique des tufs calcaires en domaine fluviatile ouest européen : reconstitution de variations des paléotempératures et des paléoprécipitations au cours des interglaciaires des stades 11 et 5 (These de doctorat). Paris, Muséum national d'histoire naturelle.
Dabkowski, J., Royle, S.H., Antoine, P., Marca-Bell, A., Andrews, J.E., 2015. High-resolution δ18O seasonality record in a French Eemian tufa stromatolite (Caours, Somme Basin). Palaeogeography, Palaeoclimatology, Palaeoecology 438, 277–284. https://doi.org/10.1016/j.palaeo.2015.08.017
Damnati, B., Reddad, H., 2017. Les microcharbons dans les sédiments du lac Ifrah moyen atlas (Maroc): significations climatiques depuis 24 000 ans cal. bp. Quaternaire. Revue de l'Association française pour l'étude du Quaternaire 28, 225–229.
Dansgaard, W., Johnsen, S.J., Clausen, H.B., Dahl-Jensen, D., Gundestrup, N.S., Hammer, C.U., Hvidberg, C.S., Steffensen, J.P., Sveinbjörnsdottir, A.E., Jouzel, J., 1993. Evidence for general instability of past climate from a 250-kyr ice-core record. Nature 364, 218–220.
Davies, S.J., Lamb, H.F., Roberts, S.J., 2015. Micro-XRF core scanning in palaeolimnology: recent developments, in: Micro-XRF Studies of Sediment Cores. Springer, pp. 189–226.
Dean, W.E., 1981. Carbonate Minerals and Organic Matter in Sediments of Modern North Temperate Hard-Water Lakes, in: Ethridge, F.G., Flores, R.M. (Eds.), Recent and Ancient Nonmarine Depositional Environments: Models for Exploration. SEPM Society for Sedimentary Geology, p. 0. https://doi.org/10.2110/pec.81.31.0213
Dean, W.E., Forester, R.M., Bright, J., Anderson, R.Y., 2007. Influence of the diversion of Bear River into Bear Lake (Utah and Idaho) on the environment of deposition of carbonate minerals. Limnology and Oceanography 52, 1094–1111. https://doi.org/10.4319/lo.2007.52.3.1094
Dechen, S., Aiping, S., 2012. Typical earthquake-induced soft-sediment deformation structures in the Mesoproterozoic Wumishan Formation, Yongding River Valley, Beijing, China and interpreted earthquake frequency. Journal of Palaeogeography 1, 71–89. https://doi.org/10.3724/SP.J.1261.2012.00007
Dreimanis, A., 1962. Quantitative gasometric determination of calcite and dolomite by using Chittick apparatus. Journal of Sedimentary Research 32, 520–529. https://doi.org/10.1306/74D70D08-2B21-11D7-8648000102C1865D
Dunham, R.J., 1962. Classification of Carbonate Rocks According to Depositional Textures 38, 108–121.
Einsele, G., 2000. Continental Sediments, in: Einsele, G. (Ed.), Sedimentary Basins: Evolution, Facies, and Sediment Budget. Springer, Berlin, Heidelberg, pp. 19–93. https://doi.org/10.1007/978-3-662-04029-4_2

El Azzouzi, M., Maury, R.C., Bellon, H., Youbi, N., Cotten, J., Kharbouch, F., 2010. Petrology and K-Ar chronology of the Neogene-Quaternary Middle Atlas basaltic province, Morocco. Bulletin de la Societe Geologique de France 181, 243–257. https://doi.org/10.2113/gssgfbull.181.3.243
Embry, A.F., Klovan, J.E., 1971. A LATE DEVONIAN REEF TRACT ON NORTHEASTERN BANKS ISLAND, N.W.T.1. Bulletin of Canadian Petroleum Geology 19, 730–781. https://doi.org/10.35767/gscpgbull.19.4.730
Enache, M.D., Cumming, B.F., 2007. Charcoal morphotypes in lake sediments from British Columbia (Canada): an assessment of their utility for the reconstruction of past fire and precipitation. J Paleolimnol 38, 347–363. https://doi.org/10.1007/s10933-006-9084-8
Enache, M.D., Cumming, B.F., 2006. Tracking recorded fires using charcoal morphology from the sedimentary sequence of Prosser Lake, British Columbia (Canada). Quaternary Research 65, 282–292.
Eynaud, F., de Abreu, L., Voelker, A., Schönfeld, J., Salgueiro, E., Turon, J.-L., Penaud, A., Toucanne, S., Naughton, F., Sánchez Goñi, M.F., Malaizé, B., Cacho, I., 2009. Position of the Polar Front along the western Iberian margin during key cold episodes of the last 45 ka. Geochemistry, Geophysics, Geosystems 10. https://doi.org/10.1029/2009GC002398
FAO, 2020. Standard operating procedure for soil organic carbon. Walkley-Black method: titration and colorimetric method. FAO, Rome, Italy.
Fernàndez, M., Torne, M., Vergés, J., Casciello, E., Macchiavelli, C., 2019. Evidence of Segmentation in the Iberia–Africa Plate Boundary: A Jurassic Heritage? Geosciences 9, 343. https://doi.org/10.3390/geosciences9080343
Fletcher, W.J., Sánchez Goñi, M.F.S., 2008. Orbital- and sub-orbital-scale climate impacts on vegetation of the western Mediterranean basin over the last 48,000 yr. Quaternary Research 70, 451–464. https://doi.org/10.1016/j.yqres.2008.07.002
Ford, T.D., Pedley, H.M., 1996. A review of tufa and travertine deposits of the world. Earth-Science Reviews 41, 117–175. https://doi.org/10.1016/S0012-8252(96)00030-X
Freytet, P., Verrecchia, E.P., 2002. Lacustrine and palustrine carbonate petrography: an overview. Journal of Paleolimnology 27, 221–237. https://doi.org/10.1023/A:1014263722766
Frizon de Lamotte, D., Saint Bezar, B., Bracène, R., Mercier, E., 2000. The two main steps of the Atlas building and geodynamics of the western Mediterranean. Tectonics 19, 740–761. https://doi.org/10.1029/2000TC900003
Frizon de Lamotte, D., Zizi, M., Missenard, Y., Hafid, M., Azzouzi, M.E., Maury, R.C., Charrière, A., Taki, Z., Benammi, M., Michard, A., 2008. The Atlas System, in: Michard, André, Saddiqi, O., Chalouan, A., Lamotte, D.F. de (Eds.), Continental Evolution: The Geology of Morocco: Structure, Stratigraphy, and Tectonics of the Africa-Atlantic-Mediterranean Triple Junction, Lecture Notes in Earth Sciences. Springer, Berlin, Heidelberg, pp. 133–202. https://doi.org/10.1007/978-3-540-77076-3_4
Frizon de Lamotte, D.F., Leturmy, P., Missenard, Y., Khomsi, S., Ruiz, G., Saddiqi, O., Guillocheau, F., Michard, A., 2009. Mesozoic and Cenozoic vertical movements in the Atlas system (Algeria, Morocco, Tunisia): An overview. Tectonophysics, The geology of vertical movements of the lithosphere 475, 9–28. https://doi.org/10.1016/j.tecto.2008.10.024
Gierlowski-Kordesch, E.H., 2010. Chapter 1 Lacustrine Carbonates, in: Alonso-Zarza, A.M., Tanner, L.H. (Eds.), Developments in Sedimentology, Carbonates in Continental Settings: Facies, Environments, and Processes. Elsevier, pp. 1–101. https://doi.org/10.1016/S0070-4571(09)06101-9
Gomez, F., Allmendinger, R., Barazangi, M., Er-Raji, A., Dahmani, M., 1998. Crustal shortening and vertical strain partitioning in the Middle Atlas Mountains of Morocco. Tectonics 17, 520–533. https://doi.org/10.1029/98TC01439
Gomez, F., Barazangi, M., Bensaid, M., 1996. Active tectonism in the intracontinental Middle Atlas Mountains of Morocco: synchronous crustal shortening and extension. Journal of the Geological Society 153, 389–402. https://doi.org/10.1144/gsjgs.153.3.0389
Greb, S.F., Dever, G.R., Ettensohn, F.R., Rast, N., Brett, C.E., 2002. Critical evaluation of possible seismites: Examples from the Carboniferous of the Appalachian basin. SPECIAL PAPERS-GEOLOGICAL SOCIETY OF AMERICA 109–126.
Hafid, M., Zizi, M., Bally, A.W., Ait Salem, A., 2006. Structural styles of the western onshore and offshore termination of the High Atlas, Morocco. Comptes Rendus Geoscience, Quelques développements récents sur la géodynamique du Maghreb 338, 50–64. https://doi.org/10.1016/j.crte.2005.10.007

Hakala, A., 2004. Meromixis as a part of lake evolution; observations and a revised classification of true meromictic lakes in Finland. Boreal environment research 9, 37–53.
Hakam, O., Baali, A., Ait Brahim, Y., El Kamel, T., Azennoud, K., 2022. Regional and global teleconnections patterns governing rainfall in the Western Mediterranean: case of the Lower Sebou Basin, North-West Morocco. Model. Earth Syst. Environ. https://doi.org/10.1007/s40808-022-01425-3
Håkanson, L., 1982. Bottom dynamics in lakes, in: Sly, P.G. (Ed.), Sediment/Freshwater Interaction, Developments in Hydrobiology. Springer Netherlands, Dordrecht, pp. 9–22. https://doi.org/10.1007/978-94-009-8009-9_2
Hanneman, D.L., Wideman, C.J., 2010. Chapter 5 Continental Sequence Stratigraphy and Continental Carbonates, in: Alonso-Zarza, A.M., Tanner, L.H. (Eds.), Developments in Sedimentology, Carbonates in Continental Settings: Geochemistry, Diagenesis and Applications. Elsevier, pp. 215–273. https://doi.org/10.1016/S0070-4571(09)06205-0
He, B., Qiao, X., 2015. Advances and Overview of the Study on Paleo-earthquake Events: A Review of Seismites. Acta Geologica Sinica 89, 1702–1746. https://doi.org/10.1111/1755-6724.12575
Heinrich, H., 1988. Origin and consequences of cyclic ice rafting in the northeast Atlantic Ocean during the past 130,000 years. Quaternary research 29, 142–152.
Hinaje, S., 2004. Tectonique cassante et paléochamps de contraintes dans le Moyen Atlas et le Haut Atlas central (Midelt-Errachidia) depuis le Trias jusqu'à l'Actuel. Université Mohammed V, Rabat.
Hinaje, S., El Fartati, M., Yaagoub, D., Amrani, S., Gharmane, Y., El Fellah Idrissi, B., 2019. Paleocontraintes et contexte tectonique de mise en place du volcanisme alcalin neogene et quaternaire du Moyen Atlas (Maroc). European Scientific Journal May 448–466.
Horton, B.K., Schmitt, J.G., 1996. Sedimentology of a lacustrine fan-delta system, Miocene Horse Camp Formation, Nevada, USA. Sedimentology 43, 133–155. https://doi.org/10.1111/j.1365-3091.1996.tb01464.x
Hutchinson, G.E., 1957. A treatise on limnology. Vol 1: Georgraphy, physics and chemistry. John Wiley & Sons.
Jimenez-Espejo, F.J., Martinez-Ruiz, F., Rogerson, M., González-Donoso, J.M., Romero, O.E., Linares, D., Sakamoto, T., Gallego-Torres, D., Rueda Ruiz, J.L., Ortega-Huertas, M., Perez Claros, J.A., 2008. Detrital input, productivity fluctuations, and water mass circulation in the westernmost Mediterranean Sea since the Last Glacial Maximum. Geochemistry, Geophysics, Geosystems 9. https://doi.org/10.1029/2008GC002096
Keighley, D., Flint, S., Howell, J., Moscariello, A., 2003. Sequence Stratigraphy in Lacustrine Basins: A Model for Part of the Green River Formation (Eocene), Southwest Uinta Basin, Utah, U.S.A. Journal of Sedimentary Research 73, 987–1006. https://doi.org/10.1306/050103730987
Kelts, K., 1988. Environments of deposition of lacustrine petroleum source rocks: an introduction. Geological Society, London, Special Publications 40, 3–26. https://doi.org/10.1144/GSL.SP.1988.040.01.02
Kelts, K., Hsü, K.J., 1978. Freshwater Carbonate Sedimentation, in: Lerman, A. (Ed.), Lakes: Chemistry, Geology, Physics. Springer, New York, NY, pp. 295–323. https://doi.org/10.1007/978-1-4757-1152-3_9
Kempe, S., Kazmierczak, J., 1990. Calcium carbonate supersaturation and the formation of in situ calcified stromatolites. Facets of modern biogeochemistry 255–278.
Knippertz, P., Christoph, M., Speth, P., 2003. Long-term precipitation variability in Morocco and the link to the large-scale circulation in recent and future climates. Meteorology and Atmospheric physics 83, 67–88.
Köppen, W., 1900. Versuch einer Klassifikation der Klimate, vorzugsweise nach ihren Beziehungen zur Pflanzenwelt. (Schluss). Geographische Zeitschrift 6, 657–679.
Kottek, M., Grieser, J., Beck, C., Rudolf, B., Rubel, F., 2006. World Map of the Köppen-Geiger climate classification updated. Meteorologische Zeitschrift 259–263. https://doi.org/10.1127/0941-2948/2006/0130
Kuhlmann, H., Meggers, H., Freudenthal, T., Wefer, G., 2004. The transition of the monsoonal and the N Atlantic climate system off NW Africa during the Holocene. Geophysical Research Letters 31. https://doi.org/10.1029/2004GL021267
Lacey, J.H., Leng, M.J., Höbig, N., Reed, J.M., Valero-Garcés, B., Reicherter, K., 2016. Western Mediterranean climate and environment since Marine Isotope Stage 3: a 50,000-year record from Lake Banyoles, Spain. J Paleolimnol 55, 113–128. https://doi.org/10.1007/s10933-015-9868-9

Lamb, H.F., Gasse, F., Benkaddour, A., El Hamouti, N., Van der Kaars, S., Perkins, W.T., Pearce, N.J., Roberts, C.N., 1995. Relation between century-scale Holocene arid intervals in tropical and temperate zones. Nature 373, 134–137.
Lamb, H.F., van der Kaars, S., 1995. Vegetational response to Holocene climatic change: pollen and palaeolimnological data from the Middle Atlas, Morocco. The Holocene 5, 400–408. https://doi.org/10.1177/095968369500500402
Laville, E., Pique, A., Amrhar, M., Charroud, M., 2004. A restatement of the Mesozoic Atlasic Rifting (Morocco). Journal of African Earth Sciences 38, 145–153. https://doi.org/10.1016/j.jafrearsci.2003.12.003
Lewis Jr., W.M., 1983. A Revised Classification of Lakes Based on Mixing. Can. J. Fish. Aquat. Sci. 40, 1779–1787. https://doi.org/10.1139/f83-207
Martin, J., 1981. Le Moyen Atlas central étude géomorphologique. Editions du Service géologique du Maroc.
Martrat, B., Grimalt, J.O., Lopez-Martinez, C., Cacho, I., Sierro, F.J., Flores, J.A., Zahn, R., Canals, M., Curtis, J.H., Hodell, D.A., 2004. Abrupt Temperature Changes in the Western Mediterranean over the Past 250,000 Years. Science 306, 1762–1765. https://doi.org/10.1126/science.1101706
Mattauer, M., Tapponnier, P., Proust, F., 1977. Sur les mecanismes de formation des chaines intracontinentales; l'exemple des chaines atlasiques du Maroc. Bulletin de la Société Géologique de France S7-XIX, 521–526. https://doi.org/10.2113/gssgfbull.S7-XIX.3.521
Menzies, J., van der Meer, J.J.M., Ravier, E., 2016. A kinematic unifying theory of microstructures in subglacial tills. Sedimentary Geology, The environmental significance of soft-sediment deformation 344, 57–70. https://doi.org/10.1016/j.sedgeo.2016.03.024
Merz, M.U.E., 1992. The biology of carbonate precipitation by cyanobacteria. Facies 26, 81–101. https://doi.org/10.1007/BF02539795
Miall, A.D., 2013. Principles of sedimentary basin analysis. Springer Science & Business Media.
Miall, A.D., 1977. A review of the braided-river depositional environment. Earth-Science Reviews 13, 1–62. https://doi.org/10.1016/0012-8252(77)90055-1
Michard, A., Saddiqi, O., Chalouan, A., Lamotte, D.F. de (Eds.), 2008. Continental Evolution: The Geology of Morocco: Structure, Stratigraphy, and Tectonics of the Africa-Atlantic-Mediterranean Triple Junction, Lecture Notes in Earth Sciences. Springer-Verlag, Berlin Heidelberg. https://doi.org/10.1007/978-3-540-77076-3
Middleton, G.V., Hampton, M.A., 1973. Part I. Sediment Gravity Flows: Mechanics of Flow and Deposition 1–38.
Miller, M.S., O'Driscoll, L.J., Butcher, A.J., Thomas, C., 2015. Imaging Canary Island hotspot material beneath the lithosphere of Morocco and southern Spain. Earth and Planetary Science Letters 431, 186–194. https://doi.org/10.1016/j.epsl.2015.09.026
Missenard, Y., Zeyen, H., Frizon de Lamotte, D., Leturmy, P., Petit, C., Sébrier, M., Saddiqi, O., 2006. Crustal versus asthenospheric origin of relief of the Atlas Mountains of Morocco. Journal of Geophysical Research: Solid Earth 111. https://doi.org/10.1029/2005JB003708
Montenat, C., Barrier, P., Ott d'Estevou, P., Hibsch, C., 2007. Seismites: An attempt at critical analysis and classification. Sedimentary Geology 196, 5–30. https://doi.org/10.1016/j.sedgeo.2006.08.004
Moreno, A., 2005. Links between marine and atmospheric processes oscillating on a millennial time-scale. A multi-proxy study of the last 50,000 yr from the Alboran Sea (Western Mediterranean Sea). Quat. Sci. Rev. 24. https://doi.org/10.1016/j.quascirev.2004.06.018
Moreno, A., Cacho, I., Canals, M., Prins, M.A., Sánchez-Goñi, M.-F., Grimalt, J.O., Weltje, G.J., 2002. Saharan dust transport and high-latitude glacial climatic variability: the Alboran Sea record. Quaternary Research 58, 318–328.
Moretti, M., (Tom) van Loon, A.J., Liu, M., Wang, Y., 2014. Restrictions to the application of 'diagnostic' criteria for recognizing ancient seismites. Journal of Palaeogeography 3, 162–173. https://doi.org/10.3724/SP.J.1261.2014.00050
Müller, G., Wagner, F., 1978. Holocene Carbonate Evolution in Lake Balaton (Hungary): A Response to Climate and Impact of Man, in: Modern and Ancient Lake Sediments. John Wiley & Sons, Ltd, pp. 57–81. https://doi.org/10.1002/9781444303698.ch4
Mustaphi, C.J.C., Pisaric, M.F.J., 2014. A classification for macroscopic charcoal morphologies found in Holocene lacustrine sediments. Progress in Physical Geography: Earth and Environment 38, 734–754. https://doi.org/10.1177/0309133314548886

Naughton, F., Sánchez Goñi, M.F., Kageyama, M., Bard, E., Duprat, J., Cortijo, E., Desprat, S., Malaizé, B., Joly, C., Rostek, F., Turon, J.-L., 2009. Wet to dry climatic trend in north-western Iberia within Heinrich events. Earth and Planetary Science Letters 284, 329–342. https://doi.org/10.1016/j.epsl.2009.05.001

Nourelbait, M., Rhoujjati, A., Benkaddour, A., Carré, M., Eynaud, F., Martinez, P., Cheddadi, R., 2016. Climate change and ecosystems dynamics over the last 6000 years in the Middle Atlas, Morocco. Clim. Past 12, 1029–1042. https://doi.org/10.5194/cp-12-1029-2016

Nourelbait, M., Rhoujjati, A., Eynaud, F., Benkaddour, A., Dezileau, L., Wainer, K., Goslar, T., Khater, C., Tabel, J., Cheddadi, R., 2014. An 18 000-year pollen and sedimentary record from the cedar forests of the Middle Atlas, Morocco: POLLEN/SEDIMENTARY RECORD FROM THE MIDDLE ATLAS. J. Quaternary Sci. 29, 423–432. https://doi.org/10.1002/jqs.2708

Nutz, A., Ghienne, J.-F., Schuster, M., Dietrich, P., Roquin, C., Hay, M.B., Bouchette, F., Cousineau, P.A., 2015. Forced regressive deposits of a deglaciation sequence: Example from the Late Quaternary succession in the Lake Saint-Jean basin (Québec, Canada). Sedimentology 62, 1573–1610.

Nutz, A., Kwiecien, O., Breitenbach, S.F.M., Cai, Y., Porta, G.D., Danisch, J., Kabiri, L., Bodin, S., 2019. Fluvio-lacustrine sedimentation in the Agadir-Tissint Feija (Anti-Atlas, Morocco): A promising palaeoclimate archive for the last glacial cycle in northwest Africa. The Depositional Record 5, 362–387. https://doi.org/10.1002/dep2.65

Nutz, A., Schuster, M., Barboni, D., Gassier, G., Van Bocxlaer, B., Robin, C., Ragon, T., Ghienne, J.-F., Rubino, J.-L., 2020. Plio-Pleistocene sedimentation in West Turkana (Turkana Depression, Kenya, East African Rift System): Paleolake fluctuations, paleolandscapes and controlling factors. Earth-Science Reviews 211, 103415. https://doi.org/10.1016/j.earscirev.2020.103415

Nutz, A., Schuster, M., Boës, X., Rubino, J.-L., 2017. Orbitally-driven evolution of Lake Turkana (Turkana Depression, Kenya, EARS) between 1.95 and 1.72 Ma: A sequence stratigraphy perspective. Journal of African Earth Sciences 125, 230–243. https://doi.org/10.1016/j.jafrearsci.2016.10.016

Nutz, A., Schuster, M., Ghienne, J.-F., Roquin, C., Bouchette, F., 2016. Wind-driven waterbodies: a new category of lake within an alternative sedimentologically-based lake classification. J Paleolimnol 59, 189–199. https://doi.org/10.1007/s10933-016-9894-2

Ouarhache, D., Charriere, A., Chalot-Prat, F., El-Wartiti, M., 2000. Sédimentation détritique continentale synchrone d'un volcanisme explosif dans le Trias terminal à infra-Lias du domaine atlasique (Haute Moulouya, Maroc) (Late Triassic to infra-Liassic continental detrital sedimentation synchronous with an explosive volcanic event in the Atlas area [Hgh Moulouya, Morocco]). Journal of African Earth Sciences 31, 555–570. https://doi.org/10.1016/S0899-5362(00)80007-X

Ouarhache, D., Charriere, A., Chalot-prat, F., Wartiti, M.E., 2012. Triassic to early Liassic continental rifting chronology and process at the southwest margin of the Alpine Tethys (Middle Atlas and High Moulouya, Morocco); correlations with the Atlantic rifting, synchronous and diachronous. Bulletin de la Societe Geologique de France 183, 233–249. https://doi.org/10.2113/gssgfbull.183.3.233

Owen, G., 1987. Deformation processes in unconsolidated sands. Geological Society, London, Special Publications 29, 11–24.

Owen, G., Moretti, M., 2011. Identifying triggers for liquefaction-induced soft-sediment deformation in sands. Sedimentary Geology 235, 141–147. https://doi.org/10.1016/j.sedgeo.2010.10.003

Owen, G., Moretti, M., Alfaro, P., 2011. Recognising triggers for soft-sediment deformation: Current understanding and future directions. Sedimentary Geology, Recognising triggers for soft-sediment deformation: Current understanding and future directions 235, 133–140. https://doi.org/10.1016/j.sedgeo.2010.12.010

Palomeras, I., Thurner, S., Levander, A., Liu, K., Villasenor, A., Carbonell, R., Harnafi, M., 2014. Finite-frequency Rayleigh wave tomography of the western Mediterranean: Mapping its lithospheric structure. Geochemistry, Geophysics, Geosystems 15, 140–160. https://doi.org/10.1002/2013GC004861

Payton, C.E., 1977. Seismic Stratigraphy — Applications to Hydrocarbon Exploration. https://doi.org/10.1306/M26490

Pedley, H.M., 1990. Classification and environmental models of cool freshwater tufas. Sedimentary Geology 68, 143–154.

Pentecost, A., 2005. Travertine. Springer Science & Business Media.

Pentecost, A., 1998. The significance of calcite (travertine) formation by algae in a moss-dominated travertine from Matlock Bath, England. Archiv für Hydrobiologie 487–509. https://doi.org/10.1127/archiv-hydrobiol/143/1998/487

Pentecost, A., Viles, H., 1994. A review and reassessment of travertine classification. Géographie physique et Quaternaire 48, 305–314.
Pietras, J.T., Carroll, A.R., Rhodes, M.K., 2003. Lake basin response to tectonic drainage diversion: Eocene Green River Formation, Wyoming. Journal of Paleolimnology 30, 115–125. https://doi.org/10.1023/A:1025518015341
Platt, N.H., Wright, V.P., 1991. Lacustrine Carbonates: Facies Models, Facies Distributions and Hydrocarbon Aspects, in: Lacustrine Facies Analysis. John Wiley & Sons, Ltd, pp. 57–74. https://doi.org/10.1002/9781444303919.ch3
Plaziat, J.-C., Purser, B.H., Philobbos, E.R., 1990. Seismic deformation structures (seismites) in the syn-rift sediments of the NW Red Sea (Egypt). Bulletin de la Société géologique de France 6, 419–434.
Posamentier, H.W., Jervey, M.T., Vail, P.R., 1988. Eustatic Controls on Clastic Deposition I—conceptual Framework.
Prosser, S., 1993. Rift-related linked depositional systems and their seismic expression. Geological Society, London, Special Publications 71, 35–66. https://doi.org/10.1144/GSL.SP.1993.071.01.03
Ramsey, C.B., Lee, S., 2013. Recent and Planned Developments of the Program OxCal. Radiocarbon 55, 720–730.
Reddad, H., Etabaai, I., Rhoujjati, A., Taieb, M., Thevenon, F., Damnati, B., 2013. Fire activity in North West Africa during the last 30,000 cal years BP inferred from a charcoal record from Lake Ifrah (Middle atlas–Morocco): Climatic implications. Journal of African Earth Sciences 84, 47–53.
Reimer, P.J., Austin, W.E., Bard, E., Bayliss, A., Blackwell, P.G., Ramsey, C.B., Butzin, M., Cheng, H., Edwards, R.L., Friedrich, M., 2020. The IntCal20 Northern Hemisphere radiocarbon age calibration curve (0–55 cal kBP). Radiocarbon 62, 725–757.
Renaut, R.W., Gierlowski-Kordesch, E.H., Dalrymple, R., James, N., 2010. Lakes. Facies models 4, 541–575.
Rhoujjati, A., Cheddadi, R., Taïeb, M., Baali, A., Ortu, E., 2010. Environmental changes over the past c. 29,000 years in the Middle Atlas (Morocco): A record from Lake Ifrah. Journal of Arid Environments 74, 737–745. https://doi.org/10.1016/j.jaridenv.2009.09.006
Rhoujjati, A., Nourelbait, M., Benkaddour, A., Damnati, B., Baali, A., Taieb, M., Decobert, M., Malek, F., Cheddadi, R., 2012. Significations paléoenvironnementales des dépôts du remplissage Holocène du lac Iffer (Moyen Atlas, Maroc). Quaternaire. Revue de l'Association française pour l'étude du Quaternaire 23, 241–252.
Robbins, L.L., Blackwelder, P.L., 1993. Biochemical and Ultrastructural Evidence for the Origin of Whitings-a Biologically Induced Calcium-Carbonate Precipitation Mechanism-Reply. Geology.
Rosen, M.R., 1994. The importance of groundwater in playas: A review of playa classifications and the sedimentology and hydrology of playas, in: Rosen, M.R. (Ed.), Paleoclimate and Basin Evolution of Playa Systems. Geological Society of America, p. 0. https://doi.org/10.1130/SPE289-p1
Rosenbaum, G., Lister, G.S., Duboz, C., 2002. Relative motions of Africa, Iberia and Europe during Alpine orogeny. Tectonophysics 359, 117–129. https://doi.org/10.1016/S0040-1951(02)00442-0
Rosenbaum, J.G., Kaufman, D.S., 2009. Paleoenvironments of Bear Lake, Utah and Idaho, and its catchment. Geological Society of America.
Sabatier, P., Moernaut, J., Bertrand, S., Van Daele, M., Kremer, K., Chaumillon, E., Arnaud, F., 2022. A Review of Event Deposits in Lake Sediments. Quaternary 5, 34. https://doi.org/10.3390/quat5030034
Sánchez Goñi, M., Cacho, I., Turon, J., Guiot, J., Sierro, F., Peypouquet, J., Grimalt, J., Shackleton, N., 2002. Synchroneity between marine and terrestrial responses to millennial scale climatic variability during the last glacial period in the Mediterranean region. Climate Dynamics 19, 95–105. https://doi.org/10.1007/s00382-001-0212-x
Sánchez Goñi, M.F., Landais, A., Fletcher, W.J., Naughton, F., Desprat, S., Duprat, J., 2008. Contrasting impacts of Dansgaard–Oeschger events over a western European latitudinal transect modulated by orbital parameters. Quaternary Science Reviews 27, 1136–1151. https://doi.org/10.1016/j.quascirev.2008.03.003
Scholz, D., Hoffmann, D.L., 2011. StalAge – an algorithm designed for construction of speleothem age models. Quat. Geochronol. 6. https://doi.org/10.1016/j.quageo.2011.02.002
Sha, L., Brahim, Y.A., Wassenburg, J.A., Yin, J., Lu, J., Cruz, F.W., Cai, Y., Edwards, R.L., Cheng, H., 2021. The "Hockey Stick" Imprint in Northwest African Speleothems. Geophysical Research Letters 48, e2021GL094232. https://doi.org/10.1029/2021GL094232

Sha, L., Brahim, Y.A., Wassenburg, J.A., Yin, J., Peros, M., Cruz, F.W., Cai, Y., Li, H., Du, W., Zhang, H., Edwards, R.L., Cheng, H., 2019. How Far North Did the African Monsoon Fringe Expand During the African Humid Period? Insights From Southwest Moroccan Speleothems. Geophysical Research Letters 46, 14093–14102. https://doi.org/10.1029/2019GL084879

Shanmugam, G., 2017. Global case studies of soft-sediment deformation structures (SSDS): Definitions, classifications, advances, origins, and problems. Journal of Palaeogeography 6, 251–320. https://doi.org/10.1016/j.jop.2017.06.004

Strecker, U., Steidtmann, J.R., Smithson, S.B., 1999. A Conceptual Tectonostratigraphic Model for Seismic Facies Migrations in a Fluvio-Lacustrine Extensional Basin1. AAPG Bulletin 83, 1320–1336. https://doi.org/10.1306/00AA99F8-1730-11D7-8645000102C1865D

Tabel, J., Khater, C., Rhoujjati, A., Dezileau, L., Bouimetarhan, I., Carre, M., Vidal, L., Benkaddour, A., Nourelbait, M., Cheddadi, R., 2016. Environmental changes over the past 25 000 years in the southern Middle Atlas, Morocco: PAST ENVIRONMENTAL CHANGES IN MOROCCO. J. Quaternary Sci. 31, 93–102. https://doi.org/10.1002/jqs.2841

Teixell, A., Ayarza, P., Zeyen, H., Fernàndez, M., Arboleya, M.-L., 2005. Effects of mantle upwelling in a compressional setting: the Atlas Mountains of Morocco. Terra Nova 17, 456–461. https://doi.org/10.1111/j.1365-3121.2005.00633.x

Tjallingii, R., Claussen, M., Stuut, J.-B.W., Fohlmeister, J., Jahn, A., Bickert, T., Lamy, F., Röhl, U., 2008. Coherent high- and low-latitude control of the northwest African hydrological balance. Nature Geosci 1, 670–675. https://doi.org/10.1038/ngeo289

Topal, S., Özkul, M., 2014. Soft-Sediment Deformation Structures Interpreted as Seismites in the Kolankaya Formation, Denizli Basin (SW Turkey). The Scientific World Journal 2014, e352654. https://doi.org/10.1155/2014/352654

Vail, P.R., Mitchum, R.M., Jr., Thompson, S., III, 1977. Seismic stratigraphy and global changes of sea level, part 3: relative changes of sea level from coastal onlap. Seismic Stratigraphy — Applications to Hydrocarbon Exploration. Memoir 26, 63–81.

Van Loon, A.J., 2009. Soft-sediment deformation structures in siliciclastic sediments: an overview.

Van Loon, A.T., 2014. The life cycle of seismite research. Geologos 20, 61–66.

Van Wagoner, J.C., Posamentier, H.W., Mitchum, R.M.J., Vail, P.R., Sarg, J.F., Loutit, T.S., Hardenbol, J., 1988. An overview of the fundamentals of sequence stratigraphy and key definitions.

Vázquez-Urbez, M., Arenas, C., Pardo, G., 2012. A sedimentary facies model for stepped, fluvial tufa systems in the Iberian Range (Spain): the Quaternary Piedra and Mesa valleys. Sedimentology 59, 502–526.

Vegas, J., Ruiz-Zapata, B., Ortiz, J.E., Galán, L., Torres, T., García-Cortés, Á., Gil-García, M.J., Pérez-González, A., Gallardo-Millán, J.L., 2010. Identification of arid phases during the last 50 cal. ka BP from the Fuentillejo maar-lacustrine record (Campo de Calatrava Volcanic Field, Spain). Journal of Quaternary Science 25, 1051–1062. https://doi.org/10.1002/jqs.1262

Verrecchia, E.P., 2007. Lacustrine and palustrine geochemical sediments. Geochemical sediments and landscapes 298–329.

Waldron, J.W.F., Gagnon, J.-F., 2011. Recognizing soft-sediment structures in deformed rocks of orogens. Journal of Structural Geology, Flow of Rocks 33, 271–279. https://doi.org/10.1016/j.jsg.2010.06.015

Walkley, A., Black, I.A., 1934. AN EXAMINATION OF THE DEGTJAREFF METHOD FOR DETERMINING SOIL ORGANIC MATTER, AND A PROPOSED MODIFICATION OF THE CHROMIC ACID TITRATION METHOD. Soil Science 37, 29–38.

Wang, X., Edwards, R.L., Auler, A.S., Cheng, H., Kong, X., Wang, Y., Cruz, F.W., Dorale, J.A., Chiang, H.-W., 2017. Hydroclimate changes across the Amazon lowlands over the past 45,000 years. Nature 541, 204–207. https://doi.org/10.1038/nature20787

Wassenburg, J.A., Dietrich, S., Fietzke, J., Fohlmeister, J., Jochum, K.P., Scholz, D., Richter, D.K., Sabaoui, A., Spötl, C., Lohmann, G., Andreae, M.O., Immenhauser, A., 2016. Reorganization of the North Atlantic Oscillation during early Holocene deglaciation. Nature Geosci 9, 602–605. https://doi.org/10.1038/ngeo2767

Wetzel, R.G., 2001. Limnology: lake and river ecosystems. gulf professional publishing.

Winter, T.C., 2003. The Hydrology of Lakes, in: The Lakes Handbook. John Wiley & Sons, Ltd, pp. 61–78. https://doi.org/10.1002/9780470999271.ch3

Zavala, C., Liu, H., Li, X., Arcuri, M., Di Meglio, M., Zorzano, A., Otharán, G., Hao, B., Wang, Y., 2022. Chapter 16 - Lacustrine sequence stratigraphy: New insights from the study of the Yanchang Formation

(Middle-Late Triassic), Ordos Basin, China, in: Yang, R., Van Loon, A.J. (Tom) (Eds.), The Ordos Basin. Elsevier, pp. 309–335. https://doi.org/10.1016/B978-0-323-85264-7.00012-6

Zhang, D.D., Zhang, Y., Zhu, A., Cheng, X., 2001. Physical mechanisms of river waterfall tufa (travertine) formation. Journal of Sedimentary Research 71, 205–216.

Zhang, J., Wang, H., Liu, Z., An, D., Dreybrodt, W., 2012. Spatial–temporal variations of travertine deposition rates and their controlling factors in Huanglong Ravine, China – A world's heritage site. Applied Geochemistry 27, 211–222. https://doi.org/10.1016/j.apgeochem.2011.10.005

Zielhofer, C., Fletcher, W.J., Mischke, S., De Batist, M., Campbell, J.F., Joannin, S., Tjallingii, R., El Hamouti, N., Junginger, A., Stele, A., 2017a. Atlantic forcing of Western Mediterranean winter rain minima during the last 12,000 years. Quaternary Science Reviews 157, 29–51.

Zielhofer, C., Köhler, A., Mischke, S., Benkaddour, A., Mikdad, A., Fletcher, W.J., 2019. Western Mediterranean hydro-climatic consequences of Holocene ice-rafted debris (Bond) events. Climate of the Past 15, 463–475. https://doi.org/10.5194/cp-15-463-2019

Zielhofer, C., von Suchodoletz, H., Fletcher, W.J., Schneider, B., Dietze, E., Schlegel, M., Schepanski, K., Weninger, B., Mischke, S., Mikdad, A., 2017b. Millennial-scale fluctuations in Saharan dust supply across the decline of the African Humid Period. Quaternary Science Reviews 171, 119–135. https://doi.org/10.1016/j.quascirev.2017.07.010

ANNEXE

GENERALITÉS SUR LA SÉDIMENTATION LACUSTRE ET FLUVIOLACUSTRE

1 Systèmes lacustres à dominante détritico-carbonatée

Les systèmes lacustres à dominante détritico-carbonatée sont le siège à la fois de processus purement physiques [aboutissant à la composant détritique (clastique) et aux caractères morphologiques et structurales qui lui sont associés (e.g., structures sédimentaires, géométrie des dépôts)] et d'autres purement biochimiques (contribuant à la sédimentation biochimique, généralement carbonatée). De ce fait, les systèmes lacustres sont des écosystèmes, où la chaîne trophique est bien développée, avant d'être considérés comme un milieu de dépôts, ainsi imitant en partie leurs homologues marins. En conséquence, l'exposition en bref des principaux processus physiques (régulières et extrêmes) et biochimiques dans un tel environnement de dépôt doit être procédée de prime abord avant d'entamer les différents sous-environnements de dépôts et modèles de faciès, inhérents des premiers.

1.1 Processus réguliers et événements extrêmes

1.1.1 Processus physiques

1.1.1.1 Processus hydrodynamiques sédimentaires

1.1.1.1.1 Processus hydrodynamiques modulés par le vent

Les processus physiques dans les lacs connaissant un hydrodynamisme important (classés comme '*wind-driven waterbodies*' par Nutz et al., 2016; Fig. 1) sont dominés par les vagues et les courants (Imboden, 2003) régulièrement entraînés par le vent (Sly, 1978; Håkanson, 1982; Allan et Kirk, 2000; Ashton et al., 2009; Nutz et al., 2015a). Les effets des marées sont négligeables, même dans les grands lacs (Renaut et al., 2010). Les vagues déplacent les sédiments grossiers le long du rivage et transportent les sédiments fins vers le large par des processus analogues à ceux du rivage marin (Håkanson, 1982; Nutz et al., 2015a, 2016; Schuster et Nutz, 2018; Fig. 1). Leur efficacité varie en fonction de l'orientation du lac et de son 'fetch' (longueur du segment du lac parallèle à la direction du vent) par rapport aux vents dominants (Sly, 1978; Ashton et al., 2009). Les vagues mélangent également les couches supérieures de la colonne d'eau, ce qui favorise la circulation des nutriments et aide à prévenir la stratification thermique (*cf., infra*; Renaut et al., 2010).

Dans les grands lacs, les effets géostrophiques dévient les courants d'eau vers la droite (hémisphère Nord) ou vers la gauche (hémisphère Sud), à l'instar de leurs effets dans les océans. Ceux-ci peuvent induire des mouvements verticaux très typiques, 'upwellings' et 'downwellings', et ainsi déclencher activement des écoulements sous-aquatiques favorisant une redistribution des sédiments

dans le bassin (comme les écoulements d'hyperdensité, toutefois cette fois-ci générés par les vagues) (Renaut et al., 2010; Nutz et al., 2016; Fig. 1).

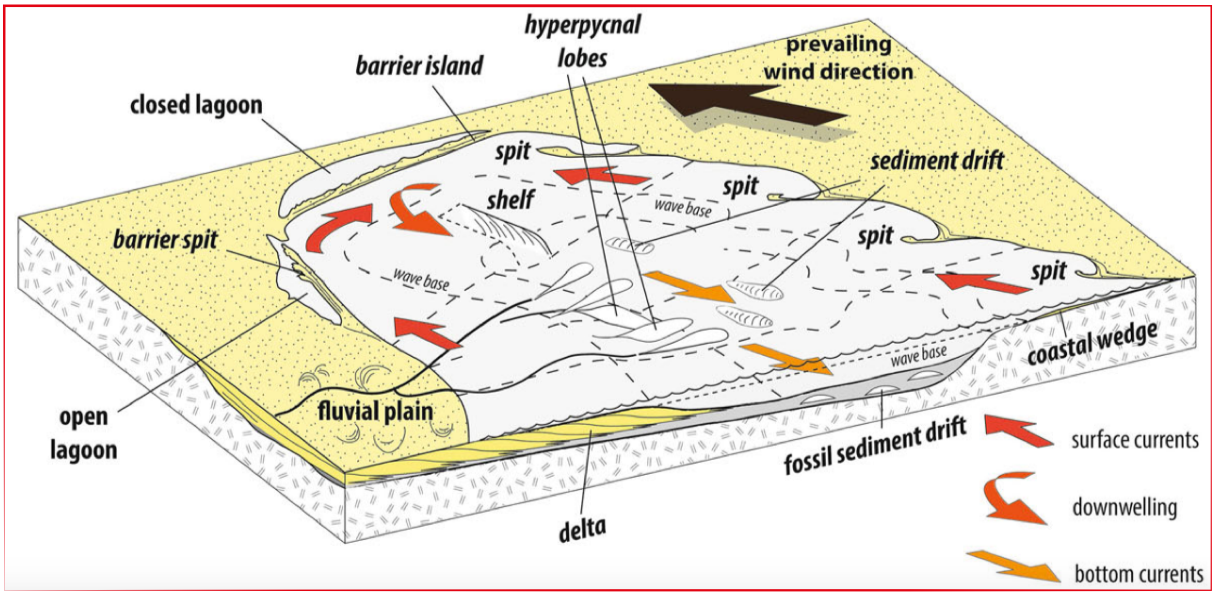


Figure 1. *Depositional model for 'wind driven waterbodies' (Nutz el al., 2015b). The shoreline shape and direction with regards to the prevailing wind direction, along with its strength, controls the occurrence of diverse kind of water current (surface current, verticals, 'downwelling' and bottom current) and sedimentary forms along lake shoreline and bottom. In addition to the straightforward wind influence, strong 'hyperpycnal' currents can be generated during strong fluvial discharges, contributing to sub-lacustrine lobes (hyperpycnal lobes). After Nutz et al., 2016.*

Figure 1*. Modèle de dépôt pour les systèmes lacustres à fort hydrodynamisme dominé par le vent ('wind-driven waterbodies' de Nutz et al., 2015b). La forme et direction du rivage par rapport au sens du vent prédominant, plus la puissance de celui-ci, conditionnent différentes sortes d'écoulements (superficiels, verticaux, 'downwelling', et profonds) et de formes sédimentaires le long du rivage et au centre du lac. Outre l'influence directe du vent, des courants 'hyperpycnales' forts peuvent être générés lors de fortes décharges fluviatiles, contribuant à des lobes sous-lacustres ('hyperpycnal lobes'). D'après Nutz et al., 2016.*

1.1.1.1.2 Processus hydrodynamiques générés par les cours d'eau

Alors que les courants et les vagues dans les lacs sont principalement dus au vent, l'écoulement inertiel des rivières au niveau de l'embouchure rehausse davantage la circulation de l'eau dans le lac (Zavala et al., 2011; Nutz et al., 2016; Zavala, 2020). Ainsi, en fonction de l'écart de densité entre celle du fluide entrant (l'eau du cours d'eau et la charge particulaire charriée par celle-ci) et celle de l'eau hébergeant le réceptacle, le lac, trois catégories d'écoulement peuvent être générées au niveau de la zone de l'ombochure (Bates, 1953; Zavala et Pan, 2018; Zavala, 2020). L'écoulement 'hypopycnal' ('hyperpycnal') se génère spontanément si la densité de l'eau, plus la charge sédimentaire, du cours d'eau est inférieure (supérieure) à celle du réceptacle, alors que l'écoulement 'homopycnal' se forme pour des valeurs semblables (Bates, 1953; *voir* Zavala, 2020) (Fig. 2). En particulier, chaque type de ceux-ci alimentent un cas typique de fameuses édifices sédimentaires

connues sous le vocable ‘deltas’ (*cf. infra*) (‘mouth delta’, delta de type ‘Gilbert’, delta sous-aquatique ; *voir* Postma, 1990; Zavala et al., 2011).

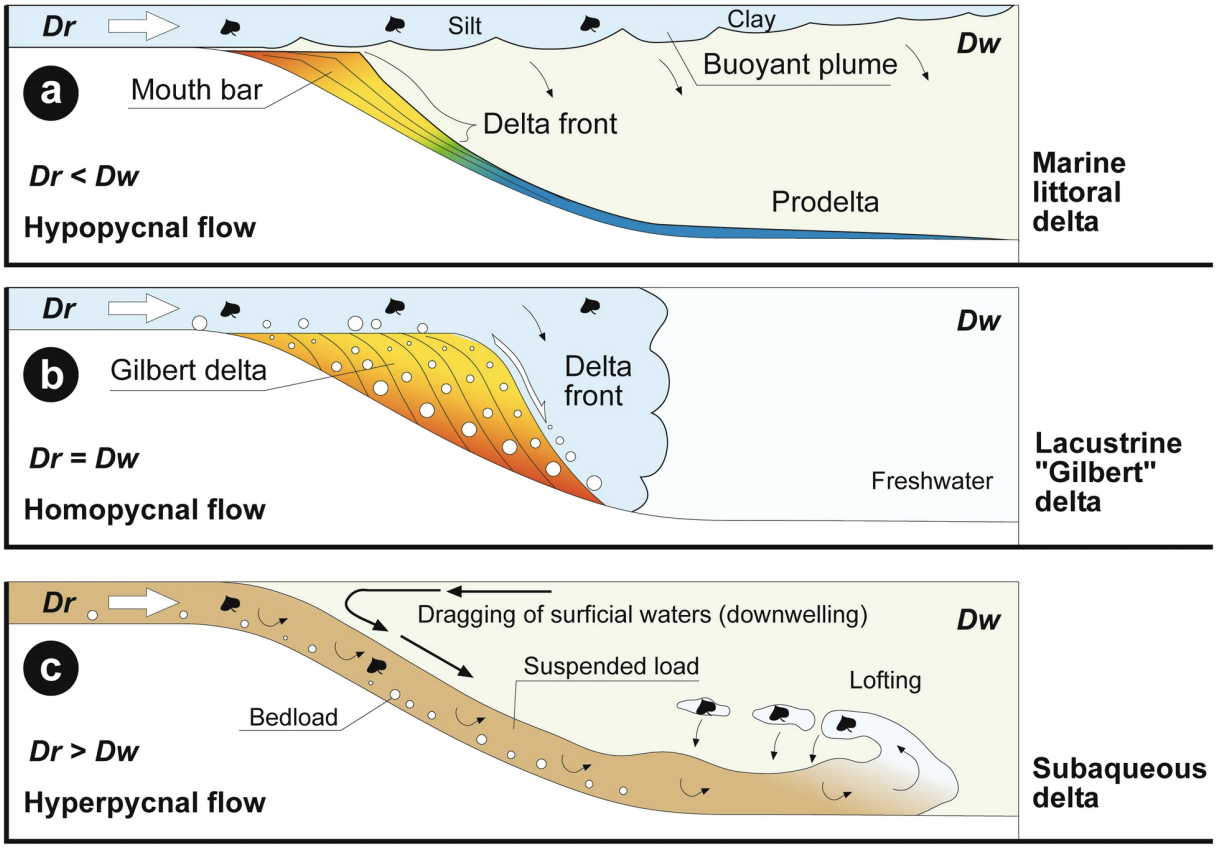


***Figure 2**. Origin of hypopycnal (a), homopycnal (b) and hyperpycnal (c) flows as a result of the density contrast between river discharge (Dr) and basin waters (Dw). Note in c that the excess in density is provided by sediments in turbulent suspension. After Zavala (2020).*

***Figure 2**. Écoulements ‘hypopycnal’ (**a**), ‘homopycnal’ (**b**), et ‘hyperpycnal’ résultant du contraste de densité entre la décharge du cours d’eau (Dr) et l’eau du bassin (Dw). L’excès de densité en **c** est conditionné par les particules turbulentes en suspension. D’après Zavala (2020).*

1.1.1.1.3 Processus associés à la déjection des sédiments : écoulements gravitaires des sédiments

En amont des versants, des écoulements de sédiments (avec une proportion d’eau modérée à faible) principalement entraînés par la gravité avec durées et densités variables (dépendantes de la proportion d’eau) peuvent se générer et alimenter des structures en éventail dites « cônes de déjection » ainsi développés en aval des versants (Baali et al., 1996; Blair et McPherson, 2009). Dans certaines circonstances, ces écoulements peuvent gagner des étendues d’eau stagnante (lac ou mer). Dès lors, en continuant leur parcours sous l’eau, ils peuvent subir des modifications considérables affectant leur rhéologie et propriétés hydrodynamiques initiales (Nemec et Steel, 1984). Ce processus peut toutefois être auto-généré dans le bassin lui-même et ainsi qualifié de ‘intra-bassin’ (*'intrabasinal'* ; Zavala et Arcuri, 2016). Ces écoulements de sédiments, conduits principalement par la gravité et,

conséquemment, leur densité apparente, sont classifiés comme des « écoulements gravitaires des sédiments » (‘*sediment gravity flows*’, SGF, *sensu* Middleton et Hampton, 1973). Ils sont distingués de leurs homologues « écoulements gravitaires fluides » (écoulements fluviatiles où le fluide, de type newtonien, est très dilué), dans lequel un fluide est déplacé, l’eau dans ce cas, par gravité et les sédiments sont entraînés passivement par les forces de cisaillement gouvernées par l’énergie cinétique du flux (Middleton et Hampton, 1973; Zavala, 2020). Conformément au mécanisme dominant de support des sédiments (‘*sediment-support mechanism’*) et leur rhéologie, plusieurs types de SGF ont été distingués (Middleton et Hampton, 1973; Carter, 1975; Lowe, 1979, 1982; Nardin et al., 1979; Postma, 1986; Haughton et al., 2009). Toutefois, des controverses et débats très sérieux se sont provoqués dont le principal problème réside toujours dans la nature fossile des dépôts empêchant une quantification explicite des caractéristiques initiales des sédiments (e.g ., densité, rhéologie de l’écoulement), la base de la classification elle-même (Lowe, 1979; Mulder et Alexander, 2001; Dasgupta, 2003). En guise de simplicité, Zavala a récemment proposé une nouvelle classification des SGF Basée sur les concepts développés par Mutti (1992), Mutti et al. (1999) et Mulder et Alexander (2001). Ainsi, quatre classes résumant les processus gravitaires de sédiments d’origine extra-bassin et intrabassin (i.e., *‘land-derived and intrabasinal sediment gravity flows’*) ont été distinguées en fonction des propriétés physiques et mécaniques initiales tirées de l’état final des sédiments impliqués dans le processus (Zavala, 2020 ; Fig. 3), à savoir : (i) *‘cohesive debris flow’* (CDF) ; (ii) *‘hyper-concentrated flows’* (HCF) ; (iii) *‘concentrated flows’* (CF) ; et (iv) *‘sediment-laden turbidity flows’* (SLTF).

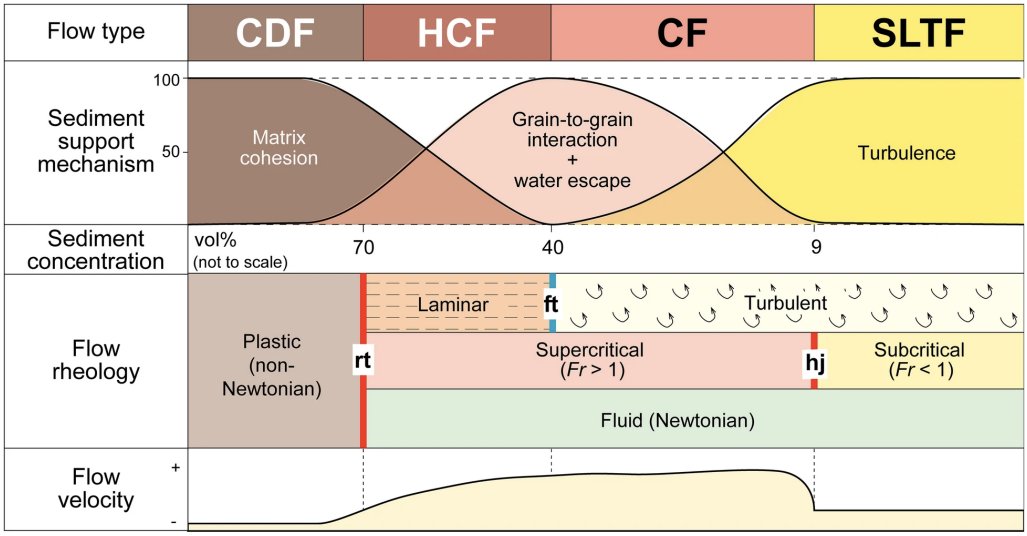


Figure 3. *Classification of sediment gravity flows after Zavala (2020, and references therein). CDF: Cohesive debris flow; HCF: Hyperconcentrated flow; CF: Concentrated flow; SLTF: Sediment-laden turbulent flow; rt.: Rheological transformation; ft.: Flow transformation; hj: Hydraulic jump; Fr: Froude number. Note that sediment concentration (% volume) is not to scale.*

***Figure 3**. Classification des écoulements gravitaires des sédiments ('sediment gravity flows') selon Zavala (2020, et références y afférentes). CDF : Cohesive debris flow ; HCF: Hyperconcentrated flow ; CF : Concentrated flow; SLTF : Sediment-laden turbulent flow; rt.:Transformation rhéologique; hj : Saut hydraulique (hydrolic jump) ; Fr : Nombre de Froude. La concentration de sédiments (en % de volume) n'est pas à échelle.*

En résumé, les trois processus physiques, laconiquement abordés, assurent le brassage du contenu fluide et la redistribution entière des sédiments dans le bassin lacustre, dès lors directement impliqué dans la sédimentologie et la stratigraphie de celui-ci. Il est à noter que ces processus varient spatialement d'importance d'un bassin à l'autre et temporellement dans le même bassin au rythme de la variabilité climatique et les contextes tectonique et morpho-structural gouvernants le bassin. Conformément à ce concept, et en s'appuyant sur des travaux pionniers de certains auteurs (e.g., Håkanson, 1982; Dam et Surlyk, 1992; Dam et al., 1993; Normandeau et al., 2013; Desiage et al., 2015), Nutz et al. (2016) ont proposé une classification ternaire basée sur la dynamique sédimentaire qui domine le bassin (Fig. 4) : systèmes lacustres à dominance éolienne (*'wind-driven* waterbodies') ; systèmes lacustres à dominance fluviatile (*'river-driven waterbodies'*) ; systèmes lacustres dominés par les processus gravitaires sous-aquatiques (*'gravity-driven waterbodies'*).

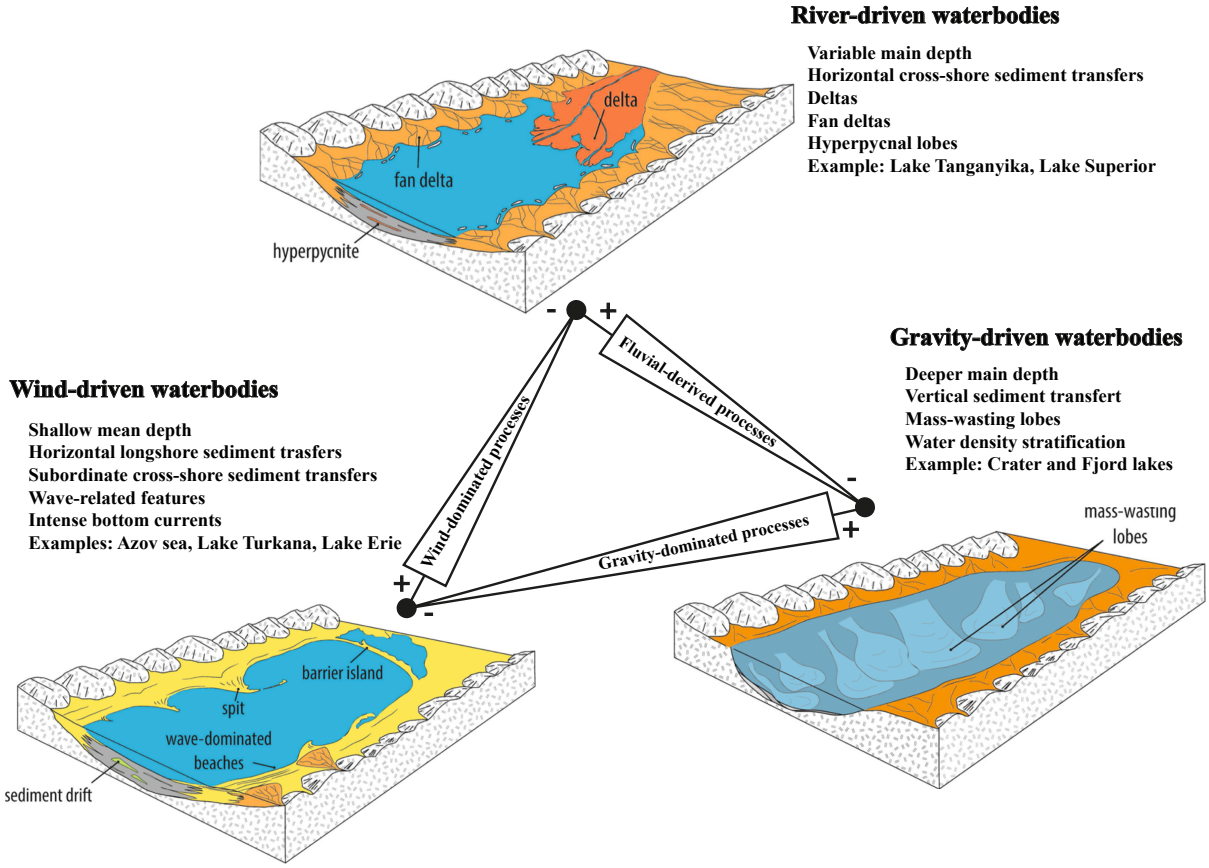


***Figure 4**. Ternary classification for lacustrine systems based on physical sedimentary dynamics. Adapted after Nutz et al. (2016).*

***Figure 4**. Classification ternaire des systèmes lacustres basée sur la dynamique sédimentaire. Adaptée d'après Nutz et al. (2016).*

1.1.1.2 Stratification et brassage des eaux

1.1.1.2.1 Stratification thermique

La sédimentation dans les lacs est forcément contrôlée par le régime thermique des eaux capable de générer une stratification (Renaut et al., 2010). En raison de l'écart vertical de l'énergie calorifique reçue par l'irradiation solaire, deux couches divisant thermiquement la colonne d'eau sont communément développées (Ullyott et Holmes, 1936; Dake et Harleman, 1969; Boehrer et Schultze, 2008; Yu et al., 2010; Kirillin et Shatwell, 2016). La couche thermique superficielle, plus chaude et généralement plus légère, est appelée « épilimnion », alors que celle se développant en bas, plus froide et généralement plus dense, est appelée « hypolimnion » (Fig. 5) (Renaut et al., 2010). La transition entre les deux couches thermiques, reflétant un changement brutal de température, est appelée « metalimnion », alors que le point de flexion de la courbe de température définit la thermocline (Fig. 5).

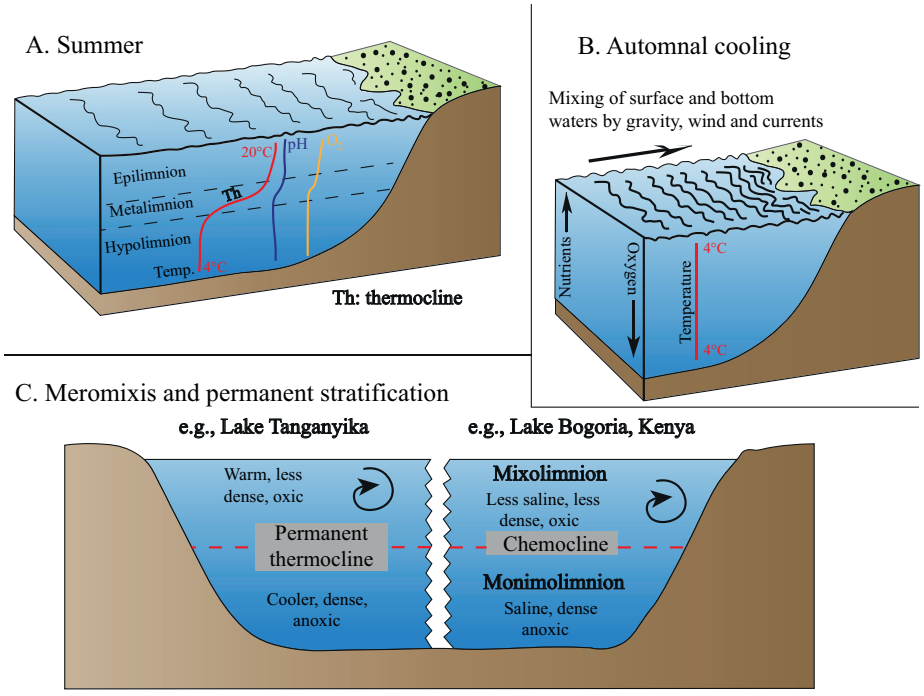


Figure 5. *Stratification in lakes.* ***A****: Vertical profile of temperature, pH and oxygen in a typical perennial lake during warm summer months. Warm, less dense surface waters lie upon denser cooler waters, separated by the thermocline.* ***B****: Breakdown of stratification during winter months when surface waters cool to 4°C and attain their maximum density. Surface and bottom waters can be mixed by wind induced currents, waves and gravity.* ***C****: Meromixis (stable stratification) can develop when surface waters are consistently warmer than the cooler, dense bottom waters or when relatively less saline surface waters lie upon denser more saline brines. Redrawn from Renault et al. (2010).*

Figure 5. *Stratification des eaux des lacs.* ***A*** *: Profil vertical de température, pH et oxygène pour un lac permanent typique pendant la saison chaude. Durant cette saison, une couche d'eau chaude, moins dense repose sur une couche froide et plus dense, séparées par la thermocline.* ***B*** *: Rupture de stratification pendant la saison froide lorsque les eaux de surface atteignent 4°C, ainsi atteignant leur densité maximum. Les eaux de surfaces et de fond peuvent dès lors se mélanger facilement via les courants induits par le vent, vagues et gravité.* ***C*** *: Meromixisme (stratification stable) peut se développer lorsque les eaux de surface sont constamment plus chaudes que les eaux de fond (cas du lac Tanganyika), ou lorsque les eaux de surface relativement moins salines reposent sur des eaux de fond plus salines (plus denses ; exemple du lac Bogoria). Redessinée d'après Renault et al. (2010).*

1.1.1.2.2 Brassages thermiques

Alors que le vent et les courants induits par les afflux dus aux rivières, comme s'est déjà démontré plus haut, peuvent entraîner le brassage de la colonne d'eau, les variations verticales de la densité de l'eau, contrôlée par la température, sont responsables de la plupart des brassages que connaissent les lacs modernes (Wetzel, 2001). Le mécanisme expliquant ceux-ci peut être résumé comme suit : étant donné que l'eau douce atteint sa densité maximale à température (T°) égale à 4 °C, la masse d'eau constituant l'épilimnion, en se refroidissant (ou se réchauffant si T° < 4 °C) et ainsi devenant aussi dense ou plus dense que la masse d'eau sous-jacente, une instabilité (dite de Rayleigh-Taylor) se crée et conséquemment force la masse d'eau de surface (de fond), plus dense (moins dense), à plonger (remonter), déclenchant ainsi un brassage complet des eaux du lac. Dans le cas où les deux masses d'eau (de surface et de fond) atteignent 4 °C (i.e., une densité uniforme), le brassage devient plus facilement abordable par la simple action du vent ou de rivière.

1.1.1.2.3 Classification et implications

En tenant compte du nombre de brassage induit par année, les limnologistes ont établi une classification descriptive (e.g., Hutchinson, 1957; Håkanson, 1982; Lewis Jr., 1983; Wetzel, 2001) en distinguant : lacs monomictiques (brassage une seule fois annuellement) ; lacs dimictiques (brassage deux fois annuellement, généralement au printemps et en automne) ; lacs polymictiques (lacs peu profonds se stratifiant temporairement pour des périodes courtes, mais se brassant librement le reste de l'année) ; et lacs meromictique (lacs restant généralement stratifiés tout au long de l'année ; Hakala, 2004).

Le régime thermal et la conséquente stratification présentent des implications directes dans la sédimentation lacustre et les caractères des faciès sédimentaire qui en découlent (Renaut et al., 2010). Ainsi, en devenant stratifiés, les eaux de fond s'isolent de l'atmosphère et deviennent à leur tour anoxique par le biais des bactéries aérobiques après avoir consommé toute la réserve en dioxygène (Renaut et al., 2010). Par conséquent, la préservation de la matière organique et de la lamination faite par les sédiments décantés est favorisée (*cf., infra*). Généralement, le brassage des eaux lacustres induit de nombreuse effets déterminants influençant à la fois l'écologie du milieu et le mode de sédimentation (Renaut et al., 2010), à savoir :

- recyclage des nutriments essentiels (N, P) du fond vers la surface, stimulant ainsi la productivité planctonique ;

- refroidissement ou réchauffement des eaux de fond et de surface imposant des modifications remarquables sur le système d'équilibre calco-carbonique et sur l'activité biologique dans son ensemble ;
- oxygénation des eaux de fond favorisant (i) l'oxydation de certains éléments réduits et donc mobile (e.g., Fe^{2+} et Mn^{2+}), ce qui cause leur précipitation en minéraux oxydés, et (ii) la bioturbation par les organismes benthiques.

1.1.2 Processus chimiques et biochimiques

Le chimisme des eaux des lacs est une variable non linéaire, ne dépendant ni du temps ni de l'espace. Ainsi, contrairement à celle de l'océan, la composition chimique des eaux lacustres est très variable, principalement contrôlée par le substrat rocheux, l'hydrologie, le climat, et le temps de résidence des eaux (Dean et al., 2007; Verrecchia, 2007; Rosenbaum et Kaufman, 2009). Que ce soit d'eau douce ou saline, les lacs sont présentés simultanément depuis les régions polaires jusqu'à l'équateur (Renaut et al., 2010). En effet, le caractère doux des eaux se présente chaque fois un drainage ouvert est maintenu (i.e., le lac est hydrologiquement ouvert) et la somme des entrées (précipitations directes, ruissèlements, recharge par la nappe) équivaut celle des sorties (flux sortant et évaporation) (Fig. 6A et B). En revanche, un lac salé est conditionné si le bassin lacustre est hydrologiquement clos en permanence, favorisant ainsi le stockage des solutés transportés (à l'exception du CO_2 hydraté qui est facilement dégazé en fonction de sa pression partielle dans l'atmosphère) par le réseau de drainage depuis le bassin versant après hydrolyse et dissolution de la roche mère. En outre la disponibilité en éléments nutritifs sépare l'état eutrophe (disponibilité importante en nutriments) de l'état oligotrophe (limitation en nutriments), eux même influencés par l'état hydrologique du lac (Fig. $6A_1$ et B_2). Le passage d'un lac d'eau douce à un lac d'eau salée est concevable. Ainsi, lorsque le taux d'évaporation plus la perte des eaux souterraines surpassent les entrées annuelles, le lac diminue de volume et devient hydrologiquement plus fermé et plus concentré en anions des halogènes et cations des alcalins susceptibles d'augmenter la conductivité (et donc la salinité de l'eau), tel est acquis le caractère salé. L'augmentation davantage des concentrations en ces ions (allogènes et alcalins) au-delà du point de saturation (sursaturation de l'eau par rapport aux espèces minérales à précipiter), ils précipitent pour former la série évaporitique classique (Fig. 6) (Renaut et al., 2010).

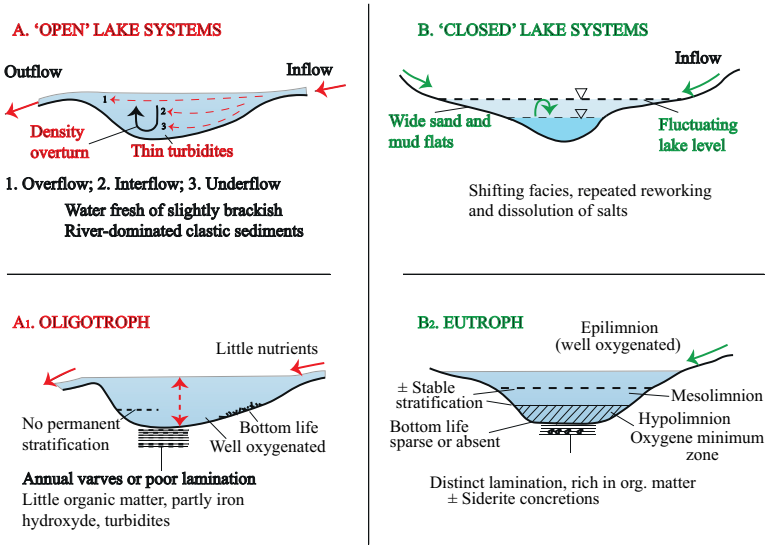


***Figure 6**. Overview of different lake systems. **A**. Open system with inflow and outflow; the lake water chemistry is river-dominated. A1. Well oxygenated, oligotrophic lake (poor in nutrients). **B**. Closed systems without outflow; concentration of dissolved species commonly increasing with lowering lake water level and time. **B2**. Stable stratification of lake water and eutrophic conditions with oxygen-deficient bottom water. Redrawn after Einsele (2000, p. 77).*

***Figure 6**. Aperçu sur les différents systèmes lacustres. **A**. Système ouvert avec flux entrant et flux sortant ; la chimie du lac est dominée par celle du cours d'eau. **A1**. Lac oligotrophe (pauvre en nutriments) bien oxygéné. **B**. Système clos (sans flux sortant) ; l'augmentation de la concentration des espèces chimiques est fonction de la variation du niveau d'eau modulée par l'évaporation/précipitation. **B2**. Stratification stable de la colonne d'eau et installation des conditions d'eutrophie (disponibilité importante en nutriments) avec déplétion en oxygène des eaux de fond. Redessinée d'après Einsele (2000, p. 77).*

En fait, les cations dominants dans la plupart des lacs d'eau douce (diluée) sont, typiquement, Na^+ et Ca^{2+} et, variablement, K^+ et Mg^{2+} qui dépendent de la nature chimique du substrat rocheux directement touché par le réseau de drainage du système lacustre. En revanche, les anions démontrent une variabilité plus prononcée (Renaut et al., 2010). Ainsi, les espèces carbonatées (e.g., HCO_3^-, CO_3^{2-}) dominent les systèmes lacustres à substrat carbonaté (e.g., calcaires et dolomies). L'altération par hydrolyse des terrains métamorphiques ou magmatiques peut aussi libérer quelques espèces carbonatées. Alors qu'elles peuvent être libérées par altération (dissolution) de certaines évaporites et présentés dans les précipitations sous forme de pluies (comme noyaux de condensation, i.e., aérosols marins), les ions sulfates sont les principaux produits de l'oxydation des sulfures (composés contenant du souffre réduit, e.g., la pyrite). D'autre part, les chlorures sont principalement originaires des aérosols marins et eaux souterraines généralement confinées, mais peuvent aussi provenir des inclusions fluides dans les évaporites ou via la dissolution de la halite (NaCl). La silice hydratée, fluorures, et nutriments (e.g., N, P) forment le reste des solutés les plus communes.

Les précipités chimiques dans les lacs d'eau douce incluent : carbonates ; minéraux associés aux changements des conditions réd-ox comme les oxy-hydroxydes de Fe et Mn ; et plus accessoirement quelques phosphates et minéraux argileux. Généralement, la précipitation des phosphates caractérise les lacs d'eau salée ou de saumures (*'brine lakes'*). Ces derniers sont très

communs dans le cas de bassins lacustres hydrologiquement fermés avec un rapport évaporation/précipitation élevé (Eugster et Hardie, 1978; Jones et Deocampo, 2003). Ils sont dominés par des processus purement chimiques où la concentration en ions est principalement gouvernée par l'excès d'évaporation (Müller et al., 1972; Morgan et Stone, 1985; Gierlowski-Kordesch, 2010). D'autre part, la précipitation des carbonates dans les lacs d'eau douce peut être directement (bio-contrôle) ou indirectement (bio-médiation) associée à l'activité biologique de certains microorganismes (e.g., cyanobactéries), faune (e.g., gastéropodes, ostracodes) et flore (e.g., chara) (Müller et Wagner, 1978; Kempe et Kazmierczak, 1990; Merz, 1992; Robbins et Blackwelder, 1993; Arp et al., 2010; Gierlowski-Kordesch, 2010). Il est important de souligner que l'accumulation des carbonates dépend forcément de la présence et abondance des roches carbonatées formant le substrat ou quelques types de roches volcaniques dont l'assemblage minéral inclut des minéraux riches en Ca (e.g., plagioclases calciques ; Renaut et al., 2010; Gierlowski-Kordesch, 2010). L'implication de l'activité biologique dans la précipitation de la calcite se voit spécialement lorsqu'il y a précipitation sans qu'il y ait de sursaturation par rapport à $CaCO_3$ (Renaut et al., 2010). Les coquilles de bivalves et de gastéropodes, tests d'ostracodes en plus de carbonates précipités par charophytes, ainsi que les éléments carbonatés détritiques gagnant le lac via le réseau de drainage, collectivement contribuent à l'accumulation dans le fond du lac de la calcite et de l'aragonite. Toutefois, nucléation et croissance de petits cristaux de carbonates peuvent avoir lieu au niveau de la zone photique (épilimnion) avant d'être forcés à décanter par la gravité (Renaut et al., 2010). Ce phénomène de nucléation induit au voisinage de la surface peut être commandé par évaporation, réchauffement saisonnier, et dégazage de CO_2, collectivement contribuent à la décroissance de la solubilité de $CaCO_3$. L'exclusion de CO_2 peut être favorisée par l'activité photosynthétique de certaines bactéries (cyanobactéries) et algues (Gierlowski-Kordesch, 2010); le carbonate de calcium précipité par ce processus est dit bio-induit.

1.1.3 Événements extrêmes et dépôts associés

Les risques naturels sont capables d'engendrer des modifications sérieuses, à la fois instantanées et brutales, sur l'infrastructure humaine et les environnements de dépôts naturels. Cet effet instantané et brutal leur attribut le qualificatif de « événements extrêmes ». La plupart de ces événements peuvent être inclus dans l'un des deux catégories : géodynamique (e.g., tremblements de terre, tsunamis, éruptions volcaniques) et climatique (e.g., crues, hurricans, avalanches) (Sabatier et al., 2022; Fig. 7). Les éventuelles empreintes de ces phénomènes sévères et périodiques dans les

sédiments lacustres devraient être une vertu incommensurable puisqu'elles auraient rehaussé davantage notre appréciation *vis-à-vis* de la période de récurrence et magnitudes de l'événement en question dans le passé. Ainsi, depuis les environnements de hautes altitudes jusqu'aux milieux côtiers, le registre géologique des lacs permet d'archiver, en allant jusqu'à plusieurs milliers d'années, une large variété d'événements (Sabatier et al., 2022), tels que crues fluviales (e.g., Wilhelm et al., 2022), crues associées à la rupture d'un barrage glaciaire retenant un lac glaciaire ('*glacial-lake outburst floods*' ; e.g., Xu et al., 2015), hurricans (e.g., Chaumillon et al., 2017), avalanches (e.g., Fouinat et al., 2018), séismes (e.g., Sims, 1975; Moernaut, 2020), tsunamis lacustres (e.g., Kremer et al., 2021), éruptions volcaniques (Van Daele et al., 2014) (Fig. 7).

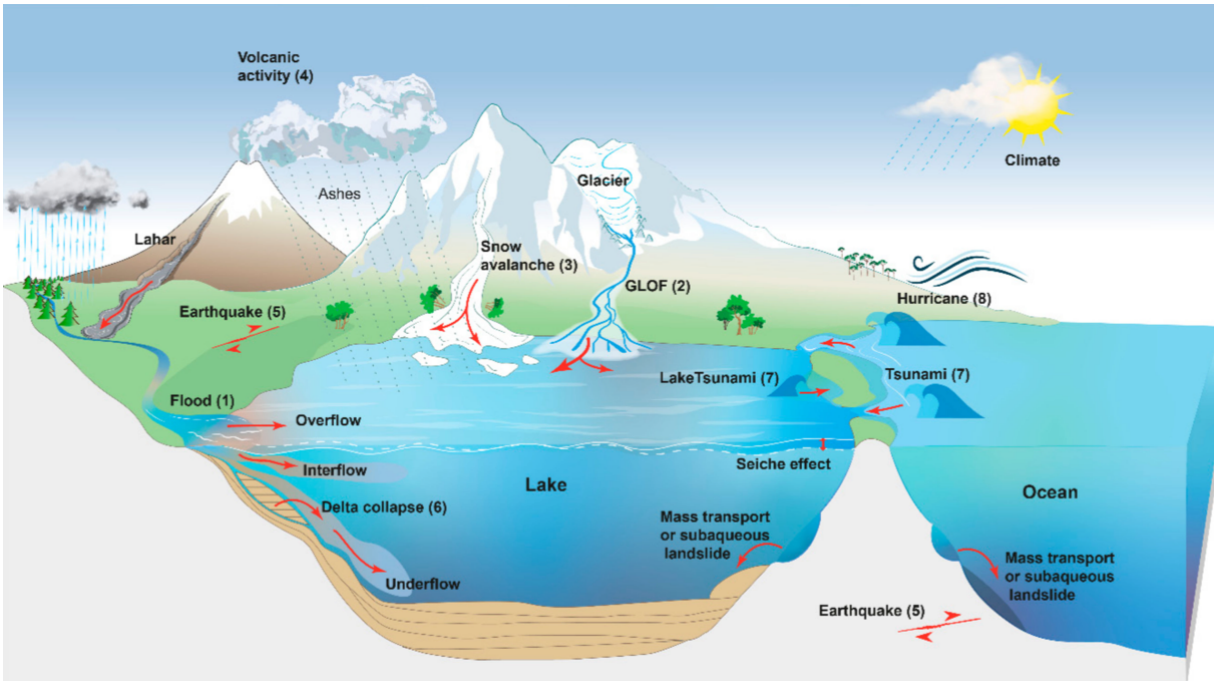


***Figure** 7. Processes at the origin of event deposits in lake systems. GLOFs: glacial-lake outburst floods. After Sabatier et al. (2022).*

***Figure** 7. Processus sur l'origine des dépôts d'événements extrêmes dans les systèmes lacustres. GLOFs : 'glacial-lake outburst floods' (crue associée à la rupture d'un barrage glaciaire retenant un lac glaciaire). D'après Sabatier et al. (2022).*

Bien que ces événements sont extrêmement différents par nature, récurrence et amplitude, leurs empreintes dans le registre géologique ne peuvent être autant différentes puisque le résultat, dans la plupart des cas, est un dépôt dit de « transport de masse » ('*mass-transport deposit*') où la dynamique du transport et de la déposition est gouvernée par des processus gravitaires (un bref aperçu sur ces dépôts est fourni dans **§1.1.1.1.3**) (Sabatier et al., 2022), ce qui rend leur décryptage depuis les sédiments hôtes un vrai défi. Cependant, d'autres processus, autres que associés au transport gravitaire, peuvent aboutir à l'enregistrement d'un ou de plusieurs types d'événements extrêmes pour autant que

le dépôt hôte soit déjà déposé et à l'état mou ('*soft-sediment*') avant que l'événement ne soit-il déclenché. En effet, il s'agit de déformations 'ductiles' ou cassantes déclenchées par l'événement (e.g., séisme, tsunami, avalanche) et guidées par des forces internes ou externe (forces motrices; Owen, 1987) après que le sédiment hôte (toujours à l'état mou) voit sa résistance au cisaillement diminue ou devenant nulle (mécanisme de déformation, *liquidization*, *sensu* Allen, 1977). Celles-ci, baptisées en anglais '*soft-sediment deformation structures*' (SSDSs), reçoivent un grand intérêt dans ce projet de thèse et sont exhaustivement communiquées dans l'article 1 présenté comme chapitre 3. Pour plus de détail sur les différents événements extrêmes, les processus géologiques qui en découlent et leurs empreintes dans le registre lacustre, le lecteur peut trouver une exhaustive révision récemment publiée par Sabatier et al. (2022) dans *Quaternary* (MDP AG). En outre, une très bonne exposition sur les SSDSs peut être trouvée dans le bouquin précurseur par Allen (1982, volume B, p. 343-393) et l'article fondateur par Owen (1987). D'autres révisions qui peuvent intéresser le lecteur sur le sujet des SSDSs, les processus de déformation et leur classification, sont, entre autres : Plaziat et al. (1990) ; Collinson (1994, 2019) ; Greb et al. (2002) ; Montenat et al. (2007) ; Van Loon (2009, 2014) ; Owen et al. (2011) ; Owen et Moretti (2011) ; Waldron et Gagnon (2011) ; Dechen et Aiping (2012) ; Moretti et al. (2014) ; Topal et Özkul (2014) ; He et Qiao (2015) ; Menzies et al. (2016) ; Shanmugam (2017).

1.2 Sédimentation et environnements de dépôts

Références. La synthèse présentée dans cette sous-section s'intéresse uniquement aux lacs d'eau douce qui peuvent être soit ouverts ou équilibrés hydrologiquement, généralement dans les régions tempérées humides à subhumides. Les lacs d'eau salée où l'évaporation l'emport largement sur les précipitations, en partie favorisé par l'état hydrologique fermé du bassin lacustre, sont hors du cadre de ce doctorat et donc totalement omis. Le lecteur intéressé à ces systèmes lacustres producteur d'évaporites peut se référer à : Eugster et Hardie (1978) ; Hardie et al. (1978) ; Lowenstein et Hardie (1985) ; Smoot et Lowenstein (1991) ; Gierlowski-Kordesch et Rust (1994) ; Rosen (1994) ; Schubel et Lowenstein (1997) ; Last et Ginn (2005) ; Benison et al. (2007). En outre, l'ensemble de références que la présente synthèse repose sur sont citées d'emblée : Kelts et Hsü (1978 ; **sédimentation carbonatée et développement des laminites**) ; Murphy et Wilkinson (1980 ; **production carbonatée en contexte d'un lac marneux**) Dean (1981; **sédimentation carbonatée et organique**) ; Dean et Fouch (1983 ; **environnements lacustres carbonatés**) ; Cohen et Thouin (1987, **sédimentation carbonatée en zones côtières**) ; Platt et Wright (1991 ; **modèles de faciès en contexte carbonaté**) Einsele (2000 ; **généralités**) ; Owen (2002 ; **précipitation des silicates amorphes**) ; Renaut et al. (2010 ; **généralités**) ; Nutz et al. (2015a, 2016 ; **sédimentation dominée par les vagues**)

1.2.1 Lacs dominés par la sédimentation détritique

La composante détritique terrigène des sédiments lacustres reflète le relief, le climat et la lithologie des roches directement impliquées dans les processus de drainage caractérisant le système lacustre. Généralement, les lacs proglaciaires et les lacs des régions montagneuses sont dominés par

les sédiments détritiques, y compris ceux de nature carbonatée. En effet, en raison d'un taux de sédimentation élevé, la sédimentation autochtone est forcément diluée, ou très faible pour être significative. De ce fait, la sédimentation dans un lac de tels caractères est largement contrôlée par les processus physiques favorisant la distribution de la charge de fond et en suspension des cours d'eau entrants le lac (*cf.*, **§1.1.1.1.2.**). Ainsi s'instaure une pléthore de sous-environments de dépôts conditionnés par les trois processus majeurs illustrés dans la figure 1 (i.e., vent, gravité, forces d'inertie des cours d'eau entrant). En raison de simplicité, on peut les regrouper en deux zonations qui se distinguent hydrodynamiquement et bathymétriquement : zone littorale ('*nearshore enironment*') et zone profonde ('*offshore environment*').

1.2.1.1 Zone littorale : modèle de faciès

La zone littorale en domaines lacustres, contrairement à leurs homologues marins, varie considérablement d'un cas à l'autre en fonction principalement de la pente, les niveaux d'énergie et qu'au type, l'apport et la texture des sédiments. Ainsi, en conditions calmes avec gradient topographique faible, certains lacs développent dans leur bordure (arrière plage, '*backshore*') de la vasière ou platière sableuse ('*mud flat*' et '*sand flat*', respectivement) où la végétation est généralement absente ou peu développée. L'accumulation des sédiments grossiers dans de telles conditions est très limitée, voire absente, rendant difficile le traçage de la ligne côtière durant n'importe quel point dans le temps. Par contre, dans le cas où l'énergie est considérable, à l'image de leurs homologues marins bien qu'à petite échelle, arrière plage ('*backshore*'), plage/estran ('*foreshore*') et avant-plage ('*shoreface*') peuvent s'individualiser (Fig. 8D), ainsi rendant possible le traçage de la ligne côtière (implication directe sur la stratigraphie séquentielle). Cependant, la transition littoral-large ('*nearshore-offshore*') est plus subtile comparée au domaine marin. Qui plus est, au niveau des zones de confluence (exutoires d'un cours d'eau), la signature fluviatile est plus remarquable et, à nouveaux, trace explicitement la ligne côtière une fois que les dépôts associés (i.e., deltaïque, *cf.,* **§1.1.1.1.2.**) sont reconnus dans le registre lacustre (Fig. 8E).

Pour plus de détail concernant ces dépôts littoraux, que ce soit dominés par les vagues (action du vent, '*wave-influenced nearshore deposits*', Fig. 8D) ou par le régime fluviatile ('*river-dominated nearshore deposits*', Fig. 8E), un exemple concret et surtout exhaustif où le lecteur peut consulter est fourni par Nutz et al. (2017, 2020) pour le lac Turkana en Kenya (système de rift Est africain).

1.2.1.2 Zone profonde : modèle de faciès

La zone centrale en domaines lacustres ('*offshore*') reçoit généralement moins d'énergie et est considérée comme un environnement calme. De ce fait, outre le transport éolien, les apports détritiques venus des cours d'eau doivent être distribués dans le centre du lac selon des mécanismes différents de

ceux évoquant l'influence directe du vent (Figs. 1 et 2). Ainsi, dans le cas de lacs profonds, une large proportion de la charge de fond d'un cours d'eau sableux ('*sandy river*') est transportée depuis le prodelta à fort pendage ('*Gilbert-type delta*') jusqu'aux milieux plus profonds, que ce soit directement par les flux profonds ('*underflows*') lors des périodes de crues fluviatiles, ou par des processus gravitaires qui évoluent par transformation en courants de turbidité, les deux discutés dans **§1.1.1.1.** (Fig. 2). Dans ce cas, la texture des sédiments hébergeant le fond de tels lacs est principalement silto-sableuse, i.e., des niveaux fins sableux ou silteux de turbidites alternant avec des niveaux plus fins (argilo-silteux, '*mud*') formés par des processus de décantation des éléments en suspension ('*suspension-fallout processes*') (Fig. 8E1). Dans le cas où l'écoulement fluviatile est chargé considérablement en charge de fond ('*sediment-laden flows*'), des chenaux sous-aquatiques avec des levées bien marquées peuvent se développer au-dessus des sédiments deltaïques, depuis la pente du prodelta vers le fond lacustre (Fig. 8A). Dans un deuxième scénario, les eaux fluviatiles chargées plutôt en suspension avec une densité plus faible que celle des eaux de fond, une composante de flottabilité se développe (effet de la poussée d'Archimède) et les flux entrants distribuant leur charge en suspension dans le lac sont plutôt intermédiaires à superficiels (*voir* Figs. 2 et 6A). Des successions rythmiques résultent de ces processus varient depuis des turbidites proximales, formées principalement de niveaux sableux, jusqu'à des sédiments semblables aux varves formées plus distalement (Fig. 8E2). En fait, la période de récurrence des événements aboutissant à des turbidites est rarement saisonnière, mais plutôt irrégulièrement contrôlée par les événements extrêmes tels que les tempêtes, qui peuvent se produire plusieurs fois par année, ou d'autres qui sont moins fréquents mais avec grande amplitude. Une présentation plus exhaustive avec plus de schémas très pédagogique sur la sédimentation détritique de large ('*offshore*') est fournie par Robin W. Renaut et Elizabeth H. Gierlowski-Kordesch dans le chapitre dédié aux lacs du bouquin 'Facies Models' (Renaut et al., 2010, p. 554-558).

1.2.2 Lacs dominés par l'activité biologique authigénique

Comme les apports détritiques originaires du bassin versant d'un système lacustre varient considérablement d'un cas à l'autre, la contribution biologique productrices des squelettes minéralisés biogéniques (e.g., microfossiles et produits des organismes nectoniques) et matière organique brute (e.g., pelotes fécales ou pellets des planctons, débris de macrophytes) en domaine lacustre dépend intimement de la chimie des eaux du lac ainsi que les nutriments transportés par le réseau de drainage. Par exemple, les eaux lacustres riches en ions alcalino-terreux, spécialement les ions ca^{2+} sont favorables pour la croissance des organismes sécréteurs de tests calcaires (précipitation bio-contrôlée), alors que les lacs pauvres en Ca^{2+} mais relativement riches en silice dissout et en nutriments (comme P et NO^{-}_{3}) favorisent plutôt une production considérable en silice opaline biogénique. En fait, les deux

lignées chimiques (carbonates et silices) sont trouvées ensemble bien qu'avec des proportions variables.

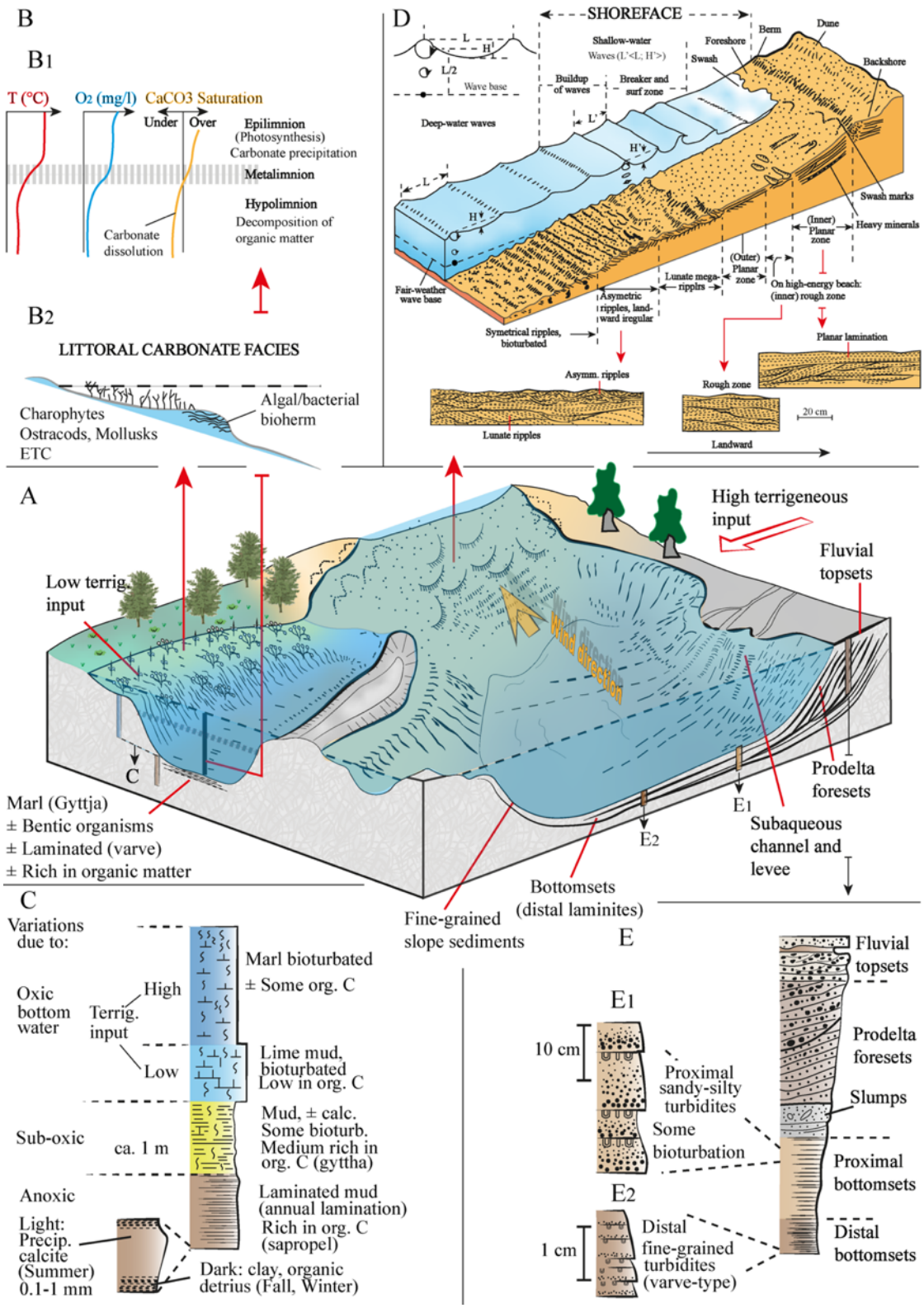


Figure 8. *Conceptual facies model.* ***A***. *3D drawing of the depositional systems for open to balanced lake system (not close or underfilled system) with clastic- (river-driven and wind-driven physical processes) and biochemical-dominated settings.* ***B1***. *Some characteristics of the epi- and hypolimnion of hard-water lakes allowing calcite precipitation in summer time.*

__B2__. Littoral carbonate facies (see __Fig. 9__ for more details). __C__. Idealised stratigraphic log showing variation in facies from the littoral zone (__B2__) towards the profundal (offshore) setting in hard-water lake due to changing terrigenous input and oxygenation of bottom water in biochemical-dominated settings. Note the occurrence of annual lamination (varve). __D__. Nearshore wind-driven clastic-dominated depositional system showing transition from deep-water waves to shallow-water waves and swash (backwash) in the shoreface zone and associated bedforms and internal sedimentary structures. __E__. Idealised stratigraphic log of river-dominated depositional system showing ideal coarsening-upward sequence (detrital clastic-dominated basin-fill), with (__E1__) proximal and (__E2__) distal (varve-like) turbidites. Redrawn with modification after Einsele (2000, his __Figs. 2.29__ and __3.1__).

***Figure 8**. Modèle conceptuel de faciès. __A.__ Illustration en perspective montrant les différents systèmes de dépôt potentiellement rencontrés dans les systèmes lacustres hydrologiquement fermés ou balancés (systèmes fermés sont exclus), avec domination détritique terrigène (processus physiques gouvernés soit par le vent ou par le cours d'eau entrant) ou biochimique. __B1__. Quelques caractéristiques de l'épilimnion et l'hypolimnion des eaux lacustres à caractère dure permettant la précipitation de la calcite pendant la saison l'été. __B2__. Facies carbonaté de la zone littorale (plus de précision en __Fig. 9__). __C__. Log stratigraphique idéalisé montrant une variation de faciès depuis la zone littorale (__B2__) jusqu'à la zone profonde comme réponse au changement de l'apport détritique ainsi que l'oxygénation du fond de lac dans un système de dépôt à dominante biochimique. Note la présence des laminites (lamines saisonnières ou varves). __D__. Système de dépôt de la zone littorale de haute-énergie à dominance détritique montrant la transition depuis les vagues des eaux profondes jusqu'aux vagues des eaux peu profondes et zone de plage. __E__. Log stratigraphique de système de dépôt dominé par les processus fluviaux (remplissage dominé par le détritisme) montrant une séquence à granoclassement négatif, avec des dépôts de turbidites (__E1__) proximaux et (__E2__) distaux (lamines semblables aux varves). Redessinée avec modification d'après Eisele (2000, ses __Figs. 2.29__ et __3.1__).*

1.2.2.1 Zone littorale : modèle de faciès

La sédimentation des carbonates biogéniques ou bio-induits dans les eaux peu profondes (>10 m) est généralement dominante. Ceci est d'autant plus prononcé que le substrat, directement impliqué dans les processus de drainage superficiel ou souterrain, est de nature carbonaté (e.g., calcaires, dolomies). En effet, la zone côtière est dominée par des produits bioclastiques et algaires cantonnés dans une matrice constituée essentiellement de la micrite. Elle est colonisée par des macrophytes aquatiques à racines bien développées. En outre, les charophytes peuvent y proliférer et s'étendre jusqu'à des profondeurs considérables (15-20 m) lorsque l'énergie est suffisamment réduite. La productivité carbonatée biogénique dans la zone littorale se produit par assimilation photosynthétique de CO_2, modifiant ainsi l'équilibre calco-carbonique et déplaçant l'équation vers le sens de la formation de $CaCO_3$, ce qui aboutit au phénomène d'incrustation carbonatée des tiges de certains macrophytes et charophytes (la contribution de certains micro-organismes épiphytes, y compris certaines cyanobactéries, est à considérer aussi), ainsi qu'à la bio-minéralisation des structures productives femelles des charophytes (oogones). Toutefois, la plupart de ces matériaux incrustés sont cassés facilement et ainsi accumulés sur le fond aboutissant à la matrice (micrite) qui cantonne les bioclastes issus des processus de bio-minéralisation contrôlée (e.g., fragments d'oogones, d'ostracodes, de gastéropodes). Toujours dans ce contexte à dominance biologique, les marges présentant un faible gradient topographique ('*backshore evironment*') peuvent héberger des marécages ('*wetlands*') colonisés par une végétation aquatique typique.

En effet, les modèles de faciès proposés pour la zone littorale dominée par la production biologique sont en fonction de la pente et du niveau d'énergie influant sur le littoral. Ainsi, quatre modèles sont proposés par Platt et Wright (1991), à savoir (Fig. 9) :

- 'banc' carbonaté à faible énergie ('*low-energy bench margin*') formé essentiellement de marnes à géométrie semblable de celle des delta de type Gilbert (i.e., avec topsets, foresets et bottomsets) ;
- 'banc' carbonaté à fort énergie ('*high-energy bench margin*'), très commun dans les lacs à large superficie, composé essentiellement de sables oïdales à texture grainestone pouvant s'accumuler pour former une barrière séparant le large du littoral ('*cross-bedded shoals*') ;
- 'ramp' carbonaté à faible énergie ('*low-energy ramp margin*'), ou autrement qualifié d'environnement palustre par d'autres auteurs (e.g., Freytet et Verrecchia, 2002; Alonso-Zarza, 2003; Alonso-Zarza et Wright, 2010), caractérisé par une production typiquement importante de la micrite avec évidences d'une fluctuation de haute fréquence de la tranche d'eau produisant des figures associées à des phénomènes subaériens pédogéniques et diagénitiques (e.g., dessiccations, dissolutions, marmorisation) ;
- 'ramp' carbonaté à fort énergie ('*high-energy ramp margin*') caractérisé par l'occurrence des stromatolithes (biohermes à base des cyanobactéries) et oolithes ou oncolithes.

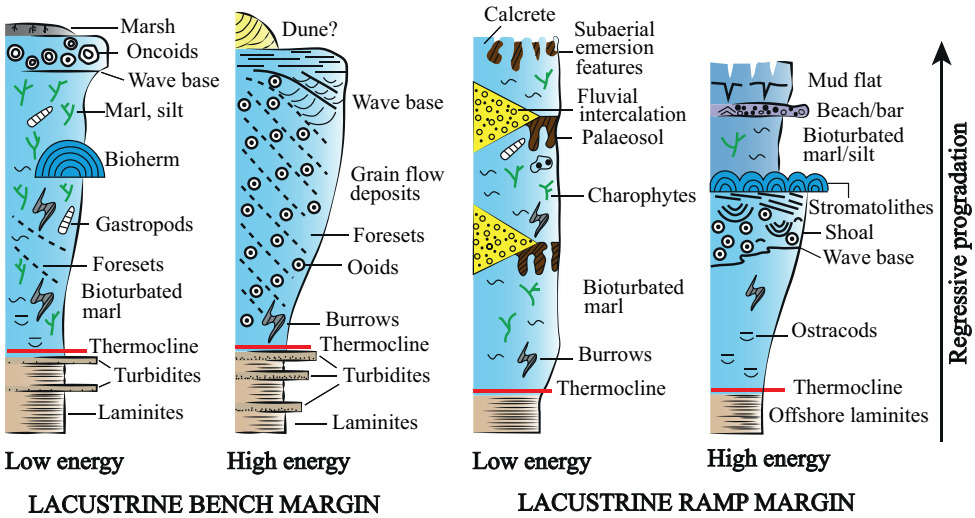


***Figure 9**. Ideal vertical sequences (facies models) of lacustrine carbonates and associated facies showing typical shallowing upwards conditioning a regressive progradation of marginal lacustrine ramp and bench. Redrawn after Platt et Wright (1991, **Fig. 2**) (see also Renaut et al., 2010, **Fig. 8**).*

***Figure 9**. Séquences verticales idéales (modèles de faciès) des carbonates lacustres et faciès associés montrant un passage vers des conditions de plus en plus peu profondes du bas en haut conditionnant une progradation régressive des faciès marginaux de 'ramp' et 'banc'. Redessinée d'après Platt et Wright (1991, **Fig. 2**) (voir aussi Renaut et al., 2010, **Fig. 8**).*

1.2.2.2 Zone centrale (pélagique et profonde) : Modèle de faciès

La sédimentation dans la zone profonde manque les évidences d'une végétation *in situ*. Au sein de la zone pélagique (zone photique), la production des carbonates de calcium est principalement assurée par bio-induction due aux phytoplanctons, bien que la précipitation inorganique puisse se produire aussi durant le brassage de lac ('*turnover*', *voir* Fig. 5 et **§1.1.1.2.**). A titre comparatif, la fraction silico-clastique dans la zone profonde est plus importante que celle de la zone littorale.

Les faciès du large ('*offshore*') sont fortement contrôlés par la dynamique lacustre associée à la stratification thermique (*voir* **§1.1.1.2.**). Par exemple, dans le cas où la stratification thermique est permanente (lacs méromictiques) les conditions anoxiques règnent le fond (hypolimnion) et ainsi favorise l'accumulation et la préservation de la matière organique (exemple modern du lac Tanganyika présenté par Cohen, 1989) (Fig. 5C). Qui plus est, le manque d'oxygène limite la bioturbation par les organismes benthiques. Ceci favorise une parfaite préservation de la succession lamines organiques/lamines carbonatées (le dépôt est *lato sensu* baptisé 'laminites', et *stricto sensu* associé aux environnements glaciaires, 'varves') originaire d'une variation saisonnière de la productivité phytoplanctonique. Ainsi, pendant la saison favorable (généralement l'été et/ou printemps), en raison de leur assimilation de CO_2, l'efflorescence des algues microscopiques conditionne la précipitation des carbonates de calcium et développement d'une lamine carbonatée claire. En revanche, en succombant pendant la saison défavorable, la sédimentation de ces phytoplanctons produit une lamine riche en matière organique (les détails de ces processus sont présentés par Kelts et Hsü, 1978). Dans l'autre cas où le brassage des eaux lacustres est commun (e.g., lacs polymictiques) ou dans le cas des lacs à tranche d'eau peu profonde, l'oxygénation du fond est commune, rehaussant ainsi la bioturbation et limitant la préservation de tels archivages de la variabilité saisonnière de la bio-productivité.
Une présentation plus exhaustive avec plus de schémas pédagogiques sur la sédimentation carbonatée due à l'activité biologique dans la zone pélagique (photique) et sur le développement des laminites dans la zone profonde est fournie par Robin W. Renaut et Elizabeth H. Gierlowski-Kordesch dans le chapitre dédié aux lacs du bouquin 'Facies Models' (Renaut et al., 2010, p. 554-558).

2 Sédimentation fluviatile à fluvio-lacustre à dominante carbonatée : tufs calcaires

Les dépôts de carbonates biogènes en domaine fluviatile actuel et ancien enregistrent une pléthore de systèmes de dépôts qui varient de contextes purement fluviatiles à fluvio-lacustres, exclusivement lacustres et palustres (Arenas-Abad et al., 2010). En fonction de la température ambiante, des conditions d'eau relativement froide à tiède ainsi que l'origine météorique du CO_2 qui participe activement à leur formation, les carbonates fluviatiles à fluvio-lacustres et leurs dépôts

associés sont classés comme des 'travertins météogènes' (Pentecost et Viles, 1994; Pentecost, 2005), aussi dénommés '*tufas*'(ou tufs calcaires) (Pedley, 1990; Ford et Pedley, 1996). Le terme tufs calcaires est communément attribué aux faciès contenant des restes de plantes incrustés ou imprégnés de carbonates de calcium (Arenas-Abad et al., 2010). En effet, Pedley (1990) a délibérément recommandé à ce que le terme 'tufs calcaires' soit employé pour les carbonates biogènes associés aux systèmes fluviatiles et fluvio-lacustres où l'origine de $\mathbf{CO_2}$ est météorique (e.g., oncolithes). Dans leur publication fondatrice, Arenas-Abad et al. (2010) ont proposé une classification descriptive de ces dépôts carbonatés fluvio-lacustres sur la base de leurs caractéristiques texturales, en s'appuyant sur le vocabulaire développé par Dunham (1962) et Embry et Klovan (1971). Cette classification est entièrement adoptée dans ce travail et a fait l'objet d'article déjà publié dans Palaeo-3 et présenté dans le chapitre 5.

2.1 Contexte de formation : aspects chimiques et biochimiques

La précipitation des carbonates de calcium dans les environnements de dépôts fluvio-lacustres est primordialement conditionnée par (i) le degré de saturation ou Indice de Saturation (IS), (ii) l'occurrence des plantes subaquatiques fournissant des sites pour le processus de nucléation et assimilant le $\mathbf{CO_2}$ par le processus de photosynthèse, ainsi que (iii) l'hydrodynamisme qui, par agitation, enclenche le dégazage de $\mathbf{CO_2}$ qui modifie directement l'équilibre calco-carbonique (Arenas-Abad et al., 2010; Arp et al., 2010). Les conditions hydrologiques/hydrogéologiques influent sur la disponibilité, débit, et vitesse de l'eau qui coulent le long du cours d'eau (Arenas et al., 2014a, 2015). Tous les systèmes carbonatés fluvio-lacustres connus sont associés à un substrat constitué de vastes successions lithologiques carbonatées, responsable des concentrations élevées en ions de bicarbonates ($\mathbf{HCO_3^-}$) et de calcium ($\mathbf{Ca^{2+}}$) dans les eaux de surface d'où ils prennent naissance ; d'autres types de roches (e.g., dépôts de gypse) peuvent toutefois contribuer aux propriétés hydro-chimiques de l'eau (Arenas-Abad et al., 2010). Les réactions essentielles qui gouvernent la précipitation chimique de carbonates de calcium sont :

$$\mathbf{CaCO_3 + CO_2 + H_2O <=> (HCO_3^-) + Ca^{2+}} \qquad \mathbf{1)}$$

$$\mathbf{CO_2 + H_2O <=> H_2CO_3 <=> H^+ + HCO_3^-} \qquad \mathbf{2)}$$

Principalement, la réaction vers le sens de formation du carbonate de calcium [sens 2 dans l'équation (1) et sens 1 dans l'équation (2)] est contrôlée par (i) la température (la solubilité de CO_2 dans l'eau est favorisée dans l'eau froide, de sorte que l'Indice de Saturation augmente quand la température augmente) et (ii) la perte en CO_2 de l'eau, qui fait augmenter le pH (Arenas-Abad et al.,

2010). En effet, la perte en dioxyde de carbone de l'eau entraîne une augmentation à la fois du pH, via la consommation de H^+ et HCO_3^-, et de CO_3^{2-}. La perte mécanique en CO_2, e.g., agitation, est considérée comme le mécanisme le plus important en matière de contribution à la précipitation de carbonates de calcium. Ainsi, le dégazage de CO_2 est favorisé en milieu montrant des conditions d'hydrodynamisme fort (forte turbulence, i.e., nombre de Reynolds élevé) telles celles rencontrées au niveau des cascades, rapides et marges lacustres agitées. Précisément parlant, le dégazage (perte mécanique) de CO_2 est promu par des processus baptisés 'effet de l'aération' ('*aeration effect*'), 'effect jet-flow' ('*jet-flow effect*') et 'effet de basse-pression' ('*low-pressure effect*'), qui, collectivement, contribuent à l'augmentation de la surface spécifique air-eau (Zhang et al., 2001; Chen et al., 2004). De ce fait, le taux de précipitation de carbonates de calcium dans les systèmes fluviatiles est proportionnel, avec une bonne corrélation, aux paramètres hydrodynamiques des cours d'eau modernes, e.g., vitesse et turbulence d'écoulement (Drysdale et Gillieson, 1997; Malusa et al., 2003; Arenas-Abad et al., 2010; Gradziński, 2010; Arenas et al., 2014a, 2015, 2019; Auqué et al., 2014; Arenas et Jones, 2017). En régions arides, l'évaporation peut s'agir d'un facteur déterminant dans le processus de dégazage de CO_2 et donc dans la précipitation physicochimique de carbonates de calcium (*voir* Pentecost, 2005).

Outre leur contribution aux attributs faciologiques caractérisant les dépôts de tufs calcaires (*cf. infra*), les plantes hygrophiles (préférant des milieux humides) constituent une composante primordiale et très typique dans les processus chimiques de précipitation de $CaCO_3$ comme elles fournissent des sites pour la nucléation et croissance de CaCO3 et le piégeage des particules carbonatées fines (Arenas-Abad et al., 2010). D'autre part, les microorganismes (e.g., cyanobactéries, certaines algues eucaryotes) et macroorganismes (e.g., mousses, roseaux) contribuent (par bio-médiation) à la production d'une biomasse carbonatée grâce à l'effet de photosynthèse (Bhaya et al., 2002; Shiraishi et al., 2008, 2010; Arp et al., 2010). L'assimilation de CO_2 par voie de photosynthèse ainsi que d'autres activités physiologiques des plantes (e.g., assimilation de bicarbonates) promeuvent la précipitation de $CaCO_3$, bien qu'avec une proportion minimale par rapport aux processus physicochimiques selon quelques études faites sur les dépôts actuels (Pentecost, 1996; Merz-Preiß and Riding, 1999; Arp et al., 2001, 2010; Shiraishi et al., 2008, 2010).

Cyanobactéries et algues sont les plus importants producteurs des 'substances polymériques extracellulaires' ('*extracellular polymeric substances*', EPS) en domaine fluviatile et faciès carbonatés associés (e.g., oncoïds, stromatolithes, tapis algaires et de mousses, tiges encroutées, *cf., infra*) qui créent des microenvironnements favorables à la précipitation des carbonates de calcium (Arp et al.,

2001; Hägele et al., 2006; Gradziński, 2010; Jones et Peng, 2014; Berrendero et al., 2016) tant que les inhibiteurs sont absents (Arenas-Abad et al., 2010; Auqué et al., 2014; Arenas et al., 2015). Il est toutefois à noter que l'élimination de HCO_3^- et Ca^{2+}, que ce soit par assimilation de CO_2 ou de HCO_3^- via les différentes activités physiologiques des plantes et microbes ou bien par la précipitation de la calcite sur la surface des EPS, aboutit à des changements minimaux de l'Indice de Saturation (par rapport à la calcite) dans la solution globale (Pentecost, 2005; Arenas-Abad et al., 2010).

La température peut jouer un rôle important sur la croissance de la flore qui, à son tour, contrôle la quantité produite de la biomasse carbonatée. Par conséquent, la variation du taux de sédimentation à l'échelle centimétrique des tufs calcaires est prévue être dans la même longueur d'onde que les variations de court-terme (saisonnière ou pluriannuelle) des changements climatiques (Arenas-Abad et al., 2010; Vázquez-Urbez et al., 2010). De plus, les variations spatiales des caractères faciologiques et géométriques des dépôts de tufs calcaires, ainsi que leur extension et épaisseur, sont en fonction de la latitude et altitude (Pentecost, 2005; Arenas-Abad et al., 2010).

2.2 Association de faciès et environnements de dépôts : séquences de faciès élémentaires

Dans leur publication fondatrice, Arenas-Abad et al. (2010) ont répertorié un nombre considérable de faciès caractérisant différents environnements et sous-environnements de dépôts carbonatés en domaine fluviatile s.s., fluvio-lacustre, à fluvio-palustre (*voir* leur tableau. 1). Certains de ces faciès se rencontrent dans des sous-environnements uniques, tels que les boundstones des plantes encroutées suspendus ('*boundstones of hanging coated plantes*') qui se forment uniquement au niveau des cascades ou barrages-cascades (Arenas-Abad et al., 2010) (Fig. 10). Toutefois, la plupart se rencontrent dans différents contextes qui vont de fluviatiles au sens stricte, fluvio-lacustres à fluvio-palustres (Fig. 10). Ceci est le cas par exemple des boundstones de bryophytes (communément des mousses) qui peuvent se former sur des cascades et marges des cours d'eau ; rudstones des oncoïdes au milieu de chenaux, au niveau des marges lacustres ; et rudstones de tiges de plantes encroutées au fond de cours d'eau et dans les marges lacustres à conditions palustres (Figs. 9, 10 et 12). Cet aspect exige une adoption d'une approche qui doit prendre en considération les associations verticales de faciès, qui sont génétiquement liés, et non pas prendre séparément chaque faciès lors d'interprétations en termes d'environnements ou sous-environnements de dépôts. Un détail de ces faciès est rapporté explicitement, avec photos de terrain très représentatives, par Arenas-Abad et al. (2010). Que ce soit en contexte fluviatile s.s., fluvio-lacustre, fluvio-palustre à exclusivement palustres, nombreuses sont les séquences verticales de faciès, ou associations de faciès génétiquement liés, qui font distinguer les

différents sous-environnements des tufs calcaires (Fig. 10, *voir* aussi Fig. 7 de Vázquez-Urbez et al., 2012 et Fig. 9 de Arenas et al., 2014b), démasquant ainsi leur diversité et complexité.

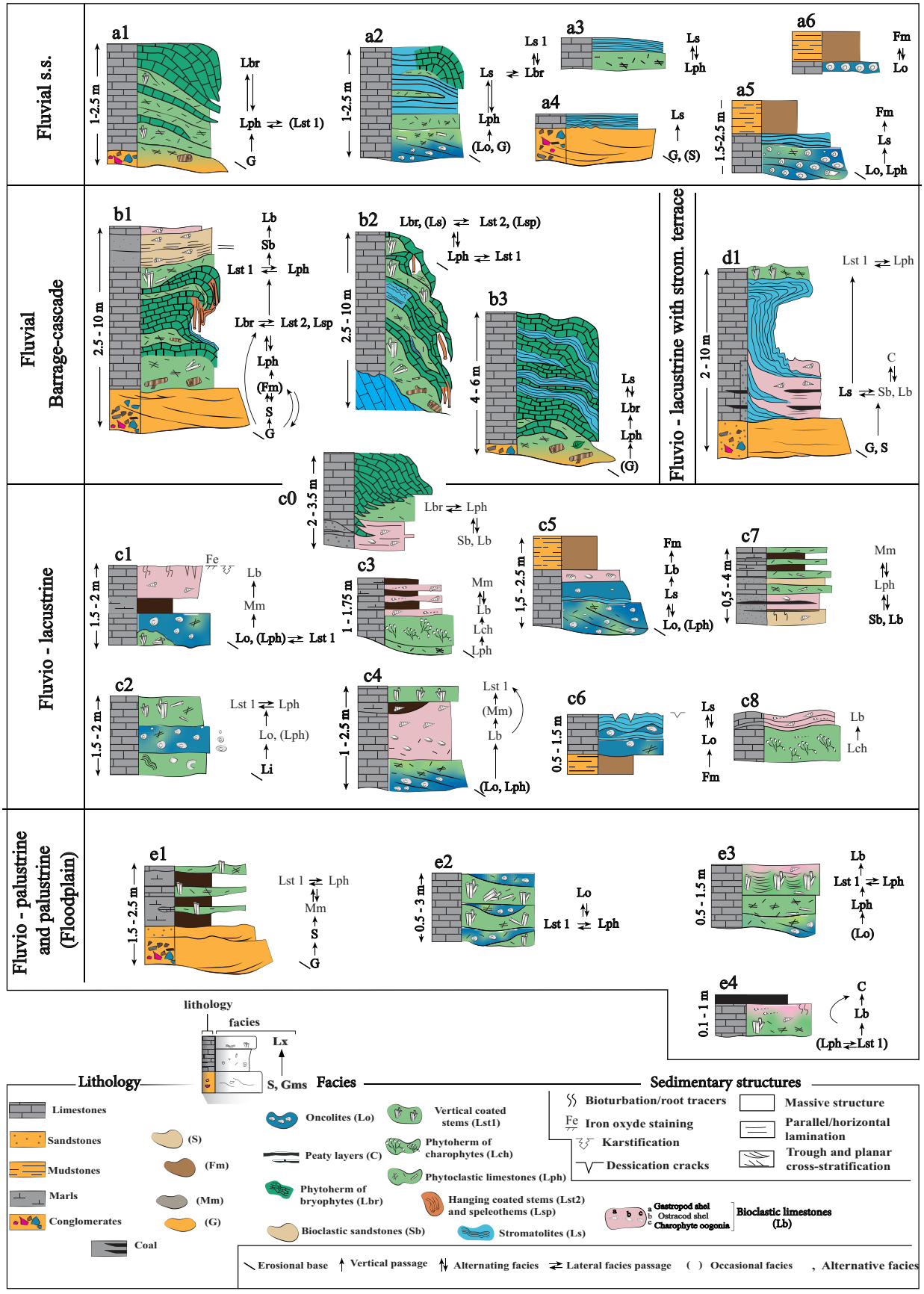


Figure 10. *Some of the most characteristic facies sequences for fluvial s.s., fluvio-lacustrine, and fluvio-palustrine carbonate systems. Compiled after Arenas- Abad et al. (2010, and references therein) Vázquez-Urbez et al. (2012), and Arenas et al. (2014).*

***Figure 10**. Séquences de faciès typiques des systèmes carbonatés fluviatiles s.s., fluvio-lacustres et fluvio-palustres. Compilé d'après Arenas- Abad et al. (2010, et références y afférentes) Vázquez-Urbez et al. (2012), et Arenas et al. (2014).*

La figure 10 exhibe une compilation d'associations verticales de faciès les plus communément reconnues dans les systèmes carbonatés fluviatiles (**a1-a6**, **b1-b3**), fluvio-lacustres (**d1**, **c0-c8**) à fluvio-palustres (**e1-e4**). Celles-ci ont été observées dans différents systèmes de dépôts associés aux contextes fluviatiles que ce soit dans les cas modernes ou fossiles (Arenas-Abad et al., 2010; Vázquez-Urbez et al., 2012; Arenas et al., 2014a, 2014b, 2015; Pla-Pueyo et al., 2017; Toker, 2017; Azennoud et al., 2022a). Les variétés observées dans chaque contexte (e.g., fluviatile s.s.) peuvent refléter (i) des cycles de variation du niveau d'eau et/ou des condition hydrodynamiques d'écoulement ou (ii) des variétés de contextes géomorphologiques (e.g., pente du cours d'eau). En revanche, il faut noter que ces séquences verticales de faciès sont idéales et donc susceptibles de variations (e.g., manque d'un faciès).

Des caractères comparables peuvent toutefois exister entre différentes séquences de faciès représentant différentes conditions de dépôts. Les dépôts détritiques grossiers (conglomérats et/ou sables) sont des exemples qui peuvent former la base des séquences carbonatées fluviatiles s.s., fluvio-lacustres et fluvio-palustres (Fig. 10). Leur présence implique une phase d'érosion prononcée des dépôts plus anciens, avec emplacement d'une incision, précédant la phase de 'bio-construction' (**a1**, **a3**, **a4**, **b1**, **d1**, **e1**). Alors qu'une présentation exhaustive de chaque séquences de faciès est fournie dans les publications originaires (Arenas-Abad et al., 2010, p. 149-155; Vázquez-Urbez et al., 2012, p. 514-517; Arenas et al., 2014b, p. 153-154), sa réitération ici est délibérément jugée superfétatoire.

Considérant l'aspect spatial tridimensionnel, l'occurrence ou non-occurrence d'une ou de plusieurs séquences, répertoriées dans la figure 10, est une fonction des caractéristiques géomorphologiques et structurales (y compris le contrôle tectonique) du substrat rocheux ainsi qu'aux paramètres climatiques qui priment la bio-calcification, cités d'emblée dans cette section. Ceci nous a mené à construire, par inférence ou explicitement, des modèles conceptuels permettant de contraindre l'occurrence de ces séquences et, par extension, de démasquer les interactions entre les différents facteurs de contrôles (climat, caractéristiques structurales et géomorphologiques du substrat) et les systèmes de dépôts qui en découlent.

2.3 Modèles conceptuels de faciès

Comparés à d'autres systèmes d'environnements carbonatés, les systèmes fluvio-lacustres et dépôts carbonatés associés se développent promptement, avec des taux de sédimentation/précipitation très élevés (Emeis et al., 1987; Drysdale et Gillieson, 1997; Merz-Preiß and Riding, 1999; Vázquez-

Urbez et al., 2010; Arenas et al., 2014a, 2015; Auqué et al., 2014; Berrendero et al., 2016). Sur cette base, un degré de complexité transcendant cerne l'étude de ces dépôts puisqu'un taux élevé de sédimentation impliquerait une migration latérale fréquente de faciès (Arenas-Abad et al., 2010). Ceci aboutirait à des successions de faciès reflétant des superpositions de sous-environnements latéralement associés par le fait de progradation, aggradation, rétrogradation et, surtout, processus de migration latérale. Qui plus est, l'érosion est un processus commun qui complique davantage la préservation des dépôts et donc limite l'extraction des signaux de contrôles sur la sédimentation. Partant de tous ces considérations, des tentatives ont été menées en guise de proposer des modèles conceptuels de faciès résumant l'occurrence simultanée de tels systèmes de dépôts (séquence de faciès) sous telles conditions, en prenant comme base les aspects interprétatifs en termes d'environnements et sous-environnements de dépôts (e.g., Pedley, 1990, 2009; Violante et al., 1994; Ford et Pedley, 1996). Cependant, ces modèles proposés ne prennent pas en considération les variétés pétrographiques, sédimentologiques et géomorphologiques à l'échelle d'un même environnement (e.g., fluviatile s.s., palustre, lacustre) ou de sous-environnement (e.g., barrage, cascade, barrage-cascade), communément observées dans des études de cas focalisant à la fois sur les dépôts actuels et anciens. Cet aspect a été parfaitement considéré et résolu par Arenas-Abad et al. (2010) en proposant deux modèles de faciès généraux sur la base du gradient topographique (i.e., fort gradient vs. faible gradient) et de la géomorphologie générale (géomorphologie 'en gradins' ou 'en escalier' vs. géomorphologie 'sans gradins' ; '*stepped vs. non-stepped fluvial geomorphology*') du cours d'eau d'où les séquences de faciès typiques résultent. Les sous-sections suivantes présentent un aperçu sur les principaux aspects caractérisant chaque modèle de faciès et ses variétés selon les travaux de Arenas-Abad et al., 2010, Vázquez-Urbez et al., 2012, Arenas et al., 2014.

2.3.1 'low-gradient, non-stepped, fluvial and fluvio-lacustrine facies model'

Comme l'indiquent ses qualificatifs, ce modèle décrit des conditions de faible gradient sans changements brusques du profil topographique (i.e., occurrence des knickpoints, *cf., infra*). Le réseau fluviatile se caractérise par un style méandriforme à sinueux avec développement typique des plaines d'inondation et ses dépôts associés (e.g., faciès **Fm**, Fig. 10). Aussi typiquement présents sont les oncolithes (faciès **Lo**, Fig. 10) qui se développent au fond de chenaux et forment les briques élémentaires des dépôts de bars et de remplissage de chenaux (**a1** et **a4**, Fig. 10), à l'instar de leur homologues cailloutis ('*gravels*') en domaines fluviatiles à dominance détritique (Fig. 11). Les stromatolithes (faciès **Ls**, Fig. 10) sont présents là où la profondeur de la tranche d'eau en écoulement est peu profonde formant des incrustations autour des dépôts carbonatés déjà mis en place (e.g.,

oncolithes) et en forme de 'biohermes', généralement pendant la période d'étiage, ainsi indiquant des conditions de faible énergie et de manque de sédiments détritiques ('*sediment-starvation conditions*') une fois identifiés dans les dépôts fossiles.

Comme les plaines d'inondation sont raisonnablement communes dans les conditions de faible gradient, des environnements palustres (*sensu* Freytet et Verrecchia, 2002, et Alonso-Zarza, 2003) peuvent y développer tant que ces plaines sont périodiquement inondées pendant les événements de haute énergie (séquences **e1**-**e4**, Fig. 10). Les parties submergées de tiges de plantes hygrophiles colonisant ces endroits sont enrobées de la calcite. Ces encroûtements cylindriques vont rester sur place après disparition du végétal, formant ainsi le faciès typique des environnements palustres associé aux systèmes fluviatiles carbonatés 'boundstones des tiges verticales' ('*boundstones of up-growing stems*', faciès **Lst 1**, Fig. 10) tant que le milieu demeure hydrodynamiquement calme. En revanche, si le milieu devient relativement plus agité, à cause par exemple de processus auto-cyclique de migration latérale des chenaux mentionné plus haut, ces encroutements cylindriques in situ se cassent pour former des détritus remobilisables dits 'phytoclastes' qui s'accumulent dans le fond de chenaux et au niveau des zones palustres situées plus en aval formant le dénommé 'rudstones de phytoclastes' (faciès **Lph**, Fig. 10). Ainsi, les fragments de plantes (encroûtés ou non) et coquilles de gastéropodes constituent les principaux nucléus des oncolithes.

Outre le développement de conditions palustres, les plaines d'inondation peuvent héberger des étangs d'eau ('*pools*') fonctionnant comme des lacs très réduits, interconnectés entre eux et/ou connectés avec les chenaux. Il s'agit de lieux d'accumulation de boues carbonatées avec bioclastes (faciès **Lb**, Fig. 10) formés de gastéropodes, ostracodes, bivalves et autres qui y vivent (Fig. 11). La matière organique est susceptible d'accumulation et de préservation dans ces conditions produisant un faciès organique (faciès **C**, Fig. 10). Les 'boundstones de mousses' (mousses encroûtées in situ formant un faciès 'bio-construit', faciès **Lbr**, Fig. 10) peuvent se développer sur les berges des cours d'eau là où le relief est suffisamment positif ou au niveau des sources, bien que leur occurrence dans de telles conditions (faible gradient avec absence de ruptures de pente) n'est pas fréquente. Dans certaines circonstances, de larges plaines d'inondation peuvent s'établir et ainsi recevant une quantité considérable de sédiments fins (silts et argiles) silico-clastiques et/ou carbonatés détritiques (faciès **Fm**, Fig. 10).

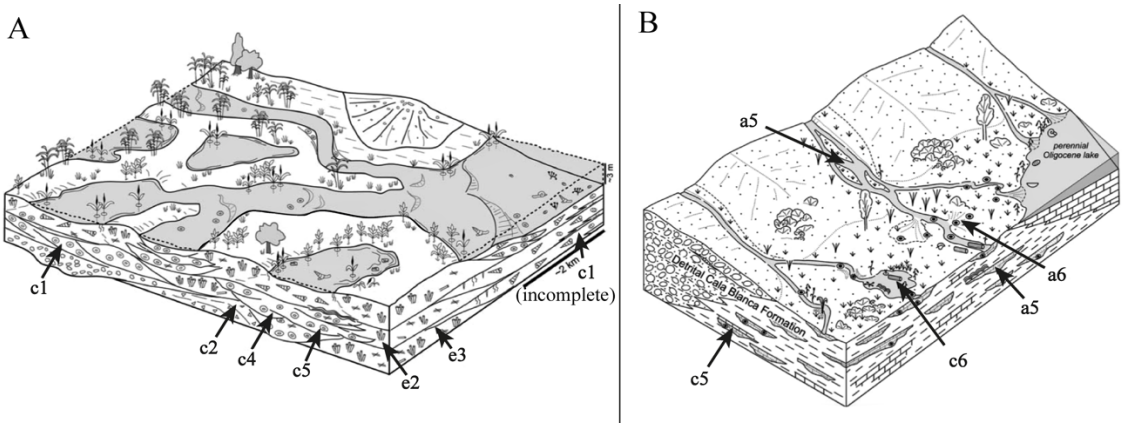


***Figure 11**. Sedimentary conceptual facies model for 'low-gradient, non-stepped conditions' with (**A**) strong development of oncolitic (facies **Lo**) and palustrine facies (e.g., facies **Lst 1**) and (**B**) strong development of oncolitic and stromatolitic (facies **Lo** and **Ls**, respectively) facies and mudstone floodplains (facies **Fm**). Facies sequences are indicated. After Arenas-Abad et al. (2010, and references therein).*

***Figure 11**. Modèle conceptuel de faciès sédimentaire à 'faible gradient à géomorphologie sans gradins' avec (**A**) développement fréquent d'oncolithes et faciès d'environnements palustres, et (**B**) développement fréquent de faciès oncolithiques et stromatolithiques (faciès **Lo** et **Ls**, respectivement) ainsi que les sédiments fins de plaines d'inondation (faciès **Fm**). Les séquences verticales de faciès sont indiquées. D'après Arenas-Abad et al. (2010, et références y afférentes).*

La figure 11A illustre un exemple concret d'une variété du modèle de faciès 'faible gradient à géomorphologie fluviatile sans gradins' ainsi qu'au système de dépôt associés (séquences verticales de faciès) élaboré par Vázquez-Urbez et al. (2002) pour le cas des dépôts de tufs carbonatés d'âge Miocène tardif dans le bassin d'Ebro en Espagne. Dans ce modèle, le système fluviatile est généralement à multi-chenaux de faible sinuosité (ressemblant le style anastomosé des systèmes fluviatiles à dominance clastique) latéralement associés à des environnements palustres et lacustres d'extension limitée. Les oncolithes constituent le faciès dominant des dépôts de chenaux. Spécifique au cas étudié mais pas à être généralisé, ce système a été connecté plus en aval à une étendue d'eau lacustre permanente où certains faciès typiques à cet environnement se développent (e.g., **Mm**, **Lb**, **Lst 1**, Fig. 10). La chose emblématique qui caractérise ce modèle est la migration latérale prompte et consistante des chenaux et ainsi des sous-environnements qui l'encadrent. En outre, le contrôle tectonique sur la topographie, un caractère déterminant dans ce modèle, a été signalé.

La figure 11B présente un autre exemple du modèle 'faible gradient à géomorphologie sans gradins' proposé par Arenas et al. (2007) sur la base des dépôts d'âge Oligocène localisés en Mallorcan (Espagne). Contrairement à ceux schématisés dans la figure 11A, ces dépôts sont caractérisés par l'occurrence de vastes plaines d'inondation, réceptacles d'une sédimentation détritique fine siliciclastique importante (faciès **Fm**, Fig. 10), développement limité de conditions lacustres et faciès associés (e.g., faciès **Lb**) ainsi qu'une mauvaise préservation des boundstones de tiges encroutées (faciès **Lst 1**). Outre les oncolithes qui existent sous différentes tailles, les fragments de carbonates

('intraclasts') sont omniprésents et remplissent le fond des chenaux. La chose typique caractérisant cette variété de modèle de faciès, comparée à celle présentée préalablement, est la migration lente de chenaux ainsi que son apport interprétatif, une fois reconnue dans les séries sédimentaires fossiles, qui assume une sédimentation dans la partie distale du réseau fluviatile.

2.3.2 'High-gradient and stepped fluvial conditions'

Considérant toujours le gradient topographique comme étant la base de la conception, ce modèle décrit des conditions avec un gradient suffisamment fort pour permettre le développement d'une géomorphologie en 'gradins' ou 'escaliers' du cours d'eau (généralement singulier contrairement à l'autre cas). Concrètement parlant, ces gradins, reflétant des changements brusques de pente (ou 'knickpoints' selon le jargon des géomorphologues), constituent des lieux d'occurrences de certaines structures emblématiques du contexte fluviatile carbonaté désignés sous les vocables : 'barrage', 'barrage-cascade', 'cascades' et 'chutes d'eaux' (distinction entre ces structures est fournie dans Arenas-Abad et al., 2010). Ainsi, étant des lieux enclins à des taux de sédimentation/précipitation élevés, en raison de dégazage intense de CO_2 (*voir* Zhang et al., 2001), les barrages peuvent servir d'obstacles enclins à conditionner des étangs d'eau (conditions palustres ou lacustres) en amont de ceux-ci et des cascades en leur aval. En termes de faciès sédimentaires, les barrages ou barrages-cascades sont formés majoritairement de boundstones de mousses (**Lbr**) se développant sur des matériaux remaniés (généralement des débris de végétaux encroûtés ou non, **Lph**). Les stromatolithes (**Ls**) sont aussi des faciès communs de ces édifices carbonatés. Ils sont communément trouvés en alternance avec les boundstones de mousses reflétant des changements dans l'hydrodynamisme (les stromatolithes tolèrent un hydrodynamisme fort). Les étendues d'eau relativement stagnante d'arrière-barrages sont le siège d'une sédimentation typiques aux zones palustres (**e1-e4**, Fig. 10) ou lacustres (**c0-c8**, Fig. 10) conformément à l'échelle en question. De ce fait, les faciès **Lst 1**, **Lb**, **Sb**, **Mm** et **C** sont susceptibles de se développer (signification des codes en Fig. 10, *voir* aussi Arenas-Abad et al., 2010, tableau 1). Outre ces caractéristiques fondamentales de ce modèle qui le distinguent facilement de celui préalablement présenté, d'autres considérations en matière d'extension et de distribution de faciès sont à souligner (i.e., variétés de ce modèle). C'est ainsi qu'Arenas et al. (2014b), sur la base des dépôts carbonatés fluviolacustres de la vallée Añamaza (Espagne), ont proposé deux variétés de ce modèle (i.e., 'à géomorphologie en gradins') selon le paramètre pente (Fig. 12B) : (i) modèle à pente modérée (1.3-2.5%) et (ii) modèle à pente forte (5.7%). En général, les deux variétés partagent les principaux systèmes de dépôts (chenaux, cascades, barrages-cascades et zones endiguées par ces barrages ou retenues), mais la différence se voit dans l'extension et la distribution de ces systèmes le

long du cours d'eau ainsi que le développement de certains environnements typiques (e.g., chenaux escarpés et cascades en escalier de taille réduite dans le modèle à forte pente).

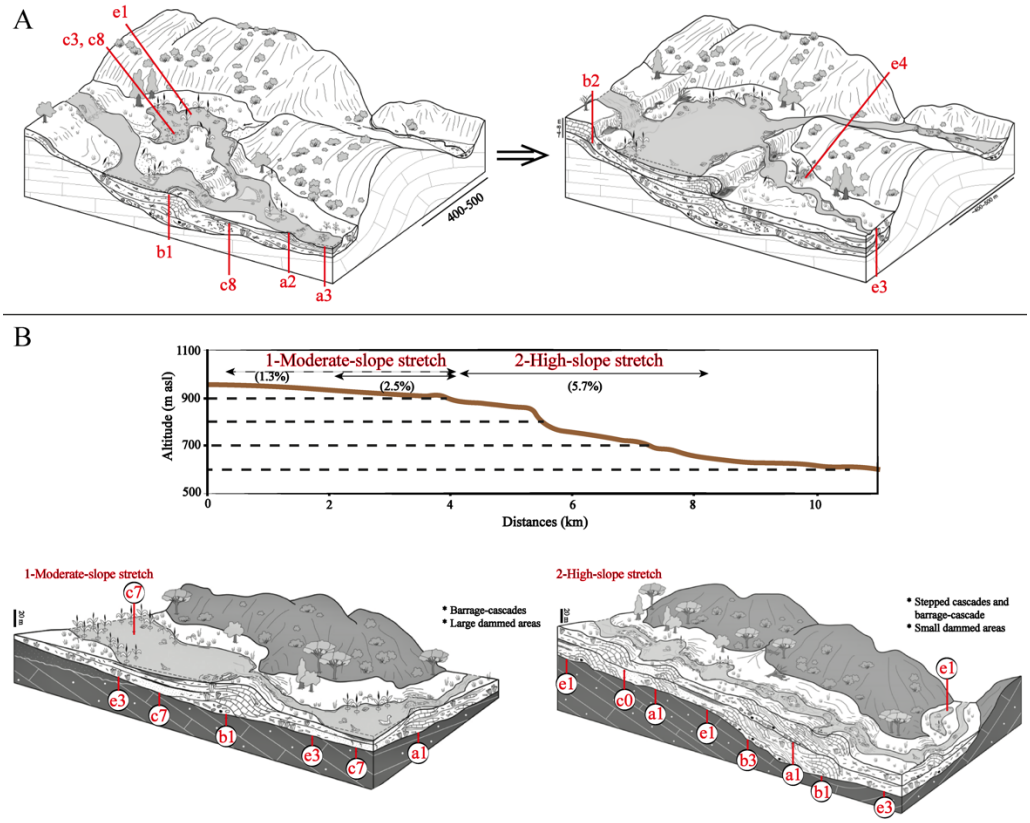


***Figure 12**. Sedimentary conceptual facies model for 'high-gradient, stepped conditions' (after Arenas-Abad et al., 2010). **A**. 3D drawings showing initial development of barrage a build-up on rudstones of phytoclasts (**Lph**) and subsequent vertical accretion by mosses giving rise to higher height/width of the build-up, thereby conditioning extensive dammed area upstream (after Vázquez-Urbez et al., 2012). **B**. Two varieties of the stepped facies models proposed for moderate slope (1.3-2.5%) and high slope (5.7%) (after Arenas et al., 2014b).*

***Figure 12**. Modèles conceptuels de faciès à 'fort-gradient à géomorphologie en gradins' (d'après Arenas-Abad et al., 2010). **A**. Représentation tridimensionnelle montrant le mécanisme de développement d'un édifice de barrage sur des rudstones de phytoclastes (**Lph**) et l'accrétion verticale subséquente conduite par le développement des mousses conditionnant un fort rapport hauteur/largeur de l'édifice, créant ainsi de l'espace en amont pour de vaste étendue d'eau plus ou moins stagnante (d'après Vázquez-Urbez et al., 2012). **B**. Deux variétés du modèle à géomorphologie 'en gradins' proposées pour une pente modérée (1.3-2.5%) et pente forte (5.7%) (d'après Arenas et al., 2014b).*

Dans le cas du modèle à forte pente, la vallée du chenal est généralement étroite et caractérisée par une série de ruptures de pente ('knickpoints') très serrées. Dans chaque rupture se développe un édifice de barrage ou barrage-cascade qui est principalement constitué sur la base des phytohermes mousse (**Lbr**) et rudstones de phytoclastes (**Lph**). Des étendues, très réduites, d'eau plus ou moins stagnantes ('*dammed area*') peuvent s'individualisées en arrière de chacun de ces édifices. Des dépôts d'extraclastes grossiers polygéniques et phytoclastes lenticulaires et en forme de coin ('*wedge-shaped*') sont présents sur les tronçons plus raides de chenaux (**a0**, Figs. 10 et 12B) et témoignent d'une activité importante d'érosion. L'association verticale entre stromatolithes et phytohermes de mousses constitue le brique élémentaire des cascades en escalier (i.e., façade avale inclinée, pas

verticale, en forme de dôme ou convexe) (**b3**, Figs. 10 et 12B) et indique des changements hydrodynamiques comme mentionnés préalablement. Généralement, ce modèle est typiquement distingué par l'occurrence fréquente des barrages, barrages-cascades et de chutes d'eau et faciès associés et par la rareté d'occurrence de phytohermes de tiges à croissance verticale (**Lst 1**) caractérisant les milieux palustres plus ou moins hydrodynamiquement stagnants.

Dans un contexte de pente modérée, la vallée se présente large et extensive dans certains tronçons, séparés par des tronçons où la vallée se montre étroite, conformément à une géomorphologie 'en gradins' plus espacés, comparée au modèle-type mentionné en haut. Ainsi, cette variété de modèle 'en gradin' caractérise des contextes hydrodynamiques avec développement de larges retenues d'eau stagnante ou à mouvement très lent, où des conditions palustres ou même lacustres peuvent se former, endiguées par des barrages ou barrages-cascades. Ces retenues ('*dammed areas*') sont le siège d'une sédimentation extensive de silts, boues (**Lb**) et sables (**Sb**) à gastéropodes alternant ou pas avec des phytoclastes et sédiments marneux et, dans certains cas, riches en matière organique (tourbe ou sapropel, faciès **C**, Figs. 10, 12B), conformément aux séquences verticales idéales **c1**, **c3 et c7** (Fig. 10). Dans des conditions peu profondes ou marges d'extensif espaces lacustres peuvent se développer des conditions palustres enclins à former les séquences verticales typiques **e2**, **e3** et la partie supérieure de **c4** (Fig. 10). Généralement, la chose importante qui distingue cette variété de modèle décrivant la géomorphologie 'en gradins' est le développement commun d'une végétation hygrophiles si bien que les espaces à hydrodynamisme faible sont fréquents, et, par conséquent, l'occurrence fréquente du faciès **Lst 1** caractérisant les conditions palustres.

Références

Allan, J.C., Kirk, R.M., 2000. Wind wave characteristics at Lake Dunstan, South Island, New Zealand. New Zealand Journal of Marine and Freshwater Research 34, 573–591. https://doi.org/10.1080/00288330.2000.9516959

Allen, J.R.L., 1982. Sedimentary structures, their character and physical basis. Elsevier.

Allen, J.R.L., 1977. The possible mechanics of convolute lamination in graded sand beds. Journal of the Geological Society 134, 19–31.

Arenas, C., Auqué, L., Osácar, C., Sancho, C., Lozano, M.V., Vázquez-Urbez, M., Pardo, G., 2015. Current tufa sedimentation in a high discharge river: a comparison with other synchronous tufa records in the Iberian Range (Spain). Sedimentary Geology 325, 132–157.

Arenas, C., Cabrera, L., Ramos, E., 2007. Sedimentology of tufa facies and continental microbialites from the Palaeogene of Mallorca Island (Spain). Sedimentary Geology 197, 1–27. https://doi.org/10.1016/j.sedgeo.2006.08.009

Arenas, C., Jones, B., 2017. Temporal and environmental significance of microbial lamination: Insights from Recent fluvial stromatolites in the River Piedra, Spain. Sedimentology 64, 1597–1629. https://doi.org/10.1111/sed.12365

Arenas, C., Osácar, M.C., Auqué, L., Sancho, C., 2019. Coupling textural and stable-isotope variations in fluvial stromatolites: Comparison of Pleistocene and recent records in NE Spain. J. Palaeogeogr. 8, 13. https://doi.org/10.1186/s42501-019-0021-y

Arenas, C., Vázquez-Urbez, M., Auqué, L., Sancho, C., Osácar, C., Pardo, G., 2014a. Intrinsic and extrinsic controls of spatial and temporal variations in modern fluvial tufa sedimentation: A thirteen-year record from a semi-arid environment. Sedimentology 61, 90–132.
Arenas, C., Vázquez-Urbez, M., Pardo, G., Sancho, C., 2014b. Sedimentology and depositional architecture of tufas deposited in stepped fluvial systems of changing slope: Lessons from the Quaternary Añamaza valley (Iberian Range, Spain). Sedimentology 61, 133–171. https://doi.org/10.1111/sed.12053
Arenas-Abad, C., Vázquez-Urbez, M., Pardo-Tirapu, G., Sancho-Marcén, C., 2010. Chapter 3 Fluvial and Associated Carbonate Deposits, in: Developments in Sedimentology. Elsevier, pp. 133–175. https://doi.org/10.1016/S0070-4571(09)06103-2
Arp, G., Bissett, A., Brinkmann, N., Cousin, S., De Beer, D., Friedl, T., Mohr, K.I., Neu, T.R., Reimer, A., Shiraishi, F., 2010. Tufa-forming biofilms of German karstwater streams: microorganisms, exopolymers, hydrochemistry and calcification. Geological Society, London, Special Publications 336, 83–118.
Arp, G., Wedemeyer, N., Reitner, J., 2001. Fluvival tufa formation in a hard-water creek (Deinschwanger Bach, Franconian Alb, Germany). Facies 44, 1–22.
Ashton, A.D., Murray, A.B., Littlewood, R., Lewis, D.A., Hong, P., 2009. Fetch-limited self-organization of elongate water bodies. Geology 37, 187–190. https://doi.org/10.1130/G25299A.1
Auqué, L., Arenas, C., Osácar, C., Pardo, G., Sancho, C., Vázquez-Urbez, M., 2014. Current tufa sedimentation in a changing-slope valley: the River Añamaza (Iberian Range, NE Spain). Sedimentary Geology 303, 26–48.
Azennoud, K., Baali, A., Ait Brahim, Y., Ahouach, Y., Hakam, O., 2022. Climate controls on tufa deposition over the last 5000 years: A case study from Northwest Africa. Palaeogeography, Palaeoclimatology, Palaeoecology 586, 110767. https://doi.org/10.1016/j.palaeo.2021.110767
Baali, A., Gourari, L., Fedan, B., 1996. Types de dépôts et processus de mise en place des cônes de déjection dans le bassin de la dayet Afourgagh (Moyen Atlas, Maroc). Bull. 1115!. ScL 51–61.
Bates, C.C., 1953. RATIONAL THEORY OF DELTA FORMATION1. AAPG Bulletin 37, 2119–2162. https://doi.org/10.1306/5CEADD76-16BB-11D7-8645000102C1865D
Benison, K.C., Bowen, B.B., Oboh-Ikuenobe, F.E., Jagniecki, E.A., LaClair, D.A., Story, S.L., Mormile, M.R., Hong, B.-Y., 2007. Sedimentology of Acid Saline Lakes in Southern Western Australia: Newly Described Processes and Products of an Extreme Environment. Journal of Sedimentary Research 77, 366–388. https://doi.org/10.2110/jsr.2007.038
Berrendero, E., Arenas, C., Mateo, P., Jones, B., 2016. Cyanobacterial diversity and related sedimentary facies as a function of water flow conditions: Example from the Monasterio de Piedra Natural Park (Spain). Sedimentary Geology 337, 12–28. https://doi.org/10.1016/j.sedgeo.2016.03.003
Bhaya, D., Schwarz, R., Grossman, A.R., 2002. Molecular Responses to Environmental Stress, in: Whitton, B.A., Potts, M. (Eds.), The Ecology of Cyanobacteria: Their Diversity in Time and Space. Springer Netherlands, Dordrecht, pp. 397–442. https://doi.org/10.1007/0-306-46855-7_15
Blair, T.C., McPherson, J.G., 2009. Processes and Forms of Alluvial Fans, in: Parsons, A.J., Abrahams, A.D. (Eds.), Geomorphology of Desert Environments. Springer Netherlands, Dordrecht, pp. 413–467. https://doi.org/10.1007/978-1-4020-5719-9_14
Boehrer, B., Schultze, M., 2008. Stratification of lakes. Reviews of Geophysics 46. https://doi.org/10.1029/2006RG000210
Carter, R.M., 1975. A discussion and classification of subaqueous mass-transport with particular application to grain-flow, slurry-flow, and fluxoturbidites. Earth-Science Reviews 11, 145–177. https://doi.org/10.1016/0012-8252(75)90098-7
Chaumillon, E., Bertin, X., Fortunato, A.B., Bajo, M., Schneider, J.-L., Dezileau, L., Walsh, J.P., Michelot, A., Chauveau, E., Créach, A., Hénaff, A., Sauzeau, T., Waeles, B., Gervais, B., Jan, G., Baumann, J., Breilh, J.-F., Pedreros, R., 2017. Storm-induced marine flooding: Lessons from a multidisciplinary approach. Earth-Science Reviews 165, 151–184. https://doi.org/10.1016/j.earscirev.2016.12.005
Chen, J., Zhang, D.D., Wang, S., Xiao, T., Huang, R., 2004. Factors controlling tufa deposition in natural waters at waterfall sites. Sedimentary Geology 166, 353–366.
Cohen, A.S., 1989. Facies relationships and sedimentation in large rift lakes and implications for hydrocarbon exploration: Examples from lakes Turkana and Tanganyika. Palaeogeography, Palaeoclimatology, Palaeoecology, The Phanerozoic Record of Lacustrine Basins and Their Environmental 70, 65–80. https://doi.org/10.1016/0031-0182(89)90080-1

Cohen, A.S., Thouin, C., 1987. Nearshore carbonate deposits in Lake Tanganyika. Geology 15, 414–418. https://doi.org/10.1130/0091-7613(1987)15<414:NCDILT>2.0.CO;2
Collinson, J., 2019. Sedimentary structures. Dunedin Academic Press Ltd.
Collinson, J., 1994. Sedimentary deformational structures, in: The Geological Deformation of Sediments. Springer, pp. 95–125.
Dake, J.M.K., Harleman, D.R.F., 1969. Thermal stratification in lakes: Analytical and laboratory studies. Water Resources Research 5, 484–495. https://doi.org/10.1029/WR005i002p00484
Dam, G., Surlyk, F., 1992. Forced regressions in a large wave-and storm-dominated anoxic lake, Rhaetian-Sinemurian Kap Stewart Formation, East Greenland. Geology 20, 749–752.
Dam, G., Surlyk, F., Posamentier, H.W., Summerhayes, C.P., Haq, B.U., Allen, G.P., 1993. Cyclic sedimentation in a large wave and storm-dominated anoxic lake; Kap Stewart Formation (Rhaetian-Sinemurian), Jameson Land, East Greenland. Sequence stratigraphy and facies associations 18, 419–448.
Dasgupta, P., 2003. Sediment gravity flow—the conceptual problems. Earth-Science Reviews 62, 265–281. https://doi.org/10.1016/S0012-8252(02)00160-5
Dean, W.E., 1981. Carbonate Minerals and Organic Matter in Sediments of Modern North Temperate Hard-Water Lakes, in: Ethridge, F.G., Flores, R.M. (Eds.), Recent and Ancient Nonmarine Depositional Environments: Models for Exploration. SEPM Society for Sedimentary Geology, p. 0. https://doi.org/10.2110/pec.81.31.0213
Dean, W.E., Forester, R.M., Bright, J., Anderson, R.Y., 2007. Influence of the diversion of Bear River into Bear Lake (Utah and Idaho) on the environment of deposition of carbonate minerals. Limnology and Oceanography 52, 1094–1111. https://doi.org/10.4319/lo.2007.52.3.1094
Dean, W.E., Fouch, T.D., 1983. Lacustrine Environment: Chapter 2: PART 1 43, 97–116.
Dechen, S., Aiping, S., 2012. Typical earthquake-induced soft-sediment deformation structures in the Mesoproterozoic Wumishan Formation, Yongding River Valley, Beijing, China and interpreted earthquake frequency. Journal of Palaeogeography 1, 71–89. https://doi.org/10.3724/SP.J.1261.2012.00007
Desiage, P.-A., Lajeunesse, P., St-Onge, G., Normandeau, A., Ledoux, G., Guyard, H., Pienitz, R., 2015. Deglacial and postglacial evolution of the Pingualuit Crater Lake basin, northern Québec (Canada). Geomorphology 248, 327–343. https://doi.org/10.1016/j.geomorph.2015.07.023
Drysdale, R., Gillieson, D., 1997. Micro-erosion meter measurements of travertine deposition rates: a case study from Louie Creek, Northwest Queensland, Australia. Earth Surface Processes and Landforms: The Journal of the British Geomorphological Group 22, 1037–1051.
Dunham, R.J., 1962. Classification of Carbonate Rocks According to Depositional Textures 38, 108–121.
Einsele, G., 2000. Continental Sediments, in: Einsele, G. (Ed.), Sedimentary Basins: Evolution, Facies, and Sediment Budget. Springer, Berlin, Heidelberg, pp. 19–93. https://doi.org/10.1007/978-3-662-04029-4_2
Embry, A.F., Klovan, J.E., 1971. A LATE DEVONIAN REEF TRACT ON NORTHEASTERN BANKS ISLAND, N.W.T.1. Bulletin of Canadian Petroleum Geology 19, 730–781. https://doi.org/10.35767/gscpgbull.19.4.730
Emeis, K.-C., Richnow, H.-H., Kempe, S., 1987. Travertine formation in Plitvice National Park, Yugoslavia: chemical versus biological control. Sedimentology 34, 595–609. https://doi.org/10.1111/j.1365-3091.1987.tb00789.x
Eugster, H.P., Hardie, L.A., 1978. Saline Lakes, in: Lerman, A. (Ed.), Lakes: Chemistry, Geology, Physics. Springer, New York, NY, pp. 237–293. https://doi.org/10.1007/978-1-4757-1152-3_8
Ford, T.D., Pedley, H.M., 1996. A review of tufa and travertine deposits of the world. Earth-Science Reviews 41, 117–175. https://doi.org/10.1016/S0012-8252(96)00030-X
Fouinat, L., Sabatier, P., David, F., Montet, X., Schoeneich, P., Chaumillon, E., Poulenard, J., Arnaud, F., 2018. Wet avalanches: long-term evolution in the Western Alps under climate and human forcing. Climate of the Past 14, 1299–1313. https://doi.org/10.5194/cp-14-1299-2018
Gierlowski-Kordesch, E., Rust, B.R., 1994. The Jurassic East Berlin Formation, Hartford Basin, Newark Supergroup (Connecticut and Massachusetts): A Saline Lake Playa Alluvial Plain System.
Gierlowski-Kordesch, E.H., 2010. Chapter 1 Lacustrine Carbonates, in: Alonso-Zarza, A.M., Tanner, L.H. (Eds.), Developments in Sedimentology, Carbonates in Continental Settings: Facies, Environments, and Processes. Elsevier, pp. 1–101. https://doi.org/10.1016/S0070-4571(09)06101-9

Gradziński, M., 2010. Factors controlling growth of modern tufa: results of a field experiment. Geological Society, London, Special Publications 336, 143–191.
Greb, S.F., Dever, G.R., Ettensohn, F.R., Rast, N., Brett, C.E., 2002. Critical evaluation of possible seismites: Examples from the Carboniferous of the Appalachian basin. SPECIAL PAPERS-GEOLOGICAL SOCIETY OF AMERICA 109–126.
Hägele, D., Leinfelder, R., Grau, J., Burmeister, E.-G., Struck, U., 2006. Oncoids from the river Alz (southern Germany): tiny ecosystems in a phosphorus-limited environment. Palaeogeography, Palaeoclimatology, Palaeoecology 237, 378–395.
Hakala, A., 2004. Meromixis as a part of lake evolution; observations and a revised classification of true meromictic lakes in Finland. Boreal environment research 9, 37–53.
Håkanson, L., 1982. Bottom dynamics in lakes, in: Sly, P.G. (Ed.), Sediment/Freshwater Interaction, Developments in Hydrobiology. Springer Netherlands, Dordrecht, pp. 9–22. https://doi.org/10.1007/978-94-009-8009-9_2
Hardie, L.A., Smoot, J.P., Eugster, H.P., 1978. Saline Lakes and their Deposits: A Sedimentological Approach, in: Modern and Ancient Lake Sediments. John Wiley & Sons, Ltd, pp. 7–41. https://doi.org/10.1002/9781444303698.ch2
Haughton, P., Davis, C., McCaffrey, W., Barker, S., 2009. Hybrid sediment gravity flow deposits – Classification, origin and significance. Marine and Petroleum Geology, Sediment Gravity Flows - Recent Insights into their Dynamic and Stratified/Composite Nature 26, 1900–1918. https://doi.org/10.1016/j.marpetgeo.2009.02.012
He, B., Qiao, X., 2015. Advances and Overview of the Study on Paleo-earthquake Events: A Review of Seismites. Acta Geologica Sinica 89, 1702–1746. https://doi.org/10.1111/1755-6724.12575
Hutchinson, G.E., 1957. A treatise on limnology. Vol 1: Georgraphy, physics and chemistry. John Wiley & Sons.
Jones, B., Peng, X., 2014. Multiphase calcification associated with the atmophytic cyanobacterium Scytonema julianum. Sedimentary Geology 313, 91–104. https://doi.org/10.1016/j.sedgeo.2014.09.002
Jones, B.F., Deocampo, D.M., 2003. Geochemistry of Saline Lakes. Treatise on Geochemistry 5, 605. https://doi.org/10.1016/B0-08-043751-6/05083-0
Kelts, K., Hsü, K.J., 1978. Freshwater Carbonate Sedimentation, in: Lerman, A. (Ed.), Lakes: Chemistry, Geology, Physics. Springer, New York, NY, pp. 295–323. https://doi.org/10.1007/978-1-4757-1152-3_9
Kempe, S., Kazmierczak, J., 1990. Calcium carbonate supersaturation and the formation of in situ calcified stromatolites. Facets of modern biogeochemistry 255–278.
Kirillin, G., Shatwell, T., 2016. Generalized scaling of seasonal thermal stratification in lakes. Earth-Science Reviews 161, 179–190. https://doi.org/10.1016/j.earscirev.2016.08.008
Kremer, K., Anselmetti, F.S., Evers, F.M., Goff, J., Nigg, V., 2021. Freshwater (paleo)tsunamis – a review. Earth-Science Reviews 212, 103447. https://doi.org/10.1016/j.earscirev.2020.103447
Last, W.M., Ginn, F.M., 2005. Saline systems of the Great Plains of western Canada: an overview of the limnogeology and paleolimnology. Aquat. Biosyst. 1, 10. https://doi.org/10.1186/1746-1448-1-10
Lewis Jr., W.M., 1983. A Revised Classification of Lakes Based on Mixing. Can. J. Fish. Aquat. Sci. 40, 1779–1787. https://doi.org/10.1139/f83-207
Lowe, D.R., 1982. Sediment gravity flows; II, Depositional models with special reference to the deposits of high-density turbidity currents. Journal of Sedimentary Research 52, 279–297. https://doi.org/10.1306/212F7F31-2B24-11D7-8648000102C1865D
Lowe, D.R., 1975. Water escape structures in coarse-grained sediments. Sedimentology 22, 157–204.
Lowenstein, T.K., Hardie, L.A., 1985. Criteria for the recognition of salt-pan evaporites. Sedimentology 32, 627–644. https://doi.org/10.1111/j.1365-3091.1985.tb00478.x
Malusa, J., Overby, S.T., Parnell, R.A., 2003. Potential for travertine formation: Fossil Creek, Arizona. Applied Geochemistry 18, 1081–1093. https://doi.org/10.1016/S0883-2927(02)00241-X
Menzies, J., van der Meer, J.J.M., Ravier, E., 2016. A kinematic unifying theory of microstructures in subglacial tills. Sedimentary Geology, The environmental significance of soft-sediment deformation 344, 57–70. https://doi.org/10.1016/j.sedgeo.2016.03.024
Merz, M.U.E., 1992. The biology of carbonate precipitation by cyanobacteria. Facies 26, 81–101. https://doi.org/10.1007/BF02539795

Merz-Preiß, M., Riding, R., 1999. Cyanobacterial tufa calcification in two freshwater streams: ambient environment, chemical thresholds and biological processes. Sedimentary Geology 126, 103–124.
Middleton, G.V., Hampton, M.A., 1973. Part I. Sediment Gravity Flows: Mechanics of Flow and Deposition 1–38.
Moernaut, J., 2020. Time-dependent recurrence of strong earthquake shaking near plate boundaries: A lake sediment perspective. Earth-Science Reviews 210, 103344. https://doi.org/10.1016/j.earscirev.2020.103344
Montenat, C., Barrier, P., Ott d'Estevou, P., Hibsch, C., 2007. Seismites: An attempt at critical analysis and classification. Sedimentary Geology 196, 5–30. https://doi.org/10.1016/j.sedgeo.2006.08.004
Moretti, M., (Tom) van Loon, A.J., Liu, M., Wang, Y., 2014. Restrictions to the application of 'diagnostic' criteria for recognizing ancient seismites. Journal of Palaeogeography 3, 162–173. https://doi.org/10.3724/SP.J.1261.2014.00050
Morgan, J.J., Stone, A.T., 1985. Kinetics of chemical processes of importance in lacustrine environments. Chemical Processes in Lakes, John Wiley and Sons, New York New York. 1985. p 389-426, 8 fig, 1 tab, 51 ref.
Mulder, T., Alexander, J., 2001. The physical character of subaqueous sedimentary density flows and their deposits. Sedimentology 48, 269–299. https://doi.org/10.1046/j.1365-3091.2001.00360.x
Müller, G., Irion, G., Förstner, U., 1972. Formation and Diagenesis of Inorganic Ca-Mg Carbonates. Naturwissenschaften 59, 158–164.
Müller, G., Wagner, F., 1978. Holocene Carbonate Evolution in Lake Balaton (Hungary): A Response to Climate and Impact of Man, in: Modern and Ancient Lake Sediments. John Wiley & Sons, Ltd, pp. 57–81. https://doi.org/10.1002/9781444303698.ch4
Murphy, D.H., Wilkinson, B.H., 1980. Carbonate deposition and facies distribution in a central Michigan marl lake. Sedimentology 27, 123–135. https://doi.org/10.1111/j.1365-3091.1980.tb01164.x
Mutti, E., 1992. Turbidite sandstones (275 pp.). San Donato Milanese, Italy: Agip-Istituto di Geologia, Università di Parma.
Mutti, E., Tinterri, R., Remacha, E., Mavilla, N., Angella, S., Fava, L., 1999. An Introduction to the Analysis of Ancient Turbidite Basins from an Outcrop Perspective. American Association of Petroleum Geologists. https://doi.org/10.1306/CE39687
Nardin, T.R., Hein, F.J., Gorsline, D.S., Edwards, B.D., 1979. A Review of Mass Movement Processes, Sediment and Acoustic Characteristics, and Contrasts in Slope and Base-of-Slope Systems Versus Canyon-Fan-Basin Floor Systems., in: Doyle, L.J., Pilkey, O.H. (Eds.), Geology of Continental Slopes. SEPM Society for Sedimentary Geology, p. 0. https://doi.org/10.2110/pec.79.27.0061
Nemec, W., Steel, R.J., 1984. Alluvial and Coastal Conglomerates: Their Significant Features and Some Comments on Gravelly Mass-Flow Deposits 1–31.
Normandeau, A., Lajeunesse, P., Philibert, G., 2013. Late-Quaternary morphostratigraphy of Lake St-Joseph (southeastern Canadian Shield): Evolution from a semi-enclosed glacimarine basin to a postglacial lake. Sedimentary Geology 295, 38–52. https://doi.org/10.1016/j.sedgeo.2013.07.005
Nutz, A., Schuster, M., Barboni, D., Gassier, G., Van Bocxlaer, B., Robin, C., Ragon, T., Ghienne, J.-F., Rubino, J.-L., 2020. Plio-Pleistocene sedimentation in West Turkana (Turkana Depression, Kenya, East African Rift System): Paleolake fluctuations, paleolandscapes and controlling factors. Earth-Science Reviews 211, 103415. https://doi.org/10.1016/j.earscirev.2020.103415
Nutz, A., Schuster, M., Boës, X., Rubino, J.-L., 2017. Orbitally-driven evolution of Lake Turkana (Turkana Depression, Kenya, EARS) between 1.95 and 1.72 Ma: A sequence stratigraphy perspective. Journal of African Earth Sciences 125, 230–243. https://doi.org/10.1016/j.jafrearsci.2016.10.016
Nutz, A., Schuster, M., Ghienne, J.-F., Roquin, C., Bouchette, F., 2016. Wind-driven waterbodies: a new category of lake within an alternative sedimentologically-based lake classification. J Paleolimnol 59, 189–199. https://doi.org/10.1007/s10933-016-9894-2
Nutz, A., Schuster, M., Ghienne, J.-F., Roquin, C., Hay, M.B., Rétif, F., Certain, R., Robin, N., Raynal, O., Cousineau, P.A., Team, S., Bouchette, F., 2015. Wind-driven bottom currents and related sedimentary bodies in Lake Saint-Jean (Québec, Canada). GSA Bulletin 127, 1194–1208. https://doi.org/10.1130/B31145.1
Owen, G., 1987. Deformation processes in unconsolidated sands. Geological Society, London, Special Publications 29, 11–24.

Owen, G., Moretti, M., 2011. Identifying triggers for liquefaction-induced soft-sediment deformation in sands. Sedimentary Geology 235, 141–147. https://doi.org/10.1016/j.sedgeo.2010.10.003
Owen, G., Moretti, M., Alfaro, P., 2011. Recognising triggers for soft-sediment deformation: Current understanding and future directions. Sedimentary Geology, Recognising triggers for soft-sediment deformation: Current understanding and future directions 235, 133–140. https://doi.org/10.1016/j.sedgeo.2010.12.010
Owen, R.B., 2002. Sedimentological Characteristics and Origins of Diatomaceous Deposits in the East African Rift System.
Pedley, H.M., 1990. Classification and environmental models of cool freshwater tufas. Sedimentary Geology 68, 143–154.
Pedley, M., 2009. Tufas and travertines of the Mediterranean region: a testing ground for freshwater carbonate concepts and developments. Sedimentology 56, 221–246.
Pentecost, A., 2005. Travertine. Springer Science & Business Media.
Pentecost, A., 1996. Moss growth and travertine deposition: the significance of photosynthesis, evaporation and degassing of carbon dioxide. Journal of Bryology 19, 229–234. https://doi.org/10.1179/jbr.1996.19.2.229
Pentecost, A., Viles, H., 1994. A review and reassessment of travertine classification. Géographie physique et Quaternaire 48, 305–314.
Pla-Pueyo, S., Viseras, C., Henares, S., Yeste, L.M., Candy, I., 2017. Facies architecture, geochemistry and palaeoenvironmental reconstruction of a barrage tufa reservoir analog (Betic Cordillera, S. Spain). Quaternary International 437, 15–36.
Platt, N.H., Wright, V.P., 1991. Lacustrine Carbonates: Facies Models, Facies Distributions and Hydrocarbon Aspects, in: Lacustrine Facies Analysis. John Wiley & Sons, Ltd, pp. 57–74. https://doi.org/10.1002/9781444303919.ch3
Plaziat, J.-C., Purser, B.H., Philobbos, E.R., 1990. Seismic deformation structures (seismites) in the syn-rift sediments of the NW Red Sea (Egypt). Bulletin de la Société géologique de France 6, 419–434.
Postma, G., 1990. Depositional Architecture and Facies of River and Fan Deltas: A Synthesis, in: Coarse-Grained Deltas. John Wiley & Sons, Ltd, pp. 13–27. https://doi.org/10.1002/9781444303858.ch2
Postma, G., 1986. Classification for sediment gravity-flow deposits based on flow conditions during sedimentation. Geology 14, 291–294. https://doi.org/10.1130/0091-7613(1986)14<291:CFSGDB>2.0.CO;2
Renaut, R.W., Gierlowski-Kordesch, E.H., Dalrymple, R., James, N., 2010. Lakes. Facies models 4, 541–575.
Robbins, L.L., Blackwelder, P.L., 1993. Biochemical and Ultrastructural Evidence for the Origin of Whitings-a Biologically Induced Calcium-Carbonate Precipitation Mechanism-Reply. Geology.
Rosen, M.R., 1994. The importance of groundwater in playas: A review of playa classifications and the sedimentology and hydrology of playas, in: Rosen, M.R. (Ed.), Paleoclimate and Basin Evolution of Playa Systems. Geological Society of America, p. 0. https://doi.org/10.1130/SPE289-p1
Rosenbaum, J.G., Kaufman, D.S., 2009. Paleoenvironments of Bear Lake, Utah and Idaho, and its catchment. Geological Society of America.
Sabatier, P., Moernaut, J., Bertrand, S., Van Daele, M., Kremer, K., Chaumillon, E., Arnaud, F., 2022. A Review of Event Deposits in Lake Sediments. Quaternary 5, 34. https://doi.org/10.3390/quat5030034
Schubel, K.A., Lowenstein, T.K., 1997. Criteria for the recognition of shallow-perennial-saline-lake halites based on Recent sediments from the Qaidam Basin, western China. Journal of Sedimentary Research 67, 74–87. https://doi.org/10.1306/D42684FA-2B26-11D7-8648000102C1865D
Schuster, M., Nutz, A., 2018. Lacustrine wave-dominated clastic shorelines: modern to ancient littoral landforms and deposits from the Lake Turkana Basin (East African Rift System, Kenya). J Paleolimnol 59, 221–243. https://doi.org/10.1007/s10933-017-9960-4
Shanmugam, G., 2017. Global case studies of soft-sediment deformation structures (SSDS): Definitions, classifications, advances, origins, and problems. Journal of Palaeogeography 6, 251–320. https://doi.org/10.1016/j.jop.2017.06.004
Shiraishi, F., Bissett, A., de Beer, D., Reimer, A., Arp, G., 2008. Photosynthesis, respiration and exopolymer calcium-binding in biofilm calcification (Westerhöfer and Deinschwanger Creek, Germany). Geomicrobiology Journal 25, 83–94.

Shiraishi, F., Okumura, T., Takahashi, Y., Kano, A., 2010. Influence of microbial photosynthesis on tufa stromatolite formation and ambient water chemistry, SW Japan. Geochimica et Cosmochimica Acta 74, 5289–5304.
Sims, J.D., 1975. Determining earthquake recurrence intervals from deformational structures in young lacustrine sediments, in: Developments in Geotectonics. Elsevier, pp. 141–152.
Sly, P.G., 1978. Sedimentary Processes in Lakes, in: Lerman, A. (Ed.), Lakes: Chemistry, Geology, Physics. Springer, New York, NY, pp. 65–89. https://doi.org/10.1007/978-1-4757-1152-3_3
Smoot, J.P., Lowenstein, T.K., 1991. Chapter 3 Depositional Environments of Non-Marine Evaporites, in: Melvin, J.L. (Ed.), Developments in Sedimentology, Evaporites, Petroleum and Mineral Resources. Elsevier, pp. 189–347. https://doi.org/10.1016/S0070-4571(08)70261-9
Toker, E., 2017. Quaternary fluvial tufas of Sarıkavak area, southwestern Turkey: Facies and depositional systems. Quaternary International, Non-marine Carbonates: A Multidisciplinary Approach 437, 37–50. https://doi.org/10.1016/j.quaint.2016.06.034
Topal, S., Özkul, M., 2014. Soft-Sediment Deformation Structures Interpreted as Seismites in the Kolankaya Formation, Denizli Basin (SW Turkey). The Scientific World Journal 2014, e352654. https://doi.org/10.1155/2014/352654
Ullyott, P., Holmes, P., 1936. Thermal Stratification in Lakes. Nature 138, 971–971. https://doi.org/10.1038/138971a0
Van Daele, M., Moernaut, J., Silversmit, G., Schmidt, S., Fontijn, K., Heirman, K., Vandoorne, W., De Clercq, M., Van Acker, J., Wolff, C., Pino, M., Urrutia, R., Roberts, S.J., Vincze, L., De Batist, M., 2014. The 600 yr eruptive history of Villarrica Volcano (Chile) revealed by annually laminated lake sediments. GSA Bulletin 126, 481–498. https://doi.org/10.1130/B30798.1
Van Loon, A.J., 2009. Soft-sediment deformation structures in siliciclastic sediments: an overview.
Van Loon, A.T., 2014. The life cycle of seismite research. Geologos 20, 61–66.
Vázquez-Urbez, M., Arenas, C., Pardo, G., 2012. A sedimentary facies model for stepped, fluvial tufa systems in the Iberian Range (Spain): the Quaternary Piedra and Mesa valleys. Sedimentology 59, 502–526.
Vázquez-Urbez, M., Arenas, C., Pardo, G., 2002. Facies fluviolacustres de la unidad superior de la Muela de Borja (Cuenca del Ebro): Modelo sedimentario. Revista de la Sociedad Geológica de España 15, 41–54.
Vázquez-Urbez, M., Arenas, C., Sancho, C., Osácar, C., Auqué, L., Pardo, G., 2010. Factors controlling present-day tufa dynamics in the Monasterio de Piedra Natural Park (Iberian Range, Spain): depositional environmental settings, sedimentation rates and hydrochemistry. International Journal of Earth Sciences 99, 1027–1049.
Verrecchia, E.P., 2007. Lacustrine and palustrine geochemical sediments. Geochemical sediments and landscapes 298–329.
Violante, C., Ferreri, V., D'Argenio, B., Golubic, S., 1994. Quaternary travertines at Rocchetta a Volturno (Isernia, Central Italy). Facies analysis and sedimentary model of an organogenic carbonate system, in: International Association of Sedimentologists, 15th Regional Meeting, Ischia, Pre-Meeting Fieldtrip Guidebook. pp. 3–23.
Waldron, J.W.F., Gagnon, J.-F., 2011. Recognizing soft-sediment structures in deformed rocks of orogens. Journal of Structural Geology, Flow of Rocks 33, 271–279. https://doi.org/10.1016/j.jsg.2010.06.015
Wetzel, R.G., 2001. Limnology: lake and river ecosystems. gulf professional publishing.
Wilhelm, B., Amann, B., Corella, J.P., Rapuc, W., Giguet-Covex, C., Merz, B., Støren, E., 2022. Reconstructing Paleoflood Occurrence and Magnitude from Lake Sediments. Quaternary 5, 9. https://doi.org/10.3390/quat5010009
Xu, M., Bogen, J., Wang, Z., Bønsnes, T.E., Gytri, S., 2015. Pro-glacial lake sedimentation from jökulhlaups (GLOF), Blåmannsisen, northern Norway. Earth Surface Processes and Landforms 40, 654–665. https://doi.org/10.1002/esp.3664
Yu, Z., Loisel, J., Brosseau, D.P., Beilman, D.W., Hunt, S.J., 2010. Global peatland dynamics since the Last Glacial Maximum. Geophysical Research Letters 37. https://doi.org/10.1029/2010GL043584
Zavala, C., 2020. Hyperpycnal (over density) flows and deposits. Journal of Palaeogeography 9, 17. https://doi.org/10.1186/s42501-020-00065-x
Zavala, C., Arcuri, M., 2016. Intrabasinal and extrabasinal turbidites: Origin and distinctive characteristics. Sedimentary Geology 337, 36–54. https://doi.org/10.1016/j.sedgeo.2016.03.008

Zavala, C., Arcuri, M., Meglio, M.D., Diaz, H.G., Contreras, C., 2011. A Genetic Facies Tract for the Analysis of Sustained Hyperpycnal Flow Deposits 31–51. https://doi.org/10.1306/13271349St613438

Zavala, C., Pan, S.X., 2018. Hyperpycnal flows and hyperpycnites: Origin and distinctive characteristics. Lithologic Reservoirs 30, 1–27.

Zhang, D.D., Zhang, Y., Zhu, A., Cheng, X., 2001. Physical mechanisms of river waterfall tufa (travertine) formation. Journal of Sedimentary Research 71, 205–216.